THEME 6: WATER RESOURCES MANAGEMENT

Editor: Amir Hashim Mohamad Kassim


IAHR
AIRH
Supported by
Spain Water
and IWHR, China
IAHR
2017
37th IAHR
WORLD CONGRESS
13-18 August, 2017
Kuala Lumpur, Malaysia
WATER RESOURCES MANAGEMENT
UNDER INCREASING UNCERTAINTY

THE DISTRIBUTION OF FRESHWATER PHYTOPLANKTON IN THE STORMWATER RUNOFF TREATMENT CONSTRUCTED WETLAND

SYAFIQ SHAHARUDDIN[1], AMINUDDIN AB. GHANI[2], NOR AZAZI ZAKARIA[3]
& WAN MAZNAH WAN OMAR[4]

[1,2,3] River Engineering and Urban Drainage Research Center (REDAC), Universiti Sains Malaysia (USM), Engineering Campus, Penang, Malaysia,
redacsyafiq@usm.my; redac02@usm.my; redac01@usm.my
[4] School of Biological Science, Universiti Sains Malaysia (USM), Main Campus, Penang, Malaysia,
wmaznah@usm.my

ABSTRACT

The impact from stormwater runoff is not only on water quality degradation, but also habitat-destroying, which can cause harm to many wildlife population such as fish and birds, and also can kill the native vegetation. Stormwater runoff issues can also cause eutrophication, when the nutrient concentration flow through the pond system is not well treated. The impact can be severe to the ecosystems, water quality and habitat sustainability. The use of constructed wetland to manage the stormwater runoff is well applicable and prove to be the most efficient and environmental friendly. However, in terms of how the impact of wetland performance to the phytoplankton or algae in the system is not well understand. The reason to understand it is as if the algae or phytoplankton overpopulated, which can cause eutrophication and if it is too low, theoretically it will cause problem to the food chain. Thus, the aim of the study is to understand the relationship of water quality performance to the distribution of phytoplankton in the free water surface (FWS) constructed wetland. The results show that freshwater phytoplankton has significantly negative relationship ($p=0.01$) with water quality index (WQI) as well as certain parameters measured such as dissolved oxygen and water temperature. The WQI value showed that the macrophytes zone was low compared to forebay zone and micropool zone. The distribution of phytoplankton was high at macrophytes zone, whereas the wetland plant is expected to contribute high favourable nutrient and other environmental variables for the high abundance of phytoplankton density. Through regression, phyla Chlorophyta shows dominance as well as high R2 value, namely more than 0.7. The constructed wetland is able to retain the sufficient amount of distribution of freshwater phytoplankton at the outlet zone, micropool, for the source of food for higher trophic level.

Keywords: Stormwater; water quality; phytoplankton; constructed wetlands; free water surface.

1 INTRODUCTION

Rapid urban growth in Malaysia over the last 30 years has resulted in increased stormwater flow into receiving waters, increases in flood peaks, and degraded water quality. In the past, stormwater runoff has been generally regarded as a nuisance that must be disposed of as quickly and efficiently as possible. The consequence of removing the stormwater from the land surface so quickly is to increase volumes and peak rates of flow discharge and finally overloading conventional drainage system. This results in a greater runoff that generally requires expensive enhancement of drainage network to reduce severity and frequency of flooding in urban areas. This also results in a higher pollutant wash off from the urban areas leading to deteriorate water quality in the receiving water bodies (Zakaria et al., 2003).

Constructed wetlands are engineered systems that had been designed and constructed to utilize the natural processes involving wetland vegetation, soils and their associated microbial assemblages to assist in treating pollutant and wastewater (Vymazal, 2007). Constructed wetlands generally used to treat various types of wastewater (Vymazal, 2010) such as stormwater runoff-residential (Bavor et al., 2001) and stormwater runoff-highway (Lv et al., 2011). Free water surface (FWS) is a one of the type of constructed wetland with emergent macrophytes is a shallow sealed basin or sequence of basins, containing 20-30 cm of rooting soil, with a water depth of 20-40 cm. The treatment studies from FWS constructed wetlands are also well documented in tropical climate region, especially in Malaysia (Mohammadpour et al., 2014; Mohammadpour et al., 2015; Mohd Noor et al., 2014). However in Malaysia, the study on how well constructed wetlands can contribute and give impact to the biodiversity is scarce. Semeraro et al. (2015) had shown the ability of constructed wetland in sustaining wildlife habitats and biodiversity at local and global scales. Hsu et al. (2011) also suggested that wetland area, cover of aquatic macrophytes and water quality are the most important factor contributing in diversity in constructed wetland. The understanding diversity in the constructed wetland had to be consider the initial stage of whole food web systems, which is phytoplankton or algae. Phytoplankton is a main source of foods to the zooplanktons, invertebrates and fish, which later affected the distribution of birds. Even though the role of phytoplankton is not only to act as a primary producer in food chains, but if it present in the highly abundance

©2017, IAHR. Used with permission / ISSN 1562-6865 (Online) - ISSN 1063-7710 (Print)

in numbers and density, it can cause eutrophication. Eutrophication is characterized by excessive plant and algal growth due to the increased availability of one or more limiting growth factors needed for photosynthesis (Schindler, 2006), such as sunlight, carbon dioxide and nutrient fertilizers. Recently, a few studied had been conducted to start to use the constructed wetland as a new approached and sustainable solution to solve the eutrophication problem (Martin et al., 2013; Calero et al., 2015). The aim of this paper to see the relationship of phytoplankton distribution and which group dominance in each zone in the system in the difference level of water quality observed during the sampling period.

2 MATERIAL AND METHODS

2.1 Site description

The constructed wetland of this study is located in the Universiti Sains Malaysia (USM) Engineering Campus, Seberang Perai Selatan District, Pulau Pinang (Figure 1). The area of the campus is about 320 acres and made up of mainly oil palm plantation land and is fairly flat. This constructed wetland was built to receive 0.0712km^2 catchment area, which comprises of faculty buildings and car park areas.

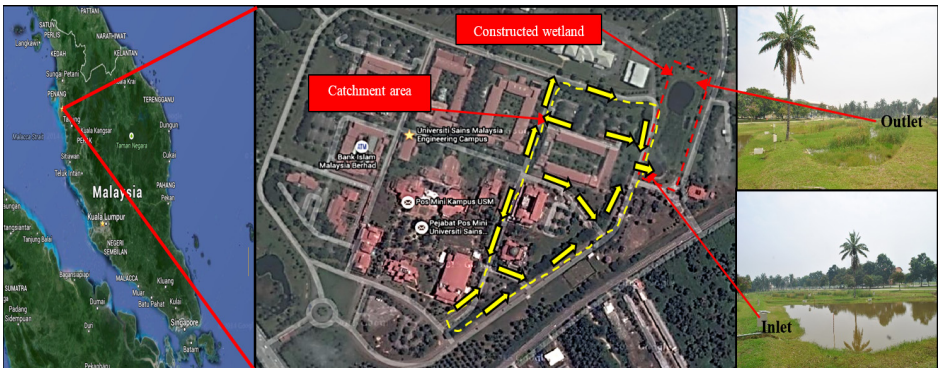

Figure 1. Location of study area of stormwater constructed wetland in USM Engineering Campus.

2.2 Sampling and analysis

The constructed wetland consists of three zones and design based on MSMA 2nd Edition (DID, 2012). The forebay zone is the first zone to receive the discharge from drainage/swales (Table 1). The macrophyte zone consists of three main sub-zones, high marsh, low marsh and deep marsh. In this zone, most of the species are emergent macrophytes. The last zone before the water is discharged from the constructed wetland is called the micropool zone (Table 1). Sampling was conducted from November 2014 until March 2015, once a month throughout the sampling period. Four sampling points were selected in the forebay, seven points were selected at the macrophytes zone and three sampling points were selected at micropool (Figure 2). Sampling time was between 9am and 12pm (3 hours) using grab samples 0.5m below the water surface.

The phytoplankton was sampled using plankton net 35µm mesh size, filtered 40L samples and preserved using formalin 5% solution and Lugol. Phytoplankton identification was done using taxonomic keys references (Shamsudin, 1990; Tomas, 1997). Enumeration of phytoplankton samples was done according to Leupold (1998). The in-situ water quality parameter was taken at the sampling point during the sampling using a YSI Pro Plus multiparameter water quality sonde and laboratory analyses followed HACH procedure (Hach, 2013). Rainfall data were collected using a rain gauge located at the constructed wetland. Pearson correlation will be used to identify the relationship of phytoplankton abundance (cell/ml) and WQI

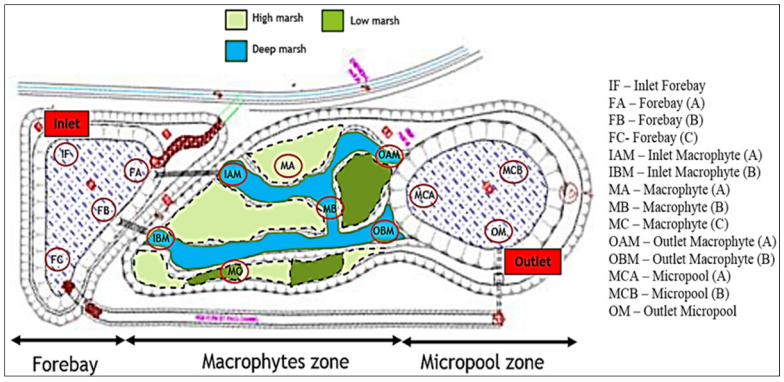

Figure 2. The sampling point and zonation of constructed wetland.

©2017, IAHR. Used with permission / ISSN 1562-6865 (Online) - ISSN 1063-7710 (Print)

Table 1. Zone characteristics (water depth and plants/macrophytes) in the constructed wetland.

Zonation		Water depth (min-max) (m)	Types of plants	Plant Density
Forebay		0.6-1.0	-	-
Macrophyte	High marsh	0-0.3	*-Donax grandis*, *-Eleocharis variegata*	1.63 ind/m^2
	Low marsh	0.3-0.5	*Phragmates karka*	58 ind/m^2
	Deep marsh	0.6-1.0	*Typha angustifolia*	29 ind/m^2
Micropool		0.7-1.4	-	-

The WQI will be adopted from the Department of Environment (DOE) [19] based on the given formula;

WQI = (0.22* SIDO) + (0.19*SIBOD) + (0.16*SICOD) + (0.15*SIAN) + (0.16 * SISS) + (0.12 * SIpH)

where;
SIDO = Sub-index DO (% saturation); SIBOD = Sub-index BOD; SICOD = Sub-index COD
SIAN = Sub-index NH3-N; SISS = Sub-index SS/TSS; SIpH = Sub-index pH

The classification of water quality concentration was based on the Table 2;

Table 2. DOE water quality index classification (DOE, 2006).

Parameters	Unit	Classes				
		I	II	III	IV	V
Ammoniacal nitrogen (AN)	mg/L	<0.1	0.1-0.3	0.3-0.9	0.9-2.7	>2.7
Biochemical oxygen demand (BOD_5)	mg/L	<1	1-3	3-6	6-12	>12
Chemical oxygen demand (COD)	mg/L	<10	10-25	25-50	50-100	>100
Dissolved oxygen (DO)	mg/L	>7	5-7	3-5	1-3	<1
pH	-	>7	6-7	5-6	<5	>5
Total suspended solid (TSS)	mg/L	<25	25-50	50-150	150-300	>300
Water quality index (WQI)	mg/L	>92.7	76.5-92.7	51.9-76.5	31.0-51.9	<31.0

3 RESULTS AND DISCUSSIONS

3.1 Mean water quality parameters

The mean water quality was presented in the Figure 3 as to observe the different in mean concentration for six main parameters for five-month sampling period and variation in the wetland zonation. Based on the results obtained, AN showed obvious variation in term of monthly comparison, in which low AN values were obtained during the wet season compared to the dry season. The decrease in concentration of AN during wet season suggest that concentration had been diluted by the inflow of water originated from rainfall. From the box plot (Figure 3), the AN concentration progressively reduced from the forebay to the micropool. The ammonia absorption through plant uptake of emergent plant species in the macrophytes zone is one of the factor affected the AN concentration (Vymazal, 2007). The average BOD5 concentration reduced from the forebay to the micropool zone suggest that not only primary mechanism of BOD removal is just involved such as sedimentation, absorption microbial metabolism, plant root from the wetland plants species may also provide a more effective settling medium and at the same time increasing attachment surface area and food sources for the microbial population (Karathanasis et al., 2003). Cattail or *Typha angustifolia* (Table 1) is a type of vegetation that can enhance substrate attenuation through its dense rooting and large surface area (Karathanasis et al., 2003). COD and TSS showed reduction from the forebay zone through discharge micropool zone in which the removal in this parameters were mainly due to physical processes (sedimentation and filtration). The pH showed acceptable values between the ranges 6.5-8.5 and it decrease from the forebay to the micropool, in which the forebay show slightly basic as compare to micropool due to initial pollutant received from the drainage system. The DO concentration in the Figure 3 varied significantly due to different type of plant and depth from the water surface.

©2017, IAHR. Used with permission / ISSN 1562-6865 (Online) - ISSN 1063-7710 (Print)

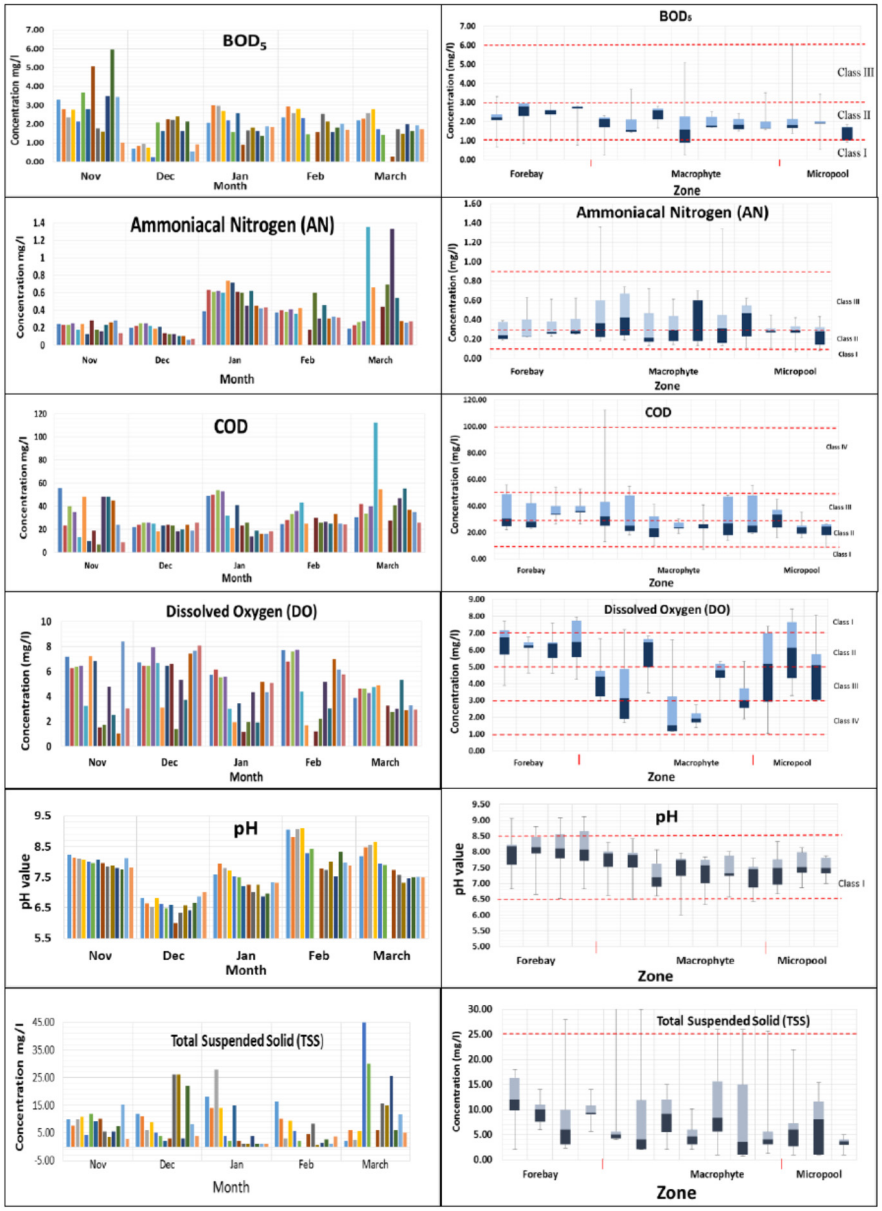

Figure 3. Monthly variation (left side) and sampling point variation (right side) in three different zone for six main parameters; (from the top to bottom) BOD, Ammoniacal nitrogen (AN), COD, DO, pH and TSS.

3.1 Monthly and zone variation of phytoplankton abundance

Figure 4 shows the distribution of phytoplankton phyla throughout the sampling period. Four main phyla were observed, with Chlorophyta being the most abundant, followed by Bacillariophyta, Cyanophyta, Chrysophyta, and Pyrrhophyta. Chlorophyta is the most common phyla in the freshwater and marine ecosystems (Graham, 2008). A few examples species observed and obtained in the constructed wetland such as *Closterium parvulum, Nitzschia longgisima, Lyngbya confervoides, Stauroneis anceps* and *Straurastrum sp*. The identity of species of is important because of their specificity as food sources for herbivorous species (Coesel, 1997). Olurin and Awolesi, 1991, found that the fish species *Tilapia mariae* and *Chromidotilapia guntheri*, fed mainly on phytoplankton largely consisting of the desmid genera Closterium and Cosmarium. Thus, Closterium sp is a desirable species in this wetland because of the dominance fish such as Tilapia sp. The variation of phytoplankton abundance can be seen in Figure 5, as the sampling point IF, FA, FB and FC were in the forebay zone; IAM, IBM, MA, MB, MC, OAM and OBM were in the macrophyte zone and; MCA, MCB and OM were in the micropool zone. Based on the Figure 5 for phytoplankton distribution in the zone, the result showed that the distribution was high in the macrophyte zone as compare to forebay zone and micropool zone. This is due to the source of nutrient available in the area as well as sufficient amount of light due to low level of water depth as compared to other zone. We assume in general that the amount of nutrient is high in macrophyte area due to low WQI valued obtained at this area. Based on WQI value in Table 2, the WQI value in the macrophyte zone fall into Class III as compared to other zone (Class II).

 ©2017, IAHR. Used with permission / ISSN 1562-6865 (Online) - ISSN 1063-7710 (Print)

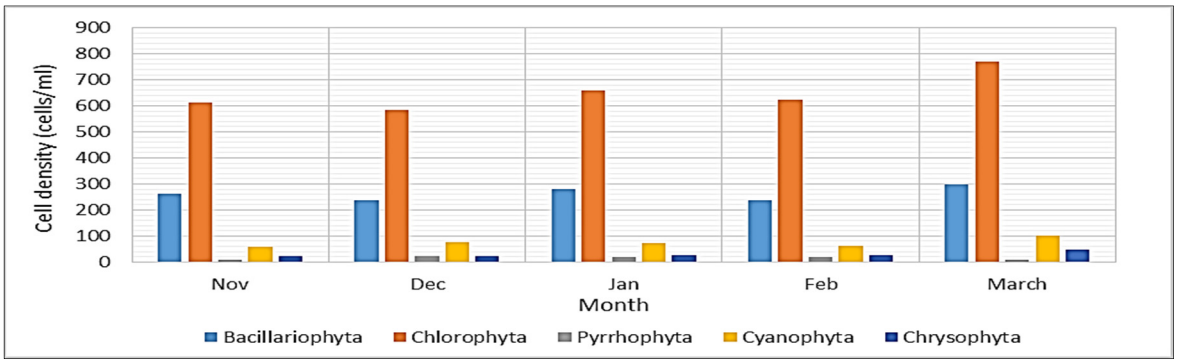

Figure 4. Monthly distribution of phytoplankton density by phylum in the constructed wetland from November 2014 until March 2015

3.2 Correlation between phytoplankton and WQI and water quality parameters

Based on the Table 3, DO concentration showed significant negative relationships (p=0.01) with all phytoplankton phyla, except for Pyrrhophyta. The pH value showed only significance positive relationship (p=0.05) with Chrysophyta. Phytoplankton density had affected the oxygen concentration in the water through decomposition by the bacteria present in the constructed wetland. As the density of phytoplankton was high, the decomposition rate may be high. The amount of oxygen used by the bacteria will be high and cause DO concentration to drop in the macrophytes zone. For the nutrients, TN showed significance positive relationship (p=0.05) with Cyanophyta and Chrysophyta. TN typically stimulates phytoplankton growth in freshwater ecosystems such as lake and wetlands (Lv et al., 2011). However the TP showed no significant relationships for all phytoplankton phyla. Based on the Figure 5, the WQI value developed from the six main parameters had showed significant negative relationships (p=0.01) with Bacillariophyta, Chlorophyta and Chrysophyta. As the WQI value drops in the macrophytes zone, with the range of 71.6-77.9, for mostly Class III, the phytoplankton density increased, which may be due to several factors. The source of nutrient, come through natural processes from the decomposition of plants and animals materials as well as surface water runoff that enters this zone from the forebay, had decrease the WQI value, and at the same time trigger the growth and numbers of density of phytoplankton. The macrophytes zone experience low water depth and received direct sunlight for phytoplankton to undergo photosynthesis process. The WQI of the outlet of this constructed wetland is high, with the range in between 83.7-85.5, Class II, which shows that the constructed wetland has improved the water quality received from the catchment area. The most important parameters for the abundance of phytoplankton based on Table 3 were DO and water temperature. The relationship in DO and water temperature involved a lot of other factors such as the respiration and decomposition rate of bacteria, which affected the concentration level of oxygen in the water. The more plants, the more places for the bacteria to inhabit. As the macrophytes zone consist high density of plants compared to other zones, most probably the amount of bacteria was high. The zone would thus have a high decomposition rate, which also involved decomposition of phytoplankton. The Figure 5 showed that Forebay has high WQI value due to certain reason and assumption. We predict that nutrient may directly flow from the forebay into the macrophyte zone without having settle during the high flow due to (i) short distance between the inlet of forebay and inlet of macrophyte and (ii) settlement period is short. As a result, more nutrient go to the macrophyte zone instead of left in the forebay, causes the WQI value to get higher. However, a few more physical parameters need to be added in to understand this situation such as flow rate and settlement rate in the forebay zone.

Table 3. The relationship (in Pearson correlation coefficient) between phytoplankton phylum and WQI and environmental variables.

Parameters	Pearson correlation coefficient				
	Baci.	Chlo	Pyrr	Cyan	Chry
BOD	-0.309	-0.253	-0.089	-0.29	-0.263
AN	0.336	0.339	0.196	0.091	0.053
COD	-0.185	-0.201	-0.052	-0.406	-0.414
DO	**-0.723****	**-0.836****	-0.526	**-0.734****	**-0.836****
pH	0.430	0.477	0.115	0.380	**580***
TSS	0.236	0.144	0.336	-0.006	-0.005
TN	0.502	0.428	0.435	**0.629***	**0.623***
TP	-0.131	-0.097	0.133	-0.188	-0.117
Temp	**-0.794****	**-0.847****	**-0.729****	**-0.699****	**-0.721****
WQI	**-0.720****	**-0.852****	**-0.593***	**-0.650***	**-0.736****

©2017, IAHR. Used with permission / ISSN 1562-6865 (Online) - ISSN 1063-7710 (Print)

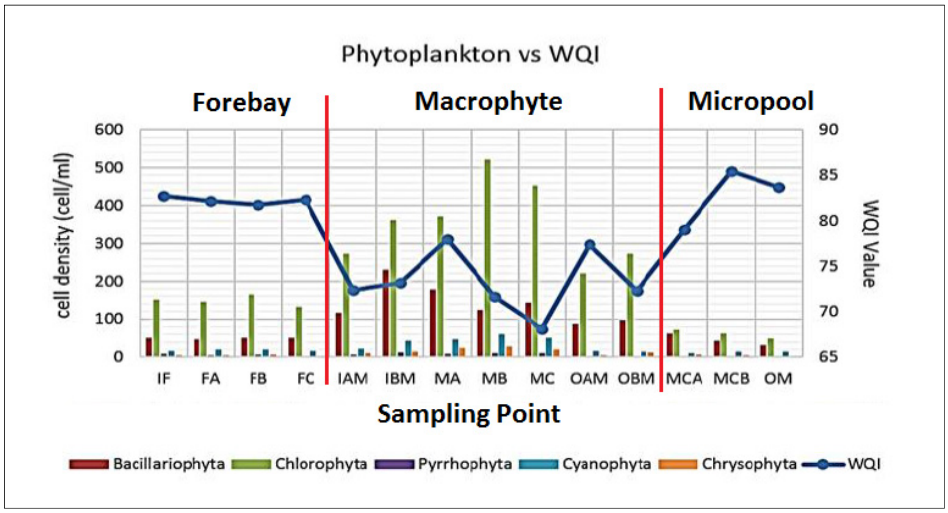

Figure 5. WQI and phytoplankton density pattern for sampling station in the constructed wetlands.

4 CONCLUSIONS

As a conclusion, this free water surface constructed wetland was able to control the distribution of freshwater phytoplankton and at the same time capable to improve water quality up to Class II DOE standard. Slight variation on distribution during dry and wet season for phytoplankton as the water quality parameter, also not affected monthly except for ammoniacal nitrogen. The introduction of this constructed wetland had overcome the problems of eutrophication caused by highly abundance algae or phytoplankton. However, the macrophytes area had to be carefully monitored and it is suggested to have periodically harvesting the plants, once in six months to avoid contribution of nutrient in which can affect the water quality as it also can trigger the distribution of phytoplankton based on the graph show in Figure 5. This relationship assessment will help to understand importance parameters for the phytoplankton in the constructed wetland for the sustainability habitat and biodiversity, ecological interaction and primary production in the food web under tropical climate condition in Malaysia.

ACKNOWLEDGEMENTS

The authors would like to acknowledge the financial assistance from the Ministry of Education of Malaysia (MOE) for the recognition of Higher Centre of Excellent (HICOE) in services to River Engineering and Urban Drainage Research Centre (REDAC), Universiti Sains Malaysia (USM). This study is funded under the Short Term Grant Research USM (Grant Number: 304/PREDAC/60313014).

REFERENCES

Bavor, H.J., Davies, C.M. & Sakadevan, K. (2001). Stormwater Treatment: Do Constructed Wetlands Yield Improved Pollutant Management Performance over a Detention Pond System?. *Water Science Technology*. 44(11-12), 565- 570.

Calero, S., Segura, M., Rojo, C. & Rodrigo, M.A. (2015). Shifts in Plankton Assemblages Promoted by Free Water Surface Constructed Wetlands and Their Implication in Eutrophication Remediation. *Ecological Engineering*, 74, 385-393.

Coesel, P.F.M. (1997). The Edibility of Staurastrum Chaetoceras and Cosmarium Abbreviatum (Desmidiaceae) for Daphnia Galeata/Hyalina and the Role of Desmids in the Aquatic Food Web. *Aquatic Ecology*, 31(1), 73–78.

Department of Irrigation and Drainage (DID). (2012). *Urban Stormwater Management Manual for Malaysia*, (MSMA) 2th Edition, Malaysia.

Department of Environment (DOE). (2006). *Malaysia Environmental Quality Report 2006*, Sasyaz Holdings Sdn. Bhd., Chapter C3, 24-41.

Graham, L.E., Graham, J.M. & Wilcox, L.W. (2008). *Algae* (*2nd Edition)*, Benjamin Cummings (Pearson), San Francisco, CA.

Hach (2013). *Water Analysis Handbook 5th Edition*. Hach Company, Loveland, CO, USA

Hsu, C.B., Hsieh, H.L., Yang, L., Wu, S.H., Chang, J.S., Hsiao, S.C., Su, H.C., Yeh, C.H., Ho, Y.S. & Lin, H.J. (2011). Biodiversity of Constructed Wetlands for Wastewater Treatment. *Ecological Engineering*, 37(10), 1533-1545.

Karathanasis, A.D., Potter, C.L. & Coyne, M.S. (2003). Vegetation Effects on Fecal Bacteria, BOD, and Suspended Solid Removal in Constructed Wetland Treating Domestic Wastewater. *Ecological Engineering*, 20(2), 157-169.

 ©2017, IAHR. Used with permission / ISSN 1562-6865 (Online) - ISSN 1063-7710 (Print)

Leupold, M.A. (1998). Water Quality Assessment. In Lobban, C.S., Chapman, D.J. & Kremer, B.P. (Eds.), *Experimental Phycology: A Laboratory Manual*, Cambridge Australia, 47-55.

Lv, J., Wu, H. & Chen, M. (2011). Effects of Nitrogen and Phosphorus on Phytoplankton Composition and Biomass in 15 Subtropical, Urban Shallow Lakes in Wuhan, China. *Limnologica-Ecology and Management of Inland Waters*, 41(1), 48-56.

Martin, M., Oliver, N., Crespo, C.H., Gargallo, S. & Regidor, M.C. (2013). The Use of Free Water Surface Constructed Wetland to Treat the Eutrophicated Waters of Lake LÁlbufera de Valencia (Spain). *Ecological Engineering*, 50, 52-61.

Mohammadpour, R., Shaharuddin, S., Chang, C.K., Zakaria, N.A. & Ab Ghani, A. (2014). Spatial Pattern Analysis for Water Quality in Free Surface Constructed Wetland. *Water Science and Technology*, 70(7), 1161-1167.

Mohammadpour, R., Shaharuddin, S., Chang, C.K., Zakaria, N.A., Ab Ghani, A. & Chan, N.W. (2015). Prediction of Water Quality Index in Constructed Wetlands Using Support Vector Machine. *Environmental Science and Pollution Research*, 22(8), 6208-6219.

Mohd Noor, N.A., Mohd Sidek, L., Zainal Abidin, M.R. & Ab Ghani, A. (2014). Removal Efficiency Evaluation for Constructed Wetland in Tropical Climate. *Journal of Energy and Environment*, Universiti Tenaga Nasional, 5(1), 1-6.

Olurin, K.B. & Awolesi, O.O. (1991). Food of Some Fishes of Owa Stream, South-Western Nigeria. *Archiv für Hydrobiologie*, 122, 95–104.

Shamsudin, L. (1990). *Diatom Marin di Perairan Malaysia*. Dewan Bahasa dan Pustaka, Kementerian Pendidikan Malaysia.

Schindler, D.W. (2006). Recent Advances in the Understanding and Management of Eutrophication. *Limnology and Oceanography*, 51(1), 356-363.

Semeraro, T., Giannuzi, C., Beccarisi, L., Aretano, R., De Marco, A., Pasimeni, M.R., Zurlini, G. & Petrosillo, I. (2015). A Constructed Treatment Wetland as an Opportunity to Enhance Biodiversity and Ecosystem Services. *Ecological Engineering*, 82, 517-526.

Tomas, C.R. (1997). *Identifying Marine Phytoplankton*. Academic Press.

Vymazal, J. (2007). Removal of Nutrient in Various Type of Constructed Wetland. *Science of the Total Environment*, 380(1), 48-65.

Vymazal, J. (2010). Constructed Wetland for Wastewater Treatment. *Water*, 2(3), 530-549.

Zakaria, N.A., Ab. Ghani, A., Abdullah, R., Mohd Sidek, L. & Ainan, A. (2003). Bio-Ecological Drainage System (BIOECODS) for Water Quantity and Quality Control. I*nternational Journal River Basin Management,* 1(3), 237-251.

©2017, IAHR. Used with permission / ISSN 1562-6865 (Online) - ISSN 1063-7710 (Print)

Proceedings of the 37th IAHR World Congress
August 13 – 18, 2017, Kuala Lumpur, Malaysia

PROJECTING FUTURE HYDRO-CLIMATIC CHANGES OF THE JOHOR RIVER BASIN, MALAYSIA

MOU LEONG TAN[1], VIVIEN P. CHUA[2], LIEW JUNENG[3], FREDOLIN T. TANGANG[4] & NGAI WENG CHAN[5]

[1,5] Universiti Sains Malaysia, Penang, Malaysia
mouleong@gmail.com
[2] National University of Singapore, Singapore.
[3,4] Universiti Kebangsaan Malaysia, Selangor, Malaysia.

ABSTRACT

Water resources in the Johor River Basin (JRB) are vital for the populations of Malaysia and Singapore. This study provides an overview of future hydro-climatic changes using climate projections from an ensemble of four dynamically downscaled Coupled Model Intercomparison Project Phase 5 (CMIP5) products under the Representative Concentration Pathway (RCP) 4.5 and 8.5 scenarios for the 2015-2100 period. The downscaled climate projections were incorporated into a calibrated Soil and Water Assessment Tool (SWAT) model to simulate future streamflow over the JRB. Overall, future annual precipitation, streamflow, maximum and minimum temperature are projected to change about -27.8 to 17.8%, -35.8 to 17.9%, 0.4 to 3.9^{o}C and 0.5 to 4^{o}C, respectively, under different downscaled products and RCP scenarios. The projected precipitation and streamflow show little changes under the RCP 4.5 scenario, but decrease significantly under the RCP 8.5 scenario. Therefore, we recommend development of more desalination and waste water treatment plants in both countries, and exploration of groundwater as an alternative freshwater source for Malaysia.

Keywords: Precipitation; streamflow; SWAT; Johor; CMIP5.

1 INTRODUCTION

Climate change has become an increasing concern all around the world. The Intergovernmental Panel on Climate Change (IPCC) reported that global average surface temperature has increased by 0.85^{o}C from 1880 to 2012 in the Fifth Assessment Report (AR5) (IPCC, 2013). The global warming has caused substantially changes in local hydrological cycle, thus influences the frequency and intensity of hydrological-related disasters such as floods and droughts (Zhang et al., 2016). Hence, it is very important to understand the impact of climate change on local hydrological cycle to support water resources management (Chan, 2006).

Freshwater resources in the Johor River Basin (JRB) are critical for ~7 million people in southern Peninsular Malaysia and Singapore. As a small island country with limited natural water resources, Singapore imports about 40% of the total water demand from Malaysia. Therefore, a dramatic reduction of freshwater in the JRB could affect the populations in both countries. On the other hand, flood is also a major natural disaster in JRB (Tan et al., 2015) and regularly impacts people, crops and properties. For instance, the 2006-2007 flood in JRB have affected more than 100000 people, caused damaged around USD$ 0.5 billion and resulted in 18 deaths (Kia et al., 2012; Chan, 2015).

To understand the effects of climate change on hydrological cycle of a basin, a hydro-climatic modelling should be conducted within the context of water resources management. Generally, downscaled climate projections from Global Circulation Model (GCM) are used as input to hydrological models to assess future hydro-climatic changes. The Soil and Water Assessment Tool (SWAT) model is one of the widely applied hydrological models for this purpose (Gassman et al., 2007; Krysanova and White, 2015). Tan et al. (2014) evaluated the climate change impacts on streamflow of the JRB using the GCMs from phase 5 of the Coupled Model Intercomparison Project (CMIP5) and SWAT model. Still, such hydro-climatic assessment has not been adequately studied in this region despite more projection products are recently made available from various initiatives, i.e. the Coordinated Regional Downscaling Downscaling Experiment (CORDEX).

The major objective of this study is to present a comprehensive analysis of streamflow response to climate change scenarios using multiple regional climate models (RCMs) output and SWAT model in the JRB. The most notable aspects of this study include: (1) the characteristics of future precipitation and temperature changes, (2) improvement of the SWAT model from previous study by Tan et al. (2014) and (3) future streamflow as modelled by the latest RCMs and improved SWAT model. The findings from this study could be used as a reference for water manager and local authorities regarding flood control, drought resistance and crop irrigation management.

 ©2017, IAHR. Used with permission / ISSN 1562-6865 (Online) - ISSN 1063-7710 (Print)

2 JOHOR RIVER BASIN

JRB is located in the southern Peninsular Malaysia (Figure 1). The basin has an area of 1652 km^2, covering four main districts of the Johor state including the Johor Bahru, Mersing, Kluang and Kota Tinggi. The Johor River is the main river of the basin, and has a total length of about 122 km. There are five major tributaries including the Linggiu River, Belitong River, Sayong River, Penggeli River and Jengeli River. The climate of this basin is classified as a tropical rainforest system, with a mean annual precipitation of about 2500 mm/year and a mean annual temperature of about 26ºC. Two main monsoon seasons of the JRB are the northeast monsoon (NEM) from November to February and the Southwest monsoon (SWM) from May through to August, with the latter brings lesser precipitation. There are two shorter inter-monsoon periods (March-April and September-October) that bring intense localized convective rain.

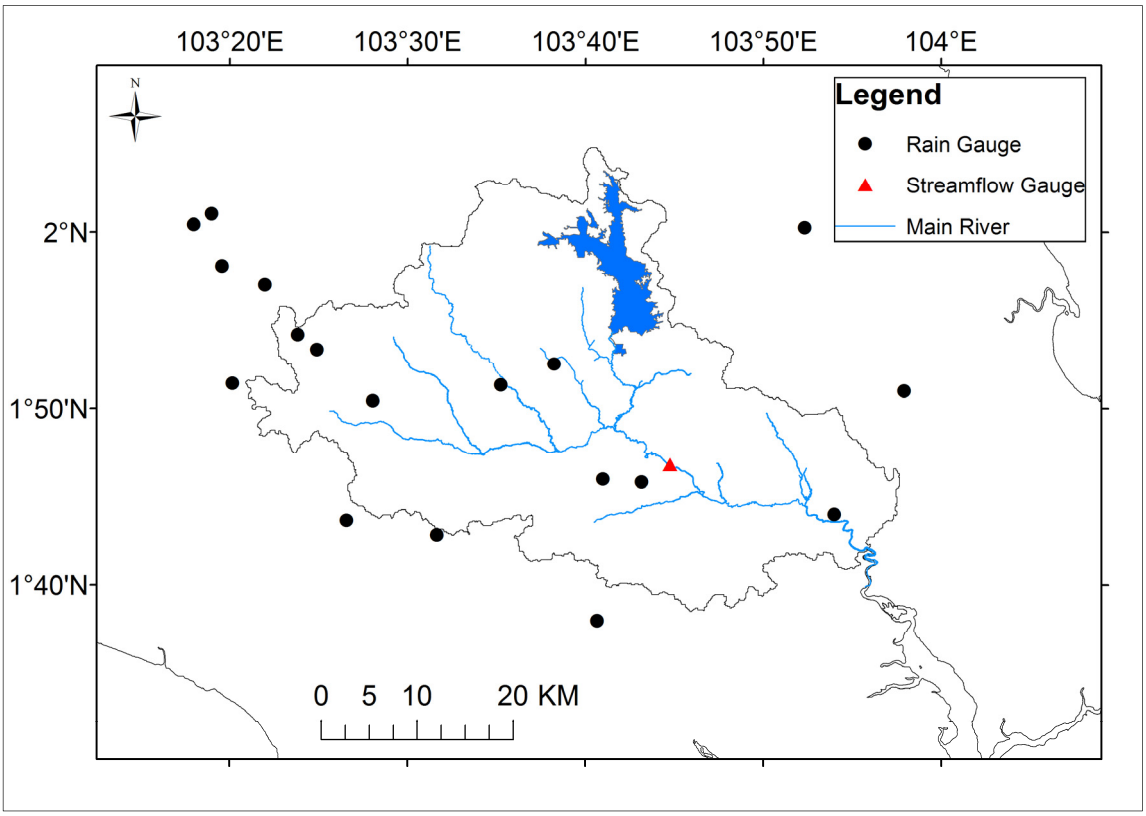

Figure 1. Johor River Basin.

3 DATA AND METHODOLOGY

3.1 Data

Daily precipitation data from 1975 to 2005 from 18 stations were collected from the Malaysia Meteorology Department (MMD) and the Department of Irrigation and Drainage Malaysia (DID) (Figure 1). Only two of the stations recorded maximum and minimum temperature. Monthly streamflow data at Rantau Panjang station from 1976 to 1989 was obtained from the DID. To develop SWAT model, spatial data such as digital elevation model (DEM), land use and soil maps are required. A 30m resolution Shuttle Radar Topography Mission (SRTM) DEM developed by the United States Geological Survey (USGS) was used. Land use and soil maps were collected from the Ministry of Agriculture and Agro-based Industry Malaysia (MOA).

3.2 Climate projections

In this study, dynamically downscaled products from the archive of the Southeast Asia Regional Climate Downscaling (SEACLID)/CORDEX Southeast Asia project was used to drive the SWAT model. These downscaled climate projections were produced at 25km x 25km based on the Representative Concentration Pathways (RCPs) 4.5 and 8.5 scenarios. More information about the SEACLID/CORDEX Southeast Asia can be found in Juneng et al. (2016) or the project website at http://www.ukm.edu.my/seaclid-cordex. Table 1 summarizes the downscaled climate change projection products used in current study. The GCMs-RCMs combination comprises of three different GCMs dynamically downscaled by three different RCMs. The downscaled GCMs include i) CNRM-CM5 from the France National Centre for Meteorological Research, ii) GFDL-ESM2M from the Geophysical Fluid Dynamic Laboratory, USA and iii) HadGEM2 from the UK Met Office. The regional model used include i) RegCM4, which is developed by International Centre for Theoretical

©2017, IAHR. Used with permission / ISSN 1562-6865 (Online) - ISSN 1063-7710 (Print)

Physics, ii) WRF, which is developed National Center for Atmospheric Research, USA and iii) RCA4, which is developed by Rossby Centre, Swedish Meteorological and Hydrological Institute.

Table 1. Climate Projections used in this study.

Driving GCM	RCM	RCP	Period
CNRM-CM5	RCA4	4.5	2006-2100
		8.5	2006-2100
GFDL-ESM2M	RegCM4	4.5	2006-2100
		8.5	2006-2100
HadGEM2	RCA4	4.5	2006-2100
		8.5	2006-2100
HadGEM2	WRF	4.5	2021-2050; 2071-2100
		8.5	2021-2050; 2071-2100

3.3 SWAT model

The SWAT model is a semi-distributed hydrological model developed by the U.S. Department of Agriculture and Texas A&M University (Arnold et al., 1998). It has been widely applied in best management practices, water resources management, climate change and land use changes assessment management and water quality analysis (Gassman et al., 2007). In SWAT, the water balance equation was used to simulate hydrological cycle, as follows:

$$SW_t = SW_o + \sum_{i=1}^{t} (R_{day} - Q_{surf} - E_a - w_{seep} - Q_{gw}) \quad [1]$$

where SW_t is the final soil water conten (mm H_2O), SW_o is the initial soil water content on day i (mm H_2O), R_{day} is the amount of precipitation on day i (mm H_2O), Q_{surf} is the amount of surface runoff on day i (mm H_2O), E_a is the amount of evapotranspiration on day I (mm H_2O), w_{seep} is the amount of water entering the vadose zone from the soil profile on day i (mm H_2O), and Q_{gw} is the amount of return flow on day I (mm H_2O).

The semi-automated Sequential Uncertainty Fitting algorithm (SUFI-2) within the SWAT Calibration and Uncertainty (SWAT-CUP) tool was used to calibrate and validate the SWAT model (Abbaspour et al., 2015). Three statistical metrics including the Nash-Sutcliffe Efficiency (NSE), the coefficient of determination (R^2) and the percentage bias (PB) were used to evaluate the ability of the SWAT model. More information on these statistical metrics can be found in Tan et al. (2017). Based on Moriasi et al. (2007, 2015), the SWAT model can be regarded as “very good” and “good” performances, if the NSE value ranges from 0.75 to 1 and 0.65 to 0.75, respectively.

4 RESULTS AND DISCUSSION

4.1 Climate projection

The annual anomaly changes of the future climate projections from 2015 to 2100 under the RCP 4.5 and 8.5 scenarios against the historical mean of the 1975-2005 period are shown in Figures 2 and 3. The ensemble of four climate projection (Table 1) shows large spread in projected future precipitation of about -27.8 to 12.5% and -27.6 to 17.8% under the RCP 4.5 and RCP 8.5 scenarios, respectively (Figure 2). Figure 3 shows that maximum and minimum temperatures are projected to increase by 0.4 to 2.1 ^oC (0.5 to 3.9^oC) and 0.5 to 2.5 ^oC (0.5 to 4^oC) under the RCP 4.5 (8.5) scenario. Interestingly, the uncertainty range of the precipitation and minimum temperature under the RCP 8.5 scenario are larger than the RCP 4.5 scenarios. A possible explanation for this might be that the RCP 8.5 scenario is a high range impact scenario that covered a wider range of possibilities.

4.2 SWAT model

Figure 5 indicates the monthly observed and simulated streamflow at the Rantau Panjang station during the calibration (1976-1985) and validation (1986-1989) periods. The NSE, R^2 and PB values were 0.85, 0.86 and 0.08%, respectively, during the calibration period. The ideal parameters that obtained from the calibration process were then implemented into the SWAT model for validation purpose. For the validation period, the NSE, R^2 and PB values were 0.72, 0.76 and 2.15%, respectively, indicating the SWAT model can satisfactorily simulate streamflow in the basin. The SWAT model performed better than previous SWAT studies in the same basin (Tan et al., 2014; 2015). In this study, we applied the latest SRTM DEM at 30m resolution, while the previous work used a coarser resolution of SRTM DEM (90m resolution).

 ©2017, IAHR. Used with permission / ISSN 1562-6865 (Online) - ISSN 1063-7710 (Print)

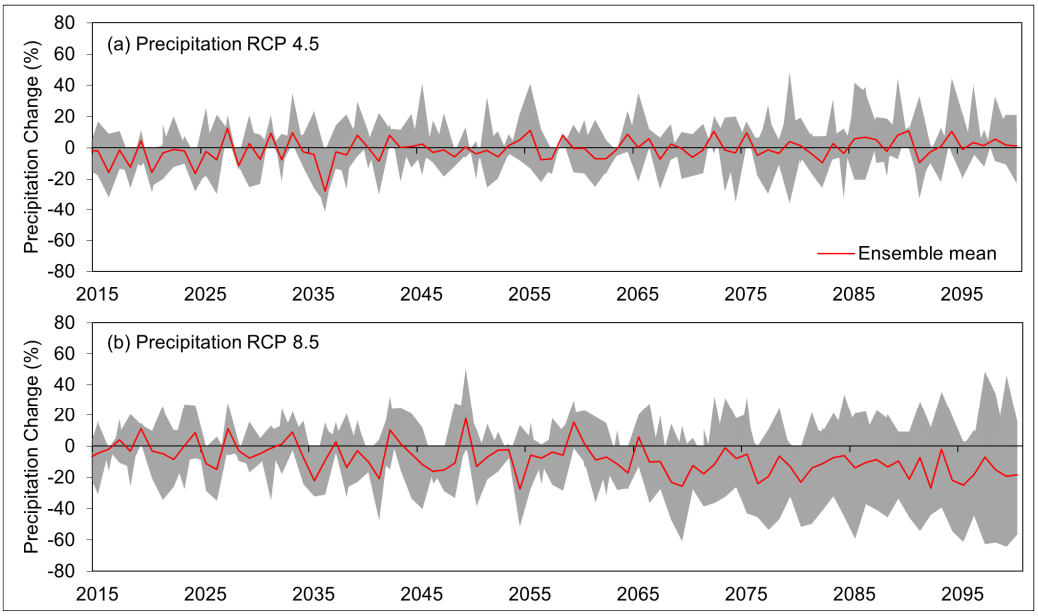

Figure 2. Anomaly changes of precipitation under (a) RCP 4.5 and (b) 8.5 scenarios against historical mean 1975 to 2005.

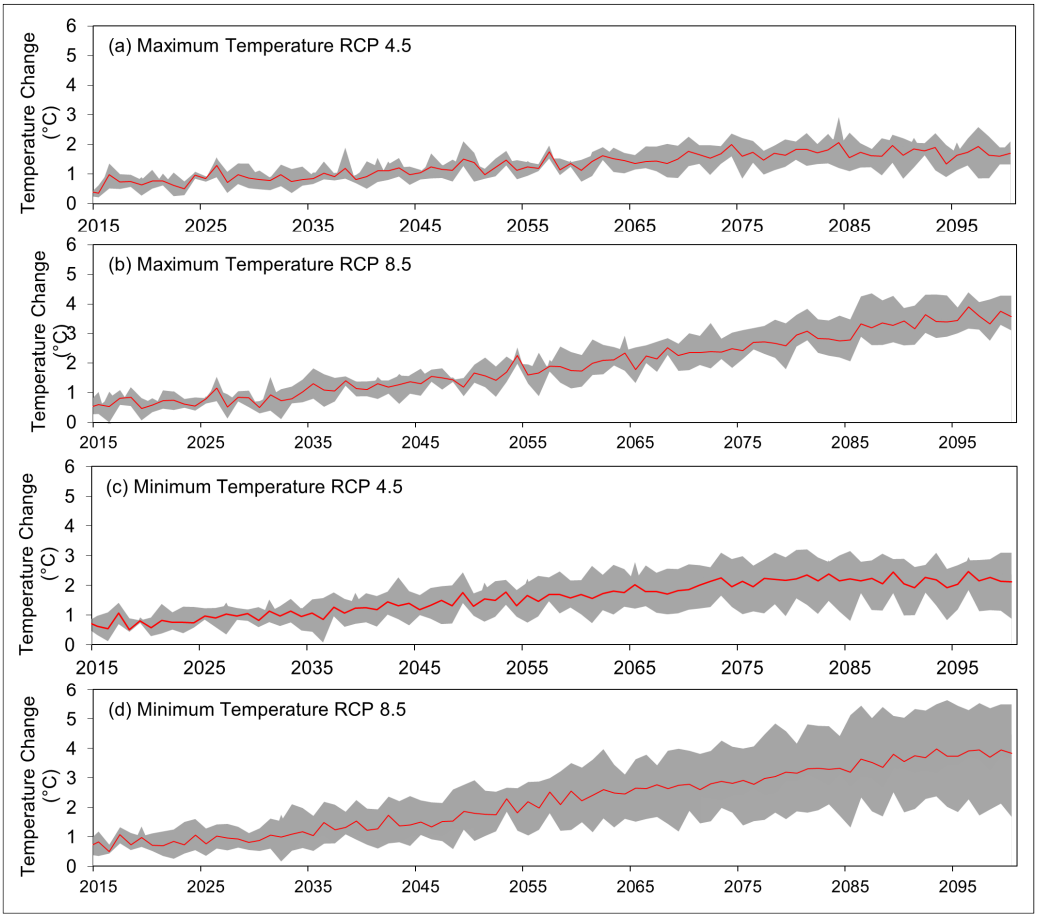

Figure 3. Anomaly changes of (a) maximum temperature RCP 4.5, (b) maximum temperature RCP 8.5, (c) minimum temperature RCP 4.5 and (d) minimum temperature 8.5 against historical mean 1975 to 2005.

©2017, IAHR. Used with permission / ISSN 1562-6865 (Online) - ISSN 1063-7710 (Print)

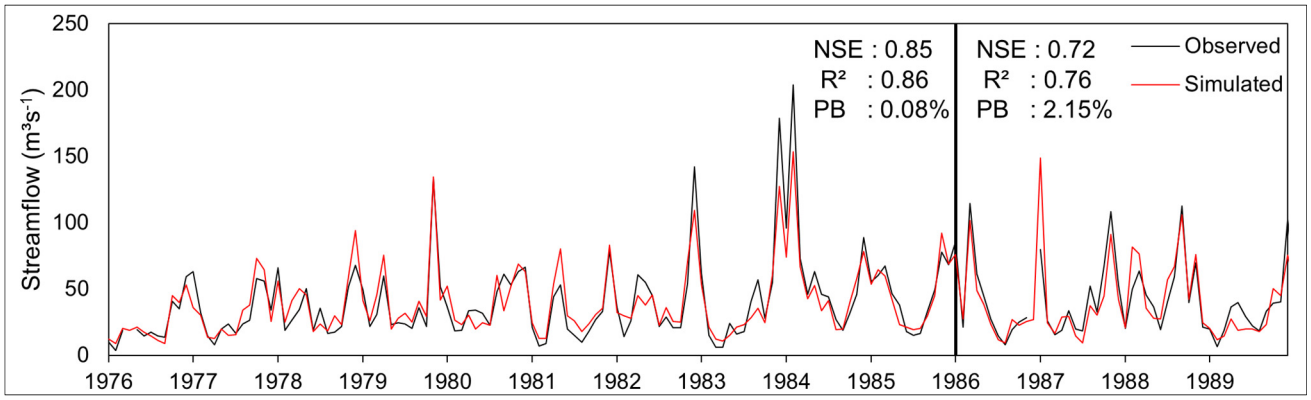

Figure 4. Comparison of monthly observed and simulated SWAT for calibration (1976-1985) and validation (1986-1989) periods.

4.3 Streamflow projection

Figure 5 shows the annual anomaly changes of streamflow in the 2015-2100 period compared to the mean 1975-2005 period at the Rantau Panjang station. The results indicate that the future annual streamflow varies from -34.4 to 16.7% and -35.8 to 17.9% under the RCP 4.5 and 8.5 scenarios, respectively. The most striking result from the figure is that the future annual streamflow in the 2066-2100 period under the RCP 8.5 scenario will be lower than the historical values. This finding is contrary to that of Tan et al. (2014) who projected the annual streamflow to increase in the same period and RCP scenario. These differences can be explained in part by the different in GCMs and downscaling approaches, where they used an ensemble of six GCMs that statistically downscaled by the delta approach.

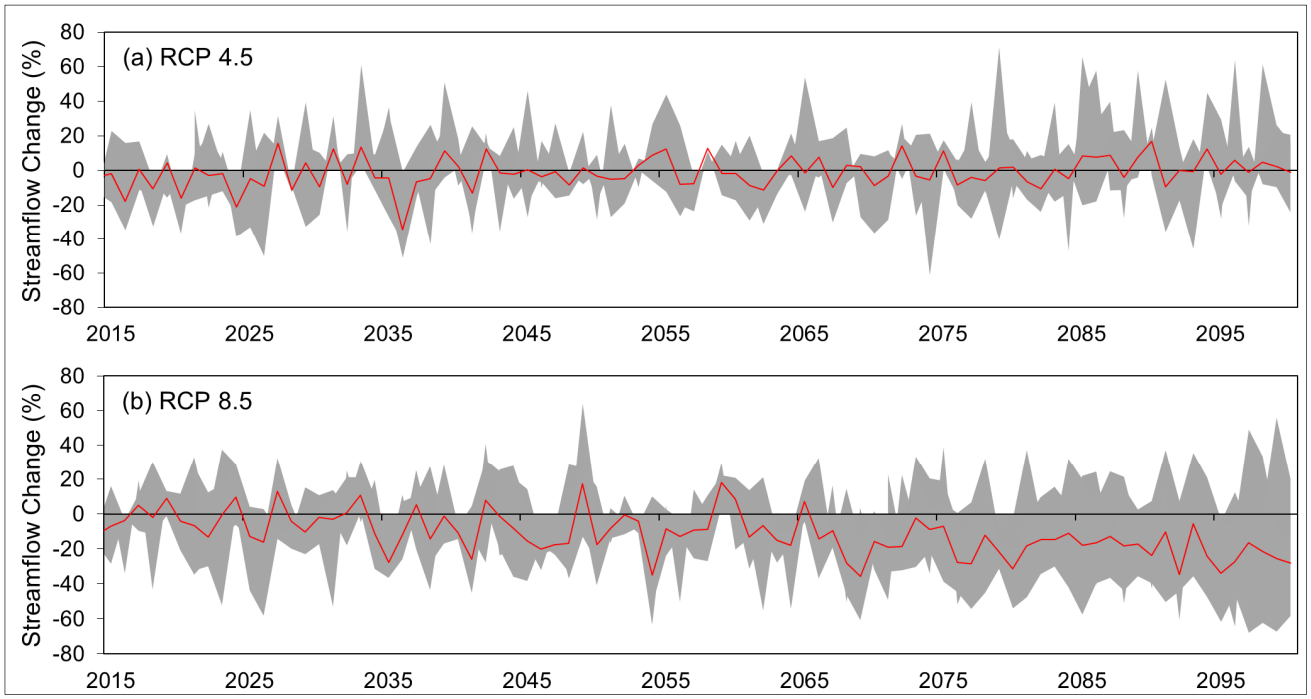

Figure 5. Anomaly changes of monthly streamflow under RCP (a) 4.5 and (b) 8.5 scenarios against mean from 1976 to 2005.

5 CONCLUSIONS

This study presents the most up-to-date projection on climate change impact assessment on water resources of the JRB, Malaysia. The climate scenarios were projected from an ensemble of four different combinations of GCMs and RCMs under RCP 4.5 and 8.5 scenarios from 2015 to 2100. The climate projections were then used as inputs into a SWAT model to project future streamflow projection. The SWAT model has been improved from previous study (Tan et al., 2014) by using a better resolution SRTM DEM.

The future annual precipitation, maximum and minimum temperatures are projected to change by -27.8 to 17.8%, 0.4 to 3.9°C and 0.5 to 4°C, respectively. These climate changes will lead to the annual streamflow change between -35.8 and 17.9%. Generally, the hydro-climatic trends of the JRB will increase slightly under the RCP 4.5 scenario. By contrast, a decreasing hydro-climatic trend is expected to occur under the RCP 8.5

 ©2017, IAHR. Used with permission / ISSN 1562-6865 (Online) - ISSN 1063-7710 (Print)

scenario. Water scarcity problems might be increased in the future if there is no implementation of climate adaptations strategies related to water resources. In this context, strategies such as groundwater, water catchment gazettement and reforestation, water demand management, rainwater harvesting and desalination should be considered to reduce climate change impacts on water resources in the KRB.

ACKNOWLEDGEMENTS

The study was funded by the Ministry of Education, Singapore (Tier 2 Grant No: 2013-T2-2-027), UKM (Grant No.: UKM-ICONIC-2013-001) and USM FRGS (Grant No. 203/PHUMANITI/6711393). Special thanks to MMD, DID and MOA for providing the hydro-climatic and spatial data used in this study. The SEACLID/CORDEX-SEA downscaled products were made available via the SEACLID/CORDEX-SEA project funded by APN (ARCP2013-17NMY-Tangang, ARCP2014-07CMY-Tangang, ARCP2015-04CMY-Tangang).

REFERENCES

Abbaspour, K.C., Rouholahnejad, E., Vaghefi, S., Srinivasan, R., Yang, H. & Kløve, B. (2015). A Continental-Scale Hydrology and Water Quality Model for Europe: Calibration and Uncertainty of a High-Resolution Large-Scale SWAT Model. *Journal of Hydrology*, 524, 733-752.

Arnold, J.G., Srinivasan, R., Muttiah, R.S. & Williams, J.R. (1998). Large area hydrologic modeling and assessment - Part 1: Model development. *Journal of the American Water Resources Association,* 34(1), 73-89.

Chan, N.W. (2006). *USM-CETDEM Climate Change Survey. Healthy Campus Series 12.* Penang: Penerbit Universiti Sains Malaysia.

Chan, N.W. (2015). Challenges in Flood Disasters Management in Malaysia. *Proceedings of the World Water Congress XV Edinburgh*, International Water Resources Association, 1-9.

Gassman, P.W., Reyes, M.R., Green, C.H. & Arnold, J.G. (2007). The Soil and Water Assessment Tool: Historical development, applications, and future research directions. *Transactions of the American Society of Agricultural and Biological Engineers*, 50(4), 1211-1250.

IPCC (Intergovernmental Panel on Climate Change). (2005). *In climate change 2013; The Physical Science Basic Contribution of Working Group 1 to the Fifth Assessment Report of the Intergovernmental Panel on Climate Change*, Cambridge University Press, Cambridge, United Kingdom and New York, USA.

Juneng, L., Tangang, F., Chung, J.X., Ngai, S.T., Tay, T.W., Narisma, G., Cruz, F., Phan-Van, T., Ngo-Duc, T., Santisirisomboon, J., Singhruck, P., Gunawan, D. & Aldrian, E. (2016). Sensitivity of Southeast Asia Rainfall Simulations to Cumulus and Air-Sea Flux Parameterizations in RegCM4. *Climate Research*, *69*(1), 59-77.

Kia, M.B., Pirasteh, S., Pradhan, B., Mahmud, A.R., Sulaiman, W.N.A. & Moradi, A. (2012). An Artificial Neural Network Model for Flood Simulation using GIS: Johor River Basin, Malaysia. *Environmental Earth Sciences*, 67(1), 251-264.

Krysanova, V. & White, M. (2015). Advances in Water Resources Assessment with SWAT—An Overview. *Hydrological Sciences Journal*, 60(5), 771-783.

Moriasi, D.N., Arnold, J.G., Van Liew, M.W., Bingner, R.L., Harmel, R.D. & Veith, T.L. (2007). Model Evaluation Guidelines for Systematic Quantification of Accuracy in Watershed Simulations. *Transactions of the Asabe*, 50(3), 885-900.

Moriasi, D.N., Gitau, M.W., Pai, N. & Daggupati, P. (2015). Hydrologic and Water Quality Models: Performance Measures and Evaluation Criteria. *Transactions of the ASABE*, 58(6), 1763-1785.

Tan, M.L., Ficklin, D.L. & Yusop, Z. (2014). Impacts and Uncertainties of Climate Change on Streamflow of the Johor River Basin, Malaysia using a CMIP5 General Circulation Model Ensemble. *Journal of Water and Climate Change*, 5(4), 676-695.

Tan, M.L., Ibrahim, A.L., Yusop, Z., Duan, Z. and Ling, L. (2015). Impacts of Land-Use and Climate Variability on Hydrological Components in the Johor River basin, Malaysia. *Hydrological Sciences Journal*, 60(5), 873-889.

Tan, M.L., Ibrahim, A.L., Yusop, Z., Chua, V.P. & Chan, N.W. (2017). Climate Change Impacts under CMIP5 RCP Scenarios on Water Resources of the Kelantan River Basin, Malaysia. *Atmospheric Research*, 189, 1-10.

Zhang, Y., You, Q., Chen, C. & Ge, J. (2016). Impacts of Climate Change on Streamflows under RCP Scenarios: A Case Study in Xin River Basin, China. *Atmospheric Research*, 178, 521-534.

©2017, IAHR. Used with permission / ISSN 1562-6865 (Online) - ISSN 1063-7710 (Print)

Proceedings of the 37th IAHR World Congress
August 13 – 18, 2017, Kuala Lumpur, Malaysia

ASSESSMENT OF CLIMATE CHANGE IMPACTS ON HYDROLOGICAL PROCESSES AND WATER RESOURCES BY WATER EVALUATION AND PLANNING (WEAP) MODEL: CASE STUDY IN THAC MO CATCHMENT, VIETNAM

BAO QUOC PHAM[1], PAO-SHAN YU[2], TAO-CHANG YANG[3], CHEN-MIN KUO[4] & HUNG-WEI TSENG[5]

[1,2,3,4,5] Department of Hydraulic and Ocean Engineering, National Cheng Kung University, Tainan, Taiwan,
pbquoc92@gmail.com

ABSTRACT

Climate change could affect the water resources system globally and particularly at the catchment level. Future changes in climate would affect streamflow and subsequent water resources. This study aims to use the Water Evaluation and Planning (WEAP) model for assessment of climate change impacts on hydrological processes and water resources in the Thac Mo catchment, which plays a vital role in the life of inhabitants at the downstream of the Thac Mo reservoir. WEAP is a powerful tool in scenario of a building for predicting climate change impacts, which has been implemented in many regions in the world. For this study, data collection and processes are conducted to input the required data into the WEAP model. Streamflow data (1978–1993) were used to calibrate and validate the WEAP hydrological model, where the period of 1978–1988 for calibration and 1989–1993 used for validation, respectively. By using WEAP and General Circulation Model (GCM) outputs, both streamflow and subsequent water shortage during the baseline period (1994 – 2003) and midterm period (2046–2064) are simulated and compared to indicate the effect of climate change. Downscaled monthly rainfalls and temperatures under B1 and A2 emission scenarios from different GCMs were used to generate streamflow through the WEAP model and subsequent water shortage. The results show that mean streamflow tends to increase around 10.1% in the wet season due to an increase in rainfall, but also tends to decrease in December (-4.4%), January (-1.0%), and February (-0.85%) of the dry season relative to the baseline scenario. Consequently, the downstream of the Thac Mo reservoir may face a big challenge in the dry season in terms of water use. In addition, water shortage at the downstream of the catchment increases around triple compared with the baseline. This scenario must be taken into consideration for a combined assessment of climate change impacts and socioeconomic development in this region.

Keywords: WEAP model; climate change; general circulation models; streamflow; water shortage.

1 INTRODUCTION

Climate change is one of the main challenges to humankind in the 21st century. The Intergovernmental Panel on Climate Change (IPCC) emphasized that climate change is an unavoidable phenomenon (IPCC, 2007). Changes in temperature and precipitation affect the hydrological processes and water availability for agricultural areas, hydropower, industrial sectors, and population. Climate change will rush the hydrological cycle with an increase trend in the temperature, change in evapotranspiration and precipitation. The change in distribution of precipitation intensity and frequency will affect the stream flow (Rochdane et al., 2012).

Climate change, population growth, and economic development will likely affect the availability of future water resources in numerous regions. The Impacts of climate change are a worldwide problem, but researchers will be most interested in the local scale effects, e.g., catchment, basin or region (Kiparsky et al., 2014). One of the most prominent results in researches on impacts of climate change is that climate change will change hydrological processes and water availability around the world (Kiparsky et al., 2014). Understanding the interaction of climate change and water resources, this can help scientists and policy makers to diminish the harmful effects by introducing correct water management plans. A number of studies have been accomplished on the impacts of climate change on hydrological processes (Devkota et al., 2015; Githui et al., 2009; Kim et al., 2009; Zhang et al., 2007; Andersson et al., 2006) indicating that streamflow variation are related to changes in temperature and rainfall.

Vietnam, located in the region of the South East Asia monsoon area, is among the countries most strongly affected by climate change. In Vietnam, the yearly mean temperature will increase 2-3°C in the late 21st century. Although annual precipitation increased in Southern Vietnam and it decreased in Northern Vietnam (MONRE, 2009). About 10-12% of Vietnam's population is directly impacted by climate change and country could lose around 10% of GDP (Vietnam government, national strategy on climate change, 2011). Although Vietnam is located in the tropical zone with high rainfall per year, water scarcity and drought still occur in some regions. It might be that the impacts of human activities and climate change will likely exacerbate water scarcity in some regions. These changes have impacted considerably on hydrology and water resources availability throughout Vietnam. These challenges require Vietnam to have appropriate

 ©2017, IAHR. Used with permission / ISSN 1562-6865 (Online) - ISSN 1063-7710 (Print)

policies to construct plans and methods to mitigate climate change impacts. In order to estimate the impacts of climate change, assessment of water resources will provide appreciated input for decision makers and also provide a comprehensive perception for communities to establish better adaptation strategies. The aforementioned serves as a motivation for this research to construct a modeling framework for assessing the variation of streamflow and subsequent water shortage by applying GCM outputs and a hydrological model.

Thac Mo catchment is located at the upstream of the Thac Mo reservoir, which plays a vital role for inhabitant in term of water supply and hydropower electricity. The downstream of the Thac Mo reservoir will experience rapid population growth and economic development in the future. Hence, water demand in 2050 is predicted to approximately triple relative to water demand in 2000 at the downstream of the reservoir. The catchment is faced with some problems, i.e. pressure of water use from irrigation, municipal, domestic, livestock, and ecological demands. The region is strongly influenced by climate change in the 21st century. Water demand can be met during the rainy season but water shortages occur in the dry period. Climate change, along with the socioeconomic development, likely leads to changes in hydrology and subsequent water scarcity. One needs to investigate the impacts of climate change on hydrological processes and water shortage for supporting decision – made on water resources planning and management in the future.

This study seeks to estimate the impacts of global climate change downscaled to a catchment scale. A modeling framework is used to estimate the effects of climate change on hydrological processes in Thac Mo catchment and subsequent water shortage at the downstream of the Thac Mo reservoir. The modeling framework used in this research consists of applying GCMs and a WEAP model (integrated hydrological – water evaluation and planning model).

WEAP model is widely used to assess the impact of climate change in the future possible climate (Santikayasa et al., 2015; Mehta et al., 2013; Alemayehu et al., 2010; Purkey et al., 2007; Rosenzweig et al., 2004) and adaptation scenarios on water resources (Joyce et al., 2011; Wilby et al., 2002). In these studies, WEAP model is used to evaluate water resources, hydropower, hydrological processes under future scenarios in many different regions. These studies showed that the WEAP model is widely used over the world and a can be a useful tool to predict changes in hydrology and water availability in the catchment scale. Therefore, integrating WEAP model and GCM outputs is possible for assessment of climate change impacts on hydrological processes and water resources, which is adopted in the study area of this research (Thac Mo catchment, Vietnam). Phu Long catchment has not been chosen for assessment of climate change impacts in previous studies, so it is necessary to have an official research to assess climate change impacts on hydrological processes and water resources. Besides, the catchment has also faced with many issues, such as the need to trade-off hydropower demand, water demand, land use change and socioeconomic development at the downstream area of the catchment. In recent years, there are many researches that are focused on climate change impacts on hydrological processes in Vietnam. Some researchers have applied different hydrological models and GCMs to assess climate change impacts, with their study areas being near the Thac Mo (Nam et al., 2016; Vo et al., 2015; Tran et al., 2011; Kawasaki et al., 2010).

The main objective of this research is to investigate the impacts of climate change on hydrological processes and water resources at the downstream of the Thac Mo reservoir. The sub-objectives of the study are: to calibrate and validate the hydrological module embedded into WEAP model for streamflow simulation at the Thac Mo station; to project and analyze changes in temperature and precipitation in the catchment under emission scenarios during 2046 – 2064; and to assess the impact of climate change on streamflow at the upstream of the Thac Mo reservoir and subsequent water shortage at the downstream of the Thac Mo reservoir.

2 STUDY AREA AND DATASET

The study was located at the upstream of Be river basin, in Binh Phuoc and Dak Nong province of Vietnam (Figure 1). It has a catchment area of 2,215km2, which lies in the tropical monsoon climate. Climatology is defined by two seasons: dry and rainy seasons. The rainy season usually starts from May to October with 85 to 90% of the total annual rainfall. The highest amount of rainfall occurs from July to September, which accounts for 50 to 60% of the annual rainfall. The dry season usually starts from November to April of the next year. Rainfall in the dry season represents about 10 to 15% of the total annual rainfall. The low rainfall season usually occurs in January and February. In aspect of climate, the Thac Mo catchment has tropical monsoon climate with the average annual temperature ranging from 25.5 - 26.7 ^{0}C, and average yearly precipitation from 2,400 - 2,800mm. An average density of the river network is about 0.56km/km^2. The study area is located in the steep area. The altitude varies from 1,000m in the highland area to 200m at the downstream area of the Thac Mo reservoir.

The terrain of Thac Mo catchment is very complex with various forms of topography: mountainous, midlands interspersed some small narrow plains and some cauldrons. The mean annual evaporation is about 1000 mm. Mean annual relative humidity in the study area is about 78.8% at the Thac Mo meteorological station. Relative humidity is high during the rainy season from May to October, reaching 85.8%. Air temperature over the study area was lowest in December and January, increasing in spring and reaching its highest values in April and May. It was observed that there was no significant difference in air temperature

©2017, IAHR. Used with permission / ISSN 1562-6865 (Online) - ISSN 1063-7710 (Print)

throughout a year. Mean annual air temperatures were found to be 25.6^{0}C. It was said that the air temperature difference in a day is approximately 7 to 8^{0}C (Nghi, 2002). In the study area, mean monthly sunshine hours vary from 4.9 hours/day in September to 8.7 hours/day in February and March with an average of 6.8 hours/day.

In this study, different types of data were collected for calibration of WEAP model as well as building scenario to predict streamflow variation in the Thac Mo catchment and subsequent water shortage at the downstream of the Thac Mo reservoir. The data consist of hydro-meteorological, reservoir characteristics, land cover, soil type, water demand at the downstream of the Thac Mo reservoir and climate scenario data were collected.

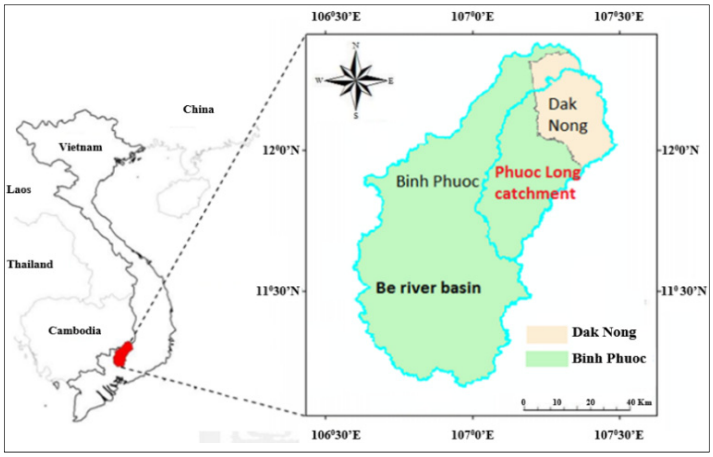

Figure 1. Location of the Thac Mo catchment.

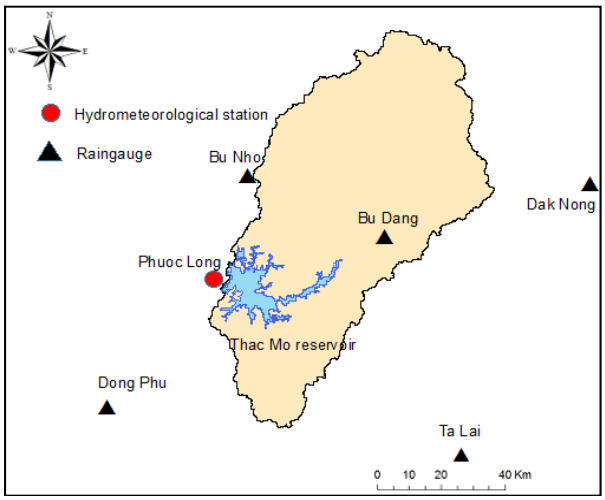

Figure 2. Location of the Thac Mo reservoir, raingauge and hydrometeorological stations.

- **Calibration process and calibration result**

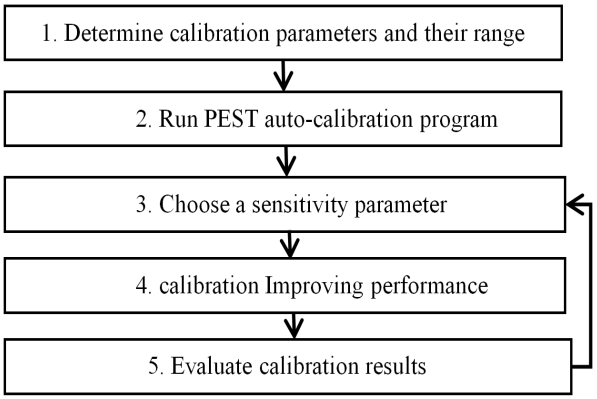

Figure 3. The framework of calibration process.

©2017, IAHR. Used with permission / ISSN 1562-6865 (Online) - ISSN 1063-7710 (Print)

In this study, calibration process was done according to the framework as shown in the Figure 3. A comparison of measured versus simulated monthly hydrographs at the Thac Mo station showed very good agreement as that shown in Figure 4. For the calibration period from 1978 to 1988, monthly RMSE was 46.5 (mm/month), Nash-Sutcliffe coefficient of efficiency (NSE), flow ratio (Vr), standard deviation ratio (RSR) of observation, percent bias (PBIAS) and correlation coefficient (CC) were 0.89, 1.01, 0.33, -3.92, 0.95, respectively (Table 1). For the validation period (1989 – 1993), all the parameters (RMSE, NSE, Vr, RSR, PBIAS, and CC) were equal to or little lower than the calibration period (1978 - 1988) with value of 49.2, 0.89, 0.92, 0.33 and 7.89, and 0.95, respectively (Table 1). According to the performance criteria of Moriasi et al. (2007), these above values showed a good WEAP model performance. These simulated results showed that hydrological processes in the WEAP model were simulated accurately at the Thac Mo catchment, which is necessary for predicting streamflow in the future scenarios. Finally, these optimal values of calibration parameters are presented in Table 2.

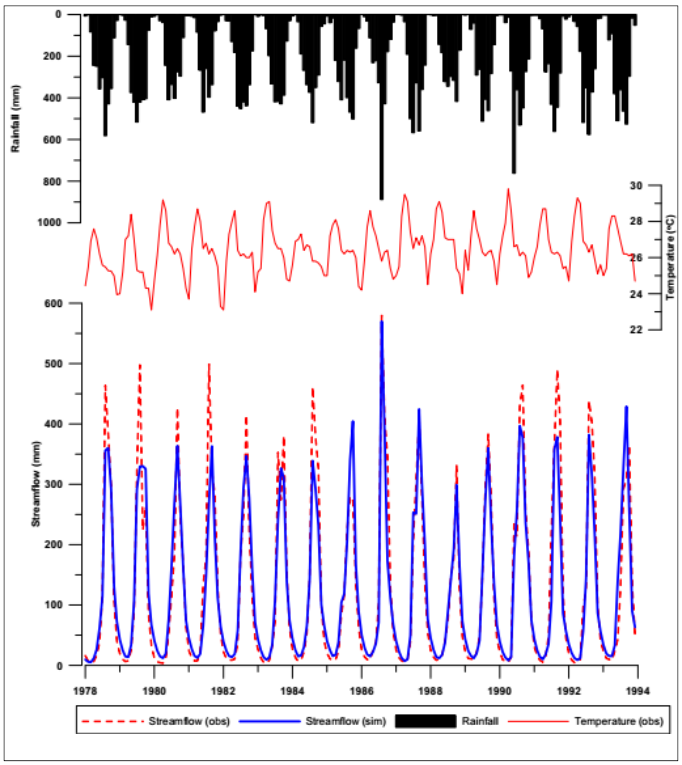

Figure 4. Observed versus simulated monthly streamflow and precipitation of Thac Mo catchment during calibration and validation periods.

Table 1. Performance criteria of simulated monthly streamflow during calibration and validation period.

Items	RMSE (mm/month)	NSE	Vr	BPIAS (%)	RSR	CC
Calibration (1978 – 1988)	46.5	0.89	1.04	-3.92	0.33	0.95
Validation (1989 – 1993)	49.2	0.89	0.92	7.89	0.33	0.95

Table 2. The calibration parameter ranges and their optimal values/

The parameter	The range	Optimal value
Soil water capacity (Sw)	0 – 1000 (mm)	969.7 (mm)
Root zone conductivity (ks)	0 – 945 (mm)	134.8 (mm)
Deep water capacity (Dw)	0 – 5000 (mm)	624.2 (mm)
Deep zone conductivity (k2)	0 – 14 (mm/month)	2.9 (mm/month)
Runoff resistance factor (LAI)	5.1 – 6.7 (no dimension)	6.7 (no dimension)
Preferred flow direction (f)	0 – 1 (no dimension)	0.98 (no dimension)

3 IMPACTS OF CLIMATE CHANGE ON HYDROLOGICAL PROCESSES AND WATER RESOURCES

3.1 Impacts of climate change on streamflow

In this section, the former projections of rainfall and temperature under B1 and A2 emission scenarios were used to simulate streamflow using the WEAP model. Averaged by the approach of multi-model

©2017, IAHR. Used with permission / ISSN 1562-6865 (Online) - ISSN 1063-7710 (Print)

ensemble (MME), results showed that an increase trend in streamflow in both the dry and wet seasons under both B1 and A2 emission scenarios. As shown in the Figure 5, the differences of seasonal changes on streamflows between the B1 and A2 emission scenarios are not apparent. Therefore, only the B1 emission scenario was selected for presenting the changes on monthly streamflows for the five GCMs. Figure 6 shows the projected changes on the average monthly streamflow in the period of 2046 – 2064 under B1 emission scenario compared with the baseline scenario. The MME values indicate that the average monthly streamflows have an increase tendency from the baseline scenario to the future scenario for most of months in a year excluding January, February, September, and December. The increment in streamflow can be explained by a tight correlation between rainfall and streamflow, when the total amount of rainfall increases the streamflow rises up accordingly. Streamflow reduction in December, January and February will likely exacerbate water shortage in the dry season. The results of water shortage are discussed in section D.

Furthermore, the MME results indicated that the timing of the projected maximum streamflow in the period of 2046 - 2064 is approximately one month earlier than that in the baseline scenario. This is mainly because maximum rainfall will likely occur earlier in the study area in the future scenario.

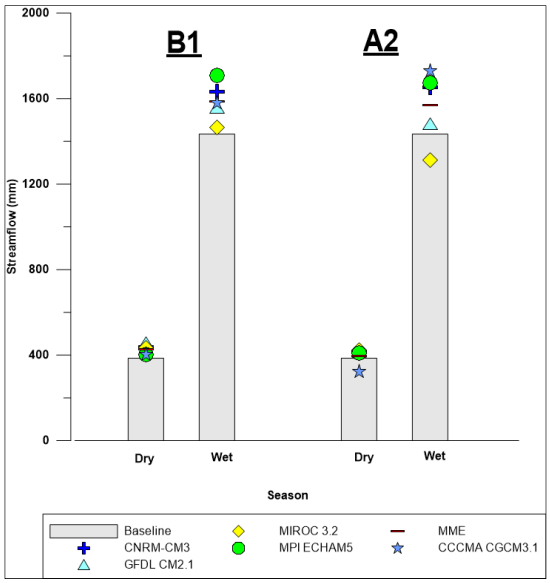

Figure 5. Simulated mean seasonal streamflow for the future and baseline scenarios using the five GCMs under B1 and A2 emission scenarios.

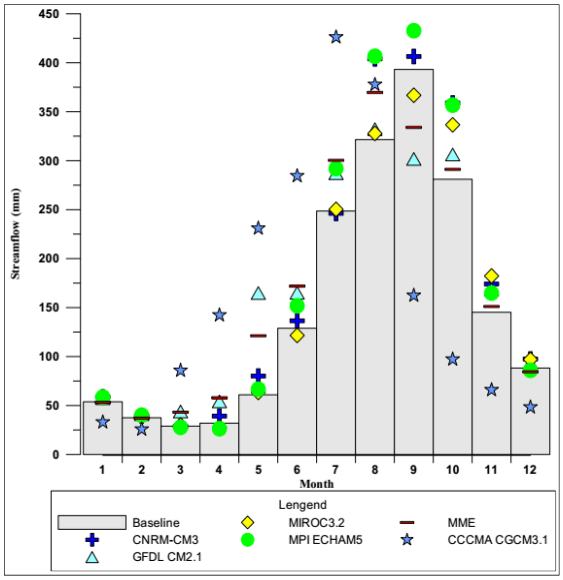

Figure 6. Simulated monthly streamflow for the future and baseline scenarios by five GCMs and MME under the B1 emission scenario.

3.2 Impacts of climate change on water resources at downstream of Thac Mo catchment

In this section, two scenarios (Scenario I and Scenario II) were suggested to assess impacts of climate changed due to socioeconomic development in the study area on water shortage in the future. Scenario I was

 ©2017, IAHR. Used with permission / ISSN 1562-6865 (Online) - ISSN 1063-7710 (Print)

generated with water demand in the baseline year 2000 and climatic condition during 2046 – 2064.The Scenario II was generated with water demand in the year 2050 and climatic condition during 2046 – 2064. The only difference between Scenario I and Scenario II was the water demand data.

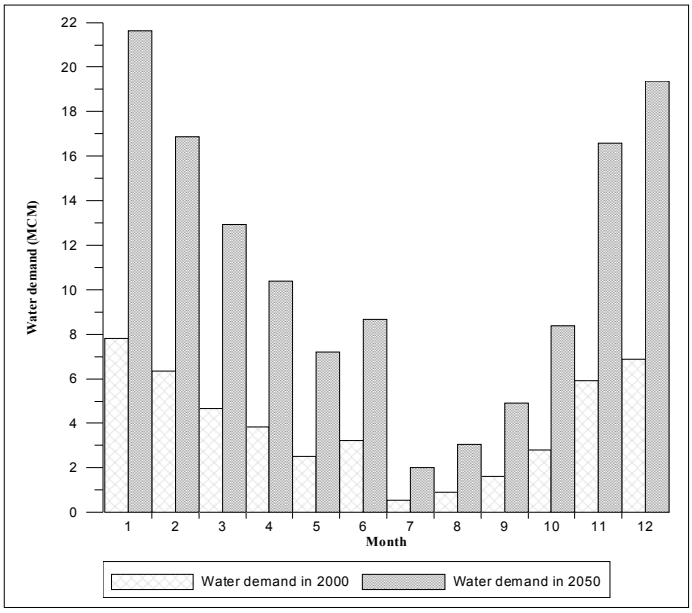

Figure 7. Water demand at the downstream of the Thac Mo reservoir in 2000 and 2050.

The Scenario I was generated with total water demand (agricultural, livestock, domestic and industrial demand) in the baseline year 2000 (Figure 7) and climatic condition during 2046 – 2064. The major water demand at the downstream of the Thac Mo reservoir is mainly for agricultural demand sites, which accounts for approximately 92% of the total water demand. This scenario was generated to assess only the impacts of climate change on the water shortage, the socioeconomic is assumed to remain constant over time at the downstream of the Thac Mo catchment.

Scenario II was generated with total water demand in the year 2050 and climatic condition during 2046 – 2064 to investigate the water shortage. The water demand that was estimated by SIWRP in 2050 was taken into account due to increasing water demand due to population growth and socioeconomic growth. Therefore, this scenario will likely reflect realistically on water scarcity at the downstream of the Thac Mo reservoir in the future. Due to population growth and socioeconomic development at the downstream of the Thac Mo reservoir, water demand in 2050 increases to approximately triple compared with water demand in 2000 (Figure 7).

3.2.1 Water shortage under Scenario I

The modeled seasonal water shortage for the baseline and future scenarios for the five GCMs under the B1 and A2 emission scenarios are presented in Figure 8. Under the B1 emission scenario, water shortage for the five GCMs vary between -9.2% and 89.8% (mean: 12.2%) for the dry season and between -79.4% and -3.1% (mean: -29.4%) for the wet season. Under the A2 emission scenario, water shortage for the five GCMs varied from -8.4% to 71.6% (mean: 19.4%) for the dry season and -82.5% to -17.5% (mean: -15.4%) for the wet season. Water shortage tends to decrease in the rainy season and increase in the dry season in both emission scenarios. For the dry season, the mean increase (19.4%) under the A2 emission scenario is greater than that (12.2%) under the B1 emission scenario. For the wet season, the mean that decreases (-15.4%) under the A2 emission scenario is less than that (- 29.4%) under the B1 emission scenario. Since seasonal impacts on water shortage between the two emission scenarios are not apparent, only the B1 emission scenario was chosen for further presenting the monthly impacts on water shortage for the five GCMs in the future. The simulated mean monthly water shortage for the baseline future scenarios for the five GCMs under the B1 emission scenario are presented in Figure 9 under Scenario I. From March to August, the reservoir inflows of the Thac Mo reservoir tend to increase that leads to reduce water shortage at the downstream of the Thac Mo reservoir. Water shortage will tend to increase from September to February of the following year due to the reduction of inflows during this period in the future. The aforementioned results advised that the water use during the dry season may encounter a big task while the streamflow is reduced in the future.

3.2.2 Water shortage under Scenario II

The modeled mean seasonal water shortage for the baseline scenario and the future scenario for the five GCMs under the B1 and A2 emission scenarios under Scenario II are shown in Figure 10. Under B1 emission

©2017, IAHR. Used with permission / ISSN 1562-6865 (Online) - ISSN 1063-7710 (Print)

scenario, water shortage for the five GCMs vary between 189.2% and 495.4% (mean: 255.6%) for the dry season and between –22.4% and 203.9% (mean: 124.6%) for the wet season. Under the A2 emission scenario, the ranges of percentage change in water shortage for the five GCMs are 187.4% to 445.4% (mean: 278.8%) for the dry season and -31.1% to 278.1% (mean: 171.1%) for the wet season. Water shortage tends to increase in the dry season as well as in the wet season under both emission scenarios.

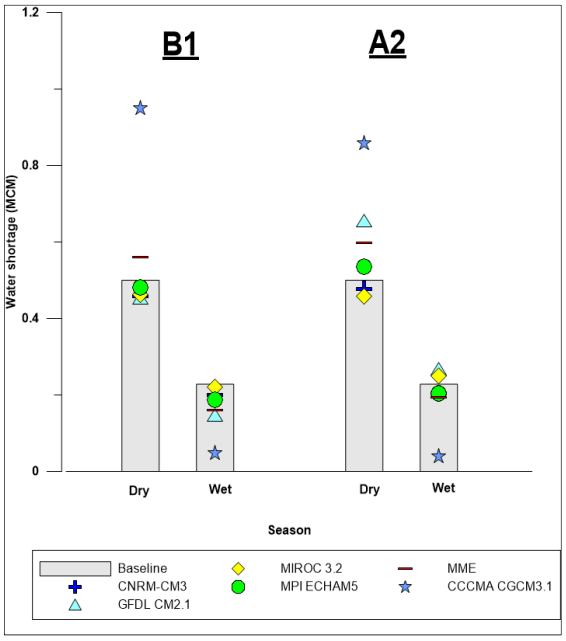

Figure 8. Simulated mean seasonal water shortage in the future and baseline scenarios using the five GCMs under B1 and A2 emission scenarios under Scenario I.

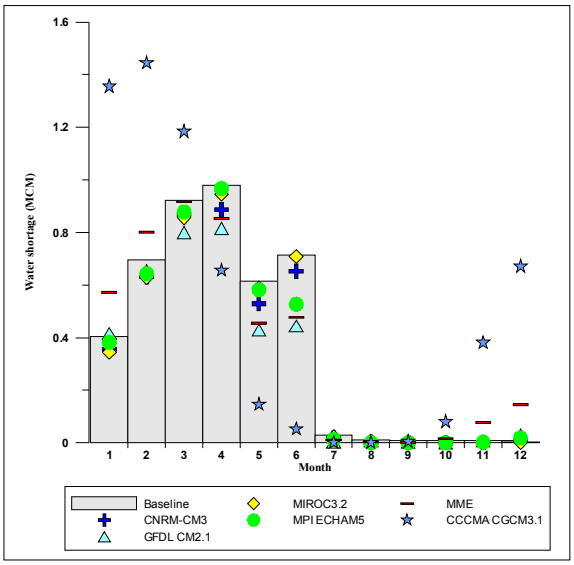

Figure 9. Modeled monthly water shortage for the future and baseline scenarios by five GCMs and MME under the B1 emission scenario under Scenario I.

For the dry season, the mean increased (278.8%) under the A2 emission scenario was greater than that (255.6%) under the B1 emission scenario. For the wet season, the mean increase (171.1%) under the A2 emission scenario is also greater than that (124.6%) under the B1 emission scenario. The B1 emission scenario was chosen for further presenting the monthly impacts on water shortage for the five GCMs. Under B1 emission scenario, the MME results indicated that the simulated monthly water shortages tend to increase from the baseline scenario to the future scenario for all months (Figure 11). The increases or decreases of simulated average monthly mean water shortage by the five GCMs range from -0.5 MCM/month to 3.8 MCM/month. Although water demand in the Scenario II increases approximately triple than the baseline year, an increase in average monthly mean water shortage during July – December is not much (0.9 MCM/month) compared to an increase in average monthly mean water shortage during January – June (4.1 MCM/month), which implies that abundant rainfall in the catchment area and water storage in the reservoir could meet

 ©2017, IAHR. Used with permission / ISSN 1562-6865 (Online) - ISSN 1063-7710 (Print)

90.1% water demand at the downstream of the Thac Mo reservoir during the wet season. However, an increase in water shortage is inevitable from January to June because the dry period occurs in the catchment and water users need a lot of water supply (12.9 MCM/month) during that time, so water storage in the reservoir could meet only 68.3% water demand at the downstream of the Thac Mo reservoir.

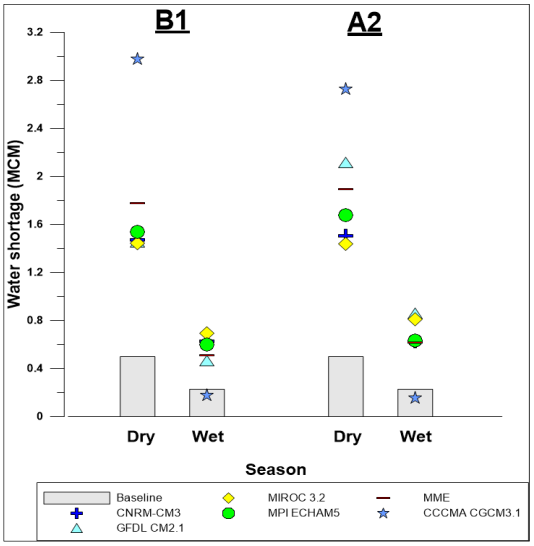

Figure 10. Simulated mean seasonal water shortage for the baseline scenario and the future scenario using the five GCMs under B1 and A2 emission scenarios under Scenario II.

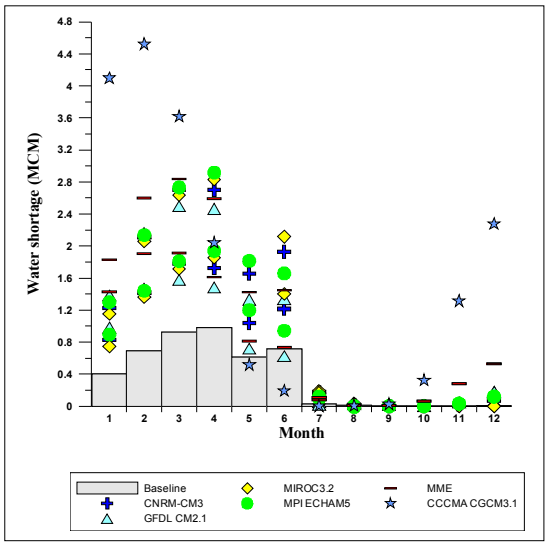

Figure 11. Modeled monthly mean water shortage for the future and baseline scenarios by five GCMs and MME values under the B1 emission scenario under Scenario II.

4 CONCLUSIONS

This study offered a simple process for investigating climate change impacts on streamflow and subsequent water shortage at the downstream of the Thac Mo reservoir. A case study was implemented in the Thac Mo catchment, Vietnam. By integrating the GCMs output and the WEAP model, the streamflow and subsequent water shortage for the baseline (1994–2003) and future scenario (2046–2064) were simulated. By paralleling the results during the baseline and the future scenario, the climate change impacts on the streamflow and subsequent water shortage; a combined assessment of the impacts of climate change and socioeconomic development on water shortage were assessed.

The WEAP model was effectively applied in the study area of the Thac Mo catchment, to assess the impacts of climate change on hydrological processes and subsequent water shortage. The model calibration and validation results showed that the WEAP model could be a useful tool for evaluating the impacts of climate change on hydrological processes and water shortage in the study area.

For both the calibration and validation periods, the results show that NSE and CC are equal to 0.89 and 0.95, respectively; RSR and the absolute value of PBIAS are less than or equal to 0.33 and 7.89, respectively; Vr is equal to 1.04 and 0.92, respectively. These results indicate that WEAP model is suitable for the study

©2017, IAHR. Used with permission / ISSN 1562-6865 (Online) - ISSN 1063-7710 (Print)

area. Annual temperature and rainfall were projected to increase in the future. Annual temperatures were projected to increase by 0.3 ^{0}C and 0.7 ^{0}C under B1 and A2 emission scenarios, respectively. The differences of seasonal impacts on rainfall between the two emission scenarios are not apparent. Under B1 emission scenario, the MME results showed that mean monthly rainfalls have an increase tendency from the baseline scenario to the future scenario for most of months of the year excluding February, September, and December. The simulated monthly temperatures tend to increase from the baseline scenario to the future scenario for most of months of the year excluding January, March, and November under B1 emission scenario. Under A2 emission scenario, the MME results indicate that the simulated monthly temperature tend to increase from the baseline scenario to the future scenario for all months. The MME results indicate that the seasonal mean streamflows were projected to increase in the future under both B1 and A2 emission scenarios for both the wet and dry seasons. The differences of seasonal impacts on streamflow between the two emission scenarios are not apparent. The streamflow projections for this study is consistent with the IPCC report (2007) which indicated that streamflow will increase in Southeast Asia due to the impacts of climate change. However, the increase in rainfall is not distributed at similar levels for all months of the year. A decrease was also found in January, February, September and December. The seasonal mean water shortages were projected to increase in the dry season and decrease in the wet season under both B1 and A2 emission scenarios in Scenario I. This result stressed that the impacts of climate change will likely exacerbate water scarcity in the dry season at the downstream of the Thac Mo reservoir. From March to August, the MME results indicate that water shortage is reduced at the downstream of the Thac Mo reservoir. Water shortage will tend to increase from September to February of the following year in the future.

A combined assessment of the impacts of climate change and socioeconomic development on water shortage at the downstream of the Thac Mo reservoir was conducted in Scenario II. The results showed that water shortage during 2046 – 2064 increase approximates triple than the baseline year 2000, which imply that the water use during the dry season might encounter an immense challenge while the water shortage is increased. Although the Thac Mo catchment has abundant rainfall and water storage in the reservoir, water scarcity is inevitable from January to June.

Despite several limitations of this study, it might provide coarse results for investigating the hydrological processes and water resources under climate change scenarios and socioeconomic development. These results could be considered adequate to estimate the variations in hydrological processes and water resources in terms of total discharges and seasonal impacts. This study provides a convenient model to evaluate the impacts of climate change on prospective water availability, and support for water management and planning in the future. The results also provided useful insights for decision-makers on how to trade-off water resources management issues under future climate change.

5 SUGGESTIONS

In terms of calibration results, the WEAP model underestimated when simulating the streamflow in the catchment. The main reason might come from scarcity of rain gauges in the catchment, only one rain gauge was located inside of the catchment and other rain gauges are located outside of the catchment (Figure 2). In addition, these limitations might come from lack of some rainfall data during calibration and validation periods. The catchment rainfall data was the most important input in the WEAP model, and the model was mainly sensitive to it. The quality of the rainfall data will solidly affect the precision of the simulations. Hence, a catchment rainfall data recovery approach of improving the precision of catchment area rainfall estimation was proposed by Chu et al. (2012) can be applied in the future to the Thac Mo catchment which had a low density of the rain gauge network. Another reason might be that WEAP model embedded PEST software for auto-calibration; however, PEST software uses the single objective function for the calibration process. Therefore, WEAP model can be linked to other software using multi- objective functions such as genetic algorithm II (NSGA-II) to improve WEAP model calibration performance and thus streamflow prediction might be more confident in the future.

Along with climate change, vegetation pattern and reservoir operating rules may change over time and thus have an effect on hydrological processes in the future. However, land use and reservoir operating rules changes are not considered in this study. Improvement might be to include estimates of uncertainty in terms of how the reservoir might be operated in the future, and the uncertainty in the types of crops that might be used in the future. These improvements would help to make the model more detailed.

In addition, this study only has a rough estimate of the monthly streamflow and water shortage, which based on the uncertainty in rainfall and temperature from five GCMs. The use of GCM outputs in climate change scenarios is uncertain. In this study, GCMs were selected only based on the correlation coefficient between local data and GCM outputs. In the next steps of this study, to provide higher levels of confidences for each climate scenario, the super higher resolution global climate model (20 km grid cell distance) which is experimented by the Meteorological Research Institute and Japan Meteorological Agency (MRI and JMA) could be considered as well as IPCC - Fifth Assessment Report (AR5) could be used for better results.

 ©2017, IAHR. Used with permission / ISSN 1562-6865 (Online) - ISSN 1063-7710 (Print)

REFERENCES

Alemayehu, T., McCartney, M. & Kebede, S. (2010). The Water Resource Implications of Planned Development in the Lake Tana Catchment, Ethiopia. *Ecohydrology & Hydrobiology*, 10(2), 211-221.

Andersson, L., Wilk, J., Todd, M.C., Hughes, D.A., Earle, A., Kniveton, D. & Savenije, H.H. (2006). Impact of Climate Change and Development Scenarios on Flow Patterns in the Okavango River. *Journal of Hydrology*, 331(1), 43-57.

Chu, J., Zhang, C., Wang, Y., Zhou, H. & Shoemaker, C.A. (2012). A Watershed Rainfall Data Recovery Approach with Application to Distributed Hydrological Models. *Hydrological Processes*, 26(13), 1937-1948.

Devkota, L.P. & Gyawali, D.R. (2015). Impacts of Climate Change on Hydrological Regime and Water Resources Management of the Koshi River Basin, Nepal. *Journal of Hydrology: Regional Studies*, 4, 502-515.

Githui, F., Gitau, W., Mutua, F. & Bauwens, W. (2009). Climate Change Impact on SWAT Simulated Streamflow in Western Kenya. *International Journal of Climatology,* 29(12), 1823-1834.

Intergovernmental Panel on Climate Change (IPCC). (2007). *Climate Change 2007: Synthesis Report*, IPCC, Geneva.

Joyce, B.A., Mehta, V.K., Purkey, D.R., Dale, L.L. & Hanemann, M. (2011). Modifying Agricultural Water Management to Adapt to Climate Change in California's Central Valley. *Climatic Change*, 109(1), 299-316.

Kawasaki, A., Takamatsu, M., He, J., Roger, P. & Herath, S. (2010). An Integrated Approach to Evaluate Potential Impact of Precipitation and Land-Use Change on Streamflow in Srepok River Basin. *Theory and Applications of GIS,* 18(2), 9-20.

Kim, U. & Kaluarachchi, J.J. (2009). Climate Change Impacts on Water Resources in the Upper Blue Nile River Basin, Ethiopia. *Journal of the American Water Resources Association,* 45(6), 1361-1378.

Kiparsky, M., Joyce, B., Purkey, D. & Young, C. (2014). Potential Impacts of Climate Warming on Water Supply Reliability in the Tuolumne and Merced River Basins, California. *PLoS One*, 9(1), doi:10.1371/journal.pone.0084946.

Mehta, V.K., Haden, V.R., Joyce, B.A., Purkey, D.R. & Jackson, L.E. (2013). Irrigation Demand and Supply, Given Projections of Climate and Land-Use Change, in Yolo County, California. *Agricultural Water Management*, 117, 70-82.

Ministry of Natural Resources and Environment (MONRE). (2009). *Climate Change, Sea Rise Scenarios for Vietnam*, Hanoi.

Moriasi, D.N., Arnold, J.G., Van Liew, M.W., Bingner, R.L., Harmel, R.D. & Veith, T.L. (2007). Model Evaluation Guidelines for Systematic Quantification of Accuracy in Watershed Simulations. *Transactions of the ASABE*, 50(3), 885-900.

Nam, D.H., Udo, K. & Mano, A. (2012). Climate Change Impacts on Runoff Regimes at a River Basin Scale in Central Vietnam, Terr. *Atmos. Ocean Sci.,* 23(5), 541-551.

Nghi, V.V. (2002). Rainfall-Runoff and Hydrodynamic Modelling in the Dong Nai River Basin, Vietnam, *MSc Thesis*, HH 429, International Institute for Infrastructural, Hydraulic and Environmental Engineering (IHE), Delft, the Netherlands.

Purkey, D.R., Huber-Lee, A., Yates, D.N., Hanemann, M. & Herrod-Julius, S. (2007). Integrating a Climate Change Assessment Tool into Stakeholder-Driven Water Management Decision-Making Processes in California. *Water Resources Management*, 21(1), 315-329.

Rochdane, S., Reichert, B., Messouli, M., Babqiqi, A. & Khebiza, M.Y. (2012). Climate Change Impacts on Water Supply and Demand in Rheraya Watershed (Morocco), with Potential Adaptation Strategies. *Water*, 4(1), 28-44.

Rosenzweig, C., Strzepek, K.M., Major, D.C., Iglesias, A., Yates, D.N., McCluskey, A. & Hillel, D. (2004). Water Resources for Agriculture in a Changing Climate: International Case Studies. *Global Environmental Change*, 14(4), 345-360.

Santikayasa, I.P., Babel, M.S. & Shrestha, S. (2015). Assessment of the Impact of Climate Change on Water Availability in the Citarum River Basin, Indonesia: The Use of Statistical Downscaling and Water Planning Tools. *Managing Water Resources under Climate Uncertainty*, 45- 64.

Thai, T.H. & Thuc, T. (2011). Impacts of Climate Change on the Flow in Hong-Thai Binh and Dong Nai River Basins. *Journal of Science, Earth Sciences,* 27(2), 98-106.

Vietnam Government Portal (2011). *National Strategy on Climate Change,* Vietnam.

Vo, N.D., Gourbesville, P., Vu, M.T., Raghavan, S.V. & Liong, S.Y. (2015). A Deterministic Hydrological Approach to Estimate Climate Change Impact on River Flow: Vu Gia–Thu Bon Catchment, Vietnam. *Journal of Hydro-Environment Research*, 11, 59-74.

Wilby, R.L., Dawson, C.W. & Barrow, E.M. (2002). SDSM—A Decision Support Tool for the Assessment of Regional Climate Change Impacts. *Environment Modelling Software,* 17(2), 145–157.

Zhang, X., Srinivansan, R. & Hao, F. (2007). Predicting Hydrologic Response to Climate Change in the Luohe River Basin Using SWAT Model. *Transactions of the ASABE*, 50(3), 901-910.

©2017, IAHR. Used with permission / ISSN 1562-6865 (Online) - ISSN 1063-7710 (Print)

Proceedings of the 37th IAHR World Congress
August 13 – 18, 2017, Kuala Lumpur, Malaysia

ANALYSIS OF THE RELATIONSHIP BETWEEN SNOW DEPTH AND TOPOGRAPHY IN A MOUNTAINOUS REGION USING AIRBORNE LASER SCANNING DATA

TERUMASA NISHIHARA[(1)], ATSUSHI TANISE[(2)] & KAZUYOSHI WATANABE[(3)]

[(1,2)] Civil Engineering Research Institute for Cold Region of Public Works Research Institute, Sapporo, Japan, Nishihara-t22aa@ceri.go.jp
[(3)] Hokkaido Regional Development Bureau, Ministry of Land, Infrastructure, Transport and Tourism, Kushiro, Japan

ABSTRACT

In cold and snowy regions, the snowmelt water stored in dams in early spring is important to meet the water demand until summer. In water resource management, it is very important to estimate snow depth distribution in the catchment basin as accurately as possible before the snow starts to melt. We conducted airborne laser scanning twice, in 2012 and in 2015, to measure the snow depth distribution in the same range of mountainous regions. The pattern of snow depth distribution in two years was almost similar. We found there is a linear relationship between snow depth and elevation in forests and the linear relationship between snow depth overground-openness in the high elevations above the forest line.

Keywords: Snow depth distribution; forest; high elevations above the forest line; overground-openness; airborne laser scanning.

1 INTRODUCTION

In snowy cold regions, the snowmelt water stored in dams in early spring is important for meeting the water demand until summer. However, snowmelt water also can cause snowmelt flood disasters. Therefore, at dams in Hokkaido, Japan, snow surveys are conducted every March, when the snow water equivalent in the catchment basin is approaching its peak, and the total snow water equivalent in the catchment basin is estimated. In water resource management and in disaster prevention, it is very important to clarify the total water snow water equivalent for the catchment basin as accurately as possible before the snow starts to melt. However, sites where snow surveys can be conducted are limited, because there is the risk of avalanches. At high elevations above the forest line, it is particularly difficult to set survey points other than at or near ridges. Snow depths that represent each elevation range have not been systematically measured.

The snow depth distribution in mountainous areas, such as the snow distribution in the catchment basin of a dam, greatly differs for low-elevation sites in forests versus high-elevation sites above the forest line (Yamada et al., 1979; Nishihara et al., 2013). Many studies have addressed the snow depth distribution in forested areas in Japan (Yamada, 1983; Shimamura et al., 2005; Nishihara et al., 2013). These studies have reported that the snow depth and the snow water equivalent increase linearly with increase in elevation. Elevation's relationships with snow depth and with snow water equivalent have been used in standard methods for estimating the total snow water equivalent for the catchment basin in dam management in Japan.

In recent years, the acquisition of high-density, three-dimensional spatial data for wide areas has become possible by using airborne laser scanning. An example was reported of a survey conducted from the air for an area that was inaccessible by land. Nishihara et al. (2013) measured snow depths by conducting an airborne laser scanning survey at high elevations above the forest line in the Chubetsu Dam basin, which is in the Taisetsu Mountains of Hokkaido, Japan. Those researchers analyzed the relationship between snow depth and topography by using the results of measurement. The analysis found that the snow depth at high elevations above the forest line had a linear relation with overground-openness, which is an index of topographic unevenness. The analysis also showed that it was possible to appropriately estimate the snow depth distribution at high elevations by applying the relationship between snow depth and overground-openness, and that it was possible to accurately estimate the total snow water equivalent for the catchment basin of a dam and the dam inflow during a snowmelt season.

However, the generalizability for the analysis results of Nishihara et al. (2013) has not been investigated, because there have been very few reports on surveys of snow depth distribution at high elevations. We conducted our second measurement in 2015 using airborne laser scanning to measure the snow depth in the areas for which the relationship between the snow depth and the topography had been analyzed based on the first airborne survey of 2012. A purpose of the present study was to examine the relationship between snow depth and topography based on measurements done for two years.

 ©2017, IAHR. Used with permission / ISSN 1562-6865 (Online) - ISSN 1063-7710 (Print)

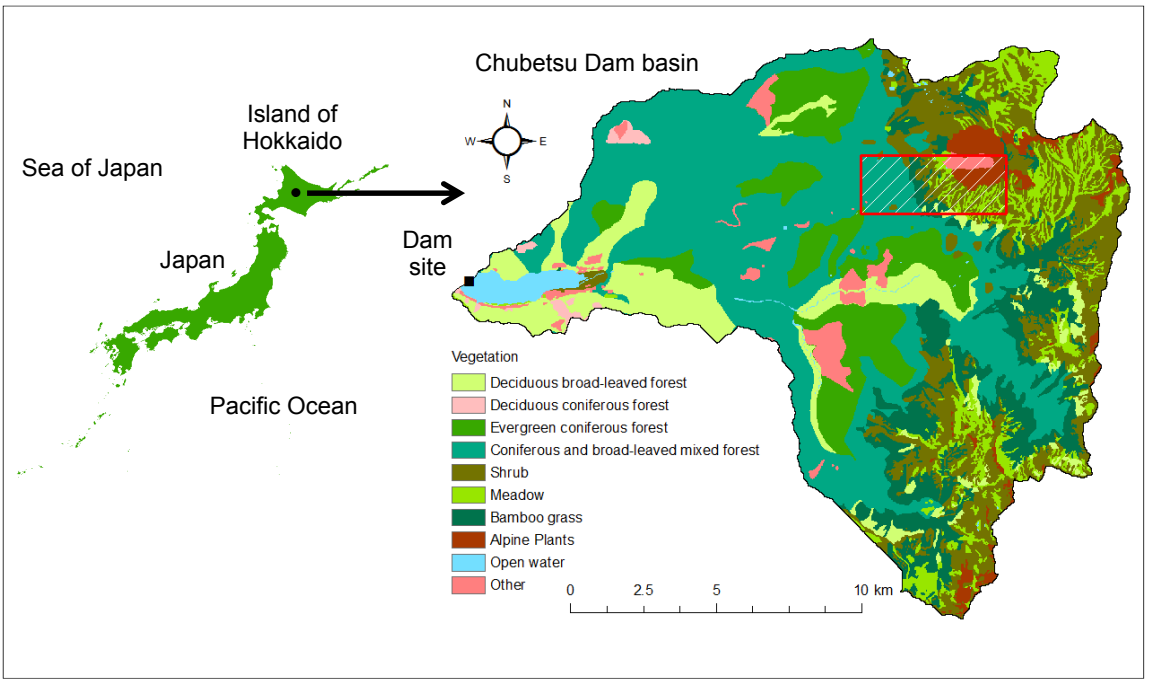

Figure 1. Target dam basin.

2 DATA AND METHOD

As shown in Figure 1, the survey was conducted at the Chubetsu Dam basin. The Chubetsu Dam is at the upper reaches of the Chubetsu River in the Ishikari River System. The catchment basin is 239km^2 in area, and its elevations are between 400m and 2,300m. Figure 1 shows the vegetation in the target basin according to 10 classifications, as determined from the results of the National Survey on the Natural Environment. The white line in the figure is the contour line for the 1,400m elevation. The main vegetation is divided by the 1,400m elevation contour into forest at lower elevations (forests) and grass, bamboo and plants other than trees at higher elevations (alpine zone). In the catchment basin, about 60% of the vegetation is forest and about 40% is non-forest.

The airborne laser scanning was conducted in the area enclosed in the red square in Figure 1. It was conducted from September 22 to 25, 2009 (during the snow-free period) and on March 10, 2012 and on March 27, 2015 (during the snowy period). Digital elevation models (DEMs) of the ground surface and the snow surface were created from the airborne laser scanning data. The horizontal resolution of the DEMs was 5m. The snow depth was calculated as the difference between the elevation of the DEMs in the period with snow and that in the period without snow. The accuracy of the calculated snow depth is about ± 30cm.

Figure 2 shows the orthophoto and the distribution of topography in the survey area. The orthophoto was taken at the time of the airborne laser scanning in 2009 and the aspect and the overground-openness were calculated by the DEMs of the ground surface. The 10km^2 survey area was at elevations between 1,100m and 2,300m and included the peak of Mt. Asahidake. The forest line in the survey area was at the elevation of about 1,450m (the red lines in the figures). At elevations higher than 1,450m, 98% of the vegetation area is non-forest. The survey area mainly consists of west-facing slopes. When winter storms occur on the Japan Sea side of Hokkaido, strong westerly winds tend to blow. Most of the slopes in the survey area are windward during these storms. The east side of the Mt. Asahidake peak in the survey area faces east, and this area is a leeward slope during these storms. The overground-openness index was developed by Yokoyama (1999) to quantify how far a target point is above or below the surrounding surface Overground-openness is determined by using Eq. [1].

$$\Phi = (\phi_0 + \phi_{45} + \phi_{90} + \phi_{135} + \phi_{180} + \phi_{225} + \phi_{270} + \phi_{315})/8 \qquad [1]$$

where, Φ: overground-openness (°), and ϕ_i: the max zenith angle (°) with which it is possible to see the sky along azimuth i° within the specified search distance from the target point. In determining overground-openness, the search distance was set to 100m. It is an index that is not dependent on azimuth or local topography, because the average value of the zenith angles along eight azimuths was determined. The overground-openness for the target points of a valley, a ridge and a flatland are$\Phi < 90°$, $\Phi > 90°$ and$\Phi = 90°$, respectively. In the figure of overground-openness, valleys and ridges were clearly identified according to the alpine zone. The overground-openness of the area for which airborne laser scanning was done roughly distributes between 55° and 100°. The frequency of overground-openness between 80° and 90° was high in the alpine zone above the forest line, as shown in Figure 3.

©2017, IAHR. Used with permission / ISSN 1562-6865 (Online) - ISSN 1063-7710 (Print)

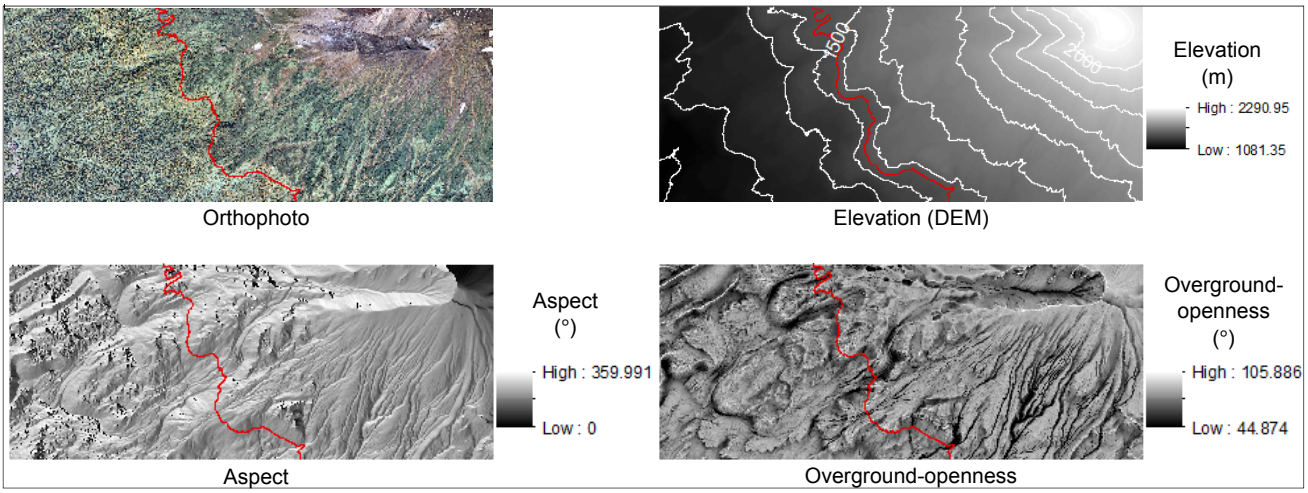

Figure 2. Orthophoto and topography of survey area.

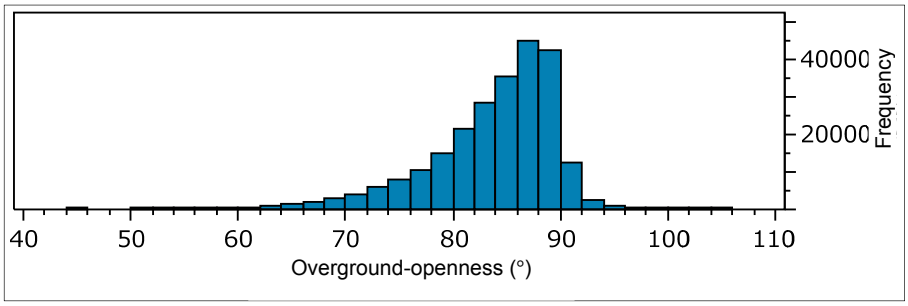

Figure 3. Frequency distribution of overground-openness in the alpine zone.

3 RELATIONSHIP BETWEEN TOPOGRAPHY AND SNOW DEPTH

3.1 Overview

Figure 4 shows the snow depth distribution calculated from airborne laser scanning data. The red lines in the figures are forest lines. The areas to the left of the red lines are forests, and those to the right of the red lines are alpine zones. The snow depth in 2015 was greater than that in 2012 in the survey area. Many previous studies reported that the characteristics of snow depth distribution in forest are different from those in the alpine zone, as Figure 4 clearly shows. In the forests, there are many dark colors. Therefore, we can say that the snow depths were small and were distributed in a narrow range. In the alpine zone, both dark colors and clear colors are found. This indicates that the snow depths were distributed in a wide range. Actually, the areas with great snow depth are distributed in valleys and these with small snow depth are distributed at ridges in the alpine zone. And the pattern of snow depth distribution between two years was similar.

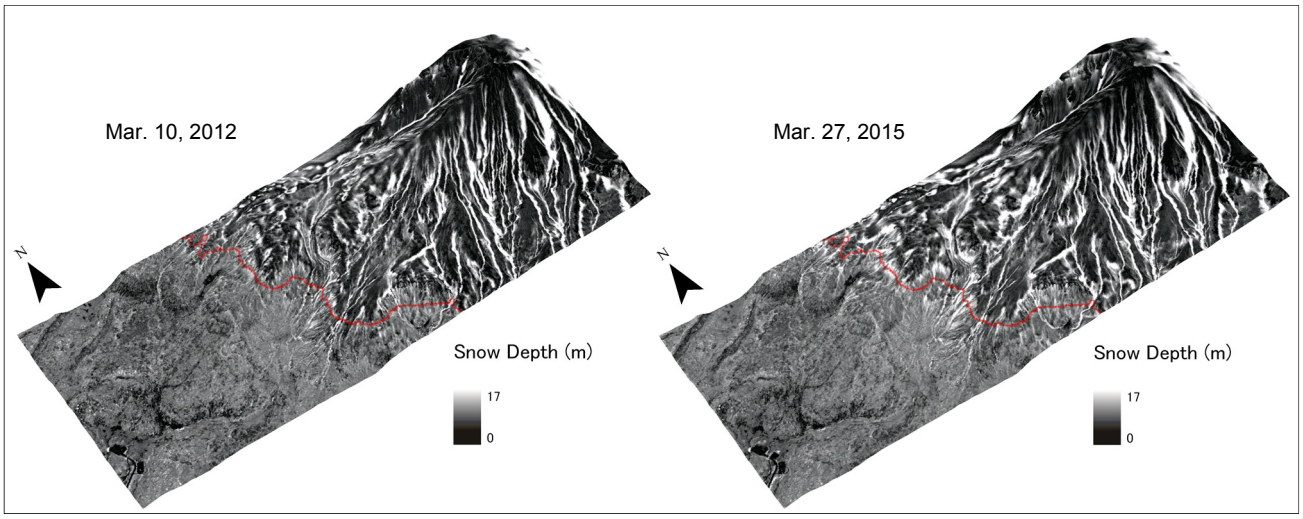

Figure 4. Snow depth distribution calculated from airborne scanning data.

©2017, IAHR. Used with permission / ISSN 1562-6865 (Online) - ISSN 1063-7710 (Print)

3.2 Relationship between elevation and snow depth

400,000 data points were used in the DEMs. Clarification of the relationship between topography and snow depth was difficult by using so many data points. Therefore, the data were grouped into 25m elevation ranges. The average snow depth in each 25m elevation range was determined, and the relationship between the determined snow depth and topographic factors was examined (Nishihara et al., 2013).

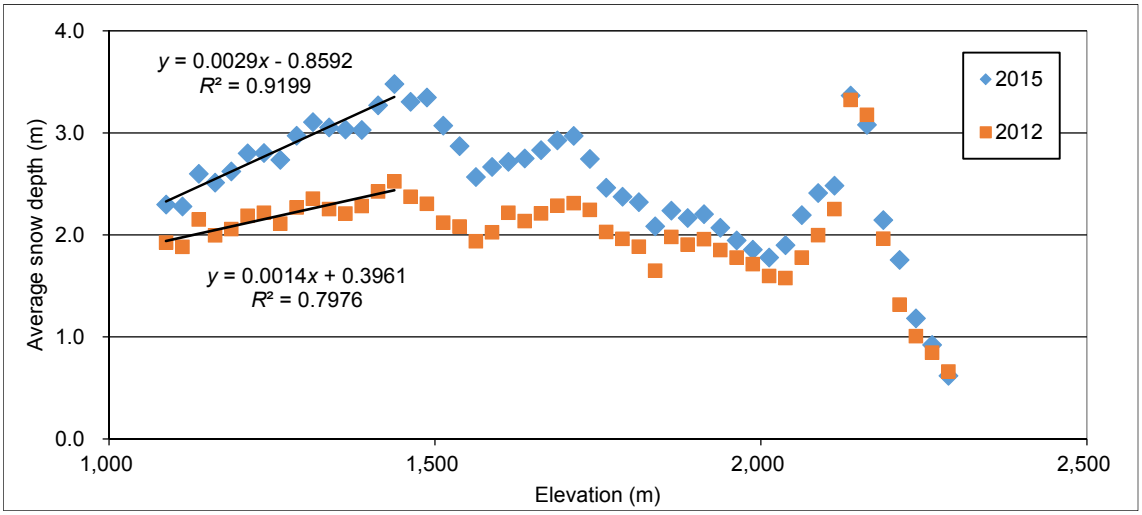

Figure 5. Relationship between snow depth and elevation.

Figure 5 shows the relationship between elevation and average snow depth. When the measurement results for 2012 and 2015 (Figure 4) are roughly examined, the tendencies in the relationship between snow depth and elevation are roughly equal for the two years. Elevations up to 1,450m correspond to forests. At these elevations, as in previous studies, the elevation and snow depth are found to have a linear relationship with a high correlation. At elevations above 1,450m, the alpine zone, the snow depth greatly varies by elevation.

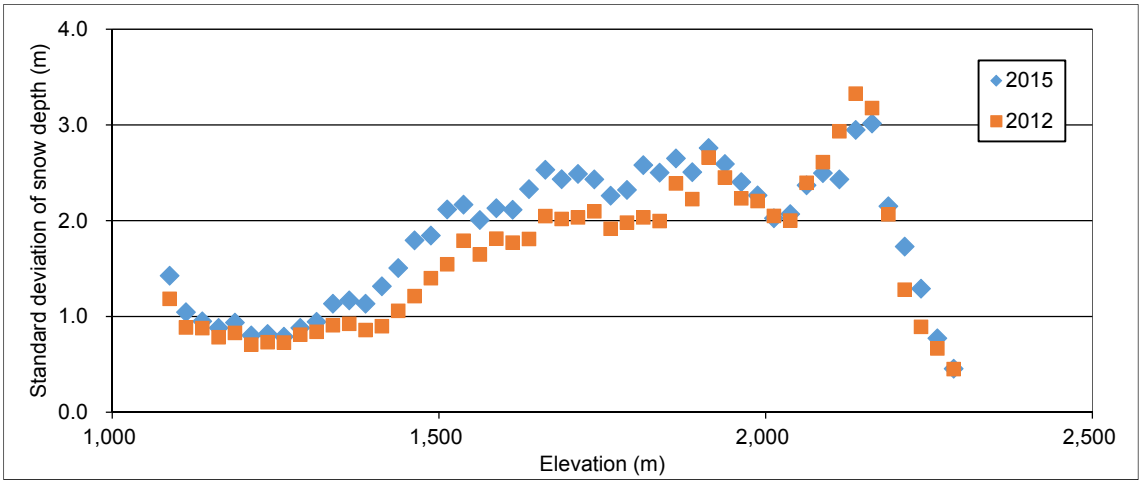

Figure 6. Relationship between standard deviation of snow depth and elevation.

The 25m elevation range was used in analyzing the relationship between elevation and snow depth. Therefore the standard deviation of snow depth for each 25m elevation range can be determined. Figure 6 shows the relationship between the elevation and the standard deviation of snow depth. Similar to Figure 5, the tendencies in the relationship between the snow depths and elevations were similar for the two years. The standard deviation was roughly 1.0m or less in the forests, and it gradually increases with increase in elevation like at elevations around 1,450m, which is the forest line. The standard deviation is about 2.0m to 3.0m in the alpine zone. The standard deviation of snow depth in forest agrees with the standard deviation of snow depth at elevations with forest in a report by Nishihara et al. (2012), in which the snow depth measured by airborne laser scanning in the Jozankei Dam basin of Hokkaido, Japan, was analyzed using the same method as above. As the reason for the gradual increase in standard deviation with increase in elevation at elevation ranges below and above the forest line, it is assumed that the main vegetation in these elevation ranges gradually with transitions from forest to non-forest. The reason that the standard deviation at elevations of 2,200m and higher

©2017, IAHR. Used with permission / ISSN 1562-6865 (Online) - ISSN 1063-7710 (Print)

was small was thought to be due to the inclusion of the Mt. Asahidake peak. The area around the peak has many ridges, and snow does not accumulate there.

To analyze the transitions in standard deviation in detail, the frequency distribution of snow depths for the 100m elevation ranges that are shown in Figure 7 was examined. Figure 7 shows the graphs of the four zones: one for elevations from 1,200m to 1,300m, in forest, for which the standard deviation does not greatly vary; one for elevations from 1,400m to 1,500m, which includes the forest line; one for elevations of 1,700m to 1,800m, in the alpine zone, for which the standard deviation does not greatly vary; and one for elevations of 2,200 and higher, which is near the mountain peak. The frequency of great snow depths was higher in 2015 than that in 2012 because the snow depth in the survey area was greater in 2015 than in 2012. For elevations from 1,200m to 1,300m, which have forest vegetation, the snow depth histogram exhibits a nearly normal distribution. This relationship between elevation and snow depth distribution agrees with that given in the report by Nishihara et al. (2012). The snow depths at elevations from 1,700m to 1,800m and at elevations of 2,200m and higher, which are in the alpine zone, exhibits a roughly exponential distribution. In the graph for elevations from 1,400m to 1,500m, which includes the forest line, the frequency distribution of snow depths slightly deviates from the normal distribution. This deviation showed that the snow depth distribution shifts from that in forest to that in the alpine zone. As the main vegetation gradually shifts from forest to alpine vegetation, the plotted width of the frequency distribution of snow depth becomes great, and then that width becomes small at elevations near the mountain peak. Accumulated snow in forest tends not to move, because the wind is abated in forest. Conversely, accumulated snow in the alpine zone, where the wind is strong, tends to move. In the alpine zone, strong winds carry away snow to create locations with very little snow or no snow cover, including ridges, and locations with much snow, including valleys and locations with snowdrifts. Zones with extremely great or small snow depths tend to appear in the alpine zone.

When we compare the frequency distribution of overground-openness in the alpine zone (Figure 3) to that of snow depths in the alpine zone (the second figures from the bottom in Figure 7), the shapes of the distributions were similar; the area with great snow depth corresponds to valley, and the area with small snow depth corresponds to ridge.

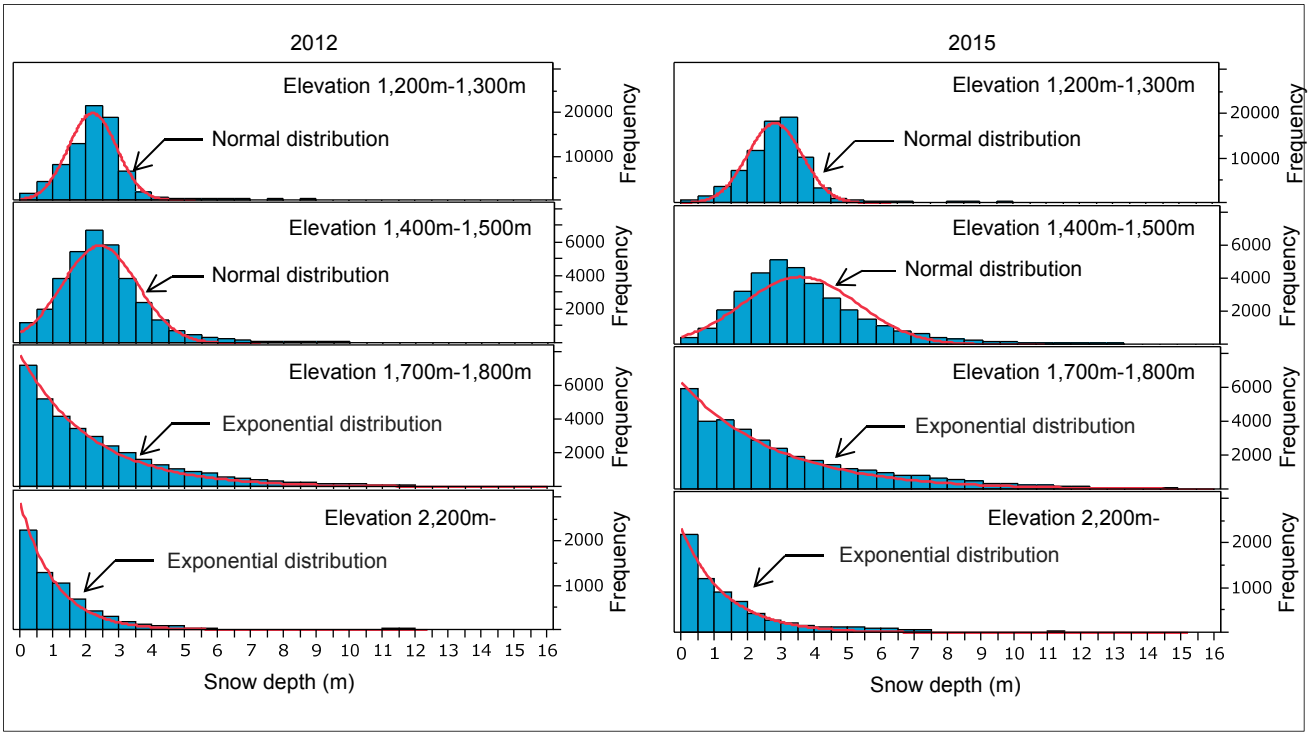

Figure 7. Frequency distribution of snow depths.

3.3 Relationship between overground-openness and snow depth in the alpine zone

Nishihara et al. (2013) reported that the snow depth in the alpine zone has a linear relationship with overground-openness. Here, this linear relationship was verified using two snow depth distributions calculated from airborne laser scanning data.

The relationship between overground-openness and snow depth is shown in Figure 8. The snow depths for the elevations of 1,450m (the forest line) and higher were extracted. The data were grouped into 5° overground-openness ranges, and the snow depth was the average value for each range. The figure showed that, for both 2012 and 2015, the snow depth decreases linearly with increase in overground-openness. The correlation between the two is high. The reason for the great snow depth in 2015 and the great slope of the

 ©2017, IAHR. Used with permission / ISSN 1562-6865 (Online) - ISSN 1063-7710 (Print)

linear equation is that more snow accumulated in 2015 than in 2012. That the snow depth in a valley is great and the snow depth at a ridge is small is a characteristic of the snow depth distribution after winds have moved the snow cover (Ohara, 2014). The snow depth distribution in the alpine zone measured by airborne laser scanning is thought to be the distribution of snow depths after the snow cover had been blown by wind and re-accumulated.

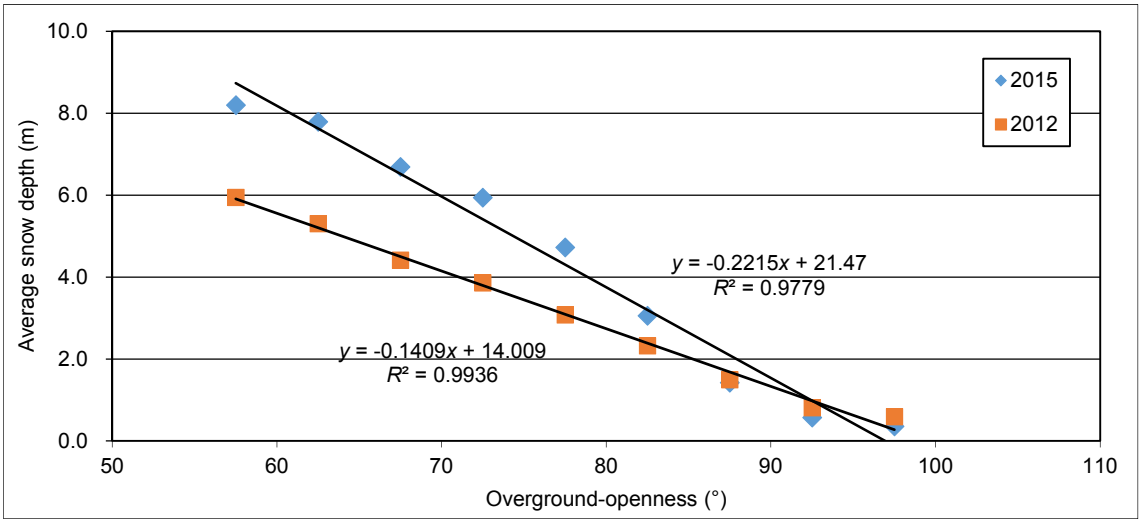

Figure 8. Relationship between snow depth and overground-openness in the alpine zone.

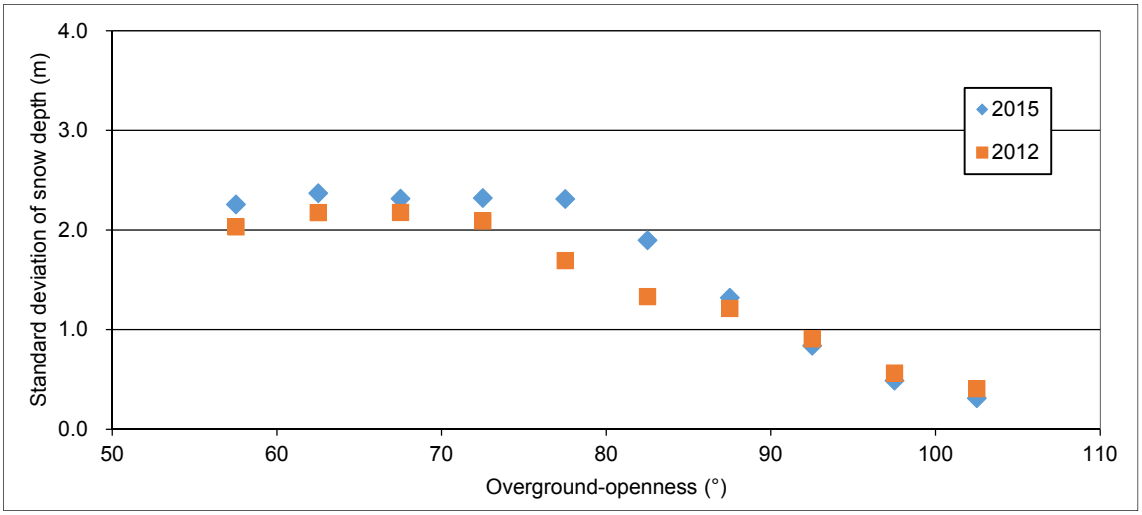

Figure 9. Relationship between standard deviation of snow depth and overground-openness in the alpine zone.

As overground-openness was determined at 5° intervals, the standard deviation of the snow depth in one section can be determined. Figure 9 shows the relationship between overground-openness and the standard deviation of snow depth. The standard deviation for 2012 and that for 2015 roughly agreed, even though they slightly differ around the overground-openness of 80°. The standard deviation showed a roughly constant value of about 2.0m up to about an overground-openness of 80°. Once the overground-openness exceeds 80°, the standard deviation decreases at a constant rate.

To track the transition in standard deviation in detail, the frequency distribution of snow depths in three sections with 5° overground openness are shown in Figure 10. Three graphs showed overground-openness for the section from 65° to 70°, that for the section from 80° to 85° and that for the section from 90° to 95°, which are typical values for a valley, a transition area from valley to ridge, and a ridge, respectively. The graph for overground-openness from 65° to 70° showed that the frequency distribution of snow depth for a valley had roughly a normal distribution and that the snow depths distribute over a wide range. There were locations with about 0m snow depth and locations with snow depths that exceeded 10m. The graph for overground-openness from 90° to 95° showed that the frequency distribution of the snow depth at a ridge has a roughly exponential distribution and that the frequencies for snow depths of 1m and smaller are very high. The variation in the standard deviation is thought to correspond to the variation in the snow depth distribution, which varies with the shifts in topography from valley to ridge. In the graph for overground-openness from 80° to 85°, the frequency

©2017, IAHR. Used with permission / ISSN 1562-6865 (Online) - ISSN 1063-7710 (Print)

distribution of snow depths slightly deviates from the normal distribution. This deviation shows that the snow depth distribution shifts from that in valley to that in ridge.

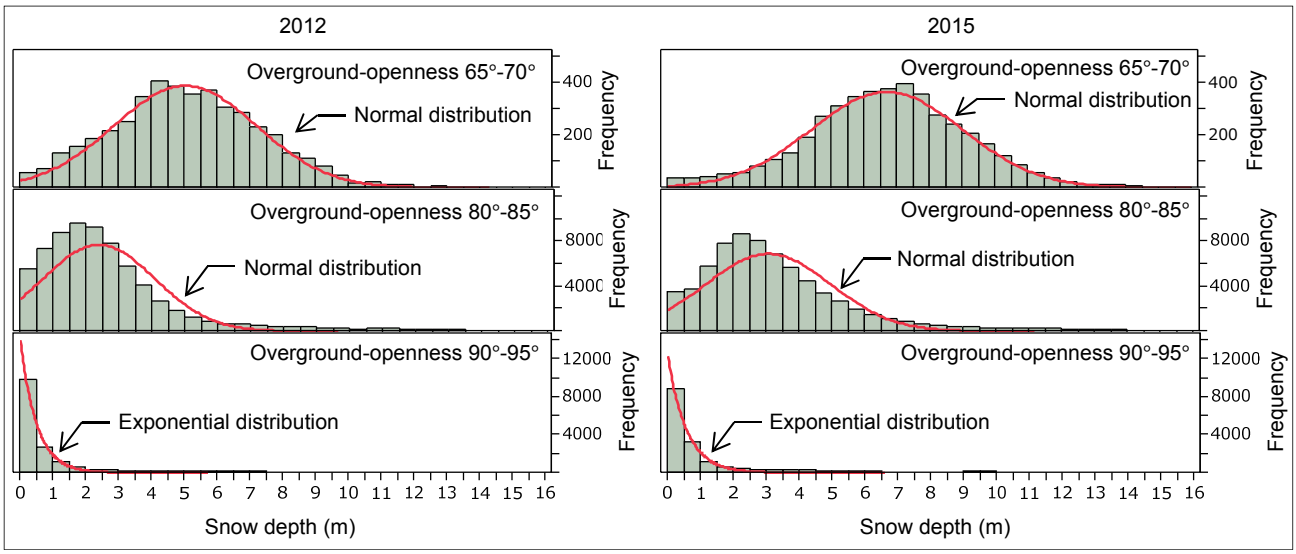

Figure 10. Frequency distribution of snow depths in the alpine zone.

Lastly, the data shown in Figure 8 were divided into 100m elevation ranges, and the relationship between the snow depth and the overground-openness by altitude range is shown in Figure 11. The figures showed only the cases with sample numbers exceeding 100, because when the number of samples was small, the resulting values are likely to be extremely large or small. From the figures, the snow depths in a valley at elevations exceeding 2,000m were somewhat small; however, linear relationships were seen between snow depth and overground-openness for each elevation range. Regression analysis was done for the data shown in the figures. The obtained equations resembled that obtained for the data of 2012 and 2015, respectively in (Figure 8). Therefore, it was found that the snow depths in the alpine zone were not dependent on elevation; only the overground-openness should be considered when estimating snow depth at locations outside forests.

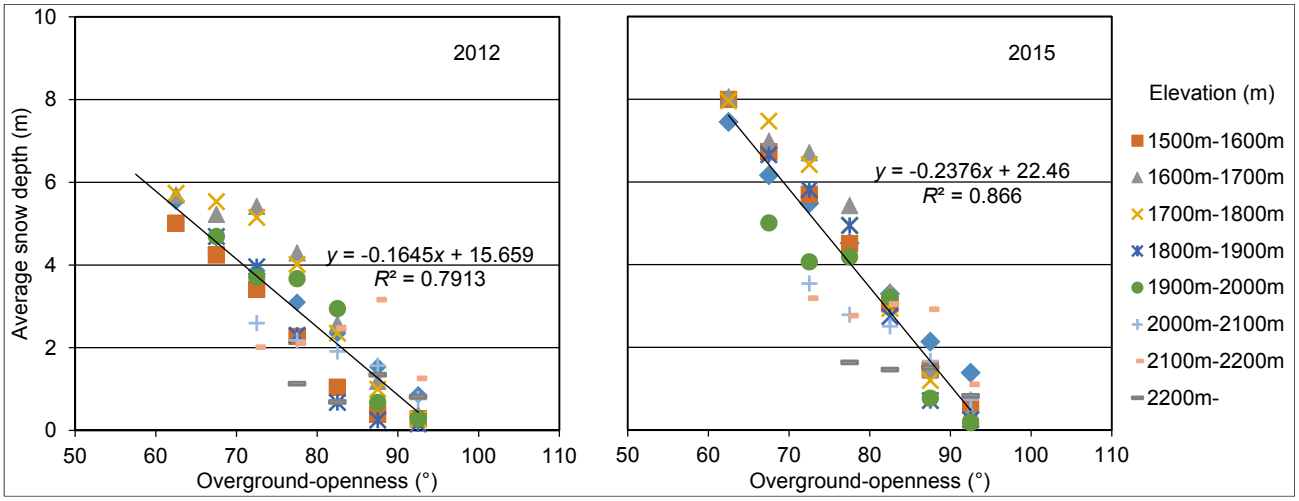

Figure 11. Relationship between snow depth and overground-openness in 100m elevation ranges in the alpine zone.

3.4 Relationship between aspect and snow depth

The distribution of snow depth frequency is strongly affected by wind at elevations above the forest line. To analyze how wind affects snow depth, we divided the forest area and the alpine zone of the survey area into 16 zones each, and we calculated the average snow depth for each zone.

As shown in Figure 12, the snow depth was nearly evenly distributed in the forest area in 2012 and 2015. In contrast, the distribution of snow depth in the alpine zone showed greater snow depths in the ranges between northeast and southeast than in the ranges between northwest and southwest. Strong winds that can transport snow on the ground surface tend to be westerly when winter storms occur on the Japan Sea side of Hokkaido. We can assume that these westerly winds blow snow on the ground and caused uneven distributions of snow

 ©2017, IAHR. Used with permission / ISSN 1562-6865 (Online) - ISSN 1063-7710 (Print)

accumulation, even though measurements of wind direction and speed have not been available in areas where snow depth was determined by airborne laser scanning.

Figure 13 diagrams the phenomena. The wind hits the western side of the ridge (the windward slope) and tracts surface snow, and that snow accumulates on the east slope (the leeward slope), where the ridge blocks the wind. As shown by the broken line in Figure 13, the snow depth on the windward slope differs from that on the leeward slope, even though these slopes have the same overground-openness. However, we did not get enough data to analyze the relationship between snow depth and topography on the leeward slope because the survey area where we conducted airborne laser scanning focused mainly on windward slopes. In the future, we will be measuring the snow depth using airborne laser scanning in an area that has mainly leeward slopes and analyzing the relationship between snow depth and topography there.

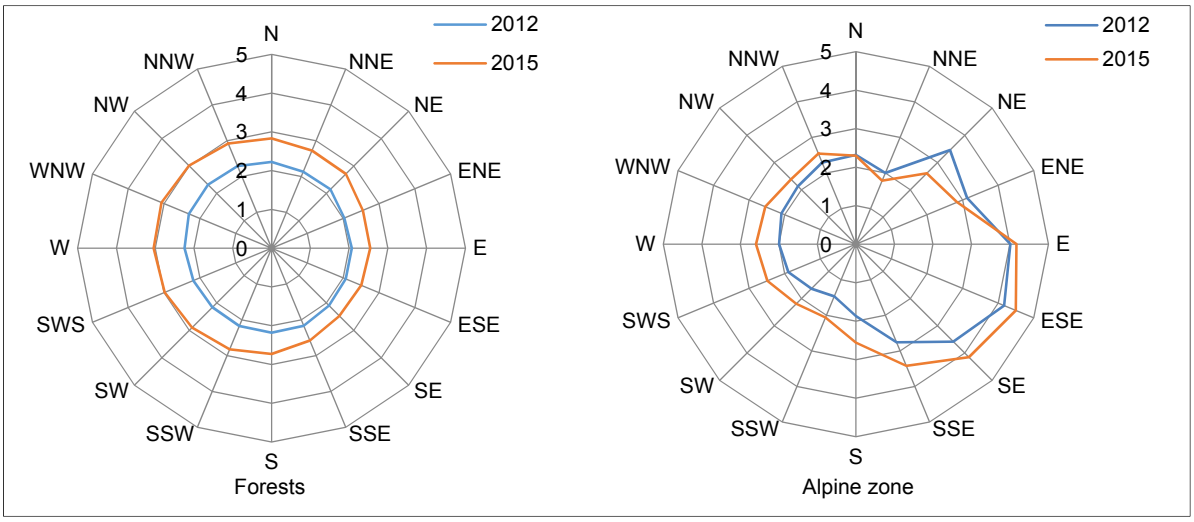

Figure 12. Average snow depth in 16 zones.

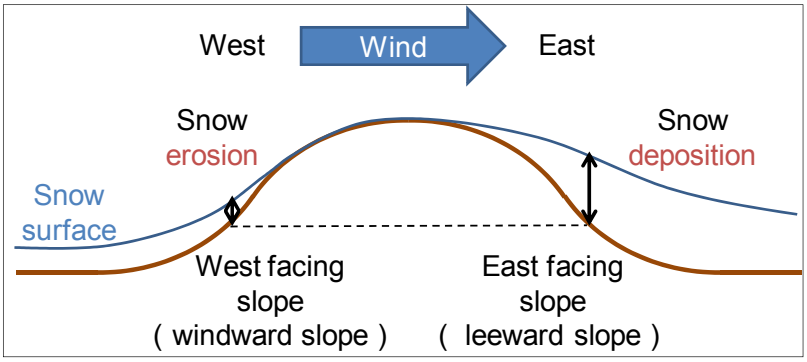

Figure 13. Image of snow erosion and deposition by the wind.

4 CONCLUSIONS

In this study, the relationship between snow depth and topography was analyzed using the measurement results from two airborne laser scanning surveys on snow depth. The following results were obtained.

The data from the two airborne laser scanning surveys verified that there is a linear relationship between snow depth and elevation in forest.

The data from the two airborne laser scanning surveys verified that there is a linear relationship between snow depth and overground-openness in the alpine zone and that the snow depth in the alpine zone does not depend on elevation.

The authors examined the snow depth distribution with respect to the elevation and clarified that the snow depth distribution shifts from a normal distribution to an exponential distribution as the main vegetation shifts from forest to non-forest. Furthermore, it is clarified in the examination using overground-openness that the distribution of the snow depth in the alpine zone shifts from a normal distribution to an exponential distribution as the topography shifts from valley to ridge. These distribution characteristics are found regardless of the survey year.

We divided forest and the alpine zone of the survey area into 16 zones each and calculated the average snow depth for each zone. The snow depth was nearly evenly distributed for the 16 zones in forest. In contrast, the distribution of snow depth in the alpine zone showed greater snow depths at leeward slopes than at windward slopes. This uneven distribution may have resulted from the strong winds of winter storms.

©2017, IAHR. Used with permission / ISSN 1562-6865 (Online) - ISSN 1063-7710 (Print)

ACKNOWLEDGEMENTS

We are grateful to WAKASA RESORT Co., Ltd., Asahidake ropeway and Hokkaido regional development bureau, MLIT for supporting our research.

REFERENCES

Nishihara, T., Nakatsugawa, M. & Hamamoto, S. (2012). The Estimate of Snow Depth Distribution in a Bam Basin Using Airborne Laser Scanning. *Advances in River Engineering*, 19, 465-470, (in Japanese with English abstract).

Nishihara, T. & Nakatsugawa, M. (2013). Estimation of Snow Water Equivalent Distribution Outside Forests Using Airborne Laser Scanning. *Journal of Japan Society of Civil Engineers, Ser. B1 (Hydraulic Engineering)*, 69(4), 409-414.

Ohara, N. (2014). A Practical Formulation of Snow Surface Diffusion by Wind for Watershed-Scale Applications. *Water Resour. Res.*, 50(6), 5074-5089.

Shimamura, Y., Izumi, T. & Matsuyama. H. (2005). Estimation of Snow Water Resources in Mountains Based on Snow Surveys and Remote Sensing Analyses - A Case Study Around the Joetsu Border of Niigata Prefecture in Japan. *J. Japan Soc. Hydrol. and Water Resour.,* 18(4), 411-423, (in Japanese with English abstract).

Yamada, T., Nishimura, H., Suizu, S. & Wakahama, G. (1979). Distribution and Process of Accumulation and Ablation of Snow on the West Slope of Mt. Asahidake, Hokkaido. *Low Temperature Science, Ser. A*, 37, 1-12, (in Japanese with English abstract).

Yamada, T. (1983). Studies on Accumulation-Ablation Processes and Distribution of Snow in Mountain Regions, Hokkaido. *Contributions from the Institute of Low Temperature Science*, A31, 1-33.

Yokoyama, R., Shirasawa, M. & Kikuchi, Y. (1999). Representation of Topographical Features by Opennesses. *Journal of the Japan Society of Photogrammetry and Remote Sensing*, 38(4), 26-34, (in Japanese with English abstract)

 ©2017, IAHR. Used with permission / ISSN 1562-6865 (Online) - ISSN 1063-7710 (Print)

CHALLENGE IN FLOOD FORECASTING USING RATING CURVE OF UNSTABLE RIVER SYSTEMS: THE BRAHMAPUTRA

MD ATIKUL ISLAM[1], JAMES E BALL[2], ASIF M. ZAMAN[3] & S M MAHBUBUR RAHMAN[4]

[1]PhD Student, School of Civil and Environmental Engineering, University of Technology Sydney, Broadway, NSW, Australia; mdatikul.islam@student.uts.edu.au
[2]Associate Professor, School of Civil and Environmental Engineering, University of Technology Sydney, Broadway, NSW, Australia; james.ball@uts.edu.au
[3]Water Resources and DSS Specialist, Water Resources Planning Division, Institute of Water Modelling, Dhaka, Bangladesh; amz@iwmbd.org
[4]Director, Water Resources Planning Division, Institute of Water Modelling, Dhaka, Bangladesh; smr@iwmbd.org

ABSTRACT

A reliable and comprehensive flood warning system is one of the key factors to minimize damage and disruption create by a flood. Ganges and Brahmaputra is the major river system of Bangladesh and authorities of Bangladesh use gauging data of this two rivers for their flood forecasting. This study only focuses on Brahmaputra River, which is still a morphologically very active river. This paper discusses how the prediction can be biased using conventional method for flood prediction, i.e. using only stage-discharge relationship. In this study, we used 1,687 observations (discharge, water level, river width and cross-sectional area) at Bahadurabad station of Brahmaputra River selected from 1976 to 2009. We examined the stationarity of river cross-section and water level-discharge relationship. The study shows that the relationship between water level and river flow changes every year significantly and without any indication which way it may change in the next year. The relationship of stage discharge is so wide that the river may experience approximately double of the calculated flow. Therefore, river water management and flood forecasting would require comprehensive method rather than relying only on stage discharge correlation. Moreover, there is also trend in river geometry which may create more uncertainty in flood forecasting.

Keywords: stage-discharge; unstable river geometry; discharge estimation; flood forecasting.

1 INTRODUCTION

Hydrological investigation and water resources management largely depend on the instantaneous discharge (Fenton & Keller, 2001). The accuracy of water level estimation by modelling, which is the major part of flood risk management, depends on the confidence level of discharge estimation/measurement (Dottori et al., 2009). Discharge is usually estimated from the stage-discharge relationship as direct measurements are typically expensive, time-consuming and sometimes not feasible e.g. during a high flood (Guven et al., 2012; Jalbert et.al, 2011). However, this method cannot guarantee the accuracy of discharge estimation especially for unsteady flow situation (Dottori et al., 2009). Schmidt (2002) states that uncertainty in river geometry is one of the key factors which influence the stage-discharge relationship and finally in real-time flood forecasting. Guerrero et al. (2012) mentioned only five studies work with the effect of unstable river geometry on the uncertainty of stage-discharge relation. However, in our knowledge, no one works with stationarity of river geometry and stage-discharge for a large river, especially braided river.

Bangladesh experiences devastating floods regularly in monsoon season by runoff generated by Ganges-Brahmaputra-Meghna. Authorities of Bangladesh use gauging data for flood forecasting collected at Hardinge Bridge on the Ganges and Bahadurabad on the Brahmaputra as well as some other stations in Bangladesh (Webster et al., 2010). Therefore, estimating discharge at Bahadurabad and Hardinge Bridge are of prime important for flood risk management of Bangladesh, and this study only focuses on Bahadurabad gauging station (Figure 1). The objective of this study is to find the stationarity analysis of river geometry and stage-discharge relationship and how it can influence on flood forecasting.

2 STUDY AREA AND LITERATURE REVIEW

The Brahmaputra River originates in Tibet on the north slope of the Himalayas (Coleman, 1969) and flows through the Tibetan Plateau, the Himalaya Mountains, the Assam Plains and the Delta in Bangladesh (Gupta, 2008). The total length of the river is about 2,840 km (Bristow, 1987) with 550,000 sq. km. of catchment area (Mondal and Chowdhury, 2013). The Brahmaputra River can be classified as a braided river with low hydraulic efficiency and heavy sediment load. It is one of the largest sand-bed braided river (Sarker et al., 2014) and the annual load is approximately 580 million tonnes which is the highest in term of sediment yield (Gupta, 2008). The Brahmaputra flows nearly 240 km in Bangladesh before joining the Ganges at

©2017, IAHR. Used with permission / ISSN 1562-6865 (Online) - ISSN 1063-7710 (Print)

Goalanda and distance from confluence to Bahadurabad station is about 130 km (Mondal and Chowdhury, 2013). The confluence point is about 241 km away from the sea “the Bay of Bengal” (Coleman, 1969). Therefore, the study location is free from tidal influences (Figure 1).

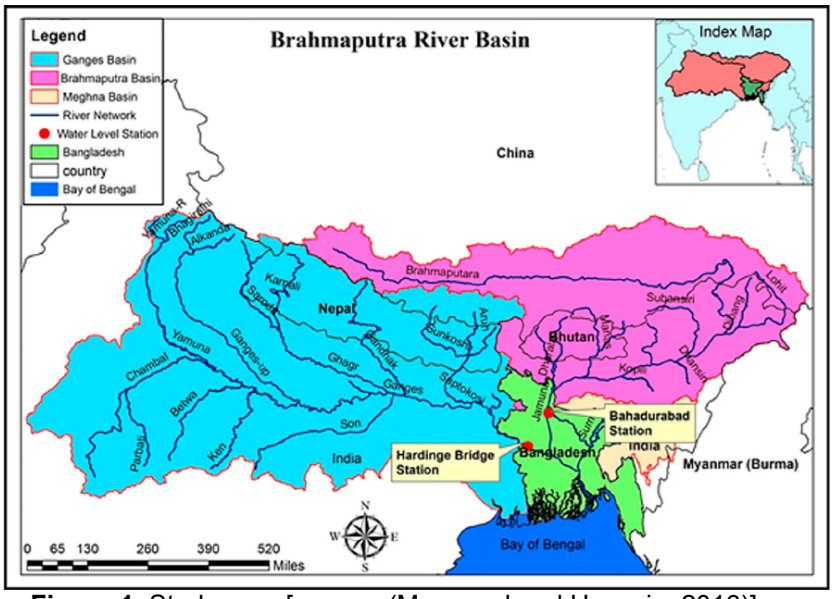

Figure 1. Study area [source: (Maswood and Hossain, 2016)].

Coleman (1969) studies bankline migration of Brahmaputra river using aerial photography and maps for the period 1944-1952 and 1952-1963. Bristow (1987) analyze channel movements and sediment characteristics of Brahmaputra River using literature review, field observations, maps and images. Again, Sarker et al. (2014) investigated the time-series of available satellite images for the period 1973 to 2010 to identify changes of Brahmaputra river width. In all studies, they agree that there is a defined movement of river banks in both ways significantly. However, as far as our understanding, most of the studies use maps/images and some study use measured cross-section for a couple of years. None of the studies uses time series of actual cross-sectional area or width to analyze Brahmaputra River geometry, especially at Bahadurabad gauging station.

3 DATA AVAILABILITY AND QUALITY CHECKING

Gauging data of the Bahadurabad station (Station ID: SW46.9L) of Brahmaputra river was collected from Bangladesh Water Development Board (BWDB). The database contains observed discharge (Q), water level (WL), river width (RW) and cross-sectional area (RA) for the period 1976 to 2009. For this study, we only selected the dates where all four types of data are available (Q, WL, RW and RA) and at least one observation per month in a year. However, due to significant gaps in data, we excluded all data before 1983 and after 2005. We only select 19 number of years from 1983 to 2005, which contains 1,687 no. of observations; lowest number of observation is 30 in 1988 and highest is 211 in 1994 (Figure 2).

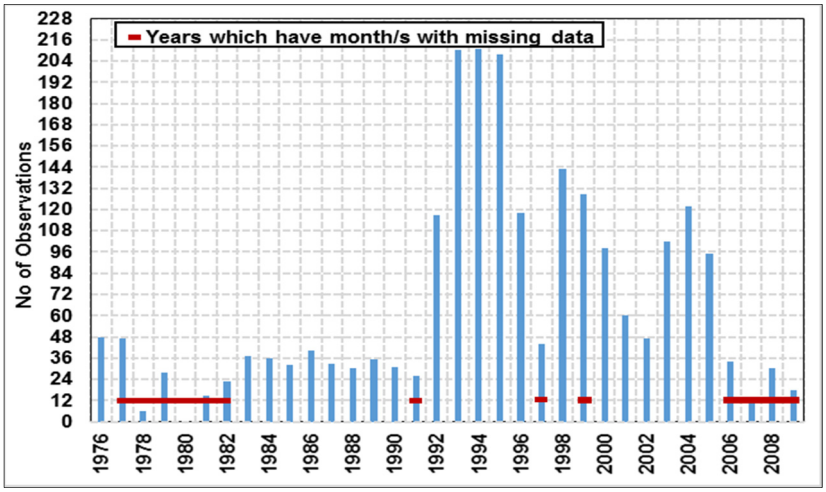

Figure 2. Data availability.

 ©2017, IAHR. Used with permission / ISSN 1562-6865 (Online) - ISSN 1063-7710 (Print)

For data quality checking, we compared each data with other corresponding data as well as previous observations and identified suspicious data and finally excluded from this study. The outliers found in the cross-sectional area and river width are presented in Figure 3. However, we have not seen any significant inconsistency in water level and discharge data.

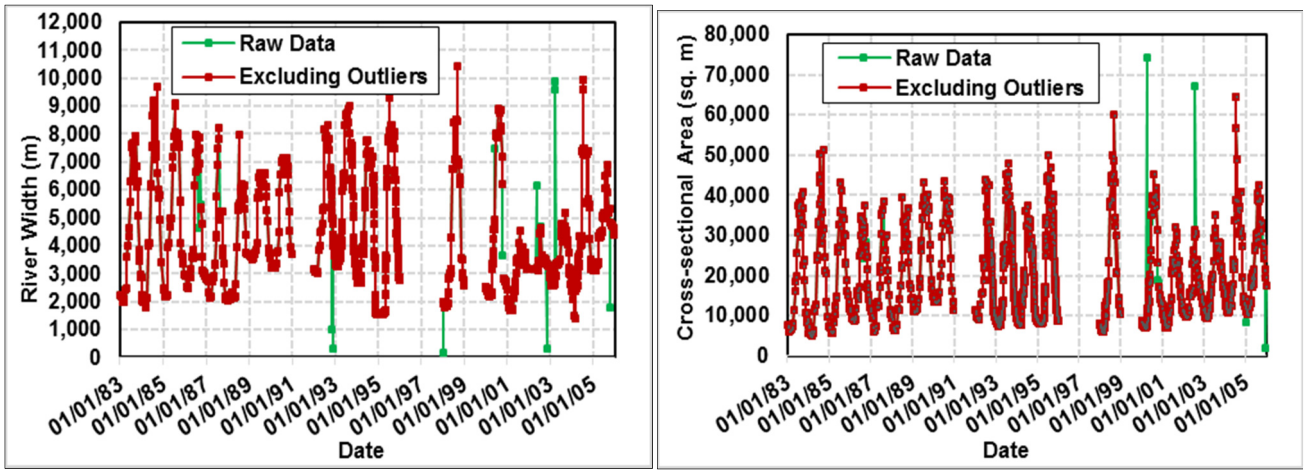

Figure 3. Data quality checking.

4 ANALYSIS OF STAGE-DISCHARGE RELATION AND RIVER GEOMETRY

The relationship between water level and discharge varies significantly during 1983 to 2004. The variation becomes larger with an increase in water level. Figure 4 shows, at 16m water level, recorded discharge varies between 10,000 to 22,000 m^3/s and at 18.5m water level, recorded discharge varies between 32000 to 50000 m^3/s. Again, at danger level (19.5 m), observed discharge fluctuates between 58,000 to 82,000 m^3/s. The figure also implies that there is no defined pattern of changes in the relationship i.e. every year the shape can change in any directions.

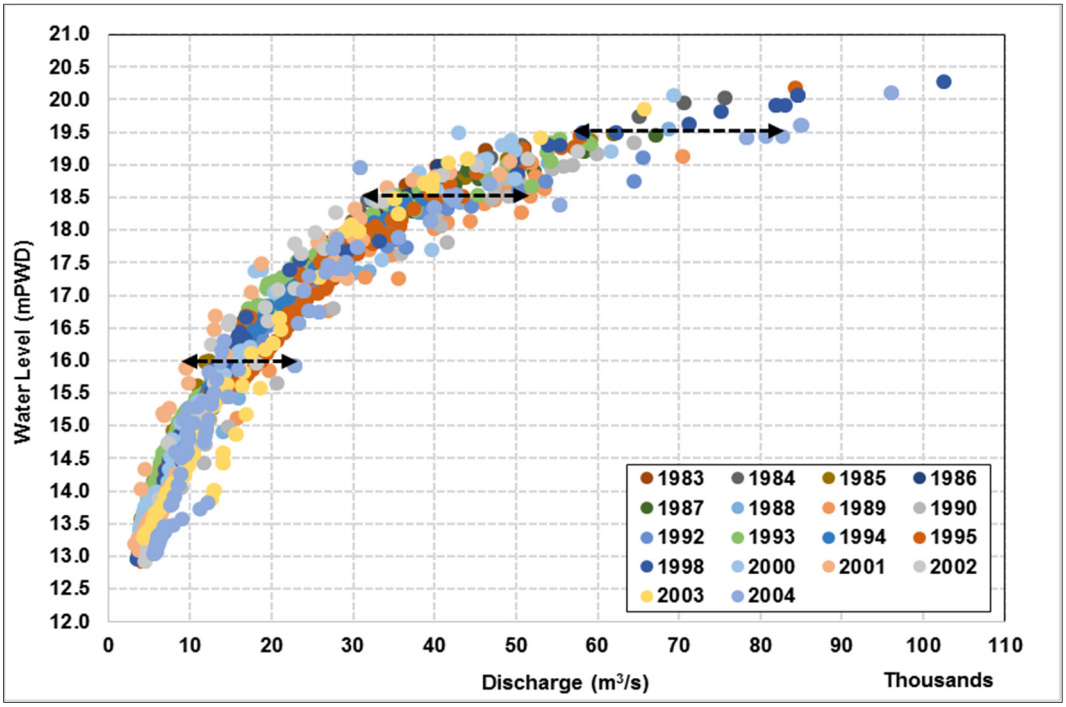

Figure 4. Stage-discharge relationship at Bahadurabad station of Brahmaputra River.

Again, to analyze river geometry, we calculated hydraulic mean depths (HMD) by dividing cross-sectional area with water surface width (Mayor-Mora, 1977; Meselhe & Sotiropoulos, 2000; Naqvi, 2003). The calculation showed that there is a tendency of increasing hydraulic mean depth over the study period. The rate of increasing is 0.0296m/ year.

For a rectangular channel, the hydraulic depth and flow depth are identical (Naqvi, 2003). Though the Brahmaputra River is a natural channel, this concept is incorporated in this study due to lack of actual cross-sectional profiles. We calculated bed level of Brahmaputra River at Bahadurabad station by subtracting

©2017, IAHR. Used with permission / ISSN 1562-6865 (Online) - ISSN 1063-7710 (Print)

hydraulic mean depth from water level elevation. The figure shows that there is a tendency of decreasing in estimated bed level at a rate 0.073 m/year.

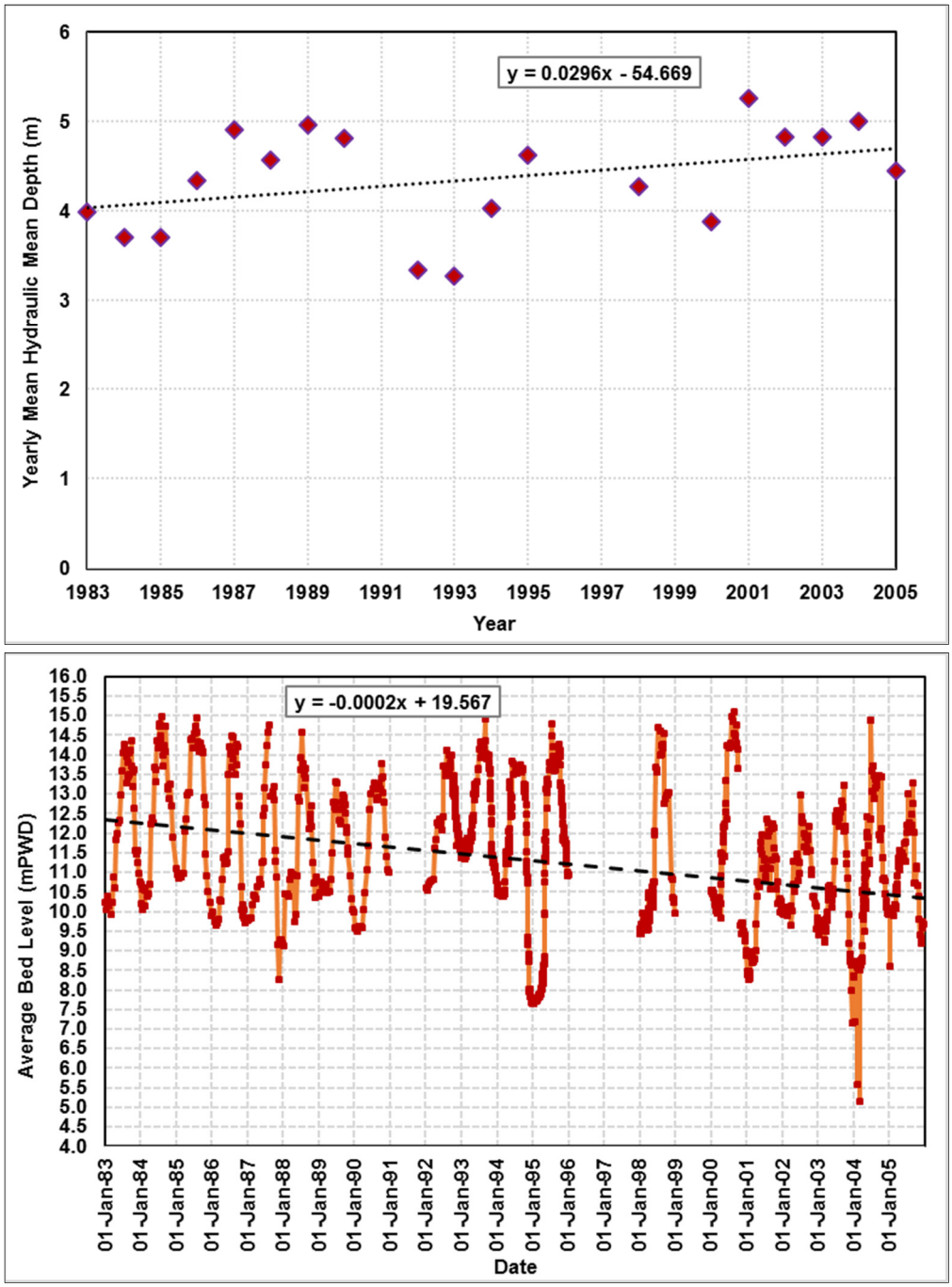

Figure 5. Trend of Brahmaputra River geometry at Bahadurabad station.

5 DISCUSSION

Advance flood forecasting system and a reliable and comprehensive flood warning is one of the key strategies to minimize damage and disruption created by flood. However, from the analysis, we can say that using a simple stage-discharge relationship of Bahadurabad gauging station of Brahmaputra River may lead to significant misleading information. Figure 4 shows that with the equal amount of water level, the difference in discharges can be as high as nearly 100%. Moreover, there is a trend of hydraulic mean depth, which implies that there is a possibility of a non-stationary relation between water level and discharge of Brahmaputra River at Bahadurabad gauging station.

In addition, to understand the likely consequences of using the relationship of stage-discharge developed in last year, we analyzed how much average monthly water level changed over the study period between any consecutive two years. To do so, we drew a reference line (Figure 6) and calculated the difference from reference line for each observation which are presented in Table 1. The results show that there is a significant

 ©2017, IAHR. Used with permission / ISSN 1562-6865 (Online) - ISSN 1063-7710 (Print)

difference in average monthly water level from immediately preceding year over the study period, sometimes as high as 98%. The differences in average monthly water level during monsoon seasons, (June-September) when Bangladesh usually experiences catastrophic flood (Ali et al., 1989), are between 0 to 81% with an average of 22%.

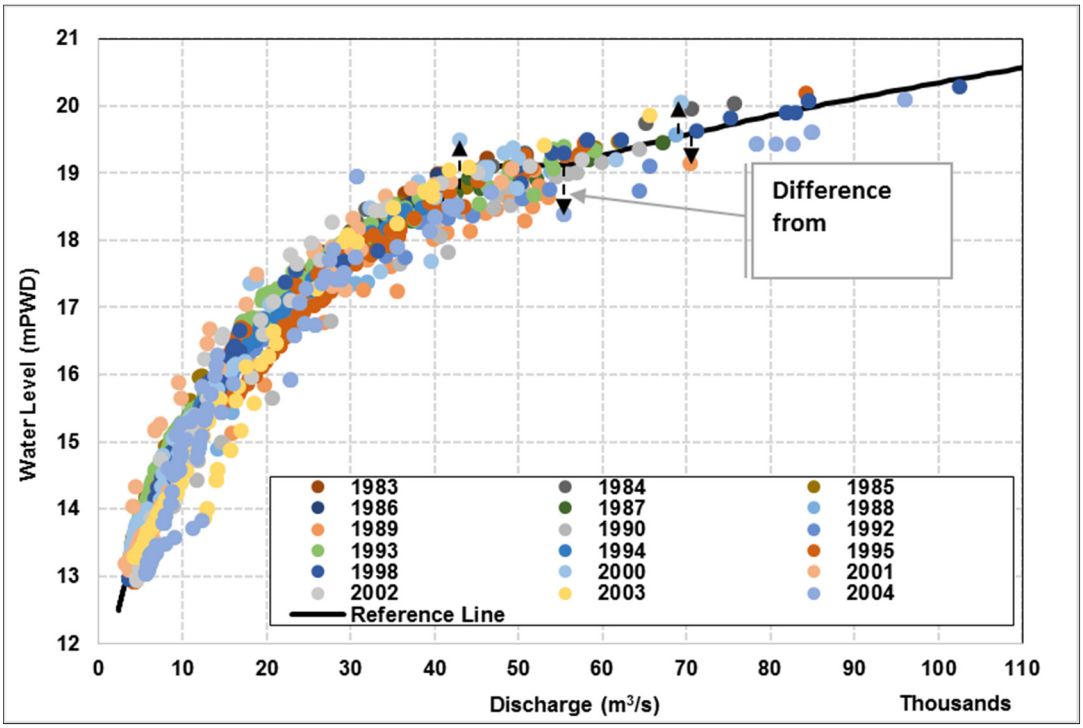

Figure 6. Reference line to estimate change in water level from previous year.

Table 1. Average monthly change in water level from previous year.

Year	Jan	Feb	Mar	April	May	June	July	Aug	Sept	Oct	Nov	Dec
1983	26%	18%	10%	-8%	22%	23%	-2%	-18%	10%	7%	65%	68%
1984	4%	13%	1%	-2%	-2%	-23%	-10%	7%	11%	24%	24%	31%
1985	33%	34%	22%	33%	44%	33%	-13%	-19%	-31%	-25%	-29%	-56%
1986	-26%	-22%	-10%	-51%	-51%	-20%	-1%	2%	21%	22%	11%	24%
1987	-8%	0%	1%	14%	1%	-8%	-28%	-23%	-24%	-22%	-20%	-16%
1988	26%	3%	20%	5%	-3%	-7%	22%	-10%	-49%	-46%	-68%	12%
1989	-31%	-10%	-34%	-60%	-25%	-56%	-41%	-57%	9%	-27%	-11%	-25%
1990	3%	2%	-15%	-13%	1%	-3%	19%	35%	14%	20%	-13%	-49%
1992	2%	22%	30%	68%	16%	31%	-34%	5%	3%	40%	81%	66%
1993	21%	2%	20%	24%	37%	26%	46%	39%	33%	32%	38%	15%
1994	-16%	-34%	-37%	-32%	-29%	0%	15%	8%	9%	-22%	-25%	-28%
1995	-36%	-29%	-23%	-11%	7%	17%	-1%	-17%	-13%	-25%	-20%	47%
2000	43%	38%	35%	5%	7%	-52%	-10%	16%	48%	35%	27%	4%
2001	-33%	-16%	-21%	61%	74%	76%	11%	-2%	-11%	13%	-17%	-29%
2002	-40%	-50%	-47%	-71%	-65%	32%	22%	6%	-2%	-58%	-29%	-5%
2003	24%	25%	29%	-37%	-61%	-81%	6%	-1%	2%	-3%	-41%	-98%
2004	-96%	-58%	-43%	50%	15%	-12%	-74%	-59%	-42%	7%	45%	85%

6 CONCLUSIONS

Webster et al. (2010) stated nicely that full flood control is impossible in Bangladesh as floods are so severe. It takes on 2-3 days to reach the river flow in the sea through Bangladesh, which is a very short period regarding preparation for the flood. Such limitations on flood forecast lead times are costly. Economic analyses showed that a 7-day flood forecast has the potential of reducing post-flood household and agricultural costs in Bangladesh by as much as 20% compared to 3% for a 2-day forecast. Thus, there are clear and tangible benefits for increasing the forecast horizon of river discharge. This study found that the relationship between water level and river flow changes every year and without indication which way may change in next year. The relationship of stage and discharge is so widely spread that river may experience as high as twice of the calculated flow. Therefore, river water management and flood forecasting would require comprehensive method rather than relying only on stage-discharge correlation. Moreover, there is also a trend in river geometry which may create more uncertainty in flood forecasting. We also recommend to carry more research to understand the behavior of river geometry and its relation with water level and discharge.

©2017, IAHR. Used with permission / ISSN 1562-6865 (Online) - ISSN 1063-7710 (Print)

ACKNOWLEDGEMENTS

We are grateful to Bangladesh Water Development Board (BWDB) for access to data and to the University of Technology Sydney for administrative and logistic support.

REFERENCES

Ali, A., Quadir, D. A. & Huh, O. K. (1989). Study of River Flood Hydrology in Bangladesh with AVHRR Data. *International Journal of Remote Sensing,* 10(12), 1873-1891.

Bristow, C. S. (1987). Brahmaputra River: channel migration and deposition. *Recent Developments in Fluvial Sedimentology*, 39, 63-74

Coleman, J. M. (1969). Brahmaputra River: Channel Processes and Sedimentationbrahmaputra River: Channel Processes and Sedimentation. *Sedimentary Geology,* 3(2), 129-239.

Dottori, F., Martina, M. & Todini, E. (2009). A Dynamic Rating Curve Approach to Indirect Discharge Measurement. *Hydrology and Earth System Sciences,* 13(6), 847-863.

Fenton, J. D. & Keller, R. J. (2001). *The Calculation of Streamflow From Measurements of Stage*, CRC for Catchment Hydrology, Report 01/6.

Guerrero, J.-L., Westerberg, I. K., Halldin, S., Xu, C.-Y. & Lundin, L.-C. (2012). Temporal Variability in Stage–Discharge Relationships. *Journal of Hydrology,* 446*,* 90-102.

Gupta, A. (2008). *Large Rivers: Geomorphology and Management*. John Wiley & Sons, Biik, 1-712.

Guven, A., Aytek, A. & Azamathulla, H. M. (2012). A Practical Approach to Formulate Stage–Discharge Relationship in Natural Rivers. *Neural Computing and Applications,* 23(3), 873-880.

Jalbert, J., Mathevet, T. & Favre, A.-C. (2011). Temporal Uncertainty Estimation of Discharges from Rating Curves using a Variographic Analysis. *Journal of Hydrology,* 397(1–2), 83-92.

Maswood, M. & Hossain, F. (2016). Advancing River Modelling in Ungauged Basins using Satellite Remote Sensing: The Case of The Ganges–Brahmaputra–Meghna Basin. *International Journal of River Basin Management,* 14(1), 103-117.

Mayor-Mora, R. E. (1977). *Laboratory Investigation of Tidal Inlets on Sandy Coasts*. California Univ Berkeley Hydraulic Engineering Lab.

Meselhe, E. & Sotiropoulos, F. (2000). Three-Dimensional Numerical Model for Open-Ehannels with Free-Surfaee Variations. *Journal of Hydraulic Research,* 38(2), 115-121.

Mondal, M. S. & Chowdhury, J. U. (2013). Generation of 10-Day Flow of the Brahmaputra River using a Time Series Model. *Hydrology Research,* 44(6), 1071-1083.

Naqvi, M. M. (2003). *Design of Linear Drainage Systems*, Thomas Telford, Book, 1-246.

Sarker, M. H. Thorne, C. R., Aktar, M. N. & Ferdous, M. R. (2014). Morpho-dynamics of the Brahmaputra–Jamuna River, Bangladesh. *Geomorphology,* 215, 45-59.

Schmidt, A. R. (2002). Analysis of Stage-Discharge Relations for Open-Channel Flows and Their Associated Uncertainties*, Ph.D Thesis.* University of Illinois at Urbana-Champaign.

Webster, P. J., Jian, J., Hopson, T. M., Hoyos, C. D., Agudelo, P. A., Chang, H.-R. & Subbiah, A. (2010). Extended-Range Probabilistic Forecasts of Ganges and Brahmaputra Floods in Bangladesh. *Bulletin of the American Meteorological Society,* 91(11), 1493.

 ©2017, IAHR. Used with permission / ISSN 1562-6865 (Online) - ISSN 1063-7710 (Print)

DEVELOPMENT AND EVALUATION OF DAM INFLOW DROUGHT INDEX BASED ON DAM OPERATION RULE

MINSUNG KWON[1] & KYUNG SOO JUN[2]

[1,2] Graduate School of Water Resources, Sunkyunkwan Univ., Suwon, Korea,
kwon.ms@skku.edu ;ksjun@skku.edu

ABSTRACT

This study develops a Dam Inflow Drought Index (DIDI) for Chungju Dam in Korea and evaluates the usability of the DIDI by comparing with Surface Water Supply Index (SWSI) and Standardized Precipitation Index (SPI). DIDI is calculated by the cumulative difference between the critical inflow and the observed inflow. The critical inflow means the essential inflow keeping the water supply criteria of the dam. Considering the limit of dam capacity, the upper limit of the cumulative difference, i.e., threshold, has to be determined, and the threshold is estimated by performing Receiver Operating Characteristics (ROC) analysis. The Optimal threshold is determined by a value that represents maximum ROC score. The maximum ROC score of the DIDI was 0.93, and the threshold at this point was 630 $\times 10^6$ m^3. The maximum ROC score of the DIDI was 0.21 higher than the score of SWSI and 0.33, 0.22, 0.16, and 0.17 greater than the score of SPI(3), SPI(6), SPI(9), and SPI(12), respectively. DIDI shows much better performance in monitoring dam droughts than SWSI and short-term and long-term SPI. The DIDI is useful for monitoring the dam inflow drought, and its application could help mitigate drought damages.

Keywords: Dam Inflow Drought Index (DIDI); drought; ROC analysis; threshold.

1 INTRODUCTION

The latest 2014-2015 drought in Korea caused water scarcity of multipurpose dams which supply the living and industries the water and led to difficulty with water management. This drought was so severe that it was recorded as an unprecedented event. Drought affects more people than other natural disasters and results in an enormous social, economic and environmental cost (Wilhite, 2006). Sheffield et al. (2012) expected that the frequency and severity of drought would increase due to global climate change. A regional drought is not limited to regional damages, but affecting food and economic matters over wide areas (Sternberg, 2011).

Wilhite and Glantz (1985) classified drought into meteorological drought, agricultural drought, hydrological drought, and socioeconomic drought. Therefore, drought indices are estimated using rainfall, evapotranspiration, runoff, soil moisture, and water supply ability in accordance with study objective. Numerous drought indices had been developed to express droughts which resulted in various social effects. Typical drought indices are Standardized Precipitation Index (SPI) (McKee et al., 1993), Palmer Drought Severity Index (PDSI) (Palmer, 1965), Surface Water Supply Index (SWSI) (Shafer and Dezman, 1982), Standardized Precipitation Evapotranspiration Index (SPEI) (Vicente-Serrano et al., 2010). However, most drought indices are calculated by the lack of amount over the normal phenomenon or the occurrence probability, which has a problem that does not reflect the water supply systems. Modern water use mainly depends on reservoir's water supply system. Therefore, to respond drought in a timely manner and mitigate drought damages, the drought index which considers the dam operation is needed instead of evaluating the shortage of the average or the probability of occurrence.

This study developes a Dam Inflow Drought Index (DIDI) which considers the criteria for reduction in water supply related to dam operation during a drought. DIDI needs threshold of the cumulative difference between the critical inflow and the observed inflow. In this study, optimal threshold is calculated by Receiver Operating Characteristics (ROC) analysis. ROC analysis is commonly used in verification of whether forecast (Mason, 1982), but it is also used in verification of drought indices compared with actual drought cases (Kim and Lee, 2011; Bae et al., 2013; You et al., 2013).

The DIDI could be used as the drought monitoring tool that can effectively detect drought of dam basin. Droughts, unlike floods, are characterized by slow progress. Appropriate drought index reflecting the characteristic of water supply system such as the DIDI would contribute to coping with drought and mitigating drought damages.

©2017, IAHR. Used with permission / ISSN 1562-6865 (Online) - ISSN 1063-7710 (Print)

2 METHOD

Multipurpose dams in Korea have the criteria for reduction in water supply during the drought. When using this criteria, we can calculate critical inflow for keeping the criteria by Eq. [1].

$$I_{C,i} = AC_i - AC_{i-1} + S_{P,i} \quad [1]$$

Where, I_C is the critical inflow, AC is the storage of the water supply adjustment criteria, S_P is the amount of the planned water supply, and i is the month.

The difference between the observed inflow and the critical inflow for each month can be calculated by Eq. [2], and cumulative the anomalies are calculated by Eq. [3]. And then the DIDI can be calculated by Eq. [4].

$$DI_i = I_{O,i} - I_{C,i} \quad [2]$$

$$CDI_i = CDI_{i-1} + DI_i \quad [3]$$

$$DIDI = \frac{CDI}{\sigma(CDI)} \quad [4]$$

Where, DI is the difference in inflows, I_O is the observed inflow, CDI is the cumulative difference in inflows, and $\sigma(\ )$ is standard deviation.

However, when calculating CDI in Eq. [3], the upper limit on CDI has to be considered because a considerable amount of inflows that cannot be stored at the reservoir are not associated with the future water use. In order to determine a threshold, this study calculated Eq. [3] and [4] repeatedly with varying the threshold and then conducted Receiver Operating Characteristics (ROC) analysis.

ROC analysis is commonly used in verification of whether forecast, but it is also used in verification of drought indices compared with actual drought cases. This study set ROC model as Table 1. ROC analysis is separated into observed value and prediction value. In this study, the observed value is defined as “Water supply” and the prediction value is defined as “DIDI” in Table 3. If an actual event occurs and an event predicted in the forecast result, it is expressed as “Hit (*H*).” Whereas, if an actual event occurs and an event did not predict in the forecast result, it is expressed as “Missing (*M*).” If an actual event does not occur and an event is predicted in the forecast result, it is expressed as “False (*F*).” On the other hands, if an actual event does not occur and an event is not predicted in the forecast result, it is expressed as “Negative hit (*N*).”

Table 1. ROC classification model.

		Water supply	
		Reduction	**Normal**
DIDI	Drought	Hit (*H*)	False (*F*)
	Normal	Missing (*M*)	Negative Hit (*N*)

The “Water supply” in Table 3 means that water supply is reduced or normal when dam operation is simulated using the water supply adjustment criteria and historical inflow data. “Drought” in Table 1 means that DIDI is less than zero and “Normal” of DIDI means that DIDI is equal or greater than zero. *H*, *F*, *M*, and *N* with various thresholds can be calculated using ROC classification model in Table 1. And then “Hit rate (*HR*)” and “False Alarm Rate (*FAR*)” can be estimated by Eq. [5] and [6].

$$HR = \frac{H}{(H+M)} \quad [5]$$

$$FAR = \frac{F}{(F+N)} \quad [6]$$

Finally, ROC score has to be calculated to evaluate results of ROC analysis quantitatively. ROC score, which indicates how well the drought index can reproduce actual water shortage, is calculated as the area shown in Figure 1.

The procedure for calculating the DIDI described above is shown in Figure 2, and the optimal DIDI is the DIDI to which the threshold value having the maximum ROC score applied.

 ©2017, IAHR. Used with permission / ISSN 1562-6865 (Online) - ISSN 1063-7710 (Print)

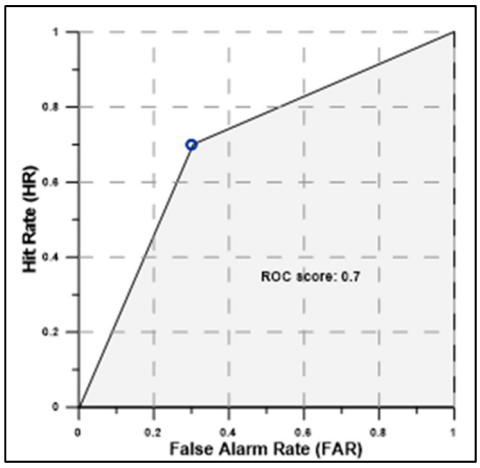

Figure 1. The description of ROC score.

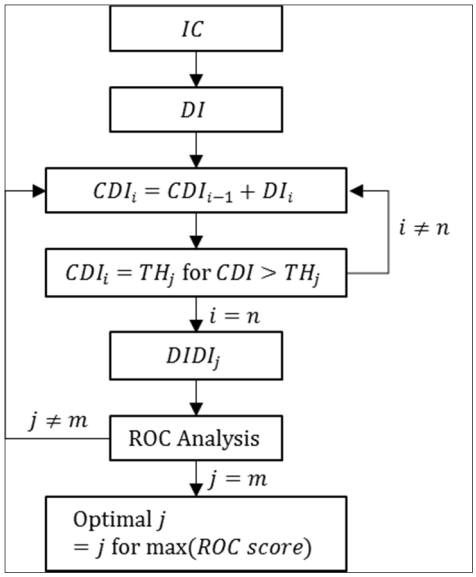

Figure 2. The description of ROC score.

3 RESULTS AND DISCUSSION

3.1 Application of DIDI

This study focused on Chungju Dam in Han River basin. The Chungju Dam, built in the Southern Han River basin which crosses the center of Korean, is the biggest concrete gravity dam in Korea. Table 2 shows detailed dimensions of Chungju Dam.

Table 2. Dimensions of Chungju Dam.

Height (m)	**97.5**	**Length (m)**	**530**
Volume (10^6 m^3)	902	Basin areas (km^2)	6,648
Annual mean inflow (10^6 m^3)	4,888	Annual water supply (10^6 m^3)	3,380
Storage capacity (10^6 m^3)	2,750	Storage for flood control (10^6 m^3)	616
Effective storage capacity (10^6 m^3)	1,789	Low water storage (10^6 m^3)	596

K-water developed Water Supply Adjustment Criteria (WSAC) to cope with a shortage of water resources in the dam. Drought response strategies of WSAC is divided into four stages, level1 to level4, according to the degree of water shortage. In this study, the starting point, at which the water supply reduced, is used for ROC analysis. Table 3 indicates volumes of WSAC's level1 for each month.

The critical inflow can be calculated by Eq. [1] using the volume in Table 3. Figure 3 shows critical inflows of Chungju Dam for each month.

©2017, IAHR. Used with permission / ISSN 1562-6865 (Online) - ISSN 1063-7710 (Print)

Table3. Volume of WSAC's level 1.

Month	Jan	Feb	Mar	Apr	May	Jun
Volume (10^6 m^3)	1,021.90	878.9	783.9	787.6	792.6	698.1
Month	Jul	Aug	Sep	Oct	Nov	Dec
Volume (10^6 m^3)	836.1	1,200.40	1,462.20	1,443.10	1,334.90	1,198.90

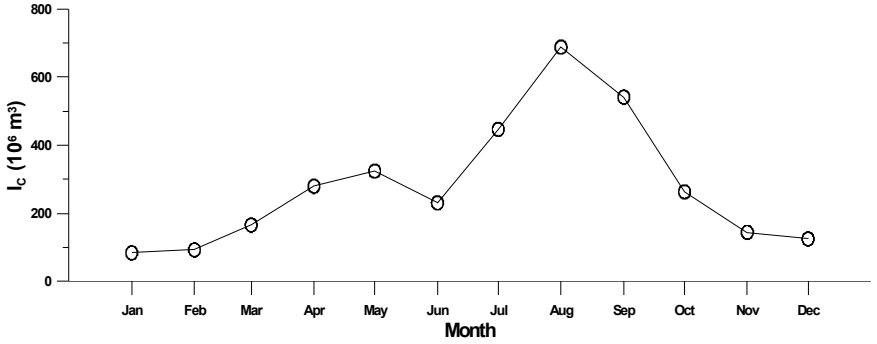

Figure 3. Critical inflows of Chungju Dam

Figure 4 shows observed monthly inflow of Chungju Dam, and the difference between the observed inflow and the critical inflow can be calculated by Eq. [2]. Figure 5 shows the difference during entire period. The CDI can be calculated by adding up the $DI$of Figure 5 in a cumulative manner. However, if the upper limit of the CDI is not set, DI continuously increases. Therefore, a threshold for CDI is needed to estimate optimal DIDI.

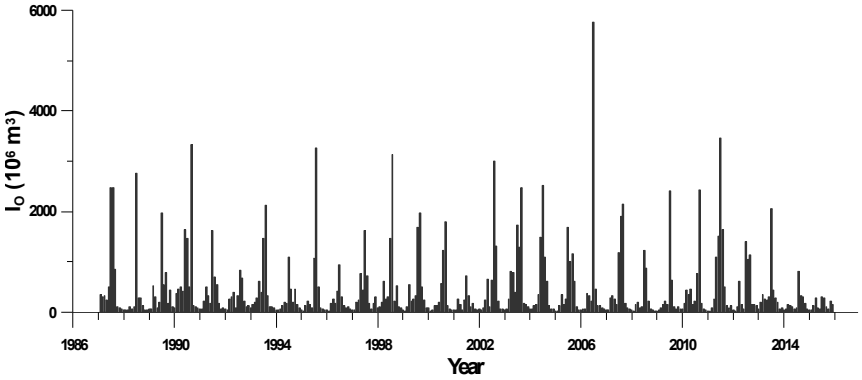

Figure 4. Observed monthly inflows of Chungju Dam

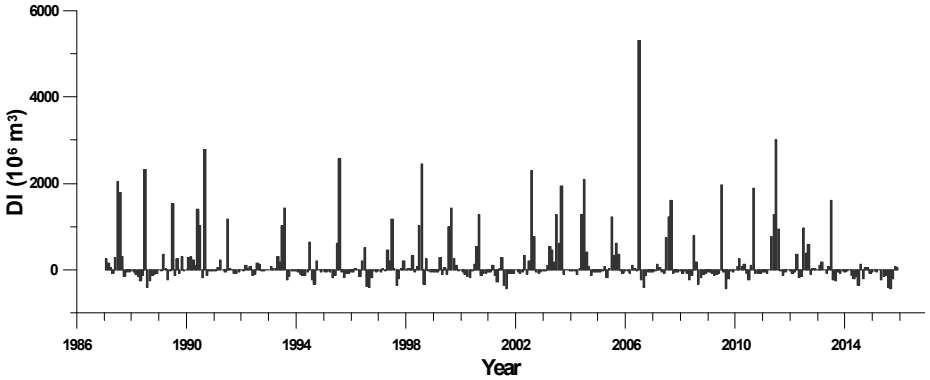

Figure 5. Difference between the observed inflow and critical inflow.

To determine the threshold of CDI, this study performed ROC analysis. Dam operation simulation was implemented from 1987 to 2015 using observed monthly inflow data and volumes of WSAC's level1. Figure 6 shows the point at which water supply reduced and the amount of reduction in water supply. This point becomes "Reduction" in Table 3 and ROC analysis performs using this point. Figure 7 shows results of ROC scores according to the change in threshold. A threshold value for maximum ROC score was determined as optimal threshold value, which was 630 × 10^6 m^3.

 ©2017, IAHR. Used with permission / ISSN 1562-6865 (Online) - ISSN 1063-7710 (Print)

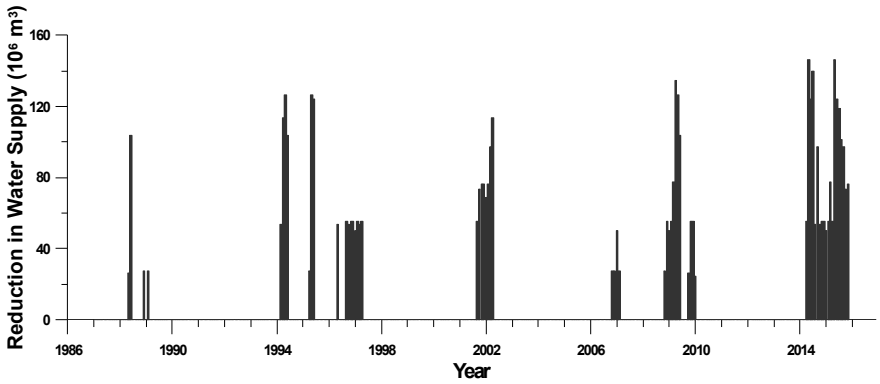

Figure 6. The point at which water supply reduced and the amount of reduction in water supply

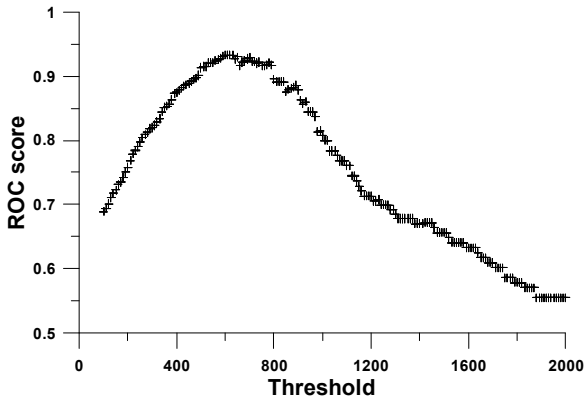

Figure 7. ROC scores according to the change in threshold.

Figure 8 shows the cumulative difference between the observed inflow and the critical inflow when adapting the optimal threshold. Figure 9 shows DIDI and the point at which water supply reduced. This Figure indicates that DIDI adequately expresses the water reduction timing of Chungju Dam.

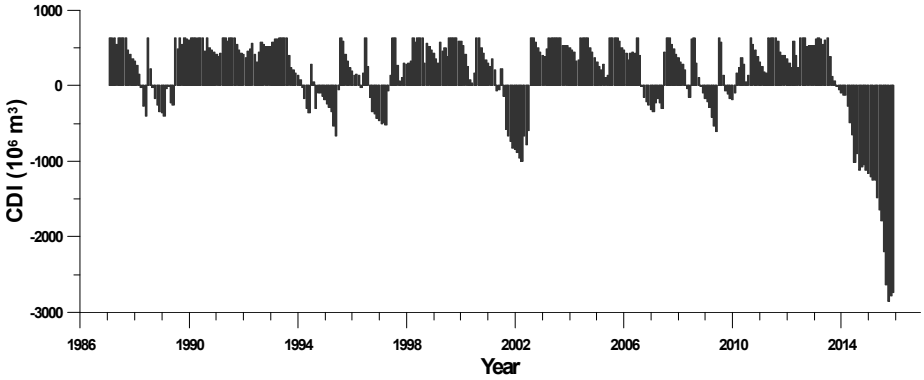

Figure 8. Cumulative difference between the observed inflow and the critical inflow with the threshold value 630×10^6 m^3.

©2017, IAHR. Used with permission / ISSN 1562-6865 (Online) - ISSN 1063-7710 (Print)

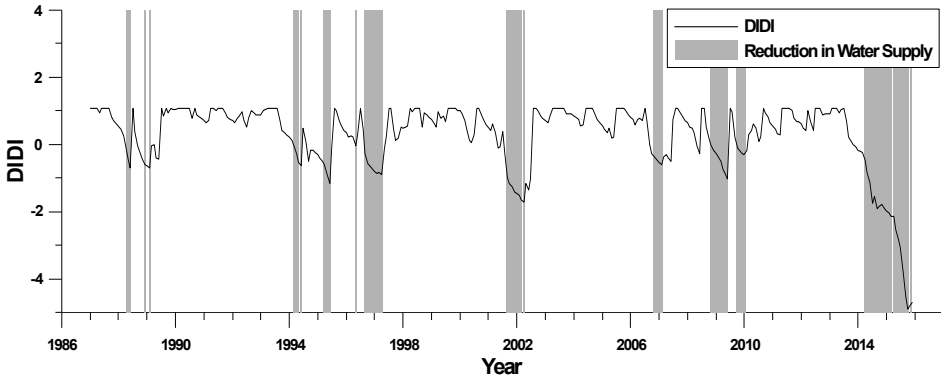

Figure 9. DIDI and reduction in water supply

3.2 Comparison with typical drought indices

This chapter compared DIDI with typical drought indices such as SWSI and SPI. SWSI and SPI are widely used drought indices. SWSI is calculated by monthly precipitation, snowpack, streamflow, and reservoir storage. SWSI is estimated by Eq. [7].

$$\mathrm{SWSI} = \frac{(\mathrm{a} \times \mathrm{PN_{sp}} + \mathrm{b} \times \mathrm{PN_{pcp}} + \mathrm{c} \times \mathrm{PN_{sf}} + \mathrm{d} \times \mathrm{PN_{rs}} - 50)}{12} \qquad [7]$$

Where a, b, c, and d are the weights for each component $(a + b + c + d = 1)$, PN is the non-exceedance probability (%), sp is snowpack, pcp is precipitation, sf is streamflow, and rs is reservoir storage.

In this study, snowpack data cannot collected, so the component was ignored. Figure 9 shows DIDI is compared with SWSI. SWSI defines -1 or less as drought. The SWSI indicates drought at the time of reduction in water supply adequately, but it can be seen that the drought which SWSI expresses is very common even in the normal water supply condition.

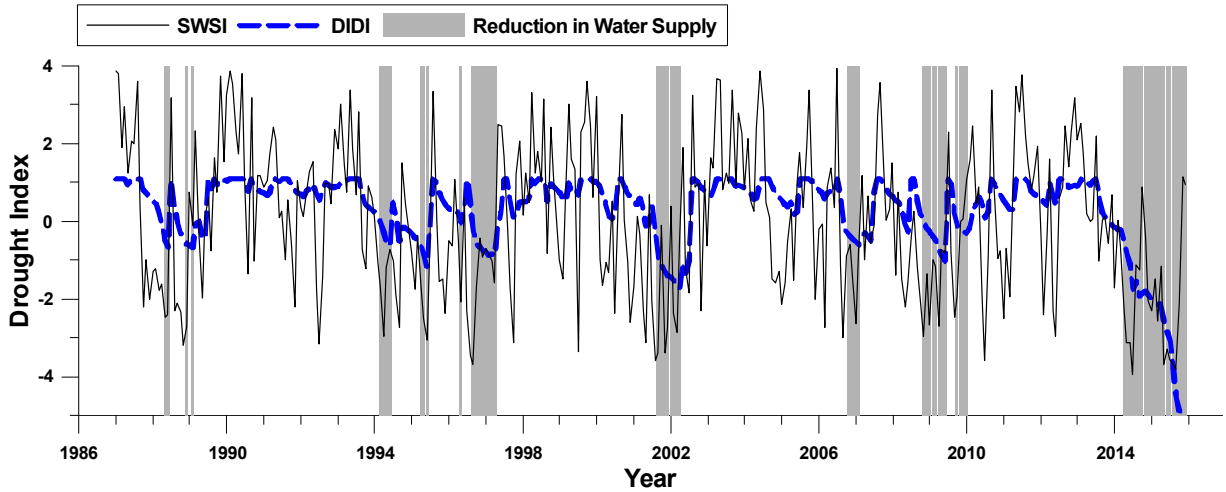

Figure 10. Comparison with DIDI and SWSI.

SPI is the most widely used drought index and it was agreed at 'The Inter-Regional Workshop on Indices and Early Warning Systems for Drought' held at the University of Nebraska-Lincoln to use SPI as universal drought index to cope with climate risks. SPI can simply calculate and easily collect data due to it uses rainfall only. SPI is calculated by standardizing value of cumulative distribution function (CDF) of Gamma distribution which is estimated using sums of rainfall for a preset period (3 months, 6 months, 12 months, etc.).

SPI is calculated by standardizing the gamma Cumulative Distribution Function (CDF). Eq. [8] is the gamma CDF. Eq. [9] is the CDF considering the time when any cumulative precipitation is zero, and the reason for using the equation is that the gamma function is not defined at zero.

$$\mathrm{G(x)} = \frac{1}{\beta^{\alpha}\Gamma(\alpha)} \int_0^{\mathrm{x}} \mathrm{x}^{\alpha-1} \mathrm{e}^{-\mathrm{x}/\beta} \mathrm{dx} \qquad [8]$$

$$\mathrm{H(x)} = (1 - \mathrm{q})\mathrm{G(x)} + \mathrm{q} \qquad [9]$$

©2017, IAHR. Used with permission / ISSN 1562-6865 (Online) - ISSN 1063-7710 (Print)

Where α is shape parameter, β is scale parameter,$q = m/n$, m is the number of times that cumulative rainfall is zero, and n is the entire number of year of used data.

SPI is calculated by standardizing $H(x)$ using the inverse standard normal CDF. Eq. [10] is Normal CDF, and when average is zero and standard deviation is one, Eq. [10] becomes standard normal CDF. Finally, SPI can be calculated by substituting $H(x)$ into Eq. [11].

$$\mathrm{F}(\mathrm{x}|\mu,\sigma) = \frac{1}{\sigma\sqrt{2\pi}}\int_{-\infty}^{\mathrm{x}} \mathrm{e}^{\frac{-(\mathrm{x}-\mu)^2}{2\sigma^2}}\mathrm{dx} \qquad [10]$$

$$\mathrm{SPI} = \mathrm{F}^{-1}(\mathrm{H}(\mathrm{x})|0,1) \qquad [11]$$

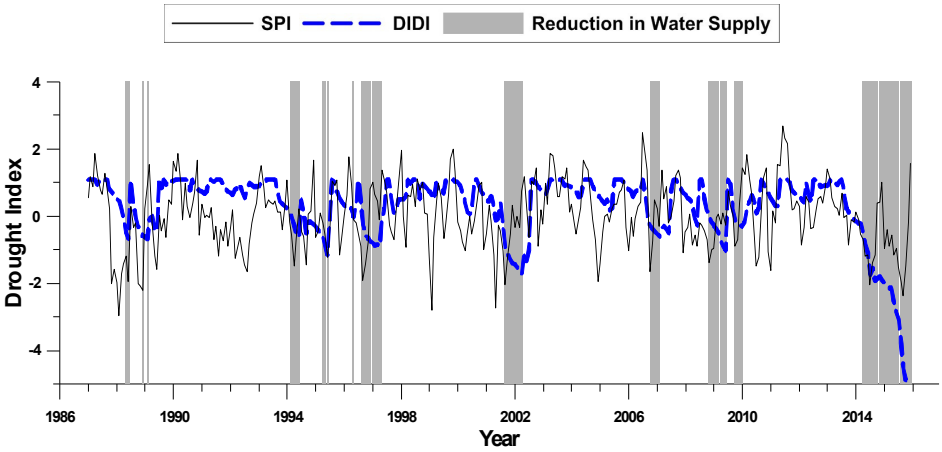

(a) SPI(3)

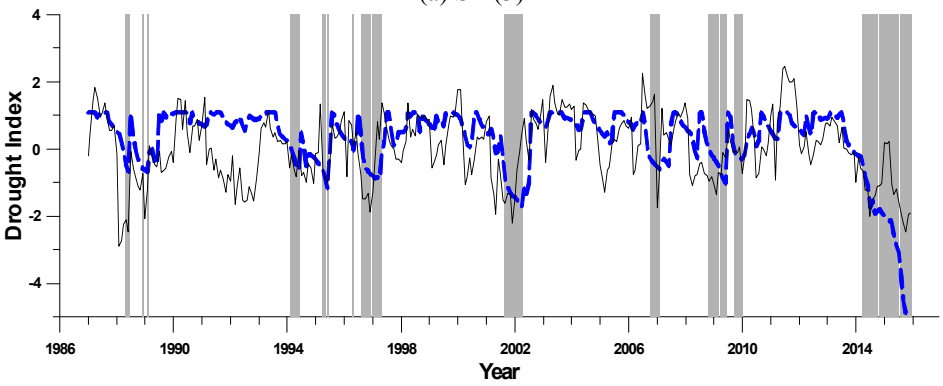

(b) SPI(6)

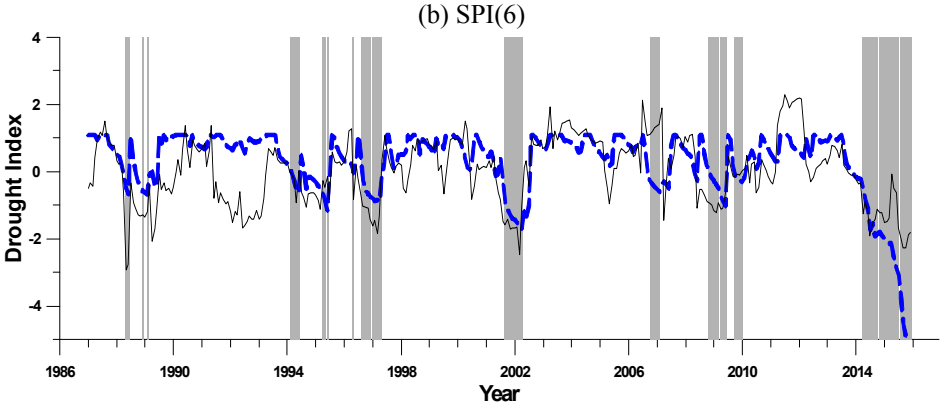

(c) SPI(9)

©2017, IAHR. Used with permission / ISSN 1562-6865 (Online) - ISSN 1063-7710 (Print)

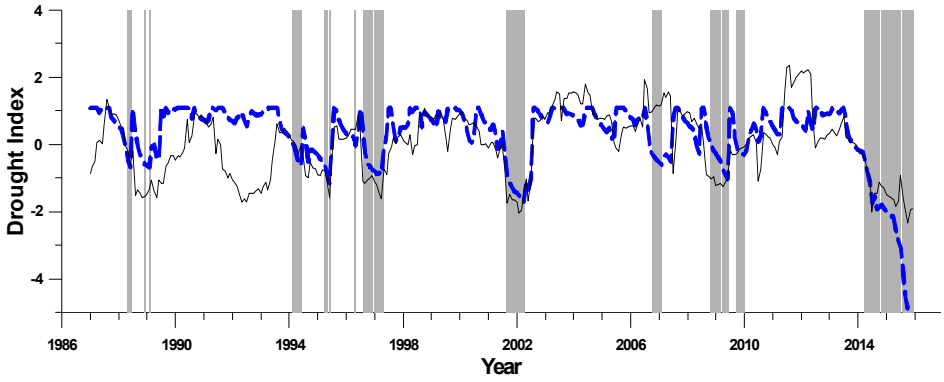

(d) SPI(12)

Figure 11. Comparison with DIDI and SPI.

Figure 11 shows DIDI and SPI of 3, 6, 9, and 12 months. When visually confirmed, DIDI seems to reflect the point of the water supply reductions better. As shown in Figure 11, one can see that 6-months and 12-months SPIs that show long-term drought are able to monitor drought better than 3-month and 6-month SPIs that show short- and mid-term. In order to evaluate the drought monitoring ability of SWSI and SPI, ROC analysis was also conducted. Figure 12 shows results of ROC analysis and Table 3 indicates ROC scores of DIDI, SWSI, SPI(3), SPI(6), SPI(9), and SPI(12). ROC score of DIDI was 0.93 which was 0.22 greater than it of SWSI and 0.33, 0.22, 0.16, and 0.17 greater than it of SPI(3), SPI(6), SPI(9), and SPI(12), respectively.

By applying the dam operation and threshold, DIDI was able to express the drought of dam inflow adequately, which indicates that the DIDI is useful for monitoring and responding the drought, and its application would help to mitigate drought damages.

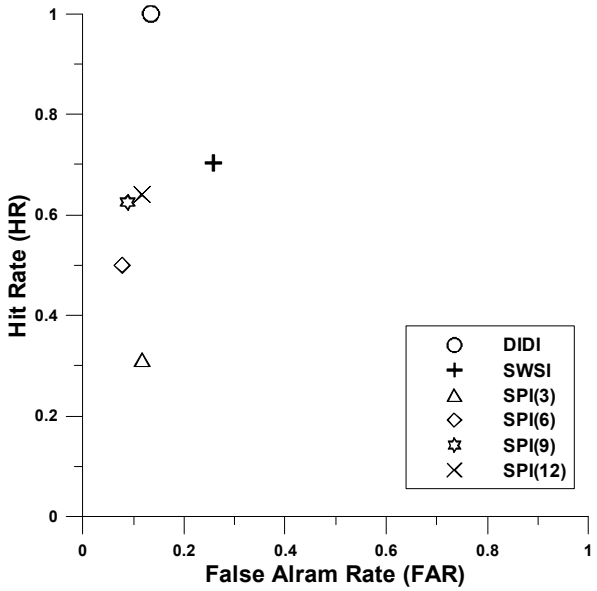

Figure 12. ROC analysis results of DIDI and SWSI.

Table3. Comparison of ROC score

	DIDI	SWSI	SPI(3)	SPI(6)	SPI(9)	SPI(12)
ROC score	0.93	0.72	0.60	0.71	0.77	0.76

4 CONCLUSIONS

This study developes and evaluates Dam Inflow Drought Index (DIDI) for Chungju Dam in Korea. The DIDI is calculated with the consideration of the dam operation. Critical inflows for each month are calculated using the criteria for water supply adjustment. The DIDI can be estimated by dividing the cumulated difference between the observed inflow and critical inflow (CDI) by its standard deviation. Considering the limit of dam storage, the upper limit of CDI, i.e., threshold, has to be determined, and the threshold was estimated by RCO analysis. ROC analysis is implemented using results of the dam operation simulation and DIDI for various thresholds. Optimal threshold of Chungju Dam was calculated as 630 $\times 10^6$ m^3, and with DIDI applying the threshold expressed the drought at the time of reduction in water supply adequately. And also the DIDI showed much better performance in monitoring dam droughts than SWSI and short- and long-term SPI (3-, 6-,

 ©2017, IAHR. Used with permission / ISSN 1562-6865 (Online) - ISSN 1063-7710 (Print)

9-, and 12-months SPI). The DIDI is useful for monitoring and responding the drought of dam inflow, and its application could help to mitigate drought damages.

REFERENCES

Bae, D.H., Son, K.H. & Kim H.A. (2013). Derivation and Evaluation of Drought Threshold Level Considering Hydro-Meteorological Data on South Korea. *Journal of Korea Water Resources Association*, 46(3), 287-299.

Kim, G. & Lee, J. (2011). Evaluation of Drought Indices Using the Drought Records. *Journal of Korea Water Resources Association*, 44(8), 639-652.

Mason I. (1982). A Model for Assessment of Weather Forecasts. *Australian Meteorological Magazine*, 30, 291-303.

Mckee, T.B., Doesken, N.J. & Kleist, J. (1993). The Relationship of Drought Frequency and Duration to Time Scales. *Proceedings of the 8th Conference on Applied Climatology*, Boston, MA, USA, 17(22), 179-183.

Palmer, W.C. (1965). *Meteorological Drought.* Washington, DC, USA: US Department Of Commerce, *30,* 58.

Shafer, B.A. & Dezman, L.E. (1982). Development of a Surface Water Supply Index (SWSI) to Assess the Severity of Drought Conditions in Snowpack Runoff Areas. *Proceedings of the Western Snow Conference*, Fort Collins, CO, 50, 164-175.

Sheffield, J., Wood, E.F. & Roderick, M.L. (2012). Little Change in Global Drought over the Past 60 Years. *Nature*, 491(7424), 435-438.

Sternberg, T. (2011). Regional Drought Has a Global Impact. *Nature*, 472(7342), 169-169.

Vicente-Serrano, S.M., Beguería, S. & López-Moreno, J.I. (2010). A Multiscalar Drought Index Sensitive to Global Warming: The Standardized Precipitation Evapotranspiration Index. *Journal of Climate*, 23(7), 1696-1718.

Wilhite, D.A. (2006). *Drought Monitoring and Early Warning Concepts, Progress and Future Challenges*. World Meteorological Organization, 24.

Wilhite, D.A. & Glantz, M.H. (1985). Understanding: The Drought Phenomenon: The Role of Definitions. *Water International*, 10(3), 111-120.

©2017, IAHR. Used with permission / ISSN 1562-6865 (Online) - ISSN 1063-7710 (Print)

Proceedings of the 37th IAHR World Congress
August 13 – 18, 2017, Kuala Lumpur, Malaysia

ESTIMATION OF DIRECT AND INDIRECT IMPACTS OF CLIMATE CHANGE ON GROUNDWATER LEVEL IN A GROUNDWATER DEPENDENT IRRIGATED REGION

GOLAM SALEH AHMED SALEM [1], SO KAZAMA [2] & SHAMSUDDIN SHAHID [3]

[1] Graduate School of Environmental Studies, Tohoku University, Sendai, Miyagi, Japan.
salem.golam.saleh.ahmed.t3@dc.tohoku.ac.jp
[2] Department of Civil Engineering, Tohoku University, Sendai, Miyagi, Japan
so.kazama.d3@tohoku.ac.jp
[3] Faculty of Civil Engineering, Universiti Technologi Malaysia, Johor Bahru, Malaysia.
sshahid@utm.my

ABSTRACT

Groundwater can balance large swings in climate and therefore, it is considered as a reliable source for irrigation to ensure food security in the context of climate change. The objective of the present study is to quantify the direct and indirect impacts of climate change on groundwater level in Bangladesh. A Support Vector Machine (SVM) model is developed to simulate groundwater level from rainfall, evapotranspiration, groundwater abstraction, and irrigation return flow for the period 1994-2010. The study reveals the significant correlation of groundwater level with rainfall, temperature and irrigation demand. The one-degree increase of temperature is found to cause a decrease in groundwater level during irrigation period by 0.65%, and 1% increase of rainfall is found to cause an increase of groundwater table by 0.05%. Similarly, 1% increase in groundwater abstraction is found to cause a decrease in groundwater table by 1.14 %. On the other hand, one- degree increases of temperature cause an increase in irrigation demand by 2.48%, which may cause a declination of groundwater level by 2.93 %. On the other hand, 1% increase of rainfall causes a decrease in groundwater abstraction by 0.59%, which increase of groundwater table by 0.48%. The study reveals the indirect impact of climate change on groundwater level through the changes in irrigation demand will be higher than direct impact due to changes in groundwater recharge. The study also reveals that impact of temperature rise on groundwater level would be much higher compared to changes in rainfall. As groundwater is the major source of irrigation in many developing countries, it is expected that the finding of the study will help in climate change adaptation and mitigation planning.

Keywords: Irrigation demand; groundwater abstraction; climatic influence; support vector machine (SVM); Northwest Bangladesh.

1 INTRODUCTION

Groundwater is a primary source of irrigation in many countries across the world. About 38% of global irrigated land is equipped for groundwater base irrigation (Siebert et al., 2010). Groundwater use in irrigation and food production is still increasing both in absolute terms and in the percentage of total irrigation, particularly in densely populated countries. For example, groundwater-based irrigated agriculture has grown more than 500% in India over the past three decades (Shah, 2008). The total number of mechanized wells has increased from barely a few thousand to millions in last few decades in Pakistan (Shah et al., 2003). The contribution of groundwater to irrigation has increased from 4% in 1971 to 85% at present in Bangladesh (Shahid et al., 2014). Groundwater based irrigated agriculture is one of the major source of global food production as well a prime sector of the rural economy. Therefore, it plays a major role in food security and poverty alleviation in many countries across the world. Groundwater has the capacity to balance large swings in precipitation and associated increase in demands during drought (Gurdak et al.,2012; Taniguchi and Hiyama, 2014). Consequently, many countries are gradually shifting to groundwater based irrigated agriculture for food security in the context of climate change.

It has been projected that by 2050 the world's population will reach more than 9.6 billion (United Nations, 2013). Food production will have to increase by 70% in order to feed the growing population. This will cause a vast expansion of irrigated agriculture globally (FAO, 2009). Evidence suggests that existing surface water resources will be far less than sufficient to provide necessary water for irrigation in many regions around the world (Watto and Mugera, 2014). From the present trend, it can be anticipated that a major portion of increased water demand will be met through abstraction of groundwater. Therefore, it can be remarked that groundwater based irrigation will continue to play an important role in food production in many countries around the world.

Rapid increase of irrigated agriculture to feed the growing population and inappropriate irrigation practice has caused overexploitation of groundwater at an alarming rate in many regions. Over-extraction has caused lowering of the groundwater table, decrease in well yield, increase of pumping cost and consequently,

 ©2017, IAHR. Used with permission / ISSN 1562-6865 (Online) - ISSN 1063-7710 (Print)

increase of crop production cost (Sharif and Ashok, 2011; Shahid et al., 2014). This has seriously affected the livelihood of a farmer in many countries. It is anticipated that climate change will pose another major threat to groundwater resources in the near future. As groundwater is closely interrelated to the environment, any changes in atmospheric precipitation will inevitably cause changes in the groundwater regime. Studies from different parts of world showed that increased temperature and changing rainfall pattern due to climate change will significantly affect groundwater recharge and storage (Shahid and Hazarika, 2010; Kumar, 2012; Jyrkama and Sykes, 2007; Davidson and Yang, 2007). Changes in precipitation pattern will alter runoff and consequently, groundwater recharge. Changes in soil moisture level due to climate change may reduce groundwater availability (Green et al., 2011). Higher temperatures will cause higher evaporation and plant transpiration rates, hence more drying up of soils, which will entail higher losses of soil moisture and groundwater recharge. Climate change may also lead to vegetation changes which may also affect groundwater recharge (Bobba, 2002; Sherif and Singh, 1999). All of these negative impacts together may cause shifting of groundwater level within the exploitable limit (Erturk et al., 2014; Hashemi et al., 2014). Furthermore, groundwater level may be indirectly affected due to increased abstraction of groundwater to meet the increased irrigation demand under a condition of higher temperature. Increased irrigation cost due to the lowering of groundwater table may seriously affect the livelihood of a farmer in the vast regions where groundwater is used as the major source of irrigation. Mitigation of Climate change impacts on groundwater resources to limit the irrigation cost and ensure farmer's profit will be a major challenge in the near future, particularly in agricultural based developing countries.

The effects of climate variability on groundwater have been less well explored than the effects on surface water (Green et al., 2011). This is particularly more appropriate for tropical region. Furthermore, though few studies have been conducted to assess the direct impact of climate change on groundwater level, no study has been conducted so far to assess the impact of climate change on groundwater level in a holistic way by considering both direct and indirect impacts. The objective of the present study is to quantify the direct and indirect impacts of climate change on groundwater level. The Northwest Bangladesh is selected as the study area, where groundwater is the sole sources irrigation. Declination of groundwater level due to overexploitation and consequent increase in irrigation cost is a major concern in the region. It is expected that the methodology presented in this study can be used to assess possible changes in irrigation cost due to the changes in groundwater level in any other parts of the world in order to facilitate adaptation and mitigation planning.

2 STUDY AREA

The study area located in northwest Bangladesh is a part of the Ganges River basin (Figure 1). The study area extends from (23.87ºN, 88.30ºE) to (24.78ºN, 88.89ºE) is extremely flat with some upland elevated 23 m above mean sea level (MSL) in the northwest. Surface geology of the area consists of sedimentary formations of alluvial sand, silt and clay of riverine origin (Haque et al., 2012). The maximum depth of groundwater level from the land surface varies from 2 to 20 meters in the area.

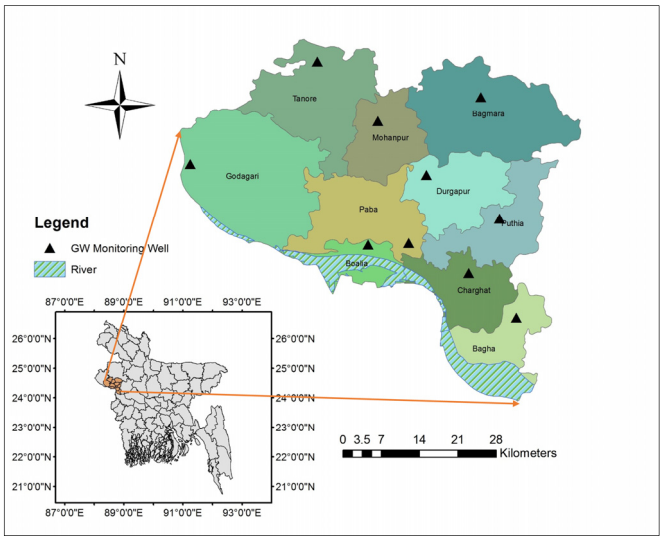

Figure 1. Location of study area and groundwater sampling point.

Climatically, the study area belongs to a dry and humid tropical zone with annual average rainfall varying between 1400 mm to 1900 mm. Almost 92.7% of rainfalls occur during May to October. Less than 6% of rainfalls occur during the irrigation period of dry season of *Boro* rice field (January to April). Annual variability of non-monsoon rainfall is also as high as 50%. Temperature in the region ranges from 25^{0}C to 40^{0}C during

the hottest season and 8^0C to 25^0C during the coolest season. Climate projection in Bangladesh using various climate modelling experiments indicates a little increase in rainfall during irrigation period. On the other hand, the temperature is projected to increase more in winter compared to other seasons (Ahmed and Alam, 1999; Manabe et al., 1992; Rajib et al., 2011).

3 DATA AND METHODS

3.1 Data and sources

Bi-monthly data of groundwater level recorded at ten observation wells (Figure 1) across the study area for a period 1994-2010 were collected from Bangladesh Water Development Board (BWDB). Daily rainfall and temperature recorded at Rajshahi station, located within the study area over the period 1973-2011 were collected from Bangladesh Meteorological Department (BMD).

3.2 Methods

The procedure used to assess the direct and indirect impacts of climate change on the groundwater level is outlined below.

a) The crop evapotranspiration was computed from crop coefficient and reference evapotranspiration estimated using Thornthwaite method.
b) The net water required for irrigation was estimated using FAO-56 model. The amount of groundwater abstraction was considered equal to the amount of groundwater required for irrigation.
c) Irrigation return flow from paddy field was estimated from soil properties.
d) A support vector machine (SVM) model was developed to simulate groundwater level from rainfall, evapotranspiration, groundwater abstraction and irrigation return flow for the period 1994-2010.
e) The rainfall and evapotranspiration values in FAO-56 model were varied to estimate the sensitivity of rainfall and temperature on irrigation demand.
f) The rainfall, evapotranspiration and irrigation demand values in SVM model were varied to estimate the direct and indirect impact of climate change on groundwater level.

Details of the methodology used are discussed below. The net irrigation water required in paddy field (W_N) was estimated using FAO-56 model (Brouwer and Heiblone, 1986),

$$W_N=ET_C+W_{RC}-P_E \quad [1]$$

Where, W_{RC} is the total amount of water required for land preparation, seepage loss from paddy field and standing water in the field (mm/day); P_E is the effective precipitation (mm/month); and ET_C is the crop evapotranspiration from paddy field (mm/day) estimated as, $ET_C= EC \times ET_O$ (mm/day), where, EC is the crop coefficient (dimensionless) and ET_O is the reference evapotranspiration estimated using Thornthwaite method. Details of the method used for estimation of W_{RC} and P_E can be found in (Shahid, 2011).

In the present study, the crop coefficient values provided by Food and Agricultural Organization (FAO) for different growing stages of rice (Brouwer and Heibloen, 1986) were used. Water required for irrigation was estimated monthly basis for the time period 1994-2010. The irrigation in the study area is mainly conducted from January to April. Therefore, Irrigation requirement was estimated only for those irrigation months.

Irrigation return flow to groundwater or the water loss through percolation from the paddy field was calculated from soil parameter. Following (Brouwer and Heibloem, 1986), it was considered that percolation loss for a sandy, clay and loom soil are 8, 4 and 6 mm/day, respectively.

SVM was used to model the function (f) dependence of the dependent variability variable y on a set of independent variables x are estimated,

$$y=f(x)=\mathbf{w}\cdot\phi(x)+b \quad [2]$$

Where, $\mathbf{w}$ and b are weight vector and bias, respectively; ϕ denotes a nonlinear transfer function that maps the input vectors into a high-dimensional feature space, in which theoretically, a simple linear regression can cope with the complex nonlinear regression of the input space. The nonlinear regression function using optimization problem with a ε insensitivity loss function can be solved SVM.

$$\frac{1}{2}\left(\mathbf{w}^T\mathbf{w}\right)+C\sum_{i=1}^{N}\left(\xi_i+\xi_i^*\right)=0 \quad [3]$$

This function can be minimized using following criteria,

$$\mathbf{w}^T\phi(x_i)-y_i+b \le \varepsilon+\xi_i^*$$
$$y_i-\mathbf{w}^T\phi(x_i)-b \le \varepsilon+\xi_i$$

 ©2017, IAHR. Used with permission / ISSN 1562-6865 (Online) - ISSN 1063-7710 (Print)

$$\xi_i \xi_i^* \geq 0, i=1,2,\ldots\ldots N$$

Where, ξ_i and ξ_i^* denote slack variable which is the distance of the training data set points from the region to an error tolerance ε. The trade-off between the flatness of f(x) and deviations greater than ε are tolerance depicted by C >0, where C is a positive constant that inducing the degree of penalized loss when there are errors during training.

A lot of conceptual and process-based modelling techniques have been established for simulating groundwater level in a variety of hydrogeological setting (Coppola et al., 2005; Coppola et al., 2003; Coulibaly et al., 2001; Uddameri, 2007). However physically based models are very intensive for data (Nikolos et al., 2008). Therefore, the machine learning method, SVM is used to develop an empirical model of groundwater level simulation.

4 RESULTS AND DISCUSSION

4.1 Historical changes in climate

The climate in the study area is changing in line with global climate change. Trends in temperature and rainfall in the study area for the period 1973-2011 was analysed using non-parametric Mann-Kendall test (Kendall 1975). Obtained results are shown in Figure 2**.** The results showed a significance increase in temperature in the region at a rate of 0.12ºC per decade, but no significant change in rainfall for the period.

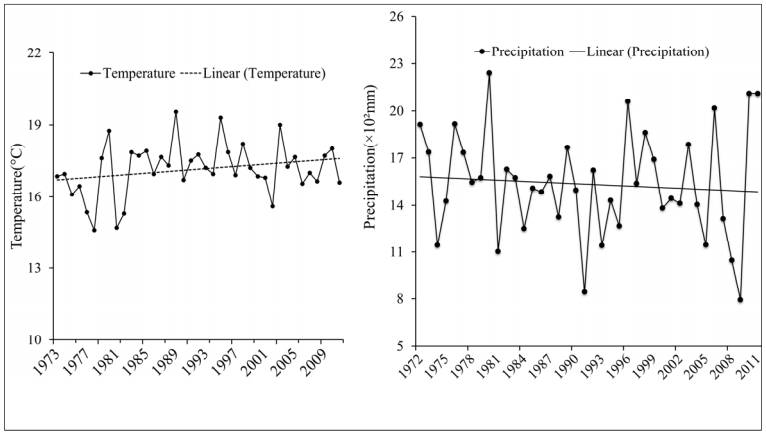

Figure 2. Trends in daily mean temperature and annual precipitation in the study area.

4.2 SVM model calibration and validation

The SVM model was developed to simulate depth to groundwater level from rainfall, evapotranspiration, groundwater abstraction and irrigation return flow for the period 1994-2010. The SVM model was calibrated and validated with 70% and 30% of observed data, respectively. The observed and SVM predicted depth to groundwater level during model calibration and validation in a water well in the study area is shown in Figure 3. The figure shows good match between observed and simulated groundwater level during both model calibration and validation. The SVM model was calibrated and validated separately at all the locations.

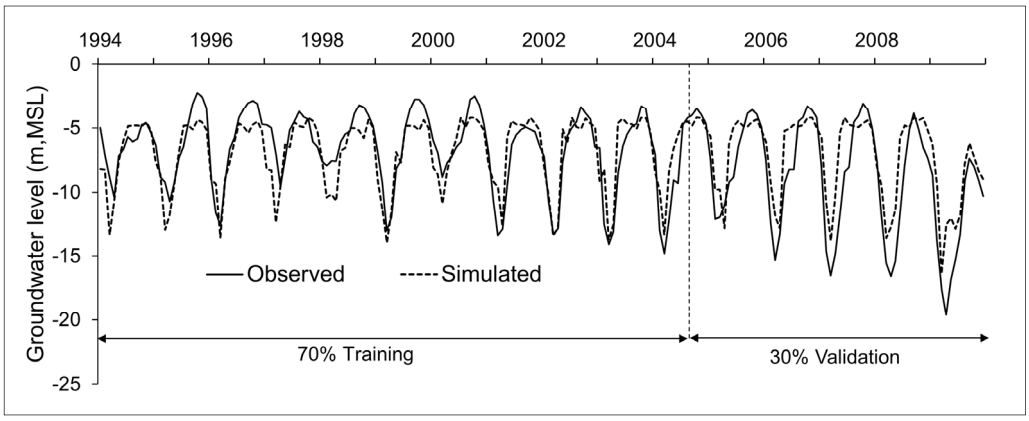

Figure 3. Observed and simulated depth to groundwater table during model calibration and validation at Mohonpur station.

The performance of SVM model was assessed using statistical indicators, namely Nash-Sutcliff efficiency (NSE), correlation coefficient (R^2), and root mean square error (RMSE). The obtained results at four locations during SVM model calibration and validation are given in Table 1. The table shows that the RMSE values are low, and the R^2 and NSE values are greater than 0.5 during both model calibration and validation at all the locations. Moriasi et al. (2007) reported that model performance is acceptable if NSE is greater than 0.5 and RMSE values are less than 50% of the standard deviation of the dependent variable. Therefore, it can be considered that the SVM model developed in the study can be used for reliable simulation of groundwater level.

Table 1. The RMSE, R^2 and NSE values obtained during SVM model calibration and validation at few selected locations

Station Name	Calibration			Validation		
	RMSE	NSE	R^2	RMSE	NSE	R^2
Charghat	1.03	0.79	0.78	0.99	0.8	0.8
Durgapure	1.694	0.663	0.823	1.708	0.632	0.815
Bagmara	1.44	0.72	0.73	1.48	0.71	0.71
Puthia	1.34	0.77	0.78	1.33	0.78	0.79

4.3 Influence of climate change on groundwater abstraction and indirect impacts on groundwater level

About 100% of water for irrigation for dry season rice cultivation in the study area comes from groundwater. Furthermore, farmers use at least 20% more water for irrigation compared to that required. Therefore, groundwater abstraction is considered as total water requirement for irrigation estimated using FAO-56 model (Equation 1) plus the 20% of the estimated water requirement for irrigation. To assess the impacts of climate variability on irrigation water demand, temperature (evapotranspiration) and rainfall values were varied in FAO-56 model. The changes in irrigation demand due to the changes in temperature and rainfall were incorporated in SVM model in order to assess the indirect impact of climate change to groundwater level. Obtained results are presented in Figure 4. The figure shows that 1ºC increase in temperature from the reference period (1994-2010) causes an increase in groundwater demand by 2.48%. On the other hand, 1% increase in rainfall from the same reference period causes a decrease in groundwater demand by 0.59%. When the changes in irrigation demand were incorporated in SVM model by keeping other inputs of the model constant, it was found that groundwater level declines 2.9% of the reference period (1994-2010) due to indirect impact (via the changes in irrigation demand) of 1ºC temperature rise. On other hand, 1% increase in rainfall indirectly elevates groundwater level by 0.48% of the reference period.

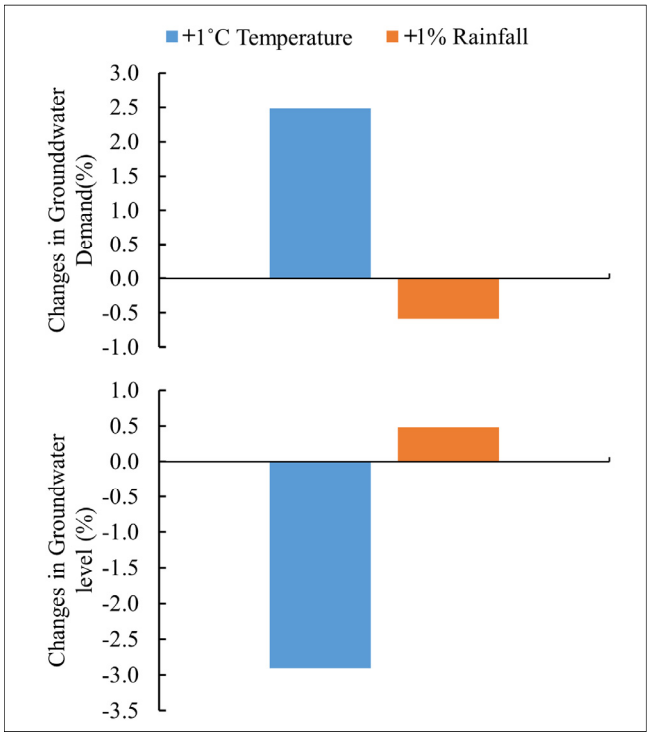

Figure 4. Changes in average groundwater demand and average depth to groundwater table during the irrigation period (January to April) due to the changes in rainfall and temperature.

 ©2017, IAHR. Used with permission / ISSN 1562-6865 (Online) - ISSN 1063-7710 (Print)

4.3.1 Direct impact of climate change on groundwater level

Rainfall, evapotranspiration (estimated from temperature) and groundwater abstraction values were varied separately in the SVM model while keeping others parameters constant in order to estimate the direct impact of climate change on groundwater level. The obtained results are represented in Figure 5. It was observed that 1% increase in rainfall from the reference period (1994-2010) causes a rise of groundwater level during irrigation period by 0.05%. A change in evapotranspiration due to 1ºC increase in temperature from the same reference period cause a decrease in groundwater level during irrigation period by 0.65%. Similarly, 1% increase in groundwater abstraction from the reference period was found to cause a decrease in groundwater table by 1.14%.

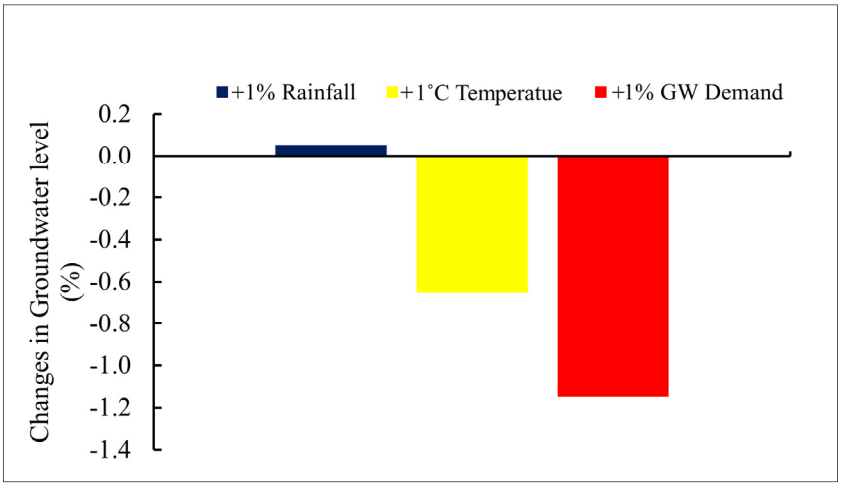

Figure 5. Sensitivity of groundwater level depth to rainfall, temperature and groundwater abstraction.

4.3.2 Changes in spatial distribution of groundwater level due to climate change

Sensitivity of rainfall and temperature on groundwater abstraction and total impacts on groundwater level at all the points were estimated separately. The obtained values were interpolated to prepare the thematic maps to show the direct and indirect impacts of climatic change on groundwater level in Northwest Bangladesh. Spatial distribution of simulated groundwater depth due to changes in rainfall and temperature is shown in Figure 6. The figure shows major impact of climate change in the study area due to climate change induced changes in groundwater abstraction followed by temperature rise. Areal extent of groundwater level drop was found higher for the increase in groundwater abstraction due to temperature rise. The highest impact occurred when temperature rise affected groundwater level directly and indirectly through the increase in groundwater abstraction.

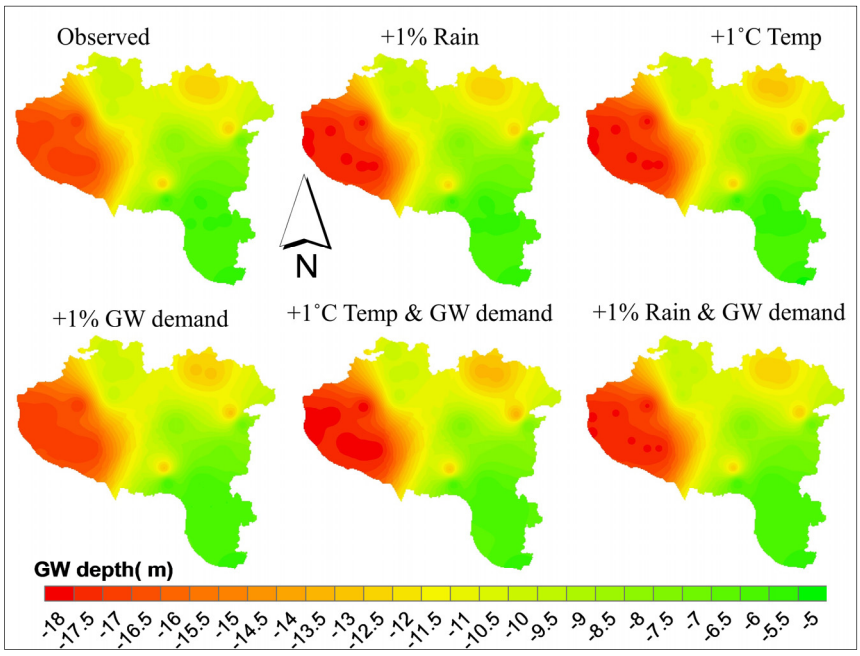

Figure 6. Changes in groundwater table depth during the irrigation period (January to April) under the influence of climate change.

©2017, IAHR. Used with permission / ISSN 1562-6865 (Online) - ISSN 1063-7710 (Print)

Rainfall during irrigation period in the study area is very scarce. The rainfalls that occur during this period (mainly in March and April) are in the form of thunderstorm. The short and intense thunderstorm rainfall produces much runoff compared to groundwater recharge. Therefore, the increase of pre-monsoon rainfall does not affect groundwater recharge much. Similar finding has also been reported in other regions. IPCC (2007) reported that 9% increase of runoff due to short and intense rainfall increases groundwater recharge only by 2%. On the other hand, temperature during March and April is higher compared to other months which cause higher evapotranspiration from paddy field. Higher evapotranspiration decreases soil moisture as well as groundwater recharge, and thereby groundwater level. Therefore, groundwater level in the study area is more sensible to temperature compared to rainfall. Chen *et al*. (2004) also reported that sensitivity of groundwater towards temperature is more at higher temperature. Water demand for irrigation is also more sensitive to temperature compared to rainfall in the region. As the rainfall during irrigation period is scarce, increase in a few percentage of rainfall does not affect irrigation demand. On the other hand, small increase in temperature significantly increases evapotranspiration from flooded rice field and thereby, increases irrigation demand significantly. Therefore, when both of the direct and indirect impacts of climate change on groundwater level are considered in an intense groundwater depended irrigated region in tropics, temperature plays the most significant role in determining groundwater level.

5 CONCLUSIONS

A study has been carried out to quantify the direct and indirect impacts of climate change on groundwater level in groundwater dependent irrigated region. The results showed that groundwater level is most sensitive to the changes in irrigation demand or groundwater abstraction due to temperature rise. The results revealed that 1˚C increase of temperature would cause a decrease in average groundwater level by 0.65% from the reference period. On the other hand, 1˚C increase in temp causes an increase in irrigation demand by 2.48%, which may cause a declination of groundwater level by 2.9%. It can be concluded that temperature rise will play the most important role in groundwater level drop and consequent increase in irrigation cost in groundwater dependent irrigated region of tropics.

ACKNOWELEDGMENTS

This research was supported by the Environment Research and Technology Development Fund (S-14) of the Ministry of the Environment Japan.

REFERENCES

Ahmed A.U. & Alam M. (1999). *Development of Climate Change Scenarios with General Circulation Models*. Vulnerability and Adaptation to Climate Change for Bangladesh, 13-20.

Brouwer C. & Heibloem M. (1986). *Irrigation Water Management: Irrigation Water Needs,* Training Manual, 3.

Chen Z., Grasby S.E. & Osadetz K.G. (2004). Relation between Climate Variability and Groundwater Levels In The Upper Carbonate Aquifer, Southern Manitoba, Canada. *Journal of Hydrology,* 290: 43-62.

Coppola E.A., Jr, Rana A.J., Poulton M.M., Szidarovszky F. & Uhl V.W. (2005). A Neural Network Model for *Predicting* Aquifer Water Level Elevations. *Groundwater*, 43(2), 231-241.

Coppola E.A., Szidarovszky F., Poulton M. & Charles E. (2003). Artificial Neural Network Approach for *Predicting* Transient Water Levels in a Multilayered Groundwater System Under Variable State, Pumping, And Climate Conditions. *Journal of Hydrologic Engineering*, 8(6), 348-360.

Coulibaly P., Anctil F., Aravena R. & Bobee B. (2001). Artificial Neural Network Modeling of Water Table *Depth* Fluctuations. *Water Resources Research*, 37(4), 885-896.

Davidson S. & Yang L. (2007). Impacts of Climate Variability and Changes on Groundwater Recharge in the Semi-Arid Southwestern United States. *United States Geological Survey,* 1-4.

Erturk A., Ekdal A., Gurel M., Karakaya N., Guzel C. & Gonenc E. (2014). Evaluating the Impact of Climate Change on Groundwater Resources in A Small Mediterranean Watershed. *Science of the Total Environment*, 499, 437-447.

FAO. (2009). How to Feed the World in 2050. *Proceedings of the Expert Meeting on How to Feed the World in 2050.* FAO Headquarters, Rome, 24-26.

Green T.R., Taniguchi M., Kooi H., Gurdak J.J., Allen D.M., Hiscock K.M., Treidel H. & Aureli A. (2011). Beneath the Surface of Global Change: Impacts of Climate Change on Groundwater. *Journal of Hydrology*, 405(3), 532-560.

Gurdak J.J., Mcmahon P.B. & Bruce B.W. (2012). *Climate Change Effects on Groundwater Resources.* A Global Synthesis of Findings and Recommendations, 145 – 168 pp.

Haque M.A.M., Jahan C.S., Mazumder Q.H., Nawaz S.M.S., Mirdha G.C., Mamud P. & Adham M.I. (2012). Hydrogeological Condition & Assessment of Groundwater Resource Using Visual Modflow Modeling, Rajshahi City Aquifer, Bangladesh. *Journal of the Geological Society of India*, 79(1), 77-84.

Hashemi H., Uvo C.B. & Berndtsson R. (2014). An Extended Modeling Approach to Assess Climate Change Impacts on Groundwater Recharge and Adaptation in Arid Areas. *Hydrology and Earth System Sciences Discussions*, 11(10), 11797-11835.

 ©2017, IAHR. Used with permission / ISSN 1562-6865 (Online) - ISSN 1063-7710 (Print)

Intergovernmental Panel on Climate Change, (IPCC). (2007). *Climate Change: Impacts, Adaptation and Vulnerability.* Contribution of Working Group II to The Fourth Assessment Report of The Intergovernmental Panel on Climate Change, Cambridge University Press, Cambridge, UK; 976.

Jyrkama M.I. & Sykes J.F. (2007). The Impact of Climate Change on Spatially Varying Groundwater Recharge in the Grand River Watershed (Ontario). *Journal of Hydrology*, 338(3), 237-250.

Kumar C.P. (2012). Climate Change and Its Impact on Groundwater Resources. *International Journal of Engineering Science*, 1(5), 43-60.

Manabe S., Spelman M.J. & Stouffer R.J. (1992). Transient Responses ff A Coupled Ocean-Atmosphere Model to Gradual Changes of Atmospheric CO2. Part II: Seasonal Response. *Journal of Climate*, 5(2), 105-126.

Nikolos I.K., Stergiadi M., Papadopoulou M.P. & Karatzas G.P. (2008). Artificial Neural Networks as an Alternative Approach to Groundwater Numerical Modelling and Environmental Design. *Hydrological Processes*, 22(17), 3337-3348.

Rajib M.A., Rahman M.M., Islam A. & Mcbean E.A., (2011). Analyzing the Future Monthly Precipitation Pattern in Bangladesh from Multi-Model Projections Using Both GCM And RCM. *World Environmental and Water Resources Congress*, 3843-3851.

Shah T. (2008). Taming the Anarchy: *Groundwater Governance in South Asia 2008 Resources for the Future,* Press, Washington (DC).

Shah T., Roy A.D., Qureshi A.S. & Wang J. (2003). *Sustaining Asia Groundwater Boom: an Overview of Issues and Evidence.* Natural Resources Forum, Wiley Online Library, 130-141.

Shahid S. & Hazarika M.K., (2010). Groundwater Drought in The Northwestern Districts of Bangladesh. *Water Resources Management*, 24(10), 1989-2006.

Shahid S., Wang X.J., Rahman M.M., Hasan R., Harun S.B. & Shamsudin S. (2014). Spatial Assessment of Groundwater Over-Exploitation in Northwestern Districts of Bangladesh. *Geological Society of India*, 85(4), 463-470.

Sharif M. & Ashok K.R., (2011). Impact of Groundwater Over-Draft on Farm Income and Efficiency in Crop Production. *Agricultural Economics Research Review*, 24(2).

Sherif M.M. & Singh V.P. (1999). Effect of Climate Change on Sea Water Intrusion in Coastal Aquifers. Hydrological *Processes*, 13(8), 1277-1287.

Siebert S., Burke J., Faures J.M., Frenken K., Hoogeveen J., Doll P. & Portmann F.T. (2010). Groundwater Use for Irrigation- Global Inventory. *Hydrology and Earth System Sciences*, 14(10), 1863-1880.

Taniguchi M. & Hiyama T. (2014). *Groundwater as a Key for Adaptation to Changing Climate and Society*. *Global Environmental Studies, Springer.*

Uddameri V. (2007). Using Statistical and Artificial Neural Network Models to Forecast Potentiometric Levels at a Deep Well in South Texas. *Environmental Geology*, 51(6), 885-895.

United Nations. (2013). *World Population Prospects: The 2012 Revision, Highlights and Advance Tables (Working Paper No. ESA/P/WP. 228)*, New York: United Nations Publications.

Watto M.A. & Mugera A.W. (2014). Econometric Estimation of Groundwater Irrigation Efficiency of Cotton Cultivation Farms in Pakistan. *Journal of Hydrology: Regional Studies*, 4(A), 193-211.

©2017, IAHR. Used with permission / ISSN 1562-6865 (Online) - ISSN 1063-7710 (Print)

Proceedings of the 37th IAHR World Congress
August 13 – 18, 2017, Kuala Lumpur, Malaysia

STUDY ON THE TOTAL WATER AMOUNT CONTROL FOR DECREASING GROUNDWATER OVEREXPLOITATION IN THE HAIHE RIVER BASIN

GUIYU YANG[1], HAO WANG[2], WEIWEI SHAO[3], YANGWEN JIA[4] & LIN WANG[5]

[1,2,3,4,5] State Key Laboratory of Simulation on Regulation of Water Cycle in River Basin, China Institute of Water Resources and Hydropower Research, Beijing, China,
guiyuy@iwhr.com; Wanghao@iwhr.com; shaoww@iwhr.com; Jiayw@iwhr.com; iwhrwl@163.com

ABSTRACT

The groundwater over-exploitation in the Haihe River Basin, China is very serious, which has drawn lots of attention around the world. The key solution for this problem is rational utilization of water resources. In the framework of the maximum available consumption of water resources consumption (MAWRC) in the water cycle, five controlling indicators are introduced upon the water supply sources and the water consumption. To quantitatively determine these indicators in future, 3 scenarios are set on the conditions of the drought hydrological series from 1980 to 2005 associating to the amount of water utilization between 2020 and 2030 planning level years. The 5 indicators are quantified in different scenarios by employing the “natural-social” dualistic model. The results showed that the amount of the MAWRC should be $1675\times10^8m^3$ and $1685\times10^8m^3$ in 2020 and 2030, respectively. Under the corresponding condition, the amounts of water consumption in 2020 and 2030 respectively should be restricted as following: the national economy water utilizations are $400\times10^8m^3$, $411\times10^8m^3$; and the artificial eco-environmental water utilizations mount to $17\times10^8m^3$ and $20.9\times10^8m^3$. The surface water supplies are $230\times10^8m^3$ and $260\times10^8m^3$ with groundwater exploration quantities at $188\times10^8m^3$ and $172\times10^8m^3$. If the total amount of water supply was strictly constrained in this way, the efficiency of water resources consumption and basin ecosystem will be greatly improved.

Keywords: The controlling indicates; groundwater; surface water; the Haihe River Basin.

1 INTRODUCTION

With the development of economy and the growth of population, the water resources scarcity and a series of water-related eco-environment issue are daily focused globally. In the Haihe River Basin, because of the poor natural water resources basic condition, together with the effect of the high strength human activity and climate change, the shortage of water resources is more prominent, which already affects the sustainable development in the whole basin. Groundwater over-exploitation, is one of the results caused by water scarcity, has become increasingly prominent, and this form the largest groundwater funnel area in the world with the increasing of the water demand, the groundwater encounters over-exploitation problem. To alleviate the groundwater exploitation, China issued the No.1 document, which demanded to "carry out the experimental work of the comprehensive treatment of groundwater over-exploitation in Hebei Province, North China in advance." Hebei became a national pilot province for the comprehensive treatment of groundwater over-exploitation in 2014. In 2014 and 2015, Hebei Province has carried out the comprehensive treatment of groundwater over-exploitation in its plain areas, and further focused on the treatment of groundwater over-exploitation in four and five prefecture-level cities covering Hengshui, Cangzhou, Handan, and Xingtai and Shijiazhuang. By the implementation of the agricultural and water conservancy measures, the situation of the groundwater over-exploitation has improved. However, the effect of the comprehensive treatment mainly was in the pilot area. Thus, it is difficult to provide the guide in the whole basin. Therefore, based on the balance between supply and drainage in the whole water cycle, this paper constructed the total amount of controlling indicators from the source of water supply and water users. Later the quantity of the controlling indicators in scenarios was implemented by employing the “natural-social” dualistic model. It is significant to treat groundwater over- exploitation in macro-scale.

2 HAHE RIVER BASIN OUTLINE AND ITS WATER CYCLE CHARACTERISTICS

The Haihe River Basin is located in eastern China between 112°E–120°E and 35°N–43°N. The basin, a political and cultural center that covers Beijing, Tianjin, Hebei and five other provinces (autonomous regions and municipalities), and has a total area of 320,000km^2. It accounts for 3.3% of the national area. The total population reached 1.5×10^8 in 2015, accounting for 11% of the national population; and the gross domestic product (GDP) of 8.2×10^8 Yuan accounts for 13% of the national GDP. The irrigation area reaches 550×10^4ha respectively.

However, there was little optimism for the basin’s water resources condition. According to the statistics (seen Figure 1), the precipitation has a declined trend with the multi-annual average precipitation lying at a

 ©2017, IAHR. Used with permission / ISSN 1562-6865 (Online) - ISSN 1063-7710 (Print)

value of 535mm in the basin from 1956 to 2005. The amount of water resources strictly reduce the trend to $260\times10^8m^3$ in 2015 from $483\times10^8m^3$ in 1950s. At the same time，the amount of water utilization appears to continue increasing (Figure 2). In 2015, The total amount of water utilization is $346\times10^8m^3$，where the rate of the water resources development and utilization was at 118%. This is far more than its international alert line of 40%，and more than the water availability rate of 63%. These lead to groundwater over-exploitation for long periods. The cumulative of over-exploitation reached about $1000\times10^8m^3$ (Wang, 2002) in the plain zone. The over-exploitation area is above 90% of the plain area, which lead to a concentration and contiguous development trend of groundwater funnel. Moreover, the total area of Baiyangdian, Qilihai and 10 other major wetlands was only 1/6 of the area in the 1950s (Han, 2008). The amount of water flowing into BoHaiyu sea decreased to $17\times10^8m^3$ in early of the 21 century from the $207\times10^8m^3$ in 1950s. Hence, faced with the serious groundwater over-exploitation situation, it is very meaningful to control the rational amount of water resources supply and the amount of water utilization for the water resources shortage

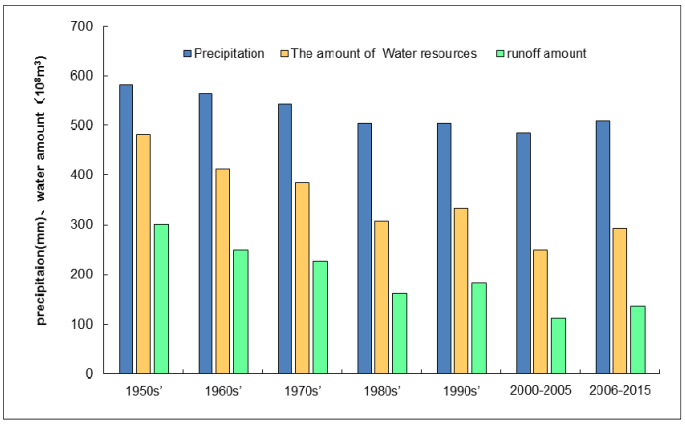

Figure 1. The change of water resources.

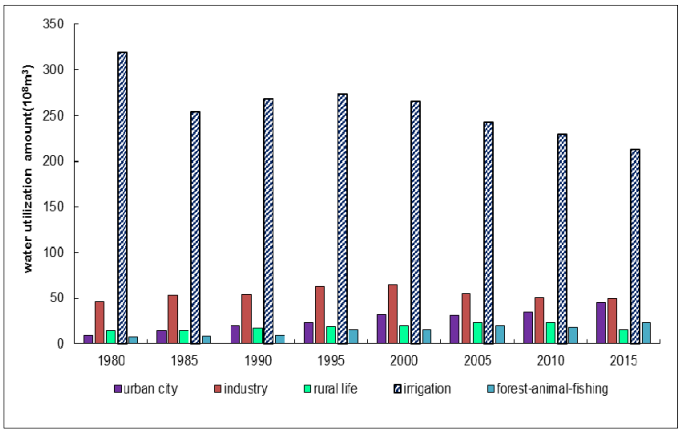

Figure 2. The change of the water supply and water use.

3 THE DESCRIPTION FOR THE CONTROLLING INDICTORS AND THEIR CALCULATION METHODS

3.1 The controlling indicators introduction

The amount of water supplied and that of the utilization is closely related to the development of social-economy in the region/basin, which directly appears in social water cycle process with “fetch-use-drainage-reuse” linkage base on the constrain of the allowable utilization amount. For the allowable utilization amount, it was decided by the incoming water amount including precipitation and water-diversion, and the natural-ecological water demand amount. Comprehensively according to the above two aspects, this paper provides 5 water amount controlling indicators according to the supply water sources and water users. The 5 controlling indicators were as following:

i. the controlling amount of the water resources consumption associating to the regional/basin rational water use structure, alleviate as the maximum available consumption;
ii. the total amount of the fetching surface water under the constrain amount of the maximum available consumption;
iii. the allowable groundwater exploitation amount;
iv. the controlling amount of the total water resources utilization to the national economy associating of

©2017, IAHR. Used with permission / ISSN 1562-6865 (Online) - ISSN 1063-7710 (Print)

the regional/basin rational water use structure;

v. the controlling amount of ecology and environment utilization associated to the regional/basin rational water use structure.

3.2 The calculation methods for the controlling indicators

The maximum available amount of consumption of water resources in the region/basin, is the maximum constrains for water resources available to be utilized, and embodies this in every water cycle link. Due to the evapotranspiration, the main part in all the consumption, the maximum amount available for consumption of water resources will also briefly be called as the object ET_{max}. It can be indicated by the Eq. [1] according to the water amount balance in region/basin.

$$ET_{\max} = P + In_w + D_{in} + G_a - Out_w + \Delta S \quad [1]$$

where P is the amount of precipitation, also known as wide-sense water resources amount(Wang et al., 2006) including the amount of runoff, soil water resources, canopy interception, and depression amount; In_w is the water amount entering into the basin; D_{in} is the water amount diverted into the basin; G_a is the available exploitation groundwater; Out_w is the amount of water flowing out of the basin; ΔS mainly is the amount of the surface water storage variance where the soil water storage variability that equal to zero under the multi-annual average conditions persist. the groundwater storage variance was already considered in the amount of the available exploitation of groundwater. The ET_{max} may be initially determined by the water balance method in the basin when the precipitation, allowable groundwater exploitation, diverted water and the amount of water flowing into sea is obtained.

The other controlling indicators were calculated by employing “natural-social” dualistic water cycle model (referred to as the dualistic model). The dualistic water cycle model of the Hai River Basin was coupled with the WEPLAR, ROWAS and DAMOS module, which together may be used for hierarchical decomposition at the macro-, meso- and micro-scales, and may also be nested with analog feedback, so as to achieve the integrated simulation of the “natural-social” dualistic water cycle process. The amount of water supply and that of the water use may be obtained in different linkage. The special calculation process was showed in Figure 3. The above modules constitute the dualistic model. The detail information of the model and the module feedback process could be shown in the reference (Jia, 2010).

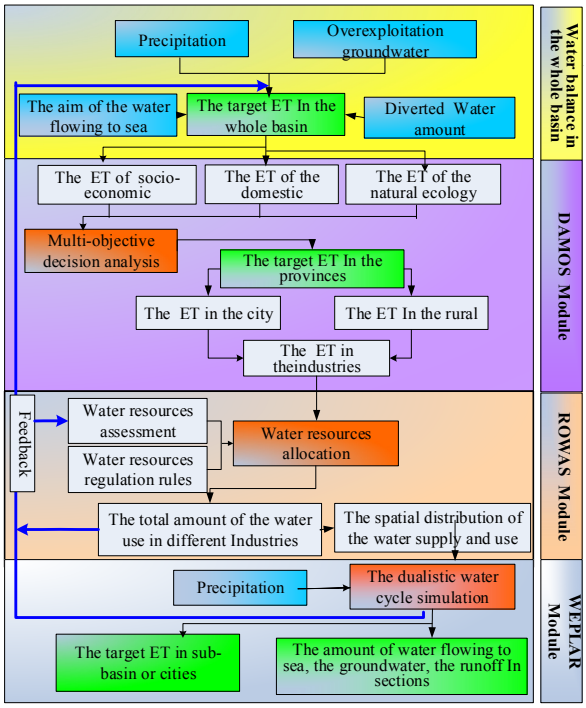

Figure 3. Calculation process of the total control indicators in the dualistic model.

 ©2017, IAHR. Used with permission / ISSN 1562-6865 (Online) - ISSN 1063-7710 (Print)

4 THE CALCULATION AND ANALYSIS OF THE CONTROLLING INDICES IN SCENARIOS IN HAIHE RIVER BASIN

4.1 Scenarios

According to the basic water resources condition and the available water resources amount, only 3 scenarios were set under the drought hydrological series. The basic condition of the 3 scenarios are as following:

Table 1. Scenarios of water quantity control. unit: $10^8 m^3$

Level year	Precipitation	Over Exploitation of Groundwater	Water Amount to Sea	South-to-North Water Diversion		Water Diverted from Yellow River
				Mid-route	East-route	
2005	1596.2	80	35	0	0	46.2
2020	1596.2	27	55	58.7	14.2	47
2030	1596.2	0	93	83.9	31.3	43.3

The specific constrain condition is as following for the water resources input aspect: (1) Groundwater use: groundwater overexploitation was at $80\times10^8 m^3$ and it is the benchmark of 2005. This scenario is now supporting the reduction of usage of groundwater to $27\times10^8 m^3$ and zero in 2020 and 2030, respectively;(2) South-to-North Water Diversion (from the Yangtze River) had no transfer in the benchmark situation where full transfer ability of the Middle route and east route in 2020, and the total water diversion is $72.9\times10^8 m^3$; the twice-stage full diversion ability of the two routes in 2030, will amount the diversion at $114.2\times 10^8 m^3$. In addition, the water diverted from Yellow River also should be included, where the water transfer of $46.2 \times 10^8 m^3$ in the benchmark situation will be achieved. $45.91\times 10^8 m^3$, in which $1.056\times10^8 m^3$ of seepage would be transferred from the Yellow River into the Haihe Basin (come from of Integrated Water Resources Planning) in 2020; and the less decreasing water transfer of $43.3\times10^8 m^3$ will occur in 2030.

The output of water resources aspect where the water resources output includes not only the amount of economy water requirement but also the reserved water amount flowing into Bohai Sea to guard fair and sustainable development in the whole basin. The amount of the water flowing into sea was, respectively at $35\times10^8 m^3$ in benchmark of level year (that is the average value of the water flowing into sea from 1980 to 2005). Besides that, $55\times10^8 m^3$ is one of third of average natural runoff amount from 1980 to 2005 and $93\times10^8 m^3$ is the average value of the water flowing into sea from 1956 to 2005.

In addition, to realize the development of economy and the protection of eco-environment system, the water resources regulation measures were also considered which associates it to the current management measures where the water saving measure and policy are promoted in the future.

4.2 Results analysis

The controlling indicators were calculated under the condition of food safety guarded and eco-environment, where this will be well developed in the future by employing the calibrated dualistic model. The results (seen in Table 2) shows that the maximum available consumption of water resources in the whole basin should be maintained at $1675\times10^8 m^3$ and $1685\times10^8 m^3$ for the year 2020, 2030. This situation could be under a drought hydrological situation. Under the condition of the total consumption constrain, the national economy use of $400 \times10^8 m^3$, $411\times10^8 m^3$, and the artificial eco-environment water use of $17\times10^8 m^3$, $20.9\times10^8 m^3$ should be constrained in year 2020 and 2030, respectively. Meanwhile, the amount of groundwater exploitation should be controlled below $188 \times10^8 m^3$ to $172 \times10^8 m^3$, and the amount of the surface fetched water should be increased from $230 \times10^8 m^3$ to $260 \times10^8 m^3$.

The code in the table 2 means that: OEG indicated as groundwater overexploitation; SWD indicated as surface water drawing; NEU indicated as national economy use; EEU is indicated as the eco-environment use; and WFS indicated as water flowing to sea.

Table 2. The controlling indices in the Hai River Basin scenarios. unit: $10^8 m^3$

Level year	ET_{max}	the OEG Amount*	the SWD Amount*	the NEU Amount*	the EEU Amount*	the WFS Amount*
2005	1661	248.7	135.6	381.1	3.5	43.1
2020	1675	187.5	230.2	400	17.14	71.13
2030	1685	171.9	260.2	410.9	20.9	86.4

Associating to the efficiency of water resources consumption (Wang et al., 2009), the consumption structure and the consumption efficiency will be improved. It can be seen in Table 3 and Table 4, soil water in the unsaturation zone is the maximum consumption, accounting to the 72% of the total evapotranspiration amount. Compared with the consumption structure of the benchmark year, the water resources consumption structure will appeared to be following evolution character where the decreasing of groundwater utilization

©2017, IAHR. Used with permission / ISSN 1562-6865 (Online) - ISSN 1063-7710 (Print)

amount, and increasing of the surface water utilization, as well as the increasing the transpiration in soil water consumption will be studied. For the efficiency of water resources consumption, comparing with that of the benchmark level year, the amount of the high efficiency consumption increases and the low efficiency consumption and non-production decreases

In general, the groundwater over-exploitation will be rationally controlled by constrain that are available for water amount with improve to the consumption efficiency of the soil water resources. The land ecology under the total controlling amount of water resources utilization also was improved.

Table 3. Water resource consumption structure in the Hai River Basin in the different period. unit: mm

Level year	The Evaporation (E)of Interception Water Amount		The Evapotranspiration(ET) of The Soil Water and Groundwater				
	Impervious area	Pervious area	Forest land T	Grass land T	Farm field T	Soil E	Total ET
2005	7.6	110.5	47.1	30.1	126.3	152.2	355.7
2020	7.6	110.2	47.4	30.1	122.0	149.6	349.1
2030	7.3	122.6	52.7	30.0	123.5	139.0	345.2

Table 4. The analysis of the water resource consumption efficiency in the Hai River Basin. unit:10^8m^3

Level year	The no-controllable ET	The Controllable Consumption(ET)				The Ratio of Different ET to The Total ET		
		The total ET	Productive High efficiency*	Productive low efficiency*	No-productive*	High efficiency	Low-efficiency	No-productive
2005	571.40	1085.44	489.41	496.06	99.97	45.09	45.70	9.21
2020	629.70	1016.12	463.72	443.95	108.46	45.64	43.69	10.67
2030	632.72	1043.38	473.43	445.66	124.30	45.37	42.71	11.91

5 CONCLUSIONS

The groundwater over-exploitation is serious under the joint action between the severe water shortage and the increasing demand of water resources in the Haihe River Basin. To rationally manage the limited water resources, this paper has put forward the five controlling indicators from the water supply sources and the water users, based on the maximum available consumption of water resources and consumption in the water cycle. To quantitatively determine these indicators in future, the 3 scenarios were set under the drought hydrological series from 1980 to 2005. Employing the dualistic model, the quantitative results of these indicators were obtained. The results have shown that the maximum available consumption of water resources were $1675\times10^8m^3$ and $1685\times10^8m^3$ in 2020 and 2030, respectively. Under the corresponding condition, water utilization of $400\times10^8m^3$ to $411\times10^8m^3$ for the national economy, and the total amount of the artificial eco-environmental water utilization of $17\times10^8m^3$ and $20.9\times10^8m^3$ should be strictly controlled. The amount of the surface water supply of $230\times10^8m^3$ and $260\times10^8m^3$, groundwater exploration will be reduced to $188\times10^8m^3$ and $172\times10^8m^3$ where this should be controlled in the planning year itself. Then, the serious situation of groundwater over-exploitation could be improved. At same time, the eco-environment also might be better by the rational allocation of water resources and the increase in the efficiency of water resources.

ACKNOWLEDGEMENTS

The authors express their sincere gratitude to all who provided help in the study. Supported by the National Basic Research Program of China (“973” project) (Grant No. 2006CB403404).

REFERENCES

Wang, Z.M. (2002). Target and Countermeasures of Water Ecological Environment Recovery in the Haihe River Basin (in Chinese). *China Water Resources*, 4, 12-13.

Han, P. & Zhou, Y.J. (2008). Water Resources Comprehensive Management in Haihe River Basin (in Chinese). *Haihe Water Resources,* 5, 4-7.

Jia, Y.W., Wang, H., Zhou, Z.H., You, J.J., Gan, Z.G., Qiu, Y.Q., Lu, C.Y. & Luo, X.Y. (2010). Development and Application of Dualistic Water Cycle Model in Haihe River Basin: I. Model Development and Validation (in Chinese). *Advance in Water Science,* 21(1), 1-8.

Wang, H., Yang, G.Y., Jia, Y.W. & Qin, D.Y. (2009). Study on Consumption Efficiency of Soil Water Resources in the Yellow River Basin Based on Regional ET Structure. *Science in China Series D: Earth Sciences*, 51(3), 456-468.

 ©2017, IAHR. Used with permission / ISSN 1562-6865 (Online) - ISSN 1063-7710 (Print)

DERIVATION OF AREAL REDUCTION FACTOR FOR STORM DESIGN APPLICATION IN MALAYSIA USING GRID-BASED APPROACHES

KAHHOONG KOK[1], WANSIK YU[2], LARIYAH MOHD SIDEK[3] & KWANSUE JUNG[4]

[1,4] Department of Civil Engineering, Chungnam National University, Yuseong-gu, Daejeon, Korea
kahhoong_kok@yahoo.com; ksjung@cnu.ac.kr
[2] International Water Resources Research Institute, Chungnam National University, Yuseong-gu, Daejeon, Korea
yuwansik@gmail.com
[3] Sustainable Technology & Environment Group, Institute for Energy Infrastructure,
Universiti Tenaga Nasional, Selangor, Malaysia
lariyah@uniten.edu.my

ABSTRACT

In this study, ARF estimations in Malaysia have been reviewed as some shortcomings were noticed in the existing technical manual. Apart from that, rainfall time series data are examined by several statistical tests to determine existence of trends and increasing trends are observed in the point of rainfalls and areal rainfalls especially for short rainfall interval. In this study, grid-based approach of Average-Point rainfall tracking method is adopted to compute the Maximum Areal Average Rainfall (MAAR). Average-Point rainfall tracking method improves the estimation of maximum areal rainfall by considering spatial and temporal distribution of a storm multilaterally. A slight increment was obtained from the ARF derived in this study when compared to the ARF presented in the existing technical manual. The increment could be explained by the changes of rainfall characteristics as concluded by the results obtained from the statistical tests done on the rainfall time series data. In conclusion, the ARF derived from this study offers the engineers or hydrologists in Malaysia with the updated information and references for storm design applications of local concerns as the outdated technical manual which was developed 30 years ago is still regarded by most of the local practitioners as the authoritative reference document.

Keywords: Areal reduction factor (ARF); change point test; trend test; average-point rainfall tracking method.

1 INTRODUCTION

Hydrological studies are the crucial procedures which cannot be omitted in any water resources management projects. Furthermore, Malaysia is located in a region with high rainfall intensity especially during the monsoon seasons which contributes to estimating an appropriate design of rainfall for a catchment area where it requires extra and careful considerations. Local practitioners always refer to *Water Resources Publication No.17: Variation of Rainfall with Area in Peninsular Malaysia* (DID, 1986) and *Review and Updated the Hydrological Procedure No.1: Estimation of Design Rainstorm in Peninsular Malaysia* (NAHRIM, 2010) as the guidelines for hydrological studies of local concerns. However, there are some shortcomings in these guidelines which need to be reviewed for the following reasons. The areal reduction factor (ARF) developed in *Water Resources Publication No.17: Variation of Rainfall with Area in Peninsular Malaysia* (DID, 1986) was based on the rainfall data recorded up to 1980 only. The latest rainfall data shall be included for the derivation of ARF in order to improve its practicability for the present use as present rainfall pattern and intensity may influence the climate change. Apart from that, the average length of records used in the analysis of the technical manual was less than 20 years and some were even less than 10 years. Thus, more data shall be used to improve the precision of the derivation with the aid of latest refined computation methods. In fact, the manual has been once reviewed in 2010 and the results are presented in *Review and Updated the Hydrological Procedure No.1: Estimation of Design Rainstorm in Peninsular Malaysia* (NAHRIM, 2010). However, the reviewed manual receives comments and was criticizes from the local practitioners that the derivation methods and the results are implausible. Thus, even though the results presented in the olden manual are outdated, the olden manual is still regarded by most of the local practitioners as the authoritative reference document for hydrological studies in Malaysia.

In view of the above discussion, it is thought that there is an urgent need to review the ARF estimation for the design of rainfall application in Malaysia. The objectives of this study are to review the existing ARF in Malaysia by incorporating more current data and latest computation methods as well as considering the changes in rainfall pattern and intensity. The final outcomes are to derive empirical formulae for ARF estimations and publish/distribute the results to the local practitioners for application of design rainfall in Malaysia.

©2017, IAHR. Used with permission / ISSN 1562-6865 (Online) - ISSN 1063-7710 (Print)

2 STUDY AREA AND RAINFALL TIME SERIES DATA

There are total 9 rainfall stations located in the vicinity of Kuala Lumpur and the rainfall time series data for interval of 1-hour, 3-hour, 6-hour, 12-hour, and 24-hour were extracted from these selected rainfall stations for the analysis of this study. All of the selected rainfall stations were able to provide data from year 1980-2015 and no missing data was observed during the study period. The information and the geographical coordinates of the rainfall stations are depicted in Table 1.

Table 1. Rainfall stations in Kuala Lumpur with their geographical coordinates.

Station Number	Station Name	Coordinates	
		Latitude	Longtitude
3116003	Pejabat JPS Malaysia	03° 09′ 05″N	101° 41′ 05″E
3116006	Ldg. Edinburgh Site 2	03° 11′ 00″N	101° 38′ 00″E
3117070	Pusat Penyelidikan JPS Ampang	03° 09′ 11″N	101° 44′ 56″E
3216001	Kg. Sg. Tua	03° 16′ 20″N	101° 41′10″E
3217001	Ibu Bekalan Km. 16	03° 16′ 05″N	101° 43′45″E
3217002	Empangan Genting Klang	03° 14′ 10″N	101° 45′10″E
3217003	Ibu Bekalan Km. 11	03° 14′ 10″N	101° 42′50″E
3217004	Kg.Kuala Seleh	03° 15′ 30″N	101° 46′05″E
3 317004	Genting Sempah	03° 22′ 05″N	101° 46′15″E

Fixed square boundaries of 100km^2, 196km^2, 484km^2, 784km^2, and 1024km^2 were plotted for computation of areal rainfalls for the respective fixed boundary area. Square boundary was preferred rather than circular boundary as it was convenient to compute the maximum areal rainfall for square fixed area using Average-Point tracking method. Actually, it had been suggested in the previous research (Bell,1976) that it may be worthwhile to carry out further ARF researches on non-circular fixed areas. The fixed boundaries and the contained rainfall stations for each fixed boundary are illustrated in Figure 1.

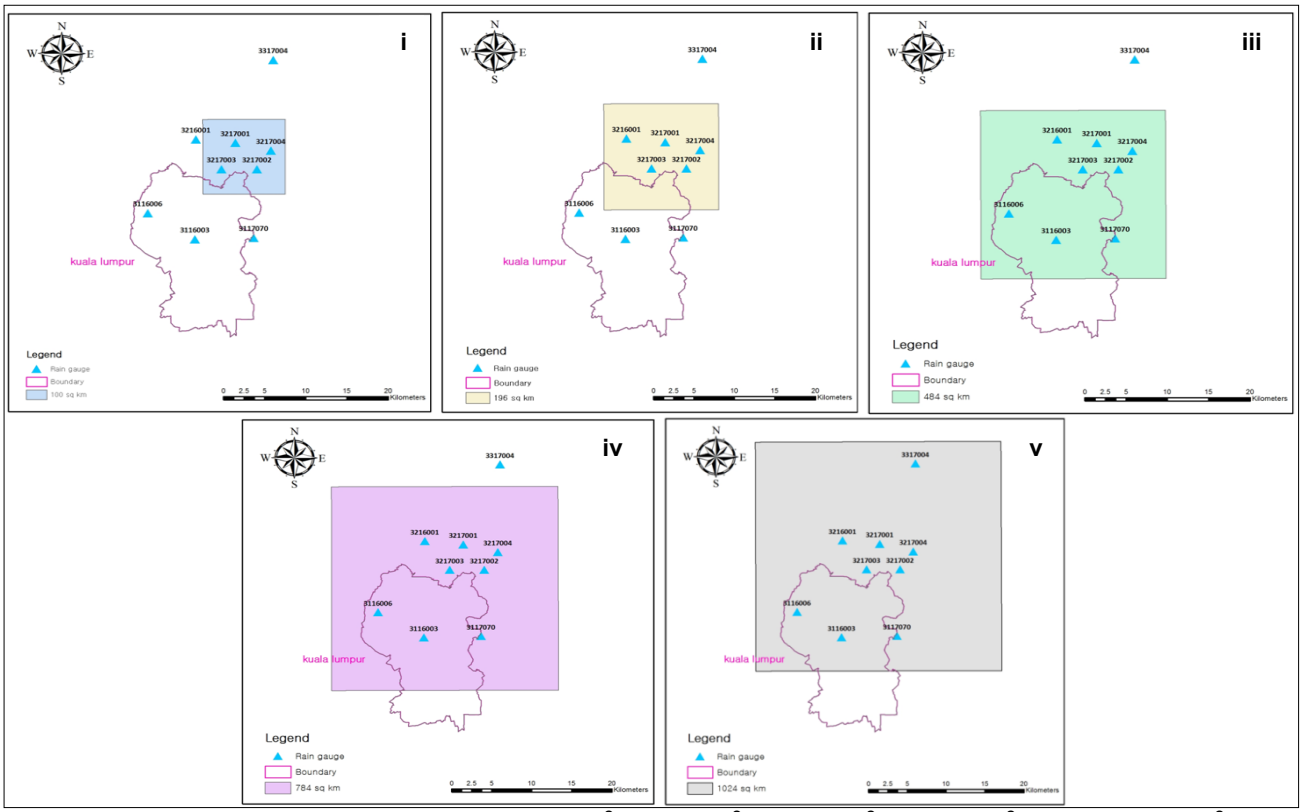

Figure 1. Fixed square boundaries of 100km^2(i), 196km^2(ii), 484km^2(iii), 784km^2(iv), and 1024km^2(v).

 ©2017, IAHR. Used with permission / ISSN 1562-6865 (Online) - ISSN 1063-7710 (Print)

3 ANALYSIS ON RAINFALL TIME SERIES DATA

Change point tests and trend tests had been conducted on the rainfall time series data of different intervals in order to identify any changes on the rainfall data statistically. 36 years of annual maximum rainfall data for intervals of 1-hour, 3-hour, 6-hour, 12-hour, and 24-hour were retrieved from each rain gauge station within the study area. We strived to conduct the statistical tests for the collected rainfall data which are at least 30 years or above in order to meet the requirement of central limit theorem.

Change points are times of discontinuities in a time series that can be induced from changes in observation locations, equipment, measurement techniques, environmental changes and so on (Reeves et al., 2006). However, it was assumed that the rainfall time series data in this study were quality guaranteed which implies that the possibility of changes or trends detected in the observed rainfall time series due to anthropogenic and equipment errors was very low. Change point tests were also known as absolute homogeneity tests as they are performed to identify the homogenous characteristic of the time series data as well as to detect breaks in the time series data. Four statistical tests were conducted to identify any change points or breaks of the rainfall time series data in this study which are *Buishand range test, Standard Normal Homogeneity Test (SNHT), Pettitt test, and von Neumann ratio test*. The first three tests were able to identify years that may contain breaks whereas the last only allows estimation of presence of breaks within a time series (Hawkins, 1977). The results of the change point tests were classified according to Schonwiese and Rapp (1977) and Wijngaard et al. (2003). There are three classes which are class 1(useful), class 2(doubtful), and class 3(suspect). The descriptions of each of the category are depicted in Table 2.

Table 2. Classification of change point test.

Class	Description	Remark
1	One or zero test rejects the null hypothesis. No clear signal of an inhomogeneity in the time series data is apparent.	Useful
2	Two tests reject the null hypothesis. Indications are present for an inhomogeneity of a magnitude that exceeds the level expressed by the inter-annual standard deviation of the time series data.	Doubtful
3	Three tests reject the null hypothesis which indicates that high possibility that an inhomogeneity is present that exceeds the level expressed by the inter-annual standard deviation of the time series data. This indicates there may be some changes in the time series data.	Suspect

The trend of the rainfall time series data in this study was investigated through performing the *Mann-Kendall test* which requires distribution-free input data which was less sensitive to outliers than other alternative methods. This test had been widely recommended by the World Meteorological Organization (WMO) for public application (Mitchell et al., 1996). If increasing or decreasing trend is detected for a rainfall time series data, its mono-trend magnitude will be determined by *Theil* and *Sen's* Slope Estimator which is a non-parametric median based slope estimator proposed by Theil (1950) and Sen (1968) and extended by Hirsch et al. (1982).

4 ESTIMATION OF MAXIMUM AVERAGE AREAL RAINFALL (MAAR)

Rainfall tracking method was applied to compute the maximum average areal rainfall (MAAR) instead of the conventional *Thiessen polygon* method for the pre-specified fixed catchment area in this study. The MAAR estimated from the tracking method was used to derive the ARF for the respective catchment areas and rainfall intervals by dividing it to maximum point rainfall. There are three kinds of tracking methods: Box (B), Point (P), and Average-Point (AP) rainfall tracking method. These tracking methods are able to consider actual temporal and spatial distribution of rainfall more accurately and thus enhancing the accuracy of MAAR. The main theory behind the rainfall tracking method is the "sub-duration". The concept of "sub-duration" is introduced to explain the accumulated duration which was needed to estimate the probable maximum rainfall per accumulated area. This concept was introduced as rainfall distribution is always changing according to the duration and thus the interval of duration plays an important factor in estimating the altering rainfall distribution. An interested duration of rainfall may consist of several numbers of sub-duration. The number of sub-duration can be obtained by applying Eq. [1].

$$S^{D}_{Trackingmethod} = 1,...,L-D \qquad [1]$$

where *L* is the interested total interval of rainfall (total rainfall event period), *D* is the sub-duration, and *S* is the number of sub-duration. The number of sub-duration ranges from 1 to *L-D* for each total interval of rainfall. According to Shin (2013), Point tracking outperformed Box tracking and Average-Point tracking method

©2017, IAHR. Used with permission / ISSN 1562-6865 (Online) - ISSN 1063-7710 (Print)

yielded most promising results and thus it was recommended for computing MAAR over the studied catchment area. Average-Point tracking method is applied to estimate MAAR in this study. Actually, Average-Point tracking is the combination of Point tracking and Box tracking. It combines the merits of both methods and gets rid of the demerits from both methods. Its basic is same with Point tracking but additional concept of averaging is introduced into the Point tracking procedures.

Point tracking is a 3-dimensional tracking method which considers all the grids contained within the catchment area. Firstly the catchment area is divided into rows and columns of small grids with grid size of 1km x 1km. Grid size of 1km x 1km was recommended by Shin (2013) for Point tracking analysis as it was found that the MAAR might be over-estimated for smaller grid size (less than 1km^2). Each grid contains a rainfall value which is interpolated from the observed rainfall data (rain gauges) within the catchment area. Interpolation method of Inverse Distance Squared Weighting (IDW2) was applied to interpolate the observed rainfall data over the catchment. Then an initial grid cell with the MAAR value is searched throughout the area (spatially) as well as the designated sub-durations (temporally) as a starting point. After that, the cell adjoining below, above, right, and left from the starting point was searched again for all sub-durations simultaneously to locate the 2nd MAAR cell. This iteration was performed until all the grid cells within the catchment have been considered. The description of Point tracking is illustrated in Figure 2.

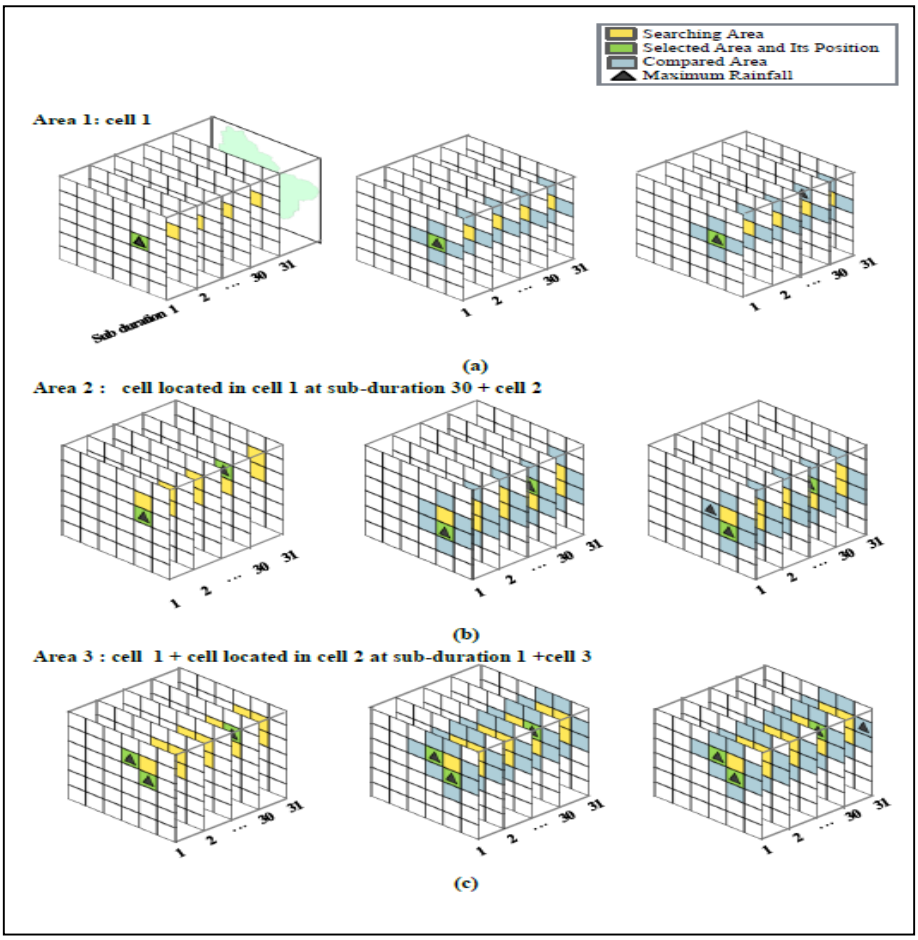

Figure 2. Illustration of 3-dimensional Point tracking method (Shin, 2013).

Maximum of 3 storm centers is available for analysis using Average-Point tracking. However, only 1 storm center is possible for analysis using Point tracking. In other words, it was assumed that maximum of 3 grid cells have the possibility to be the storm centers in Average-Point tracking which implies that Average-Point tracking aims to search a convex surface of the rainfall data physically at the grid-cells which is over the average rainfall in each sub-duration when the z-axis is rainfall. The 3 storm centers grid cells were filtered through the condition of the cells which have rainfall value larger than the adjoining 8 cells provided that the distance between the storm centers to be greater than 5km. Figure 3 shows the illustration of Average-Point tracking method. The computer program which was developed using FOTRAN (Shin, 2013) is applied to perform the calculations of Average-Point tracking.

 ©2017, IAHR. Used with permission / ISSN 1562-6865 (Online) - ISSN 1063-7710 (Print)

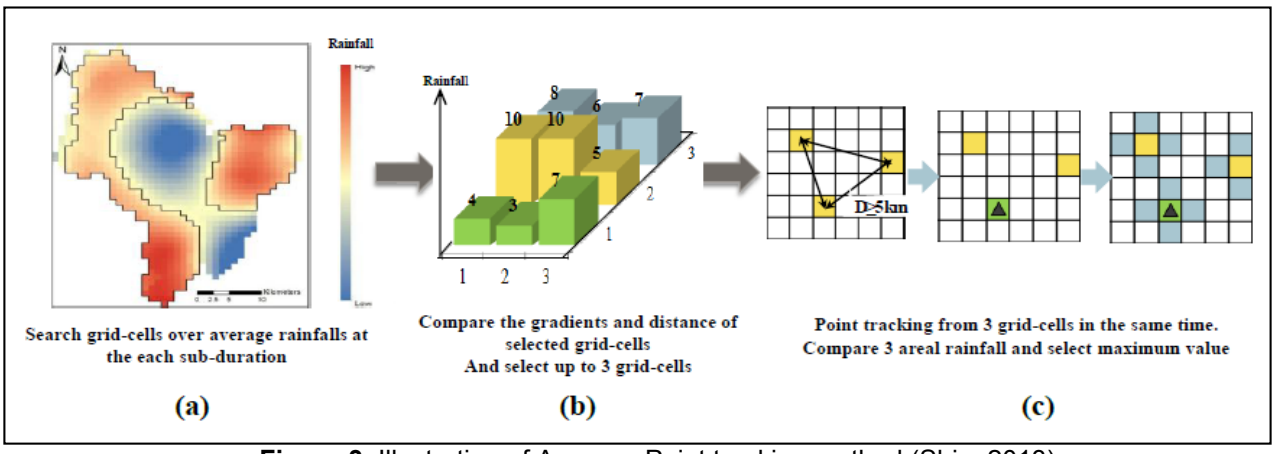

Figure 3. Illustration of Average-Point tracking method (Shin, 2013).

5 DERIVATION OF AREAL REDUCTION FACTOR

In this study, the derivation procedures of USWB (1957) using fixed area method were adopted to compute the ARF. Firstly, the annual maximum areal rainfall for particular fixed area boundary and storm duration as well as the annual maximum point rainfalls were observed from each rain gauge within that fixed area boundary were determined also. The annual maximum areal rainfall (R_a) was computed from Average-Point tracking method as mentioned in the previous section while the annual maximum point rainfall (R_p) for the same boundary and storm duration was obtained by averaging the annual maximum point rainfall recorded in each rain gauge located within the boundary. And ARF for a certain year was estimated by dividing the annual maximum areal rainfall (R_a) of that year to the annual maximum point rainfall (R_p) of the identical year which was expressed in Eq. [2]. Finally, same procedures were executed to obtain ARF for other years and obtaining grand average of ARF for the whole study period.

$$ARF = \frac{R_a}{R_p} \qquad [2]$$

6 RESULTS AND DISCUSSIONS

The results of *Mann-Kendall test* for different rainfall intervals were depicted in Table 3-5. The number of stations showing increasing trend decreased as the rainfall interval increased. For 1-hour rainfall interval, 6 out of 9 selected stations showed statistically significant increasing trend while only 2 stations were showing increasing trend for 3 and 6-hour rainfall interval. The *Mann-Kendall* tests results tell that increasing trend of annual maximum rainfall diminished as rainfall interval increased. The magnitude of increasing trend was also depicted in Table 3-5 by the *Sen's Slope*. For 1-hour rainfall interval, maximum rate of 1 mm/year was estimated for station 3217002 and minimum rate of 0.4 mm/year was estimated for station 3116003. These results could tell us that total increment of 36 mm was estimated for station 3217002 if a mono increasing trend was considered for the study period of 36 years. These findings are similar to the findings that concluded from IPCC which stated that increasing rainfall extremes have been observed for short rainfall duration in some parts of the world (IPCC, 2007).

Table 3. *Mann-Kendall test* results for 1-hour rainfall interval.

Station Number	Station Name	*P*-value	α-value	Trend	*Sen's Slope*
3116003	Pejabat JPS Malaysia	0.039	0.05	Increasing	0.414
3116006	Ldg. Edinburgh Site 2	0.001	0.05	Increasing	0.700
3117070	Pusat Penyelidekan JPS Ampang	0.039	0.05	Increasing	0.500
3216001	Kg. Sg. Tua	0.089	0.05	No trend	-
3217001	Ibu Bekalan Km. 16	0.014	0.05	Increasing	0.515
3217002	Empangan Genting Klang	< 0.0001	0.05	Increasing	1.000
3217003	Ibu Bekalan Km. 11	0.012	0.05	Increasing	0.704
3217004	Kg.Kuala Seleh	0.094	0.05	No trend	-
3317004	Genting Sempah	0.134	0.05	No trend	-

©2017, IAHR. Used with permission / ISSN 1562-6865 (Online) - ISSN 1063-7710 (Print)

Table 4. *Mann-Kendall test* results for 3-hour rainfall interval.

Station Number	Station Name	*P*-value	α-value	Trend	*Sen's Slope*
3116003	Pejabat JPS Malaysia	0.196	0.05	No trend	-
3116006	Ldg. Edinburgh Site 2	0.0027	0.05	Increasing	0.936
3117070	Pusat Penyelidekan JPS Ampang	0.105	0.05	No trend	-
3216001	Kg. Sg. Tua	0.089	0.05	No trend	-
3217001	Ibu Bekalan Km. 16	0.06	0.05	No trend	-
3217002	Empangan Genting Klang	0.002	0.05	Increasing	1.010
3217003	Ibu Bekalan Km. 11	0.429	0.05	No trend	-
3217004	Kg.Kuala Seleh	0.070	0.05	No trend	-
3317004	Genting Sempah	0.165	0.05	No trend	-

Table 5. *Mann-Kendall test* results for 6-hour rainfall interval.

Station Number	Station Name	*P*-value	α-value	Trend	*Sen's Slope*
3116003	Pejabat JPS Malaysia	0.414	0.05	No trend	-
3116006	Ldg. Edinburgh Site 2	0.014	0.05	Increasing	0.833
3117070	Pusat Penyelidekan JPS Ampang	0.301	0.05	No trend	-
3216001	Kg. Sg. Tua	0.068	0.05	No trend	-
3217001	Ibu Bekalan Km. 16	0.016	0.05	No trend	-
3217002	Empangan Genting Klang	0.026	0.05	Increasing	0.902
3217003	Ibu Bekalan Km. 11	0.935	0.05	No trend	-
3217004	Kg.Kuala Seleh	0.072	0.05	No trend	-
3317004	Genting Sempah	0.258	0.05	No trend	-

Same results were observed for the change point tests. Table 6 shows that 7 out of 9 stations showed statistically significant inhomogeneous characteristics for the 1-hour rainfall interval. All of them were classified as 'suspect' which mean that at least 3 of the statistical tests rejected the null hypotheses and accepted the alternative hypotheses. In other words, it was very likely that change points occurred in the time series data. Table 7-8 depicts the change point tests results for rainfall interval of 3-hour and 6-hour. Again, the results are same with the Mann-Kendall test. The inhomogeneous characteristics diminished as the rainfall interval increased. Figure 4 illustrates the change point tests of 1-hour rainfall interval for station 3116006 and station 3217002. It could be observed from the figures that the change point occurred on 1995 for both stations for rainfall interval of 1-hour.

Table 6. Change point test results for 1-hour rainfall interval.

Station Number	Station Name	*P*-value				Class
		Buishand	*SNHT*	*Pettitt*	*Von Neumann*	
3116003	Pejabat JPS Malaysia	0.104	0.273	0.101	0.932	Useful
3116006	Ldg. Edinburgh Site 2	< 0.0001	< 0.001	< 0.0001	0.0031	Suspect
3117070	Pusat Penyelidekan JPS Ampang	0.007	0.018	0.005	0.088	Suspect
3216001	Kg. Sg. Tua	0.014	0.034	0.017	0.061	Suspect
3217001	Ibu Bekalan Km. 16	0.007	0.024	0.008	0.035	Suspect
3217002	Empangan Genting Klang	< 0.0001	< 0.001	< 0.0001	0.001	Suspect
3217003	Ibu Bekalan Km. 11	0.001	0.005	0.003	0.095	Suspect
3217004	Kg.Kuala Seleh	0.027	0.207	0.014	0.012	Suspect
3317004	Genting Sempah	0.233	0.487	0.153	0.020	Useful

Table 7. Change point test results for 3-hour rainfall interval.

Station Number	Station Name	*P*-value				Class
		Buishand	*SNHT*	*Pettitt*	*Von Neumann*	
3116003	Pejabat JPS Malaysia	0.396	0.523	0.422	0.866	Useful
3116006	Ldg. Edinburgh Site 2	0.0004	0.001	0.0002	0.083	Suspect
3117070	Pusat Penyelidekan JPS Ampang	0.040	0.096	0.05	0.060	Useful
3216001	Kg. Sg. Tua	0.093	0.326	0.063	0.06	Useful
3217001	Ibu Bekalan Km. 16	0.039	0.158	0.018	0.168	Doubtful
3217002	Empangan Genting Klang	0.005	0.011	0.003	0.171	Suspect
3217003	Ibu Bekalan Km. 11	0.159	0.372	0.160	0.160	Useful
3217004	Kg.Kuala Seleh	0.070	0.273	0.147	0.233	Useful
3317004	Genting Sempah	0.596	0.438	0.363	0.06	Useful

 ©2017, IAHR. Used with permission / ISSN 1562-6865 (Online) - ISSN 1063-7710 (Print)

Table 8. Change point test results for 6-hour rainfall interval.

Station Number	Station Name	*P*-value				Class
		Buishand	*SNHT*	*Pettitt*	*Von Neumann*	
3116003	Pejabat JPS Malaysia	0.423	0.640	0.546	0.793	Useful
3116006	Ldg. Edinburgh Site 2	0.002	0.0003	0.0007	0.193	Suspect
3117070	Pusat Penyelidekan JPS Ampang	0.178	0.425	0.236	0.160	Useful
3216001	Kg. Sg. Tua	0.194	0.380	0.166	20101	Useful
3217001	Ibu Bekalan Km. 16	0.135	0.198	0.069	0.330	Useful
3217002	Empangan Genting Klang	0.029	0.065	0.041	0.597	Doubtful
3217003	Ibu Bekalan Km. 11	0.352	0.683	0.356	0.099	Useful
3217004	Kg.Kuala Seleh	0.155	0.400	0.140	0.619	Useful
3317004	Genting Sempah	0.509	0.308	0.429	0.020	Useful

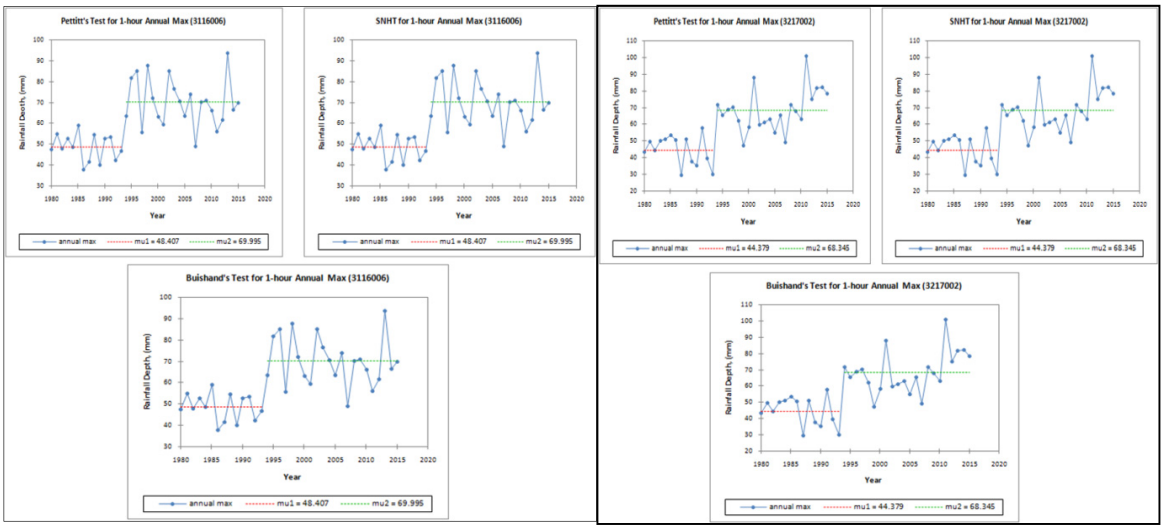

Figure 4. Change point tests of 1-hour rainfall interval for station 3116006 (left) and 3217002 (right).

It was also found that increasing trend was observed from the areal rainfall as they were computed from the point rainfall observed from the rainfall stations which showed increasing trends as discussed in the previous section. Without a doubt, the increasing trend also diminished as the rainfall interval increased. Thus, it could be concluded from the change point tests and trend test that there might be some changes for the rainfall observed in the study area which might influence the derivation of ARF as point rainfall and areal rainfall are the dependent variables for derivation of ARF.

Figure 5 shows the derived ARF diagrams for the study area by fitting the average annual ARF to the logarithmic curves. Table 9 depicts the derived ARF empirical formulae for different rainfall duration along with the coefficient of determinations for each empirical formula and the variable *x* represents the catchment area in km^2. The ARF for other rainfall durations can be interpolated from the empirical formulae listed in Table 9. As expected, the derived ARF increased as the rainfall interval increased. Apart from that, the gap between two curves is becoming smaller as the rainfall interval increased which tells us that ARF would not vary much for longer rainfall duration in the study area. Table 10 shows the comparisons of the ARF estimated from this study with the ARF presented in *Water Resources Publication No.17: Variation of Rainfall with Area in Peninsular Malaysia* (DID,1986). The comparisons were done for catchment area until 200km^2 as the manual only provided ARF values up to 200km^2. Therefore, the ARF presented in the manual might be over-estimated as they were derived from a small catchment area and also short rainfall time series data. Estimation of areal rainfall using *Thiessen Polygon* method in the manual might also cause over-estimation of ARF. However, a slight increment was observed from comparisons of all rainfall intervals. The increasing trends found in the point of rainfalls as well as the areal rainfalls could explain the slight increment found from the comparisons.

©2017, IAHR. Used with permission / ISSN 1562-6865 (Online) - ISSN 1063-7710 (Print)

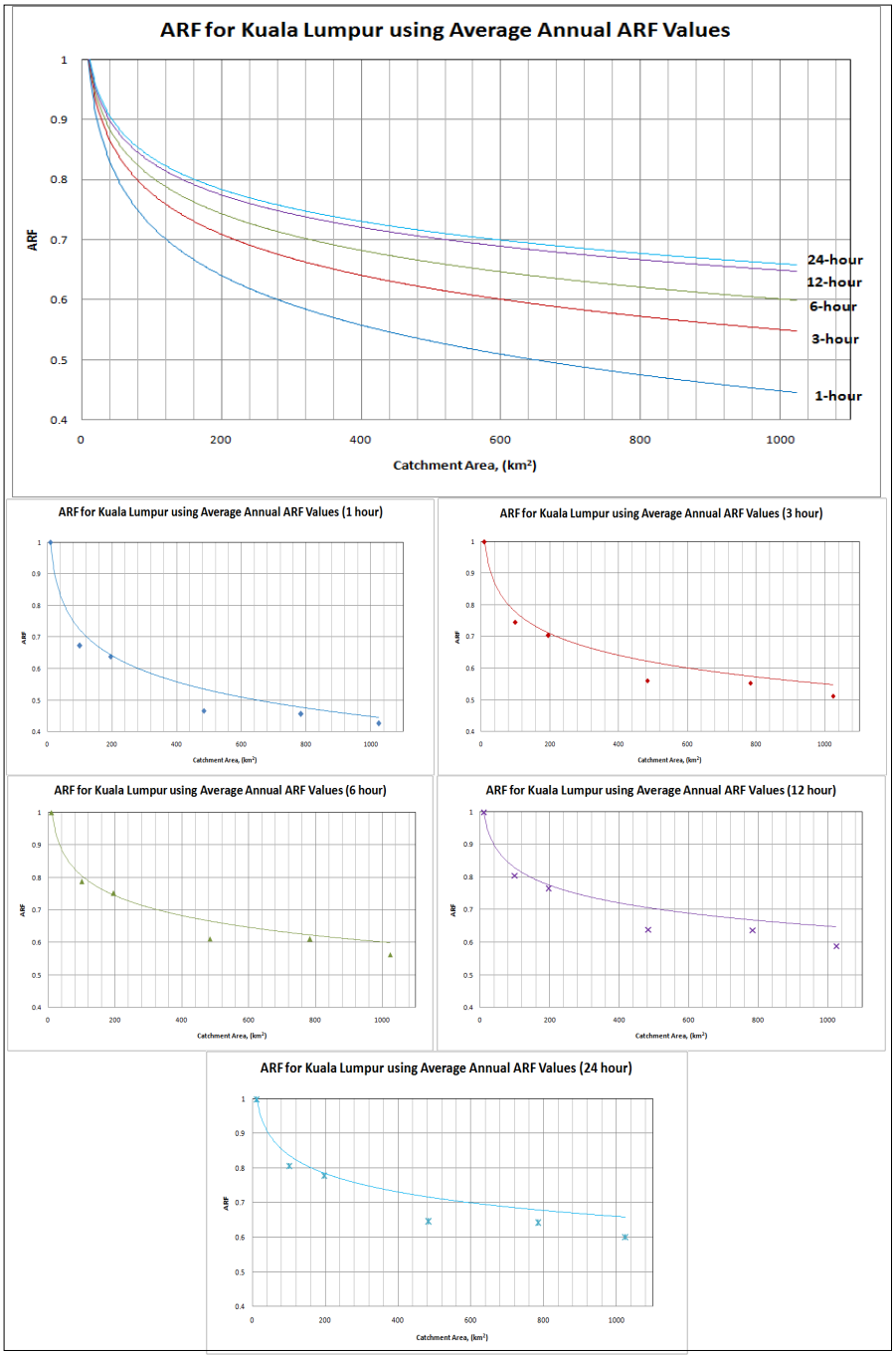

Figure 5. ARF diagrams for Kuala Lumpur using average annual ARF values.

Table 9. Derived ARF empirical formulae.

Rainfall Duration (hr)	Empirical formula	R^2
1	-0.12*lnx*+1.277	0.965
3	-0.10*lnx*+1.241	0.958
6	-0.09*lnx*+1.222	0.964
12	-0.08*lnx*+1.200	0.920
24	-0.08*lnx*+1.210	0.908

©2017, IAHR. Used with permission / ISSN 1562-6865 (Online) - ISSN 1063-7710 (Print)

Table 10. Comparisons of ARF (2016) with *Water Resources Publication No.17* (DID,1986).

Catchment area (km^2)	50		100		150		200	
Duration (hr)	*2016*	*1986*	*2016*	*1986*	*2016*	*1986*	*2016*	*1986*
1	0.81	0.79	0.72	0.70	0.68	0.64	0.64	0.63
3	0.85	0.83	0.78	0.75	0.74	0.72	0.71	0.70
6	0.87	0.86	0.81	0.79	0.77	0.75	0.75	0.74
12	0.89	0.87	0.83	0.80	0.80	0.77	0.78	0.76
24	0.90	0.88	0.84	0.81	0.81	0.79	0.79	0.78

7 CONCLUSIONS

The outdated ARF estimations presented in the olden technical manual have been reviewed by incorporating longer time series of latest rainfall data. Analysis on the point of rainfall time series data as well as the areal rainfall time series data indicated increasing trends especially for short rainfall intervals which eventually resulted in changes in ARF estimations as well. Average-Point rainfall tracking method which is able to consider spatial of temporal characteristics of rainfall storm has been applied in this study instead of conventional *Thiessen Polygon* method to compute the Maximum Average Areal Rainfall (MAAR) in order to increase the precision in estimating areal rainfall. Since increasing trends are observed in the rainfall time series data, the reviewed empirical formulae for ARF estimations yield higher values than the previous ARF estimations listed in the olden technical manual. Further studies will be continued on derivation of ARF using remote sensing equipment such as precipitation radar and satellite in estimation of areal rainfall.

ACKNOWLEDGEMENTS

This research is supported by a grant (16AWMP-B079625-03) from Water Management Research Program funded by Ministry of Land, Infrastructure and Transport of Korean government.

REFERENCES

Bell, F.C. (1976). *The Areal Reduction Factor in Rainfall Frequency Estimation*, Institute of Hydrology, Report No 35, Swindon, UK, Natural Environment Research Council.

Department of Irrigation and Drainage Malaysia (DID). (1986). *Variation of Rainfall with Area in Peninsular Malaysia,* Water Resources Publication No.17.

Hawkins, D.M. (1977). Testing a Sequence of Observations for a Shift in Location. *Journal of the American Statistical Association*, 72(357), 180-186.

Hirsch, R.M., Slack, J.R. & Smith, R.A. (1982). Techniques of Trend Analysis for Monthly Water Quality Data. *Water Resour. Res.,* 18(1), 107-121.

IPCC. (2007). *Understanding and Attributing Climate Change*. In Climate Change 2007, The Physical Science Basis. Contribution of Working Group I to the Fourth Assessment Report of the Intergovernmental Panel on Climate Change. Cambridge University Press, Cambridge, United Kingdom and New York, NY, USA.

Mitchell, J.M., Dzezerdzeeskii, B., Flohn, H., Hofmeyer, W.L., Lamb, H.H., Rao, K.N. & Wallen, C.C. (1966). *Climate Change.* WMO Technical Note 79, WMO No. 195, TP-100, World Meteorological Organization (WMO), Geneva, 79.

National Hydraulic Research Institute of Malaysia (NAHRIM). (2010). *Estimation of Design Rainstorm in Peninsular Malaysia*, Review and Updated the Hydrological Procedure No.1, Department of Irrigation and Drainage Malaysia.

Reeves, J., Chen, J., Wang, X.L., Lund, R., Lu Q.Q. (2007). A Review and Comparison of Change Point Detection Techniques for Climate Data. *Journal of Applied Meteorology and Climatology*, 46(6), 900-915.

Schonwiese, C.D., Rapp, J. (1997). Climate Trend Atlas of Europe Based on Observation 1891-1990. *International Journal of Climatology,* 18, 580-598.

Sen. P.K. (1968). Estimates of the Regression Coefficients Based on Kendall's Tau. *Journal of the American Statistical Association*, 63(324), 1379-1389.

Shin, Y.A. (2013). Grid-Based Spatial and Temporal Approaches to Depth-Area-Duration Rainfall Analysis, *MSc Thesis*. Department of Civil and Earth Resources Engineering, Kyoto University.

Theil, H. (1950). A Rank Invariant Method of Linear and Polynomial Regression Analysis. Part III, *Proceeding of the Royal Netherlands Academy of Sciences*, 53, 1397-1412.

United States Weather Bureau (USWB). (1957). Rainfall Intensity-Frequency Regime. Technical paper 29, United States Department of Commerce, Washington DC.

Wijngaard, J.B., Klein, T.M. & Konnen, G.P. (2003). Homogeneity of 20th Century European Daily Temperature and Precipitation Series. *International Journal of Climatology*, 23(6), 679-692.

©2017, IAHR. Used with permission / ISSN 1562-6865 (Online) - ISSN 1063-7710 (Print)

Proceedings of the 37th IAHR World Congress
August 13 – 18, 2017, Kuala Lumpur, Malaysia

PREDICTING THE COMBINED EFFECT OF CLIMATE CHANGE AND RAPID URBANIZATION ON WATER QUALITY OF PASIG-MARIKINA RIVER, MANILA

PANKAJ KUMAR [(1)*], YOSHIFUMI MASAGO [(2)], BINAYA KUMAR MISHRA [(3)], AMMAR RAFIEIEMAM [(4)] & KENSUKE FUKUSHI [(5)]

[(1, 2, 3, 4)] United Nations University – Institute for the Advanced Study of Sustainability, Tokyo, Japan;
[(5)] Integrated Research System for Sustainability Science, University of Tokyo
kumar@unu.edu

ABSTRACT

Considering the finite volume of fresh water resources, managing its quality and quantity sustainably is one of the greatest challenges because of the complex global changes. This work strives to predict the combined effect of urbanization and climate change on water quality in Pasig-Marikina River considering its criticalities to develop proactive plan by policy makers working in water sectors. Pasig-Marikina River is an important source of water for different usage, viz., domestic, industrial, agriculture and recreation in the National Capital Region (NCR) in Philippines. However, rapid urbanization and weak/non-structured government policies result in severe pollution, making a long section of the river unsuitable for any use in recent past. Therefore presenting a comprehensive spatio-temporal status of river water quality will be valuable to guide and implement better management policies within governance structure. In this study, status of water quality of the Pasig-Marikina River was analyzed for current and future timescale using population growth, land use change, wastewater production and treatment scenarios. Water Evaluation and Planning (WEAP) model was used to model river pollution scenarios. Five indicators that are important for aquatic ecosystem health, viz., Dissolved Oxygen (DO), Biochemical Oxygen Demand (BOD), Chemical Oxygen Demand (COD) and Nitrate (NO3), were simulated to assess river pollution. Water quality simulation was done along a 25 km stretch of the Pasig River from downstream of the Napindan/C6 to Manila Bay. Comparison of simulated water quality parameters for the year 2015 and 2030 with 2011 (base year) clearly indicates that the water quality at 2030 will rapidly deteriorate and will be not suitable for any aquatic life in terms of major of water quality parameters. Current planned wastewater treatment plants and policies are not sufficient enough for sustainable water resource management within NCR, Philippines and hence a call for immediate and inclusive action.

Keywords: River pollution; wastewater management; water quality modelling; Manila.

1 INTRODUCTION

Water is the vital natural resource with social and economical value for human being (Hanemann et al., 2006). At present around the globe, more than 1.1 billion people have inadequate access to clean drinking water (Pink, 2016). On the other hand, population growth, urbanization, economic development and rapid urbanization put constant and tremendous amount of pressure on water resources and their ecosystems (Alcamo et al., 2007). Degradation of the urban water environment is a challenging issue in developing nations despite the adoption of a number of countermeasures (Ismail and Abed, 2013; Purandara et al., 2011). Asian economies have shown impressive growth and rapid urbanization. By 2050, more than half of Asian population (approximately 3 billion) will be living in towns and cities, particularly in secondary cities. This is roughly twice the current population of 1.6 billion. The demands on water, land, and ecosystems as resources pose significant challenges in the delivery of commodities like food, energy, and water for municipal and industrial purposes. The expected impacts of climate change will further exacerbate the challenges, which are faced by planners and providers of such services. Delivery of sustainable water supply and sanitation services in growing towns and cities remains an issue. Considering the water stress and scarcity, United Nations and its associated members have unanimously called for sustainable water resource management (both quality and quantity) (Jenson, 2016).

However, the recognition of water management and climate change as multidimensional and multi-scalar concerns (Downing, 2012; Meinke et al., 2009) is the evidence of the need to integrate biophysical and social aspects looking at environmental and human contexts. In line with this, varied types of integrated modeling frameworks have been developed to address the different scales and the different dimensions of climate change, water and agriculture. Trying to better represent socio-economic issues, hydro-economic modeling has been extensively used along the last decades as a prominent tool for guiding and implementing water policy decisions (Blanco-Gutiérrez et al., 2013; Brouwer and Hofkes, 2008; Heinz et al., 2007). Mathematical models are widely used to simulate the pollution of water bodies for likely wastewater production and treatment scenarios (Deksissa et al., 2004). In case of countries with limited financial resources, for any water

 ©2017, IAHR. Used with permission / ISSN 1562-6865 (Online) - ISSN 1063-7710 (Print)

quality model to be useful, it should not be data intensive or complex to operate. The Water Evaluation and Planning model (WEAP), a decision support system of the Stockholm Environmental Institute, is widely used for integrated water resource planning and management (Sieber and Purkey, 2011). The WEAP hydrology module enables estimation of rainfall-runoff and pollutant travel from a catchment to water bodies (Ingol-Blanco and McKinney, 2013) using different scenarios. A variety of applications of WEAP for water quality modelling and ecosystem preservation have been reported previously in many studies (Slaughter et al., 2014; Assaf and Saadeh, 2008).

Manila, Capital of The Philippines, is the top contributor to the national economy. Metro Manila's population is one of the largest in the Asia Pacific Region and in the world. According to a World Bank Study (WB, 2015), Metro Manila is the 3rd largest urban agglomerations in terms of population in East Asia, excluding China. With very high GDP growth at an average rate of 7% and uncoordinated rapid urban expansion, inadequate wastewater treatment facilities and the fragile institutional capability of the concerned agencies; a huge amount of wastewater is generated, causing deterioration of surface water resources. The other problem is the rapid change of land development (from vegetation into built-up areas) around the Pasig-Marikina-San Juan River Basin area during the last three decades resulting in exaggeration in water quality deterioration and frequency of extreme weathers. So far, very few studies have addressed the status of water resources and their management strategies for the near future. Considering the facts stated above, this work intends to assess the current situation and simulated future outlook with regard to pollution in the Pasig-Marikina-San Juan River Basin area and ultimately aims to help formulate sustainable water resource management options for the area.

2 STUDY AREA

The Metropolitan Manila (Metro Manila), otherwise known as the National Capital Region (NCR), is located at 14°40' N 121°3 E. It is bounded by the Manila Bay in the west, the Laguna de Bay in the south-east, the Sierra Madre Mountain Range in the east and the fertile plains of Central Luzon in the north (Figure 1). Metro Manila has a total land area of 63,600 hectares, approximately 0.21 % of the country's land area of 30 million hectares. Based on the 2015 census of population, Metro Manila registered a population of 12,877,253 accounts for about 15% of the national population. NCR remains to be the most densely populated region in the country. With 186 persons per hectare, NCR is more than 60 times denser than at the national level. Population density changes during ten years between 2000 and 2010 are shown in figure 2. Metro Manila features a tropical wet and dry climate that borders on a tropical monsoon climate. Like the rest of the Philippines, it lies entirely within the tropics. The average temperature during the cold months of December to February is 26.1º C, while that of during the hot months of March to May is 28.8ºC. It has a distinct, though relatively short dry season from January through April, and relatively lengthy wet season from May through December with an annual average precipitation of 2670 mm (PAGASA, 2011).

Located at the mouth of the Pasig River, Metro Manila is generally flat with average elevation of about 10 meters on its western part. Five river systems, which traverse Metro Manila, are Marikina River, San Juan River, Parañaque River, Pasig River and Navotas-Malabon-Tullahan-Tenejeros (NMTT) River. Pasig River, NCR's principal river, extends from the largest freshwater lake in Southeast Asia which is Laguna Lake (Laguna de Bay), located in the south eastern part of Metro Manila. It drains at Manila Bay in the west, virtually bisecting the metropolis horizontally. It has a total length of 25 km and is a tidal estuary. Both the Marikina and San Juan Rivers are major tributaries of the Pasig River (Figure 3).

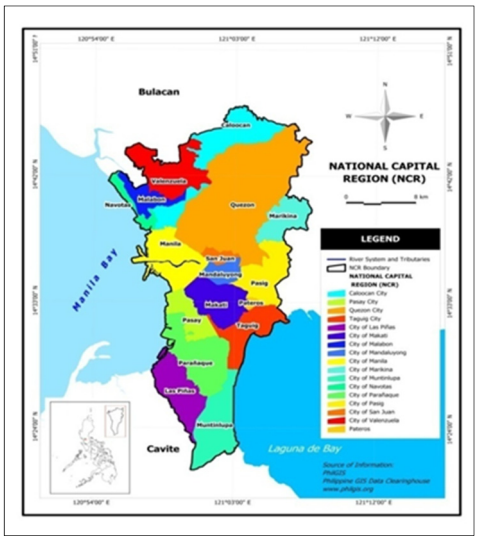

Figure 1. Administrative boundary of Metro Manila.

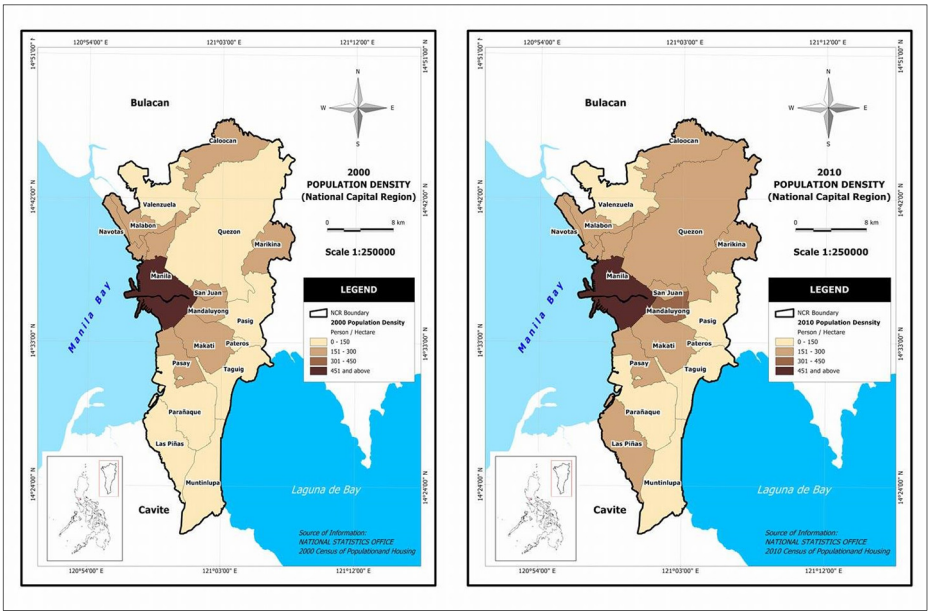

Figure 2. Population density map showing trends of population growth in Metro Manila (2000-2010).

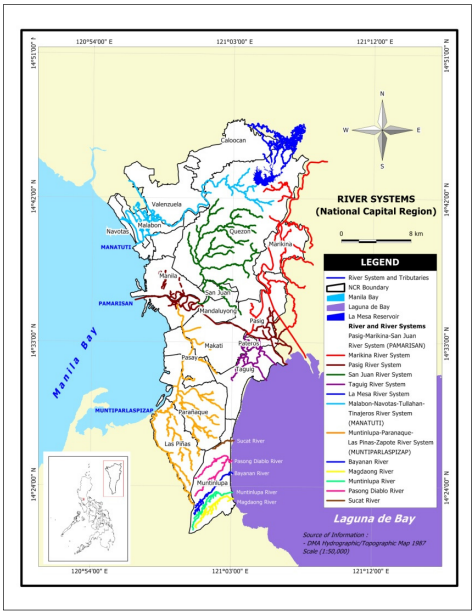

Figure 3. Map showing drainage pattern in Metro Manila.

3 METHOD

3.1 Basic information about model and data requirements

The WEAP model is used to simulate future total water demand and water quality variables in 2030 and it is useful for assessing alternative management policies in the Pasig-Marikina-San Juan River Basin. Water quality modelling requires a wide range of input data including: point and non-point pollution sources, their locations and concentrations; past spatio-temporal water quality; wastewater treatment plants (Department of Environment and Natural Resources (DENR)); historical rainfall; evaporation; temperatures (Philippine Atmospheric, Geophysical and Astronomical Service Administration (PAGASA)); drainage network (Metropolitan Waterworks and Sewerage System (MWSS)); river flow-stage-width relationships; river length; water quality at head flows; groundwater; surface water inflows and land-use/land-cover (National Water Resource Board (NWRB)). Different hydroclimatic data (monthly rainfall, air temperature, relative humidity and wind velocity) were collected for the period 1980 to 2016 and were used for model set up. Daily average stream flow data from 1984 to 2016 measured at five stations (namely Napindan, Bambang Bridge, Nagtahan Bridge, Jones Bridge and Manila Bay at Pasig River) was utilized to calibrate and validate the WEAP hydrology module simulation. Data (collected from both the local Manila government and measured at seven different locations along the Pasig River) of important water quality indicators (BOD, COD and NO_3) were

 ©2017, IAHR. Used with permission / ISSN 1562-6865 (Online) - ISSN 1063-7710 (Print)

used for water quality modelling.

A Water Evaluation and Planning (WEAP) model application was developed for the Pasig-Marikina-San Juan River Basin, having seven command areas with inter-basin transfers. Hydrologic modelling requires the entire study area to be split into smaller catchments with consideration for confluence points, physiographic and climatic characteristics. The WEAP hydrology module computes catchment surface pollutants generated over time by multiplying runoff volume and concentration or intensity of different types of land use. During simulation, land use information was broadly categorized into three categories viz.: agricultural, forested, and built-up areas. Soil data parameters were identified using previous secondary data and literature (Clemente et al., 2001).

3.2 Stream water quality modelling

The water quality module of the WEAP tool makes it possible to estimate pollution concentrations in water bodies and is based on the Streeter–Phelps model. In this model, two processes govern the simulation of oxygen balance in a river: consumption by decaying organic matter and reaeration induced by an oxygen deficit (Sieber and Purkey, 2011). BOD removal from water is a function of water temperature, settling velocity, and water depth Eq. [1 to 4]:

$$BOD_{final} = BOD_{init} \exp^{\frac{-k_{rBOD}L}{U}} \quad [1]$$

$$\text{Where, } k_{rBOD} = k_{d20}^{1.047(t-20)} + \frac{v_s}{H} \quad [2]$$

where, BOD_{init} = BOD concentration at the beginning of reach (mg/l), BOD_{final} = BOD concentration at the end of reach (mg/l), t = water temperature (in degrees Celsius), H = water depth (m), L= reach length (m), U = water velocity in the reach, v_s = settling velocity (m/s), k_r, k_d and k_a = total removal, decomposition and aeration rate constants (1/time), k_{d20} = decomposition rate at reference temperature (20° Celsius). Oxygen concentration in the water is a function of water temperature and BOD:

$$\text{Oxygen saturation or } OS = 14.54 - (0.39t) + (0.01t^2) \quad [3]$$

$$O_{final} = OS - \left(\frac{k_d}{k_a - k_r}\right)\left(\exp^{-k_r L/U} - \exp^{-k_a L/U}\right)BOD_{init} - \left[(OS - O_{initial})\exp^{-k_a L/U}\right] \quad [4]$$

where, O_{final} = oxygen concentration at end of reach (mg/l), $O_{initial}$ = oxygen concentration at beginning of reach (mg/l)

Ideally, field measurements should be carried out and analyzed to obtain values for the different parameters. However, extensive time and money requirements restrict the use of field measurements to directly identify several water quality module parameters. Therefore, most water quality modelling parameters are estimated using established literature and reports (Bowie et al., 1985). Similarly, simulation for Chemical Oxygen Demand (COD) and Nitrate (NO_3) is done considering consumption by decaying organic and inorganic matter and reaeration induced by oxygen deficit.

3.3 Model set-up

The whole problem domain (and its different components (Figure 4)) was divided into seven catchments, which were further subdivided into thirteen sub-basins, so as to consider influent locations of major tributaries. Other major considerations were fourteen demand sites and one wastewater treatment plant to accurately represent the problem domain. Here, demand sites were meant to identify domestic (population) and industrial centres are defined with their attributes explaining water consumption and wastewater pollution loads per capita, water supply source and wastewater return flow. Dynamic attributes are described as functions of time and include population and industries. WWTP are pollution handling facilities with design specifications including total capacity and removal rates of pollutants. The flow of wastewater into the Pasig-Marikina-San Juan River mainly feeds through domestic, industrial and storm water runoff routes. No precise data is available regarding the total volume of wastewater production from different sources. In the absence of detailed information, the daily volume of domestic wastewater generation was based on an estimated 130 litres of average daily consumption per capita.

©2017, IAHR. Used with permission / ISSN 1562-6865 (Online) - ISSN 1063-7710 (Print)

Scenario analysis is carried out by defining a time horizon for which alternative wastewater generation and management options are explored. The business as usual condition was represented by a reference scenario with selection of all the existing elements as currently active. Different alternative wastewater management options were introduced by proposing changes vis-à-vis the reference scenario. These changes may include activating, deactivating or modifying attributes of elements or parameters. Information on each object can easily be retrieved by selecting the corresponding graphical element. The baseline year under the current reference scenario in this study is 2011.

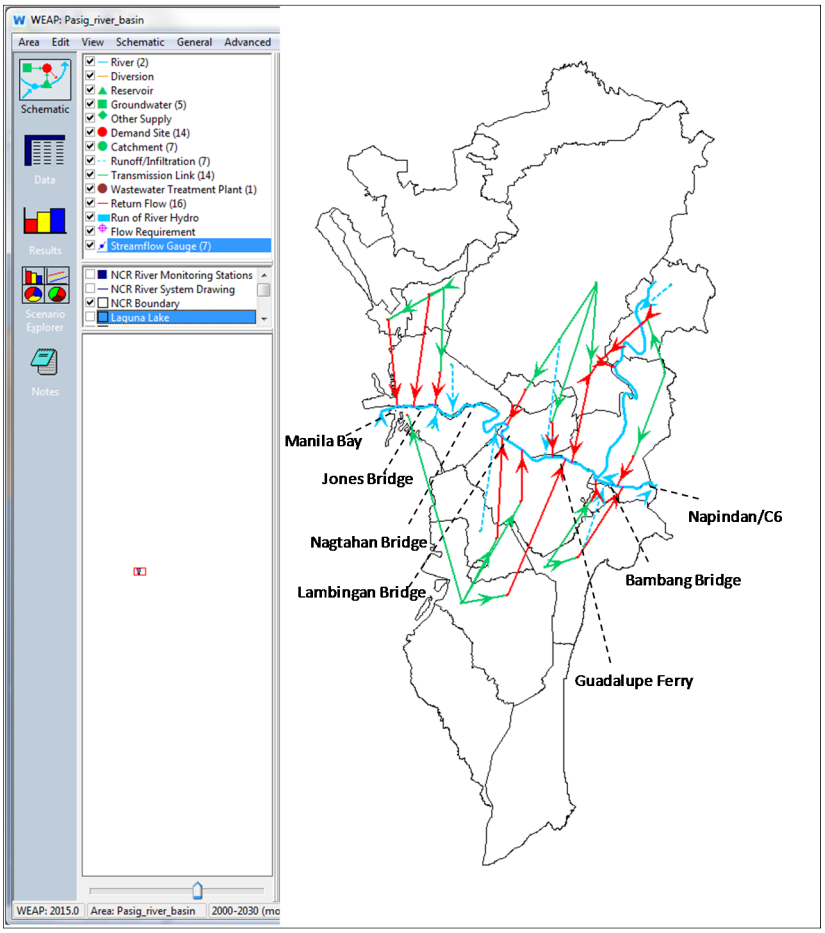

Figure 4. Schematic diagram showing problem domain for water quality modelling in Metro Manila using WEAP interface.

4 RESULTS AND DISCUSSION

4.1 Model performance evaluation

Before doing future scenario analysis, performance of the WEAP simulation was verified with significant correlation between observed and simulated values of water quality parameters. The hydrology module simulation performance was evaluated for the period from 2011 to 2014. Adjustments to hydrology module parameters were made with consideration for both quantitative and qualitative evaluation of the hydrologic response at the Sugutamu command area or monitoring station. Hydrology module parameters were adjusted in order to reproduce the observed monthly stream flows. Figure 5(a) compares monthly simulated and observed stream flows at Jones Bridge, showing that they largely match for most months, with an average error of 7%. On the other hand, the simulation performance of the water quality module was evaluated by comparing BOD value also at Jones Bridge. Selection of this location was made on the basis of consistent availability of observed water quality data. Results show a significant correlation between these two (Figures 5b) confirming suitability of the model performance in the study area.

 ©2017, IAHR. Used with permission / ISSN 1562-6865 (Online) - ISSN 1063-7710 (Print)

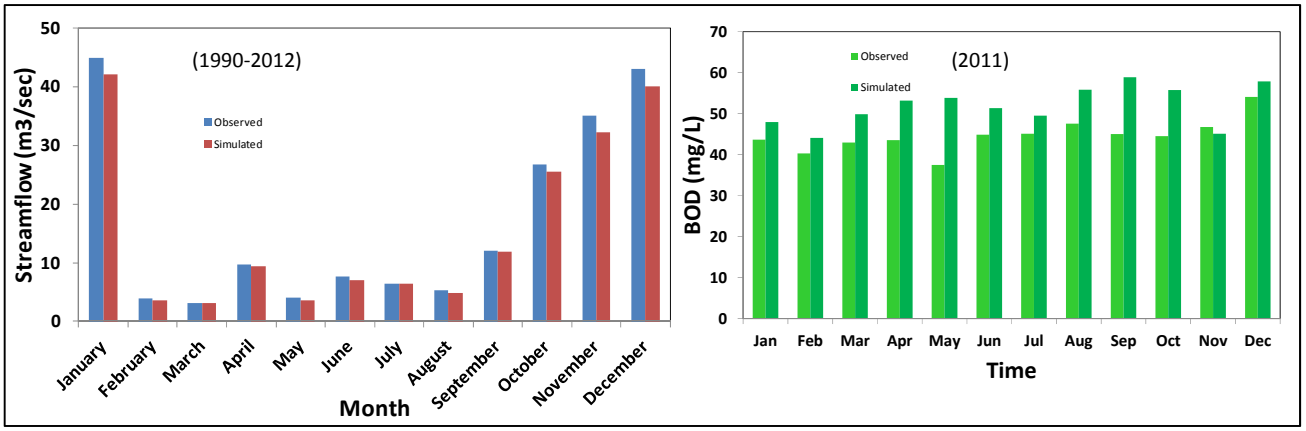

Figure 5. Validation of the model by comparing simulated and observed (a) monthly discharge, (b) BOD values at Jones Bridge.

4.2 Scenario analyses

Future simulation for both water quality of selected parameters and total water demand was done for the years 2015 and 2030, while utilising scenarios considering business as usual and possible future involvement to give a potential solution for the water related problems. Spatio-temporal simulation and prediction of water quality parameters was done using 2011 as a reference or base year. The results for total water demand are shown in Figure 6, indicating that annual water demand for the year 2030 will be approximately 1.34 billion cubic meters, approximately 2.5 times greater than that of the year 2000 i.e. 0.55 billion cubic meters. Difference of water demand between 2007 and 2010 is significantly higher than the normal trend may be justified because of high rate of migration from suburban areas to Metro Manila and relatively higher amount of construction activities. This rapid growth calls for water planners to take appropriate action in due course so as to provide sustainable water management for future generations. Results for simulated water quality using three parameters (namely NO3, BOD and COD) are shown in Figure 7. Simulation was done for the years 2015 and 2030 using 2011 as reference year with consideration for population increase, land use change, wastewater generation and its treatment at waste water treatment facilities. Based on the water quality parameters, a general trend found here is that water quality deteriorates from upstream to downstream because of the addition of anthropogenic output.

The results clearly show a high concentration of nitrate, indicating the influence of agricultural activities, fertilizer use, microbial mineralization, untreated sewerage input and animal waste. In general most water samples were safe for aquatic systems in terms of NO3 except those taken from the Manila Bay and Jones Bridge location. However, with business as usual, water quality will be deteriorating at other locations as well. The value for BOD varies from 30 to 146 mg/L, clearly indicating that all of the water samples are moderately to extremely polluted with reference BOD required value to safe aquatic system i.e. 6 mg/L (WHO, 2002). The COD value, a commonly used indicator of both organic and inorganic nutrients in water samples, increases with the course of time. This suggests that current management policies are not enough to keep the pollution level in check within a desirable limit and calls for transdisciplinary research for sustainable water resource management.

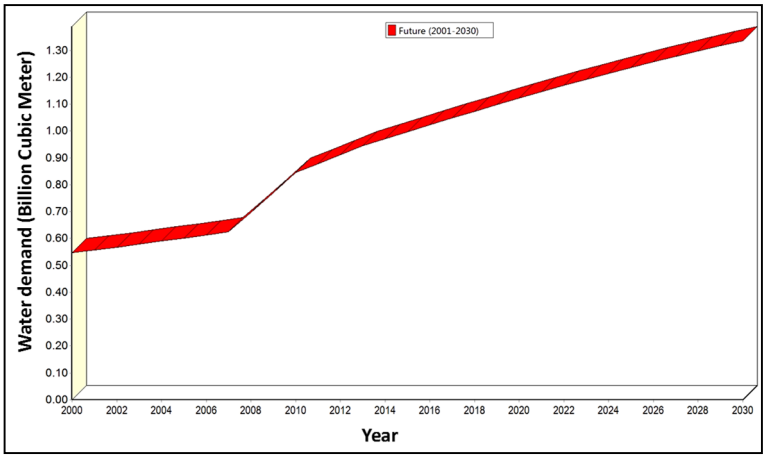

Figure 6. Simulation results for total water demand in the study area

©2017, IAHR. Used with permission / ISSN 1562-6865 (Online) - ISSN 1063-7710 (Print)

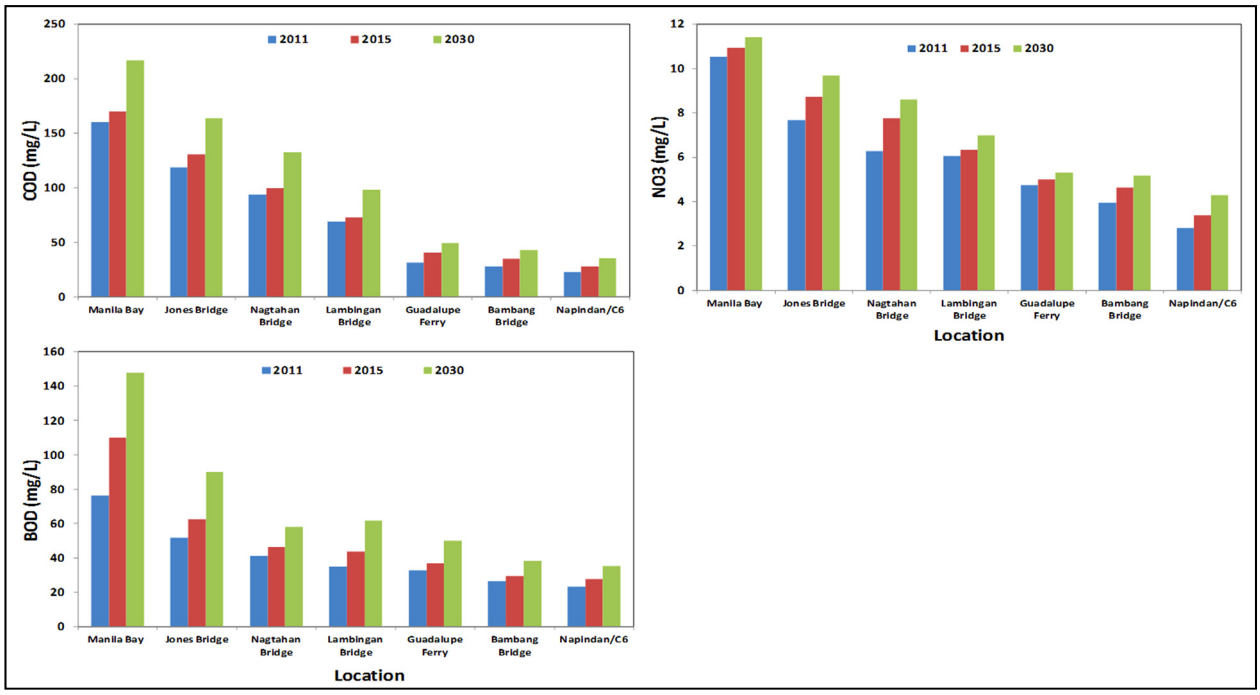

Figure 7. Simulation results of annual average value for COD, BOD and NO3 at seven different locations in 2011, 2015 and 2030.

5 CONCLUSIONS

This research work briefly sketches the quality and quantity of current and future water resources. A significant correlation between simulated and observed values indicates that hydrology and water quality modules in the WEAP model can efficiently replicate stream flows and water quality variables. Based on an exponential increase in the total demand for water resources, promotion of water reuse and water recycling in industry can also contribute toward the restoration and reclamation of water resources and can reduce urban water demand. Results indicate that water quality is moderately to extensively polluted throughout the Pasig-Marikina-San Juan River Basin. Therefore, improved regulation of wastewater treatment and sectoral water usage practice based on water quality should be put in place to preserve precious water resources.

ACKNOWLEDGMENTS

The authors would like to acknowledge support by the Water and Urban Initiative (WUI) project of the United Nations University and the Institute for the Advanced Study of Sustainability (UNU-IAS) for financial and other logistic support in conducting this research.

REFERENCES

Alcamo, J., Flörke, M. & Märker, M. (2007). Future Long-Term Changes in Global Water Resources Driven by Socio-Economic and Climatic Changes. *Hydrological Sciences Journal*, 52(2), 247-275.

Assaf, H. & Saadeh, M. (2008). Assessing Water Quality Management Options in the Upper Litani Basin, Lebanon, Using an Integrated GIS-Based Decision Support System. *Environmental Modelling & Software*, 23, 1327–1337.

Blanco-Gutiérrez, I., Varela-Ortega, C. & Purkey, D.R. (2013). Integrated Assessment of Policy Interventions for Promoting Sustainable Irrigation in Semi-Arid Environments: A Hydro-Economic Modeling Approach. *Journal of Environmental Management*, 128, 144–160.

Bowie, G.L., Mills, W.B., Porcella, D.B., Campbell, C.L., Pagenkopf, J.R., Rupp, G.L., Johnson, K.M., Chan, P.W.H. & Gherini, S.A. (1985). *In Rates, Constants and Kinetics Formulations in Surface Water Quality Modeling.* 2nd Ed. US EPA, Athens, Georgia EPA 600/3-85/040.

Brouwer, R. & Hofkes, M. (2008). Integrated Hydro-Economic Modelling: Approaches, Key Issues and Future Research Directions. *Ecological Economics*, 66, 16–22.

Clemente, R., Guillermo, S., Tabios, Q., Ramon, P., Abracosa, C., David, C. & Inocencio, A.B. (2001). Groundwater Supply in Metro Manila: Distribution, Environmental and Economic Assessment, Philippine Institute for Development Studies. *Discussion Paper*, Series No. 2001-06.

Deksissa, T., Meirlaen, J., Ashton, P.J. & Vanrolleghem, P.A. (2004). *Simplifying Dynamic River Water Quality Modelling: A Case Study of Inorganic Dynamics in the Crocodile River, South Africa.* Water Air Soil Pollution, 155, 303–320.

Downing, T.E. (2012*).* Views of the Frontiers in Climate Change Adaptation Economics. *Wires Climate Change,* 3, 161–170.

 ©2017, IAHR. Used with permission / ISSN 1562-6865 (Online) - ISSN 1063-7710 (Print)

Hanemann, W.M. (2006). The Economic Conception of Water. *Water Crisis: Myth or Reality*, 61-91.

Heinz, I., Pulido-Velazquez, M., Lund, J.R. & Andreu, J. (2007). Hydro-Economic Modeling in River Basin Management: Implications and Applications for the European Water Framework Directive. *Water Resource Management*, 21, 1103–1125.

Ingol-Blanco, E. & Mckinney, D. (2013). Development of a Hydrological Model for the Rio Conchos Basin. *Journal of Hydrologic Engineering*, 18(3), 340–351.

Ismail, A.H. & Abed, G.A. (2013). BOD and DO Modeling for Tigris River at Baghdad City Portion Using QUAL2K Model. Journal of Kerbala University, 11(3), 257-273.

Meinke, H., Howden, S.M., Struik, P.C., Nelson, R., Rodriguez, D. & Chapman, S.C. (2009). Adaptation Science for Agriculture and Natural Resource Management—Urgency and Theoretical Basis. *Current Opinion in Environmental Sustainability*, 1, 69–76.

Philippine Atmospheric, Geophysical and Astronomical Services Administration, (PAGASA). (2011). Climatological Normals: Rainfall Normal Values (Mm) 1981-2010. Http://Pagasa.Dost.Gov.Ph/Index.Php/Climate/Climatological-Normals. Downloaded On December 2014.

Pink, R.M. (2016). *Introduction Water Rights in Southeast Asia and India*. Palgrave Macmillan US, 1-14.

Purandara, B.K., Varadarajan, N., Venkatesh, B. & Choubey, V.K. (2011). Surface Water Quality Evaluation and Modeling of Ghataprabha River, Karnataka, India. *Environmental Monitoring and Assessment,* 184(3), 1371-8.

Sieber, J. & Purkey, D. (2011). *Water Evaluation and Planning (WEAP),* User Guide, Stockholm Environment Institute, USA.

Slaughter, A.R., Mantel, S.K. & Hughes, D.A. (2014). Investigating Possible Climate Change and Development Effects on Water Quality within an Arid Catchment in South Africa: A Comparison of Two Models. *Proceedings of the 7th International Congress on Environmental Modelling and Software,* San Diego, California, USA.

World Bank. (2015). *East Asia's Changing Urban Landscape, Measuring a Decade of Spatial Growth,* Urban Development Series. Washington, DC: World Bank.

World Health Organization. (2002). *Global Water Supply and Sanitation Assessment 2002,* Report WHO and UN Children's Fund: New York.

©2017, IAHR. Used with permission / ISSN 1562-6865 (Online) - ISSN 1063-7710 (Print)

Proceedings of the 37th IAHR World Congress
August 13 – 18, 2017, Kuala Lumpur, Malaysia

PREPARATION OF A NEWLY FUNCTIONALIZED POLYMERIC ADSORBENT FOR THE ENHANCED TREATMENT OF TEXTILE CONTAMINANT

SITI NURZAHIDAH RAMLI[(1)], KENG YUEN FOO[(2)] & NOR AZAZI ZAKARIA[(3)]

[(1)]School of Health Sciences, Universiti Sains Malaysia, Health Campus, Kubang Kerian, Malaysia
ieyda_wirama86@yahoo.com
[(2,3)]River Engineering and Urban Drainage Research Centre (REDAC), Universiti Sains Malaysia, Engineering Campus, Nibong Tebal, Malaysia
redac01@usm.my, k.y.foo@usm.my

ABSTRACT

To date, water pollution is a global top agenda that requires on-going evaluation and revision of water resource management at all levels. It occurs when pollutants are directly or indirectly discharged into the water bodies without the implementation of good management and treatment strategy. It has been reported that approximately 5 to 10 billion tons of industrial wastes are generated annually, many of which are pumped untreated into rivers, oceans or groundwater, with an estimated production of 1,500 km^3/year, six times higher than the river water volume. These effluents could be a major threat to the natural environmental and induce a potentially carcinogenic, mutagenic and allergenic impact to the aquatic environment and ecosystems. This has prompted an urgent need for the exploration of a low cost, reliable, and simple treatment technique. Among all, adsorption process has been identified to be a feasible treatment method for the pre-treatment of water pollutants. In this study, a new functionalized polymeric adsorbent was prepared, and its potential for the adsorptive treatment of textile effluent was evaluated using methylene blue (MB) as the model adsorbate. The prepared adsorbent was characterized by Scanning Electron Microscopy (SEM), Fourier Transform Infrared Spectroscopy (FTIR) and nitrogen adsorption-desorption curve. The effects of modification agents, initial concentrations, contact time and solution pH on the adsorption performance were examined. Glutamic acid modification has shown the best adsorption capacity, with the monolayer adsorption capacity for MB of 205.99 mg/g. Equilibrium data were best confronted to the pseudo-second-order kinetic equation, while the adsorptive process was satisfactory described by the Langmuir isotherm model. Regeneration studies showed that the adsorptive uptake remain at 180.37 mg/g even after five adsorption regeneration cycles. The findings revealed the great potential of the functionalized adsorbent for the successive treatment of contaminated textile water.

Keywords: Adsorption Dye; Functionalization; Polymeric adsorbent; Textile Contaminant.

1 INTRODUCTION

Commercially available Amberlite XAD resins are a synthetic group of cross-linked polymer, which derives its properties from the macroreticular structure, characterized by an inert, high physical and chemical stability, great porosity, uniform pore size distribution, homogenous, and non-ionic structure. It is considered to be one of the best commercially available macroporous poly (styrene-co-divinylbenzene) adsorbents, to support the impregnation or immobilization of chelating agents, with a variety of hydrophobic and hydrophilic parts in their molecules (Lee et al., 1988). Among them, Amberlite XAD-4 has been known to be a non-ionic polymeric sorbent material, with superior physical properties, economical, easily available and thermally stable to remove large quantities of hydrophobic pollutants, surfactants and organic species from the aqueous solutions, notably pharmaceuticals, chlorinated organics and pesticides (Uzun et al., 2001). Unlike most other adsorbents, the spent resins could be easily regenerated by the desorption of organic chemicals to offer great economical advantages (Kennedy, 1973). However, the polystyrene matrix of the XAD-4 is highly hydrophobic, making it very difficult in contacting with aqueous solutions, to induce a relatively smaller adsorption capacity towards the hydrophilic organic compounds (Hubbard et al., 1999; Li et al., 2001).

To improve the adsorptive property of the macroporous polymeric adsorbents for hydrophilic organic compounds, the modification or functionalization of XAD-4 resin has been designed. The modification by the introduction of organic and inorganic chelating ligands or reagents could significantly alter the surface chemistry, specific surface area, porosity, or generation of specific functional groups on the matrix of adsorbents to optimize their applications (Dos Santos et al., 2011). Today, a considerable amount of modification procedures have been reported. Among all, chemical modification is widely adopted as a viable and attractive alternative to the synthesis of new polymers, to enhance the selectivity (Zheng et al., 2007; Valderrama et al., 2007) and to increase the number of surface active sites, contact area, surface energy and surface porosity (Schwantes et al., 2016; Mikati et al., 2013). The modification process is driven mainly by the acid or base reagents, which are expected to improve the pollutant removal efficiency by manipulating the functional groups, alteration of surface charge and introduction of new active binding sites (Owabor et al.,

 ©2017, IAHR. Used with permission / ISSN 1562-6865 (Online) - ISSN 1063-7710 (Print)

2012; Chen and Wu, 2004; Fathy et al., 2013; Marshall et al., 1999). However, there are limited researches that have been conducted to provide an overview of these modification agents on the alteration of the adsorptive property of the Amberlite resins (Argun and Dursun, 2006).

The present work was carried out to examine the effect of modification agents on the adsorptive property of Amberlite XAD-4 resin. To achieve the purpose, the copolymer was nitrated, reduced to the corresponding amine, converted to the diazonium salt with nitrite, and reacted with different modification agents to produce a series of new functionalized XAD-4 resins. The applicability was investigated for the effective treatment of methylene blue solution. The effects of operating conditions, isotherm modelling and the reusability of the newly prepared resins were elucidated.

2 MATERIALS AND METHODS

2.1 Adsorbate

Methylene Blue, (MB) a cationic dye, difficult to be degraded in the natural environment was chosen as the model adsorbate in this study. The standard stock solution was prepared by dissolving an accurately weighed amount of MB in distilled water to a concentration of 500 mg/L. Working solutions of desired concentrations were prepared by diluting the stock solution in accurate proportions to different initial concentrations.

2.2 Preparation of functionalized XAD-4 derived adsorbents

Amberlite XAD-4, a non-ionic macroreticular resin generally applied for the removal of low molecular weight pollutants was selected as the raw precursor in this work. The specification of Amberlite XAD-4 resin is given in Table 1.

Table 1. Properties of polymeric adsorbent Amberlite XAD-4.

Properties	Description
Matrix	Macroreticular crosslinked aromatic polymer
Surface area	≥ 750 m^2/g
Porosity	≥ 0.50 ml/ml
Particle size	
Harmonic mean size	0.49 – 0.69 mm
Uniformity coefficient	≤ 2.0
Fines content	< 0.350 mm : 5.0 % max
Coarse beads	>1.18 mm : 5.0 % max
Moisture holding capacity	54 to 60 %
Specific gravity	1.01 to 1.03

The resin was purified by the diluted methanol rinsing, subsequent by repeated washing with deionized water to remove the surface impurities. The functionalization of Amberlite XAD-4 resins was performed by the treatment of resin beads in 1 M of nitric acid and sulphuric acid solution at 60 °C for 30 minutes. The reaction mixture was inhibited in an ice water mixture, subsequently by repeated washing with deionised water. The resin beads were added to the reducing mixture of $SnCl_2$, concentrated hydrochloric acid and ethanol where the system was refluxed for 10 h at 90 °C. The produced precipitate was rinsed with distilled water and 2 M of NaOH solution to obtain the free amino polymer according to the reaction (Kara et al., 2005):

$$(RNH_3)_2SnCl_6 + 8OH^- \rightarrow 2RNH_2 + SnO_3^{2-} + 6Cl^- + 5H_2O \quad [1]$$

The diazotized resin was filtered, washed and functionalized with glutamic acid (XAD-4-GMA), potassium carbonate (XAD-4-PC) or sulphuric acid (XAD-4-SA) in 10% NaOH and stored at 0-4 °C for 24 h. The functionalized resins were washed extensively with deionized water and air dried prior to use. The reaction sequence is provided in Figure 1.

2.3 Physical and chemical characterizations

The surface physical properties were characterized with Micromeritics ASAP 2020, using N_2 as the adsorbate at 77 K. The sample was degassed for 2 h under vacuum prior to the measurement. The textural structure was evaluated using Scanning Electron Microscopy (Zeiss Supra 35VP), while the surface functionality were detected using the Fourier transform infrared (FTIR) spectroscopy (FTIR-2000, Perkin Elmer) from the scanning range of 4000–400 cm^{-1}. The zero point of charge (pH_{pzc}) was determined by adjusting the pH of the 0.1 M of NaCl solution mixture of 0.15 g of resin and 50 mL of NaCl solution to a value between 2- 12. The final pH (pH_{final}) was measured after 48 h of agitation. The pH_{pzc} is the point where $pH_{initial} - pH_{final}=0$.

©2017, IAHR. Used with permission / ISSN 1562-6865 (Online) - ISSN 1063-7710 (Print)

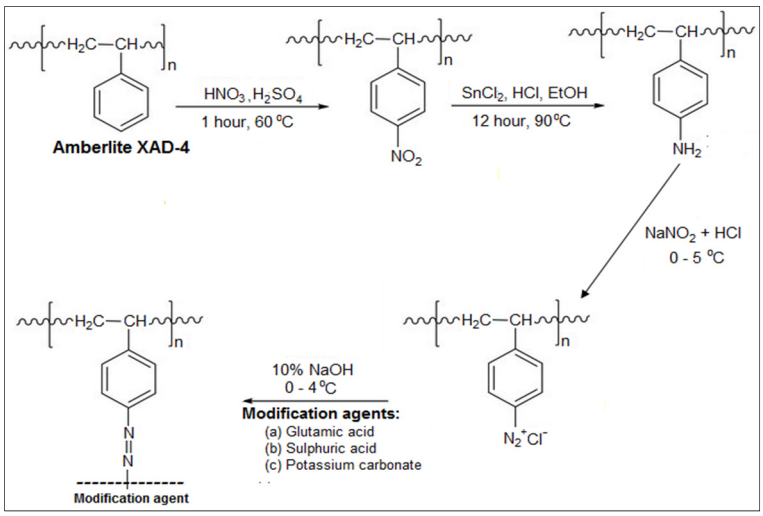

Figure 1. Reaction sequence for the preparation of functionalized XAD-4 resins.

2.4 Batch adsorption experiments

The batch adsorption experiments were carried out in a set of Erlenmeyer flask containing 0.2 g of adsorbent and 200 mL of methylene blue (MB) solutions in an isothermal water bath shaker at 120 rpm and 30 °C until the equilibrium is reached. The concentration of the supernatant solution was measured using a double beam UV-Visible spectrophotometer (UV-1801 Shimadzu, Japan) at 663 nm. Each experiment was duplicated under identical conditions. The adsorptive uptake of MB at time t, q_t (mg/g) and equilibrium, q_e (mg/g) was calculated by:

$$q_t = \frac{(C_0 - C_t)V}{M} \quad [2]$$

$$q_e = \frac{(C_0 - C_e)V}{M} \quad [3]$$

Where C_0 (mg/L) is the initial concentrations, and C_t (mg/L) and C_e (mg/L) are the concentrations of dye solution at time t and equilibrium, respectively. V is the volume of solution (L) and M (g) is the mass of adsorbent. The effect of pH on dye removal was examined by regulating the pH from 2 to 12 using 0.1 M of NaOH or HCl solutions. The pH was measured using a pH meter (Fischer Scientific Accumet XL200).

3 RESULTS AND DISCUSSION

3.1 Effect of modification agents

Figure 2 illustrates the effect of modification agents on the adsorptive property of the Amberlite XAD-4 resin. Generally, acid and base modified resins demonstrated a greater adsorptive behaviour for MB as compared to the raw and purified forms. Interestingly, acid treatment showed a dramatic improvement as compared to the base modification. The incorporation of acidic functional groups has successfully enhanced the feasibility on the adsorptive uptake of MB, due to the hydrophilic properties of resin, making them more dispersed in aqueous solutions (Li et al., 2011). Moreover, the abundant presence of oxygen-containing groups could induce an electron-withdrawing characteristic that corresponds to the reduction of electron density on the resin surface, with a repulsive force for anionic species and good anchoring sites for cationic dyes, contributing to the preferable adsorption of the basic MB molecules (Foo and Hameed, 2010).

The highest quantitative uptake of MB was evident with glutamic acid-functionalization (XAD-4-GMA). The affinity of XAD-4-GMA surface toward MB was remarkably improved by organic acid treatment, owing to the outstanding enhancement of carboxyl and hydroxyl groups. According to Rajan and Martell (1967), the presence of these two carboxylic groups in the structure of glutamic acid itself may increase the hydrophilicity of the polymeric adsorbent resin to facilitate a better contact, whereby the equilibrium between the adsorbent surface and the MB ions could be achieved, thereby enhancing the efficiency of the adsorption process. Inorganic acid modification with sulphuric acid was less favourable for the adsorptive uptake of MB molecules, mainly attributed to the strong acidic characteristics of inorganic acid that may significantly destroy the textural structure by breaking of some chemical surface bondings of the XAD-4-SA (Liu et al., 2014). Similarly, base

 ©2017, IAHR. Used with permission / ISSN 1562-6865 (Online) - ISSN 1063-7710 (Print)

treatment with the attachment of more basic functionalities did not show great improvement to the adsorptive uptake of MB molecules.

In the present work, the adsorptive uptakes of MB for raw, purified, potassium carbonate, sulphuric acid and glutamic acid-modified resin were identified to be 5.65, 16.30, 52.74, 116.22 and 193.69 mg/g, respectively. The findings was in agreement with previous researches on the organic acid modification of XAD resins (Memon et al., 2005; Islam et al., 2013; Khazaeli et al., 2013; Sharma and Pant, 2009; Tokalioglu et al., 2008; Tewari and Singh, 1999; Metilda et al., 2005; Cekic et al., 2004). The obtained result supported the application of glutamic acid for the modification of Amberlite XAD-4 resin.

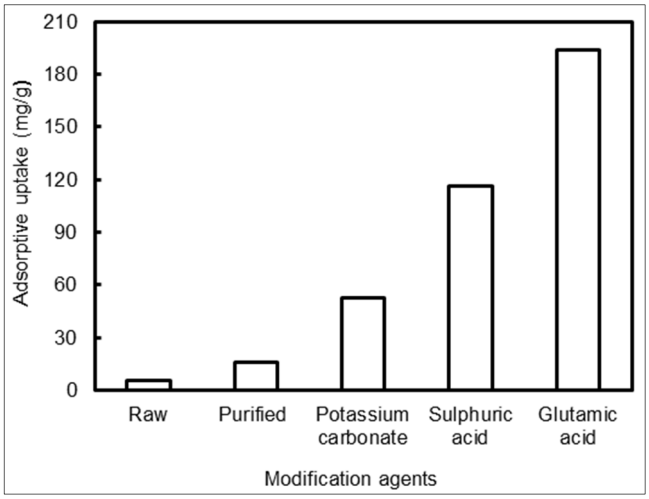

Figure 2. Effect of modification agents on the adsorptive uptake of MB.

3.2 Effect of contact time and initial concentrations

The effects of contact time and initial concentrations on the adsorptive uptake of MB are displayed in Figure 2. Generally, the adsorptive uptake of MB increased by prolonging the contact time. At the initial stage, the dye adsorbed rapidly onto the adsorbent surface, and the adsorption process was gradually decreased, and reached to a plateau as the equilibrium approached. The time required to attain this state of equilibrium is termed as equilibrium time (Wang et al., 2009).

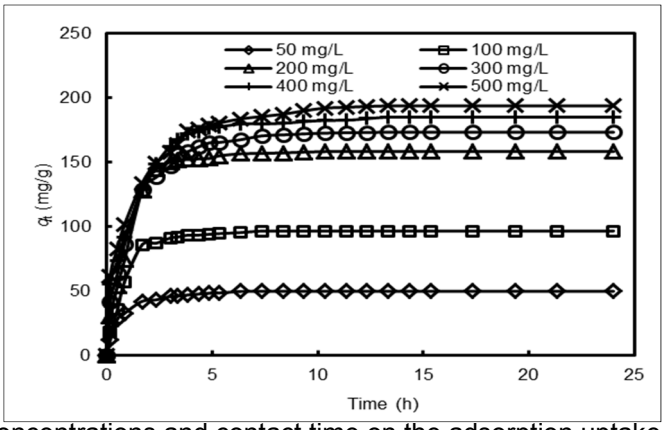

Figure 3. Effect of initial concentrations and contact time on the adsorption uptake of MB onto XAD-4-GMA.

The rapid sorption during the first few hours of contact time could be explained by the presence of large numbers of vacant active sites, and these surface active sites would reach to the saturation as the equilibrium is attained. The equilibrium time for the adsorption of MB with the initial concentration of 50 mg/L was achieved within 6 h. However, a longer equilibrium time of 9 h was required for the higher concentrations of 100 to 500 mg/L. In the present study, the adsorption equilibrium of MB, q_e increased from 49.95 to 193.69 mg/g with an increase in the initial concentration from 50 to 500 mg/L, indicating a higher concentration gradient to support the adsorption process, and greater driving force between the liquid and the solid phase at higher initial concentration range (Han et al., 2010).

3.3 Effect of solution pH

Solution pH is an important variable affecting the electrostatic interactions between the adsorbent and the adsorbate molecules (Hu et al., 2013). It affects not only the surface charge of the adsorbents, but also the

degree of ionization of the dye molecules (Foo and Hameed, 2012). Figure 3 illustrates the adsorption behaviour of MB onto XAD-4-GMA as a function of solution pH. It was evident that by increasing the solution pH from 2 to 12 showed an increase in q_e from 49.44 to 248.55 mg/g. This phenomenon can be explained in term of zero point of charge (pH_{pzc}) of XAD-4-GMA which was found to be at 7.60. At pH<pH_{pzc}, the adsorbent could be positively charged, due to the present of H^+ ions. The observed low adsorption of MB onto XAD-4-GMA at low solution pH may be attributed by the effective competition of H^+ ions with the dye cations. Under such conditions, repulsion between the MB dye cations and the adsorbent may be expected. At pH>pH_{pzc}, the adsorbent surface is negatively charged, and greatly contributed to the accumulation of OH^- ion on the XAD-4-GMA surface. This interaction could induce a strong electrostatic interaction between the COOH groups incorporated into the polymeric adsorbent by glutamic acid modification with the MB molecules to facilitate the adsorption process. A similar finding has been reported for the adsorption of MB onto anaerobic granular sludge and activated carbon (Liu et al., 2010; Reddy et al., 2015).

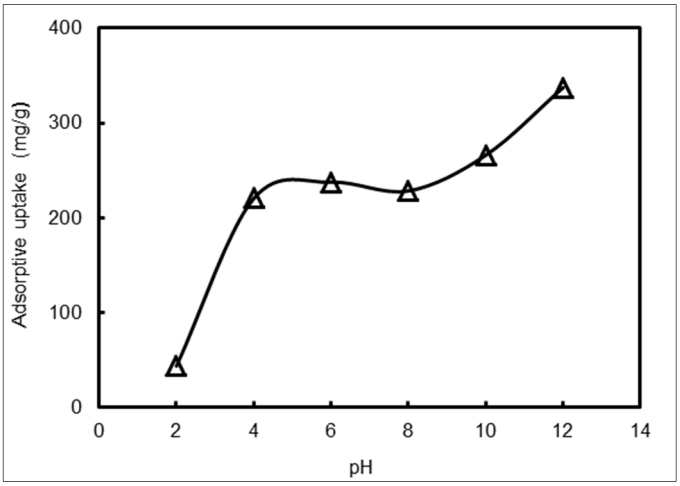

Figure 4. Effect of solution pH on the adsorptive uptake of MB onto XAD-4-GMA.

3.4 Adsorption isotherm

Adsorption isotherm is an invaluable tool describing the specific relationship between the adsorbents and adsorbate molecules at the equilibrium. It is crucial for the prediction of adsorption parameters, and quantitative comparison of the adsorbent behaviour. The correlation of equilibrium data is essential for the practical design and operation of the adsorption systems (Foo and Hameed, 2010). In this work, the nonlinear Langmuir, Freundlich and Tempkin isotherm models were established.

Langmuir isotherm model (Langmuir, 1918) was developed based on the assumption that adsorption takes place at a fixed number of accessible homogeneous surface that are identical, with no transmigration of adsorbates in the plane of the neighbouring surface. The Langmuir equation is suitable for homogeneous adsorption, and obeys Henry's law at low concentrations. The nonlinear form of Langmuir isotherm model is expressed as:

$$q_e = \frac{Q_0 K_L C_e}{1 + K_L C_e} \qquad [4]$$

where K_L (L/g) is the adsorption intensity or Langmuir coefficient, and Q_0 (mg/g) is the isotherm constant related to adsorption capacity.

The Freundlich isotherm model (Freundlich, 1906) is an empirical equation widely applied to multilayer adsorption, with non-uniform distribution of adsorption heat and affinity over the heterogeneous surface. The heterogeneity arises from the presence of different functional groups on the adsorbent surface, and from the different adsorbent–adsorbate interactions. The nonlinear Freundlich isotherm is expressed by:

$$q_e = K_F C_e^{1/n} \qquad [5]$$

where K_F and n are the Freundlich isotherm constants that indicate the extent of the adsorption, and the degree of nonlinearity between the solution concentration and the adsorption process, respectively.

Temkin isotherm model (Tempkin and Pyzhev, 1940) was derived based on the assumption that the heat of adsorption of all molecules in the layer would decrease linearly rather than logarithmically with surface coverage. This isotherm assumes that: (i) the heat of adsorption of all the molecules in the layer decreases linearly with coverage due to adsorbate–adsorbate interactions, and (ii) adsorption is characterized by a

 ©2017, IAHR. Used with permission / ISSN 1562-6865 (Online) - ISSN 1063-7710 (Print)

uniform distribution of binding energies, up to some maximum binding energy (Tempkin and Pyzhev, 1940), and is commonly used in the form:

$$q_w = B \ln(AC_e) \quad [6]$$

where B = RT/b and b (J/mole) and A (L/g) are the isotherm constants, R (8.314 J/mole K) is the universal gas constant and T (K) is the absolute temperature.

The applicability of the isotherm models was judged by determining the correlation coefficients, R^2, where the higher the R^2 value, the better the fit is. The validity of the models was further verified by root-mean-square deviation (RMSD), the commonly used statistical tool measuring the predictive power of a model derived as:

$$RMSD = \frac{\sqrt{\sum_{i=1}^{n}(q_{\exp} - q_p)^2}}{n-1} \quad [7]$$

where q_{exp} (mg/g) and q_p (mg/g) are the experimental and theoretical adsorption capacities, respectively. Due to the inherent bias resulting from linearization, the alternative isotherm parameter sets were determined by non-linear regression (Foo and Hameed, 2010). This provides a mathematically rigorous method for determining isotherm parameters using the original form of the isotherm equations.

The isotherm parameters are presented in Table 2. The experimental data for the adsorption of MB onto XAD-4-GMA showed good agreement with the Langmuir isotherm model, with the highest R^2 value and lowest RMSD among the tested models. Similar observation was reported for the adsorption of MB onto papaya leaves, baker's yeast and pineapple leaf powder (Krishni et al., 2013; Yu et al., 2009; Weng et al., 2009). The applicability of the Langmuir isotherm model suggested that the adsorption process is monolayer, with each molecule poses equal enthalpies and activation energy. The results also illustrated no interaction and transmigration of dyes in the plane of the neighbouring surface (Foo and Hameed, 2012). The correlation coefficient, R^2 values fitted with the Freundlich and Temkin models were found to be much lower than the Langmuir isotherm model (0.99), thus ascertained the homogenous nature of the surface interaction.

Table 2. Langmuir, Freundlich and Temkin isotherm parameters for the adsorption of MB onto XAD-4-GMA.

Langmuir isotherm				Freundlich isotherm				Temkin isotherm			
K_L (L/mg)	Q_0 (mg/g)	R^2	RMSD	n	K_F (mg/g)(L/mg)$^{1/n}$	R^2	RMSD	A (L/g)	B	R^2	RMSD
0.0447	205.99	0.997	1.247	3.528	40.59	0.896	6.329	0.579	38.95	0.967	3.569

3.5 Characterization of XAD-4-GMA

The representative FTIR spectrum of the XAD-4-GMA before and after the adsorption of MB is shown in Table 3. The broad band at 3443/3417 cm^{-1} is assigned to the O-H groups. The region between 2926-2921 cm^{-1} is attributed to the C-H stretching of methyl groups and the signal at 2358/2352 cm^{-1} is ascribed to the vibration of -COOH structure. The sharp peak at 1732 cm^{-1} is associated to the carbonyl group, while the intensity at 1629/1600 cm^{-1} is related to the aromatic rings. The transmittance appears at 1491 cm^{-1} showed the presence of C=O group, ascribed to the ketones, aldehyde, lactone, and carboxyl derivatives. The bending vibration of C-H of methyl and C-O groups was illustrated by the signals at 1441/1440 cm^{-1}, 1380-1388 cm^{-1} and 1281/1239 cm^{-1}. The band at 1174/1171 cm^{-1} is due to the C-CH_3 stretching vibration and the bands appeared at 1134 and 1098 cm^{-1} are corresponded to the ether linkage. The transmittance at 883-606 cm^{-1} could be due to the C–H and O–H bending in aromatics, respectively. The obtained FTIR spectra elaborated well the alteration of surface chemistry of XAD-4-GMA, with some shift, disappearance and formation of new peaks after the adsorption process, suggesting the possible involvement of these functional groups in the adsorption of MB molecules.

Scanning electron microscopy (SEM) provides essential topographic information of the newly prepared XAD-4-GMA as depicted in Figure 4. The surface morphology of the modified resin has a rough appearance of small crystalline with needle-like projections, which is in contact with resin surface after glutamic-acid treatment. As compared with the smooth surface of unmodified XAD-4 resin (figure not shown), the changing of substrate surface after the functionalization verified the attachment of glutamic acid onto the surface resin.

©2017, IAHR. Used with permission / ISSN 1562-6865 (Online) - ISSN 1063-7710 (Print)

Table 3. FTIR spectrum of XAD-4-GMA before and after the adsorption process.

IR peak	Before adsorption	After adsorption	Assignment
1	3443	3417	O-H stretching
2	2926	2921	C-H stretching
3	2353	2358	-COOH group
4	1629-1550	1732-1491	C=O stretching
5	1440	1441	C=C stretching
6	1380	1388-1335	C-H bending
7	1282	1239	C-O stretching
8	1174	1171	C-CH_3 stretching
9	1098	1134	C-O-C stretching
10	707	883-606	C-H bending

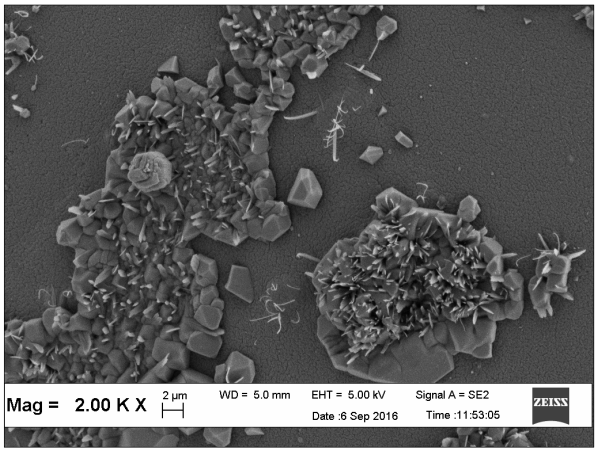

Figure 5. Scanning electron micrograph of XAD-4-GMA.

3.6 Regeneration study

Regeneration study is an important and crucial tool to ascertain the economic and environmental feasibility of the adsorption system. In this work, the regeneration study was carried out by rinsing the dye-loaded resins with 0.1 M of HCl solution. The regenerated sample was washed repeatedly with double distilled water, and air dried prior to use in the subsequent regeneration cycle. The adsorption-regeneration experiment was conducted under the prefixed conditions continuously for five repeated cycles. As depicted in Figure 5, it was observed that the adsorptive uptake of MB could remain at 180.37 mg/g even after five regeneration cycles. The findings illustrated the excellent reusability and stability of this modified resin to be applied for real practical applications.

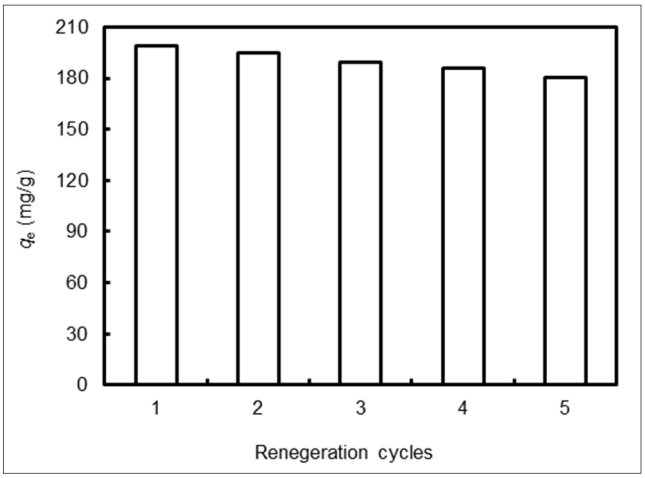

Figure 6. The adsorption-desorption cycles for MB onto XAD-4-GMA.

However, the slight decrease of the adsorption capacity after several adsorption-desorption cycles may be attributed to the incomplete desorption of the adsorbed MB molecules from the surface of XAD-4-GMA, and the loss of the XAD-4-GMA resin during the washing and filtration process (Zhou et al., 2015). A comparison of the monolayer adsorption capacity of MB onto various adsorbents is presented in Table 4. It can be concluded that the XAD-4-GMA resin prepared in this work showed relatively high adsorption capacity as compared to some previous works as reported in the literature. The findings demonstrated the high

 ©2017, IAHR. Used with permission / ISSN 1562-6865 (Online) - ISSN 1063-7710 (Print)

potential of XAD-4-GMA resin to be employed as a cost-effective alternative for the adsorptive treatment of textile effluents.

Table 4. Comparative evaluation of monolayer adsorption capacity of MB onto different adsorbents.

Adsorbent	Monolayer adsorption capacity (mg/g)	Reference
XAD-4-GMA resin	205.99	Present study
Pyrolytic tire char	65.81	Makrigianni et al. (2015)
Fc modified cation exchange resin	10.01	Wang et al. (2014)
Amberlite XAD-4 resin	21.00	Zhang et al. (2006)
ZCH-101 resin	20.90	
Amberlite XAD-16	21.55	Kerkez et al. (2012)
Amberlite XAD-7 HP	2.72	
Diatomite treated with NaOH	27.86	Zhang et al. (2013)
Zerolit DM-F resin	24.75	Khan et al. (2013)
Polydopamine microspheres	90.70	Fu et al. (2014)
Ultrasonic surface modified chitin	26.69	Dotto et al. (2015)
Multi-wall carbon nanotubes	62.50	Tabrizi and Yavari, (2015)
Magnetic $ZnO/ZnFe_2O_4$ particles	37.27	Feng et al. (2015)
Anaerobic granular sludge-based biochar	90.91	Shi et al. (2014)
Poly(cyclotriphosphazene-co-4,4-sulfonyldiphenol) nanotubes	69.16	Chen et al. (2014)

4 CONCLUSION

This study revealed the potential of the newly modified XAD-4 resin as a suitable adsorbent for the adsorptive removal of MB dyes from the aqueous water streams. The integration of glutamic acid modification has successfully established azo-bridge linking structure to improve the hydrophilicity, and adsorption capability for different water pollutants. Equilibrium data were best fitted to the Langmuir isotherm model, with a monolayer adsorption capacity for MB of 205.99 mg/g. FTIR and SEM morphology studies elaborated the successful attachment of glutamic acid onto the XAD-4 resin. The adsorption performance did not show appreciable reduction even after five adsorption–desorption cycles. These findings verified the high economical feasibility and efficiency of XAD-4-GMA as an excellent adsorbent for the adsorptive treatment of water pollutants.

ACKNOWLEDGEMENTS

The authors acknowledge the financial support provided by Universiti Sains Malaysia under the RUI (Project No: 1001/PREDAC/814272) and RU-PRGS (Project No: 1001/PPSK/8144015) grant schemes.

REFERENCES

Argun, M.E. & Dursun, S. (2006). Removal of Heavy Metal Ions using Chemically Modified Adsorbents. *Journal of International Environmental Application & Science*, 1 (1-2), 27–40.

Cekic, S.D., Filik, H. & Apak, R. (2004). Use of an O-aminobenzoic Acid-functionalized XAD-4 Copolymer Resin for the Separation and Preconcentration of Heavy Metal (II) Ions. *Analytica Chimica Acta*, 505, 15–24.

Chen, Z., Zhang, J., Fu, J., Wang, M., Wang, X., Han, R. & Xu, Q. (2014). Adsorption of Methylene Blue onto Poly(cyclotriphosphazene-co-4,4'-sulfonyldiphenol) Nanotubes: Kinetics, Isotherm and Thermodynamics Analysis. *Journal of Hazardous Materials*, 273, 263–271.

Chen, J.P. & Wu, S. (2004*). Acid/Base-Treated Activated Carbons: Characterization of Functional Groups and Metal Adsorptive Properties*. Langmuir, 20, 2233–2242.

Dos Santos, V.C.G., De Souza, J.V.T.M., Tarley, C.R.T., Caetano, J. & Dragunski, D.C. (2011). Copper Ions Adsorption from Aqueous Medium using the Biosorbent Sugarcane Bagasse In Natura and Chemically Modified. Water, *Air and Soil Pollution*, 216, 351–359.

Dotto, G.L., Santos, J.M.N., Rodrigues, I.L., Rosa, R., Pavan, F.A. & Lima, E.C. (2015). Adsorption of Methylene Blue by Ultrasonic Surface Modified Chitin. *Journal of Colloid Interface Science*, 446, 133–140.

Fathy, N.A., El-Shafey, O. I. & Khalil, L.B. (2013). *Effectiveness of Alkali-Acid Treatment in Enhancement the Adsorption Capacity for Rice Straw: The Removal of Methylene Blue Dye*. ISRN Physical Chemistry, 2013, 1–15.

Feng, J., Wang, Y., Zou, L., Li, B., He, X., Ren, Y., Lv, Y. & Fan, Z. (2015). Synthesis of Magnetic $ZnO/ZnFe_2O_4$ by a Microwave Combustion Method, and its High Rate of Adsorption of Methylene Blue. *Journal of Colloid and Interface Science*, 438, 318–322.

Foo, K.Y. & Hameed, B.H. (2010). Insights into the Modeling of Adsorption Isotherm Systems, *Chemical Engineering Journal*, 156, 2–10.

©2017, IAHR. Used with permission / ISSN 1562-6865 (Online) - ISSN 1063-7710 (Print)

Foo, K.Y. & Hameed, B.H. (2012). Preparation, Characterization and Evaluation of Adsorptive Properties of Orange Peel Based Activated Carbon via Microwave Induced K_2CO_3 Activation. *Bioresource Technology*, 104, 679–686.

Foo, K.Y. & Hameed, B.H. (2012). A Rapid Regeneration of Methylene Blue Dye-Loaded Activated Carbons with Microwave Heating. *Journal of Analytical and Applied Pyrolysis*, 98, 123–128.

Freundlich, H. (1906). Über Die Adsorption in Lösungen (Adsorption in Solution), Zeitschrift fur Physikalische Chemie, 57, 384–470.

Fu, J., Chen, Z., Wang, M., Liu, S., Zhang, J., Zhang, J., Han, R. & Xu, Q. (2014). Adsorption of Methylene Blue by a High-Efficiency Adsorbent (Polydopamine Microspheres): Kinetics, Isotherm, Thermodynamics and Mechanism Analysis. *Chemical Engineering Journal*, 259, 53–61.

Han, R., Zhang, L., Song, C., Zhang, M., Zhu, H. & Zhang, L. (2010). Characterization of Modified Wheat Straw, Kinetic and Equilibrium Study about Copper Ion and Methylene Blue Adsorption in Batch Mode. *Carbohydrate Polymer*, 79, 1140–1149.

Hu, Y., Guoa, T., Ye, X., Li, Q., Guo, M., Liu, H. & Wu, Z. (2013). Dye Adsorption by Resins: Effect of Ionic Strength on Hydrophobic and Electrostatic Interactions. *Chemical Engineering Journal*, 228, 392–397.

Hubbard, K.L., Finch, J.A. & Darling, G.D. (1999). Thiol and Disulfide Addition to the Pendant Vinylbenzene Groups of Poly (divinylbenzene-co-ethylvinylbenzene), including Amberlite XAD-4. *Reactive & Functional Polymer*, 40, 61–90.

Islam, A., Laskar, M.A. & Ahmad, A. (2013). Preconcentration of Metal Ions Through Chelation on a Synthesized Resin Containing O, O Donor Atoms for Quantitative Analysis of Environmental and Biological Samples. *Environmental Monitoring and Assessment*, 185, 2691–2704.

Kara, D., Fisher, A. & Hill, S.J. (2005). Preconcentration and Determination of Trace Elements with 2,6-diacetylpyridine Functionalized Amberlite XAD-4 by Flow Injection and Atomic Spectroscopy. *Analyst,* 130, 1518–1523.

Kennedy, D.C. (1973). Treatment of Effluent from Manufacture of Chlorinated Pesticides with a Synthetic, Polymeric Adsorbent, Amberlite XAD-4. *Environmental Science and Technology*, 7, 138–141.

Kerkez, Ö., Bayazit, Ş.S. & Uslu, H. (2012). A Comperative Study for Adsorption of Methylene Blue from Aqueous Solutions by Two Kinds of Amberlite Resin Materials. *Desalination and Water Treatment*, 45, 206–214.

Khan, M.A., Alothman, Z.A., Naushad, M. & Khan, M.R. (2013). Adsorption of Methylene Blue on Strongly Basic Anion Exchange Resin (Zerolit DMF): Kinetic, Isotherm, and Thermodynamic Studies. *Desalination and Water Treatment*, 1–9, 37–41.

Khazaeli, S., Nezamabadi, N., Rabani, M. & Panahi, H.A. (2013). A New Functionalized Resin and its Application in Flame Atomic Absorption Spectrophotometric Determination of Trace Amounts of Heavy Metal Ions after Solid Phase Extraction in Water Samples. *Microchemical Journal*, 106, 147–153.

Krishni, R.R., Foo, K.Y. & Hameed, B.H. (2013). Adsorption of Methylene Blue onto Papaya Leaves: Comparison of Linear and Nonlinear Isotherm Analysis. *Desalination and Water Treatment*, 52, 6712–6719.

Langmuir, I. (1918). The Adsorption of Gases on Plane Surfaces of Glass, Mica and Platinum, *Journal of the American Chemical Society*, 57, 1361–1403.

Lee, D.W., Eum, C.H., Lee, I.H. & Jeon, S.J. (1988). Adsorption Behavior of 8-Hydroxyquinoline and Its Derivatives on Amberlite XAD Resins, and Adsorption of Metal Ions by Using Chelating Agent-Impregnated Resins. *Analytical Sciences*, 4(5), 505–510.

Li, A., Zhang, Q., Chen, J., Fei, Z., Long, C. & Li, W. (2001). Adsorption of Phenolic Compounds on Amberlite XAD-4 and its Acetylated Derivative MX-4. *Reactive & Functional Polymers*, 49, 225–233.

Li, J., Chen, S., Sheng, G., Hu, J., Tan, X. & Wang, X. (2011). Effect of Surfactants on Pb(II) Adsorption from Aqueous Solutions using Oxidized Multiwall Carbon Nanotubes. *Chemical Engineering Journal*, 166, 551–558.

Liu, F., Teng, S., Song, R. & Wang, S. (2010). Adsorption of Methylene Blue on Anaerobic Granular Sludge: Effect of Functional Group. *Desalination*, 263, 11–17.

Liu, L., Wang, L., Yin, L., Song, W., Yu, J. & Liu, Y. (2014). Effects of Different Solvents on the Surface Acidic Oxygen-containing Functional Groups on Xanthoceras Sorbifolia Shell. *BioResources*, 9(2), 2248–2258.

Makrigianni, V., Giannakas, A., Deligiannakis, Y. & Konstantinou, I. (2015). Adsorption of Phenol and Methylene Blue from Aqueous Solutions by Pyrolytic Tire Char: Equilibrium and Kinetic Studies. *Journal of Environmental Chemical Engineering*, 3, 574–582.

Marshall, W.E., Wartelle, L.H., Boler, D.E., Johns, M.M. & Toles, C.A. (1999). Enhanced Metal Adsorption by Soybean Hulls Modified with Citric Acid. *Methods*, 69, 263–268.

Memon, S.Q., Hasany, S.M., Bhanger, M.I. & Khuhawar, M.Y. (2005). Enrichment of Pb(II) Ions using Phthalic Acid Functionalized XAD-16 Resin as a Sorbent. *Journal of Colloid and Interface Science*, 291, 84–91.

Metilda, P., Sanghamitra, K., Mary Gladis, J., Naidu, G.R.K. & Prasada Rao, T. (2005). Amberlite XAD-4 Functionalized with Succinic Acid for the Solid Phase Extractive Preconcentration and Separation of Uranium(VI). *Talanta*, 65, 192–200.

 ©2017, IAHR. Used with permission / ISSN 1562-6865 (Online) - ISSN 1063-7710 (Print)

Mikati, F.M., Saade, N.A., Slim, K.A. & El Jamal, M.M. (2013). Biosorption of Methylene Blue on Chemically Modified Chaetophora Elegans Alga by HCL and Citric Acid. *Journal of Chemical Technology and Metallurgy*, 48, 61–71.

Owabor, C.N., Ono, U.M. & Isuekevbo, A. (2012). Enhanced Sorption of Naphthalene onto a Modified Clay Adsorbent: Effect of Acid, Base and Salt Modifications of Clay on Sorption Kinetics. *Advances in Chemical Engineering and Science*, 2, 330–335.

Rajan, K.S., & Martell, A.E. (1967). Equilibrium Studies of Uranyl Complexes—IV. Reactions with Carboxylic Acids. *Journal of Inorganic and Nuclear Chemistry*, 29, 523.

Reddy, P.M.K, Krushanmurty, K., Mahammadunnisa, S.K., Dayamani, A. & Subrahmanyam, C. (2015). Preparation of Activated Carbons from Bio-Waste: Effect of Surface Functional Groups on Methylene Blue Adsorption. *International Journal of Environmental Science and Technology*, 12, 1363–1372.

Schwantes, D., Goncalves Jr, A.C., Coelho, G.F., Campagnolo, M.A., Dragunski, D.C., Tarley, C.R.T., Miola, A.J. & Leismann, E.A.V. (2016). Chemical Modifications of Cassava Peel as Adsorbent Material for Metals Ions from Wastewater. *Journal of Chemistry*, 2016.

Sharma, R.K. & Pant, P. (2009). Preconcentration and Determination of Trace Metal Ions from Aqueous Samples by Newly Developed Gallic Acid Modified Amberlite XAD-16 Chelating Resin. *Journal of Hazardous Material*, 163, 295–301.

Shi, L., Zhang, G., Wei, D., Yan, T., Xue, X., Shi, S. & Wei, Q. (2014). Preparation and Utilization of Anaerobic Granular Sludge-based Biochar for the Adsorption of Methylene Blue from Aqueous Solutions. *Journal of Molecular Liquids*, 198, 334–340.

Tabrizi, N.S. & Yavari, M. (2015). Methylene Blue Removal by Carbon Nanotube-based Aerogels. *Chemical Engineering Research and Design*, 94, 516–523.

Tempkin, M.J. & Pyzhev, V. (1940). Kinetics of Ammonia Synthesis on Promoted Iron Catalyst. Acta Physiochimica URSS, 12, 217–222.

Tewari, P.K. & Singh, A.K. (1999). Amberlite XAD-2 Functionalized with Chromotropic Acid: Synthesis of a New Polymer Matrix and its Applications in Metal Ion Enrichment for Their Determination by Flame Atomic Absorption Spectrometry. *Analyst* 124, 1847–1851.

Tokalioglu, S., Çetin, V. & Kartal, S. (2008). Amberlite XAD – 1180 Modified with Thiosalicylic Acid : A New Chelating Resin for Separation and Preconcentration of Trace Metal Ions. *Chemia Analityczna*, 53(2), 263–276.

Uzun, A., Soylak, M. & Elci, L. (2001). Preconcentration and Separation with Amberlite XAD-4 Resin; Determination of Cu, Fe, Pb, Ni, Cd and Bi at Trace Levels in Waste Water Samples by Flame Atomic Absorption Spectrometry. *Talanta*, 54, 197–202.

Valderrama, C., Cortina, J.L., Farran, A., Gamisans, X. & Lao, C. (2007). Kinetics of Sorption of Polyaromatic Hydrocarbons onto Granular Activated Carbon and Macronet Hyper-Cross-Linked Polymers (MN200). *Journal of Colloid and Interface Science*, 310, 35–46.

Wang, Q., Zhang, D., Tian, S. & Ning, P. (2014). Simultaneous Adsorptive Removal of Methylene Blue and Copper Ions from Aqueous Solution by Ferrocene-modified Cation Exchange Resin. *Journal of Applied Polymer Science*, 131 (21).

Wang, S.B., Ma, Q. & Zhu, Z.H. (2009). Characteristics of Unburned Carbons and Their Application for Humic Acid Removal from Water, *Fuel Processing Technology*, 90, 375–380.

Weng, C.H., Lin, Y.T. & Tzeng, T.W. (2009). Removal of Methylene Blue from Aqueous Solution by Adsorption onto Pineapple Leaf Powder. *Journal of Hazardous Material*, 170, 417–24.

Yu, J., Li, B., Sun, X., Jun, Y. & Chi, R. (2009). Adsorption of Methylene Blue and Rhodamine B on Baker's Yeast and Photocatalytic Regeneration of the Biosorbent. *Biochemical Engineering Journal*, 45, 145–151.

Zhang, J., Ping, Q., Niu, M., Shi, H. & Li, N. (2013). Kinetics and Equilibrium Studies from the Methylene Blue Adsorption on Diatomite Treated with Sodium Hydroxide. *Applied Clay Science*, 83–84, 12–16.

Zhang, X., Li, A., Jiang, Z. & Zhang, Q. (2006). Adsorption of Dyes and Phenol from Water on Resin Adsorbents: Effect of Adsorbate Size and Pore Size Distribution. *Journal of Hazardous Material*, 137, 1115–1122.

Zheng, K., Pan, B.C., Zhang, Q.J., Han, Y.H., Zhang, W.M., Pan, B.J., Xu, Z.W., Zhang, Q.R., Du, W. & Zhang, Q.X. (2007). Enhanced Removal of p-Chloroaniline from Aqueous Solution by a Carboxylated Polymeric Sorbent. *Journal of Hazardous Materials*, 143, 462–468.

Zhou, Q., Gao, Q., Luo, W., Yan, C., Ji, Z. & Duan, P. (2015). One-Step Synthesis of Amino-Functionalized Attapulgite Clay Nanoparticles Adsorbent by Hydrothermal Carbonization of Chitosan for Removal of Methylene Blue from Wastewater. *Colloids Surfaces A: Physicochemical and Engineering Aspects*, 470, 248–257.

©2017, IAHR. Used with permission / ISSN 1562-6865 (Online) - ISSN 1063-7710 (Print)

Proceedings of the 37th IAHR World Congress
August 13 – 18, 2017, Kuala Lumpur, Malaysia

COPING WITH MULTI-YEAR DROUGHTS IN SOUTH KOREA: LESSONS FROM THE 2014-2015 DROUGHT

TAE-WOONG KIM[1], KYUNG SOO JUN[2], JOO-HEON LEE[3], JAE-HYUN AHN[4], MINSUNG KWON[5], DONG-HYEOK PARK[6], HYUNGSUN CHA[7], YOUNG HO SHIN[8], YONGHO KANG[9] & JISEON SONG[10]

[1] Department of Civil and Environmental Engineering, Hanyang University, Ansan, Korea, twkim72@hanyang.ac.kr
[2,5] Graduate School of Water Resources, Sungkyunkwan University, Suwon, Korea, ksjun@skku.edu; kwon.ms@skku.edu
[3] Dept. of Civil Engineering, Joongbu University, Goyang, Korea, leejh@joongbu.ac.kr
[4] Dept. of Civil Engineering, Seokyeong University, Seoul, Korea, wrr@skuniv.ac.kr
[6] Dept. of Civil and Environmental Engineering, Hanyang University, Seoul, Korea, smilehyuki@naver.com
[7,8,9,10] Water Resources Investigation & Planning Department, K-water, Daejeon, Korea, chasun@kwater.or.kr; yhshin@kwater.or.kr; hanmirr@kwater.or.kr; jiseon1987@kwater.or.kr

ABSTRACT

This study investigated the recent multi-year drought in South Korea from various perspective of hydro-meteorology and water resources management, and drew lessons for coping with extreme droughts under the changing climate. The 2014-2015 drought was an unprecedented event that occurred in January 2014 due to lack of precipitation and intensified during August and September over Seoul-Gyeonggi and Gangwon provinces. The drought continued and spread across the nation and became most severe during August and November 2015. In the southern provinces of Chungcheong, especially, the Boryung dam which provides waters for residence, industry and agriculture, reached the lowest water level in its history and encountered emergency circumstance to restrict water supplies. In order to cope with the 2014-2015 drought, the Korean government set up and operated the joint emergency task force team to implement preemptive drought response measures preventing of stopping water supply.

Keywords: Multi-year drought; response measure; emergency task force team; saving water; water management.

1 INTRODUCTION

Drought is a prevailing natural disaster affecting more people and resulting in more social, economic and environmental costs than other natural disasters. Drought is expected to increase in frequency and severity in the future as a result of climate change (Wilhite, 2006; WMO, 2009). Drought can occur in wide area and can cause food and economic problems (Sternberg, 2011). Since the local communities are interconnected, drought occurring within a specific region can have a global impact on food supplies and undermine the economics and stability of governments. Unlike flood, however, drought is a slow-onset and creeping natural disaster. Thus, we have sufficient time to reduce the drought damages through effective responses even during drought progresses. During the drought period, it is necessary to establish countermeasures to cope with drought by analyzing the weather and drought situation considering the reasons and types of drought (Wilhite and Glantz, 1985).

This study investigated the recent multi-year drought of 2014-2015 in South Korea, as well as the past severe droughts from various perspective of hydro-meteorology and water resources management, such as drought characteristics, drought damages, and existing countermeasures. This study also drew lessons for coping with extreme droughts under the changing climate.

2 MAJOR DROUGHTS IN THE PAST

The first drought records in Korea can be found in the Three Kingdoms period over 2,000 years ago. Ancient literature showed that people suffered from drought, and drought occurred in the spring and summer because of lack of rainfall. The severe droughts before 2013 is summarized in Table 1. Before 1940, there was no apparent response to the drought and there were periodic droughts with shortage of drinking water and agricultural water. Severe droughts occurred between 1960 and 2000. However, several institutional supports such as budgeting and tax reduction have been provided, and the development of agricultural well and groundwater has been facilitated. Since 1990, drought damage has decreased due to the development of irrigation technology and the construction of dams. After 2000, extreme droughts occurred. In 2001, drought occurred in Gyeongg-do, Gangwon-do and Chungcheong-do. In 2008-2009, drought occurred in Gyeongsangnam-do, Jeollanam-do and Gangwon-do. In addition, there was a nationwide drought in 2012.

 ©2017, IAHR. Used with permission / ISSN 1562-6865 (Online) - ISSN 1063-7710 (Print)

Due to the drought that occurred after 2000, there were problems in supplying agricultural water and domestic water. Although the government imposed limited water supply and provided measures to secure water resources, due to climate change/variability and urban development, people and society still face drought.

Table 1. Past droughts before 2013.

Period	Consequences
1927~1928	Lack of drinking water, Lack of agricultural water, Water dispute
1937~1939	Depletion of surface water, Reduction of rice production (37%)
1942~1944	Power generation water shortage
1958~1959	Agriculture and water shortage, Shutdown of the plant, Lack of drinking water (Seoul)
1967~1968	Lack of drinking water (Seoul), Reduction of rice production (18%)
1976~1978	Agricultural and industrial water shortage
1981~1982	River and a reservoir depletion, City water shortage
1994~1995	Lack of domestic water and industrial water, Crops and animal damage, Pollution of drinking water sources, Low water rate and reservoir depletion
2001	Domestic and agricultural water shortage, Deteriorating river water quality
2008~2009	Lack of drinking water (Taebaek), Crops and animal damage
2012	Domestic and agricultural water shortage

3 DROUGHT CONSEQUENCES (2014~2015)

3.1 Precipitation

The average precipitation in South Korea during the last 30 years is 1,333.3mm, and the precipitation in 1988 was the lowest in most watersheds except Nakdong River Basin. During 2014-2015, the precipitation of Han River basin recorded the second lowest. In 2015, the Han Rriver basin recorded the first lowest precipitation, and Geum river basin recorded the second lowest precipitation, in history, as shown in Table 2. The development of meteorological droughts is shown in Figure 1 using the standardized precipitation index with 6-month (SPI(6)).

3.2 Multipurpose dam reservoir

Figure 2 shows the status of multi-purpose dams in December 2014. Boryeong Dam, Hoengseong Dam and Yongdam Dam has recorded the lowest water level. Most of dams reached the caution and serious stages. It was estimated that the amount of water has decreased due to decrease in precipitation since 2014. The small precipitation in the Han River basin affected the decrease of the storage capacity of Soyang River dam, Chungju Dam and Hoengseung Dam. In particular, Boryeong Dam has a serious level of water storage because the amount of rainfall during the flood season in 2015 was less than one third of the previous year's amount. The average inflow of multi-purpose dams in 2015 was 7.83 billion m^3, which was 43.7% of the previous year's amount.

3.3 Drought affected area

The drought of 2014-2015 caused water supply damage. The largest water supply damages in 2015 were on June 19, with 26 cities, counties and districts, 51,241 households and 117,472 people affected. In Sokcho, 80,500 people in 36,100 households were subjected to water restriction for 8 hours (22:00 ~ 06: 00) for 9 days (Jun 17 ~ Jun 25), as shown in Figure 3. On the other hand, Boryeong Dam, which is responsible for water supply in western Chungcheong province, reached the lowest water storage rate (18.9%, 2015.11.6.), as shown in Figure 4. Although the supply of water was limited, damage did not occur due to preemptive response such as adjustment of the water supply system, water saving subsidy system, autonomous water supply adjustment and construction of Boryeong dam waterway.

©2017, IAHR. Used with permission / ISSN 1562-6865 (Online) - ISSN 1063-7710 (Print)

Table 2. Precipitation ranks.

	Total	Han River	Nakdong River	Geum River	Seomjin River	Youngsan River
Average (1981~2010)	1,333.3	1,366.7	1,227.8	1,272.1	1,428.1	1,383.6
Minimum (Year)	831.1 (1988)	965.5 (1988)	794.5 (1994)	783.7 (1988)	808.0 (1988)	803.2 (1988)
2014 (Rank)	1,157.0 (12)	873.3 (2)	1,225.0 (16)	1,096.1 (10)	1,526.8 (23)	1,367.2 (14)
2015 (Rank)	942.9 (4)	813.6 (1)	931.6 (6)	832.4 (2)	1,130.2 (7)	1,118.3 (8)

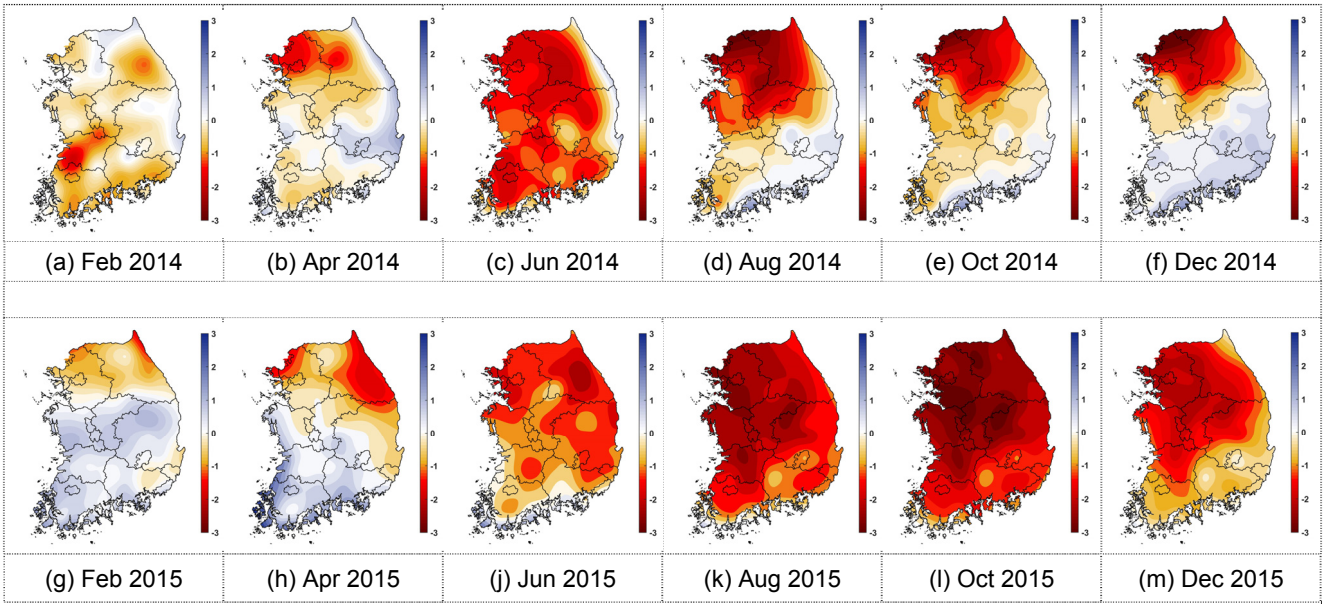

Figure 1. Temporal and spatial changes in SPI(6) during the 2014-2015 drought.

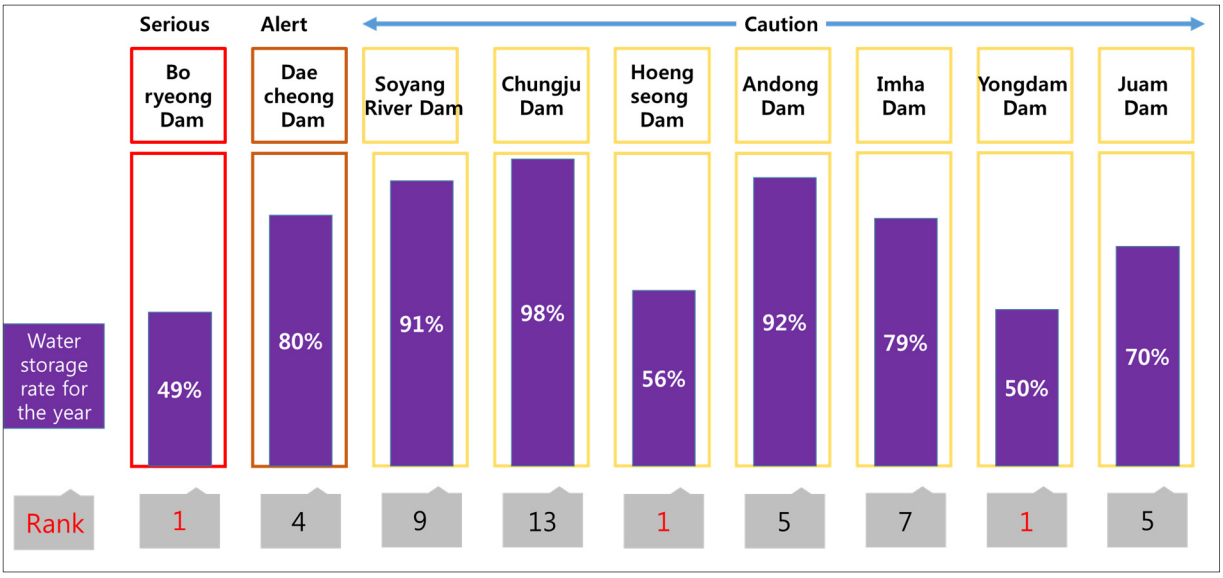

Figure 2. Water storage rate compared to previous years (2015.12).

©2017, IAHR. Used with permission / ISSN 1562-6865 (Online) - ISSN 1063-7710 (Print)

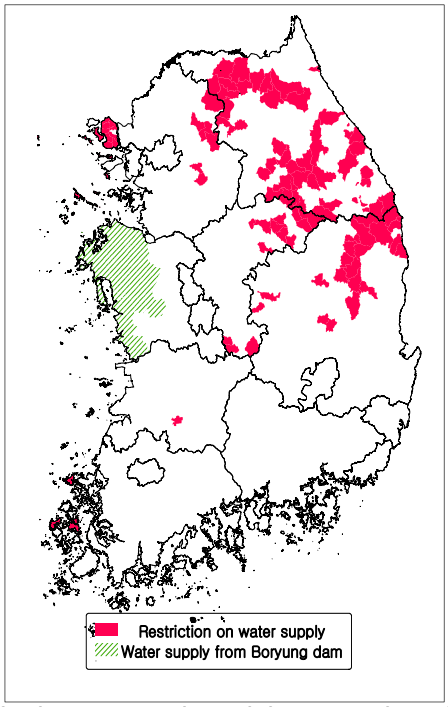

Figure 3. Areas affected by the limited water supply and the area where Boryeong dam provides water.

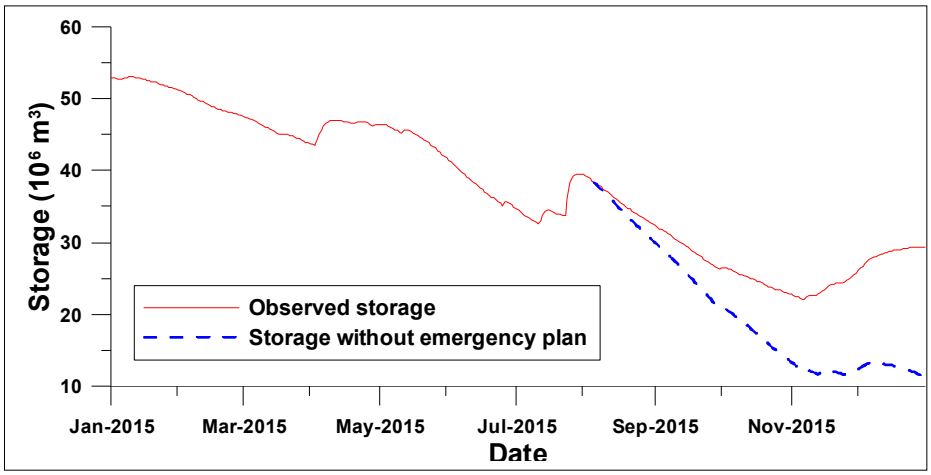

Figure 4. Comparison of the dam storages between when implementing the project to respond drought (solid line) and not (dashed line).

4 2014~2015 DROUGHT

4.1 Meteorological cause of drought

Various analysis were conducted to analyze the 2014~2015 drought. Considering the characteristics of climate change according to El Niño, we analyzed the cause of drought in 2014~2015. After the El Niño in June 2014, the sea surface temperatures differ by more than 3 °C in 2015. The precipitation was the lowest and the temperature was the highest of the Han River basin. When El Niño occurred, the high pressures of the western Pacific increased and drought and high temperature phenomena occurred in Asia. In South Korea, an abnormal high temperature occurred in January 2015, as shown in Figure 5. In addition, there have been abnormal high temperatures, heat waves, tropical nights, and annual precipitation (common year 72%).

4.2 Operational perspective of drought

The management of water resources is important because of the seasonal changes in South Korea. Since 1965, living and industrial water use has increased as the level of living and industry has increased. On the other hand, the use of agricultural water decreased as the share of agriculture decreased. In addition, water resources are limited in South Korea, but as water usage per person increased, thus water shortage occurred.

In South Korea, the average annual precipitation is 1.6 times that of the world average, and the amount of water resources is 135.6 billion m^3/year. However, due to the high density of population, annual

©2017, IAHR. Used with permission / ISSN 1562-6865 (Online) - ISSN 1063-7710 (Print)

precipitation per person is 2,673m^3. In particular, the amount of precipitation concentrated in the summer makes the water management more difficult. In addition, the water price for living, agriculture and industry is cheap and the use of water is increasing. Due to the low water rate, it is difficult to reinvest the facility for improvement. Thus, from a long-term point of view, stable water supply is very challenging to be achieved.

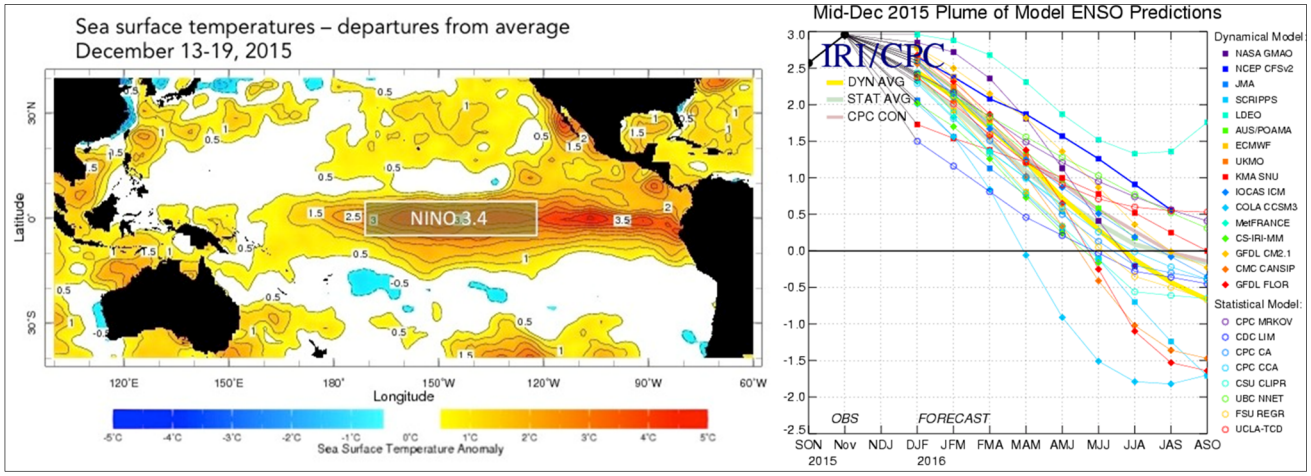

Figure 5. Temperature variation of sea surface (December 2015, left), Sea surface temperature of El Nino surveillance area (right).

4.3 Drought management system

Unlike flooding, drought has a long-term impact on society. Structural measures to secure water resources have been proposed to reduce drought damage. However, it is limited to overcome drought only by structural measures. Structural measures and drought management systems should be used for preemptive response, recovery, and planning for drought. Current drought management is inefficient and there is no integrated control agency. In addition, the construction and sharing of data of drought were not well performed during decision-making process. There is no division of information for public organizations, and public institutions are not closely linked to determine the stages of drought. To solve these problems, system development, information sharing, and system for drought management are needed.

4.4 Countermeasures to overcome drought

Including the western region of Chungcheongnam-do, many communities suffered due to the drought in 2014~2015. Precipitation was only 31.9% (257mm) in July to September 2015 and cumulative rainfall was the lowest since the dam construction. Boryeong Dam recorded a low rate (18.9%) in November 2015, but the severe damage did not occur in the following responses.

i. (Water system adjustment) Supply of 31,000m^3/day to Dangjin-si and Seocheon-gun by using nearby waters;
ii. (Water saving fund) Signed a water conservation agreement with city government and power plant (2015.10~12, 2,808m^3 water saving) (Table 3);
iii. (Autonomous water adjustment) 20% reduction by autonomous water saving;
iv. (Leakage reduction business) Emergency leakage project (5 local governments including Boryeong-si) (Table 4);
v. (Boryeong dam construction of waterway) Construction of waterway connecting Boryeong Dam and Geum River;
vi. (Sprinkler cart and water bottle support) Preemptively use sprinkler cart and water bottles to prepare for emergencies;
vii. (Water conservation public relations) Build consensus on water conservation.

Table 3. Effect of water saving with granting the Incentive.

	Total	Dangjin	Boryeong	Seosan	Seocheon	Yesan	Cheongyang	Taean	Hongseong
Amount of water saving (million m^3)	2,808	480	425	739	193	190	54	332	395
Participation rate (%)	47.2	42.4	51.5	58.1	42.3	42.0	48.1	47.9	42.3

 ©2017, IAHR. Used with permission / ISSN 1562-6865 (Online) - ISSN 1063-7710 (Print)

Table 4. Results of implementing the project to reduce water leaks.

	Total	Boryeong	Hongseong	Taean	Cheongyang	Dangjin
Exploration / Restoration (cases)	252/207	78/57	82/77	63/62	10/7	19/4
Amount of water saving (m^3/day)	7,420	3,078	2,542	1,082	306	412

5 CONCLUSIONS

Water management has been challenging in recent time, due to continuous droughts between 2014 and 2015. However, agricultural and living water encountered damage that was significantly reduced compared to the past droughts, because of the well-timed establishment and implementation of proper drought countermeasures. When this is compared with that in the past drought response measures, it was made after the damage occurred. In order to cope with the 2014-2015 drought, the Korean government set up and operated the joint emergency task force team to implement preemptive drought response measures preventing stopping water supply; (1) adjusting the water supply system. Using surplus water in a nearby inter-regional water system, municipal water was delivered to drought-affected areas within Chungcheong province (providing waters of 31,000 m^3/day); (2) granting incentive of water saving. Communities that receive waters from the Boryung dam made an agreement to implement water saving and to provide the incentive of water saving (saving waters of 2,808m^3 from October to December 2015); (3) promoting the voluntary water saving campaign. The residents of drought-affected areas voluntarily participated in the water-saving campaign (saving resident waters by 20%); (4) reducing water leaks. The local governments of drought-affected areas implemented the emergency works for reducing water leaks; (5) constructing the emergency waterway from the Geum River to the Boryung dam (providing waters of 115,000m^3/day).

In summary, the Ministry of Land, Infrastructure and Transport and K-water reserved the water before the drought and Ministry of Agriculture, Food and Rural Affairs and Korea Rural Corporation minimized drought damage by storing water in reservoirs. Along with these measures local governments also need tailored measures, as shown in Figure 6. To do this, local governments need to provide laws and guidelines to establish regular and concrete drought measures.

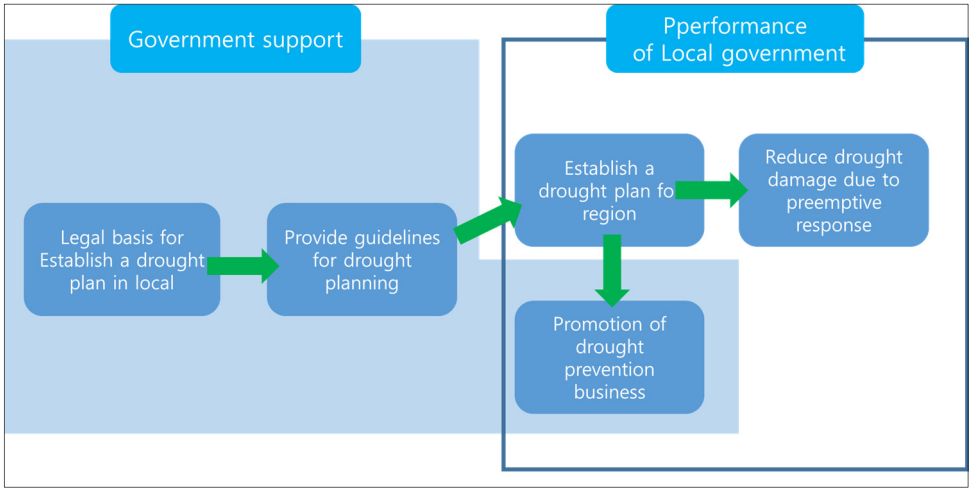

Figure 6. Relations between central and local governments for drought mitigation.

ACKNOWLEDGEMENTS

This research is supported by grants (14AWMP-B082564-01 and 16AWMP-B079625-03) from Advanced Water Management Research Program funded by Ministry of Land, Infrastructure and Transport of Korean government.

REFERENCES

Sternberg, T. (2011). Regional Drought Has a Global Impact. *Nature*, 472(7342), 169.

Wilhite, D.A. (2006). *Drought Monitoring and Early Warning: Concepts, Progress and Future Challenges*. World Meteorological Organization.

Wilhite, D.A. & Glantz, M.H. (1985). Understanding: The Drought Phenomenon: The Role of Definitions. *Water International*, 10(3), 111-120.

World Meteorological Organization (WMO). (2009). *Experts Agree on a Universal Drought Index to Cope with Climate Risks*, WMO Press Release No. 872, http://www.wmo.int/pages/prog/wcp/agm/meetings/wies09/documents/872_en.pdf.

©2017, IAHR. Used with permission / ISSN 1562-6865 (Online) - ISSN 1063-7710 (Print)

Proceedings of the 37th IAHR World Congress
August 13 – 18, 2017, Kuala Lumpur, Malaysia

ASSESSING UNCERTAINTY OF VARIABLE SOURCE AREA, HYDROLOGICAL MODEL IN HARANGI WATERSHED, KARNATAKA STATE, INDIA

KUMAR RAJU B.C[(1)] & LAKSHMAN NANDAGIRI[(2)]

[(1)] Department of Civil Engineering, ACS College of Engineering, Kambipura, Bangalore, India, kumarrajubc@gmail.com
[(2)] Department of Applied Mechanics & Hydraulics National Institute of Technology Karnataka, Surathkal, Mangalore, India, lnand@rocketmail.com

ABSTRACT

Assessing uncertainty associated with distributed Variable Source Area (VSA) hydrological models are essential for accurate simulation of stream flows of the humid tropical watersheds. The present study is taken up to assess the uncertainties associated with the Soil and Water Assessment Tool – VSA (SWAT-VSA) model using Generalized Likelihood Uncertainty Estimation (GLUE) technique. The study is carried out in Harangi watershed (538.8km^2) located in the humid region of Karnataka State, India. The goodness-of-fit and efficiency of the model have been tested using the Nash-Sutcliffe efficiency (E_{NS}) as the objective function. Sensitivity analysis indicated that model parameters CN_2, Alpha_Bf and Sol_Awc are important for simulating uncertainty associated with stream flows. The P-factor, which is the percentage of observed data bracketed by the 95% prediction uncertainty (95PPU), was 43% and 48% during calibration and validation periods. The results indicated that the GLUE technique applied on the SWAT-VSA model performed well in quantifying uncertainties in stream flow estimates at the outlet of the Harangi watershed.

Keywords: Hydrological modeling; uncertainty analysis; curve number (CN); variable source area (VSA); SWAT.

1 INTRODUCTION

In recent times, it is widely accepted that all hydrological modeling exercises must provide a detailed report of the associated uncertainty in predictions. Proper consideration of uncertainty in hydrological modeling is essential for assessment of water balance components and optimal planning and management of water and land resources (Wagener and Gupta, 2005). Uncertainty analysis is a process of identifying and quantifying uncertainties associated with model structure, input data and parameters of a hydrological model (Beven and Binley, 1992; Muleta and Nicklow, 2005). The uncertainty associated with model structure and its parameter and input data affects the efficiency of the predictions of hydrological models. The various sources of error and uncertainty in hydrological modeling have been analyzed by various researchers (Beven and Freer, 2001; Schaefli et al., 2007; Ewen et al., 2006). Ewen et al. (2006) gave a comprehensive description of the error sources in hydrological modeling, which were categorized into three groups: 1) model structure error 2) model parameter error and 3) run time error. These three components contributed to the "integrated" model output error, but the individual contribution of each error cannot be isolated because it is difficult to understand hydrologic responses of the watersheds

Many uncertainty analysis methods have been introduced in hydrological modeling, which includes Generalized Likelihood Uncertainty Estimation (GLUE) (Beven and Binley, 1992), Importance sampling (Kuczera and Parent, 1998), Markov Chain Monte Carlo (MCMC) (Kuczera and Parent, 1998; Vrugt et al., 2003), Sequential Uncertainty Fitting (SUFI-2) (Abbaspour et al., 2004), Parameter solutions (ParaSol) (Van Griensven et al., 2006), Ensemble Kalman Filter (EnKF) (Vrugt et al., 2005), Bayesian Recursive Estimation (BaRE) (Thiemann et al., 2001), and Bayesian Model Averaging (BMA) (Ajami et al., 2007; Duan et al., 2007, Vrugt and Robinson, 2007). Among the many uncertainty analysis methods that have been introduced in hydrological modeling, GLUE and SUFI-2 use the flexible likelihood function to assign different levels of confidence to different parameter sets or models.

2 STUDY AREA AND DATA

The Harangi river originates in the Pushpagiri Hills of Western Ghats and joins the Cauvery near Kudige in Madkeri. The watershed is located in Karnataka State and has an area of 538.8km^2 (Figure 1). Elevation in the Harangi watershed ranges from 818m to 1635m. While average annual rainfall exceeds 3000mm, the mean maximum and minimum temperatures are 36^{0}C and 4.8^{0}C respectively. The major LU/LC categories in the Harangi watershed included forest (62.39%), agricultural (32.80%), urban (1.57%) and water bodies/reservoirs (3.24%). Daily stream flow output from the watershed was monitored as inflow into the Harangi dam (Figure 1). The LU/LC map and characteristics of the Harangi watershed are shown in Figure 2 and Table 1 respectively.

 ©2017, IAHR. Used with permission / ISSN 1562-6865 (Online) - ISSN 1063-7710 (Print)

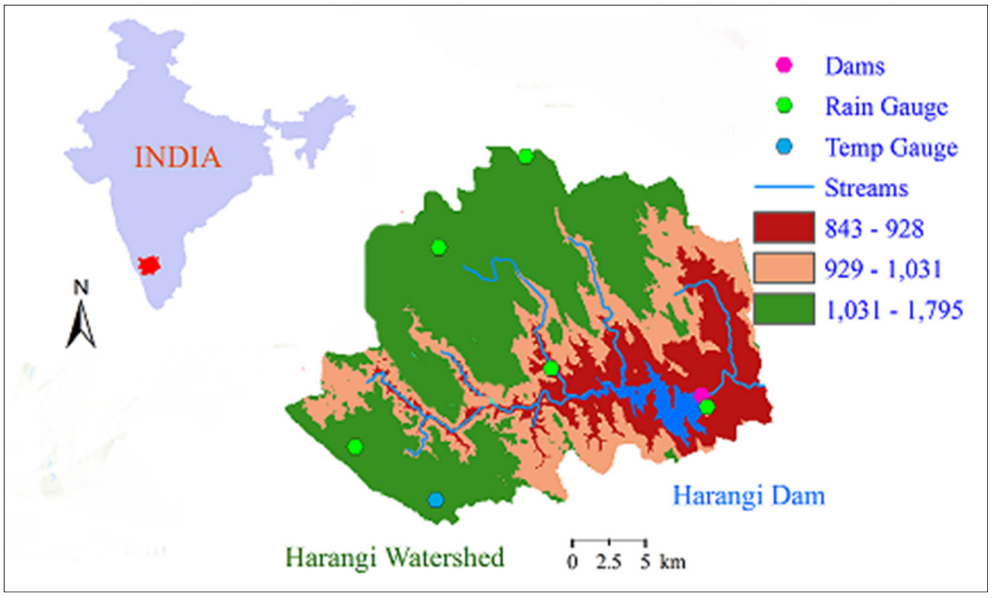

Figure1. Location Maps of Harangi watershed showing elevations, stream network and location of dams, rain gauges and climate stations.

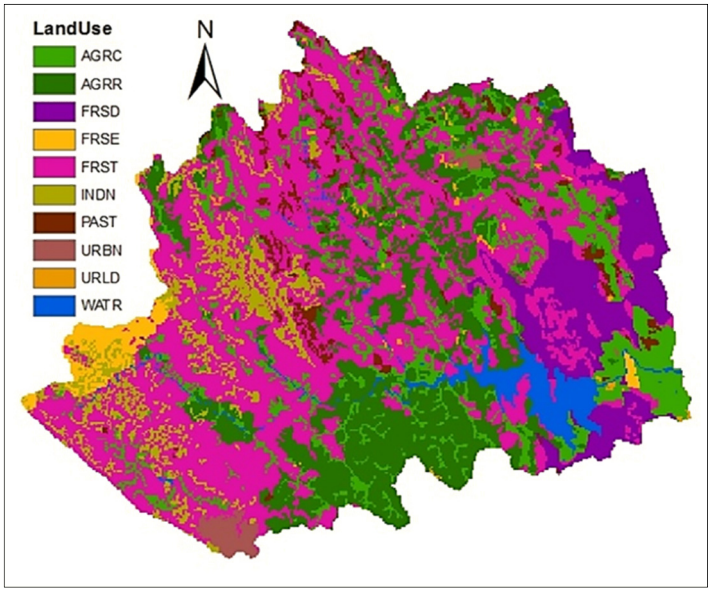

Figure 2. LU/LC of the Harangi watershed.

Table 1. Characteristics of LU/LC in the Harangi watershed.

Land use	Class	Area (km^2)	Watershed area (%)
Residential	URBN	6.07	1.13
Residential-Low Density	URLD	2.46	0.46
Agricultural Land-Close-grown	AGRC	72.21	13.40
Agricultural Land-Row Crops	AGRR	104.87	19.46
Forest-Evergreen	FRSE	10.46	1.94
Forest-Deciduous	FRSD	45.08	8.37
Forest-Mixed	FRST	232.84	43.21
Pasture	PAST	13.59	2.52
Water	WATR	17.45	3.24
Indian grass	INDN	33.77	6.27

©2017, IAHR. Used with permission / ISSN 1562-6865 (Online) - ISSN 1063-7710 (Print)

3 METHODS

3.1 SWAT-VSA

The SWAT-VSA model (Easton et al., 2008) incorporates VSA hydrology in terms of CN-VSA equation for capturing the spatial pattern of saturation excess runoff from source areas. The re-conceptualization of SWAT model helps in modeling VSAs without any modification in the code of the original model and thus provides an efficient and easy way of capturing spatially variant saturation excess runoff processes from the landscape. CN-VSA hydrology distinguishes between unsaturated and saturated areas in the catchment and assumes that all rainfall infiltrates in the unsaturated areas and all rain falling on saturated areas is converted into runoff. Based on this assumption, Steenhuis et al. (1995) derived the following equation for the fractional runoff contributing area for a rainfall event (A_f):

$$A_f = 1 - \frac{S_e^2}{\left(P_e + S_e\right)^2} \quad [1]$$

According to Eq. [1], runoff only occurs from areas that have local effective storage, σ_e, which is less than effective precipitation. By substituting σ_e for P_e in Eq. [1], with the purpose of making local effective soil water storage less than or equal to σ_e for a specified overall watershed storage of S_e, a relationship for a fraction of watershed area A_s can be expressed as (Steenhuis et al., 1995):

$$A_s = 1 - \frac{S_e^2}{\left(\sigma_e + S_e\right)^2} \quad [2]$$

According to Schneiderman et al. (2007), runoff for an area, q_i (mm), can be expressed as:

$$q_i = P_e - \sigma_e \qquad \text{for } P_e > \sigma_e, \quad [3]$$

For $P_e \leq \sigma_e$ the unsaturated portion of the watershed, $q_i=0$. To avoid changing the SWAT code, Easton et al. (2008) proposed approximating Eq. [3] with the CN equation:

$$Q_{surf} = \frac{P_e^2}{\left(P_e - \sigma_e\right)} \quad [4]$$

The SWAT-VSA model uses Soil Topographic Index (STI) in place of soil input and the area of each HRU was defined by the concurrence of land use and STI. STI classifies each unit of a watershed into a relative tendency to become saturated and producing a saturation excess response to runoff. The STI map is generated by using the following equation:

$$STI = \ln\left(\frac{a}{T\tan\beta}\right) \quad [5]$$

where 'a' is the upslope contributing area for the cell per unit of contour line (m), $\tan\beta$ is the topographic slope of the cell and T is the transmissivity of the uppermost soil layer (m^2/d). The local storage deficit of each wetness class ($\sigma_{e,i}$) is determined by integrating Eq. [4] over the fraction of the watershed represented by that wetness class (Schneiderman et al., 2007):

$$\sigma_{e,i} = \int_{A_{s,i}}^{A_{s,i+1}} \sigma_e * d\overline{A}_s$$

$$= \frac{2S_e\left(\sqrt{1-A_{s,i}} - \sqrt{1-A_{s,i+1}}\right)}{\left(A_{s,i+1} - A_{s,i}\right)} - S_e \quad [6]$$

where the fractional area ($A_{s,i}$) corresponded to each wetness index class that is bounded one side by the fraction of watershed that is wetter and other side by the fraction of the watershed that is dryer.

 ©2017, IAHR. Used with permission / ISSN 1562-6865 (Online) - ISSN 1063-7710 (Print)

3.2 Generalized Likelihood Uncertainty Equation (GLUE)

GLUE is motivated by sampling and regional sensitivity analysis of hydrological modeling. GLUE assumes that, in the case of large over-parameterized models, there is no unique set of parameters, which optimizes goodness-of fit criteria. The sources of uncertainties associated with the input, model structure and its parameter were accounted through parameter uncertainty (Beven and Binley, 1992). Parameter uncertainty was described as a set of discrete behavioural parameter sets with corresponding likelihood weights. The following steps were used in the GLUE uncertainty analysis as described by (Yang et al., 2008):

1) After the detention of the generalized likelihood measure L(θ), a large number of parameter sets were randomly sampled from prior uniform distribution and each parameter set was assessed as either behavioral or non-behavioural through a comparison of the likelihood measured with a selected threshold value.
2) Each behavioural parameter set was given a likelihood weight according to:

$$W_i = \frac{L(\theta_i)}{\sum_{k=1}^{N} L(\theta_k)} \quad [7]$$

where N is the number of behavioural parameter sets.

3) The uncertainty was described by quantile of the cumulative distribution realized from the weighted behavioural parameter sets. In the literature, the most frequently used likelihood measure for GLUE is the Nash–Sutcliffe efficiency (E_{NS}), which is also used in the SWAT-CUP program:

$$E_{NS} = 1 - \frac{\sum_{t_i=1}^{n} \left(y_{t_i}^{m}(\theta) - y_{t_i}\right)^2}{\sum_{t_i=1}^{n} \left(y_{t_i} - \bar{y}\right)^2} \quad [8]$$

where n is the number of the observed data points, y_{t_i} and $y_{t_i}^{m}(\theta)$ represents the observation and model simulation with parameters θ at time t_i respectively and $\bar{y}$ is the average value of the observations.

4 RESULTS AND DISCUSSIONS

4.1 Sensitivity analysis using GLUE

The five sensitive parameters Alpha_Bf, CN_2, Gwqmn, Sol_Awc and Esco were considered for performing uncertainty analysis of the SWAT-VSA model using GLUE technique. For the Harangi watershed, differences in parameter relative sensitivity of the model for the techniques are shown in Table 2. The dotty plots shown in Figure 3 demonstrate that for each parameter, solutions with equally good values of the E_{NS} efficiency can be found within the complete prior range of the GLUE for SWAT-VSA model. Moderate levels of good simulation could be found for both the techniques with E_{NS} efficiency above 0.70. Also, these plots clearly showed that there was no single optimum parameter, but many parameter sets can provide similar E_{NS} efficiency values.

Table 2. Parameter sensitivities for Harangi Watershed.

Parameter	t-stat	P-value
CN_2	11.89	0
Esco	-1.868	0.062
Gwqmn	-1.14	0.254
Alpha_Bf	16.36	0
Sol_Awc	1.632	0

©2017, IAHR. Used with permission / ISSN 1562-6865 (Online) - ISSN 1063-7710 (Print)

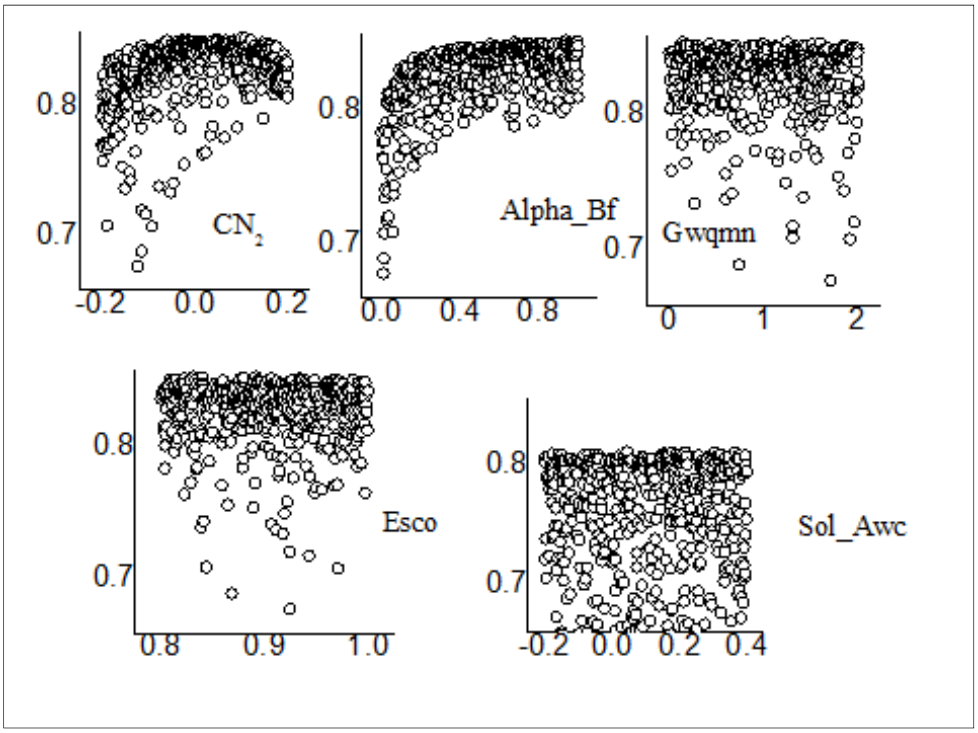

Figure 3. Dotty plot of ENS efficiency (y-axis) against each aggregate SWAT-VSA parameter (x-axis) conditioning with GLUE for Harangi watershed.

4.2 Uncertainty analysis using GLUE and SUFI-2

GLUE technique was used for calibration and uncertainty analysis of the SWAT-VSA model using daily observed dam inflow data of Harangi dam for Harangi watershed for the period of January 01, 2000 to December 31, 2003. Daily observed dam inflow data from January 01, 2004 to December 31, 2006 was used to validate the models. Model performances evaluated using four statistical measures: P-factor, R-factor, E_{NS} and R^2 are shown both for calibration and validation phases in Table 3. The comparison between the observed and simulated streamflow indicated that there is a good agreement between the observed and simulated streamflow which was verified by higher values of R^2 and E_{NS}. Figure 4 show the time series graph for observed and simulated streamflow (m^3/s) with the 95% prediction uncertainty (95PPU) band for the GLUE. From these figures, it was noticed that during the calibration and validation phase, observed streamflow was simulated reasonably well by SWAT-VSA model for the Harangi watershed. For the Harangi watershed, GLUE results indicated that the P-factor brackets of 43% and 48% of the observation and R-factor value of 0.35 and 0.39 during calibration and validation periods respectively for SWAT-VSA model. Its observed that GLUE predicted lower values of P-factor and R-factor for SWAT-VSA model.

Table 3. Performance evaluation criteria for the SWAT-VSA during calibration and validation for Harangi Watershed.

Phase	Statistical Criteria	Calibration	Validation
	P-factor (%)	43	48
	R-factor	0.35	0.39
	R^2	0.84	0.84
	E_{NS}	0.83	0.83

 ©2017, IAHR. Used with permission / ISSN 1562-6865 (Online) - ISSN 1063-7710 (Print)

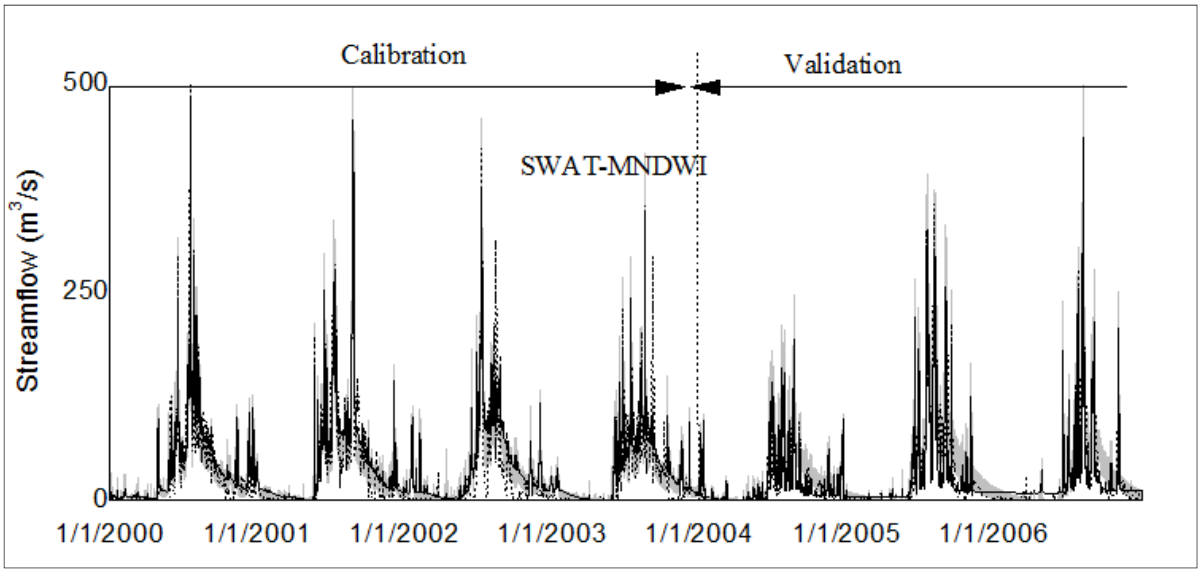

Figure 4. 95PPU (shaded area) derived by GLUE during calibration and validation period. The black dash line corresponds to the observed discharge at the outlet, while the black solid line represents the best simulation obtained for Harangi watershed.

5 CONCLUSIONS

The SWAT-CUP tool was used for automatic calibration and uncertainty analysis of developed hydrological models.GLUE technique is implemented to SWAT-VSA model and applied to Harangi watershed. For the Harangi watershed CN_2 and Sol_Awc are the important parameters but Alpha_Bf also proved to be an important parameter with P-value equal to zero. The performance of the above technique is good at bracketing uncertainty in the models using 95PPU band.For GLUE, R-factor during the validation phase in the Harangi watershed is 0.39 for the SWAT-VSA model. The Nash-Sutcliffe efficiency values (E_{NS}) estimated by GLUE is 0.84 and coefficient of determination (R^2) is 0.83. Overall results indicated that the GLUE technique applied on the SWAT-VSA model performed best to quantify the prediction of uncertainty of stream flows at the outlet of watershed.

REFERENCES

Abbaspour, K.C., Johnson, C.A. & Van Genuchten, M.T. (2004). Estimating Uncertain Flow and Transport Parameters Using a Sequential Uncertainty Fitting Procedure. *Vadose Zone Journal*, 3(4), 1340-1352.

Ajami, N.K., Duan, Q. & Sorooshian, S. (2007). An Integrated Hydrologic Bayesian Multimodel Combination Framework: Confronting Input, Parameter, and Model Structural Uncertainty in Hydrologic Prediction. *Water Resources Researc*h, 43(1).

Beven, K. & Binley, A. (1992). The Future of Distributed Models: Model Calibration and Uncertainty Prediction. *Hydrological Processes*, 6(3), 279-298.

Beven, K. & Freer, J. (2001). Equifinality, Data Assimilation, and Uncertainty Estimation in Mechanistic Modelling of Complex Environmental Systems Using the GLUE Methodology. *Journal of Hydrology*, 249(1), 11-29.

Duan, Q., Ajami, N.K., Gao, X. & Sorooshian, S. (2007). Multi-Model Ensemble Hydrologic Prediction Using Bayesian Model Averaging. *Advances in Water Resources*, 30(5), 1371-1386.

Easton, Z.M., Fuka, D.R., Walter, M.T., Cowan, D.M., Schneiderman, E.M. & Steenhuis, T.S. (2008). Re-Conceptualizing the Soil and Water Assessment Tool (SWAT) Model to Predict Runoff from Variable Source Areas. *Journal of Hydrology*, 348(3), 279-291.

Ewen, J., O'Donnell, G., Burton, A. & O'Connell, E. (2006). Errors and Uncertainty in Physically-Based Rainfall-Runoff Modelling of Catchment Change Effects. *Journal of Hydrology*, 330(3), 641-650.

Kuczera, G. & Parent, E. (1998). Monte Carlo Assessment of Parameter Uncertainty in Conceptual Catchment Models: The Metropolis Algorithm. *Journal of Hydrology*, 211(1), 69-85.

Muleta, M.K. & Nicklow, J.W. (2005). Sensitivity and Uncertainty Analysis Coupled with Automatic Calibration for a Distributed Watershed Model. *Journal of Hydrology*, 306(1), 127-145.

Schaefli, B., Talamba, D.B. & Musy, A. (2007). Quantifying Hydrological Modeling Errors Through a Mixture of Normal Distributions. *Journal of Hydrology*, 332(3), 303-315.

Schneiderman, E.M., Steenhuis, T.S., Thongs, D.J., Easton, Z.M., Zion, M.S., Neal, A.L., Mendoza, G.F. & Todd Walter, M. (2007). Incorporating Variable Source Area Hydrology into a Curve-Number-Based Watershed Model. *Hydrological Processes*, 21(25), 3420-3430.

©2017, IAHR. Used with permission / ISSN 1562-6865 (Online) - ISSN 1063-7710 (Print)

Steenhuis, T., Winchell, M., Rossing, J., Zollweg, J. & Walter, M. (1995). SCS Runoff Equation Revisited for Variable-Source Runoff Areas. *Journal of Irrigation and Drainage Engineering*, 121(3), 234-238.

Thiemann, M., Trosset, M., Gupta, H.V. & Sorooshian, S. (2001). Bayesian Recursive Parameter Estimation for Hydrologic Models. Water Resources Research, 37(10), 2521-2535.

Van Griensven, A., Meixner, T., Grunwald, S., Bishop, T., Diluzio, M. & Srinivasan, R. (2006). A Global Sensitivity Analysis Tool for the Parameters of Multi-Variable Catchment Models. *Journal of Hydrology*, 324(1), 10-23.

Vrugt, J.A., Diks, C.G.H., Gupta, H.V., Bouten, W. & Verstraten, J.M. (2005). Improved Treatment of Uncertainty in Hydrologic Modeling: Combining the Strengths of Global Optimization and Data Assimilation. *Water Resources Research*, 41(1).

Vrugt, J.A., Gupta, H.V., Bouten, W. & Sorooshian, S. (2003). A Shuffled Complex Evolution Metropolis Algorithm for Optimization and Uncertainty Assessment of Hydrologic Model Parameters. *Water Resources Research*, 39(8), 1201.

Vrugt, J.A. & Robinson, B.A. (2007). Treatment of Uncertainty Using Ensemble Methods: Comparison of Sequential Data Assimilation and Bayesian Model Averaging. *Water Resources Research*, 43(1).

Wagener, T. & Gupta, H.V. (2005). Model Identification for Hydrological Forecasting under Uncertainty. *Stochastic Environmental Research and Risk Assessment*, 19(6), 378-387.

Yang, J., Reichert, P., Abbaspour, K.C., Xia, J. & Yang, H. (2008). Comparing uncertainty Analysis Techniques for a SWAT Application to the Chaohe Basin in China. *Journal of Hydrology*, 358(1), 1-23.

 ©2017, IAHR. Used with permission / ISSN 1562-6865 (Online) - ISSN 1063-7710 (Print)

ANALYSIS ON REGIONAL SOCIO-ECONOMIC WATER CONSUMPTION REGULATION BASED ON MATHEMATICAL PROGRAMMING

HONGYUAN FANG[1], CHENGLING LIU[2] & CHEN CHEN[3]

[1,2,3] School of Hydraulic, Energy and Power Engineering, Yangzhou University, Yangzhou, China,
hyfang4936@aliyun.com; 862239647@qq.com; 398022755@qq.com

ABSTRACT

Proceeded from significance of industrial structure adjustment and water use efficiency control to the Hydrosocial-Cycle regulation, the present work, takes Yancheng City, a typical area in Jiangsu Coastal District as case study region where the nonlinear programming model is proposed by using Logarithmic Mean Divisia Index approach and mathematical programming method to study regional socio-economic water consumption regulation strategy. The model contains the constraints on total water-use quantity limit, water-use efficiency and quantization equations of driving factors decomposition effect. It also takes full account of socio-economic development at present situation and plan, water resources utilization strategy and target plus saving-water society construction planning. For analysis period of 2010 to 2016 year, the rational scheme on Yancheng City's socio-economic development size, industrial structure proportion and water resources utilization efficiency is obtained by solving the model. According to computation results corresponding to water utilization, industrial structure, economic development level and population scale, the characteristic of driving factors effects are analyzed, as well adjustment policy of the primary industry, secondary industry and tertiary industry, and water consumption regulation measures were drawn out.

Keywords: Regional water resources; total water-use quantity limit; factors decomposition; socio-economic water consumption; mathematical programming model.

1 INTRODUCTION

Water resources are one of the most important internal driving forces and restriction factors to impact regional economic development and industrial structure change characteristics. Reasonable adjustment of industrial structure is conducive to the balance of supply and demand of regional water resources and promotion of the sustainable utilization of water resources (Lei et al., 2004; Wang et al., 2003; Xu et al., 1997). In the process of hydrosocial-cycle regulation, industrial structure adjustment and water quota management of socio-economy (*i.e.* water efficiency control) play a key role, because the development of socio-economy consequentially promote the growth of water demand, and with the increase of water the regional development and utilization of water resources will be strengthened. Thus, the further development of regional economy is affected and the change of ecological environment is caused. The causal relationship between water demand growth and socio-economic development and ecological system degradation will force adjusting regional economic structure, and improving water use efficiency through implementing regional water-saving measures (Wang et al., 2014; Wang et al., 2011; Chen, 2006).

In the present work, the Yancheng City, which is located in the Jiangsu coastal development district, is taken as the study region. According to the socio-economic situation and development plan, strategic objectives of water resources development and utilization, water-saving society construction planning and other specific circumstances are achieved by using the driving factor analysis of water resources utilization and mathematical programming method and the analytical model. These models are established to obtain the reasonable plan ensuring the planning of socio-economic scale, industrial structure ratio and water efficiency to satisfy total water-use quantity limit within the planning period of study region.

2 DRIVING FACTOR ANALYSIS OF WATER RESOURCES UTILIZATION

In the reasons analysis of energy and resource utilization, as well as carbon emissions change, IDA (Index Decomposition Analysis) was widely used in many countries. IDA is the method applying index concepts into the decomposition analysis, by which actually the total amount was expressed as the product of components, where several factors, and decomposition procedure was determined based on the adopted methods of decomposition weight calculation. This is to obtain the incremental share of each index. Among several existing exponential decomposition methods, Logarithmic Mean Divisia Index (LMDI) method was widely used (Ang, 2004; Ang et al., 2001), due to resolving reasonably the residuals problem. Through comparative analysis for a series of decomposition methods, Ang and Liu (2001) pointed out that the decomposition of LMDI does not produce residuals, with some advantages such as full decomposition, no residual items, consistent polymerization, and flexibility. Since the subjectivity and arbitrariness of parameter

©2017, IAHR. Used with permission / ISSN 1562-6865 (Online) - ISSN 1063-7710 (Print)

estimation can be avoided and the calculation is simple, the LMDI method was applied to related fields by many researchers.

The related literatures showed that there were many applications of the exponential decomposition method into energy consumption, CO_2 emissions and other issues in some countries (Zhao, 2010; Ma et al., 2008; Sun, 1998). In China, the related researches mainly started from the beginning of this century, and concentrated on the industrial sector energy consumption structure changes, energy consumption and CO_2 emission change characteristics of regional industry, terminal energy consumption changes and the contribution degree of main influence factors, Chinese energy intensity change structure and efficiency factor contribution etc. In the analysis on driving factors of regional water resources utilization and impact of economic structure on water resources utilization has made Chinese water science researchers in recent years to focus on application of index decomposition model. Jia et al. (2004) conducted a quantitative analysis on the water saving effect of economic structure adjustment in Beijing city by the principle of factors decomposition. Sun and Wang (2009) studied the driving force and model of temporal and spatial variation of water utilization change in Liaoning province using index decomposition model. Zhang et al. (2011) made analysis on the change of characteristic of water resources utilization during the period of 1980-2009 in the Dalian city, Liaoning Province by using LMDI method which accounted for the key driving factors of water resources utilization of the city from the aspects of social and economic scale, industrial structure and so on. However, the application of different factor decomposition models in explaining driving factors of regional water resources utilization is still at the stage of exploration and development.

According to the characteristics of socio-economic water consumption, the factors that affected regional water consumption mainly included the characteristics of industrial structure, water efficiency of various industries, regional socio-economic level and population size, etc.

Let W_t be total amount of water consumption during the period of time t, $W_{i,t}$ is water consumption of i-th industrial sector during the period of time t, GDP_t is the regional gross domestic product for the period of time t, $GDP_{i,t}$ is GDP of i-th industrial sector during the period of time t, $S_{i,t}$ is the structure proportion of i-th industrial sector during the period of time t, and $S_{i,t} = GDP_{i,t} / GDP_t$. I_t is the water quota of the period of time t (expressed by the water consumption amount of per 10^4-yuan output value), and $I_t = W_t / GDP_t$. $I_{i,t}$ is the water quota of i-th industrial sector during the period of time t, namely $I_{i,t} = W_{i,t} / GDP_{i,t}$. P_t is the region total population of the period of time t. Y_t is per capita GDP during the period of time t, namely $Y_t = GDP_t / P_t$. N is the number of industrial sector classification. Then the decomposition of total water consumption and its driving factors during the period of time t can be expressed as follows:

$$\begin{aligned} W_t &= \sum_{i=1}^{N} W_{i,t} = \sum_{i=1}^{N} \left(\frac{W_{i,t}}{GDP_{i,t}} \times \frac{GDP_{i,t}}{GDP_t} \times \frac{GDP_t}{P_t} \times P_t\right) \\ &= \sum_{i=1}^{N} I_{i,t} \times S_{i,t} \times Y_t \times P_t \end{aligned} \quad [1]$$

Let W_0 and W_T denote the total water consumption of region in the base year and the planning term (T year), respectively. By Eq. [1], water consumption variation from the base year to T year, ΔW_{tot}, can be expressed as:

$$\Delta W_{tot} = W_T - W_0 = \Delta W_I + \Delta W_S + \Delta W_Y + \Delta W_P \quad [2]$$

where ΔW_I denotes the effect of water consumption quota, which reflects the contribution to water consumption variation produced by water efficiency change due to technological progress and management of water resources. ΔW_S is the effect of industrial structure, which expresses the contribution to water consumption variation from the adjustment of industrial structure due to consideration of regional water resources endowment conditions. ΔW_Y is the effect of economic level, which reflects contribution from the regional socio-economic scale and the level of social welfare. ΔW_P is the effect of the population scale, which is the contribution to water consumption variation, resulting from population scale factors.

The water consumption variation driving factors of the planning time period t are computed according to following equations:

$$\Delta W_I^{\,t} = \sum_i B_{it} \times \ln(W_{it} / (GDP_{it} I_{i0})) \quad [3]$$

$$\Delta W_S^{\,t} = \sum_i B_{it} \times \ln(S_{it} / S_{i0}) \quad [4]$$

 ©2017, IAHR. Used with permission / ISSN 1562-6865 (Online) - ISSN 1063-7710 (Print)

$$\Delta W_Y{}^t = \sum_i B_{it} \times \ln(GDP_t/(P_t Y_0)) \quad [5]$$

$$\Delta W_P{}^t = \sum_i B_{it} \times \ln(P_t / P_0) \quad [6]$$

where ΔW_I^t、ΔW_S^t、ΔW_Y^t、ΔW_P^t respectively is the contribution to total water consumption variation from the water quota, industrial structure, per capita GDP and population size of the planning time period *t*, which was derived from the LMDI decomposition method. $B_{it} = (W_{it} - W_{i0})/(\ln W_{it} - \ln W_{i0})$. W_{i0}、I_{i0}、S_{i0} respectively denote the annual water consumption, water quota and ratio of *i*-th industrial sector in the base year of planning. Y_0 and P_0 is GDP per capita GDP and population size in the base year of planning, respectively.

3 MODEL OF INDUSTRIAL STRUCTURE AND WATER EFFICIENCY ANALYSIS BASED ON TOTAL WATER-USE QUANTITY LIMIT

Eq. [1] and [2] can be used for quantitative analysis on the driving factors of regional water consumption variation for a certain period of time. To identify the contributions to regional water consumption variation result from regional water quota, industrial structure, economic level and population size and other factors are taken into account. Because the driving factors include regional water quota and the industrial structure, therefore, the mathematical programming model can be established based on LMDI decomposition method, so as to make analysis on optimization of the regional industrial structure and regional water quota within total water-use quantity under a limit.

3.1 Objective function

The purpose of analysis on optimizing the regional industrial structure and regional water quota within total water-use quantity limit is to seek the reasonable proportion of industrial structure and water use efficiency. The premise of not breaking the regional total water-use quantity control targets, for obtaining the balanced socio-economic development and the maximum gross domestic product to adapt to regional water resources were also available. Therefore, the objective of optimization model can be defined as minimizing an absolute difference between the amount of water demand and total water-use quantity control threshold.

$$Min\left|W_{1t} + W_{2t} + W_{3t} - W_m\right| \quad [7]$$

where W_{1t} 、W_{2t}、W_{3t} denote the water consumption of the primary industry, secondary industry and tertiary industry corresponding to the period of time *t*, respectively. W_m is total water-use quantity control threshold.

3.2 Constraint conditions

(1) Regional GDP target requirements:

$$GDP_{1t} + GDP_{2t} + GDP_{3t} \geq GDP_m \quad [8]$$

where GDP_m is regional GDP target requirement in the period of time *t*. GDP_{1t}、GDP_{2t}、GDP_{3t} is the product of the primary industry, secondary industry and tertiary industry in the period of time *t*.

(2) Population size constraints:

$$P_t \leq P_0(1+r)^T \quad [9]$$

where P_0 and P_t is the population size of the base year and the planning period *t*, respectively. *r* is the population natural growth rate controlled by regional social economic development plan. *T* is years from the base year to the planning term.

(3) Per capita GDP target requirements:

$$(GDP_{1t} + GDP_{2t} + GDP_{3t})/P_t \geq Y_m \quad [10]$$

where Y_m is per capita GDP target of the planning time period *t*, and Y_t is per capita GDP value of the planning time period *t*.

(4) Regional comprehensive water efficiency constraint:

$$(W_{1t} + W_{2t} + W_{3t})/GDP_t \leq C_m \quad [11]$$

©2017, IAHR. Used with permission / ISSN 1562-6865 (Online) - ISSN 1063-7710 (Print)

where C_m is the water consumption amount of per 10^4 yuan GDP value derived from the comprehensive planning of water resources and the planning of water-saving society construction.

(5) Regional total water-use quantity control constraint:

$$W_0 + \sum_i \mathrm{B}_{it} \times \ln(W_{it} /(GDP_{it} I_{i0})) + \sum_i B_{it} \times \ln(S_{it} / S_{i0}) + \sum_i B_{it} \times \ln(GDP_t /(P_t Y_0)) + \sum_i B_{it} \times \ln(P_t / P_0) \le W_m \quad [12]$$

where W_m is regional total water-use quantity control target issued by Jiangsu provincial water resources administration department.

(6) Regional industrial structure proportion constraint:

$$GDP_{1t} + GDP_{2t} + GDP_{3t} = GDP_t \quad [13]$$

where $GDP_{i,t}$ is GDP of i-th industrial sector during the period of time t. To study the region, appropriate compression of the primary industry ratio, emphasis on the secondary industry development, and gradually promotion of the tertiary industry development of the socio-economic development policy in planning time period must be taken into account. Therefore, the proportion of the primary industry, secondary industry and tertiary industry should be regulated appropriately.

$$GDP_{1t} /(GDP_{1t} + GDP_{2t} + GDP_{3t}) \le S_{1,0} \quad [14]$$

$$GDP_{2t} /(GDP_{1t} + GDP_{2t} + GDP_{3t}) \ge S_{2,0} \quad [15]$$

$$GDP_{3t} /(GDP_{1t} + GDP_{2t} + GDP_{3t}) \ge S_{3,0} \quad [16]$$

where $S_{1,0}$、$S_{2,0}$、$S_{3,0}$ respectively is the proportion of the primary industry, secondary industry and tertiary industry in the base year of planning. （7）Non negative constraint of decision variables. In the model, the decision variables include $W_{i,t}$, $GDP_{i,t}$, P_t. Non-negative constraints as follows:

$$W_{i,t}, GDP_{i,t}, P_t \ge 0, i = 1,2,\cdots, N \quad [17]$$

where N is the number of industrial sectors.

3.3 Solution method of the model

The proposed model is a non-linear programming model with the decision variables, $W_{i,t}$, $GDP_{i,t}$, P_t, and was solved by the convenient tool software Lingo. Solving the above non-linear model would need adequate trials of choosing several initialization values of decision variables to avoid being incapable of iteration or trapped in local optimum. It's also worth mentioning that varied starting values of $GDP_{i,t}$, P_t should be chosen in advance based on information from regional water resources comprehensive planning and national economic and social development plan, etc. Then corresponding local optimum solutions were searched for and compared gradually until the proper optimal solution is identified.

4 CASE STUDY

4.1 General situation of study region

The Yancheng City of Jiangsu province is located in the eastern part of the Jianghuai plain. It belongs to radiation range of the Pudong Economic Development Zone and the Yangtze River Delta, with administrative area of 16972km^2. The study region is in transition zone from subtropics to warm temperate zone with average annual precipitation of 867.7mm. The Yancheng City water resources bulletin showed that the city's total water consumption of 5335 million m^3 in 2012, and water use amount of the primary industry was 4429.1 million m^3 which accounted for 88.4% of the water use amount of production. That the usage of secondary industry was 535.9 million m^3, which accounted for 10.7% of the water use amount of production, in which water usage for thermal power plant is 213 million m^3, water usage for general industry production is 298.9 million m^3 and water usage for construction business is 24.1 million m^3. The water use amount for tertiary industry is 45.3 million m^3 which was accounted for 0.9% of water use of production.

According to Yancheng City Statistical Yearbook, in 2012, regional GDP of Yancheng is 312 billion yuan, with the primary industrial earning value was 45.613 billion yuan, the secondary industrial earning value was

 ©2017, IAHR. Used with permission / ISSN 1562-6865 (Online) - ISSN 1063-7710 (Print)

1472.87 billion, and the tertiary industrial earning value was 1191 billion yuan. The proportion of three industries in Yancheng City was adjusted to 14.62:47.21:38.17 in 2012 from 45.05:33.48:21.47 in 1990. The primary industrial added value revealed rapid decline, but still much higher than 6.3% of the average of whole Jiangsu province (China Statistics Press, 2012). The proportion of the secondary industry and the tertiary industry had been greatly improved, but the proportion of the three industries was still not rational. Since 1990, the percentage of the primary industrial output had been declining, and one of the secondary and tertiary industrial outputs had been increasing. Up to 1995, output of the secondary industry exceeded that of the primary industry for the first time where the production centers gradually transferred to secondary industry. The proportion of three industries was changed to 36.91:38.10:24.99. After 1995, the tertiary industry had been developing and raised the percentage of 31.27% in 2000, which was more than 30.10% of the primary industry. During 1995-2012, the secondary industry always occupied the dominant position, the proportion of primary industry dropped to a lower value. Compared with the law of industrial development, the secondary industry dominates the Yancheng's local national economy and the tertiary industry sustains rapid development. So, it is concluded that socio-economic development situation of Yancheng is in the middle stage of industrialization.

4.2 Driving factors decomposition calculation based on LMDI

Based on the above LMDI decomposition method, the contributions of four factors including industrial structure, water quota, economic level and population size to the variation of total water consumption in Yancheng City was analyzed quantitatively. Putting Yancheng's GDP and its components, the industrial water use and population data into Eq. [3] to [6], the driving factors effect values can be calculated for three time periods of 2006 to 2008 year, 2008 to 2010 year and 2010 to 2012 year, as shown in Table 1.

Table 1 shows the effects of water quota in three time periods of 2006 to 2008, 2008 to 2010 and 2010 to 2012 were always negative, and the degree of negative effect was more and more obvious over time. It indicates that while Yancheng City vigorously improves the city's policy situation of energy saving and emission reduction, the development, utilization, management and protection of water resources is worsening gradually. Under the relevant water-saving policy guidance, more and more industrial departments actively promote technological progress to implement the most stringent water management system. The city strives hard to implement water-saving society, construction planning where the water use efficiency of the city gradually increased. The effects of industrial structure in three periods were negative, but the numerical values had a fluctuation. This was because since 2006, Yancheng City had been adjusting the regional industrial structure according to the national and provincial economic development planning. local economic and social development situation and target, the actual water resources natural conditions, water resources development and utilization characteristics, and water resources utilization technology level were also being regulated. From China's current social and economic development characteristics, although water supply and demand situation was not the only factor determining the characteristics of regional industrial structure, but its importance can't be ignored, and the industrial structure change effect on the characteristics of development and utilization of regional water resources is getting more obvious.

Table 1. Driving factors affect values of water resources utilization in Yancheng.

Time period	driving factors effect values（million m³）				
	water quota	industrial structure	economic level	population size	Total effect
2006-2008	-507.5	-730.7	1403.8	400	2056
2008-2010	-1007.1	-284.3	1683.0	268	4184
2010-2012	-1348.8	-425.7	1585.9	390	-1496

The driving factor effects of both population size and economic level were positive; it indicates that they have a promoting function on regional water consumption growth. In the three time periods of 2006 to 2008, 2008 to 2010 and 2010 to 2012, the effect value of population size may vary, but not greatly. This shows that in the analysis period, due to the characteristics of Yancheng City's economic development scale and obtaining employment opportunities, the influence of population floating on the total regional population was not marked up highly. In addition, due to implementation of the family planning policy, the natural growth rate had been controlled within a certain range and resulted in little change in the size of the city population. The quantization value of driving effect of economic factors, expressed as level of per capita GDP, is significantly greater than the population size, and by which the increased effect to regional water amount is higher than the population size. Because GDP and population size will change over time, so the economic level factor evaluated by these two parameters has characteristic of few fluctuations and changes with time. From the connotation of economic level adopted in this paper, it involves two parameters of GDP (*i.e.* economic scale) and population number (*i.e.* population size), which are typical index of socio-economic development. The quantization values of this factor affect in three time periods, as shown in Table 1, indicated that the characteristic of current Yancheng City development will still belong to initial-middle industrialization stage.

©2017, IAHR. Used with permission / ISSN 1562-6865 (Online) - ISSN 1063-7710 (Print)

The improvement of socio-economic level needs heightening of science and technology and optimization of the industrial structure.

4.3 Analysis on industrial structure and water quota with total quantity limit

Based on the mathematical programming model of optimizing regional industrial structure and water quota with the total water consumption limit, the present work takes 2016 year as the research planning term period to verify the applicability of the model, while selecting 2012 as the base year. Relevant statistics showed that in 2012, the population of Yancheng City was 8.224 million, the amount of total water use was 5335 million m^3, in which the primary industrial water consumption was 4429.1 million m^3, secondary industrial water consumption was 535.9 million m^3 and tertiary industrial water consumption was 45.3 million m^3. The city's GDP of 312 billion yuan and the per capita GDP of 37938 yuan should also be noted. According to the status of socio-economic development in recent years and the national economic development plan, the natural population growth rate should be maintained at less than 4 per thousand to the end of the city's planning term period.

According to the city's value of total water consumption limit issued by Jiangsu Province, in 2016, the total water amount of Yancheng City should be controlled within 5400 million m^3. Based on the Yancheng City water resources planning and water saving planning, the comprehensive water consumption per ten thousand yuan output should not exceed 146 m^3 at the end of planning term period. The Yancheng City's recent economic and social development trends and national economic targets showed the regional GDP target value should be more than 360 billion yuan, the per capita GDP amounted to 42000 yuan in 2016. Eq. [7] to [17] will be used in a mathematical programming tool software known as Lingo 11 to solve the model where three industrial water consumptions, production output and total population in 2016 may be computed. The results are shown in Table 2.

From the model calculation results listed in Table 2, if the value of total water consumption limit and the expected target of the socio-economic development were guaranteed, at the end of 2016, Yancheng City's proportions of the three industrial structure should be respectively 13%, 48.83% and 38.17%. Compared to 2012 year statistics, the proportion of the primary industry declines and reduces by 11.08%, while the proportion of the secondary industry had an increase of 3.43%, the proportion of the tertiary industry remains almost unchanged with only an increase of 0.1%. At the same time, the primary industrial water consumption of per ten-thousand-yuan output value was reduced from 970.99m^3 to 734.73m^3, a reduction by 24.33%. The secondary industrial water consumption of per ten thousand yuan output value decreased from 36.38m^3 to 30.50m^3, a reduction by 16.17%. The tertiary industrial water consumption of per ten thousand yuan output value boosts from 3.8m^3 to 5.01m^3, an increment by 31.71%. Based on the proportion of industrial structure and corresponding industrial water quota calculation, Yancheng City's water consumption in 2016 is 5400 million m^3 that meets the permission of total water consumption limit.

The analysis on calculated results shows that similar to most parts of the country, although agriculture is still an important basic industry in Yancheng City, but the water use amount is enormous and use of efficiency is still not high. Therefore, the agricultural development should take water saving as the leading direction, and reduce the planting industry with high water consumption, vigorously develop water-saving agriculture, ecological agriculture and forestry and animal husbandry. The saved water resources should be used for other industries to achieve high efficient allocation and sustainable utilization of water resources. The secondary industry with relatively large proportion plays an important role in the regional economic development, because the increased output value of secondary industry was higher than the ones of the primary industry and the tertiary industry which possess greater contribution to regional GDP. At the end of 2016, the proportion of secondary industry still should be increased in the industrial structure, but the higher water consumption, higher energy consumption and higher pollution industries should be reduced or eliminated by the internal structure adjustment. At present, the tertiary industrial pressure on water resources in the region is still relatively small, but its output value is generally higher, so while the secondary industry is strengthened, in the near future, a stable and efficient development of the tertiary industry should be maintained. According to the characteristic of tertiary industry, the industrial projects should focus on internal structure optimization of local tertiary industry in Yancheng City, in order to effectively promote regional ecological environment maintenance and improve the quality of people's life and health level.

 ©2017, IAHR. Used with permission / ISSN 1562-6865 (Online) - ISSN 1063-7710 (Print)

Table 2. Model computation values of 2016 year.

Decision variable (units)	W_{1t} (mil. m^3)	W_{2t} (mil. m^3)	W_{3t} (mil. m^3)	GDP_{1t} (bil. yuan)	GDP_{2t} (bil. yuan)	GDP_{3t} (bil. yuan)	P_t (ten thous. person)
model value	4592	716	92	62.499	234.752	183.505	828.40
Statistical variables (units)	S_{1t} (%)	S_{2t} (%)	S_{3t} (%)	I_{1t} (m^3/ ten thous. yuan)	I_{2t} (m^3/ ten thous. yuan)	I_{3t} (m^3/ ten thous. yuan)	Total water amount (mil. m^3)
model value	13.00	48.83	38.18	734.73	30.50	5.01	5400

5 CONCLUSIONS

The adjustment of socio-economic industrial structure and water efficiency control is an important basic measure of regulation of hydrosocial-cycle process. Based on this cognition, through using the regional water resources utilization driving factor analysis method and mathematical programming method, an analytical model is proposed for analysis on proportion of industrial structure and water quota in Yancheng City, Jiangsu province. It may provide a quantitative analysis means for regional socio-economic development planning, industrial structure adjustment and the water resources utilization regulation and prediction. This research shows that making full use of the opportunities policy of the Jiangsu coastal development strategy is a breakthrough in promoting Yancheng City economic development speed and quality. The city must have advanced consciousness, rational target positioning and planning as well as a good infrastructure for its construction and development is bound to adapt to the whole region's socio-economic development strategy and resource development and utilization of environment. In the process of development, the city should have a reasonable layout of industrial structure, and strict limit of the development of high water consumption industries, adequately build the economic structure system to suit conditions in water resources and water environment carrying capacity, and strengthen water conservation and improve water use efficiency.

ACKNOWLEDGEMENTS

The research work is supported by the National Natural Science Foundation of China (No. 51379181).

REFERENCES

Ang, B.W. (2004). Decomposition Analysis for Policymaking in Energy: Which is the Preferred Method? *Energy Policy*, 32(9), 1131-1139.

Ang, B.W. & Liu, F.L. (2001). A New Energy Decomposition Method: Perfect Decomposition and Consistent in Aggregation. *Energy*, 26(6), 537-548.

Chen, Q.Q. (2006). *Research on Pollution Reduction and Water-Saving of City in Pearl River Delta*. Chinese Water Conservancy and Hydropower Press, Beijing.

Jia, S.F., Zhang, S.F., Xia, J. & Yang, H. (2004). Effect of Economic Structure Adjustment on Water Saving. *Journal of Hydraulic Engineering*, 3,111-116.

Lei, S.P., Xie, J.C. & Ruan, B.Q. (2004). Industrial Structure and Water Resources Related Theory and the Analysis of the Empirical. *Operations Research and Management Science*, 2,100-105.

Ma, C.B. & Stern, D.I. (2008). China's Changing Energy Intensity Trend: A Decomposition Analysis. *Energy Economics*, 30(3), 1037-1053.

Sun, C.Z. & Wang, Y. (2009). Driving Force Measurement of Water Utilization Change in Liaoning Province and Analysis of Their Spatial-Temporal Difference Based on Factor Decomposition Model. *Arid land and Geograph*., 32(6),850-858.

Sun, J.W. (1998). Accounting for Energy Use in China, 1980 - 1994. *Energy*, 20, 835-849.

Wang, H., Long, A.H., Yu, F.L. & Wang, D.X. (2011). Study on Theoretical Method of Social Water Cycle I: Definition and Dynamical Mechanism. *Journal of Hydraulic Engineering*, 42(4), 379-387.

Wang, J.H. & Wang, H. (2014). *Principle and Regulation of Social Water Cycle*. Science Press, Beijing.

Wang, S.H., Wang, Z.J. & Xiong, Y.H. (2003). Some Problems in Modern Water Resources Planning and Their Solutions and Technical Methods. *Haihe Water Resources*, 4,15-18.

Xu, X.Y., Wang, H., Gan, H., et al. (1997). *The Theory and Method of the Water Resources Planning and Macro-Economy in North China Area*. The Yellow River Water Conservancy Press, Zhengzhou.

Yancheng City Bureau of Statistics (2012). *Yangcheng Statistical Yearbook*. Statistics Press, Beijing, China, 2006-2012.

Zhang, Q., Wang, B.D. & Cao, M.L. (2011). Analysis of Water Resources Utilization Change Based on Factor Decomposition Model. *Journal of Natural Resources*, 26(7),1209-1216.

Zhao, X.L., Ma, C.B. & Hong, D.Y. (2010). Why did China's Energy Intensity Increase During 1998-2006: Decomposition and Policy Analysis. *Energy Policy*, 38(3), 1379-1388.

©2017, IAHR. Used with permission / ISSN 1562-6865 (Online) - ISSN 1063-7710 (Print)

Proceedings of the 37th IAHR World Congress
August 13 – 18, 2017, Kuala Lumpur, Malaysia

THROUGHPUT OF THE DONGTING LAKE INFLUENCED BY THE THREE GORGES RESERVOIR DURING THE PERIOD OF IMPOUNDMENT

HUA GE[(1)] & LINGLING ZHU[(2)]

[(1)] Changjiang River Scientific Research Institute, Wuhan, China,
gh-102@126.com
[(2)] Hydrology Bureau, Yangtze River Water Resources Commission, Wuhan, China,
zhull1012@foxmail.com

ABSTRACT

During the period of the impoundment of Three Gorges Reservoir, there was a significant water level drop downstream reservoir in middle Yangtze River. It has exerted an obvious influence on the throughput of Dongting Lake. Based on a well verified numerical model of the river-lake nets, the throughput of Dongting Lake influenced by the Three Gorges Reservoir during the period of impoundment was analyzed in this article, by employing the inflow and outflow of Three Gorges Reservoir from 2009 to 2012 as the boundaries. The results show that, because of the impoundment, the inflow and outflow of the Dongting Lake has been seriously reduced, combined by the water level drop in the lake. At the same time, the ability to outthrow the water from Dongting Lake to Yangtze River has been slightly strengthen. It will seriously worsen the water resource and the environment in Dongting Lake during dry season.

Keywords: Three Gorges Reservoir; Dongting Lake; impoundment; low water level; water resource and environment.

1 INTRODUCTION

The Dongting Lake, which is connected to the middle Yangtze River by three inlets, known as Songzi, Taiping and Ouchi in Jingjiang reach and one outlet at Chenglingji (as shown in Figure 1), has been significantly influenced by the impoundment of the Three Gorges Reservoir (TGR) since 2003. The impact was mainly embodied in two aspects. On the one hand, the water level drop in Jingjiang reach (from Zhicheng to Chenglingji), caused by the reduction of the discharges from TGR, will obviously decrease the water amount splitting into the Dong-ting Lake by worsening the hydrological boundary conditions of the flow diversion at the three inlets. On the other hand, the water level drop at Chenglingji will accelerate the outflow by weakening the backwater effect at the export of Dongting Lake. The relationship between the Yangtze River and the Dongting Lake has been obviously changed, and is getting more and more complicated. It has become attractive to many researchers who are paying close attention to the water resource and environment in Dongting Lake. At present, most of the studies were focused on the changes of the water and sediment splitting ratio of the three inlets (XU et al., 2009; GUO et al., 2014; QU et al., 2014; FANG et al., 2014) by the analysis of the measured data, and less attention has been paid to the backwater effect of the outlet. In this article, a one dimensional unsteady flow numerical model of river-lake nets, including the Yangtze River and the Dongting Lake, was established and well verified. Then, by taking the inflow and outflow of the TGR as the boundaries, the calculations were carried out to analyze the throughput of the Dongting Lake influenced by the Three Gorges Reservoir during the period of impoundment. The results show that, both the inflow and the outflow of the Dongting Lake has been obviously reduced, especially the inflow. And at the same time, a water level drop has occurred in the lake area. This phenomenon has suggested a slight strengthen of the ability to out throw the water from Dongting Lake to Yangtze River. This will seriously worsen the water resource and environment in Dong-ting Lake during the dry season.

 ©2017, IAHR. Used with permission / ISSN 1562-6865 (Online) - ISSN 1063-7710 (Print)

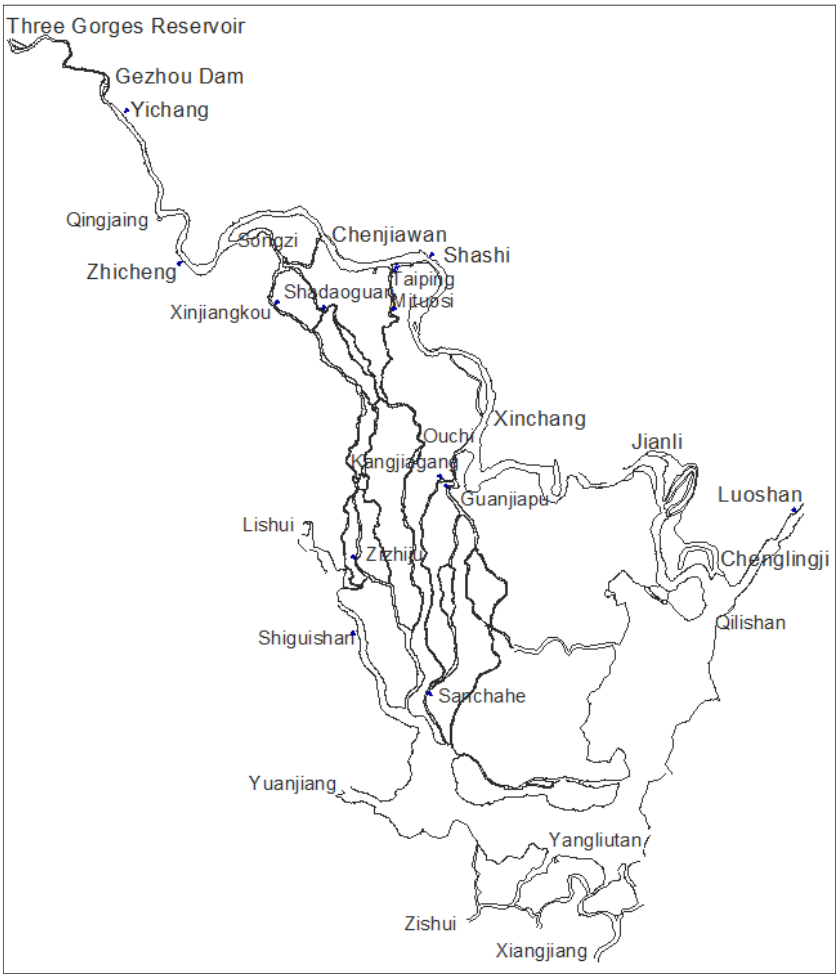

Figure 1. Map of the study region.

2 NUMERICAL MODEL

2.1 Establishment

The one dimensional unsteady flow numerical model of the river-lake nets takes the Yichang to Luoshan reach and the Dongting Lake area as the computational region, which was shown in Figure 1. In this region, 63 nodes and 87 reaches were generalized to represent the study area. The Reaches consist of 3726 cross sections. The average separation distance between these sections was about 440m. The governing equations of the numerical model were the de Saint-Venant system of equations, written as follows:

$$\frac{\partial Q}{\partial x} + B\frac{\partial z}{\partial t} = 0 \qquad [1]$$

$$\frac{\partial Q}{\partial t} + \frac{\partial}{\partial t}\left(\alpha\frac{Q^2}{A}\right) + gA\frac{\partial z}{\partial x} + gn^2\frac{Q|Q|}{AR^{4/3}} = 0 \qquad [2]$$

where,

$Q =$ *flow quantity*

$z =$ *water level*

$B =$ *river width*

$A =$ *area of the wetted cross – section*

$g =$ *gravity acceleration*

$n =$ *roughness factor*

$R =$ *hydraulic radius*

$\alpha =$ *momentum correction coefficient*

$x, t =$ *spatial and temporal axes*

©2017, IAHR. Used with permission / ISSN 1562-6865 (Online) - ISSN 1063-7710 (Print)

After the difference by using the Preissmann scheme and the linearization, the Eq. [1] – [2] can be changed into:

$$a_i \Delta Z_{i+1} + b_i \Delta Q_{i+1} = c_i Z_i + d_i \Delta Q_i + e_i \quad [3]$$

$$a_i' \Delta Z_{i+1} + b_i' \Delta Q_{i+1} = c_i' Z_i + d_i' \Delta Q_i + e_i' \quad [4]$$

where,

$\Delta Q, \Delta Z =$ *changes of the flow quantity and water level from* $t = t_0$ *to* $t = t + \Delta t$
$a, b, c, d, e =$ *coefficients related to the flow variables at* $t = t_0$
$i =$ *subscript of cross – section*

By the variable substitution, the unknowns of the internal cross-sections were eliminated, and only the unknowns of the first and last cross-sections in one reach were reserved, written as:

$$\Delta Q_1 = E_1 \Delta Z_1 + F_1 + H_1 \Delta Z_{\text{num}} \quad [5]$$

$$\Delta Q_{\text{num}} = E_1' \Delta Z_1 + F_1' + H_1' \Delta Z_{\text{num}} \quad [6]$$

where,

$E, F, H =$ *coefficients coming from the substitution*
$1, num =$ *index of the first and last cross – sections*

Based the law of the water continuity at a river node, the governing equations of the river nets can be derived by combining the Eq. [5] or 6 for each node:

$$[A]\{\Delta Z_{\text{nod}}\} = \{B\} \quad [7]$$

where,

$[A]$ *is a matrix of coefficients*
$[B]$ *is a vector consists of constant terms*
$\Delta Z_{nod} =$ *changes of the water level at river nodes*

The junctions-group method (LI 1997) was use to solve the Eq. [7]. After the grouping, the Eq. [7] for a group of nodes, with the exception of the first and last group, can be written as:

$$[R]_{\text{ng}} \{\Delta Z\}_{\text{ng-1}} + [S]_{\text{ng}} \{\Delta Z\}_{\text{ng}} + [T]_{\text{ng}} \{\Delta Z\}_{\text{ng+1}} = \{V\}_{\text{ng}} \quad [8]$$

where,

$ng =$ *index of the group*
$[R], [S], [T], [V] =$ *matrix of coefficients*

The governing equations for the first and last group can be written as:

$$[S]_1 \{\Delta Z\}_1 + [T]_1 \{\Delta Z\}_2 = \{V\}_1 \quad [9]$$

$$[R]_{\text{gnum}} \{\Delta Z\}_{\text{gnum}-1} + [S]_{\text{gnum}} \{\Delta Z\}_{\text{gnum}} = \{V\}_{\text{gnum}} \quad [10]$$

 ©2017, IAHR. Used with permission / ISSN 1562-6865 (Online) - ISSN 1063-7710 (Print)

where,

$$gnum = number\ of\ the\ groups$$

The solving started from the first group of nodes. By the use of variable substitution method gradually, the unknowns in each group were eliminated. After the solving of the water level changes for each node, the flow quantity can be derived by the back substitution of ΔZ to Eq. [5] – [6]. Then, the flow and water level for internal cross-sections can be obtained by E. [3] – [4].

In this article, all the nodes in the study region were divided into five groups.

2.2 Verification

The verification of the numerical model was carried out by using a series of day-averaged hydrology data of the hydrologic stations in this study region, from 2006-1-1 to 2009-12-31. The inflow of the region was controlled by six hydrologic stations as follows:

Yichang - controlling station of Yangtze River;
Gaobazhou - controlling station of the Qingjiang;
Xiangtan - controlling station of the Xiangjiang;
Taojiang - controlling station of the Zishui;
Taoyuan - controlling station of the Yuanjiang;
Shimen - controlling station of the Lishui.

The lower boundary of the numerical model was controlled by the water level of the Luoshan hydro-logic station, which was located at the export of the study region. The verification was proceeded based on the measured terrain data. The terrain of the Yangtze River was measured in 2006, and that of the Dongting Lake was measured in 2011.

Both the level-flow relationship of the typical hydrologic stations in this study area, and the correlation of the splitting ratio of the three inlets in Jingjiang reach were included in the verification. Figure 2 gives the comparison of the calculated and measured level-flow relationship for the typical hydrologic stations both in Yangtze River and the Dongting Lake. Figure 3 shows the comparison of the calculated and measured correlation between the amount of the flow splitting into Dongting Lake and the water level at the three inlets. It can be clearly seen that the calculated ones agree well with the measured ones from the Figure 2 and Figure 3. That is to say that, the numerical model established in this article can well reflect the hydraulic characteristics of the water movement in this region and this has laid a solid foundation for the calculations carried out in the following.

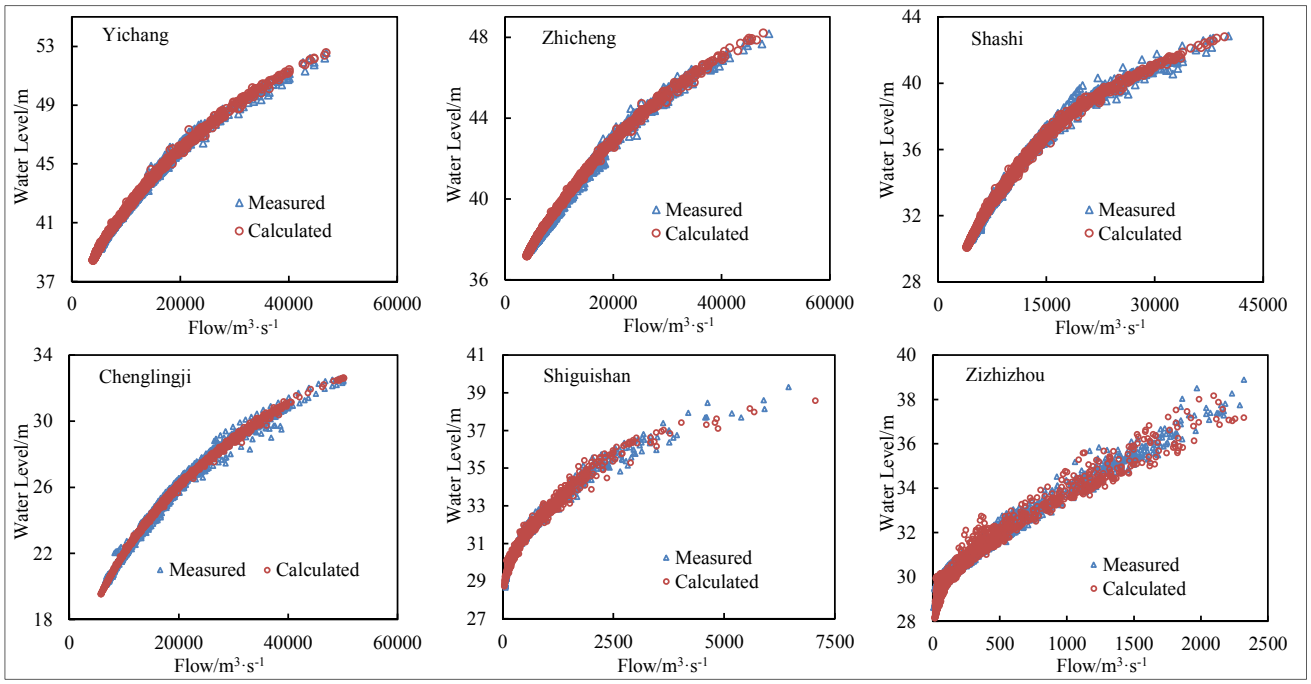

Figure 2. Comparison of the calculated and measured level-flow relationship for the typical hydrologic stations.

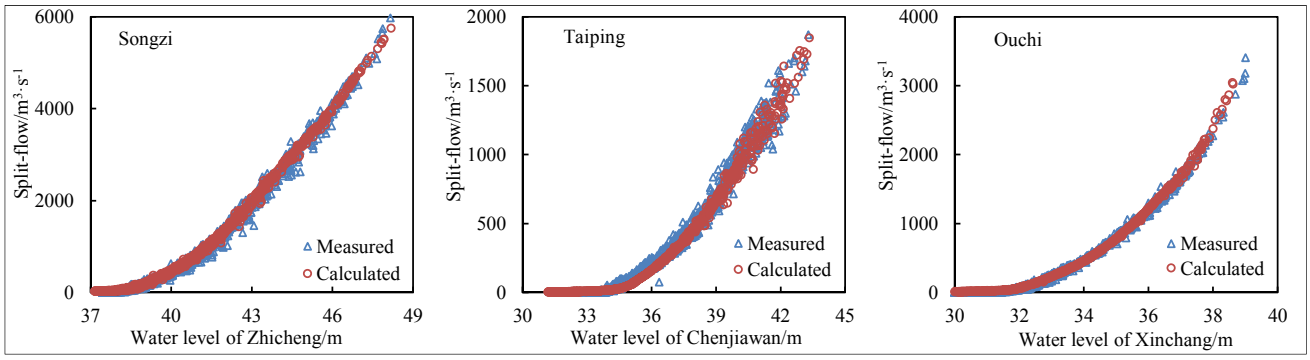

Figure 3. Comparison of the calculated and measured correlation between the split-flow and the water level at the three inlets.

3 CALCULATION AND ANALYSIS

3.1 Boundaries of the calculation

Since the experimental impoundment from 2008, the TGR has successfully raised the storage level to the normal storage water level (175m) from 2010 to 2012. Based on the above actual situation, the calculation was carried out by using the inflow and out-flow data of TGR from 2009 to 2012, which was published by the China Three Gorges Corporation (http://www.ctgpc.com). Two conditions were considered to analyze the influence on the throughput of the Dongting Lake after the impoundment of the TGR. The inflow data of the TGR was firstly used as the boundary to provide the situation without the influence of TGR. Then, the outflow of TGR was used to carry out the calculation to proceed a contrastive analysis on the throughput of the Dongting Lake. The process of the inflow and outflow of TGR were shown as Figure 4. During the calculation, the day-averaged measured data of the controlling hydro-logic stations were used as the inflow of the Qingjiang, Xiangjiang, Zishui, Yuanjiang and Lishui. The water level-flow relationship curve of the Luoshan hydrologic station, which was derived from the measured data from 2009 to 2012, was taken as the lower boundary of the numerical model. The curve was shown in Figure 5.

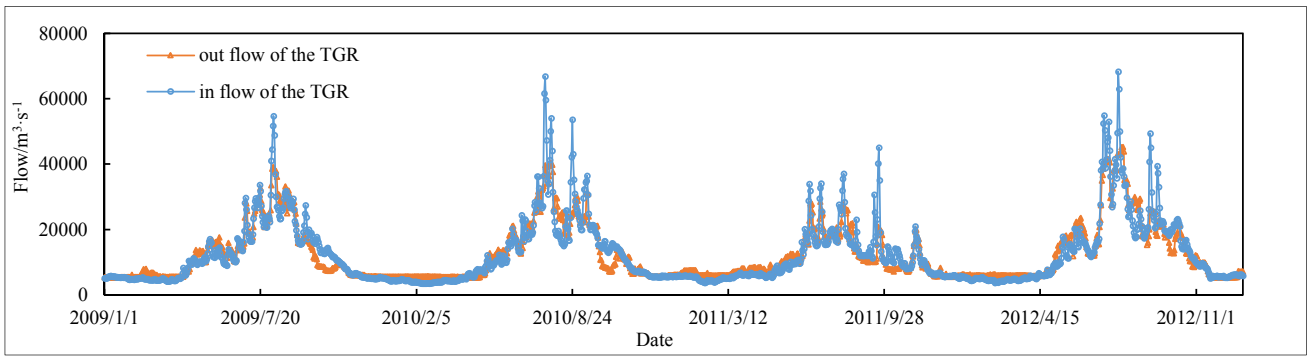

Figure 4. The process of inflow and outflow of TGR from 2009 to 2012.

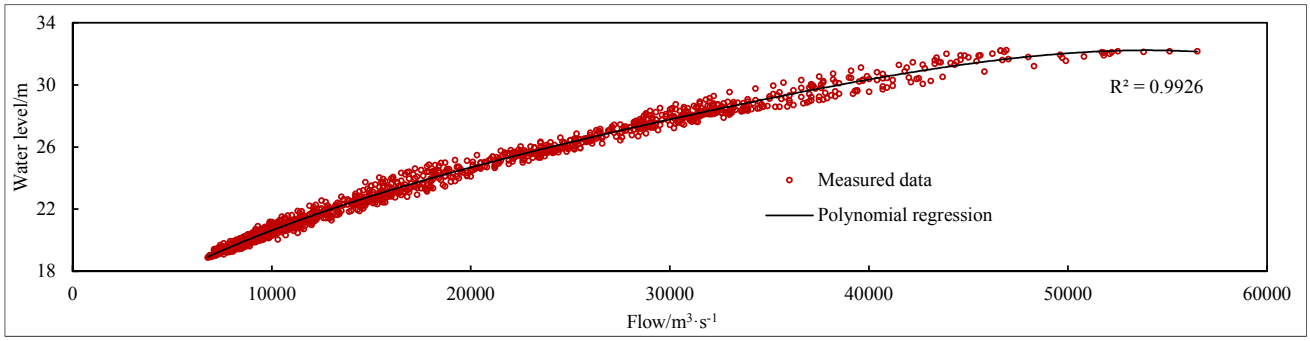

Figure 5. Level-flow relationship at the Luoshan hydrologic station from 2009 to 2012.

3.2 Analysis

The flow splitting into the Dongting Lake from Yangtze River was controlled by the three inlets, and the outflow of the Dongting Lake was controlled by the Qilishan hydrologic station, which is located at the outlet of the lake. Based on the results of the calculation, the process of the throughput of the Dongting Lake, before

 ©2017, IAHR. Used with permission / ISSN 1562-6865 (Online) - ISSN 1063-7710 (Print)

and after TGR, was described as Figure 6, as well as the inflow and out-flow of the TGR. A statistics of the changes, both for the runoff and the water level in the Dong-ting Lake, are also given in Table 1 and Table 2.

By a careful analysis of the Figure 6 and Table 1, it can be easily concluded that, during the period of the impoundment of TGR, there has been a significant decrease in the inflow and outflow of the Dongting Lake, especially the inflow. Taking the data of 2012 for example, the storage of TGR was about $130.9\times10^8m^3$ during the period of impoundment, while there was a $36.5\times10^8m^3$ reduction in the inflow of Dongting Lake, mainly because of reduction of the Songzi inlet with 20.5×108m3. At the same time, the outflow of the Dongting Lake has been reduced by $55.1\times10^8m^3$. The same law was also reflected in the other years.

By subtracting the variation of outflow from in-flow, the net outflow of Dongting Lake has shown a slight increase, especially in 2012. This is mainly due to the weakening of the backwater effect at the out-let of Dongting Lake. During the period of the impoundment, the water level of the Chengling hydro-logic station, locating at the outlet of Dongting Lake, has been shown an significant drop, about 0.98m to 1.45m as shown in Table 2. The drop of the level at the outlet will enlarge the water surface slope in the lake area, and the velocity of the outflow will increase, accordingly. The serious consequence of the increased outflow was the worsening of the water resource and environment in Dongting Lake during the dry season. As shown in Table 2, the water level in the Dongting Lake region, has shown an obvious drop during the impoundment, ranging from 0.2m to 0.5m.

Table 1. Statistics of the variation of runoff. (Units: 10^8m^3).

Year		2009	2010	2011	2012
Storage of TGP		173.6	124.8	168.8	130.9
Variation of throughput	Songzi	-23.0	-16.4	-23.1	-20.5
	Taiping	-6.9	-5.3	-7.1	-6.6
	Ouchi	-6.9	-6.6	-8.4	-9.4
	Inflow	-36.8	-28.2	-38.6	-36.5
	Outflow	-36.9	-37.0	-41.1	-55.1
Net outflow		-0.1	-8.8	-2.5	-18.6

Table 2. Statistics of the variation of water level. (Units: m).

Year	Shiguishan	Sanchahe	Yangliutan	Chenglingji
2009	-0.46	-0.40	-0.18	
2010	-0.36	-0.26	-0.21	-1.05
2011	-0.50	-0.47	-0.27	-1.45
2012	-0.44	-0.36	-0.34	-0.98

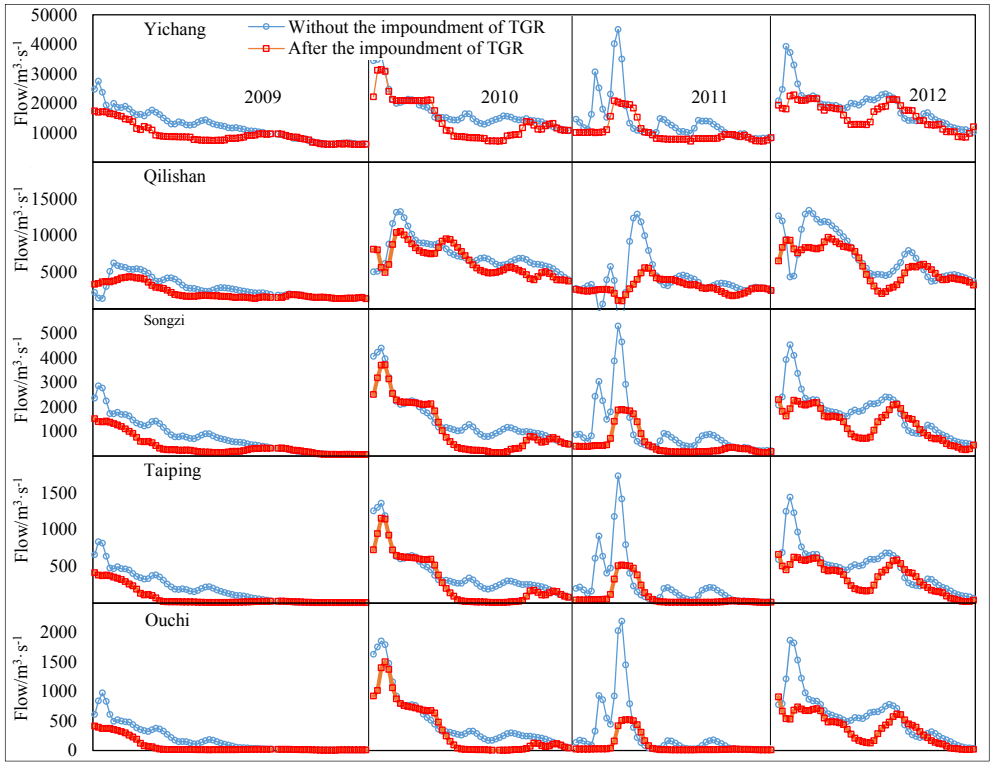

Figure 6. Inflow and outflow of the Dongting Lake before and after the impoundment of TGR.

©2017, IAHR. Used with permission / ISSN 1562-6865 (Online) - ISSN 1063-7710 (Print)

4 CONCLUSIONS

A one dimensional unsteady flow numerical model of the river-lake nets was established and well verified by using the measured data from 2009 to 2012. Both the Dongting Lake area and the Yangtze River downstream the Three Gorges Reservoir from Yichang to Luoshan reach were included in the model. By using this model, calculations were carried out by employing the series of the inflow and outflow data of the TGR from 2009 to 2012. Then, the conclusion, based on the analysis of the calculation results, was derived. It indicates that, the inflow and the outflow of the Dongting Lake has been obviously reduced during the period of the impoundment of the Three Gorges Reservoir, especially the inflow. At the same time, the water level in the Dongting Lake region has also shown a corresponding drop. This phenomenon has suggested a slight strengthen of the ability to outthrow the water from Dongting Lake to Yangtze River. It will seriously worsen the water resource and environment in Dongting Lake during the dry season.

ACKNOWLEDGEMENTS

This work was financially supported by the National Natural Science Foundation of China (No. 51209013) and the national science and technology supported program (No. 2013BAB12B01 & 2013BAB12B02).

 ©2017, IAHR. Used with permission / ISSN 1562-6865 (Online) - ISSN 1063-7710 (Print)

INTEGRATED WATER RESOURCES MANAGEMENT IN THE KISO RIVER SYSTEM

YOSHINOBU SATO[(1)]

[(1)] Faculty of Agriculture, Ehime University, 3-5-7, Tarumi, Matsuyama, 790-8566, Japan
sato@agr.ehime-u.ac.jp

ABSTRACT

This paper shows numerical simulation results for integrated water resources management in the Kiso river system. The numerical model applied in this study includes a distributed hydrological model (Hydrological river Basin Environment Assessment Model: Hydro-BEAM) for runoff simulation, reservoir operation model for flood control and water supply, and water withdrawal model for drinking and agricultural water use. Furthermore, the influence of an inter basin water transfer by new channel network facility, which is under review is also considered for mitigating extreme drought. The results show the inter basin water transfer facility will shorten the period of drought by at least 1 week. The additional coordinated support from upstream dams will also contribute to mitigate the risk of water shortage of the basin.

Keywords: Integrated water resources management; water supply; water use; reservoir operation; distributed hydrological model.

1 INTRODUCTION

The Kiso River System consisting of three river system (Kiso River, Nagara River and Ibi River), is one of the largest river systems (9,100 km^2) in Japan. For effective use of these huge water resources, lots of water utilization facilities have been operated since 1950s. In order to maximize the effectiveness of multipurpose dams in the river system, all the information about water utilization is controlled by the Ministry of Land, Infrastructure, and Transportation (MLIT) and Japan Water Agency (JWA). The water in the Kiso River System is used as the source of agricultural, drinking, industrial and hydraulic power generation. Therefore, to promote proper use of the limited water resources, various data including river water flow, water storage at dams, and amount of water withdrawal are monitored and controlled under long-term strategies for the integrated water resources management. However, the Kiso river system has been suffering from severe drought by huge water demand and the low amount of rainfall in recent years. Under these circumstances, the project of water channel network facility in the Kiso River System is now under review. The water channel network facility in the Kiso River System will lead the water made available from the Tokuyama dam (the largest dam in Japan) at the upper reaches of the Ibi River to the Kiso River, in order to provide municipal water for Nagoya city (population: approx. 2.2 million) and other cities in Aichi prefecture, and to improve the river environment during the extreme drought event. This water channel will provide 1.7 m^3/s of water to the Nagoya city and 2.3 m^3/s of water to the Aichi prefecture and provide 12.0 m^3/s of water additionally for improving river environment. In the present study, a drought analysis of Kiso River System using a distributed hydrological model (Hydro-BEAM), which can consider actual reservoir operations, water intake from river channels and the water transfer by the virtual water channel network facility was conducted.

2 STUDY AREA

Figure 1 show the location, water utilization facility and population density of the study area.

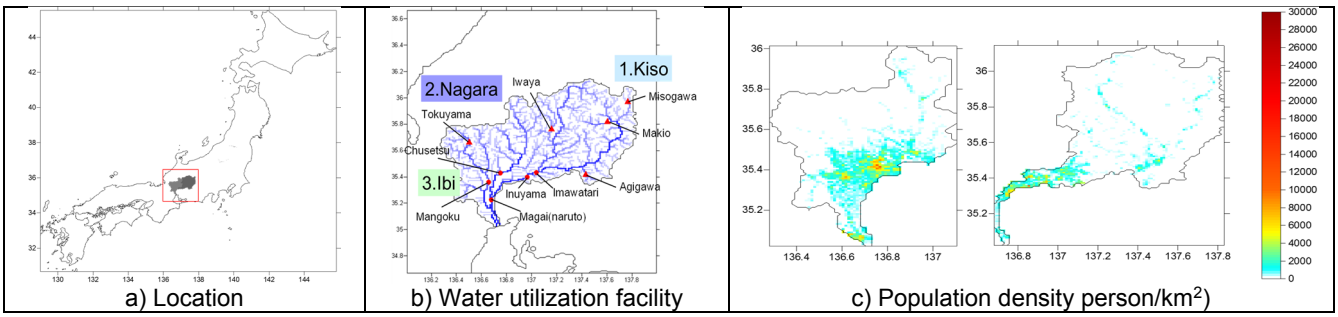

a) Location b) Water utilization facility c) Population density person/km^2)

Figure 1. Study area.

©2017, IAHR. Used with permission / ISSN 1562-6865 (Online) - ISSN 1063-7710 (Print)

Kiso river system located in the central part of Japan (Tokai Region), which consists of three rivers: 1. Kiso River (5275 km^2, 229km), 2. Nagara River (1985km^2, 166km), and 3. Ibi River (1840km^2, 121km), from East to West. More than 80% of each river basin is covered by forest and the population density is concentrated in the lower reaches. Thus, most of available water resources are located in the upstream forest area and the most water users are in the highly populated lower reaches.

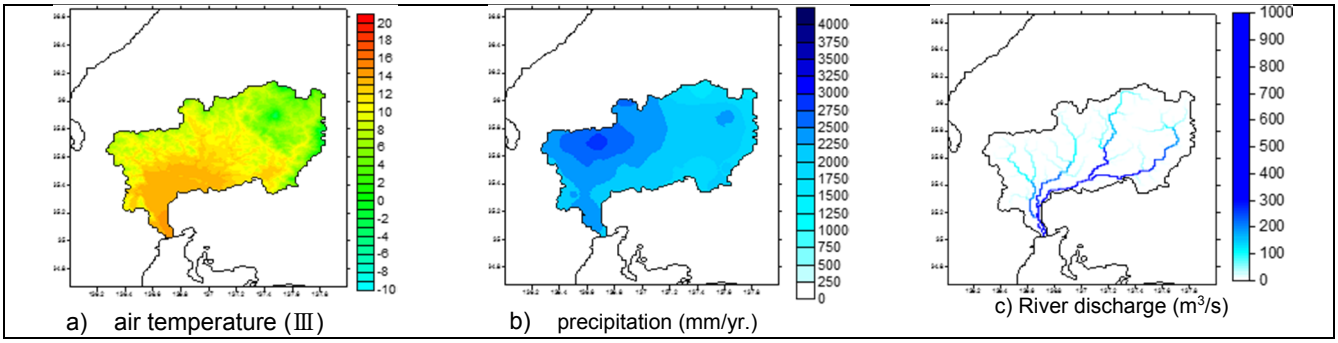

Figure 2. Climate and runoff situation of Kiso River system (1979-2003).

The average air temperature of the Kiso river system is 9.7 °C (Figure 2a), and the period (1979-2003) average annual total precipitation is 2247mm (Figure 2b). Although, the most of precipitation is concentrated in the upstream of the Ibi River basin, the annual average river discharge of Ibi River is relatively small compared with Kiso River (Figure 2c). This is mainly due to the differences of basin area and topographic conditions.

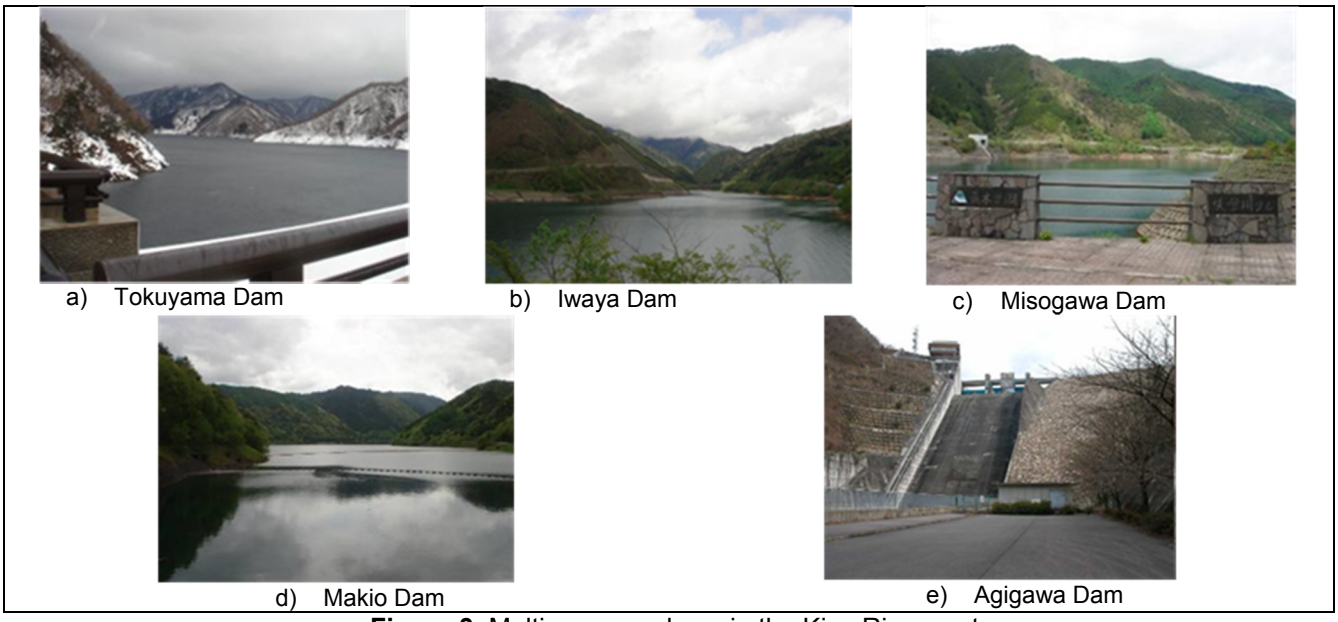

Figure 3. Multi-purpose dams in the Kiso River system.

Figure 3 shows major multi-purpose dams in the Kiso River systems. The location of each dam is indicated in the Figure 1b, and these specifications are summarized in Table 1.

Table 1. Specifications of each Multi-purpose dams in the Kiso river system.

	Tokuyama	Iwaya	Misogawa	Makio	Agigawa
River basin	Ibi	Kiso	Kiso	Kiso	Kiso
Purpose*	F.N.W.I.P.	F.A.W.I.P.	F.N.W.I.P.	A.W.I.P.	F.N.W.I.
Catchment Area (km^2)	254.5	264.9	55.1	304.0	81.8
Flood control capacity (M m^3)	123	50	120	-	160
Water supply capacity (M m^3)	1150	1000	310	680	220

*F: Flood Control, N: Natural function (for Environmental protection), W: Drinking water supply, I: Industrial water supply, P: Hydraulic power generation.

Figure 4 shows major water intake facilities in the Kiso River systems. The schematic drawing of water supplier, allocated water right (m^3/s), location of water withdrawal facilities are summarized in Figure 5.

 ©2017, IAHR. Used with permission / ISSN 1562-6865 (Online) - ISSN 1063-7710 (Print)

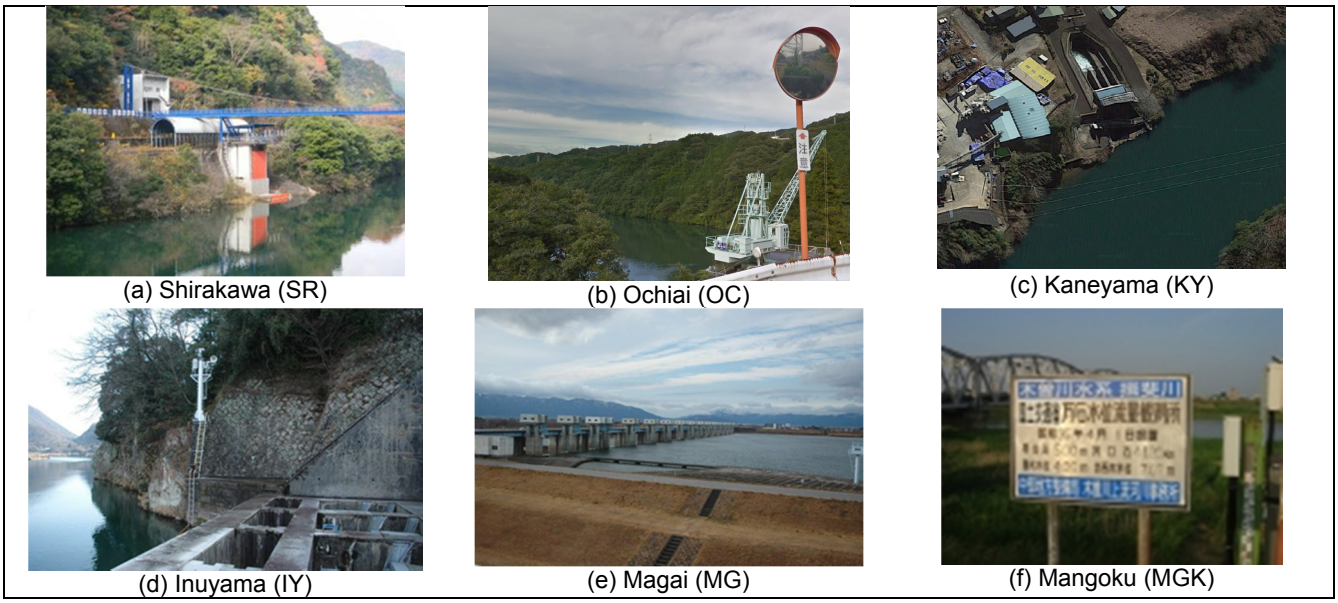

Figure 4. Major water intake facilities in the Kiso River system.

In the Kiso River system, there are two water rights: 1. Customary (Vested) water rights which has no restriction for water withdrawal from river channel and 2. Authorized water right which is restricted by the river administrator depending on the flow condition of each river. In Figure 5, red colored numbers represent vested water right and blue colored numbers are authorized water rights. Furthermore, in order to adapt the extreme water shortage, the inter basin water transfer channel from Tokuyama Dam (Ibi River) to Kiso River is now in the planning stage.

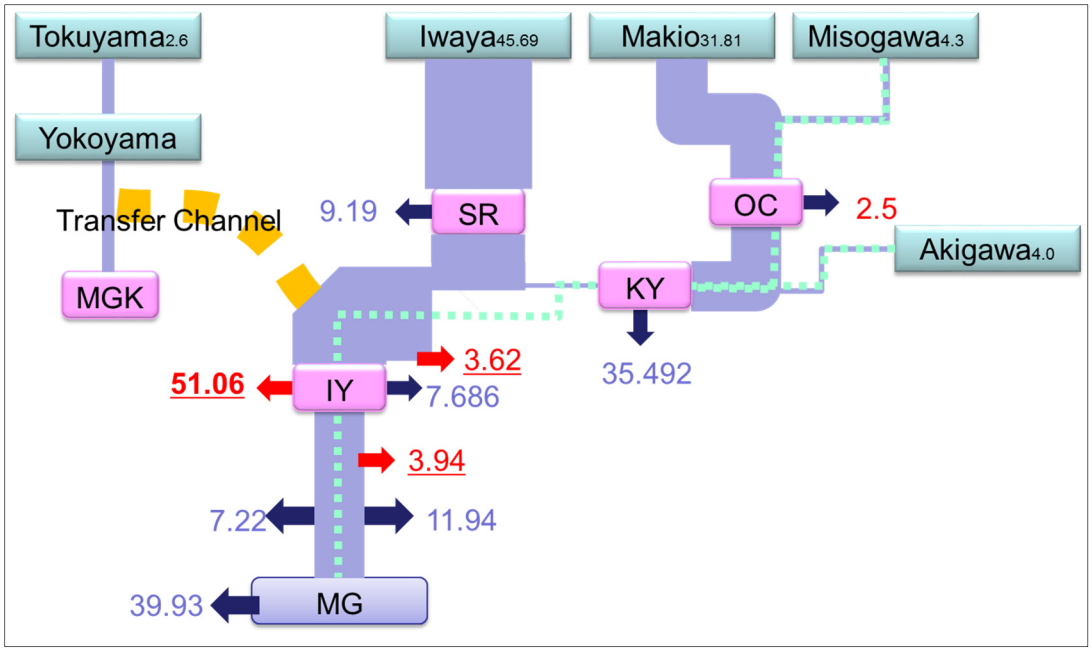

Figure 5. Schematic drawing of water supplier, allocated water right (m^3/s), location of water withdrawal facilities.
SR: Shirakawa; OC: Ochiai; KY: Kaneyama; IY: Inuyama; MG: Magai; MGK: Mangoku.

However, these allocated water right is the maximum value for water intake from river channel. So, in order to represent the actual condition of the water use, we used actual water use data from 1984 to 2008 obtained from MLIT and JWA. The monthly average actual water use patterns of each intake point is shown in Figure 6. The error bars in the Figure 6 represents standard deviation of each month.

©2017, IAHR. Used with permission / ISSN 1562-6865 (Online) - ISSN 1063-7710 (Print)

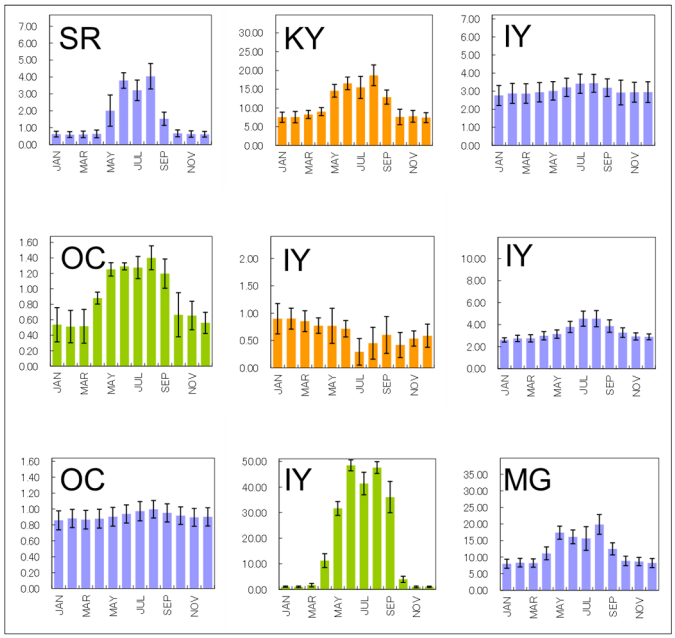

Figure 6. Monthly average actual water use pattern (m^3/s) in the Kiso river system.
SR: Shirakawa; OC: Ochiai; KY: Kaneyama; IY: Inuyama; MG: Magai; MGK: Mangoku.
The color of each figure indicates different division of water: Kiso river (Blue); Aichi (Orange); Other (reen).

3 METHODS

3.1 Hydrological model

As input variables for the hydrological model, we used surface meteorological data observed by the Japan Meteorological Agency (JMA). These data were applied to the Soil Vegetation Atmosphere Transfer (SVAT) scheme, a land surface heat-balance model, to estimate the amount of snowmelt and potential evaporation. Details of the SVAT model were summarized by Sato et al. (2008). To assess the rainfall–runoff process at a regional scale, we used a high-resolution (1-km grid scale and 10-min time step) distributed hydrological model called the Hydrological River Basin Environment Assessment Model (Hydro-BEAM) developed by Kojiri (2006). The model parameters are pre-calibrated by using observed river discharge data.

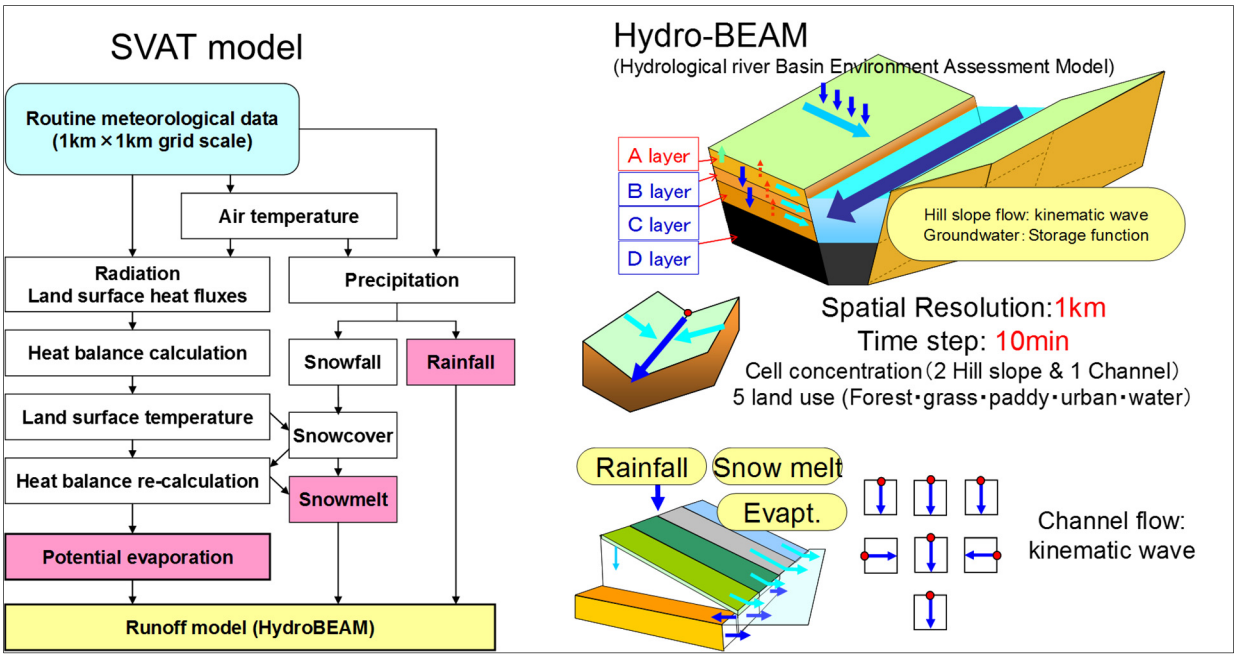

Figure 7. Outline of SVAT model and the basic structure of Hydro-BEAM.

The model is a cell concentration-type model that divides each cell into two pairs of rectangular hillslopes and one river channel. The surface and subsurface flow from each hillslope and the channel flow are

 ©2017, IAHR. Used with permission / ISSN 1562-6865 (Online) - ISSN 1063-7710 (Print)

calculated by a kinematic wave model. The groundwater discharge from each cell is calculated by a multi-layered linear storage model. The discharge from each grid cell then accumulates in the river channel, and the river flow is simulated by a river routing model (included in Hydro-BEAM) according to the channel network. The channel network and land-use type were determined from a 50-m digital elevation model (DEM) and the digital national information database developed by the Geographical Survey Institute (GSI) of Japan. Figure 7 represents an outline of the SVAT model and the basic structure of Hydro-BEAM.

3.2 AGCM

In order to clarify the impact of climate change, an AGCM (Atmospheric general circulation model) of the MRI (MRI-AGCM3.2S) was used for the experiment. The MRI-AGCM3.2S is based on a model developed jointly by the JMA and the MRI (Mizuta et al., 2006). The transform grid was composed of 1960 x 960 grid cells, corresponding to approximately 20-km grid intervals. It had 60 vertical layers (top at 0.01 hPa). As the lower boundary conditions, observed sea-surface temperatures (SSTs) and sea-ice concentrations were used for the current climate simulation (1979–2003). For the climate simulations of the end of the 21st century (2075–2099), the SSTs projected by the Coupled Model Intercomparison Project phase 3 (CMIP3) multi-model ensemble (MME) dataset were used. These data were based on the A1B scenario of the Special Report on Emission Scenarios (SRES) in the Fourth Assessment Report (AR4) of the Intergovernmental Panel on Climate Change.

3.3 Inter river basin water transfer model

The inter river basin water transfer plan is a water supply project from Tokuyama Dam located in the upstream of the Ibi River to the lower reach of the Kiso River via the Nagara River to mitigate extreme water shortage of the Kiso River which is the source of water for Nagoya city (one of the mega cities in Japan). In the normal situation, water shortage of the Kiso River basin is handled by several dams located in the upstream of the Kiso River basin itself. However, in the Kiso River basin, severe drought occurred frequently in recent years. Thus, to mitigate the risk of water shortage, the inter river basin water transfer plan is now under review.

In order to clarify the influence of the inter river basin water transfer, three numerical simulations (SIM-1~ SIM-3) were conducted (Figure 8). In the case of water shortage of Kiso River, SIM-1 assumes that water supply 0.5m^3/s from the Misogawa Dam. SIM-2 is the inter river basin water transfer 4.0m^3/s from Tokuyama Dam. In the case of sever water shortage, additional emergency water supply for river environment conservation 8.0m^3/s is operated. SIM-3 is the water supply from the estuary barrage of the Nagara River 2.0m^3/s. These three simulations correspond to basic water supply plan. The water shortage is when the situation of the river discharge at MG (magai) is less than 50m^3/s, and severe water shortage is that of less than 40m^3/s. The river discharge at MG is calculated by the Hydro-BEAM which includes the normal reservoirs operation and water withdrawal from upstream river channels.

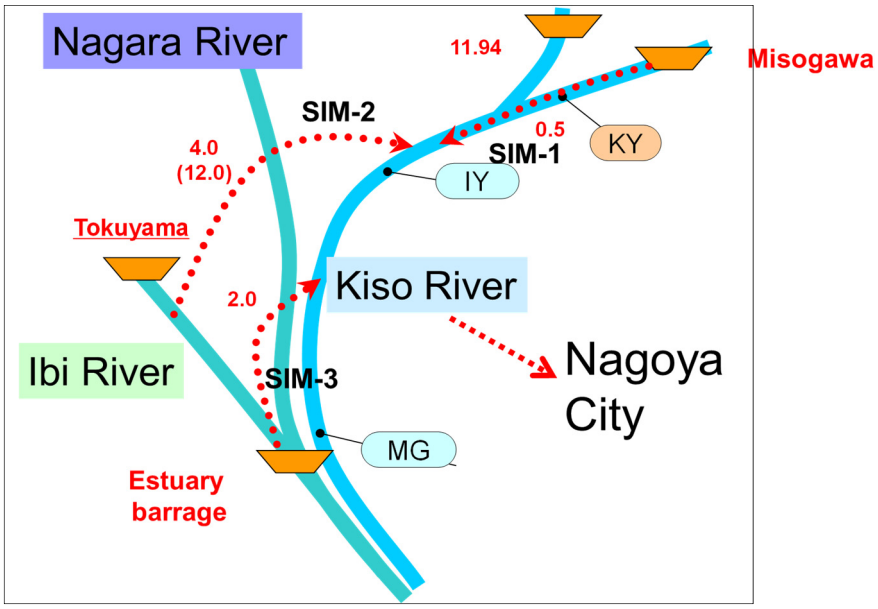

Figure 8. Outline of inter river basin water transfer simulation (SIM-1~SIM-3).

Furthermore, some combinations are considered such as SIM-4 (SIM-2 + SIM-3), SIM-5 (SIM-1 + SIM-2 + SIM-3). Above all these simulation results were compared with the control run (SIM-0: normal operation and water withdrawal only) under the present climate condition (1979-2003). Then, by using AGCM data, near

©2017, IAHR. Used with permission / ISSN 1562-6865 (Online) - ISSN 1063-7710 (Print)

future (2015-2039) and far future (2075-2099) simulation was conducted assuming SIM-1, SIM-2, and SIM-3 to clarify the impact of climate change. In this analysis, the bias correction of the AGCM does not considered, because only the relative changes between present and future climate condition are discussed in this paper.

4 RESULTS AND DISSCUSSIONS

4.1 Projected climate change and estimated change of river discharge by the MRI-AGCM

Figure 9 represents the change of air temperature (°C), evapotranspiration (mm/yr.), and precipitation (mm/yr.) projected by MRI-AGCM3.2S, and river discharge at river mouth calculated by the Hydro-BEAM between present (1979-2003) and future (near: 2015-2039, far: 2075-2099) climate conditions.

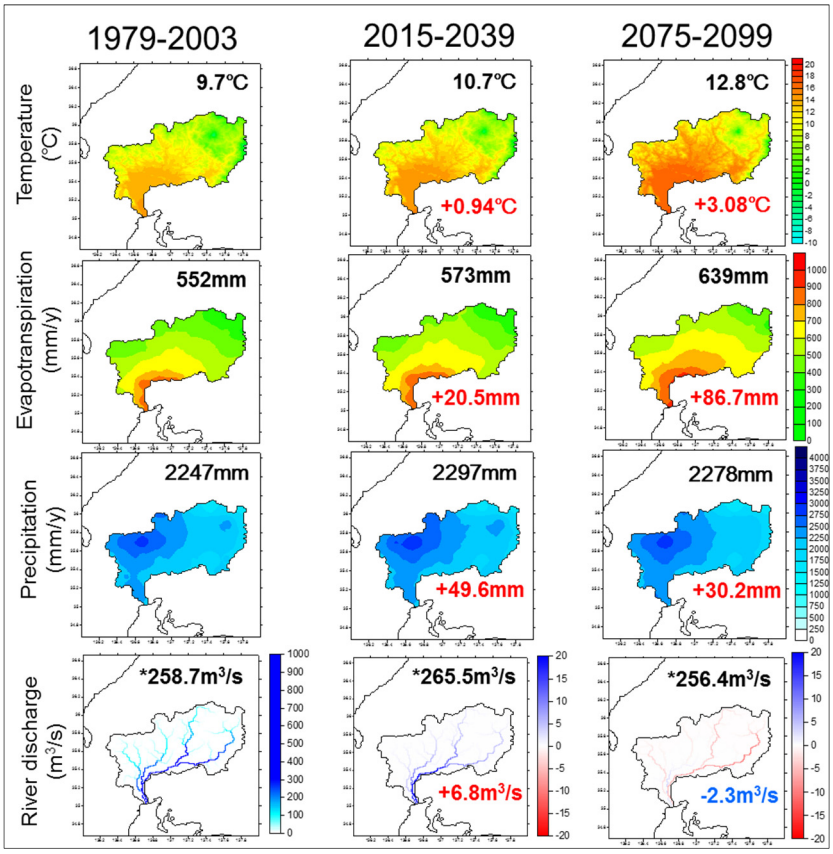

Figure 9. Climate change in the Kiso River system projected by the MRI-AGCM3.2S.

According to the MRI-AGCM3.2S based on SRES A1B scenario, the annual average air temperature will rise 0.94°C in the near future and will rise 3.08°C in the far future climate condition. Accordingly, annual amount of evapotranspiration will increase 20.5mm (near future) and 86.7mm (far future), respectively. In the same way, the amount of annual total precipitation will increase 49.6mm (near future), and 30.2mm (far future). Consequently, the annual average river discharge at river mouth of Kiso River basin will increase 6.8m^3/s (near future), and decrease 2.3m^3/s (far future). These differences mainly due to the difference of water balance between near and far future climate conditions.

4.2 Effects of inter basin water transfer under present climate condition (2000-2009)

Figure 10 shows the number of total drought days at IY (inuyama) and MG (magai) among deferent water management measures. In this figure, “normal” means normal drought condition: less than 100m^3/s at IY or less than 50m^3/s at MG, and “sever” means severe drought condition: less than 40m^3/s at MG. The differences of SIM-1 to SIM-5 are described in section 3.3. In these simulations, all meteorological variables for input data to Hydro-BEAM are obtained from raw MRI-AGCM3.2S output without bias collection. So, the result of control run “SIM-0” does not agree with the actual number of drought days (“Observed”). According to the results of SIM-1, there is no deference to SIM-0. It suggests that all the supplied water from Misogawa dam (0.5m^3/s) was consumed in the upstream of IY and MG. On the other hand, the water supply from Tokuyama Dam by the inter river basin water transfer channel (4.0m^3/s, 12.0m^3/s) showed a significant effect to reduce the number of drought days (SIM-2). In the case of SIM-3 (water supply from estuary barrage of Nagara River: 2.0m^3/s) also showed an effect to reduce drought days, however, the influence was relatively small compared with SIM-2 (inter basin water transfer channel). Furthermore, the influence of the combination

 ©2017, IAHR. Used with permission / ISSN 1562-6865 (Online) - ISSN 1063-7710 (Print)

of these water supply facilities: SIM-4 (SIM-2 + SIM-3), SIM-5 (SIM-1 + SIM-2 +SIM-3) does not show a large deference compared with SIM-2. Thus, the impact of SIM-2 seemed to be the best water resource management for drought mitigation in the Kiso River system.

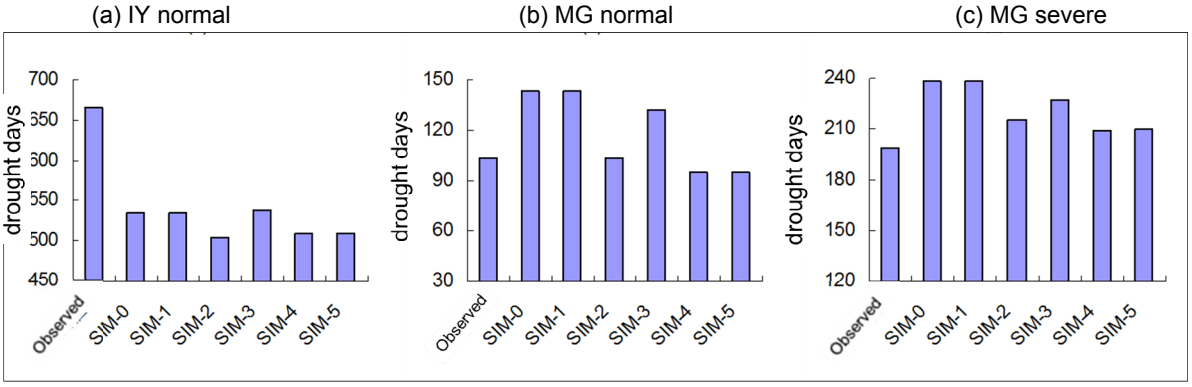

Figure 10. Annual average drought days under the present climate condition (2000-2009).

4.3 Effects of inter basin water transfer under future climate condition (2015-2039/2075-2099)

According to the actual water resources management plan, in the case of severe drought situation, the water supply facilities are used from small water storage capacities to preserve water for extreme water shortage situation. Thus, the following situation were conducted: SIM-1: water supply from Misogawa Dam only (0.5m^3/s), SIM-2: SIM-1 + water supply from estuary barrage of Nagara River (2.0m^3/s), and SIM-3: SIM-2 + water supply from Tokuyama Dam using inter river basin water transfer channel (12.0m^3/s).

Figure 11 shows the deference of total drought days under present and future climate conditions at IY and MG assuming a severe drought conditions of each point. Then, the change/effect of each simulation (SIM-1 ~ SIM-3) to control run (SIM-0) are shown in Figure 12.

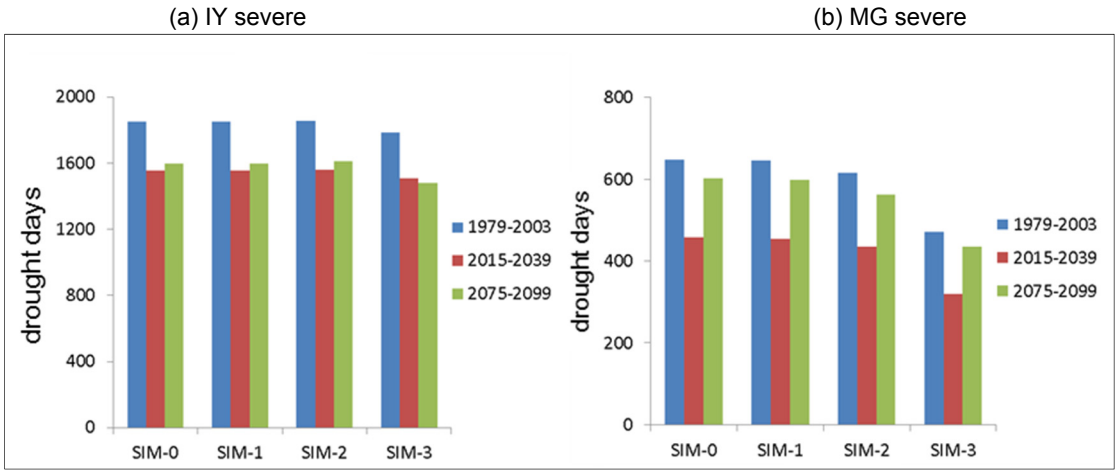

Figure 11. Difference of drought days under present and future climate condition.

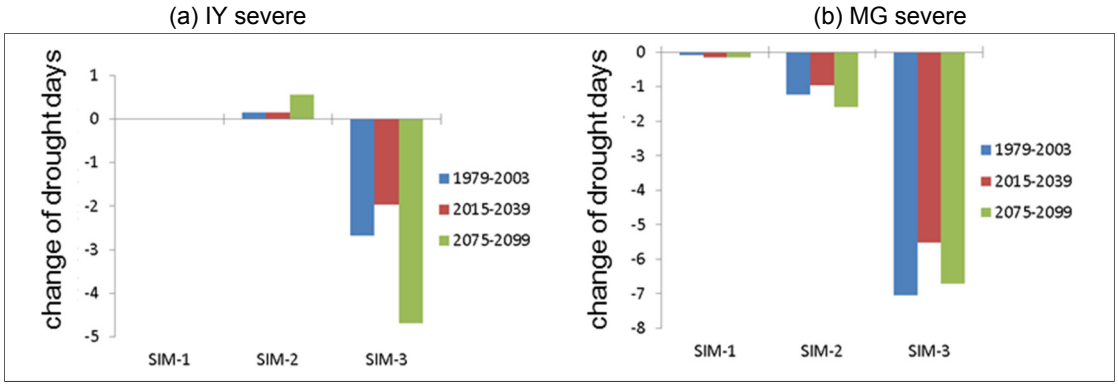

Figure 12. Change of drought days under present and future climate condition.

©2017, IAHR. Used with permission / ISSN 1562-6865 (Online) - ISSN 1063-7710 (Print)

As already mentioned in section 4.2., SIM-1 (0.5m^3/s of water supply from Misogawa Dam) does not improve the drought situation of each point (IY and MG). In the case of SIM-2, the number of drought days does not change so much at IY, but decreased approximately 1 day at MG. Because, as shown in figure 8, the water from estuary barrage of Nagara River is supplied in the downstream of IY. Finally, in the case of SIM-3, largest decrease of drought days appeared at both of IY and MG point. These results indicated that the water channel network can mitigate the drought situation significantly by shortening the period of drought approximately 7 days per year at MG and approximately 2 ~ 5 days at IY. The drought situation between present and future climate condition and influence of water supply facilities might not change so much.

5 CONCLUSIONS

In order to clarify the effect of inter river basin water transfer channels for extreme drought mitigation in the Kiso River system, several numerical simulation were conducted considering actual reservoir operation, water withdrawal and future climate change conditions. The obtained results suggest that the influence additional water supply from existing dam of Kiso River (Misogawa Dam) is almost negligible and water supply from adjacent (Nagara) river's estuary barrage seems relatively small. However, by using inter river basin water transfer channel, the drought situation of Kiso River basin will be improved significantly. In the present study, the influence of climate change does not find under the A1B scenario projected by MRI-AGCM3.2S. For the next step, multi-model ensemble and bias collection should be considered for reducing the uncertainties of the impact assessment of climate change.

ACKNOWLEDGEMENTS

This work was conducted under the framework of the "Precise Impact Assessments on Climate Change" of the Program for Risk Information on Climate Change (SOUSEI Program) supported by the Ministry of Education, Culture, Sports, Science, and Technology-Japan (MEXT). This work was also supported by JSPS KAKENHI Grant Number JP26420496.

REFERENCES

Kojiri, T. (2006). *Hydrological River Basin Environment Assessment Model (Hydro-BEAM)*. Watershed Models. Taylor & Francis, CRC Press, Florida, 613-626.

Mizuta, R., Oouchi, K., Yoshimura, H., Noda, A., Katayama, K., Yukimoto, S., Hosaka, M., Kusunoki, S., Kawai, H. & Nakawaga, M. (2006). 20-km-Mesh Global Climate Simulations using JMA-GSM Model. *Journal of the Meteorological Society of Japan,* 84(1), 165–185.

Sato, Y., Ma, X.Y., Xu J.Q., Matsuoka, M., Zheng, H.X., Liu, C.M. & Fukushima, Y. (2008). Analysis of Long-Term Water Balance in the Source Area of the Yellow River Basin. *Hydrological Processes*, 22(11), 1618–1629.

 ©2017, IAHR. Used with permission / ISSN 1562-6865 (Online) - ISSN 1063-7710 (Print)

MALAYSIAN NATIONAL WATER BALANCE SYSTEM (NAWABS) FOR IMPROVED RIVER BASIN MANAGEMENT: CASE STUDY IN THE MUDA RIVER BASIN

MOHD. RAZALI HUSAIN[(1)], ASNOR MUIZAN ISHAK[(2)], NURHAREZA REDZUAN[(3)], TERRY VAN KALKEN[(4)] & KATHERINE BROWN[(5)]

[(1,2,3)] Drainage and Irrigation Department, Kuala Lumpur, Malaysia
asnor@water.ov.my
[(4,5)] DHI Water & Environment, Kuala Lumpur, Malaysia,
tvk@dhigroup.com

ABSTRACT

Water resources management in Malaysia faces significant challenges from changing climate, growing population, increased water demand and pollution. Often water planning decisions are made without a full understanding of the impacts in the target and neighboring river basins. In daily operations, river basin managers face difficult decisions in balancing the short and long term demands with the available and predicted supplies in the basin. The National Water Balance System (NAWABS) being developed by the Malaysia Drainage and Irrigation Department (DID) aims to provide a comprehensive river basin management instrument to provide river basin managers with the tools and knowledge needed to make better informed planning and operational decisions. The core components of NAWABS are hydrological, hydraulic and basin allocation models which will be used initially to assess the current water availability and demands on a basin scale and determine water management strategies going forward to ensure the adequacy of future supply. These strategies include a range of supply augmentation measures coupled to demand management options during times of water stress. The NAWABS operational system will combine real time data and climate forecasts with the models to provide information on current and projected water availability and demands on a basin scale, including uncertainty and risk. NAWABS will provide multiple functions including current and project water availability, water use accounting, flow dependability, an assessment tool to evaluate short term operation options to ensure for efficient water allocation and a forecasting system and to assist in the decision management process. The NAWABS system is initially being implemented in the Muda River basin, in the northeast sate of Kedah on Peninsular Malaysia. The Muda basin is facing increased water demands from within the basin and neighboring basins, at the same time as long term climate change predicts decreasing rainfall in the future.

Keywords: River basin; management; modeling; decision support; Malaysia.

1 INTRODUCTION

Malaysia is blessed with one of the most abundant sources of water on the planet. Lying just north of the equator, its tropical climate delivers an average annual precipitation of 2940mm. The annual average rainfall varies between Peninsular (west) Malaysia (2490mm) and the less populated eastern states of Sarawak (3640mm) and Sabah (2560mm) on north Borneo. Rainfall is concentrated around the two monsoonal periods, between November-February and May-August.

The total annual runoff is estimated as 494 billion m^3, compared to an existing water demand of 14.7 billion m^3 and a project total demand by 2050 of 18.2 billion m^3 (Source National Water Resource Study, 2011). The total available water storage in Malaysia is 12 billion m^3, with the net supplied by direct river abstractions.

Despite this apparent abundance of water, the supply is not evenly distributed, neither spatially nor temporally. Water shortages in the capital of Kuala Lumpur and nearby Negeri Sembilan and Selangor states were apparent in 2014 due to lack of rainfall and low storage levels coupled with high demands. The “food basket” states of Kedah and Perlis in north east Peninsular Malaysia have also suffered in recent times from water stress which has affected irrigation water supplies, which are in conflict with the provision of potable water supplies being transferred from Kedah to Penang.

©2017, IAHR. Used with permission / ISSN 1562-6865 (Online) - ISSN 1063-7710 (Print)

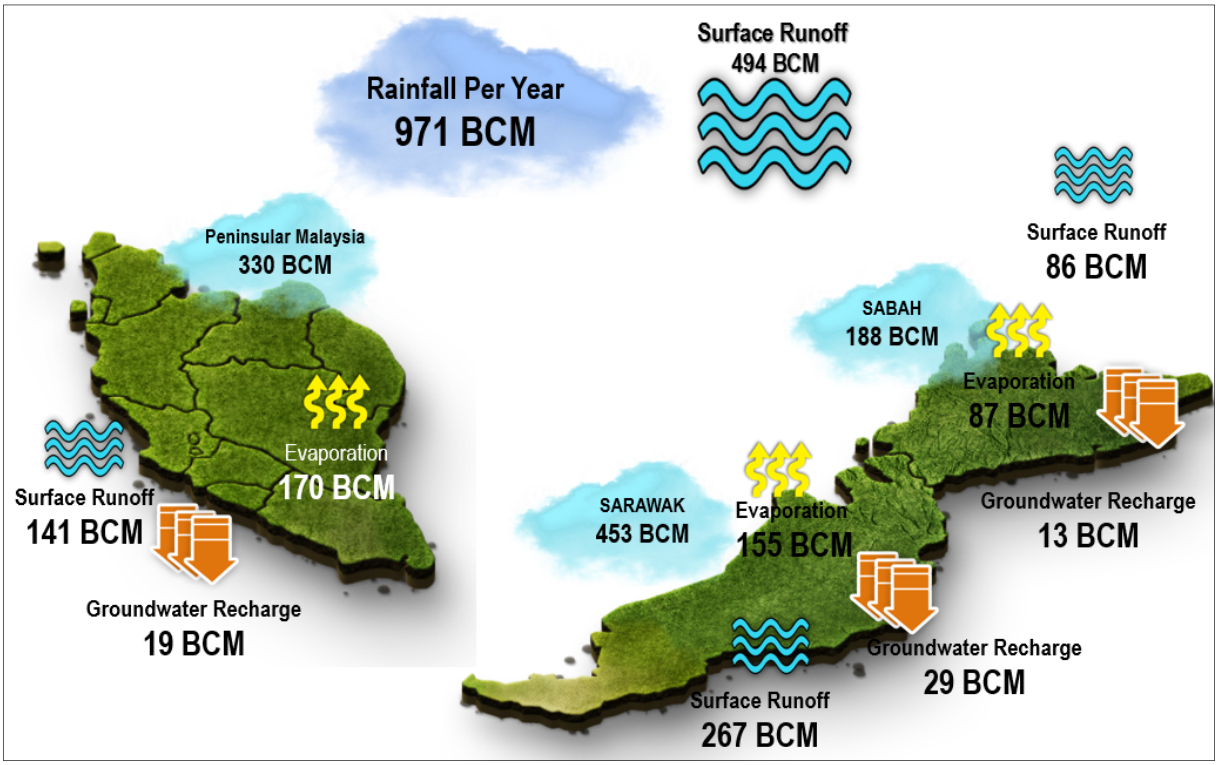

Figure 1. National water balance for Malaysia [Source: Review of National Water Resources Study (2011)].

In recent years therefore, due to development pressures, water mismanagement, and climate change, the water supply situation in Malaysia has changed from "one of relative abundance to one of relative scarcity" (Zakaria et al., 2013). In response, the Malaysian Government in February 2012 formulated and endorsed the National Water Resources Policy (NWRP). The policy sees a shift in focus on water as a resource, away from the earlier view of equating water management solely with the water supply industry alone. NWRP outlines the various strategies and action plans to address the problems and concerns for both immediate and long-term to manage water resources availability and demand in the country. With the following policy statement, NWRP provides clear directions and strategies in water resources management to ensure water security and sustainability:

"The security and sustainability of water resources shall be made a national priority to ensure adequate and safe water for all, through sustainable use, conservation and effective management of water resources enabled by a mechanism of shared partnership involving all stakeholders."

The National Water Balance System (NAWABS) is born directly from the vision of the NWRP. NAWABS is proposed as a comprehensive river basin management instrument that will facilitate a coordinated planning approach to water resources development as well as provide river basin manages with a means to more effectively operate the river basin in the short to medium term. The Malaysia Drainage and Irrigation Department is the implementing agency for NAWABS and has selected the water stressed Muda River basin in Kedah state as the first basin to be incorporated into the new system.

2 THE ROLE OF MODELLING IN RIVER BASIN MANAGEMENT

The NAWABS system is an implementation of an Integrated Water Resources Management (IWRM) approach that is *"a process, which promotes the coordinated development and management of water, land and related resources, in order to maximize the resultant economic and social welfare in an equitable manner without compromising the sustainability of vital ecosystems"* (GWP, 2000).

Models describing the physical river basin processes of runoff and river flow as well as human interactions of reservoir and dam operations and diversions are commonly used to support water management planning and decision making. Refsgaard (2007) illustrates the interactions between modelling and water management processes as shown in Figure 2. The main steps in the modelling process are described in the following:

i. Identification including assessment of present status, analysis of impacts and pressures and establishment of environmental objectives. Modelling may be useful for establishing the baseline conditions identifying impacts of the various pressures. (European Commission, 2004);

 ©2017, IAHR. Used with permission / ISSN 1562-6865 (Online) - ISSN 1063-7710 (Print)

ii. Designing including the set up and analysis of a program of measures designed to be able in a cost-effective way to reach the environmental objectives. Here modelling will typically be used for supporting assessments of the effects and costs of various measures under consideration;
iii. Implementing the measures. Here on-line modelling in some cases may support the operational decisions to be made;
iv. Evaluation of the effects of the measures on the environment. Here modelling may support the monitoring in order to extract maximum information from the monitoring data, e.g. by indicating errors and inadequacies in the data and by filtering out the effects of climate variability.

Modelling will play an important role in NAWABS. Defining the water balance requires a whole of catchment approach that considers not just surface water resources but groundwater resources as well. Integrated surface-groundwater assessments will be undertaken using the MIKE SHE model (Graham and Butts, 2006). River basin water allocation and prioritization for various water users, as well as an assessment of the potential for shortages and surpluses will be investigated using the MIKE HYDRO BASIN model (DHI, 2016). Once established, the model can be run using long-term rainfall or runoff timeseries to assess water availability and fine tune allocations and priority of use. The models will be used both as a long-term planning tool as well as to support short-medium term operations, including possible groundwater exploitation, if this option proves to be viable.

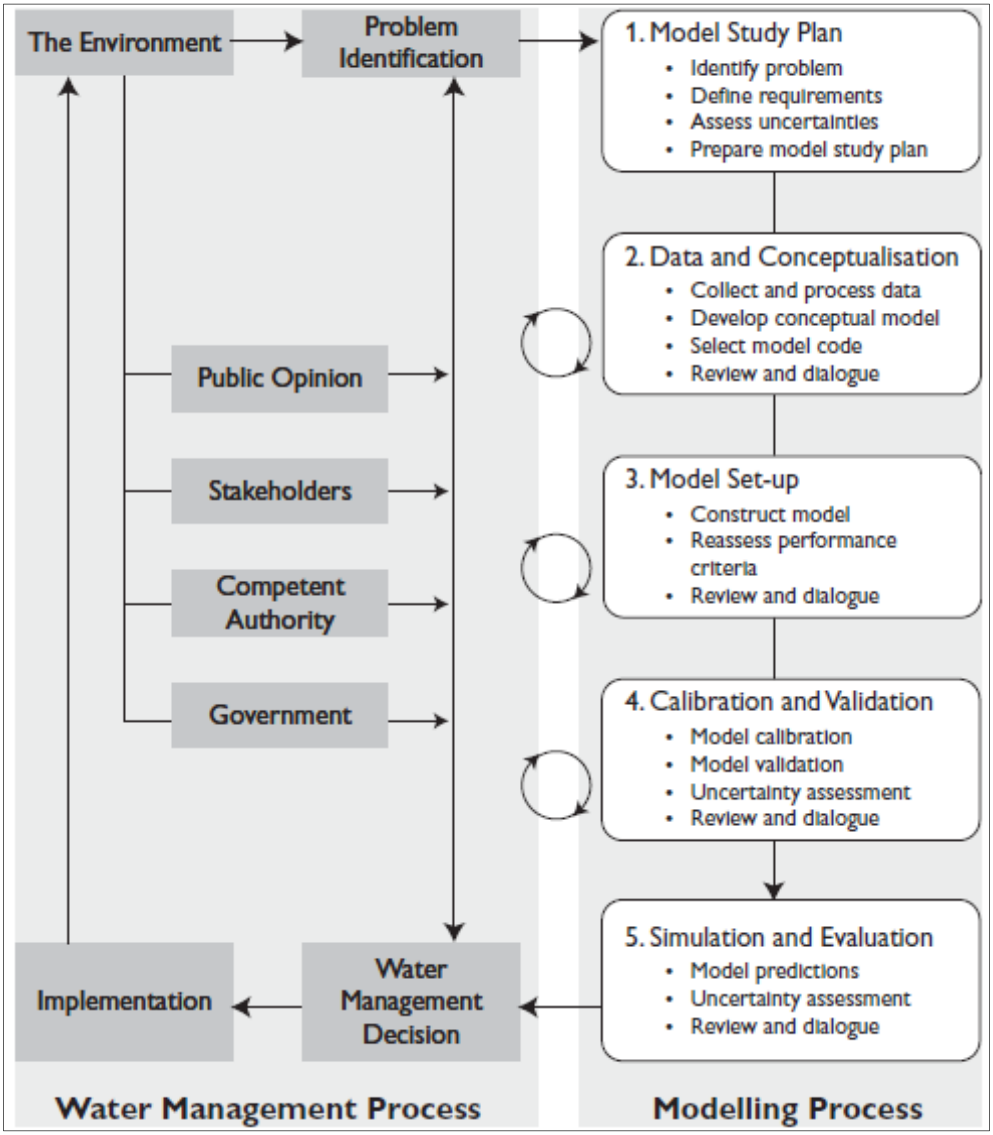

Figure 2. The role of the modelling process and the water management decision process [after Refsgaard, (2007) and inspired from Pascual et al. (2003).].

3 THE NATIONAL WATER BALANCE SYSTEM FOR MALAYSIA

3.1 Objectives

NAWABS provides a framework for sharing knowledge, understanding river system behavior, evaluating alternative developments and operational management schemes. It will also support informed decision-making from a river basin and inter-state planning perspective with the shared objective of developing the water resources in a cooperative manner, sharing socio-economic benefits, and promoting efficient water utilization.

3.2 Approach

The NAWABS system will be built around a comprehensive Decision Support System (DSS) framework that will be customized specifically to support the NAWABS operational objectives, with further local customizations for each river basin as needed. In recent years, the use of DSS is increasingly accepted by water agencies, donors and at the political level for IWRM, as a useful and sometimes a necessary approach to address operational, management or planning issues at local and/or river basin level, especially in a trans-boundary context (Malmgren-Hansen et al., 2016).

The DSS framework will be based on MIKE Customized (DHI, 2016c). MIKE Customized was originally developed as a generalized DSS for the Nile Basin Initiative (NBI, see Sørensen et al 2015). The NBI required a system that could support river basin management issues within the Nile Basin riparian countries and which could be easily adapted and customized to other river basins in Africa and elsewhere. Both parties recognized a mutual interest in DHI's commercialization of the system. The developed Nile Basin DSS and its commercial development, MIKE Customized, is an integrated solution with four main components: (see Figure 3).

i. An information management system that comprises a relational database management system to store all information in one repository;
ii. A geographic information system (GIS) to process all geo-referenced information;
iii. A time series management toolkit to process and analyze time-series data;
iv. A set of analytical and modelling tools including:

- a water resources modelling platform that allows plugging-in and linking of water;
- balance and allocation, rainfall-runoff and hydrodynamic models (an open modelling framework);
- scenario management including key performance indicator (KPI) calculations for scenario comparison;
- ensemble generator for probabilistic analyses;
- climate downscaling tools based on global circulation models;
- multi-objective optimization and trade-off analysis;
  economic cost-benefit-analyses, and multi-criteria- analysis to support a structured stakeholder involvement and decision making process.

Figure 3. MIKE customized components.

3.3 Expected outcomes

The developed models and NAWABS DSS will be used to assess the existing water balance and future scenarios, as well as an operational system for real time decision making and water accounting. Real time inputs will include rainfall, river levels and flows, pumped extractions and structure operations. Short term

 ©2017, IAHR. Used with permission / ISSN 1562-6865 (Online) - ISSN 1063-7710 (Print)

forecasts will be based on available weather forecast data from Malaysia Meteorological department whereas longer term assessments including uncertainty will be based on ensemble climate forecasts from NOAA's NCEP datasets. Model results will be processed and aggregated to provide information on 9 key outputs comprising:

- Water accounting – river basin inflows and outflows;
- Water availability – flows and river levels at key demand points;
- Water quality – key water quality parameters;
- Water storages – available dam storages and timing and volume of dam releases;
- Water and drought resources index – calculation of indices to gauge the current and forecast state of the river basin;
- Water audits – accounts of all water movements in the river basin;
- Water allocation;
- Alternative demand options;
- Water priorities.

4 THE MUDA RIVER BASIN

4.1 Description

The Muda River is the largest river in the State of Kedah, see Figure 4. The water resources in the basin developed over the past several decades and are used for irrigated agriculture and potable water supply in Kedah and Penang. Management of water resources in the catchment has multiple stakeholders, including the federal and state arms of the Drainage and Irrigation Department, Muda Agricultural Development Agency (MADA), and water supply authorities for Kedah (SADA) and Penang (PBA) Both the long-term sustainability of water resources in the basin, as well as short-term operational considerations are important in order to ensure the equitable distribution of water to all users during periods of excess and well as water stress.

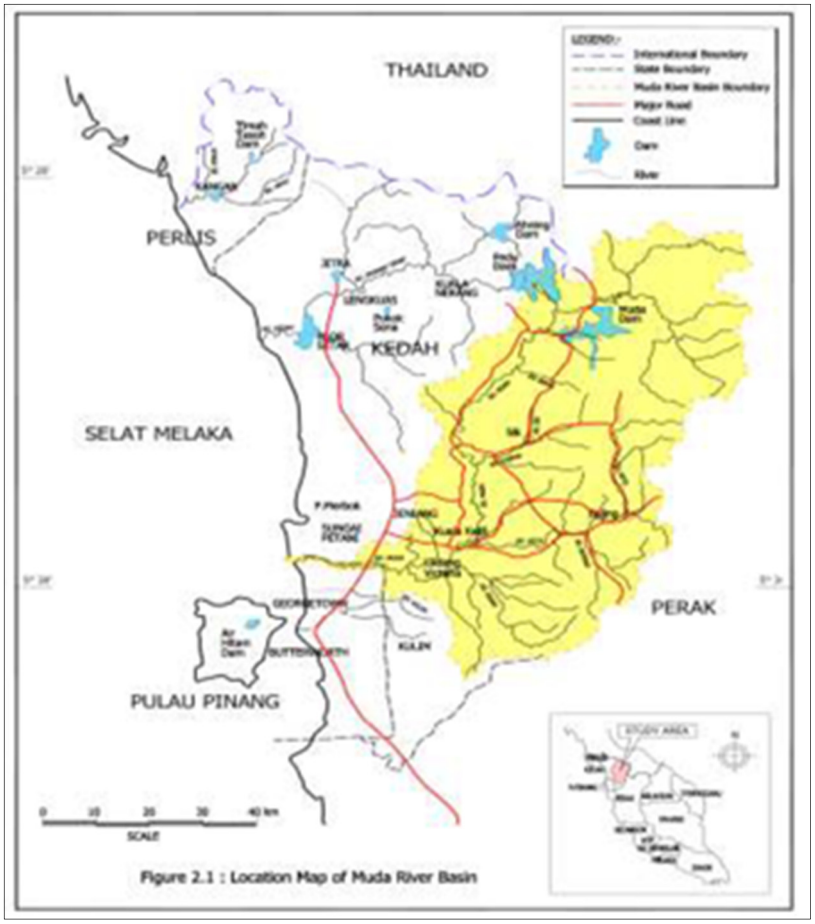

Figure 4. Muda River Basin location.

Key considerations include:

- Multiple stakeholders have different priorities;
- Water resources in the basin are now deemed to be limited;

©2017, IAHR. Used with permission / ISSN 1562-6865 (Online) - ISSN 1063-7710 (Print)

- Key hydraulic infrastructure in the basin is managed by different authorities, and their operation needs to be coordinated;
- Future changes in land use and climate will affect the supply and demand for water;
- The groundwater resource potential is yet to be fully explored.

The uncertainty of the total water resource in the basin and lack of modern river management tools hinders fully informed decision making. This, combined with the water shortages commonly experienced in the basin, have resulted in DID promoting the Muda basis as the first to be implemented in the NAWABS system.

4.2 Physical setting

The Muda basin has a catchment area of 4210 km^2. The upper tributaries drain mountainous areas where elevations reach a maximum of 1860 m. The lower reach of the Muda catchment comprising about 45% of the total area is generally flat with the elevation ranging from a minimum 2.5 m at the river mouth which gradually increases to about 70 m towards the east to the hilly areas.

The Muda basin experiences two monsoons annually, namely the northeast monsoon and southwest monsoon. The northeast monsoon usually occurs from November to February. During this monsoon, the north-easterly winds prevails the southwest monsoon reaches the west coast of Peninsular Malaysia from the Indian Ocean and prevails over Peninsular Malaysia from May to August causing the westerly and/or north-westerly winds. In the transition period between the two monsoons, from September to November, the western wind prevails and the equatorial through tends to lie over Malaysia.

The annual rainfall depth in the study area ranges between 2,000 to 3,000 mm. The heavy annual rainfall is observed around the central mountain of Gunong Jerai and the southern mountainous areas declining northward and to the river mouth. The annual average evaporation is approximately 1,635 mm (4.5 mm/day).

Land use in the basin is very much dictated or constrained by the hilly topography which make up about 70% of the basin area. As such about 60% of the area still remains forested while the balance is mostly used for agriculture involving rubber and oil palm in the upper areas while paddy is cultivated in the downstream part of the river basin.

The river experiences high flows during two periods a year corresponding to monsoon rains, one from September to November, and the other from April to May. Lowest flows usually occur either in the month of February or March. The river water is used extensively for irrigation and other commercial purposes. In order to provide a stable supply a number of large water storages in the basin have been constructed in the basin, see Table 1. These comprise the Muda Dam with a catchment area of 984 km^2 and Beris Dam (116 km^2). Water in Muda dam is mostly diverted to the neighboring Kedah River catchment via the Saiong tunnel to Pedu Dam from where it is released to supply the MADA irrigation scheme.

Table 1. Dam storages in Muda and Kedah basins.

Dam	Basin Area (km^2)	Active Storage (Mm^3)	Gross Storage (Mm^3)
Muda	84	154	171
Pedu	171	1080	1205
Ahning	122	275	319
Beris	116	114	122

Downstream from the dams a large unregulated catchment drains via the Ketil (868 km^2), Chepir (335 km^2) and Sadim Rivers (626 km^2) toward Sungai Petani, the largest town in the catchment. Two barrages, separately operated by DID and PBA, operate to exclude saline tidal flows and maintain water levels for irrigation purposes and facilitate water extraction. The first barrage as constructed around 1957 mainly to block saline water. It is currently operated by PBA. Beside the old barrage, a new barrage was constructed as part of the Sg Muda flood mitigation project. The new barrage started operation in 2004 and its operation is managed by DID.

Water is extracted from the river upstream of the barrage for irrigation and water supply purposes. A total of 8 pump stations are operated by JPS for irrigation with a combined capacity of 2280MLD. SADA and PBA operate a further 9 with a total capacity of 1300MLD. Figure 5 shows the existing water users in the basin.

 ©2017, IAHR. Used with permission / ISSN 1562-6865 (Online) - ISSN 1063-7710 (Print)

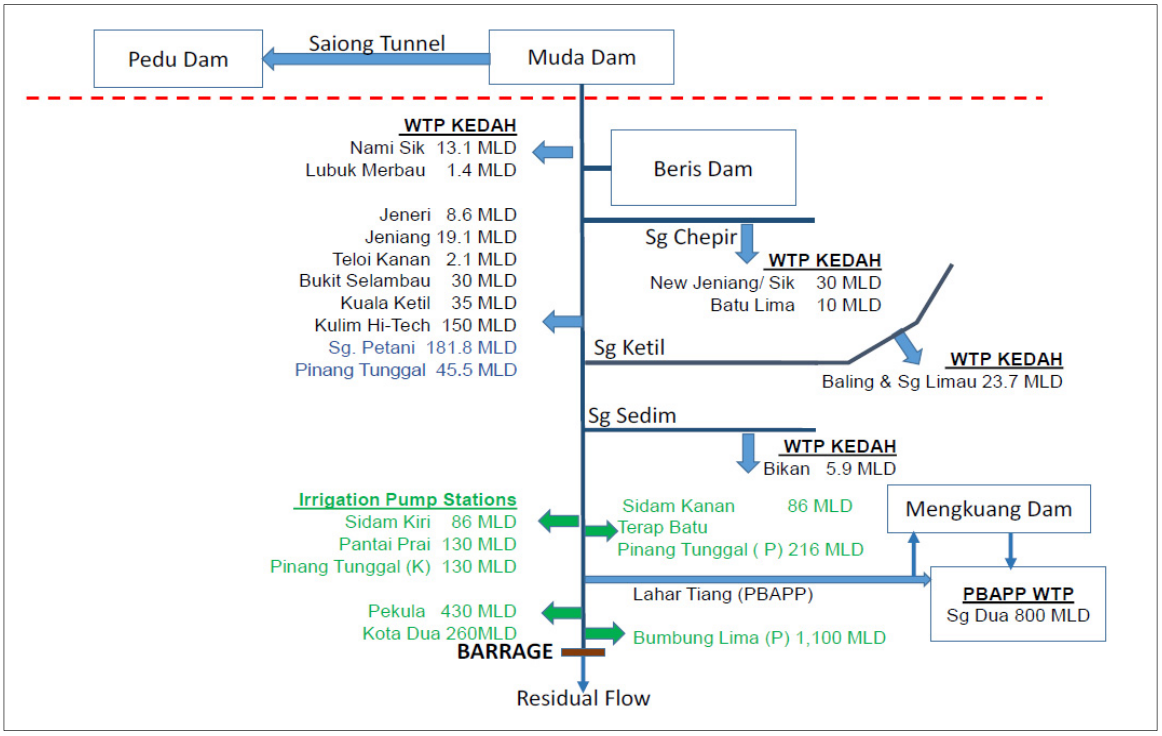

Figure 5. Existing water use in Muda River Basin.

4.3 Current challenges

The water resources of the Sg. Muda basin are in high demand for agriculture and water supply to towns and industry. Water from Muda Dam is also diverted to Pedu dam which has the biggest storage capacity at 1,080 MCM among the four dams. This arrangement is part of a comprehensive freshwater distribution system that covers the irrigation and potable water needs of Kedah and southern Perlis. The biggest user of water benefitting from this system is MADA granary area which has a size of 97,000 ha. The Muda River supplies about 32% of the MADA area irrigation needs. The Pulau Pinang granary area which stands at 9,800 ha receives irrigation water directly from the lower part of the Muda River. The total irrigation water use is estimated at 3,800 MLD on average while potable water use is at 1,160 MLD. About 80% and 96% of public water supply need for Pulau Pinang and Kedah is derived from the Muda River respectively.

According to National Water Resources Study (2011), the state of Kedah is currently in deficit for water based on available rainfall and consumptive demands. The shortfall is made up via the major water storages. Projected domestic demands are predicted to increase due to population growth while at the same time irrigation demands are predicted to decrease assuming improved future efficiencies.

In view of the increasing water demand, the government has embarked to identify and develop several projects which include the followings: (see Figure 6):

- Upgrading of Irrigation System at MADA Granary Area This project is implemented by the Ministry of Agriculture and it comprises upgrading of tertiary canals, farm road and associated facilities. Detailed design for the project has been completed and now awaiting approval for construction;
- New/Upgrading of Treatment Plants in Kedah This program is implemented by SADA which involves among others new treatment plants in Langkawi and Jenun in Pendang;
- Jeniang Transfer Scheme and Naok Reservoir (Dam), Kedah This project is implemented by the Ministry of Agriculture and comprises Jeniang Barrage, transfer canal, Naok Dam and connection to the Southern Canal at MADA Granary Area. This project when completed will allow diversion of water from the Muda River including releases from Beris Dam to the MADA area in the neighboring Kedah basin;
- Upgrading of Mengkuang Dam. This project is implemented by Kementerian Tenaga, Teknoloji Hijau dan Air (KeTTHA) and is almost completed. Under this project, the existing Mengkuang Dam capacity is increased from 22 MCM to 73.5 MCM. Water is supplied by direct pumping from the Muda River upstream of the barrages. With this increase the Sungai Dua water treatment plant production capacity can be increased from 300 MLD to 1,000 MLD.

Other issues facing the basin are:

- Pressure for land development and potential for changes in land use to impact the basin;
- Deforestation in the basin which threatens the hydrological response, sediment runoff and biodiversity;

©2017, IAHR. Used with permission / ISSN 1562-6865 (Online) - ISSN 1063-7710 (Print)

- Climate change;
- Water quality, particularly in the lower reaches;
- Severe flooding in the area;
- Lack of collaborative planning between stakeholder agencies.

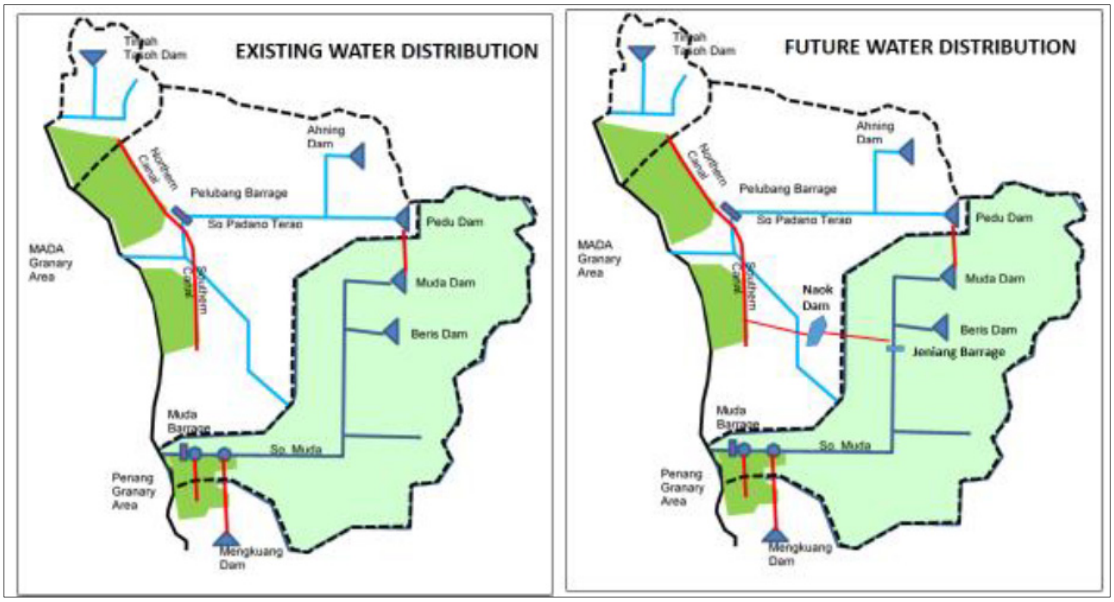

Figure 5. Existing and proposed diversions Muda River Basin.

4.4 NAWABS implementation in the Muda River Basin

An initial water balance study where the main modelling will be developed to quantify the overall resource availability and assess existing and future demands, including environmental demands. Incorporation of the developed models with a MIKE Customized DSS framework and linking to real time and forecast data sources, to provide an operational water management tool for the river basin managers.

4.4.1 Water balance study

The National Water Resource study provides a solid foundation for the current project to build on. The water balance study will be based on a validation and update of the previous work and provide a quantitative assessment of:

- Existing and future sources of supply, including surface water, groundwater, dams, inter-basin transfers;
- Existing and future demands, including surface water and groundwater abstractions, environmental flows;
- An examination of the priorities for water delivery and how demands can be managed in times of water stress;
- Potential surplus / deficits, now and in the future, under different development and demand management scenario, allowing for climate change impacts;
- Infrastructure operations now, and in the future, to meet all needs, including necessary additional development of water resources.

The water balance study will be supported by a number of sub-studies comprising:

- Demand management study – investigate current water use efficiencies, how demands are influenced by economic, climate and other factors (should include comprehensive assessment of all water demands);
- Water Resources Conservation Plan – investigate how land use and water supply/demand are tied. Recommend land use map (with catchment protected areas);
- Environmental flow study – to determine environmental flow requirements;
- Water, Energy, Food Nexus study – determine the relationships between food, energy and water in the basin, and determine the water footprint.

The water balance study requires a whole of catchment approach that considers not just surface water resources but groundwater resources as well. The MIKE SHE model provides a suitable platform on which to undertake this assessment. While there is sufficient information for the surface water modelling, hydrogeological data is sparse and additional data is likely to be required.

 ©2017, IAHR. Used with permission / ISSN 1562-6865 (Online) - ISSN 1063-7710 (Print)

Water allocation and prioritization for various water users, as well as an assessment of the potential for shortages and surpluses will be investigated using the MIKE HYDRO BASIN model. Once established the model will be run using long-term rainfall timeseries to assess water availability and fine tune allocations and priority of use.

Water quality is also an issue for the river basin. The quantification of non-point and point source pollution loads to the river system and movement of these in the river channels will be handled through the water quality extension of the MIKE HYDRO BASIN model.

The models will underpin the overall water balance assessment which will include recommendations for managing existing operations as well as future water developments, including possible groundwater exploitation, if this option is viable.

Stakeholder engagement is an important aspect of the study. Early stakeholder consultations are important to initiate awareness of the project and determine what relevant data may be available. A number of workshops have been held and more are planned to obtain a comprehensive view of the data available, the current water management arrangements in the basin and to discuss what additional information could be generated from NAWABS and how it can be best disseminated.

4.4.2 Decision management support system

The decision management support system (DMSS) will provide water managers with the ability to undertake long-term planning investigations, as well as support short and medium-term operations. The developed MIKE SHE and MIKE HYDRO BASIN models will be incorporated into the DMSS and will form the basis for decision making. The outputs from the operational models will be used to generate a set of indicators which will be used in a Multi-Criteria Analysis tool to aid decision making. The Muda Basin NAWABS DMSS will be designed to operate on a range of timescales, utilizing different spatial and temporal inputs appropriate to each subject scenario. The overall workflows of the DMSS are shown in Figure 7.

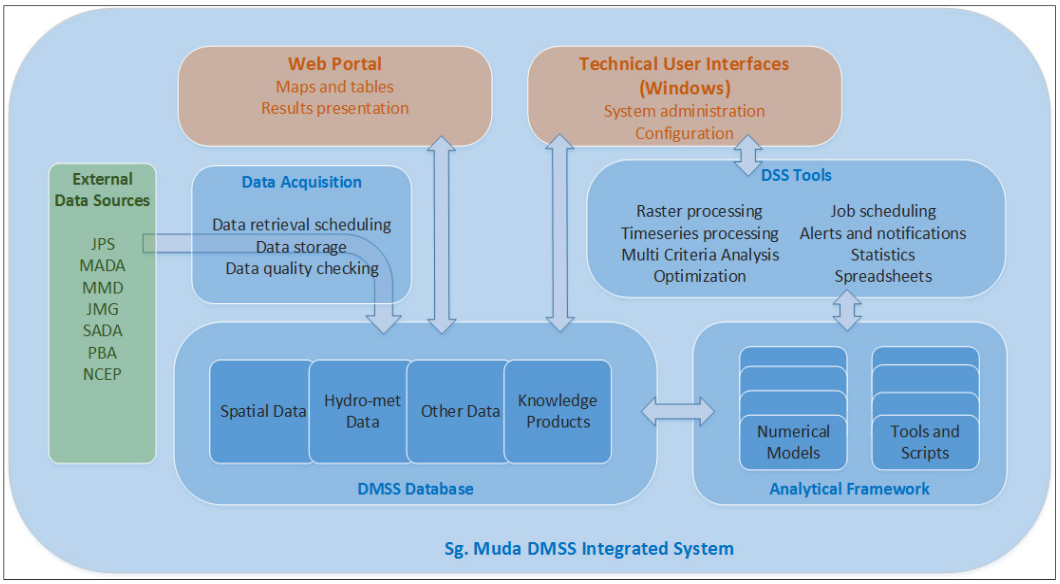

Figure 7. Muda River Basin NAWABS DMSS components.

5 FUTURE DEVELOPMENTS

The NAWABS implementation for the Muda basin represents is being undertaken as a first phase of the National NAWABS rollout. In order to ensure scalability of the Muda basin implementation of NAWABS a common DMSS platform (MIKE Customized) will be used. Data importing and processing tools, as well and model post-processing tools and web based interfaces are expected to be commonly used for all NAWABS implementation and therefore the development of these products will take into account possible future requirements in order to ensure these can be easily accommodated.

The MIKE Customized platform includes built in support for expandability with facilities to allow for the distribution of various tasks such as data acquisition, model simulations, database management and web interfaces, see Figure 8. As the MIKE Customized (and MIKE modelling) software continues to develop new functionalities will become available that may be relevant for NAWABS. Ongoing system maintenance and support is therefore an important aspect of the Muda basin implementation and this will ensure the system remains up to data and can take advantage of the latest developments.

©2017, IAHR. Used with permission / ISSN 1562-6865 (Online) - ISSN 1063-7710 (Print)

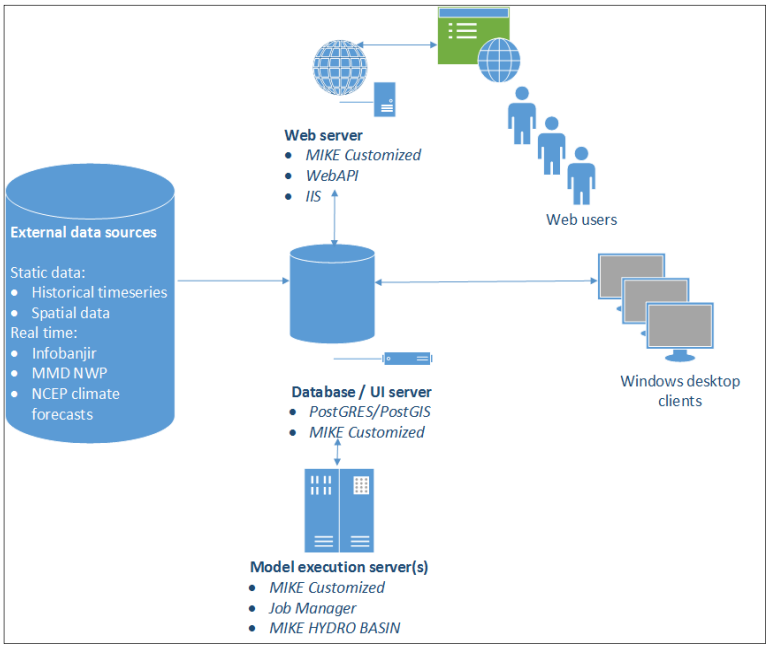

Figure 8. NAWABS system architecture.

6 CONCLUSIONS

The National Water Balance System for Malaysia is an implementation of an Integrated Water Resource management (IWRM) framework that supports the objectives of the National Water Resources Policy. Embedded in a solid scientific foundation and understanding of basin scale processes it will enable decision makers to have an improved understanding of the overall water availability within the target river basin and allow for the formulation of improved plans policies for water resource developments and allocations.

The operational system will enable river basin managers to better balance supply and demands through an improved assessment of the future flow conditions and the ability to assess the risk of various operational strategies. The Muda river basin is selected as the first basin the Malaysia to be incorporated in NAWABS. The developed system will have the ability to be scaled and expanded to other river basins in the future.

REFERENCES

Graham, D.N. & Butts M.B. (2006). *Flexible, Integrated Watershed Modelling with MIKE SHE*. Watershed Models. CRC Press, 245-272.

European Commission (2004). *Common Implementation Strategy for the Water Framework Directive (2000/60/EC)*, Guidance Document No 32, Pressures and Impacts, IMPRESS.

GWP (2000). *Integrated Water Resources Management*, TAC Background Papers No. 4. Global Water Partnership, Stockholm.

Malmgren-Hansen, A., Storm, B. & Olesen, K.W (2016). Decision Support System for River Basin Planning: A Case Study for the Shire Basin. (awaiting publication).

Pascual, P., Steiber, N. & Sunderland, E. (2003). *Draft Guidance on Development, Evaluation and Application of Regulatory Environmental Models*, The Council for Regulatory Environmental Modeling. Office of Science Policy, Office of Research and Development. US Environmental Protection Agency, Washington D.C, 60.

Ranhill. (2011). *National Water Resources Study*.

Refsgaard, J.C. (2007). Hydrological Modelling and River Basin Management, *Phd Thesis*. University of Copenhagen.

Sørensen, H.R., Beyene, M. & Ammentorp, H.C. (2015). The Nile Basin Decision Support System, *Hydrolink,* 4, IAHR.

Zakaria, N.A., Ab Ghani, A., Talib, S.A., Chan, N.W. & Desa, M.N.N. (2013). Urban Water Cycle Processes, Management, and Societal Interactions: Crossing From Crisis To Sustainability. *World Environmental and Water Resources Congress, Showcasing the Future, Cincinnati, ASCE*, Ohio, 1240-1246.

 ©2017, IAHR. Used with permission / ISSN 1562-6865 (Online) - ISSN 1063-7710 (Print)

SEASONAL FORECASTING OF RESERVOIR INFLOWS AND THEIR UNCERTAINTIES

MICHAEL BUTTS[1], ROAR JENSEN[2], JACOB LARSEN[3], HENRIK MUELLER[4], BERTRAND RICHAUD[5], PETER LARSEN[6], MIGUEL ÁNGEL CORCUERA BARRERA[7], BASEL DRAW[8] & ALEJANDRO E. LASARTE[9]

[1,2,3,4,5,8] DHI Denmark, Hoersholm, Denmark,
mib@dhigroup.com, raj@dhigroup.com, jla@dhigroup.com, hgm@dhigroup.com, ber@dhigroup.com, b.draou@gmail.com
[6] DHI Spain, San Sebastián, Spain
ptl@dhigroup.com
[7] Aguas del Añarbe - Añarbeko Urak, San Sebastián, Spain
mcorcuera@agasa.es
[9] DHI Brasil Ltda., Florianópolis, Brasil
ael@dhigroup.com

ABSTRACT

Seasonal forecasting has the potential to impact decision making in many water-related sectors such as energy, agriculture and water supply. Typical applications include, long-term contingency planning for floods and droughts, water demands and allocation for irrigation or domestic/industrial water use, energy production forecasting, environmental monitoring and climate adaptation. Hydrological seasonal forecasts over periods of weeks to months are particularly useful for water resources management where future flows depend on storages such as snow accumulation or man-made reservoirs. Despite its potential value both in terms of economics and for climate adaptation, seasonal forecast information is currently under-exploited. There are two reasons which are often cited for this. The first is the relatively large scale at which seasonal meteorological forecasts are provided, whereas water resources or reservoir managers operate at much smaller scales. Therefore, the effective downscaling approaches are required for operational forecasting. The second challenge is the perception that the seasonal forecasts are highly uncertain and unreliable. Ensemble seasonal forecasts from the latest generation of climate-ocean models address both the need to quantify the forecast uncertainties and improve reliability. Nevertheless, recent work suggests that the performance of both meteorological and hydrological seasonal forecasting at smaller scales must be evaluated separately in each case. In order to effectively use seasonal forecasts to improve decision-making, there is a strong need for decision support tools that provide seasonal forecasting information in a useful and intuitive manner. In this study, we describe the development of a generic decision support system for reservoir inflow and operations to address these challenges. We investigate the different contributions to seasonal forecast accuracy using two case studies in Spain and Chile.

Keywords: Climate variability; forecasting; climate adaptation; water resources management; reservoir operation.

1 INTRODUCTION

Seasonal forecasting has the potential to impact decision making in many water-related sectors, e.g. hydropower, agriculture and water supply, where outcomes are dependent on climate variability. Hydrological seasonal forecasts can therefore provide highly valuable information to water resource managers and decision-makers. Despite the significant potential value of such information, seasonal forecasting is currently under-exploited.

There are a number of important challenges to be addressed. Firstly, climate models used for seasonal meteorological forecasts operate at large spatial scales and provide seasonal forecasts of precipitation and temperature at these large scales. On the other hand, operational decisions in water resources, particularly for reservoirs are carried out at the (smaller) catchment scales. Higher resolution modelling or effective methods of downscaling to hydrological scales are needed.

Secondly, there is a clear perception that the general quality of seasonal forecasts is poor, (Rayner et al., 2005). Seasonal forecasting skill in water resources depends on the skill of both the meteorological and hydrological forecasts and there are strong cases for expecting improvements in skill for both. The latest generation of climate model-based forecasts includes both the atmosphere and the ocean, which means that they include sea surface temperature (SST) processes, which have longer memory than the atmospheric processes. In addition, previous studies indicated that there are connections between large-scale atmospheric behaviour (teleconnections) and precipitation in certain regions. This includes the North Atlantic Oscillation (NAO) in Iberian peninsula, (Bierkens and Beek, 2009; Trigo et al., 2004) and the El Niño–Southern Oscillation ENSO in South America.

©2017, IAHR. Used with permission / ISSN 1562-6865 (Online) - ISSN 1063-7710 (Print)

The skill of seasonal hydrological (streamflow) forecasting depends not only on the skill of forecasting the meteorological variables but is strongly related to influence of storages within the catchment; for example, where groundwater has a strong influence or where rainfall is stored as snow, with a well-defined accumulation period and subsequent snow melt. Natural lakes may also influence the seasonal streamflow patterns and man-made reservoirs are often constructed to manage and modify the seasonal flow patterns.

Despite the potential offered by these improvements, decision-makers must be convinced. Therefore, more work is needed to evaluate the performance of seasonal forecasts at operational scales and to evaluate the decisions against uncertainty. To provide real value in the decision-making process methods are required, firstly to reduce the uncertainty, such as bias-correction of the climate model forecasts and data assimilation of the hydrological states and secondly, methods to quantify the uncertainty such as ensemble forecasting.

Finally, to be useful for decision-makers in an operational context, it is necessary to provide useful and easily understood seasonal forecast information. This includes estimates of the accuracy and reliability of the seasonal forecasts. Within the EU FP7 project EUPORIAS (http://www.euporias.eu/), DHI has been developing a prototype decision support system for water resources management, (http://wrdss.euporias.eu/en/), that exploits the latest generation of climate model-based forecasts for seasonal forecasts. In this paper, we will first examine the requirements for such a decision support system. We then evaluate the performance of seasonal hydrological forecasts and investigate the different contributions to uncertainty of hydrological seasonal forecasts in two demonstration case studies in Spain and Chile.

2 DECISION SUPPORT SYSTEMS FOR SEASONAL FORECASTING

Within the EUPORIAS project, one of the important goals was to develop climate services for water resources management that exploit the latest generation of climate model-based seasonal forecasts to improve decision-making. Figure 1 shows schematically the decision-making process for seasonal forecasting in water resource systems.

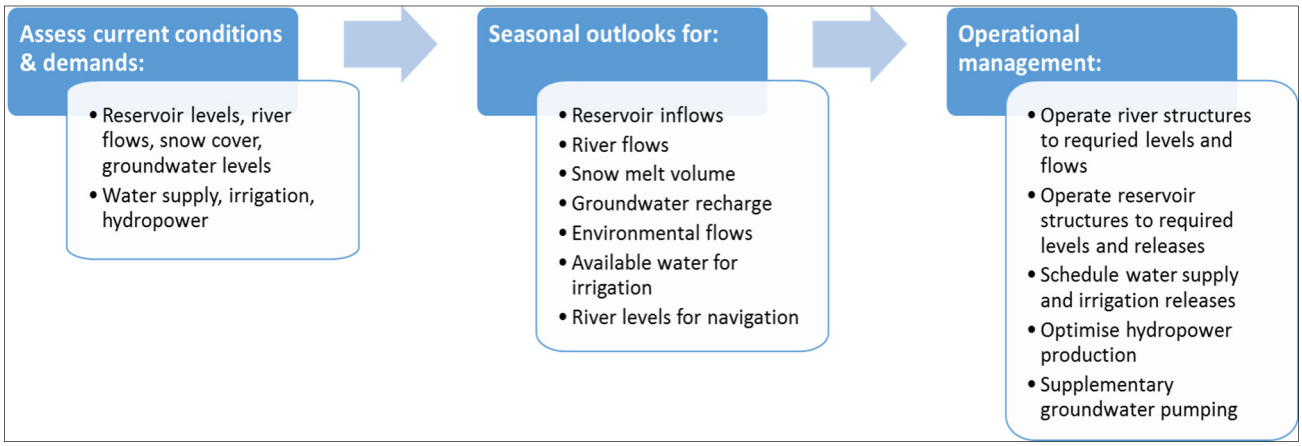

Figure 1. Schematic of the decision-making process for seasonal forecasting in water resource systems.

Decision support tools for these processes should address a number of key requirements including:

- Exploit seasonal forecasts from a range of sources;
- Support seasonal forecasts of temperature for snow accumulation, snow melt and evapotranspiration, as well as precipitation;
- Improve the forecast accuracy using bias-correction methods and by applying updating or data assimilation to reduce the uncertainty arising from initial conditions;
- Provide useful and easily understood estimates of the accuracy and reliability of seasonal forecasts if they are to be used, e.g., as the basis for operating reservoirs;
- Provide both short-term forecasting for flood management and seasonal forecasting for long-term operation and planning.

The prototype seasonal decision support tool developed by DHI in EUPORIAS is used as a starting point the generic framework developed at DHI (www.dhigroup.com/areas-of-expertise/environment-and-ecosystems/decision-support-systems-(dss)) and which formed the basis, for example, for the decision support tools for water resource planning in the Nile Basin, (Sørensen et al., 2015). An example of the information displays from the prototype, decision support tool, is given in Figure 2. This prototype was used to investigate the performance of seasonal forecasting. In this paper, we present preliminary results for the Urumea catchment, Spain and the Upper Maule, Chile.

 ©2017, IAHR. Used with permission / ISSN 1562-6865 (Online) - ISSN 1063-7710 (Print)

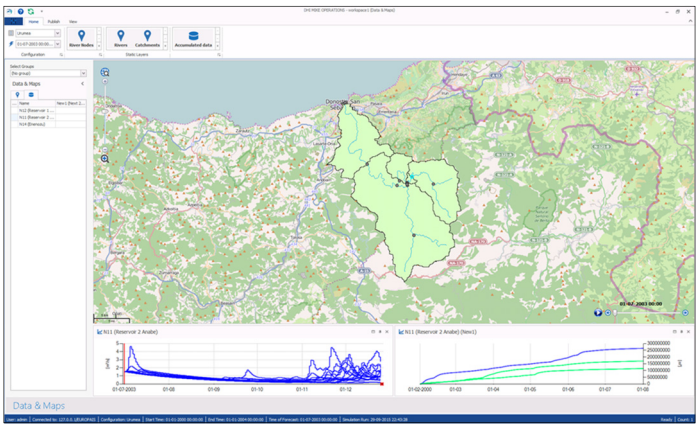

Figure 2. An example of information displays in the prototype, decision support tool for the Añarbe Reservoir, Spain.

3 CASE STUDY – URUMEA CATCHMENT ,SPAIN

3.1 Description of the study area

The Urumea catchment is representative of many areas in southern Europe that are vulnerable to floods, droughts and water scarcity due to seasonal rainfall. Figure 3 shows the location of this catchment and the subcatchments used for hydrological modelling. Rainfall in the Urumea catchment is strongly seasonal, Figure 4, with considerable variability from year to year. Previous studies have shown that the North Atlantic Oscillation (NAO) is a strong driver of interannual variability in the Iberian Peninsula, (Bierkens and Beek 2009; Trigo et al., 2004).

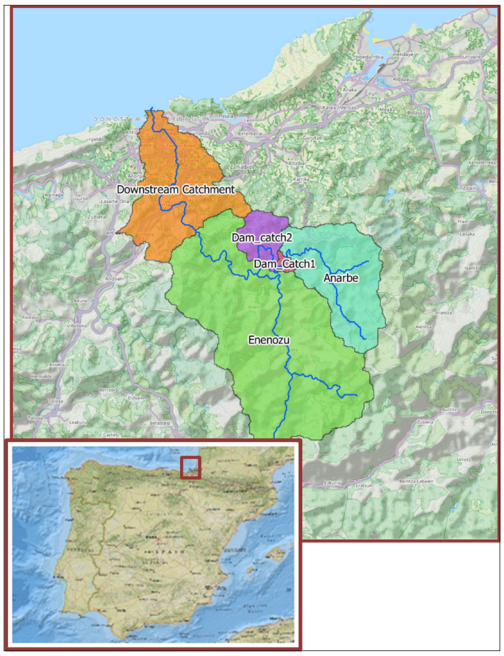

Figure 3. The location of the Urumea catchment in Spain and the hydrological model catchments.

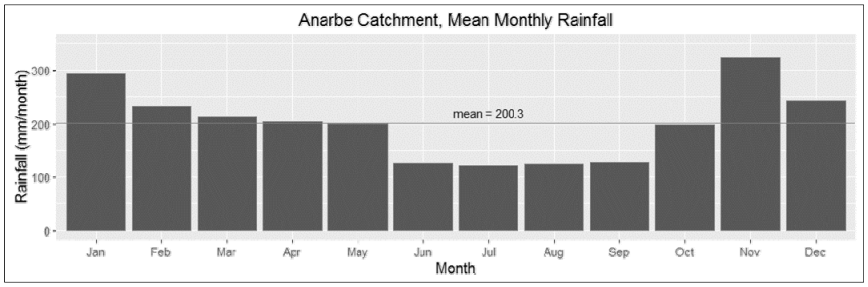

Figure 4. The mean monthly rainfall distribution derived from raingauge data within the Urumea catchment.

©2017, IAHR. Used with permission / ISSN 1562-6865 (Online) - ISSN 1063-7710 (Print)

On the Añarbe River, Aguas de Anarbe (AGASA) operates the Añarbe reservoir. This reservoir is used for water supply to the city of San Sebastian as well as hydropower, and the reservoir is operated to provide flood protection downstream and to maintain environmental flows within the Urumea. Hydrological simulations of the entire Urumea catchment, including the inflows to the Añarbe reservoir, were carried out using the MIKE NAM hydrological model to represent the rainfall-runoff processes (Butts et al., 2004) and the MIKE HYDRO Basin model (DHI, 2014; Butts et al., 2016) to represent the river network and reservoir operation. After calibration, simulations using historical rainfall data were performed over a number of years. Using historical rainfall observations and hydrological modelling to make seasonal forecasts in this manner is known as extended streamflow prediction (ESP) and was widely used in the past, (Day, 1985).

There are many different statistical measures available to measure the performance of ensemble forecasts, (Jolliffe and Stephenson, 2012). For this paper, we used a simple graphical method to illustrate the performance of ensemble model forecasts. The result of the ESP simulations were used here as a reference, as illustrated in Figure 5, we examined accumulated flows or accumulated reservoirs inflows. From the inflow forecasts, using historical rainfall, a distribution of accumulated historical inflow is derived with terciles that represent wet, normal and dry years in terms of accumulated flow, Figure 5.

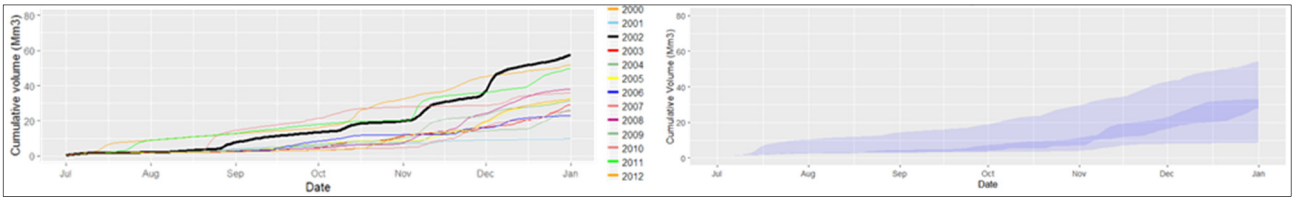

Figure 5. Inflows forecasts from historical rainfall (left) are used to derive the distribution of historical inflows (right).

The methodology used to evaluate the performance of the seasonal hydrological forecasts is illustrated in Figure 6. Using this systematic approach, we have carried out sequences forecasts to compare different downscaling methods and different climate models using both statistical and graphical measures.

In this study, seasonal forecasts of daily precipitation from two European seasonal climate models were used: the ECMWF System 4 (Molteni et al., 2011) and the Met Office GloSea5 (Johnson et al., 2016). GloSea5 is the most recent version of the Met Office seasonal forecasting system and has been operational from January 2013). System 4, the latest version of the European Centre for Medium-Range Weather Forecasts (ECMWF) seasonal forecasting system, has been operational since November 2001. Within the EUPORIAS project, retrospective forecasts were made available for this performance assessment.

Downscaling techniques are needed for two reasons. Firstly, the climate model simulations of rainfall are biased and therefore they must usually be bias-corrected before being applied to a hydrological model. Secondly, where gradients in observed rainfall within a single climate model, grid cell are found, the correction can be applied to capture these gradients.

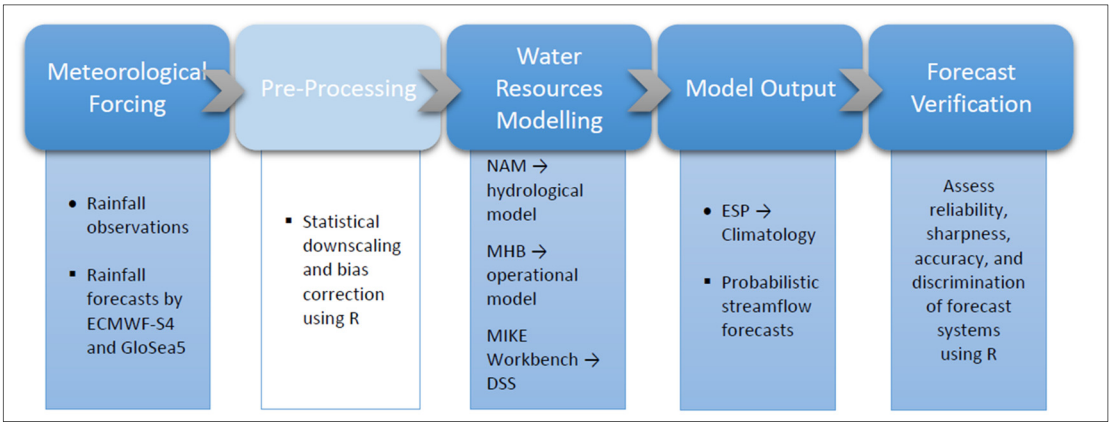

Figure 6. The methodology used to evaluate the performance of climate model–based forecasts.

Figure 7 shows inflow forecasts at different lead times during 2002 using System 4. A simple downscaling method called scaling, also known as the delta change method in climate change literature, was applied. This is a relatively wet year, historically. Figure 8 compares the performance of the ensemble forecasts for both a wet year 2002 and a dry year 2006, using another downscaling method, gamma quantile mapping (gQM) proposed by Piani et al. (2010). Ensemble forecasts were also performed for the same two years and the same downscaling approach but using the GloSea5 forecasts, Figure 9.

 ©2017, IAHR. Used with permission / ISSN 1562-6865 (Online) - ISSN 1063-7710 (Print)

These initial results suggested that the bias-corrected System 4 forecasts show better performance in predicting the wet season while bias-corrected GloSea5 forecasts seem to show better performance in predicting the dry period, at least for forecast lead times of one month. To be useful for managers of multi-purpose reservoirs like the Añarbe, seasonal inflow forecasts should be reliable both during the wet season when the reservoir is filling and dry season when water is scarce.

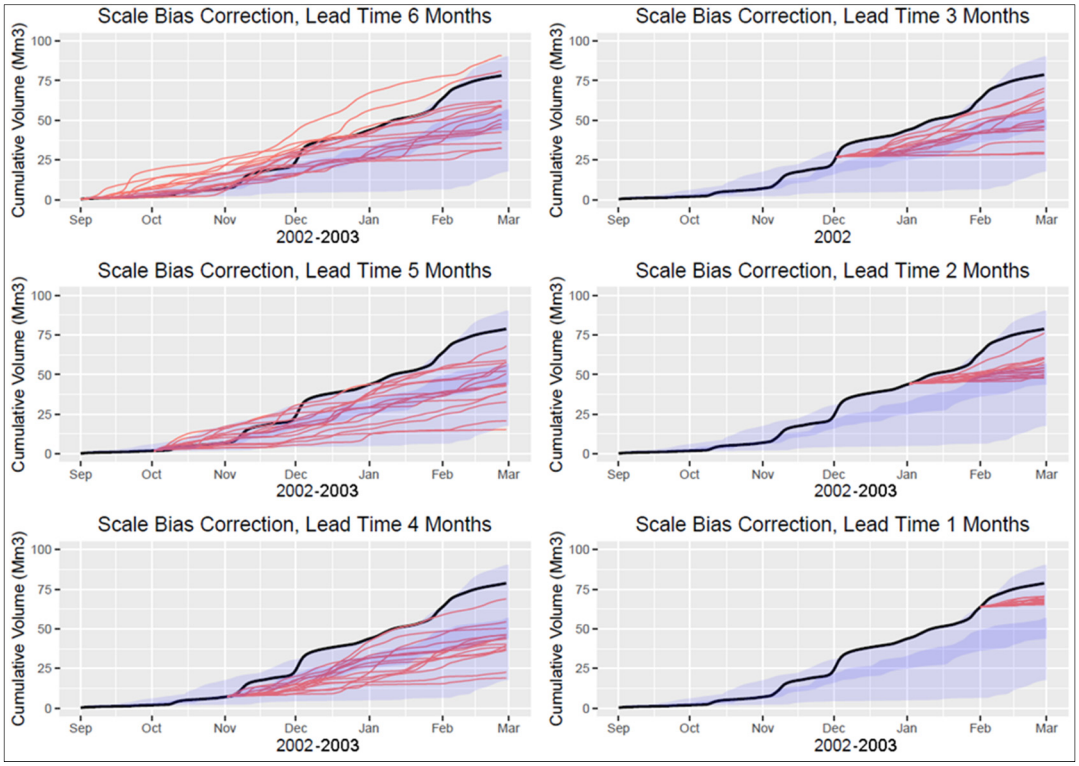

Figure 7. Accumulated inflow forecasts for lead times of 1-6 months showing the actual accumulated inflow for 2002-2003 (black) and the derived historical distribution (shaded terciles) from Figure 5. The red lines show the 15-member forecast ensemble from System 4.

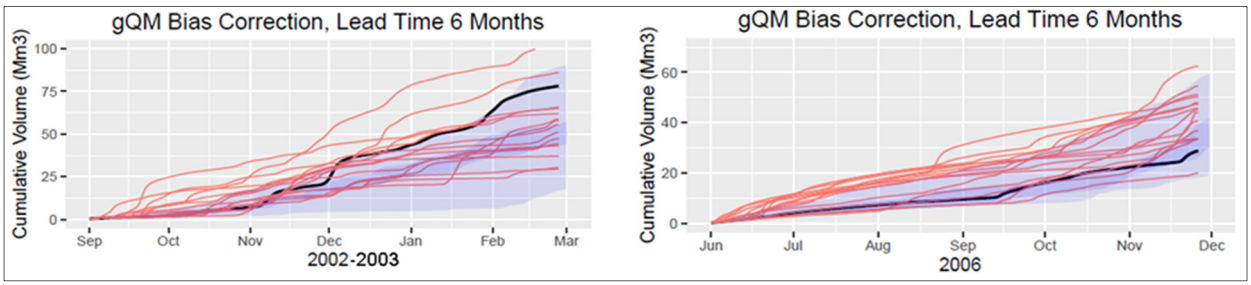

Figure 8. Six month forecasts of the wet season inflows for the wet year 2002 (left) and the dry year 2006 (right). The ensemble forecasts from System 4 were downscaled using gamma quantile mapping (gQM).

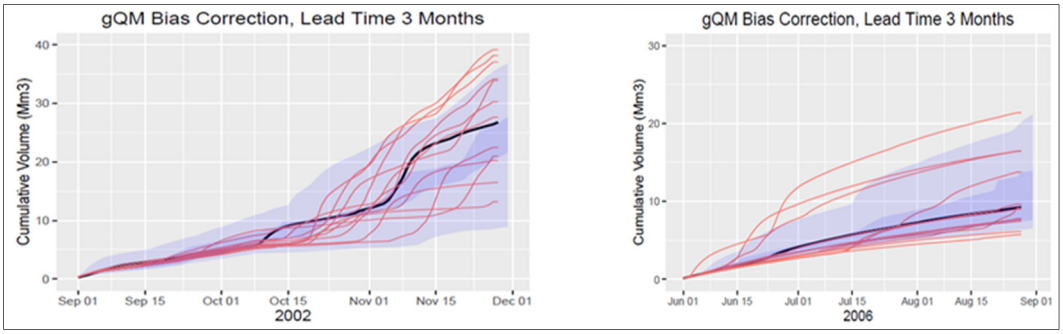

Figure 9. Three month forecasts of the wet season inflows for the wet year 2002 (left) and the dry year 2006 (right). The ensemble forecasts from GLOSea5 were also downscaled using gamma quantile mapping (gQM).

©2017, IAHR. Used with permission / ISSN 1562-6865 (Online) - ISSN 1063-7710 (Print)

4 CASE STUDY – UPPER MAULE ,CHILE

The Upper Maule catchment is located in Talca province in central Chile, Figure 10. The catchment covers an area of approximately 5740 km^2 with elevation ranges from 400 to 4000 metres above means sea level. Precipitation occurs from April to mid-September, as both rainfall and snow. During the warmer period (October - March), snowmelt becomes a major contribution to the runoff. Indeed, two peaks in runoff occur, the first from rainfall, followed by a second peak from snowmelt. The Colbún hydropower plant at the downstream end of the Maule Basin is one of the country's larger hydropower schemes. The main challenges for this reservoir are the difficulty of planning power production, the safe and economical operation of the reservoir during flood events and the provision of water for irrigation.

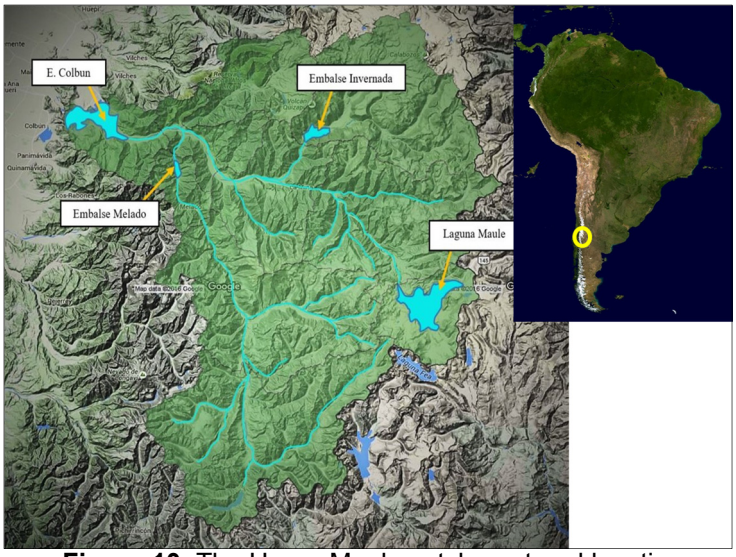

Figure 10. The Upper Maule catchment and location.

The accuracy and reliability of seasonal inflow forecasts for this reservoir depends then, not only on the accuracy of the precipitation but also of the temperature forecasts. We are currently investigating the importance of each of these climate variables on the accuracy of the hydrological forecasts. Another important contribution to the forecast accuracy, in this case, is the accurate representation of the initial conditions. In such snow-fed catchments, this includes the extent and depth of snow but the water levels in the upstream reservoirs are also important. Because of the size of the catchment, changes in levels and releases from upstream reservoirs and the snow pack may take months to propagate downstream. To capture these effects and improve the forecast accuracy, the hydrological model forecasts begin six months before the time of forecast, the warm-up period, Figure 11. Data assimilation of the reservoir levels and upstream flows is required during this warm-up period. We are also currently investigating the impact of these observations on the forecast accuracy.

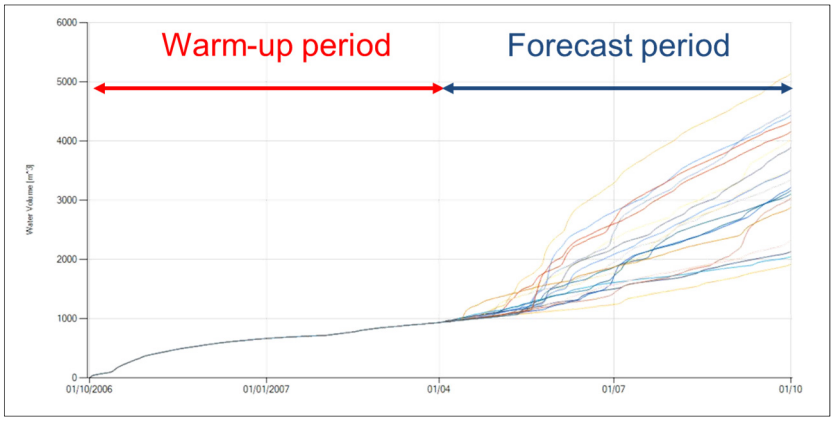

Figure 11. The initial conditions for seasonal forecasts in the Upper Maule are dependent on the snow and reservoir storages and the travel times. The accuracy of these initial conditions is ensured using a warm-up period and data assimilation.

©2017, IAHR. Used with permission / ISSN 1562-6865 (Online) - ISSN 1063-7710 (Print)

5 CONCLUSIONS

In this study, we have presented some of the current limitations and challenges in applying seasonal hydrological forecasting for water resource management. Key technical requirements for decision support tools to address these needs were formulated. These requirements were used as the basis for developing a prototype decision support tool for seasonal forecasting in water resources and reservoir management. Downscaling/bias correction of the climate model forecasts are necessary at the smaller operational scales for reservoir management.

Our preliminary results suggested that bias-corrected System 4 forecasts show better performance in predicting the wet season, while bias-corrected GloSea5 forecasts seem to show better performance in predicting the dry period, at least for forecast lead time of one month. To be useful for managers of multi-purpose reservoirs like the Añarbe, seasonal inflow forecasts should be reliable both during the wet season when the reservoir is filling and dry season when water is scarce. Based on a limited sample size, we found that the scaling and gQM methods seem to show better performance in terms of accuracy and bias with reasonable forecasting skill, again for a lead time of one month. Further work is being performed to investigate seasonal forecast accuracy in the case study in Chile, where the predictability of seasonal weather patterns is expected to be more reliable than in Europe.

ACKNOWLEDGMENTS

This work was supported by the EUPORIAS project, via funding from the European Union's Seventh Framework Programme for research, technological development and demonstration under Grant Agreement 308291.

REFERENCES

Bierkens, M.F.P. & Beek, L.P.H.V. (2009). Seasonal Predictability of European Discharge: NAO and Hydrological Response Time. *Journal of Hydrometeorology*, 10(4), 953-968.

Butts, M.B., Payne, J.T., Kristensen, M. & Madsen H. (2004). An Evaluation of the Impact of Model Structure on Hydrological Modelling Uncertainty for Streamflow Prediction, *Journal of Hydrology*, 298, 242-266.

Butts, M.B., Buontempo, C., Lørup, J.K., Williams, K., Mathison, C., Jessen, O.Z. & Jones, R. (2016). A Regional Approach to Climate Adaptation in the Nile Basin. *Proceedings of the International Association of Hydrological Sciences*, 374, 3.

Day, G.N. (1985). Extended Streamflow Forecasting using NWSRFS. *Journal of Water Resources Planning and Management*, 111(2), 157-170.

DHI (2014). *Mike Hydro User Guide*, MIKE by DHI 2014.

Johnson, S.J., Turner, A., Woolnough, S., Martin, G. & MacLachlan, C. (2016). An Assessment of Indian Monsoon Seasonal Forecasts and Mechanisms Underlying Monsoon Interannual Variability in the Met Office Glosea5-GC2 System. *Climate Dynamics*, 1-19.

Jolliffe, I.T. & Stephenson, D.B. (2012). *Forecast Verification: A Practitioner's Guide in Atmospheric Science*. John Wiley & Sons.

Molteni, F., Stockdale, T., Balmaseda, M., Balsamo, G., Buizza, R., Ferranti, L. & Vitart, F. (2011). *The New ECMWF Seasonal Forecast System (System 4)*. European Centre for Medium-Range Weather Forecasts, 49.

Piani, C., Haerter, J. O. & Coppola, E. (2010). Statistical Bias Correction for Daily Precipitation in Regional Climate Models over Europe. *Theoretical and Applied Climatology*, 99(1), 187-192

Rayner, S., Lach, D. & Ingram, H. (2005). Weather Forecasts are for Wimps: Why Water Resource Managers Do Not Use Climate Forecasts. *Climatic Change,* 69(2), 197-227.

Sørensen, H.R., Beyene, M. & Ammentorp, H.C, (2015). The Nile Basin Decision Support System. *International Association of Hydro-environment Engineering and Research (IAHR). Hydrolink* 4, 117-119.

Trigo, R. M., Pozo-Vázquez, D., Osborn, T.J., Castro-Díez, Y., Gámiz-Fortis, S. & Esteban-Parra, M.J. (2004). North Atlantic Oscillation Influence on Precipitation, River Flow and Water Resources in the Iberian Peninsula. *International Journal of Climatology*, 24(8), 925-944.

©2017, IAHR. Used with permission / ISSN 1562-6865 (Online) - ISSN 1063-7710 (Print)

Proceedings of the 37th IAHR World Congress
August 13 – 18, 2017, Kuala Lumpur, Malaysia

RESEARCH ON CLIMATE CHANGES IN JINGHE RIVER BASIN AND ITS EFFECTION ON RUNOFF

JING YIN[1], FAN HE[2], GUOYU QIU[3], SHI FENG[4], JUNJIE ZHANG[5], & SHUANG ZHANG[6]

[1,2,4,5,6] State Key Laboratory of Simulation and Regulation of Water Cycle in River Basin, China Institute of Water Resources and Hydropower Research, Beijing, China,
yinjing@iwhr.com
[3] Shenzhen Engineering Laboratory for Water Desalinization with Renewable Energy, School of Environment and Energy, Peking University, Shenzhen, Guangdong, China,
qiugy@ pkusz.edu.com

ABSTRACT

According to the long sequence observational data of 10 precipitation stations and five meteorological stations distributed in the Jinghe River Basin, the temperature and precipitation change trends of Jinghe River Basin from 1970s to the beginning of this century were analyzed. The study showed that: climate in Jinghe River Basin showed warming and drying characteristics from 1980s to 1990s, and warming and wetting characteristics from 1990 to 2005. The Soil and Water Assessment Tool (SWAT) was adopted to perform simulations. Through scenario simulation, the impact of land use/land cover change (LULC) was removed. The simulated results indicated that: the annual runoff of the basin was totally increased by 29.75 m^3s^{-1} from 1970s to 1980s under the combined effects of climate change and LULC. Wherein the annual runoff was increased by 26.07 m^3s^{-1} as a result of climate change, and the contribution percentage was 87.62%. The annual runoff was reduced by 12.59 m^3s^{-1} from 1980s to 1990s under the combined effects. Wherein climate change reduced the annual runoff by 7.04 m^3s^{-1}, and the contribution percentage was 55.92%. The annual runoff was reduced by 15.65 m^3s^{-1} from 1990s to 2005 under the combined effects. Wherein climate change reduced the annual runoff by 6.59 m^3s^{-1}, and the contribution percentage was 42.11%. The 1980s was a transition of climate change on annual runoff of the Jinghe River Basin. The annual runoff increased before 1980s, while decreased after 1980s as a result of climate change. The influence proportion of LULC was increased gradually.

Keywords: Jinghe River Basin; SWAT Model; climate change; surface runoff simulation.

1 INTRODUCTION

Global climate is changing at an unprecedented speed due to influence of human activities since the 20th century. The 20th century was the warmest century since the 16th century, and the 1990s was the warmest decade of the 20th century (Fu, 2003). Water resources shortages are aggravated due to global warming as well as ecological and hydrological environment deterioration as a result, and the water safety problem is increasingly serious, which has formed a serious threat to human survival and development. Water resources are foundational natural resources on the one hand, and they also belong to strategic economic resources and social resources on the other hand. Therefore, the safety of water resources not only belongs to an ecological environment problem, but is also related to national economic problems, social problems and political problems. We must grasp formation and evolution laws of water resources under the changing environment timely, thereby guaranteeing the safety of water resources, and realizing sustainable utilization of water resources.

2 OVERVIEW OF RESEARCH AREA

Jinghe River is located in the Central Loess Plateau, which is between Liupan Mountain and Ziwuling Mountain (106°20´-108°48´E, 34°24´-37°20´N). It is originated from east root of Guanshan Mountain in Jingyuan County of Ningxia Hui Autonomous Region. It flows through three provinces, namely Ningxia, Gansu and Shaanxi, which flows into Weihe River in Gaoling County of Shaanxi. The river basin is as long as 450km with total drop of 2180 m. It is a level I tributary of the Weihe River and level II tributary of the Yellow River. Jinghe River Basin covers an area of 45421 km^2, wherein the control area of Zhangjiashan Hydrological Station is 43216 km^2. The position of river basin in the research area is shown in Figure 1.

 ©2017, IAHR. Used with permission / ISSN 1562-6865 (Online) - ISSN 1063-7710 (Print)

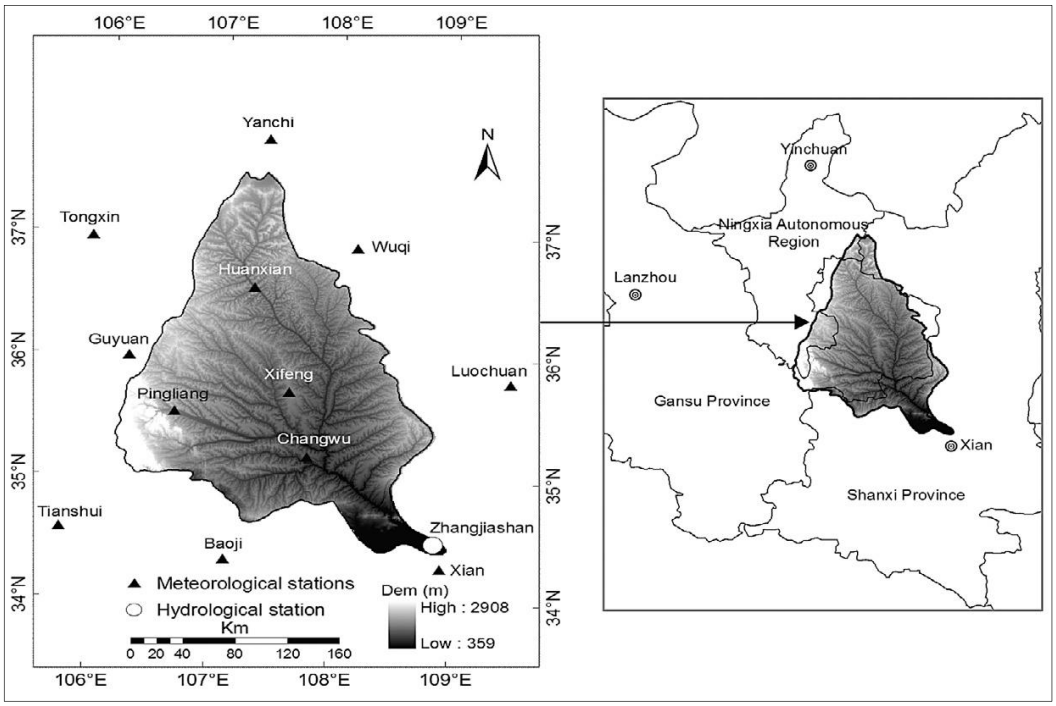

Figure 1. Location, topography, and distribution of hydrological and meteorological stations in the Jinghe River Basin.

3 CLIMATE CHANGE IN JINGHE RIVER BASIN

Four meteorological websites with consistent annual time sequences of temperature and precipitation (1970-2005) are selected in the upstream, midstream and downstream areas of Jinghe River Basin respectively: Huanxian, Xifeng, Pingliang and Changwu (Figure 1).

3.1 Characteristics of temperature change

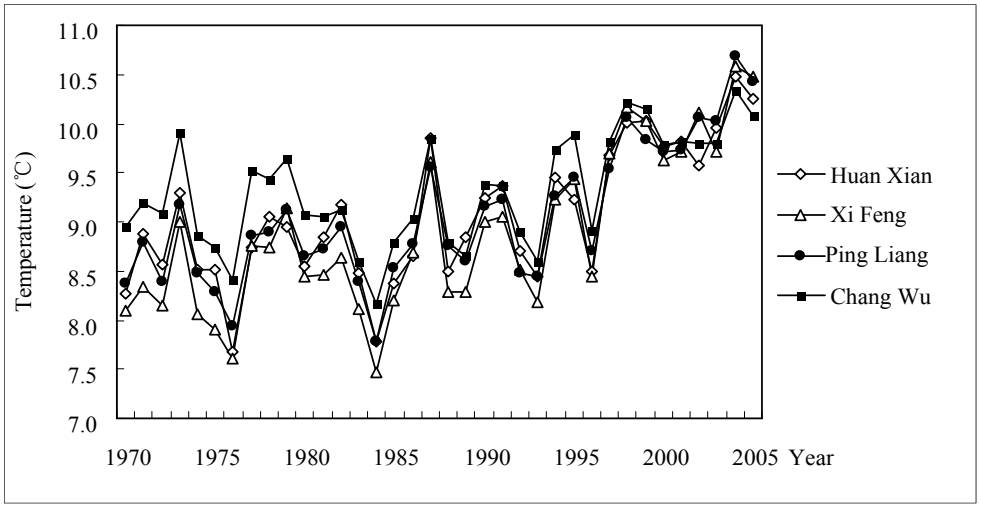

Figure 2. Annual mean temperature in the Jinghe River Basin during 1970-2005.

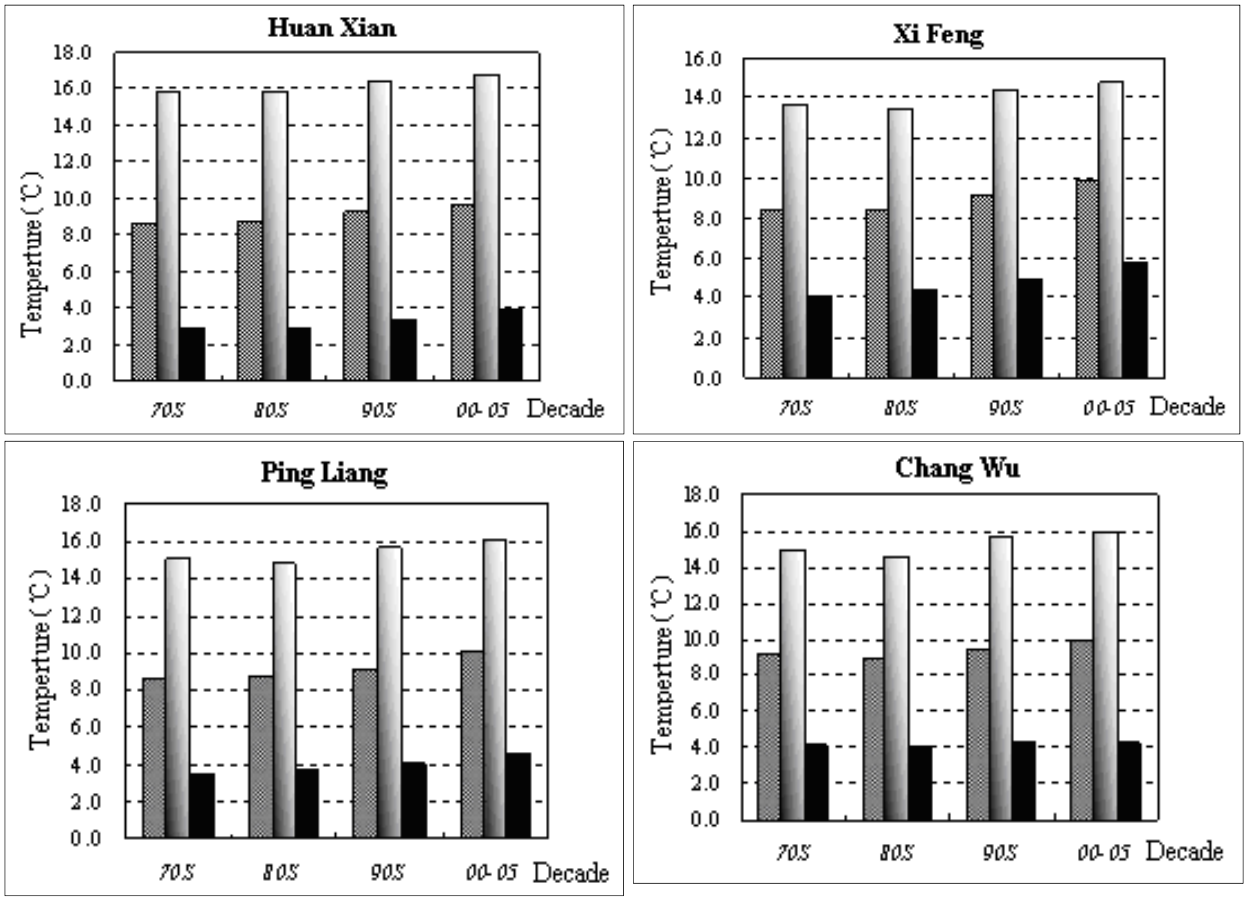

Figure 3. Annual mean temperature for 1970s, 1980s, 1990s, and 2000-2005 in the Jinghe River Basin in 1970-2005. The three columns in each figure represent the maximum (gray), average (dark), and minimum (black) temperature, respectively.

Figures 2 and 3 show that the annual mean temperature, the highest and lowest temperatures in the Jinghe River Basin, took on a rising trend during 1970-2005, a slightly increasing trend during the 1970s-1980s, followed by a more significant one during the 1980s-1990s. The maximum temperature rose precipitously. During 1990-2005, temperature in the river basin still maintained a rising trend and minimum temperature climbed most obviously.

3.2 Characteristics of precipitation change

The annual mean precipitation of Jinghe River Basin from the 1970s to 2005 was compared in pairs interannually (Figure 4, 5 and 6): the annual mean precipitation of four stations in the upstream, midstream and downstream was not different greatly in the1980s compared with that in the 1970s. During the 1980s-1990s, river basin precipitation decreased in overall, and the decline in downstream was more noticeable. During 1990-2005, overall precipitation rose, while that over midstream and downstream increased significantly. In general, the river basin climate featured warm and dry in the 1980s-1990s and presented as warm and wet during 1990-2005.

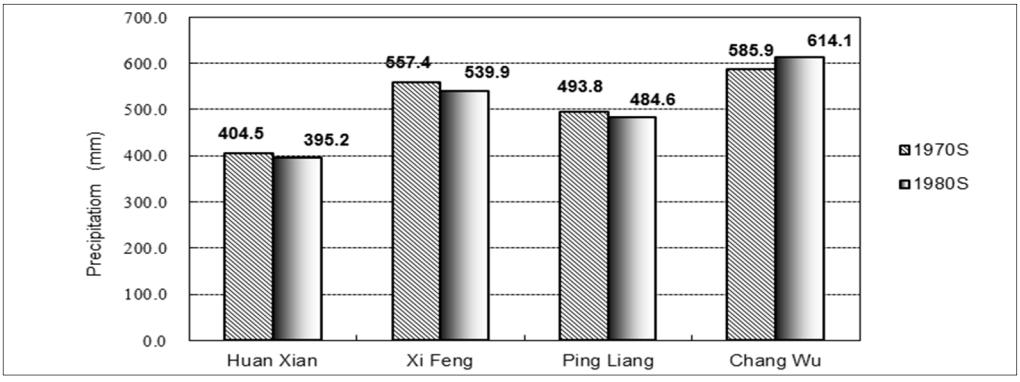

Figure 4. Annual mean precipitation in the Jinghe River Basin during 1970-1980.

 ©2017, IAHR. Used with permission / ISSN 1562-6865 (Online) - ISSN 1063-7710 (Print)

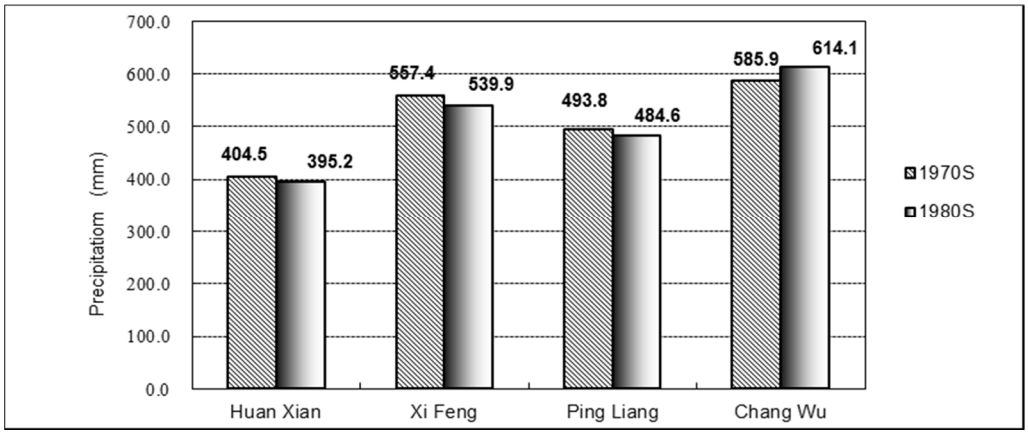

Figure 5. Annual mean precipitation in the Jinghe River Basin during 1980-1990.

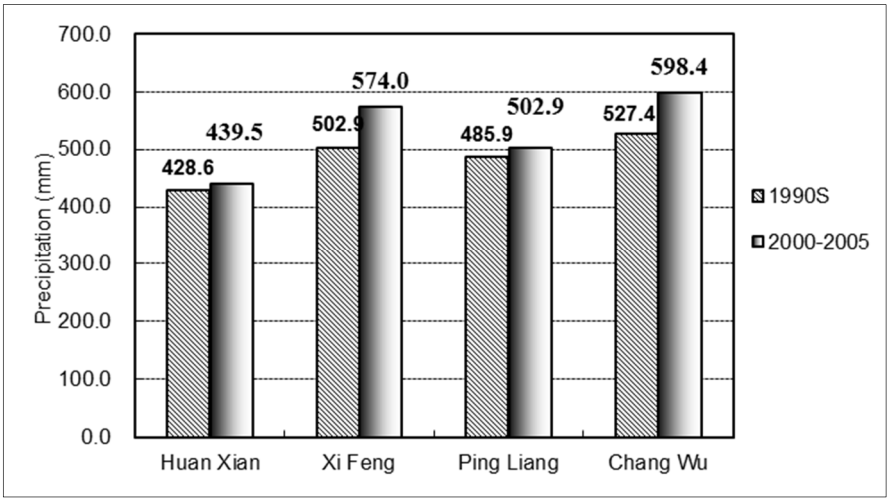

Figure 6. Annual mean precipitation in the Jinghe River Basin during 1990-2005.

3.3 Characteristics of climate change

The above analysis shows that the annual average temperature of Jinghe River Basin was increased gradually for many years as a whole from 1970s to 2005. The annual average precipitation of the river basin was decreased for many years as a whole.

In summary, the climate of the Jinghe River Basin showed warming and drying characteristics from 1980s to 1990s and showed warming and wetting characteristics from 1990 to 2005.

4 INFLUENCE OF CLIMATE CHANGE ON RUNOFF

4.1 Research method

Climate change and land use/land cover (LULC) are two main factors affecting the runoff of the river basin (Oki and Kanae, 2006; Piao et al., 2007; Wang et al., 2014). It can be approximately considered that runoff simulated by the model at different periods and the variable quantity of natural runoff are combined action results of climate changes and LULC basically. Therefore, the SWAT (Soil and Water Assessment Tool) distributed hydrological model is adopted in the research, which was more widely applied in China and foreign countries (Gassman et al., 2007; Guo et al., 2008; Fan and Shibata, 2015). The method of fixing LULC factors was adopted and the simulated scenes were input into the model. The influence mode and degree of climate change on river basin runoff are distinguished quantitatively (Elias and John, 2007; Fontaine et al., 2002; Jayakrishnan et al., 2005).

4.2 Building and verification of model

4.2.1 Model building

In summary, SWAT model database can be divided into two major categories of spatial database (also known as graph database) and attribute database (Arnold et al., 1998). The spatial database mainly includes river basin DEM graphs, legend utilization classification graphs and digital soil graphs. There are three major

©2017, IAHR. Used with permission / ISSN 1562-6865 (Online) - ISSN 1063-7710 (Print)

attribute databases for storing data related to land utilization, soil attributes, meteorological station parameters and other data. The three databases were edited and modified in the paper according to concrete conditions of the research area.

(1) Spatial database

Jinghe River DEM data belongs to 90m×90m raster data. River networks and sub-basins of Jinghe River Basin were extracted and classified on the basis of DEM (Figure 7). The river basin is divided into 30 sub-basins.

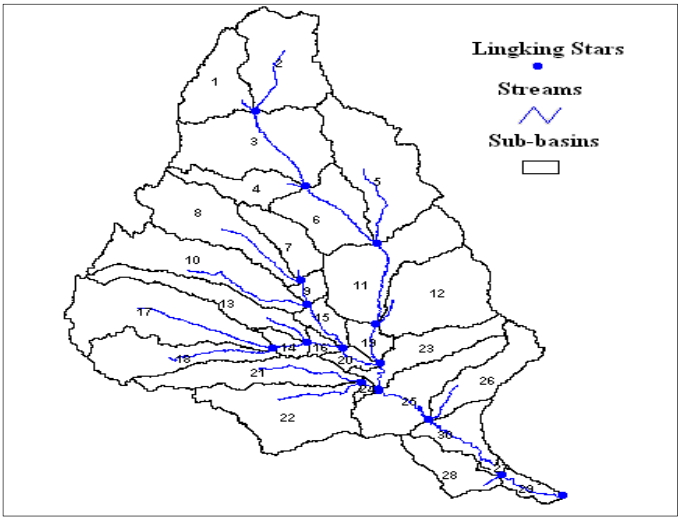

Figure 7. The river division to the Jinghe River Basin.

The TM/ETM data of Jinghe River Basin in the same season of 1979, 1989, 1999 and 2006 was classified for obtaining land utilization type maps of four periods. The land utilization types were divided into six categories according to original classification systems of land utilization types by combining with requirements on soil erosion simulation (Figure 8). Soil types of the river basin were divided into 8 soil categories and 13 subcategories. Physical property data of soil in various types were input into SWAT user-defined soil database files. Each soil type was endowed with corresponding type code and corresponding soil attribute information through reclassification.

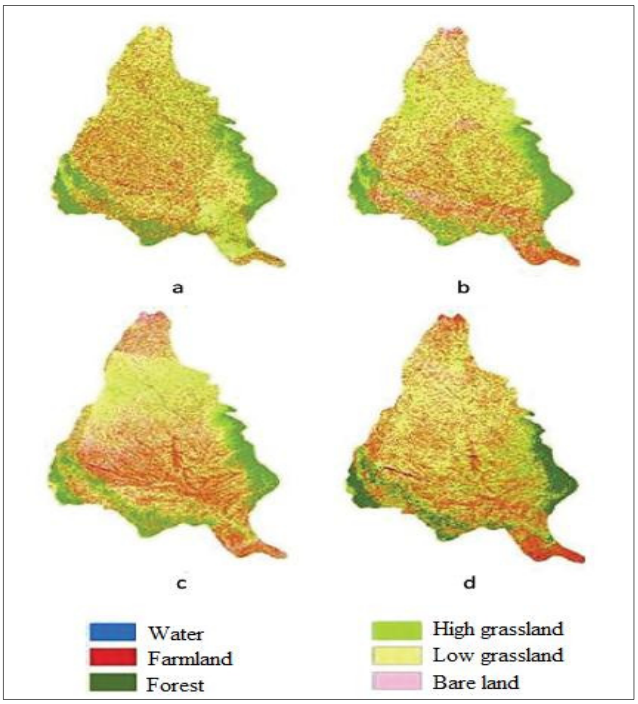

Figure 8. Land-use and land cover changes for the 1970S, 1980S, 1990S, and 2000S in the Jinghe River Basin. Data include a,b,c,d for 1979,1989,1999,2006.

 ©2017, IAHR. Used with permission / ISSN 1562-6865 (Online) - ISSN 1063-7710 (Print)

(2) Attribute database

As an important drive factors, meteorological data affecting hydrologic cycle in a distributed hydrological model. Surface energy balance, water cycle and other process in the hydrological process can be analyzed through them. The meteorological simulator embedded in the SWAT model (weather generator) can compensate insufficient meteorological data of the station or simulate insufficient meteorological data by utilizing mathematical statistics principle through mean annual monthly average meteorological data for many years input by researchers (such as monthly average data, standard deviation, etc. of temperature, precipitation, wind speed, relative humidity and solar radiation).

Long sequence meteorological data of seven meteorological stations (figure1) (Xi'an, Guyuan, Changwu, Pingliang, Xifeng, Huanxian and Tianshui) with more complete data in the research area and surrounding area were used in the research. A meteorological attribute database was established.

4.2.2 Model calibration and validation

The SWAT model of the basin was first calibrated for the period of 1971 to 1997 and was then validated for the period of 1981 to 1990. The parameter calibration results are shown in table 1. The outcome of model calibration and validation is shown in table 2.

Table 1. Calibrated values of the six parameters in SWAT.

Parameter name	Range	Parameter description	Calibrated value
CN_2	-8~+8	Runoff curve coefficient of SCS curve method	-8
ESCO	0~1	Soil evaporation compensation coefficient	0.1
SQL_AWC	0~1	Available water supply of soil	0.05
CH_K_2	0~150	Effective conductivity of river channel	0.35
ALPHA_BF	0~1	Base flow α coefficient	0.01
SURLAG	0~10	Earth surface runoff retardation time	0.85

Table 2. Runoff simulation results of model calibration and Validation.

	Year	*Ens*	*Re*	R^2
Calibration period	1971	0.64	15.58	0.903
	1972	0.85	42.82	
	1973	0.96	-3.55	
	1974	0.70	10.13	
	1975	0.98	-4.49	
	1976	0.58	-13.84	
	1977	0.81	-4.89	
	1978	0.73	4.21	
	1979	0.80	13.94	
	1980	0.53	8.39	
	Average	0.76	4.13	
Validation period	1981	0.60	-16.62	0.831
	1982	0.89	-12.36	
	1983	0.73	11.86	
	1984	0.59	12.08	
	1985	0.62	13.99	
	1986	0.90	23.63	
	1987	0.83	22.39	
	1988	0.58	-10.36	
	1989	0.88	17.55	
	1990	0.71	7.86	
Average		0.73	7.00	

The average value of runoff simulation evaluation pointer *Ens* (Nash-Sutcliffe efficiency coefficient) (Xu et al., 2011; Notter et al., 2013; Zhang et al., 2015; Liu et al., 2016; Zhao et al., 2016) reaches 0.76 and 0.73 respectively during model calibration and validation period, namely grade B of model simulation precision. The simulation results of individual years can reach grade A. It is obvious that runoff changes of the river basin can be simulated more accurately in year scale through parameter calibration and validation, and the simulation results can provide theoretical basis for water resources management of Jinghe River Basin.

4.3 Simulation results

It is well known that climate change and LULC are key factors affecting runoff of basin. The SWAT model was applied in this research. Based on setting simulated scenes, the LULC factor was fixed, the climate factor

©2017, IAHR. Used with permission / ISSN 1562-6865 (Online) - ISSN 1063-7710 (Print)

was eliminated, the simulated runoff under different climate of decades was compared and the affection of climate change to the basin runoff was analysed.

Concrete simulation steps were shown as follows: the first stage (1970-1979) was regarded as a baseline period, and the second stage (1980-1989) was regarded as a change period. The runoff simulated during the baseline period under the influence of actual climate and LULC (actual scene 1) was compared with the runoff simulated during the change period under the influence of actual climate and LULC (actual scene 2). The difference value can be regarded as the influence of climate change and LULC combined action on runoff. The runoff simulated under the simulated scene (S-C) of climate condition **in** change period and LULC in baseline period was compared with the runoff simulated under the condition of actual scene 1. The difference value can be regarded as the influence of climate change on runoff. Similarly, the runoff simulated under the simulated scene (S-L) of climate condition in baseline period and LULC in change period was compared with the runoff simulated under the condition of actual scene 1. The difference value can be regarded as the influence of LULC change on runoff. And so on for other decades. The simulation results are shown in table 3, 4, and 5.

Table 3. Contribution of climate and LULC to influence on annual runoff of Jinghe River Basin from 1970s to 1980s.

Climate change	Land use /land cover change	Scene setting	Runoff variable quantity (m^3/s)		Percentage change (%)
1970s 1980s	1970s 1980s	actual scene 1	84.1	--	--
1970s 1980s	1970s 1980s	simulated scene (S-L)	86.4	2.30	7.73
1970s 1980s	1970s 1980s	simulated scene (S-C)	110.17	26.07	87.63
1970s 1980s	1970s 1980s	actual scene 2	113.85	29.75	--
	Balance	--	--	1.38	4.64

Table 4 .Contribution of climate and LULC to influence on annual runoff of Jinghe River Basin from 1980s to 1990s.

Climate change	Land use /land cover change	Scene setting	Runoff variable quantity (m^3/s)		Percentage change (%)
1980s 1990s	1980s 1990s	actual scene 1	113.85	--	--
1980s 1990s	1980s 1990s	simulated scene (S-L)	107.02	-6.83	-54.25
1980s 1990s	1980s 1990s	simulated scene (S-C)	106.81	-7.04	-55.92
1980s 1990s	1980s 1990s	actual scene 2	101.26	-12.59	--
	Balance	--	--	1.28	10.17

Table 5. Contribution of climate and LULC to influence on annual runoff of Jinghe River Basin from 1990 to 2009.

Climate change	Land use /land cover change	Scene setting	Runoff variable quantity (m^3/s)		percentage change (%)
1990s 2000~2009	1990s 2000~2009	actual scene1	101.26	--	--
1990s 2000~2009	1990s 2000~2009	simulated scene (S-L)	90.2	-11.06	-70.67
1990s 2000~2009	1990s 2000~2009	simulated scene (S-C)	94.67	-6.59	-42.11
1990s 2000~2009	1990s 2000~2009	actual scene2	85.61	-15.65	100
	Balance	--	--	2	12.78

 ©2017, IAHR. Used with permission / ISSN 1562-6865 (Online) - ISSN 1063-7710 (Print)

Uncertainty existed in this model simulation. Our model simulation was based on the assumption that runoff is affected only by LULC change or climate change, the simulated runoff associated with changes in only one driving factor was slightly different than the runoff simulated under the combined effects of both factors due to the uncertainty in representing LULC and climate change interactions in the SWAT model. For example, in table 3, 28.37 m^3 s^{-1}, which was the combined runoff rate in S-L and S-C, was not equal to the "real runoff under combined action of climate change and LULC" (29.75 m^3 s^{-1}). This uncertainty also exists in simulation results of table 4 and 5.

5 CONCLUSIONS

The following conclusions can be obtained through the research:

(1). The mean annual temperature, maximum and minimum temperature of Jinghe River Basin showed increase trend as a whole from 1970s to 2005. The mean annual precipitation of the river basin showed a decrease trend as a whole for many years.

(2). Climate in Jinghe River Basin showed warming and drying characteristics from the 1980s to the 1990s, and warming and wetting characteristics from 1990 to 2005.

(3). The annual runoff of Jinghe River basin was increased by a total of 29.75 m^3s^{-1} from 1970s to 1980s under combined effects of climate change and LUCC, in which was increased by 26.07 m^3s^{-1} as a result of climate change and the contribution percentage of climate change to annual runoff was 87.62%. The annual runoff was decreased by a total of 12.59 m^3s^{-1} from 1980s to 1990s under the combined effects in which was reduced by 7.04 m^3s^{-1} as a result of climate change and the contribution percentage was 55.92%. The annual runoff was decreased by a total of 15.65 m^3s^{-1} from the 1990s to 2005 under the combined effects, in which was decreased by 6.59 m^3s^{-1} by climate change, and the contribution percentage was 42.11%.

(4). The 1980s was a transition of climate change on runoff of Jinghe River Basin. The annual runoff increased before 1980s, while decreased after 1980s as a result of climate change and the influence proportion of human activities was increased gradually.

ACKNOWLEDGEMENTS

This study was supported by the National Natural Science Foundation of China (grant nos. 51309246 and 31300402), and the National Basic Research Program of China (project no.2006CB400505). We thank the China Meteorological Administration for providing meteorological data.

REFERENCES

Arnold, J.G., Srinivasan, R., Muttiah, R.S. & Williams, J.R. (1998). Large Area Hydrologic Modeling and Assessment – Part 1: Model Development. *Journal of the American Water Resources Association*, 34, 73–89.

Elias, G.B. & John, W.N. (2007). Multi-Objective Automatic Calibration of SWAT using NSGA-11. *Journal of Hydrology*, 341(3-4), 165-176.

Fan, M. & Shibata, H. (2015). Simulation of Watershed Hydrology and Stream Water Quality under Land Use and Climate Change Scenarios in Teshio River Watershed, Northern Japan. *Ecology Indicator*, 50, 79–89.

Fontaine, T.A., Cruickshank, T.S., Arnold, J.G. & Hotchkiss, R.H. (2002). Development of a Snowfall-Snowmelt Routine for Mountainous Terrain for the Soil Water Assessment Tool (SWAT). *Journal of Hydrology,* 262(1-4), 209-223.

Fu, C.B. (2003). Potential Impacts of Human-Induced Land Cover Change on East Asia Monsoon. *Global Planet. Change*, 37, 219–229.

Gassman, P., Reyes, M.R., Green, C.H. & Arnold, J.G. (2007).The Soil and Water Assessment Tool: Historical Development, Applications, and Future Research Directions. *T. ASABE*, 50, 1211–1250.

Guo, H., Qi, H. & Jiang, T. (2008). Annual and Seasonal Streamflow Responses to Climate and Land-Cover Changes in the Poyang Lake Basin. *Journal of Hydrology*, 355, 106–122.

Jayakrishnan, R., Srinivasan, R., Santhi C. & Arnold, J.G. (2005). Advances in the Application of the SWAT Model for Water Resources Management. *Hydrology. Process,* 19(3), 749-762.

Liu, J., Liu, T., Bao, A.M., De Maeyer, P., Feng, X.W., Miller, S.N. & Chen, X. (2016). Assessment of Different Modelling Studies on the Spatial Hydrological Processes in an Arid Alpine Catchment. *Water Resources. Management*, 30, 1757–1770.

Notter, B., Hans, H., Wiesmann, U. & Ngana, J.O. (2013). Evaluating Watershed Service Availability under Future Management and Climate Change Scenarios in the Pangani Basin. *Physics and Chemistry of Earth*, 61–62, 1–11.

Oki, T. & Kanae, S. (2006). Global Hydrological Cycles and World Water Resources. *Science*, 313, 1068–1072.

Piao, S., Friedlingstein, P., Ciais, P., de Noblet-Ducoudré, N., Labat, D. & Zaehle, S. (2007). Changes in Climate and Land Use Have a Larger Direct Impact Than Rising CO_2 on Global River Runoff Trends. *Proceedings of the National. Academy of Sciences*, 104, 15242–15247.

©2017, IAHR. Used with permission / ISSN 1562-6865 (Online) - ISSN 1063-7710 (Print)

Wang, R., Kalin, L., Kuang, W. & Tian, H. (2014). Individual and Combined Effects of Land Use/Cover and Climate Change on Wolf Bay Watershed Streamflow in Southern Alabama. *Hydrology Process*, 28, 5530–5546.

Xu, H., Taylor, R.G. & Xu, Y. (2011). Quantifying Uncertainty in the Impacts of Climate Change on River Discharge in Sub-Catchments of the Yangtze and Yellow River Basins, China. *Hydrology and Earth System Sc*iences, 15, 333–344.

Zhang, Y., Fu, G., Sun, B., Zhang, S. & Men, B. (2015). Simulation and Classification of the Impacts of Projected Climate Change on Flow Regimes in the Arid Hexi Corridor of Northwest China. *Journal of Geophysical Research Atmos*phere, 120, 7429–7453.

Zhao, A.Z., Zhu, X.F., Liu, X.F., Pan, Y.Z. & Zuo, D.P. (2016). Impacts of Land Use Change and Climate Variability on Green and Blue Water Resources in the Weihe River Basin Of Northwest China. *CATENA*, 137, 318–327.

 ©2017, IAHR. Used with permission / ISSN 1562-6865 (Online) - ISSN 1063-7710 (Print)

ENERGY CONSUMPTION RELATED WATER DEMAND MANAGEMENT IN WUXI CITY: A FORECAST

YIHONG XIAO[1], JIANGYU DAI[2], SHIQIANG WU[3], XINGHUA XIE[4], BENYOU JIA[5], GUOYI HAN[6] & WEINBERG JOSH[7]

[1,2,3,4,5] State Key Laboratory of Hydrology-Water Resources and Hydraulic Engineering, Nanjing Hydraulic Research Institute, Nanjing, 210029, P. R. China
425627074@qq.com; jydai@nhri.cn; sqwu@nhri.cn; xiexh@nhri.cn; byjia@nhri.cn
[6] Stockholm Environment Institute, Stockholm, 115 23, Sweden
guoyi.han@sei-international.org
[7] Stockholm International Water Institute, Stockholm, 100 55, Sweden
Josh.Weinberg@siwi.org

ABSTRACT

Water and energy are the two crucial resources for the world's sustainable development. The pressures of the rapid urbanization process on water and energy demands are both significantly increasing, which must cope with the simultaneous consideration of water and energy systems. Understanding such water-energy nexus and, in turn, identifying optimal options for enhancing resource use efficiency and productivity has drawn strong attention in recent years. Wuxi is a fast-developing city in the most developed Yangtze River Delta region of China. Taking the Wuxi city as an example, this paper forecasted the water allocation required to ensure the growing energy consumption in the city by 2020 and 2030. The paper firstly maps the city's water use system, including the ecological water use. Within the water use system, three indicators are selected for in-depth analysis: the amount of production energy consumption, life power consumption and sewage discharge. Second, the paper analyzed the energy consumption of each industry and their implications on water use. Furthermore, a forecast is made on the water allocation required to enable the energy consumption by 2020 and 2030 in the city. Comparing the results with the "Water Modernization Plan of Wuxi City", the paper concludes that the Plan is generally sound, but more water can be saved through better options for efficiency gain.

Keywords: Water-energy nexus; Energy consumption; Water demand management; Forecast; Wuxi city.

1 INTRODUCTION

Water crisis has been aggravating globally, not only caused by the growing population and new industrial demands, but also the water contaminating and climate changes (Hanjra and Qureshi, 2010; Qin et al., 2010). Furthermore, uneven water distribution has complicated water problems in the world, which might be aggravated under the influence of climate changes (Brent, 2015). Energy has also encountered a similar dilemma. By 2035, the world primary energy demands will grow by 40%, compared with that in 2010 (IEA, 2012). Energy harnesses for people from conversions of resources such as fossil fuels, water, nuclear material, sunshine, wind. Fossil fuels, like coal, oil and natural gas, will reign in 2035 (Miller, 2013) and are not environmentally friendly due to large amounts of greenhouse gas emissions and mine wastewater. Saving water and energy becomes one of the most important premises to protect the sustainable development of the world.

Although water and energy are facing their own problems, the interconnection between them is intrinsic, and are receiving more and more interests in governments, institutions and businesses (Qin et al., 2015; Wang et al., 2012). Water is required for most processes of energy supply and production, and energy is essential for water extraction, desalination, conveyance, treatment and transportation (Retamal et al., 2009; Spang et al., 2014). Thus, the detailed exploration of links between energy and water, called water-energy nexus (Gleick, 1994), can provide powerful supports for resource managers to supply available water and sufficient power for sustainable developments of society, economy and ecological environments (Healy et al., 2015).

Water and energy have been managed by two different departments for a long time, people usually treat these two issues respectively (Wen et al., 2014). Although policymakers will appropriately consider energy development demand when making the energy policy or development planning, but few will take the restrict into account the energy consumption for the restriction of water resource utilization, even nearly don't focus on the energy management of urban water system and water system of water, such as different types of issues, for instance, energy consumption demand (Bao et al., 2015; Bauer et al., 2014).

Wuxi is a representative developed city in the Yangtze River Delta region of China. With the rapid process of urbanization in the three decades, this city faces great pressures from the large population (Deng

©2017, IAHR. Used with permission / ISSN 1562-6865 (Online) - ISSN 1063-7710 (Print)

et al., 2008), resource shortage (Shen et al., 2005) and environmental pollution (Peng and Bao, 2006). The rapid urbanization causes the thorough transformation of resource utilizing mode and correspondent increase of water withdraw and energy consumption, which will bring great pressures on water and energy allocation and ecological conservation. The way to harmonize the utilization of water, energy and other related resources (such as food, lands and ecosystems) is an urgent demand for orderly development in urbanization, not only for Wuxi city, but also for the whole world.

Therefore, carrying case study of Wuxi city, this paper forecasted the water allocation required to ensure the growing energy consumption in the city by 2020 and 2030. By analyzing the energy consumption of each industry and their implications on water use, we compared the results with the "Water Modernization Plan of Wuxi City" and discussed the policy implications.

2 MATERIALS AND METHODS

2.1 The establishment of water use system

The water use system divided water resources demand objects into production, living and ecology three parts, and the corresponding water requirement are the production water, living water and ecological water. On this basis, under the circumstance of meeting the basic living and basic ecological water requirement, planning the production of water requirement reasonably in order to realize the sustainable utilization of water resources and promoting the coordinated development of social economy and ecological environment.

According to different demand, the allocation system theory allocated the production water and living water with full consideration of the ecological environmental water requirements. This guarantee both the full development in social economy, and protect the regional ecological environment from destruction. Production water use mainly include primary industry, secondary industry and tertiary industry; Life water use including the urban residents, rural population and livestock water use. Ecological environment water use mainly refers to those for improving and protecting the environment, maintaining ecological own healthy development and protecting biodiversity.

The water use system theory is one of the main development direction to realize the sustainable utilization of water resources. In the face of the statistical data of different regions, different time and different fineness, the division of water system can effectively unified data caliber, which provides a convenient for the analysis and prediction on different regions and different years of water situation. Therefore, this paper selected the water use theory to divide water demand into production, life and ecological water.

2.2 Scenario simulation and Settings

Most traditional water demand management distinguished the supply and demand of water resources, very few takes into account the regional social economic development level and energy consumption. In fact, with the more and more diversified development of the region, water demand has not only affected by the growth of national economy but also by the urbanization and economic development. Rapid urbanization has made the fundamental change in the way of resource utilization, water consumption and energy consumption are increasing. Therefore, water demand management research carried out by this paper based on the energy consumption of city is of great significance.

Taking Wuxi City as a case, this paper forecasts the water allocation required to ensure the growing energy consumption in the city by 2020 and 2030. For the analysis, the paper first maps the city's water use system, including also the ecological water use. Within the water use system, three indicators are selected for in-depth analysis - the amount of production energy consumption, life power consumption and sewage discharge. Second, the paper analyzes the energy consumption of each industry and their implications on water use. By aggregation, a forecast is made on the water allocation required to enable the energy consumption by 2020 and 2030 in the city. Lastly, comparing the results with the "Water Modernization Plan of Wuxi City", this paper analyzed and evaluated the rationality of the forecasting result.

Currently, there is no clear explanation for the concept of "water demand", in practice, the concepts of "water use" , "water demand " and "water consumption" are often confused. Although there are differences between these concepts, but as a result in which there is only statistical data of water consumption of the study area is relatively complete, this paper use the "water use" approximately instead of the amount of water demand to carry on calculating.

2.3 Selection of energy index

Generally speaking, the energy consumption of urban water system mainly comes from the raw water extraction and transportation, water distribution, wastewater collection, wastewater treatment and discharge (Li et al., 2012). At present, there are many international organizations and countries that have begun to focus on the ties between water resources and energy, it's not only an opportunity but also a challenge for the resource utilization [8]. In order to realize the coordinated development of both, we need to understand clearly the basic relation between energy and water resources under the background of urbanization, so as to identify the connection of main index of energy and water resource utilization, quantitatively analyzing the relationship

 ©2017, IAHR. Used with permission / ISSN 1562-6865 (Online) - ISSN 1063-7710 (Print)

between them to make effect to coordination management policies and safeguard the coordinated and sustainable development.

As already mentioned, water resources used for production, life and ecology are mainly described with "water use system", which includes the production, life and ecology water use. Predicting the structure of water use in the future according to the existing conditions has become one of the focuses among people. Therefore, in this paper, the production system is described with water consumption of production and energy consumption of GDP. The life system is described with water consumption of life and electricity consumption of life. The ecological system is described with water consumption of ecology and discharge of wastewater.

Nowadays, the water use system including production, life and ecology has been widely used. Therefore, this paper also divides the city's total energy consumption into production, life and ecology energy consumption. The total energy consumption can be detected in Wuxi statistical yearbook, life energy consumption can be approximately calculated by life electricity consumption, ecological and energy consumption can be calculated with discharge of wastewater and power consumption of sewage treatment.

(1) Life energy consumption

With the improvement of the living standard, appliances such as refrigerators, color TV and induction cooker are essential to every household, every aspect of life is inseparable from the electricity. Suppose life energy consumption in Wuxi as E_{il}, life electricity consumption as E_{ile}. According to the National Energy Statistics System, the coefficient of electricity (equivalent value) of is 0.1229 kg of standard coal/KWh, the paper define the life energy consumption as E_{il}. The Eq. 1 shows the calculation of life energy consumption in Wuxi city.

$$E_{il} = {0.1229 \times E_{ile}} \Big/ {1000} \quad [1]$$

(2) Ecological energy consumption

Urban sewage treatment is one of energy-intensive industries, urban ecological energy consumption is mainly used for sewage treatment. At the present stage in China, sewage treatment plants are generally on a smaller scale and cost higher. In addition, the sewage treatment sludge rates were lower, but the energy consumption is very high, which to a certain extent contributed to the energy crisis in our country. At present, there is no specific studies or research data that shows the average power consumption situation of sewage treatment in Wuxi, but there are studies having shown that the energy consumption of the urban sewage treatment in China was 0.2 kWh/m^3, the average power consumption is 0.290 kWh/m^3. So this paper selects the average power consumption of Chinese urban sewage treatment plant as the one in Wuxi City, suppose ecology energy consumption in Wuxi is E_{ie}, the total amount of sewage treatment is W_i, therefore the ecology energy consumption is E_{ie}. The Eq. 2 shows the calculation of ecological energy consumption in Wuxi city.

$$E_{ie} = {0.29 \times 0.1229 \times W_i} \Big/ {10000} \quad [2]$$

(3) Production energy consumption

Production total energy consumption accounts for the largest amount of total energy consumption, it mainly includes the energy consumption of agricultural production, industrial production and service industries. Now the paper put all the energy index unit to "ten thousand tons of standard coal" (value) in order to calculate conveniently. The total amount of energy consumption in Wuxi was supposed as E_{it}, therefore the production energy consumption is E_{ip}. The Eq. 3 shows the calculation of production energy consumption in Wuxi city.

$$E_{ip} = E_{it} - E_{il} - E_{ie} \quad [3]$$

3 RESULTS AND DISCUSSION

3.1 Calculation of energy index

The energy consumption, energy consumption and the ecological life energy consumption can be calculated by the method above, the results are shown in table 1.

©2017, IAHR. Used with permission / ISSN 1562-6865 (Online) - ISSN 1063-7710 (Print)

Table 1. Calendar year energy consumption structure in wuxi city.

Years	E_{it}（value）	E_{ip}	E_{ile}/10^4kWh	E_{il}	W_i/10^4 tons	E_{ie}
2005	2580.620	2549.376	247142	30.374	24418.50	0.870
2006	2870.910	2835.137	283975	34.901	24491.50	0.873
2007	3169.130	3130.639	306054	37.614	24601.00	0.877
2008	3352.590	3309.130	346460	42.580	24705.00	0.881
2009	3539.610	3494.021	363767	44.707	24747.00	0.882
2010	3847.520	3793.524	431838	53.073	25896.75	0.923
2011	4038.648	3983.865	438110	53.844	26363.95	0.940
2012	4223.028	4163.693	475053	58.384	26681.40	0.951
2013	4374.820	4303.890	569340	69.972	26900.50	0.959

Units: 10^4 tons of standard coal

Table 2. Prediction and error analysis of life energy consumption.

	Years	Actual Value	Predictive Value	Relative Error (%)
Fitting Period	2005	30.374	33.141	9.111
	2006	34.901	36.578	4.806
	2007	37.614	40.288	7.108
	2008	42.580	44.513	4.539
	2009	44.707	48.253	7.932
	2010	53.073	54.267	2.249
Checking Period	2011	53.844	55.100	2.333
	2012	58.384	59.325	1.612
	2013	69.972	63.550	9.178
Forecast Period	2020		93.125	
	2030		135.375	

Units: 10^4 tons of standard coal

Table 3. Prediction and error analysis of ecological energy consumption.

	Years	Actual Value	Predictive Value	Relative Error (%)
Fitting Period	2005	0.720	0.714	0.841
	2006	0.722	0.721	0.159
	2007	0.726	0.728	0.368
	2008	0.729	0.735	0.914
	2009	0.730	0.742	1.710
	2010	0.764	0.749	1.881
Checking Period	2011	0.778	0.783	0.661
	2012	0.787	0.790	0.362
	2013	0.793	0.797	0.435
Forecast Period	2020		0.846	
	2030		0.917	

Units: 10^4 tons of standard coal

Table 4. Prediction and error analysis of production energy consumption.

	Years	Actual Value	Predictive Value	Relative Error (%)
Fitting Period	2005	2549.496	2587.427	1.488
	2006	2835.257	2826.736	0.301
	2007	3130.760	3066.046	2.067
	2008	3309.251	3305.356	0.118
	2009	3494.143	3544.666	1.446
	2010	3793.651	3783.975	0.255
Checking Period	2011	3983.994	4023.745	0.998
	2012	4163.824	4263.055	2.383
	2013	4304.022	4502.365	4.608
Forecast Period	2020		6177.535	
	2030		8570.635	

Units:10^4 tons of standard coal

3.2 Forecast of energy index

In the previous section, the production, living and ecological, three aspects of energy consumption were calculated and in this section, the paper uses the WEAP-LEAP model (Dale et al., 2013; Sieber, 2012) as a tool to simulate the energy consumption in Wuxi during 2005 to 2010. At the same time, this paper tests the prediction results with actual statistics from 2011 to 2013 and forecast the structure of energy consumption in 2020 and 2030. The simulation results are presented as in table 2-4.

It can be seen from table 2-4 that the WEAP-LEAP model fitting for energy consumption structure of Wuxi in present situation, relative errors are within 10%, which is within the allowed error range. The prediction

 ©2017, IAHR. Used with permission / ISSN 1562-6865 (Online) - ISSN 1063-7710 (Print)

result of production, life, ecological energy consumption of Wuxi in 2020 is respectively 6177.535 million tons of standard coal 93.125 million tons of standard coal, 0.846 million tons of standard coal. The prediction result of production, life, ecological energy consumption of Wuxi in 2020 is respectively 8570.635 million tons of standard coal, 135.375 million tons of standard coal, 0.917 million tons of standard coal.

3.3 Forecast and evaluating of water demand management model

(1) Water demand management model predict of Wuxi

Now, for there is no files related energy planning, the water consumption structure of Wuxi in the future can be predicted by reasonable planning in energy consumption structure and analyzing its relationship with the water consumption structure. In the previous chapter, the energy consumption for production, life and ecology in 2020 and 2030 has been forecasted, then the water consumption structure can be calculated by putting the actual value and predictive value into the model. The results are as follows.

Table 5. Energy and water consumption structure in Wuxi city.

	Production System		Life System		Ecosystem	
Years	Energy consumption /10^4 tec	Water consumption /10^8 m^3	Energy consumption /10^4 tec	Water consumption /10^8 m^3	Energy consumption /10^4 tec	Water consumption /10^8 m^3
2005	2549.496	28.43	30.374	2.74	0.720	0.09
2006	2835.257	27.68	34.901	3.15	0.722	0.27
2007	3130.760	27.23	37.614	3.39	0.726	0.29
2008	3309.251	24.98	42.580	4.62	0.729	0.32
2009	3494.143	24.78	44.707	4.54	0.730	0.33
2010	3793.651	29.60	53.073	4.59	0.764	0.39
2011	3983.994	31.37	53.844	3.35	0.778	0.27
2012	4163.824	30.63	58.384	3.99	0.787	0.28
2013	4304.022	34.10	69.972	4.01	0.793	0.32
2020	6177.535	39.12	93.125	5.03	0.846	0.38
2030	8570.635	47.50	135.375	6.13	0.917	0.44

It can be seen from table 5 that when the energy consumption for production, life and ecology in 2020 is respectively 6177.535 million tons of standard coal, 93.125 million tons of standard coal and 0.846 million tons of standard coal, the water consumption for production, life and ecology is respectively $39.12\times10^8m^3$, $5.03\times10^8m^3$ and $0.38\times10^8m^3$; when the energy consumption for production, life and ecology in 2030 is respectively 8570.635 million tons of standard coal, 135.375 million tons of standard coal and 0.917 million tons of standard coal, the water consumption for production, life and ecology is respectively $47.50\times10^8m^3$, $6.13\times10^8m^3$ and $0.44\times10^8m^3$.

Table 6. Correlation analysis on energy index and water consumption.

Years	Index	Production System	Life System	Ecosystem
2005~2013	Correlation coefficient	0.641	0.896*	0.901*
	Significant (two-tailed)	0.063	0.016	0.014
	N	9	9	9
2005~2030	Correlation coefficient	0.950**	0.827**	0.645*
	Significant (two-tailed)	0.000	0.002	0.032
	N	11	11	11

Table 7. Forecast results of water demand in Wuxi.

		Production water requirement/10^8 m^3	Life water requirement/10^8 m^3	Ecology water requirement/10^8 m^3	Total/10^8 m^3
Reference Year	Modernization Plan	29.04	4.60	0.40	34.04
	Predictive Value	29.60	4.59	0.39	34.58
Forecast （2020）	Modernization Plan	39.86	6.76	0.94	47.56
	Predictive Value	39.12	5.03	0.38	44.75

©2017, IAHR. Used with permission / ISSN 1562-6865 (Online) - ISSN 1063-7710 (Print)

(2) Predicted results evaluation

In the previous section, the present energy index of production, life and ecosystem was simulated and the ones in the future was forecast, and according to the relations between the various industrial water consumption, this paper has carried on the reasonable forecast. In order to evaluate the rationality of the forecast results, the paper analyzed the correlation between energy index and water consumption in three systems (Table 6).

In the first column of table 6, the paper carries the correlation analysis on each industrial energy consumption and water consumption during 2005 to 2013. It can be seen that there are positively correlated relationship between energy consumption and water consumption of each industry in Wuxi especially in the life system and ecological system. It suggested that in this stage, energy consumption has great influence on water consumption, while the effect in production system is a little bit weaker than the other two because it is also affected by income water. In the second column, social and economic indexes were added to the original sequence, then the paper carried the correlation analysis again and the results showed that there is still positive correlation in the three systems. It can be concluded that the predicted results are reasonable.

In 2011, the municipal party committee municipal government of Wuxi responded to the spirit of the central file no. 1, prospectively put forward the idea of constructing national water conservancy modernization demonstration city in China, and issued the “Water Modernization Plan of Wuxi City”, which forecast the water demand of Wuxi in 2020. Comparing with the Plan, the results and basic data are roughly the same, but the predicted results are a little less than the ones in the Plan. Therefore, it can be concluded that the Plan is generally sound, but more water can be saved through better options for efficiency gain. The demand of water resources and water structure are affected by many factors, although energy consumption is not the only one but should not be ignored. Taking advantage of this, the work that this paper has done would provide a data basis for Wuxi government to make the corresponding water resources planning policies.

4 CONCLUSIONS

This paper raises the problem of energy and water nexus starting from the direction of domestic and foreign research development, and carries on the scene simulation in Wuxi city on the basis of the existing data. In order to the unified caliber, this paper maps the city’s water use system and selects energy index combined with the corresponding water data. In order to analyze the impact that energy consumption has on water consumption, the paper identifies energy consumption of GDP, electricity consumption of life and discharge of wastewater three indicators to associate with water for each industry. When having the energy consumption, the paper forecasts energy index and water consumption with the help of model. On the premise of that the results meet the accuracy requirement, the paper forecast the water consumption with the corresponding energy consumption in 2020 and 2030.

Through the correlation analysis of current and forecast data sequence, it can be seen that the relationship between water and energy in production system and life system is strong while the one in ecological system is weaker, this may be due to the lack of fieldwork and survey, the average power consumption in Chinese urban sewage treatment plant cannot reflect the one in Wuxi, which creating a certain error. At the same time, comparing with the Plan, the results and basic data are roughly the same, but the predicted results are a little less than the ones in the Plan. Therefore, it can be concluded that the Plan is generally sound, but more water can be saved through better options for efficiency gain.

As the strengthening of globalization trend, the competition of comprehensive national strength among countries proves that the resource competition, energy and water problem has become the important factors influencing social and economic sustainable development all of the world. Therefore, in light of the characteristics of Wuxi, this paper puts forward the water demand management under the influence of energy consumption, it has certain innovation and breakthrough compared to the traditional one--dominated by supply and demand. However, the research content of this paper is just a preliminary exploration, there is still many problems which exists that needed to be solved.

For example, there are still ambiguities in the influence that energy consumption has on water consumption, and due to the limitation of time and economic conditions, a lot of basic data could not be obtained through on-the-spot investigation to calculate the conversion relations of water and energy in Wuxi and as a result, it will become an important problem that needed to be solved in the future in how to describe the conversion relationship between water and energy of a specific area more accurately. At present, on the macro scale, water and energy respectively belongs to two different departments, it will become the key and challenges to the application of the research on water and energy ties in the future in how to clear the authority and functions of different stakeholders in resource management and refine the research on water resources and energy ties in social life.

ACKNOWLEDGEMENT

This work was jointly funded by the Program of International S&T Cooperation of China (2015DFA01000), the Projects of National Natural Science Foundation of China (Grant No. 51479120; 51479121; 51679146), the Special Research Funds for Public Welfare of the State Ministry of Water

 ©2017, IAHR. Used with permission / ISSN 1562-6865 (Online) - ISSN 1063-7710 (Print)

Resources (201501015-01), the Natural Science Foundation of Jiangsu Province (Grant No. BK20141075), and the Special Research Fund of Nanjing Hydraulic Research Institute (Y116006; Y116022). Finally, we are grateful to the anonymous reviewers for their constructive comments and helpful suggestions.

REFERENCES

Bao S., Jia Y., Gao X. & Cai S. (2015). Trend and Inspiration of Water and Energy Nexus. *China Water Resources*, 11, 6-9.

Bauer, D., Philbrick, M. & Vallario, B. (2014). *The Water-Energy Nexus: Challenges and Opportunities*, U.S. Department of Energy.

Brent, D.A. (2015). *Book Review: Living with Water Scarcity*. Water Economics and Policy, 1, 1580003.

Dale, L.L., Millstein, D., Karali, N., Vicuna, S., Purkey, D. R. & Heaps, C. (2013). Energy-Water Integrated Assessment of the Sacramento Area and a Demonstration of WEAP-LEAP Capability. *Power Engineering*, 22, 1795-1800.

Deng, X., Huang, J., Rozelle, S. & Uchida, E. (2008). Growth, Population and Industrialization, and Urban Land Expansion of China. *Journal of Urban Economics*, 63, 96-115.

Gleick, P.H. (1994). Water and Energy. *Annual Review of Energy and the Environment*, 19(1), 267-299.

Hanjra, M.A. & Qureshi, M.E. (2010). Global Water Crisis and Future Food Security in an Era of Climate Change. *Food Policy*, 35(5), 365–377.

Healy, R.W., Alley, W.M., Engle, M.A., McMahon, P.B. & Bales, J.D. (2015). *The Water-Energy Nexus: an Earth Science Perspective*, (No. 1407), US Geological Survey.

IEA. (2012). *Emissions from Fuel Combustion, Highlights*. Paris, France: International Energy Agency.

Li, L., Chen, Y., He, X. & Gu, D. (2012). Studies on Water-Energy Relationship in Urban Water System. *China Water Resources*, 6, 22-25.

Miller, C.A. (2013). Energy Resources and Policy: Vulnerability of Energy Resources and Resource Availability– Fossil Fuels (Oil, Coal, Natural Gas, Oil Shale). *Climate Vulnerability*, 3, 37-51.

Peng, S. & Bao Q. (2006). Economic Growth and Environmental Pollution: An Empirical Test for the Environmental Kuznets Curve Hypothesis in China. *Research on Financial and Economic Issues*. 8, 3-17.

Qin, B., Zhu, G., Gao, G., Zhang, Y., Wei, L. & Paerl, H.W. (2010). A Drinking Water Crisis in Lake Taihu, China: Linkage to Climatic Variability and Lake Management. *Environmental Management*, 45(1), 105-112.

Qin, Y., Curmi, E., Kopec, G.M., Allwood, J.M. & Richards, K.S. (2015). China's Energy-Water Nexus–Assessment of the Energy Sector's Compliance with the “3 Red Lines” Industrial Water Policy. *Energy Policy*, 82, 131-143.

Retamal, M., Abeysuriya, K., Turner, A. & White, S. (2009). *Water Energy Nexus: Literature Review*, University of Technology, Sydney.

Spang, E.S., Moomaw, W.R., Gallagher, K.S., Kirshen, P.H. & Marks, D.H. (2014). The Water Consumption of Energy Production: An International Comparison. *Environmental Research Letters*, 9(10), 99-112.

Shen, L., Cheng, S., Gunson, A.J. & Wan, H. (2005). Urbanization, Sustainability and the Utilization of Energy and Mineral Resources in China. *Cities*, 22, 287-302.

Sieber, J. (2012). Integrating the WEAP and LEAP Systems to Support Planning and Analysis at the Water-Energy Nexus. *World Computer Congress*, 41, 92-95.

Wang, J., Rothausen, S.G.A., Conway, D., Zhang, L., Xiong, W., Holman, I.P. & Li, Y. (2012). China’s Water–Energy Nexus: Greenhouse-Gas Emissions from Groundwater Use for Agriculture. *Environmental Research Letters*, 7, 014035.

Wen, H., Zhong, L., Fu X. & Spooner, S. (2014). *Water Energy Nexus in the Urban Water Source Selection: a Case Study from Qingdao*. World Resources Institute.

©2017, IAHR. Used with permission / ISSN 1562-6865 (Online) - ISSN 1063-7710 (Print)

Proceedings of the 37th IAHR World Congress
August 13 – 18, 2017, Kuala Lumpur, Malaysia

ON THE INFLUENCE OF LATERAL FLOWS ON THE UNCERTAINTY OF UNSTEADY OPEN CHANNEL FLOWS IN MOUNTAINOUS RIVERS

KEYUE CHEN[1], HUAN-FENG DUAN[2], XUFENG YAN[3], XIEKANG WANG[4] & XINGNIAN LIU[5]

[1,2] Department of Civil and Environmental Engineering, The Hong Kong Polytechnic University, Hong Kong, wmchky@gmail.com; hf.duan@connect.polyu.hk
[3, 4, 5] State Key Laboratory of Hydraulics and Mountain River Engineering, Sichuan University, Chengdu 610065, China, wangxiekang@scu.edu.cn

ABSTRACT

Flow modeling has become essential and crucial to the hydraulic design of river channel structures such as dams, bridges and piers and to the water resources management of river networks such as flooding control and risk analysis. However, the open channel flow process, especially for mountainous rivers, is usually unsteady and highly uncertain due to the variability and randomness in both natural and artificial characteristics of parameters such as initial and boundary conditions. This paper aims to investigate the uncertainty influence of the lateral flows along mountainous river channel to the unsteady flow process in the channel. To this end, a stochastic model based on the 1D Saint-Venant equations is firstly developed by the perturbation method to express the uncertainty propagation characteristics of the lateral flows, which is solved through finite difference method. This model includes both the spatial and temporal variation and propagation of the lateral flows along the river channel, so as to fully understand the influence of uncertain lateral flows on the unsteady flow process in the channel. The findings of this study may provide practical significance and implications to the flooding risk control and water resources management of mountainous watersheds as well as to the extension and development of unsteady open channel flow models for complex mountainous rivers.

Keywords: Uncertainty Analysis; Stochastic Model; Perturbation Method; Lateral Flow; Unsteady Open Channel Flow.

1 INTRODUCTION

Open channel flows are engaged in human daily life throughout the world. Human beings benefit from the use of open channel flows in irrigation, water transportation, drainage control, hydropower generating and so on. However, human being suffer from disasters caused by open channel flows such as flood and mudslides as well. With the global climate change, extreme weather occurs with higher frequency, leads to an even higher risk in these disasters (Fang et al., 2014; Kundzewicz, 2003). Therefore, the knowledge of open channel hydraulics is of vital importance for human beings to predict and avoid disasters, as well as to take advantage of natural rivers or design artificial open channels for irrigation and other applications.

Branches usually exist with natural rivers, and the numbers of branches would be even larger than mountain rivers. It leads to a series of research about open channel with lateral flow, or open channel networks. Schaffranek et al. (1981) developed a one-dimensional numerical model with several assumptions for simulating the unsteady flow in river networks of reaches with interconnected channels, and the four-point implicit finite-difference scheme is used to solve the equations. Swain and Chin (1990) proposed an improved numerical model which considers the effects of hydraulic structures and leakage through the riverbed. Comparison of algorithms computing gradually varied flow in open channel networks has also been investigated (Islam et al., 2005). Research about diffusive wave in open channel with uniform or concentrated lateral inflow is conducted as well (Fan and Li, 2006).

Modeling in open channel hydraulics has been an essential technique in hydraulic engineering practice such as design of river channel structures and water resources management of river networks including flood control and risk analysis, and many researches have been done to conduct analytical and numerical solution to the classic Saint-Venant equations for such purpose. However, in field applications, only a limited number of spatial locations and time intervals of input data is available (Willis et al., 1989), and thus those models can only represent a specific condition of the natural hydraulic processes in open channel, and the data used for computation are unavoidable with measurement errors. Moreover, the natural open channel flow process, especially for complex mountain rivers with great variety, is usually unsteady and highly uncertain due to the variability and randomness in both natural and artificial characteristics of parameters involved in the hydraulic process such as the boundary conditions and side inflows. Therefore, a stochastic model governing the randomness of flow process in a statistical mean would be useful for theoretical understanding of the influence of these factors and in the meanwhile, for practical design and management of hydraulic engineering project.

Stochastic analysis in engineering has been investigated for hydrosystems over many years since stochastic process occurs widely in engineering practice. Usually, both simulation and non-simulation

 ©2017, IAHR. Used with permission / ISSN 1562-6865 (Online) - ISSN 1063-7710 (Print)

methods are employed for stochastic analysis for physical problems. Simulation methods are commonly adopted in the literature for the hydrosystem analysis, which may provide detailed results for the evolution process of the system under each specific condition considered for the simulation. However, under uncertainty condition, especially for those multiple variations of the system and flow conditions, the simulation methods become impractical and inefficient for obtaining conclusive results. For example, Monte-Carlo simulation method is, from theoretical point of view, one of the robust and powerful methods to represent the stochastic process of hydrosystems, but from practical point of view, it is very time-consuming to obtain accurate results that can be used for fully describing the stochastic characteristics of the system (Tung et al., 2006).

Non-simulation methods for stochastic modeling aim to deal with the partial differential equations (PDEs) analytically. Specifically, the variables in the governing equations are treated as random functions. As a result, the governing equations can be transformed into a corresponding stochastic form of PDEs, and the solution to which also becomes stochastic functions. Non-simulation methods are usually convenient and efficient in calculation, but difficulties occur in the analytical derivation of governing equations because of the complicated mathematical work. For example, probability density function (PDF) methods are conducted by deriving probability density functions from the stochastic PDEs with particular methods. Pope (1985) introduced a method to solve a series of joint pdf, and this method was further developed and tested later in the area of hydraulic engineering (Cao et al., 2007; Sett et al., 2007; Yoon and Kavvas, 2003; Pope, 1994). However, these solution methods are based on approximation by the understanding of the system, and in more general cases, solution of stochastic PDEs are hard to obtain in a nonlinear system. Moment equations methods are adopted to investigate no-single case but the statistical moments of the stochastic processes, which may lead to less consideration of objects and efficiency in computation.

In comparison to the complicated methods as described above, the perturbation method, which is a combined method of applying non-simulation and simulation processes, is an advantageous method. In particular, this method can simply describe the stochastic process, compared to above non-simulation methods, and in the meanwhile, can efficiently obtain the results, compared to above simulation methods. This kind of method are simpler in mathematic but still efficient in application, therefore, the perturbation method has been the most popular non-sampling methods, in which the random functions are usually expanded via Taylor series around their mean and truncated to a certain order (Xiu, 2009). In details, the moment equations are derived from the stochastic PDEs and the solution of moment equations presents the statistical characteristics of the stochastic process. Therefore, this method is used and applied in this study to study the stochastic characteristics of complex rivers with lateral flows. The stochastic equation is firstly derived by this method in this paper, and after validation, it is then used to analyze the influence of the uncertainty of lateral flows on the stochastic process of open channel flows. Finally, the results are discussed for their implications to the design and management of open channel flows in complex mountain rivers.

2 STOCHASTIC MODEL

The proposed method is developed with the help of perturbation method based on the 1-D Saint-Venant equations (Schaffranek, 1987) as in Eq. [1]., investigating the influence of channel side lateral-flow on open channel hydraulic process.

$$\begin{cases} B\dfrac{\partial h}{\partial t}+\dfrac{\partial Q}{\partial x}-q=0 \\ \dfrac{\partial Q}{\partial t}+\dfrac{\partial\left(\beta Q^2/A\right)}{\partial x}+gA\dfrac{\partial h}{\partial x}+\dfrac{gn^2}{AR^{4/3}}Q|Q|-qu-gS_0A+\xi B_C U_a^2\cos\alpha=0 \end{cases} \quad [1]$$

In which x is the horizontal coordinate along the channel, t is time, B is the river top width of cross section, h is the water depth normal to the horizontal coordinate, Q is the flowrate at a point, A is the area of cross-section, β is the momentum coefficient, q is the lateral inflow per unit length of channel, u is the x-component of lateral flow velocity, g is gravitational acceleration, R is the hydraulics radius, k is the flow-resistance function, ξ is the wind-resistance coefficient, B_C is the top width of conveyance part of cross section, U_C is wind velocity, and α is wind direction measured from positive x-axis.

Note that as preliminary study of method development, only simple system with rectangular cross-sectional area is considered in this study. For clarity, several assumptions and approximations are made during the analysis so as to obtain the stochastic model, as follows:

- The water is incompressible and homogeneous, and the density and viscosity of water are constant.
- The water pressure distribution is hydrostatic.
- The channel bed slope is mild and uniform.

©2017, IAHR. Used with permission / ISSN 1562-6865 (Online) - ISSN 1063-7710 (Print)

- The channel cross section is rectangular and wide, therefore, the area of cross section can be written as $A = Bh$, and the hydraulic radius could be illustrated as $R = h$.
- Frictional resistance is the same as steady flow, therefore, the Chezy or Manning's formula can be used to describe the friction loss.
- Wind resistance is negligible.

Therefore, the governing equations Eq. [1] of one-dimensional unsteady open channel flow with lateral flow in wide rectangular open channels can be transformed into:

$$\begin{cases} B\dfrac{\partial h}{\partial t} + B\dfrac{\partial hv}{\partial x} + hv\dfrac{\partial B}{\partial x} - q = 0 \\ B\dfrac{\partial hv}{\partial t} + 2\beta Bhv\dfrac{\partial v}{\partial x} + \beta v^2 h\dfrac{\partial B}{\partial x} + \beta v^2 B\dfrac{\partial h}{\partial x} + gBh\dfrac{\partial h}{\partial x} + gn^2 v^2 Bh^{-1/3} - gS_0 Bh - qu = 0 \end{cases} \quad [2]$$

where the friction slope term is expressed by Manning's formula, k are defined by $k = n^2$. The governing equations are a set of partial differential equations describe the mass and momentum conservation in simplified open channels.

As a result, by applying the perturbation analysis procedure (Li et al., 2003), the moment equations derived from the equations above can be presented as:

$$\begin{cases} B\dfrac{\partial C_{hh}}{\partial t} + B\dfrac{\partial C_{hh}v^{(0)}}{\partial x} + B\dfrac{\partial h^{(0)}C_{vh}}{\partial x} + C_{hh}v^{(0)}\dfrac{\partial B}{\partial x} + h^{(0)}C_{vh}\dfrac{\partial B}{\partial x} - C_{qh} = 0 \\ B\dfrac{\partial C_{hh}v^{(0)}}{\partial t} + B\dfrac{\partial h^{(0)}C_{vh}}{\partial t} + +2\beta BC_{hh}v^{(0)}\dfrac{\partial v^{(0)}}{\partial x} + 2\beta Bh^{(0)}C_{vh}\dfrac{\partial v^{(0)}}{\partial x} + 2\beta Bh^{(0)}v^{(0)}\dfrac{\partial C_{vh}}{\partial x} \\ +2\beta v^{(0)}C_{vh}B\dfrac{\partial h^{(0)}}{\partial x} + \beta v^{(0)^2}B\dfrac{\partial C_{hh}}{\partial x} + 2\beta v^{(0)}C_{vh}h^{(0)}\dfrac{\partial B}{\partial x} + \beta v^{(0)^2}C_{hh}\dfrac{\partial B}{\partial x} + gBC_{hh}\dfrac{\partial h^{(0)}}{\partial x} + gBh^{(0)}\dfrac{\partial C_{hh}}{\partial x} \\ +2gn^2v^{(0)}C_{vh}B\left(h^{(0)}\right)^{-\frac{1}{3}} + gn^2v^{(0)^2}B\left(h^{(0)}\right)^{-\frac{1}{3}}\left(-\dfrac{1}{3}\dfrac{C_{hh}}{h^{(0)}}\right) - gS_0BC_{hh} - \langle q\rangle C_{uh} - C_{qh}\langle u\rangle = 0 \end{cases} \quad [3]$$

$$\begin{cases} B\dfrac{\partial C_{hh}}{\partial t} + B\dfrac{\partial C_{hh}v^{(0)}}{\partial x} + B\dfrac{\partial h^{(0)}C_{vh}}{\partial x} + C_{hh}v^{(0)}\dfrac{\partial B}{\partial x} + h^{(0)}C_{vh}\dfrac{\partial B}{\partial x} - C_{qh} = 0 \\ B\dfrac{\partial C_{hh}v^{(0)}}{\partial t} + B\dfrac{\partial h^{(0)}C_{vh}}{\partial t} + +2\beta BC_{hh}v^{(0)}\dfrac{\partial v^{(0)}}{\partial x} + 2\beta Bh^{(0)}C_{vh}\dfrac{\partial v^{(0)}}{\partial x} + 2\beta Bh^{(0)}v^{(0)}\dfrac{\partial C_{vh}}{\partial x} \\ +2\beta v^{(0)}C_{vh}B\dfrac{\partial h^{(0)}}{\partial x} + \beta v^{(0)^2}B\dfrac{\partial C_{hh}}{\partial x} + 2\beta v^{(0)}C_{vh}h^{(0)}\dfrac{\partial B}{\partial x} + \beta v^{(0)^2}C_{hh}\dfrac{\partial B}{\partial x} + gBC_{hh}\dfrac{\partial h^{(0)}}{\partial x} + gBh^{(0)}\dfrac{\partial C_{hh}}{\partial x} \\ +2gn^2v^{(0)}C_{vh}B\left(h^{(0)}\right)^{-\frac{1}{3}} + gn^2v^{(0)^2}B\left(h^{(0)}\right)^{-\frac{1}{3}}\left(-\dfrac{1}{3}\dfrac{C_{hh}}{h^{(0)}}\right) - gS_0BC_{hh} - \langle q\rangle C_{uh} - C_{qh}\langle u\rangle = 0 \end{cases} \quad [4]$$

where $C_{hh}, C_{vv}, C_{vh}, C_{qh}, C_{uh}, C_{qv}, C_{uv}$ are covariance and cross-covariance of these parameters, $v^{(0)}$ and $h^{(0)}$ are the means of velocity and water depth.

For case study in this paper, the simple upstream boundary is applied and can be expressed as:

$$C_{hh}(0,t)v^{(0)}(0,t) + h^{(0)}(0,t)C_{vh}(0,t) = C_{quh}(t) \quad [5]$$

$$C_{hv}(0,t)v^{(0)}(0,t) + h^{(0)}(0,t)C_{vv}(0,t) = C_{quv}(t) \quad [6]$$

Therefore, $C_{qh}, C_{uh}, C_{qv}, C_{uv}, C_{quh}$ and C_{quv} can be solved by a series of similar equations which are not listed here subject to the limitation of pages.

The covariance and means of velocity, water depth and therefore flowrate could be computed through solving such set of equations with appropriate input data. To solve the stochastic equations, they are

 ©2017, IAHR. Used with permission / ISSN 1562-6865 (Online) - ISSN 1063-7710 (Print)

discretized with the Preissmann four-point scheme, and since these equations are linearized, they can be solved by Gaussian elimination method.

3 MODEL VERIFICATION

The accuracy of the proposed method in this paper was verified by computing a simple case, with the results compared with the solutions obtained in a previous research which was presented by both numerical simulation (i.e., simulation method) and the analytical approach (i.e., non-simulation method).

The following initial and system conditions were taken to conduct this verification: (1) cross-covariance functions C_{uqu}, C_{qqu} in equations are zero; (2) the mean velocity and water depth in Eq. [3] and [4] are steady and uniform; (3) the channel is semi-infinite so that the downstream boundary effect could be neglected. Therefore, the equations solving C_{quh} and C_{quv} can be simplified as follow:

$$\begin{cases} B\dfrac{\partial C_{hqu}}{\partial t}+B\dfrac{\partial C_{hqu}v^{(0)}}{\partial x}+B\dfrac{\partial h^{(0)}C_{vqu}}{\partial x}+C_{hqu}v^{(0)}\dfrac{\partial B}{\partial x}+h^{(0)}C_{vqu}\dfrac{\partial B}{\partial x}-C_{qqu}=0 \\ B\dfrac{\partial C_{hqu}v^{(0)}}{\partial t}+B\dfrac{\partial h^{(0)}C_{vqu}}{\partial t}++2\beta BC_{hqu}v^{(0)}\dfrac{\partial v^{(0)}}{\partial x}+2\beta Bh^{(0)}C_{vqu}\dfrac{\partial v^{(0)}}{\partial x}+2\beta Bh^{(0)}v^{(0)}\dfrac{\partial C_{vqu}}{\partial x} \\ +2\beta v^{(0)}C_{vqu}B\dfrac{\partial h^{(0)}}{\partial x}+\beta v^{(0)^2}B\dfrac{\partial C_{hqu}}{\partial x}+2\beta v^{(0)}C_{vqu}h^{(0)}\dfrac{\partial B}{\partial x}+\beta v^{(0)^2}C_{hqu}\dfrac{\partial B}{\partial x}+gBC_{hqu}\dfrac{\partial h^{(0)}}{\partial x}+gBh^{(0)}\dfrac{\partial C_{hqu}}{\partial x} \\ +2gn^2v^{(0)}C_{vqu}B\left(h^{(0)}\right)^{-\frac{1}{3}}+gn^2v^{(0)^2}B\left(h^{(0)}\right)^{-\frac{1}{3}}\left(-\dfrac{1}{3}\dfrac{C_{hqu}}{h^{(0)}}\right)-gS_0BC_{hqu}-\langle q\rangle C_{uqu}-C_{qqu}\langle u\rangle=0 \end{cases} \quad [7]$$

$$C_{hqu}(0,t)v^{(0)}(0,t)+h^{(0)}(0,t)C_{vqu}(0,t)=C_{ququ}(t) \quad [8]$$

As a result, $C_{quQ}=v^{(0)}C_{quh}+h^{(0)}C_{quv}$, which is the cross-covariance of flowrate between upstream boundary and the considered position. This set of equations are solvable through an analytical method (DOOGE et al., 1983).

The channel in this case was set to be semi-infinite with a constant bed slope $S_0=0.0005$, Manning coefficient was set to be $n=0.03$, and the uniform steady mean flow was assumed as $F_r=0.25, Q=1m^2/s$. The results were analyzed in terms of the dimensionless independent variables defined with the help of bottom slope, mean water depth and velocity as

$$L_0=h^{(0)}/s; T_0=L_0/v^{(0)} \quad [9]$$

the boundary condition which is the randomness of the upstream inflow is generated by an exponential covariance function as

$$C_{ququ}(t;\tau)=\sigma_{qu}^2\exp\left(-|t-\tau|/\lambda_{qu}\right) \quad [10]$$

where σ_{qu}^2 is the variance of inflow rate, and t, τ are the time positions of upstream boundary, λ_{qu} is the correlation length which is set to be $0.27T_0$.

Under these conditions, the results of the uncertainty of unsteady channel flows based on the developed method and procedure in this study can be obtained and shown in Figure1a, in which the results by other methods (Lu, 2008) are also plotted in Figure 1b for comparison. For illustration, only the results of the uncertainty covariance factor of C_{quQ} at the location $x=5L_0$ along the channel were extracted and shown here for the comparative analysis. For other stochastic features, similar results were obtained for the studied open channel flow system.

Figure 1 shows clearly the good agreement of the results by different methods, which confirms the validity and accuracy of the derived analytical results and the developed method procedure in this study. Therefore, the developed method is further applied to analyze the influence of the lateral flow uncertainties on the stochastic process of the unsteady open channel flows in this paper.

©2017, IAHR. Used with permission / ISSN 1562-6865 (Online) - ISSN 1063-7710 (Print)

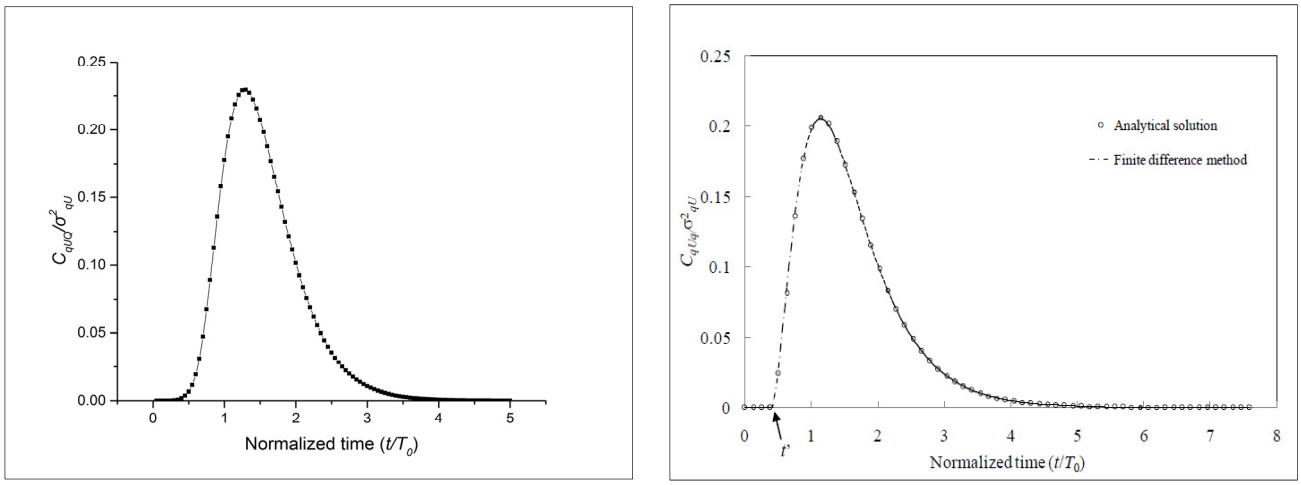

(a) (b)

Figure 1. The results of cross-covariance (x=5.0L_0) by: (a) the proposed model in this study; (b) the previous results in the literature (DOOGE et al., 1987; Lu 2008).

4 PRELIMINARY APPLICATION

Since the lateral flow of open channel is not considered in the verification case in last section, the model was applied to a similar case with lateral flow during the flow process to investigate the effects of lateral flow on the flowrate covariance.

For a preliminary application, the channel was set to be same as the simple flow system described in section 3, with lateral flow into the main channel every 6km along the channel. The quantity of lateral flow is $q = 0.025Q$ and $q = 0.05Q$ respectively and the computation results are presented in Fig. 2 below.

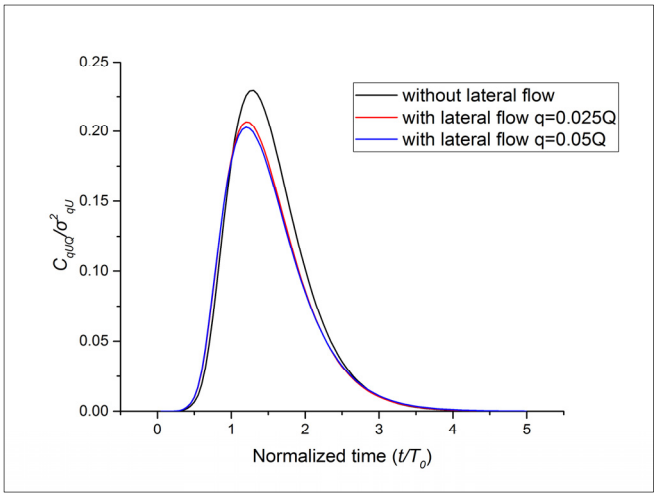

Figure 2. The comparison of different lateral flow conditions.

The result comparison in Fig. 2 shows that the lateral flow in the channel may reduce the flowrate correlation at the downstream locations with upstream uncertainty conditions, with the peaks of covariance decreased in lateral flow cases. Therefore, the lateral flow may mitigate the uncertainty propagation originated from the upstream along the flow channel. Furthermore, with higher lateral flow, the covariance becomes smaller and thus the uncertainty from the upstream will be more mitigated. However, the results also demonstrated that the mitigation effect of lateral flow on the upstream uncertainty propagation is not directly proportional to the quantity of the lateral flow, but its influence trend becomes gradually decreasing with a further increase of the lateral flow. Finally, in addition to the amplitude of uncertainty propagation, the lateral flow can also affect the speed of this propagation. Particularly, the lateral flow may speed up of the uncertainty propagation from the results of Fig. 2. This is mainly because the dynamic wave will propagate toward the downstream faster in channels with lateral flow, which results in somewhat earlier arriving of the covariance peaks in Fig. 2.

It is also noted that only the simple cases for uniform channel and constant lateral flow without variability were considered and examined in this study. More validations and applications to complex system and flow conditions are required in the future work for the developed stochastic model and method in this study.

 ©2017, IAHR. Used with permission / ISSN 1562-6865 (Online) - ISSN 1063-7710 (Print)

5 CONCLUSIONS

With the employment of the perturbation method, this study has developed a stochastic model for describing the uncertainty of 1-D open channel flows with lateral flows. The developed stochastic model of PDEs is easily solvable via Gaussian Elimination method, which has greatly improved the efficiency and accuracy of stochastic analysis of unsteady open channel flows.

With the validation by the available data in the literature, the developed model and method has been used to examine the influence of the lateral flows on the uncertainty of open channel flows. The results showed that uncertainty amplitude decreases in channels with the existence of uniform/constant lateral flow, and the uncertainty propagation speed increases with the lateral flow along the channel. From the perspective, it is necessary to consider and include the influence of lateral flows to analyze and evaluate the uncertainty and variability of unsteady open channel flows. It is also necessary to note that further validation and application in more complex channel systems will be required in the future work for the developed stochastic model and method in this study.

The results and findings are useful to the practical design and management of complex mountain rivers/watersheds where the lateral flows are common and uncertain.

ACKNOWLEDGEMENTS

This study was partially supported by: (1) the Key Program of National Natural Science Foundation of China (grant no. 51639007); (2) the open foundation of State Key Laboratory of Hydraulics and Mountain River Engineering in Sichuan University of China (grant no. SKHL1417); (3) the Hong Kong Polytechnic University (postgraduate research program and research project no. 1-ZVGF); and (4) the Hong Kong Research Grants Council (RGC) (project no. 25200616).

REFERENCES

Cao, R.R., Wang, H. & Pope, S.B. (2007). The Effect of Mixing Models in PDF Calculations of Piloted Jet Flames. *Proceedings of the Combustion Institute*, 31(1), 1543-1550.

Dooge, J.C., Kundzewicz, Z.W. & Napiórkowski, J.J. (1983). On Backwater Effects in Linear Diffusion Flood Routing. *Hydrological Sciences Journal*, 28(3), 391-402.

Fan, P. & Li, J. (2006). Diffusive Wave Solutions for Open Channel Flows with Uniform and Concentrated Lateral Inflow. *Advances in Water Resources*, 29(7), 1000-1019.

Fang, J., Du, J., Xu, W., Shi, P. & Kong, F. (2014). Advances in the Study of Climate Change Impacts on Flood Disaster. *Advances in Earth Science*, 29(9), 1085-1093.

Islam, A., Raghuwanshi, N., Singh, R. & Sen, D. (2005). Comparison of Gradually Varied Flow Computation Algorithms for Open-Channel Network. *Journal of Irrigation and Drainage Engineering*, 131(5), 457-465.

Kundzewicz, Z.W. (2003) Flood Risk Growth under Global Change-Yangtze Floods in Perspective. *Journal of Lake Sciences*, 15, 155-165.

Li, L., Tchelepi, H.A. & Zhang, D. (2003). Perturbation-Based Moment Equation Approach for Flow in Heterogeneous Porous Media: Applicability Range and Analysis of High-Order Terms. *Journal of Computational Physics*, 188(1), 296-317.

Lu, Z. (2008). *Stochastic Modeling of Unsteady Open Channels and Reliability Analysis*. Hong Kong University of Science and Technology.

Pope, S. (1994). Lagrangian PDF Methods for Turbulent Flows. *Annual Review of Fluid Mechanics*, 26(1), 23-63.

Pope, S.B. (1985). PDF Methods for Turbulent Reactive Flows. *Progress in Energy and Combustion Science*, 11(2), 119-192.

Schaffranek, R.W. (1987). *Flow Model for Open-Channel Reach or Network*, U.S Geological Survey Professional Paper, No.1384.

Schaffranek, R.W., Baltzer, R.A. & Goldberg, D.E. (1981). *A Model for Simulation of Flow in Singular and Interconnected Channels*, US Government Printing Office.

Sett, K., Jeremić, B. & Kavvas, M.L. (2007). Probabilistic Elasto-Plasticity: Solution and Verification in 1D. *Acta Geotechnica*, 2(3), 211-220.

Swain, E.D. & Chin, D.A. (1990). Model of Flow in Regulated Open-Channel Networks. *Journal of Irrigation and Drainage Engineering*, 116(4), 537-556.

Tung, Y.K., Yen, B.C. & Melching, C.S. (2006). *Hydrosystems Engineering Reliability Assessment and Risk Analysis*. McGraw-Hill Company, Inc., New York.

Willis, R., Finney, B.A., McKee, M. & Militello, A. (1989). Stochastic Analysis of Estuarine Hydraulics. *Stochastic Hydrology and Hydraulics*, 3(2), 71-84.

Xiu, D. (2009) Fast Numerical Methods for Stochastic Computations: A Review. *Communications in Computational Physics*, 5(2-4), 242-272.

Yoon, J. & Kavvas, M.L. (2003) Probabilistic Solution to Stochastic Overland Flow Equation. *Journal of Hydrologic Engineering*, 8(2), 54-63.

©2017, IAHR. Used with permission / ISSN 1562-6865 (Online) - ISSN 1063-7710 (Print)

Proceedings of the 37th IAHR World Congress
August 13 – 18, 2017, Kuala Lumpur, Malaysia

A STUDY ON THE EFFECTS OF FUTURE CLIMATE CHANGE ON WATER RESOURCES IN THE TOYOHIRA RIVER BASIN BASED ON A STATISTICAL DOWNSCALING METHOD

YOKO TANIGUCHI[(1)], MAKOTO NAKATSUGAWA[(2)] & KEIGO OTANI[(3)]

[(1)] Muroran Institute of Technology, Muroran, Japan.
17096002@mmm.muroran-it.ac.jp; mnakatsu@mmm.muroran-it.ac.jp; 13021019@mmm.muroran-it.ac.jp

ABSTRACT

This study aims at obtaining basic information toward the development of countermeasures against water resource shortages in cold, snowy areas that may result from global warming. In this study, the influence of global warming is assessed at the local level by using climatic variation projection data that is based on the IPCC Fifth Assessment Report (hereinafter: IPCC AR5) and by using the Toyohira River basin in Hokkaido as the subject area. The Representative Concentration Pathways (RCP) Scenario of the IPCC AR5 consists of four scenarios: RCP 2.6, RCP 4.5, RCP 6.0 and RCP 8.5. The radiative forcing projected for the year 2100 under these scenarios is greater for each successive scenario listed above. In this study, a statistical downscaling method is used to convert 20 km-mesh climate projection data that has been created based on these four RCP scenarios to 1 km-mesh climate projection data. The changes in water resources in the Toyohira River basin in Hokkaido are quantitatively assessed by using the downscaled model. In the Toyohira River basin, the net annual precipitation projected by using the RCP8.5 scenario is about 15% less than that of the projected present-day climate value. It is also projected that, in the year in which the decrease in the net annual precipitation is the greatest, the net annual precipitation is projected to be about half of that of the present climate. Under the RCP2.6 and RCP4.5 scenarios, in which the net annual precipitation is not much different from that of the projected present-day climate, changes are observed in hydrological variables, such as an increase in rainfall's share of total precipitation.

Keywords: Water resources; statistical downscaling; MRI-NHRCM20.

1 INTRODUCTION

This study aims at obtaining basic information toward the development of countermeasures against water resource shortages in cold, snowy areas that may result from global warming. In this study, the influence of global warming was assessed at the local level by using climatic variation projection data that is based on the IPCC Fifth Assessment Report (hereinafter: IPCC AR5) and by using the Toyohira River basin in Hokkaido as the subject area. The Representative Concentration Pathways (RCP) Scenario of the IPCC AR5 consists of four scenarios: RCP 2.6, RCP 4.5, RCP 6.0 and RCP 8.5. The radiative forcing projected for the year 2100 under these scenarios is greater for each successive scenario listed above. In this study, a statistical downscaling method was used to convert 20 km-mesh climate projection data that was created based on these four RCP scenarios to 1 km-mesh climate projection data. The changes in water resources in the Toyohira River basin in Hokkaido were quantitatively assessed by using the downscaled model. The study followed the procedure described here.

i. Downscaling of climate data for the Toyohira River basin was done by using the MRI-NHRCM20, a climate change projection model that was developed by the Japan Meteorological Agency by using the RCP Scenario of the IPCC AR5 (hereinafter: NHRCM20). First, bias correction was done based on the relationship between the present-day climate values projected using NHRCM20 and the measured values; then, this relationship was fitted into the future climate values;
ii. The changes from the present-day climate data and the hydrological data, including snowfall and snowmelt, to those in the future climate were estimated by applying a Long-term Hydrologic Assessment model considering Snow process (LoHAS) and by using the values obtained in i.

2 STUDY METHOD

2.1 Outline of the subject river basin

The Toyohira River, a primary tributary of the Ishikari River (a class A river), flows through the central area of Sapporo, the central city of Hokkaido. The Toyohira River basin accounts for about 86% of the area of Sapporo City. Sapporo uses the Toyohira River as its main water resource. The subject of this study is the catchment basin of the Toyohira River, which is important to Sapporo and its environs with respect to flood control and water utilization. Figure 1 shows the outline of the subject river basin.

 ©2017, IAHR. Used with permission / ISSN 1562-6865 (Online) - ISSN 1063-7710 (Print)

2.2 Analysis data

This study adopted the projection results of NHRCM20, which is a regional climate model that the Japan Meteorological Agency developed by applying the scenarios of the Representative Concentration Pathways (RCPs) of the IPCC AR5. The future projection scenarios used in this study were all four patterns of the RCPs. The following 6 parameters were selected for the projections in this study: precipitation (rainfall and snowfall), sea-level atmospheric pressure, ground surface wind velocity (directions: east-west and north-south), ground surface air temperature, relative humidity, and cloud cover (total and low could covers). The daily data for points of No. 1 to No. 10 on the NHRCM 20 grid, which covers the areas in and near the Toyohira River basin, were extracted and used in the calculation.

As measured values of observed climate data such as air temperature and rainfall, the values published on the websites of meteorological offices and of the Automated Meteorological Data Acquisition System (AMeDAS) were used. In Figure 1, the grid points of NHRCM20 are shown as red circles, and the meteorological observation locations near the Toyohira River basin are shown as "×"s. Table 1 outlines the climatic change projection model.

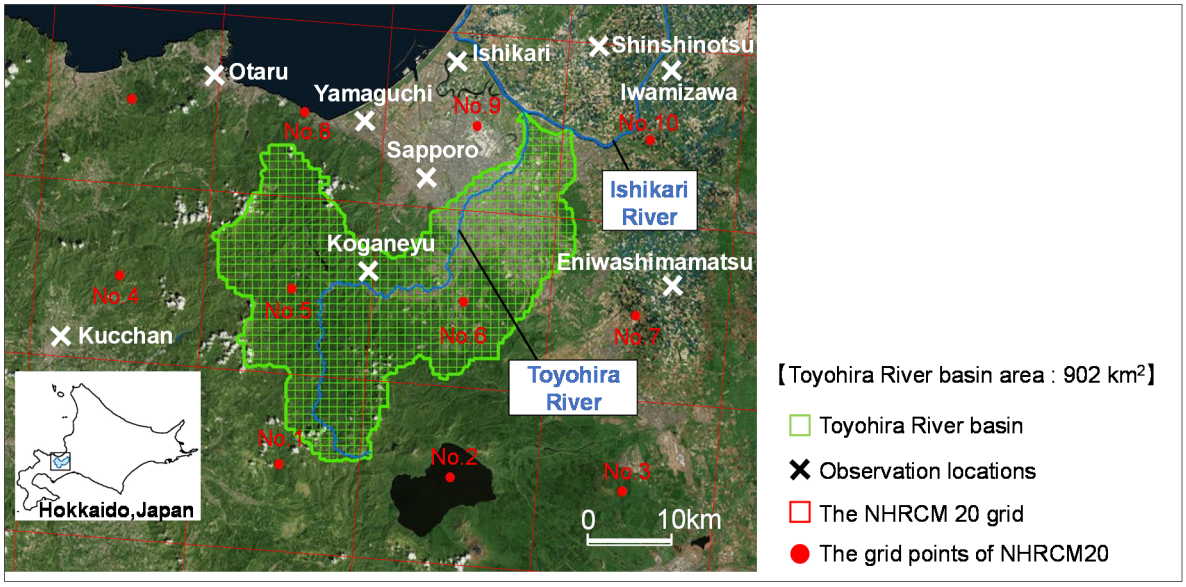

Figure 1. Subject river basin and observation locations.

Table 1. Outline of the climate change projection model.

	MRI-NHRCM20 (regional climate model)	
	Present-day climate	**Future climate**
Spatial resolution	20km	
Prediction period	1984.9～2004.8	2080.9～2100.8
Grid size	211×175 (horizontal) by 40 layers (vertical)	
Future prediction scenario	-	RCP2.6/4.5/6.0/8.5
Sea surface temperature	HadISST	SST1/SST2/SST3
Cumulus convection Scheme	Yoshimura Scheme (YS) Kain-Fritsch Scheme (KF) Arakawa-Schubert Scheme (AS)	

2.3 Statistic downscaling method

The values for the projected present-day climate did not accurately reproduce the measured values. Therefore based on previous study (Ministry of Land, Infrastructure,2016), the values for the above-stated 6 parameters extracted from MRI-NHRCM20 were bias corrected (i.e., the model outputs for monthly data were corrected based on the error rate ranking constant method, whose procedure is described below). Bias correction was done for each of grid point (No. 1 to No. 10) shown in Figure 1. After bias correction, statistical downscaling (hereinafter: SDS) from 20 km-mesh expression to 1 km-mesh expression was done by spatial interpolation. Figure 2 schematically shows the example of the process of bias correction for monthly air temperature and for SDS. The following explanation is based on the flow of this figure.

2.3.1 Spatial interpolation method

To conduct bias correction, it is necessary to compare the projected present-day climate values for the 20 km-mesh grid point to the present observation values for the same point. However, the present observation values, which scatter as point data, do not agree with the output values of the climate model, which are spatial mean values with a constant scale. Therefore, to conduct a comparison between the 20 km-mesh projected

©2017, IAHR. Used with permission / ISSN 1562-6865 (Online) - ISSN 1063-7710 (Print)

present-day climate values and the present observation values, it is necessary to spatially interpolate the present observation values into 1 km-mesh values and average those values in order to obtain the value of 20 km-mesh grid points. The following explains the procedure.

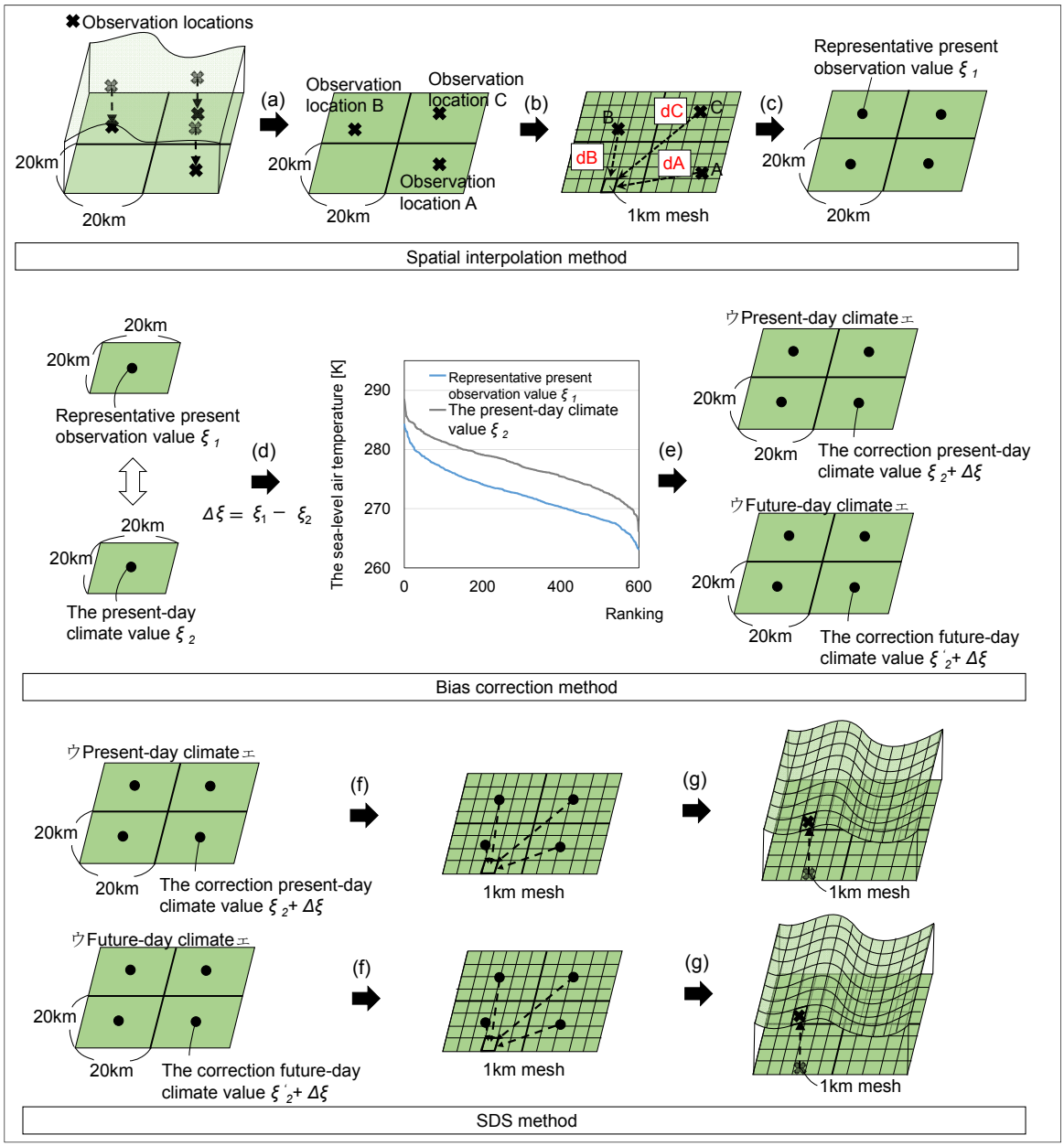

Figure 2. Schematic diagram for statistical downscaling (SDS).

i. Correction is done for the air temperature and atmospheric pressure values in the observed meteorological data for the areas in and around the Toyohira River basin so as to obtain the sea-level air temperature and atmospheric pressure values. The sea-level air temperature is obtained by adding to the observed value the value obtained by multiplying the elevation of the observation point by the temperature lapse rate γ (0.65℃/100m), and the sea-level atmospheric pressure is obtained by adding to the observed value the value obtained by multiplying the elevation of the observation point by the atmospheric pressure lapse rate γ (0.114hpa/100m). Data other than the air temperature and atmospheric pressure are used unmodified;

ii. The spatial structure of the present observation values is estimated based on a previous study (Tomohide et al., 2005) and by using Variogram. When the spatial structure can be expressed in this estimation, the spatial structure is converted into mesh data by using the Kriging method. The results of Variogram estimation of the present observation values are shown in Table 2-1. The mesh values are estimated by using the following Eq. [1], and the weight for this equation is determined by using Eq. [2] to [4]. Eq. [2] is the definition equation of Variogram;

 ©2017, IAHR. Used with permission / ISSN 1562-6865 (Online) - ISSN 1063-7710 (Print)

$$z(X_0) = \sum_{i=1}^{N} \lambda z(X_i) \quad [1]$$

$$y(d) = \frac{1}{2N(d)} \sum_{i=1}^{N(d)} \{z(X_i + d) - z(X_i)\}^2 \quad [2]$$

$$\sum_{i=1}^{N} \lambda_i \gamma(X_i - X_j) = \gamma(X_i - X_0) \quad [3]$$

$$\sum_{i=1}^{N} \lambda_i = 1 \ (i = 1, \cdots, N) \quad [4]$$

where, z (X_0) is the mesh climate value for a given mesh X_0, y (d) is the Variogram, d is the distance between two observation locations, z (X_i) and z (X_j) are the observed data at observation station X_i and that at X_j, respectively, λ_i is the weight coefficient for z (X_i), and N (d) is the number of data set pairs observed at the two observation stations that are d apart from each other.

When a clear relationship between the distance and the Variogram is not found, the distance weighting method shown as Eq. [5] is used to convert the 20 km-mesh data into the 1 km-mesh representation.

$$z(X_0) = \sum_{i=1}^{N} [z(X_i)/d_i] \Big/ \sum_{i=1}^{N} [1/d_i] \quad [5]$$

where, z (X_0) is the mesh climate value at a given mesh X_0, z (X_i) is the observed data at observation station X_i, d_i is the distance between two observation locations, and N is the number of data set pairs observed at the two observation stations that are d_i apart from each other.

Table 2. Variogram projection results of climate parameters (Observation).

Observation	Correlation equation
ground surface air temperature	$y=1.0\times10^{-4}x - 0.7059$
precipitation	$y=4.0\times10^{-4}x + 2.8340$
snowfall	$y=4.0\times10^{-4} - 3.0239$
cloud cover	$y=7.0\times10^{-7}x - 0.0097$
relative humidity	$y=1.0\times10^{-3}x + 3.0239$
sea-level atmospheric pressure	$y=1.6\times10^{-5}x - 0.4131$
ground surface wind velocity	The distance weighting method

y: Variogram, x: the distance between observation locations and any mesh

iii. The present observation values fitted to the 1 km mesh, which was obtained by using the spatial interpolation, are averaged for each 20km mesh of NHRCM20. This averaged value is used as the representative present observation value for the 20km mesh.

©2017, IAHR. Used with permission / ISSN 1562-6865 (Online) - ISSN 1063-7710 (Print)

Table 3 Variogram projection results of climate parameters (NHRCM20).

NHRCM20	Correlation equation				
	Present-day climate	**RCP2.6**	**Rcp4.5**	**RCP6.0**	**RCP8.5**
ground surface air temperature	$y=2.0\times10^{-5}x'+0.1632$	$y=2.0\times10^{-5}x'+0.1928$	$y=2.0\times10^{-5}x'+0.1993$	$y=2.0\times10^{-5}x'+0.2262$	The distance weighting method
precipitation	$y=3.0\times10^{-4}x'-2.1700$	$y=4.0\times10^{-4}x'-1.9797$	$y=4.0\times10^{-4}x'-2.2168$	$y=4.0\times10^{-4}x'-1.7456$	$y=5.0\times10^{-4}x'-1.7732$
snowfall	$y=2.0\times10^{-4}x'-3.9473$	$y=3.0\times10^{-4}x'-3.8889$	$y=3.0\times10^{-4}x'-4.2392$	$y=2.0\times10^{-4}x'-3.5195$	$y=3.0\times10^{-4}x'-4.3480$
total could covers	$y=3.0\times10^{-7}x'-0.0013$	$y=3.0\times10^{-7}x'+0.0022$	$y=3.0\times10^{-7}x'+0.0021$	The distance weighting method	The distance weighting method
low could covers	$y=2.0\times10^{-6}x'+0.0424$	$y=1.0\times10^{-6}x'-0.0001$	$y=3.0\times10^{-7}x'+0.0240$	$y=9.0\times10^{-7}x'+0.0084$	$y=9.0\times10^{-7}x'+0.0068$
relative humidity	$y=3.0\times10^{-4}x'+6.7410$	$y=3.0\times10^{-4}x'+7.4018$	$y=3.0\times10^{-4}x'+8.1625$	$y=3.0\times10^{-4}x'+6.9274$	The distance weighting method
sea-level atmospheric pressure	$y=5.0\times10^{-6}x'-0.0592$	$y=6.0\times10^{-6}x'-0.0618$	The distance weighting method	$y=6.0\times10^{-6}x'-0.0627$	$y=6.0\times10^{-6}x'-0.0612$
ground surface wind velocity	The distance weighting method	The distance weighting method	The distance weighting method	The distance weighting method	The distance weighting method

y: Variogram, x': the distance between the grid point of NHRCM20 and any mesh

2.3.2 Bias correction method

i. The monthly daily data of present observation values and those of the projected present-day climate values for each NHRCM20 grid point for each month are sorted in descending order. The ground surface wind velocity for NHRCM20 takes the square root of the sum of squares of the wind velocity in the horizontal (east-west) direction and that in the vertical (north-south) direction. The horizontal axis of the graph in Figure 2 shows the rank of data points. The total number of data points (about 600) for a certain month will be obtained by multiplying the number of days in that month by 20 years (1984 to 2004). The ranks of data points go from 1st to about 600th. Based on the ranked daily data points, the error ranking $\Delta\xi$ of the climate value ξ for the sea-level air temperature and that for the sea-level atmospheric pressure are obtained as the difference between the present observation values and the projected present-day climate values ($\Delta\xi=\xi_1-\xi_2$). The error rankings for other meteorological parameters are obtained as the ratio of the present observation values to the projected present-day climate values ($\Delta\xi=\xi_1/\xi_2$);
ii. By assuming that $\Delta\xi$, which has been obtained based on the projected present-day climate value, is the same value under the future climate, the projected present-day climate value and the future climate value for each rank are corrected by using $\Delta\xi$.

2.3.3 SDS method

The bias-corrected climate change projection data were downscaled by using the SDS and dividing the dam basins into 1 km meshes based on a study (Kazuto and Makoto, 2011). The procedure is described here.

i. The SDS is done for each 1 km mesh for the Toyohira River basin by using the bias-corrected 20 km mesh values (No. 1 to No. 10) in Figure 1. In the above, the spatial structure of NHRCM20 is estimated by using Variogram. When a correlation is found between the Variogram and the distance, the Kriging method is used for downscaling. When a correlation is not found between them, a distance weighting method is used for downscaling. Table 2-2 shows the projection results of the Variogram for the present-day climate and future climate of NHRCM20. It is assumed that the Variogram, which expresses the spatial structure of climatic factors, changes according to each climate stage;
ii. After the SDS was done on the bias-corrected project climate change data to represent the 1 km mesh on the MRI-NHRCM20 grid, the correction to obtain the temperature for 1 km-mesh grid points was done by subtracting the value obtained by multiplying the elevation of each 1 km mesh by the temperature lapse rate γ (0.65℃/100m) from the sea-level temperature, and the correction to obtain the atmospheric pressure for 1 km-mesh grid points was done by subtracting the value obtained by

 ©2017, IAHR. Used with permission / ISSN 1562-6865 (Online) - ISSN 1063-7710 (Print)

multiplying the elevation of each 1 km mesh by the atmospheric pressure lapse rate γ (0.114hPa/m) from the sea-level atmospheric pressure. The other climate valesξ are used as is, without correction on elevation.

2.4 Heat, water budget analysis model (LoHAS)

This study used the LoHAS analytical model, whose appropriateness of accuracy in hydrological estimation was verified in a previous study (Kazuto and Makoto, 2011). Based on the snowfall and snowcover conditions, daily hydrological amounts were calculated for each mesh. For LAI, bulk transfer coefficient, evaporation efficiency, albedo, and light reception coefficient ratio, the values set by their previous study (Hisashi and Makoto., 2002) were used.

3 RESULTS AND DISCUSSIONS

3.1 Examination of the validity of the SDS

A comparison was done between the average of 20 km-mesh values after bias correction and the average of 1 km-mesh value after SDS. This comparison found that appropriate downscaling was done by the SDS method used in this study, because the error rate was 1%, which means that the difference between the two averaged values is very small.

3.2 SDS results

The climate data of the 1 km mesh for the projected present-day climate and those for the future climate, which were projected by using the SDS on the Toyohira River basin, are shown in Figure 3. It is understood from Figure 3 that the decrease in snowfall in flat land areas is greater than that in mountainous areas under the RCP8.5 scenario, whose radiative forcing is high, and that the increase in the air temperature is greater in flat land areas than in mountainous areas.

The climate data of the RCP8.5 scenario, which was obtained by using SDS on the Toyohira River basin, and the climate data of projected present-day climate are shown in Figure 4. A monthly average was determined for each data set, and these averages were plotted as curves on the graph. The two temperature curves are almost parallel, and the values of the SDS projection are about 4℃ higher than the values projected under the RCP8.5 scenario all through the year. The rainfall shows small changes throughout the year; however, the snowfall shows a great decrease in the period from November to February.

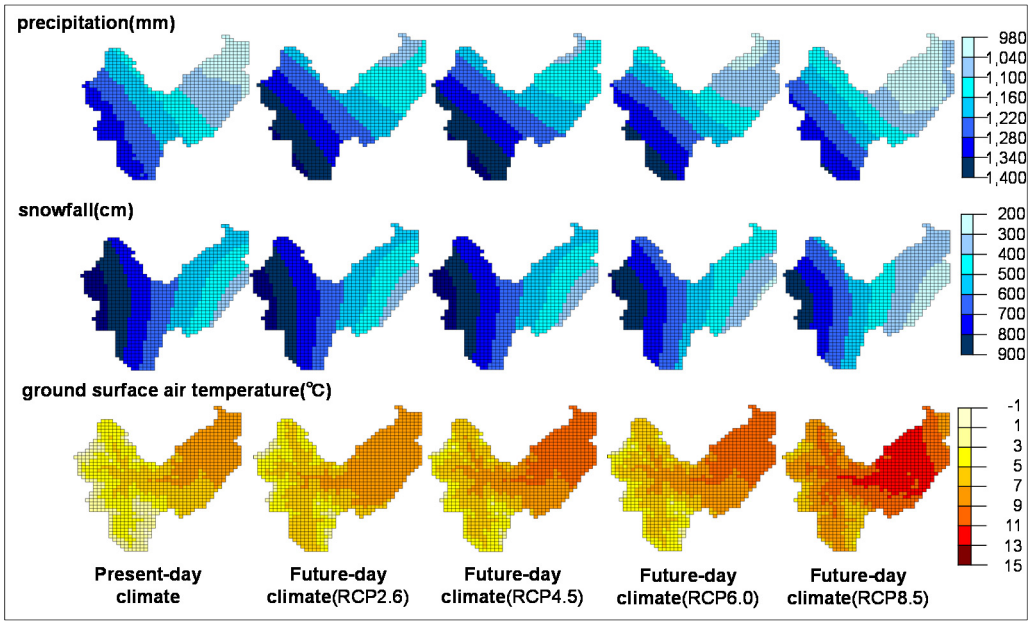

Figure 3. Spatial distribution of the annual average climate parameters in the subject basin after the SDS.

©2017, IAHR. Used with permission / ISSN 1562-6865 (Online) - ISSN 1063-7710 (Print)

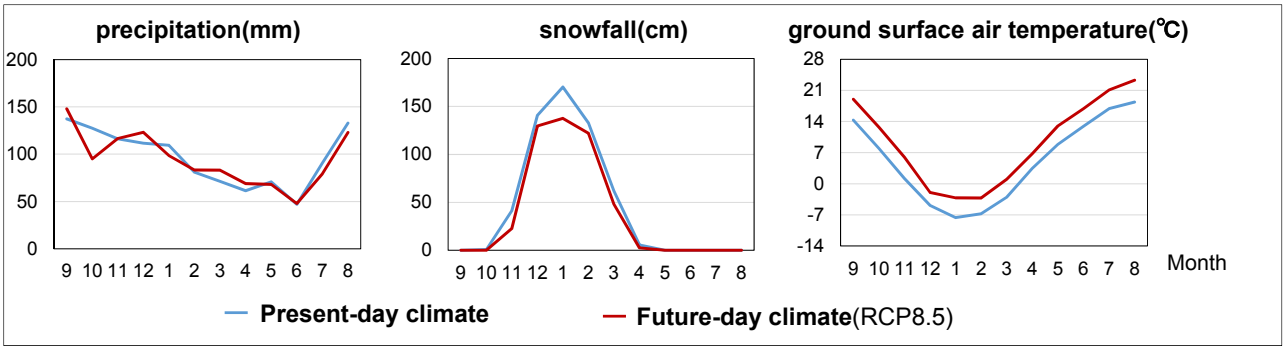

Figure 4. Monthly average values determined by SDS.

3.3 Assessment of the amount of water resource in the river basin

The net annual precipitation estimated by using LoHAS is shown in Table 3. From Table 3, it is understood that the average net annual precipitation under the RCP8.5 scenario decreases by about 15%, from 1,102 mm in the present climate to 939 mm. Under the RCP8.5scenario, the smallest net annual precipitation in one year is 563mm, which is about a 50% decrease from that of the present climate. The largest decrease in net annual precipitation under the RCP8.5 scenario from that of the present climate is calculated as 539 mm× 550 km^2 (the area of the catchment at the Ishiyama point near the water intake point on the Toyohira River) ≒0.3 billion m^3/year. When this value is compared with the present yearly amount of domestic water used by the citizens of Sapporo, which is calculated as 200 L / person / day × 1.9 million×365 days≒0.14 billion m^3/year, it is understood how greatly the decrease in net annual precipitation would affect the citizens' lives. Under the RCP2.6 and RCP4.5 scenarios, in which the net annual precipitation does not decrease, rainfall's share of precipitation increases, and rainfall's share of precipitation under the RCP8.5scenario increases from 0.37 of the present climate to 0.60. The future increase in rainfall's share of precipitation means that a portion of the snowfall will change to rainfall, whereby the water storage effect of snowfall and snowcover will be lost, which will bring about adverse conditions with regard to the stability of the water resource. Furthermore, the maximum value of rainfall under the RCP8.5 scenario is 1,622 mm, which is about 3 times the minimum rainfall (552 mm). Because of this great difference between the greatest and the smallest rainfalls, it is feared that the area may have drastic changes in climate not only in terms of changes in average rainfalls but also in terms of years of marked droughts and floods during the 20-year period.

The changes in the monthly average of snowfall and in the maximum water equivalent snowcover under the RCP8.5 scenario and those in the projected present-day climate during the 20-year period are shown in Figure 5. From this figure, it is found that the period of snowfall during the year is shorter under the RCP8.5 scenario than under the projected present-day climate, and the water equivalent snowfall is similarly smaller under this scenario than under the projected present-day climate. The maximum water equivalent snowcover under this scenario is about 120 mm less than under the projected present-day climate value in March, which is the period when the water equivalent of snow cover peaks. The water equivalent snowfall for the RCP8.5 scenario during the period from December to March is not much different from that of the projected present-day climate; however, the maximum water equivalent of snowcover for the RCP8.5 scenario during the same period is found to be much smaller than that of the projected present-day climate. The above findings suggest that, in the future, snowmelt will accelerate but snowfall will increase.

 ©2017, IAHR. Used with permission / ISSN 1562-6865 (Online) - ISSN 1063-7710 (Print)

Table 3. Projected water budget of the Toyohira River basin under each climate stage.

		Rainfall	Water equivalent snowfall	Rainfall's share of precipitation	Snowmelt	Evapotrans-piration	Annual maximum water equivalent snow cover	Net annual precipitation
		Ⓓ	Ⓔ	①/①+Ⓔ	Ⓕ	Ⓖ	Ⓗ	⑥=①+②-Ⓖ
Present-day Climate	Average	563	974	0.37	930	436	397	1,102
	Maximum	807	1,128	0.42	1,050	470	508	1,431
	Minimum	399	801	0.33	767	412	248	836
	Standard deviation	136.6	91.4	0.60	92.0	17.0	61.2	182.2
Future-day Climate (RCP2.6)	Average	676	600	0.53	887	554	395	1,158
	Maximum	1,163	808	0.59	1114	594	569	1,568
	Minimum	421	454	0.48	668	504	258	841
	Standard deviation	194.5	92.8	0.68	138.9	24.5	94.3	238.3
Future-day Climate (RCP4.5)	Average	726	884	0.45	856	469	367	1,141
	Maximum	994	1163	0.46	1,109	488	498	1,357
	Minimum	402	692	0.37	650	433	233	819
	Standard deviation	153.6	132.9	0.54	139.2	15.9	79.3	170.4
Future-day Climate (RCP6.0)	Average	896	644	0.58	628	550	325	990
	Maximum	1,226	846	0.59	846	577	498	1,304
	Minimum	553	483	0.53	488	529	217	531
	Standard deviation	171.9	103.3	0.62	107.6	14.2	83.0	230.9
Future-day Climate (RCP8.5)	Average	897	601	0.60	592	560	275	939
	Maximum	1622	808	0.67	789	598	483	1,735
	Minimum	552	454	0.55	435	517	174	563
	Standard deviation	265.7	92.8	0.74	93.5	24.6	86.1	271.5

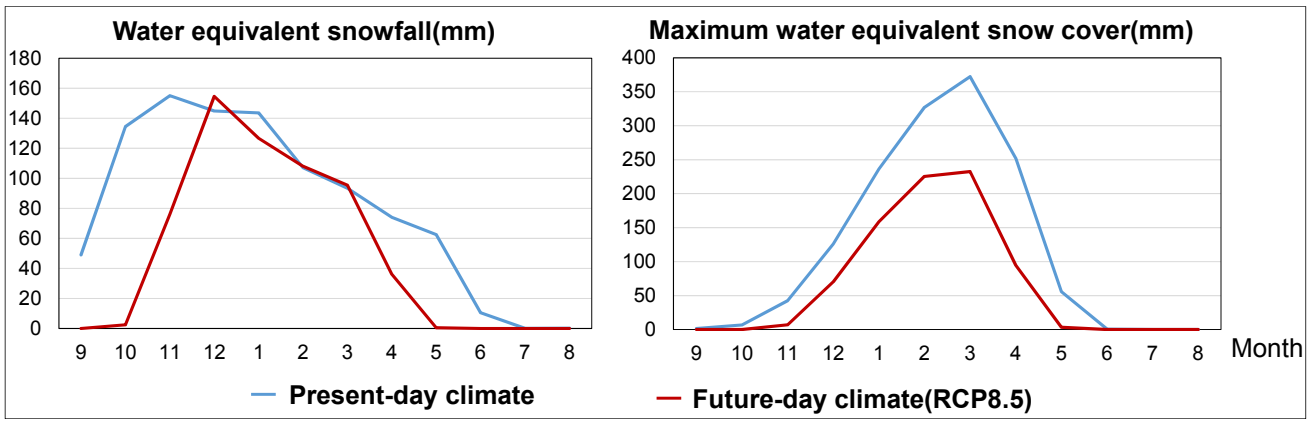

Figure 5. Changes in the monthly average water equivalent snowfall and the monthly average water equivalent of snow cover.

©2017, IAHR. Used with permission / ISSN 1562-6865 (Online) - ISSN 1063-7710 (Print)

The deviations in the annual maximum water equivalent of snow cover, which were obtained by subtracting the annual maximum water equivalent of snowfall of the future climate from that of the projected present-day climate, are shown in Figure 6 as plane distributions for the Toyohira River basin. Particularly under the RCP6.0 scenario, the deviations in the mountainous areas with high elevations are great. Under the RCP8.5 scenario, the annual maximum water equivalent of snowcover in the total area of the Toyohira River basin tends to be at least 100 mm less than that of the projected present-day climate.

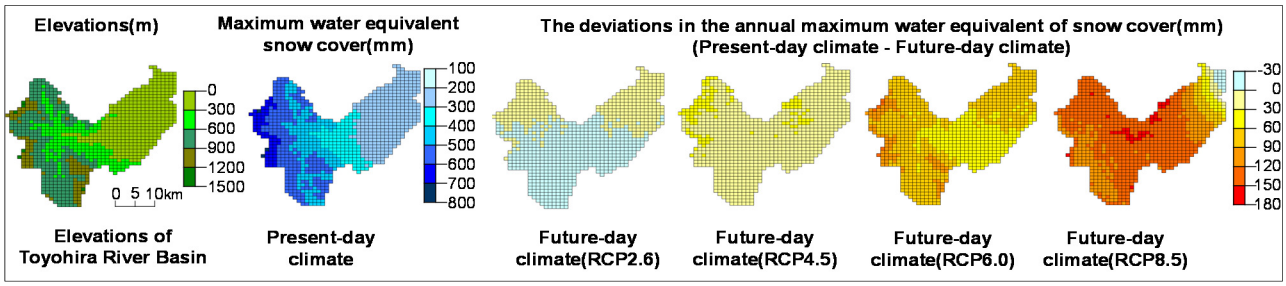

Figure 6. Elevations in the Toyohira River basin and the spatial distribution of the maximum water equivalent snowcover of each climate stage in that basin.

4 CONCLUSIONS

The results of this study are as follows:

i. When using the SDS method, the average values before the application of SDS and those after such application were compared. The comparison found that the error rate was about 1%. This comparison leads the authors to consider that the use of the SDS method in this study was appropriate;

ii. The authors were able to project the changes in the future climate in the subject area by using NHRCM20, which are the projection data based on the RCP scenarios of IPCC AR5 and by applying the SDS method. The changes in the hydrological variables of the river basin level that are predicted to occur with the changes in the future climate were able to be projected by using the Long-term Hydrologic Assessment model considering Snow process (LoHAS);

iii. In the Toyohira River basin, the net annual precipitation projected by using the RCP8.5 scenario was about15% less than that of the projected present-day climate value. It was also projected that, in the year in which the decrease in the net annual precipitation is the greatest, the net annual precipitation is projected to be about half of that of the present climate. Under the RCP2.6 and RCP4.5 scenarios, in which the net annual precipitation is not much different from that of the projected present-day climate, changes were observed in hydrological variables, such as an increase in rainfall's share of total precipitation.

ACKNOWLEDGEMENTS

This study was done with a grant from the Social Implementation Program on Climate Change Adaptation Technology (SI-CAT), a project of the Ministry of Education, Culture, Sports, Science and Technology (MEXT). Mr. Keisuke Kudo of the River Environment Division, Docon Co., Ltd., provided materials and advice on analyses using LoHAS. The authors would like to express their appreciation to the people and organizations mentioned above.

REFERENCES

Hisashi, K. & Makoto, N. (2002). Estimations of Snow Pack Condition and Evapotranspiration Based on Water and Heat Balances in Watersheds, *Monthly report of the Civil Engineering Research Institute of Hokkaido*, 588, 19-38.

Kazuto, K. & Makoto, N. (2011). Dam Management Based on an Understanding of the Effects of Dam Management on Water Use in Snowy Regions under Climatic Changes. *Advances in River Engineering*, *JSCE*, 17, 287-292.

Ministry of Land (2016). Infrastructure, Transport and Tourism. The 8th Examination Committee for Developing Measures against Climate Change in the Water Resource Field, Reference Material 3, *http://www.mlit.go.jp/mizukokudo/mizsei/mizukokudo_mizsei_fr2_000002.html* (Visited on 2016/12/8).

Tomohide, U., Makoto, N. & Keisuke, K. (2005). Quantitative Analysis of the Hydrologic Process in the Ishikari River Catchment Area, *Monthly report of the Civil Engineering Research Institute of Hokkaido*, 628, 18-34.

 ©2017, IAHR. Used with permission / ISSN 1562-6865 (Online) - ISSN 1063-7710 (Print)

A MODEL BASED APPROACH FOR DEALING WITH UNCERTAINTIES IN URBAN WATER SECURITY

FEBYA NURNADIATI[(1)], JOS TIMMERMANS[(2)], IWAN K. HADIHARDAJA[(3)] & WIL THISSEN[(4)]

[(1,2,4)] Delft University of Technology, Delft, The Netherlands,
F.N.Kusnadi-1@tudelft.nl
[(1,3)] Bandung Institute of Technology, Bandung, Indonesia,
hadihardaja@si.itb.ac.id

ABSTRACT

Urban water security indexes evaluate and compare the status of urban water systems. For example, the Asian Water Development Outlook (AWDO) Framework facilitates the assessment and comparison of the status of urban water systems of different cities based on four criteria: 1) piped urban water supply access; 2) urban wastewater collection; 3) economic damage due to floods and storms; and 4) river health. Changes in the urban water security index of a specific city are influenced by external developments like economic and population dynamics and shaped by urban water management as implemented by municipal authorities and contingent on regional or even national developments in water management, which involves identification of vulnerability and analysis of strategies under different possible futures in interaction with regional and national conditions. This complex planning challenge can be supported through Adaptive Urban Water Security Management. This paper describes the first phase in the development of this plan, the development of a fast and integrated model that can be used to explore the influence of deep uncertainty and regional interactions on urban water security. The model adopts system dynamic as its approach and use VenSim as the software platform. The model is functionally defined in terms of scenarios, policy actions, outcome indicators, and relevant processes that should be simulated. Output of the model shows the changes of the urban water security index over time in transient scenarios that include external scenarios of economic development and climate change, regional policies, investment in urban water management and autonomous responses. Three scenarios that reflect different uncertainties are used to illustrate the dynamics of the water security index of greater Jakarta.

Keywords: Model; urban water security; uncertainties; system dynamic; water management.

1 INTRODUCTION

Concept of water security has been developed from the 1990s onward and evolved significantly since then. It is discussed by policy makers and academics, including from Global Water Partnership, The World Economic Forum, UNESCO's Institute for Water Education, and Asia-Pacific Water Forum in 2007 (Cook and Bakker, 2012). Grey and Sadoff (2007) has the most widely accepted definition of water security, as " the availability of an acceptable quality and quality of water for health, livelihoods, ecosystems and productions, coupled with an acceptable level of water-related risks to people, environments, and economies". However water security is also about resolving conflict of water dispute and the tension between the various stake holders who compete for limited resources (Van Beek and Arriens, 2014), and also promotes environmental protections as well as social justice (Global Water Partnership, 2000).

Assessment of water security is important and need more attention in the years ahead. Water security indexes evaluate and compare the status of the water system (Cook and Bakker, 2012). For the example, the Asian Water Development Outlook (AWDO) Framework facilitates the assessment and comparison of the status of urban water systems based on four criteria: 1) piped urban water supply access; 2) urban wastewater collection; 3) economic damage due to floods and storms; and 4) river health (Asian Development Bank, 2013). On the other hand, managing water is also critical for modern economies (Asian Development Bank, 2013). The development of water management involves identification of vulnerability and analysis of strategies under different possible futures. The future is, however, more complex and dynamic, surrounded by large uncertainties.

A model is needed to cope the uncertainties of socio-economic, political, and also policy changes to help assessing water security condition. The model should be comprehensive integrate the water security indicators and water system. An integrated model is developed to explore the influence of possible uncertain futures to urban water security indexes. The model adopts system dynamic as its approach and use VenSim as the software platform. System dynamic approach is applicable because it clarifies the problem under study, the behavior of the result model, and the real-world effects of potential solutions (Akhtar, 2011). The process of creating the model helps clarify the problems and assumptions of the way of the explicit system works.

©2017, IAHR. Used with permission / ISSN 1562-6865 (Online) - ISSN 1063-7710 (Print)

Sehlke and Jacobson (2005) and Akhtar (2011) mention that system dynamic model allow to conduct multi-scenario, multi-attribute analyses that resulting in relative comparisons over time of many strategies.

2 CASE STUDY

This model is a simplified model to experiment with preliminary idea and elaborate the method and framework. The real case is located in Jakarta Province, Indonesia.

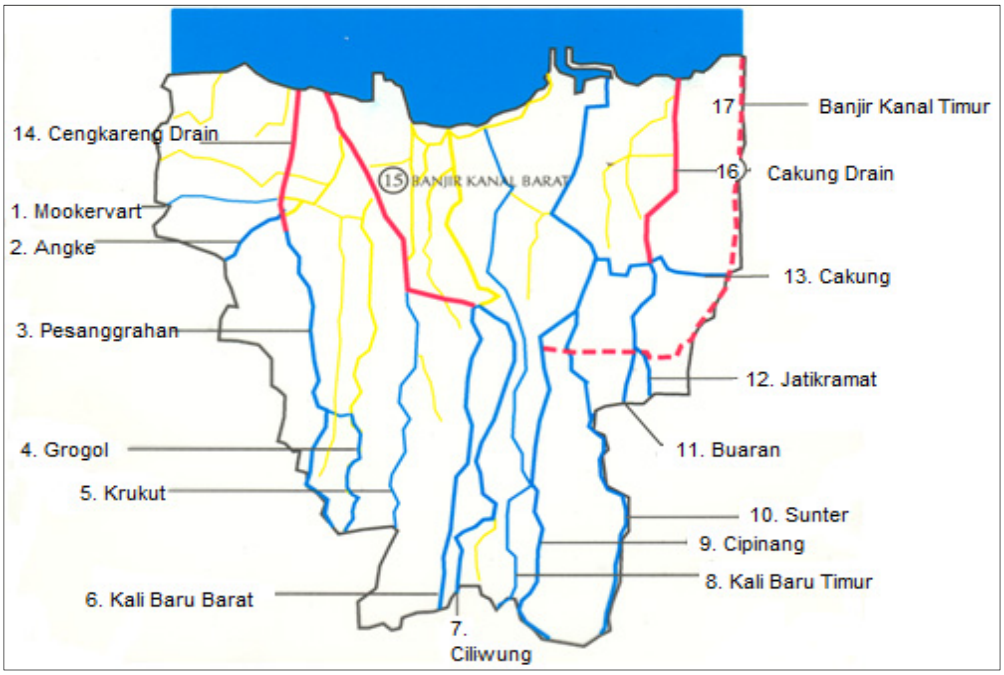

Figure 1. Map of 13 rivers in Jakarta, Indonesia (Source: PUSAIR).

Based on the data from PAM Jaya (public water company in Jakarta), in 2015 piped water connection is only able to serve in average 60.33% of the total water demand (PAM Jaya, 2015), while the rest of 38.7% is utilizing groundwater, surface water, and rainfall. Groundwater extraction is one of dominant causes of land subsidence in Jakarta (Abidin et al., 2011). So that massive uses of groundwater accelerate land subsidence in some areas in Jakarta and could cause wider expansion of (inland and coastal) flooding areas. (Abidin et al., 2011).

Floods are a recurrent problem and become a threat to the citizens of Jakarta every year, both in term of river flooding and coastal flooding. It is noted that in 2002, 2007, 2013, 2014, and 2015, there were major floods that have caused large damage. An overview of these findings is shown in Table 1. The impacts of flooding have increased in recent decades because of a large number of drivers, both physical and socio-economic in nature (Budiyono et al., 2015).

Table 1. Comparison of Jakarta flood damage in 2002 and 2007 (Bappenas, 2007).

Description	2002	2007
Precipitation	361.7 mm (mean Jakarta in 10 days)	327 mm (mean Jabodetabek in 6 days)
Inundation area	331 km^2 in Jakarta	454,8 km^2 in Jakarta
Loss of life	80 people	79 people (status of 12 February 2007)
Evacuee	381 people	590,407 people (status of 6 February 2007)
Direct losses	IDR 5.4 trillion (2002 values)	IDR 5.2 trillion (2002 values)
Indirect losses	IDR 4.5 trillion (2002 values)	IDR 3.6 trillion (2002 values)

During this time, 97% of raw water supply in Jakarta come from outside Jakarta, namely from Jatiluhur Dam, Cisadane, and Cikokol River, and only 3% were supplied from inside Jakarta. It is caused by the water quality of rivers and reservoirs in Jakarta which are generally heavily polluted (DKI Jakarta, 2014).

3 METHODOLOGY

System Dynamic (SD) is a method to describe, model, simulate, and analyze dynamically complex issues and/ or system in terms of process, information, organizational boundaries and strategies (Pruyt, 2013). System dynamic model the assumed/ previous main structure of largely closed real-world system. In SD term, a causally closed system is a system which controls action based on the previous action results (Forrester, 1994; Pruyt, 2013) which means that closed system endogenously generate their own behavior

 ©2017, IAHR. Used with permission / ISSN 1562-6865 (Online) - ISSN 1063-7710 (Print)

over time (Forrester, 1994; Pruyt, 2013). On the other hand, open systems performance is not influenced by their own pas performance, but by the external/ exogenous events or driving force. SD is often used to deal with complex issues that are not only fully closed nor entirely closed.

In SD model, diagrammatic distinctions are made between different types of variables (stocks, flows, auxiliaries, parameters, and constants). Stock variables (□) are integral equations of the flow, flow variables (⧑) and auxiliary variables (no symbol or O) are equations of other variables and parameters/ constants, and parameter/ constants assume (constant) values over a simulation run.

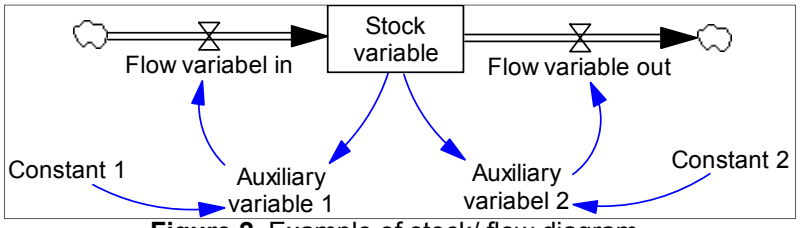

Figure 2. Example of stock/ flow diagram.

System dynamic approach is applicable because it clarifies the problem under study, the behavior of the result model, and the real-world effects of potential solutions (Akhtar, 2011). The process of creating a simulation model helps clarify the problems and makes assumptions about the way the system works explicit. Sehlke and Jacobson (2005) and Akhtar (2011) mention that system dynamic model allow to conduct multi-scenario, multi-attribute analyses that resulting in relative comparisons over time of many strategies. Therefore, this research used system dynamic approach to studies the dynamic, interrelations, and information feedbacks in water system over time.

The model used scenarios and it can be used in different ways (adopted from Haasnoot (2009); without response, with response of individual users, with response of groups, and or with automatic response by using response rules to develop many transient scenarios. However, for this simplified model, automatic response is adopted to experiment the preliminary idea and elaborate the method and framework.

4 MODEL DESCRIPTION

4.1 Model boundary

In SD term, a causally closed system is a system which controls action based on the previous action results (Forrester, 1968; Pruyt, 2013) which means that closed system endogenously generate their own behavior over time because (Forrester, 1994; Pruyt, 2013). On the other hand, open systems performance is not influenced by their own pas performance, but by the external/ exogenous events or driving force. A description of which variable area treated endogenously and exogenously in the model is presented below.

Table 2. Model boundary.

Endogenous	Exogenous
Piped water supply	Water resources
Household water demand	Population
Pipe water and wastewater infrastructure	GDP
Transition from not connected household to connected household	Investment

4.2 Model setting

A simplified model simulates a 50-year period. Several variables have used the real data of Jakarta, but the result has been synchronized to the historical planning and water security index of Jakarta. The model was simulated using time unit of years and used the Euler method. The model is constructed using VenSim Professional system dynamic software.

4.3 Sub-model

Integrated model consists of five sub-models: a simple population sub-model which is linked to water consumption sub-model and wastewater sub-model, piped water production and distribution, and investment sub-model. Each sub-model is described in detail in the following section. These descriptions provide an overview of each sub-model relation.

4.3.1 Population sub-model

This sub-model calculates the number of persons which is influenced by “births” and “deaths” (see Figure 2). More persons will influence the total number of water demand and also number of the water used. More water used means more capacity of water treatment is required.

©2017, IAHR. Used with permission / ISSN 1562-6865 (Online) - ISSN 1063-7710 (Print)

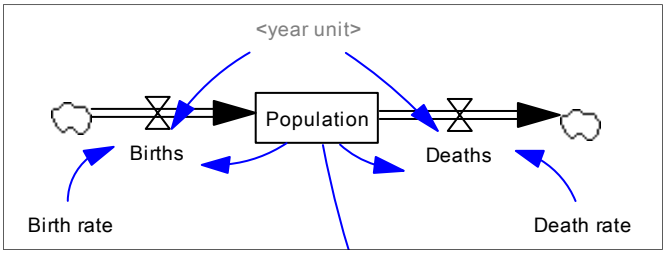

Figure 3. Population Sub-model.

4.3.2 Water production and distribution sub-model

The water production and distribution is relatively simple. The piped water supply system is not modelled as auxiliary variable and not stock variable, so the water which is not used will be directly wasted back to the river. The piped water supply is influenced by water resources and production capacity, while actual water delivered to the consumer, however, is influenced by real loss (lost water caused by the infrastructure condition) and commercial lost (lost water caused by administration issue). The difference of actual water supply to the consumer and actual used of piped water is calculated as Non Revenue Water (NRW).

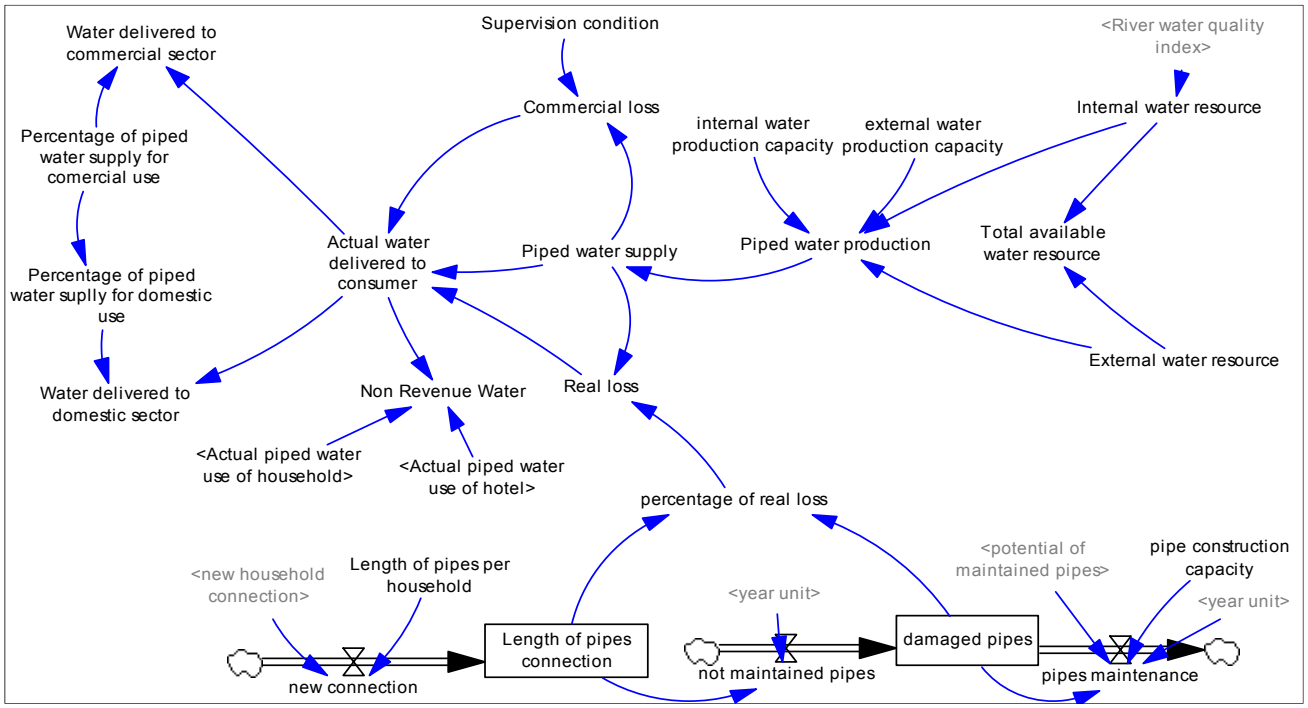

Figure 4. Water production and distribution sub-model.

4.3.3 Water consumption sub-model

The water consumption sub-model represents the actual water consumption of household. It consists of household calculation within 2 stock variables, household without piped water connection and household with piped connection. Household without piped water connection is modelled to use groundwater while household with piped connection has a choice to use both groundwater and piped water. The groundwater use and piped water consumption are influenced by piped water supply, water price, and willingness to pay for the piped water.

4.3.4 Wastewater sub-model

The wastewater sub-model represents the number of wastewater connection and number of treated and untreated water. Wastewater connection of household consists of two stock variables, households which are connected and not connected to wastewater system. The wastewater of unconnected households will directly discharge to the river, while wastewater of connected households will be treated in the wastewater treatment plan. The increment of wastewater treatment capacity will increase in line with the number of the connection. Both of the connection and wastewater treatment capacity will influence the river water quality based on the treated and untreated wastewater released to the river.

 ©2017, IAHR. Used with permission / ISSN 1562-6865 (Online) - ISSN 1063-7710 (Print)

4.3.5 Investment sub-model

The investment is very simple. It represents the investment of new piped water connection, hard maintenance of piped connection, and also new wastewater connection and wastewater treatment plan. The source of the investment budget comes from the profit percentage of piped water company and also direct investment, i.e. loan or government assistance. However, the construction of new connection will not only influenced by the amount of the investment but also construction capacity of each works.

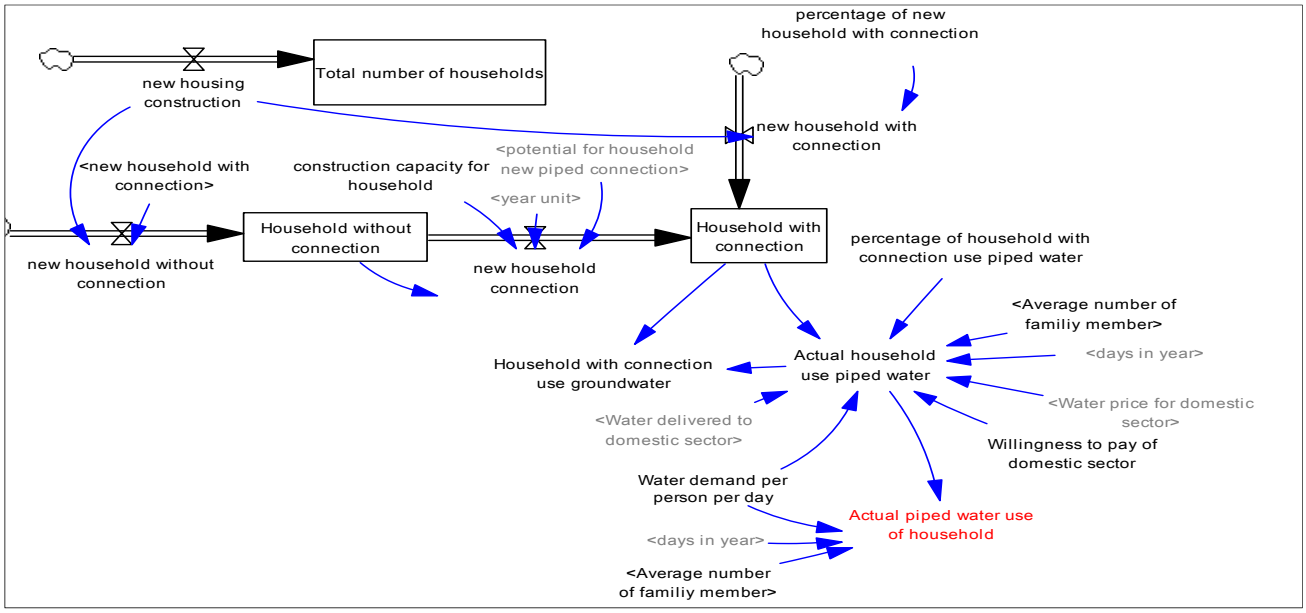

Figure 5. Water consumption sub-model.

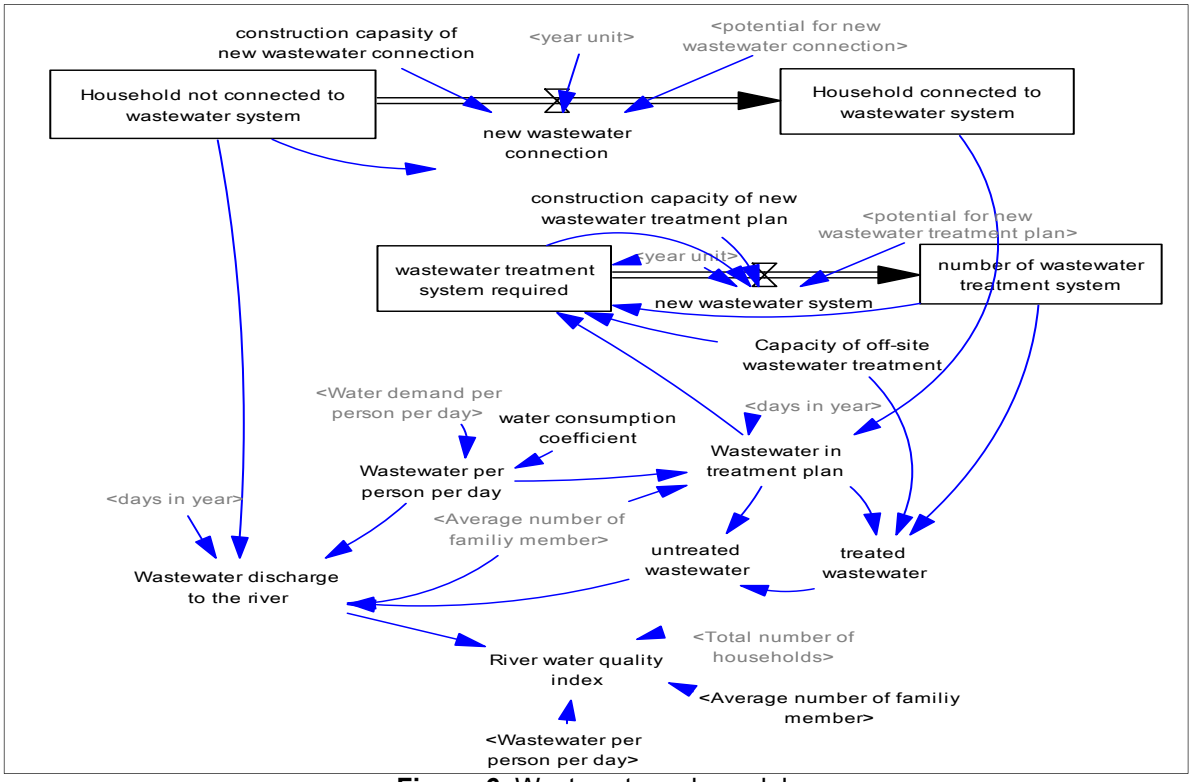

Figure 6. Wastewater sub-model.

4.4 Urban water security assessment

The integrated model has one “supplementary” variable that has no causal effect on any other variable to assess the water security index. The variables are “Urban water security index”. The formulation of this index is adopted from Asian Development Bank (2013), based on the performance of four drivers:

i. Piped water supply access (% of population): index 1-5,
ii. Urban wastewater collected (% of population): index 1-5,

©2017, IAHR. Used with permission / ISSN 1562-6865 (Online) - ISSN 1063-7710 (Print)

iii. Economic damage due to floods (% of GDP) : index 1-5,
iv. River health: index 0-1.

4.5 Model verification and validation

The integrated model was tested through process of "model debugging" to trace and correct errors preventing the model from simulating properly. It was also verified to achieve consistency between model conceptualization and specification. Unit consistency and numerical accuracy of simulation have been checked. Through the model-building process and simulation runs, structural errors have been identified and addressed iteratively.

This model is a simplified model to experiment with preliminary idea and elaborate the method and framework. It used real data of Jakarta for several variables and adjustment number for the rest of them, so for the validation process, the result of this simplified model still cannot be compared to real data. The validation test is done on the next stage of the case study model.

5 RESULTS

The results are summarized in this section by using the outputs from the model. In Figure 7 below, the urban water security index changes over time due to the condition of water supply, wastewater, drainage, and river health. Condition 0 represents the condition when we "DO NOTHING" to improve the water security index, while condition 1 and 2 are conditions when there are policy actions and investment to support the water security improvement:

1. Condition 1: the policy and investment support the improvement of piped water connection and distribution and hard maintenance,
2. Condition 2: the policy and investment support the improvement of the piped water connection, hard maintenance, and distribution, and also wastewater treatment.

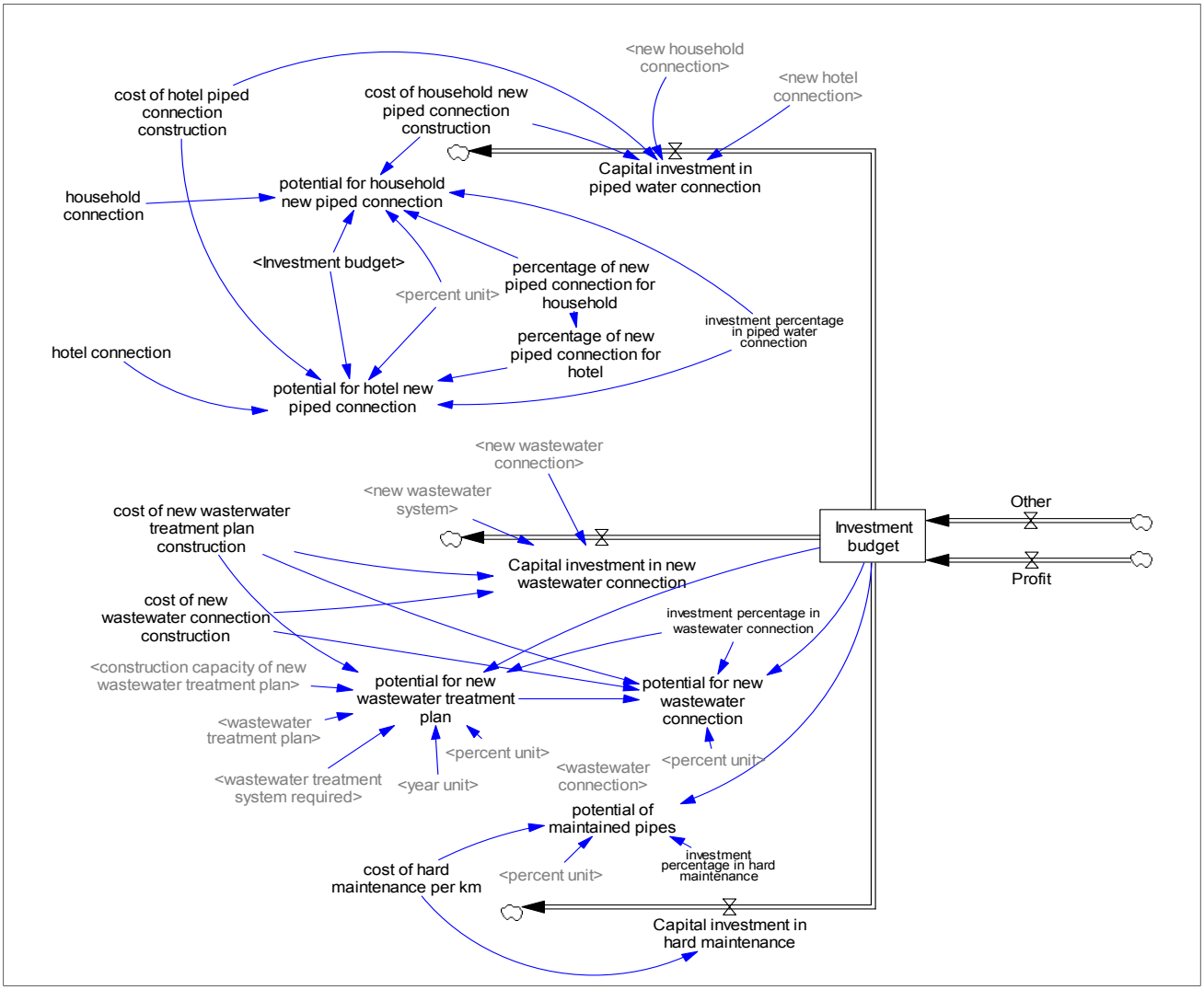

Figure 7. Investment sub-model.

 ©2017, IAHR. Used with permission / ISSN 1562-6865 (Online) - ISSN 1063-7710 (Print)

The Figure 8 below shows the changes of water consumption. In year-5, for both Condition 1 and 2, there is new policy to increase the percentage of water price subsidies, so the water price is below the willingness to pay of the household. The effect is water consumption increase from only 20% on year-0 to year-5, to around 40% on year-6 and continuously increase.

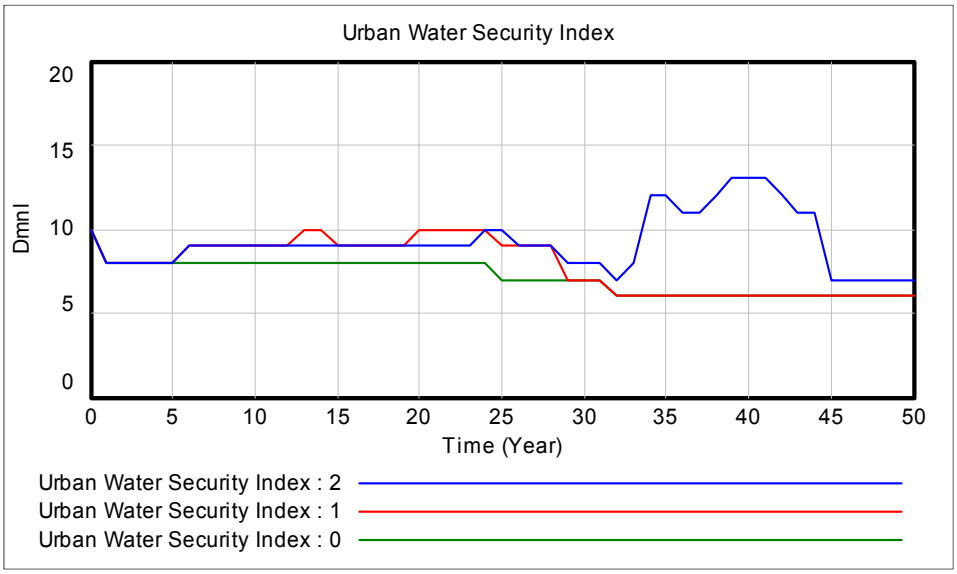

Figure 8. Urban Water Security Index (-) for 3 Scenarios.

Water demand tends to continuously increase with population growth. Therefore, it is important to maintain the water supply to meet the water needs. In year-33 onwards, graph of Condition 1 does not increase. It happens because of there is action to improve the river water quality as additional water sources. However, unlike previous condition, Condition 2 includes actions to improve the wastewater treatment which influences the water quality of the river, so that it can be used as addition sources. It can be seen by the increment of the graph in year-33 to 45, but then declined due to the water availability.

In Figure 9, for Condition 1, percentage of water supply and water supply index increase in year-5 because of high consumption of piped water and continuously decrease in year-30 due to the water shortage. There is no extra internal water sources because there is no improvement of river water quality. While for Condition 2, percentage of water supply and water supply index return to increase in year-38 because there is an action to improve the wastewater condition which effect the increment of water sources quality and quantity.

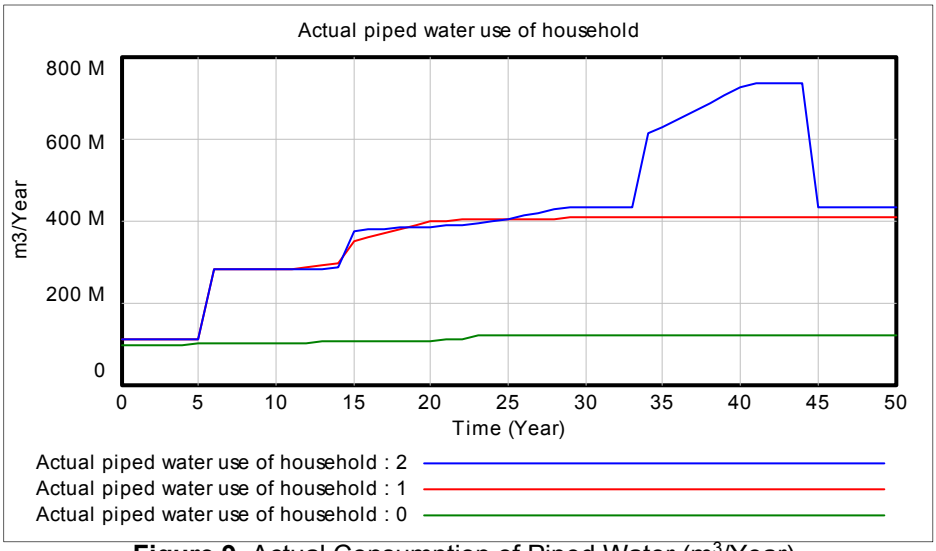

Figure 9. Actual Consumption of Piped Water (m^3/Year).

©2017, IAHR. Used with permission / ISSN 1562-6865 (Online) - ISSN 1063-7710 (Print)

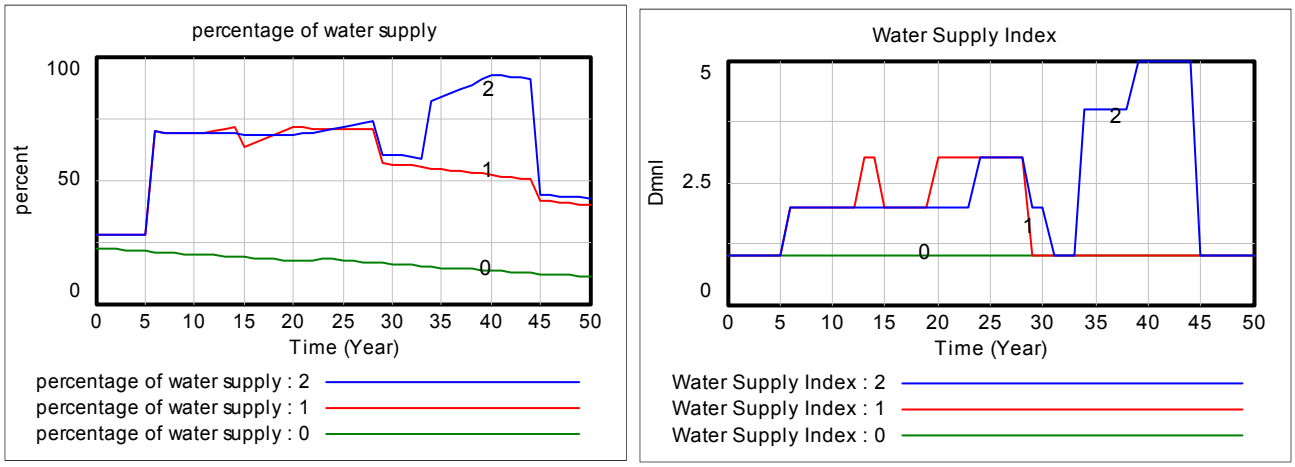

Figure 10. Percentage of Water Supply (%) and Water Supply Index (-).

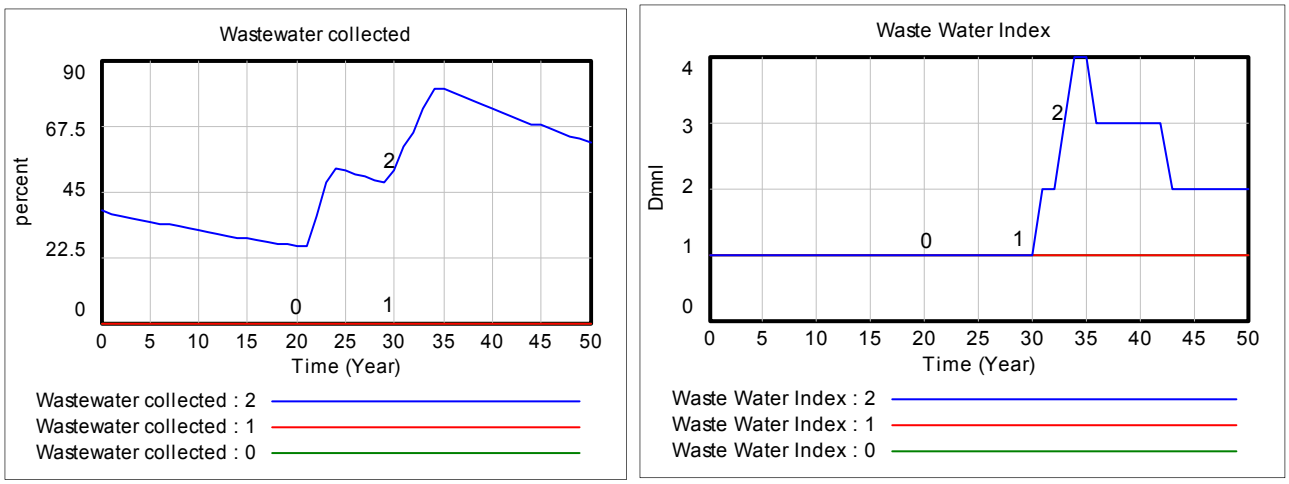

Figure 11. Percentage of Wastewater Collected (%) and Waste Water Index (-).

Based on previous explanation, in Condition 1, the policy and investment only focus on piped water connection and distribution and piped so that the percentage of wastewater collected and wastewater index are very low. While in Condition 2, the number of percentage of wastewater collected and wastewater index increase significantly because of the improvement of wastewater system.

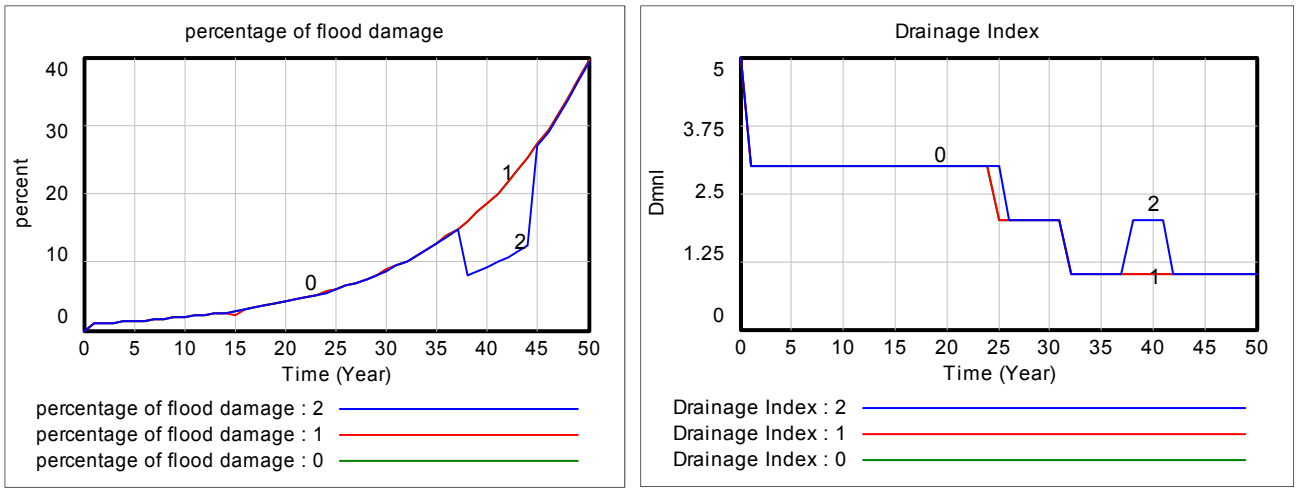

Figure 12. Percentage of Flood Damage (%) and Drainage Index (-).

In this model, flood damage is a function of groundwater, so its value is comparable to the value of groundwater use. Although the piped water supply increase, both in Condition 1 and 2, but it still cannot meet the total of water demand. So that there is still small percentage of groundwater uses which influence the flood damage due to land subsidence.

 ©2017, IAHR. Used with permission / ISSN 1562-6865 (Online) - ISSN 1063-7710 (Print)

6 CONCLUSIONS

In this paper, a simplified model using system dynamic and several scenarios was outlined, in order to assess the water security index over time due to transient policy action, investment and autonomous responses. The result shows that different policy action and also investment allocation will influence the water security index by changing the water supply and the number of connection. On the next steps, other uncertainties could be added to capture the dynamic of water security index; such as water price, willingness to pay, water availability, water demand for different household category, etc.

ACKNOWLEDGEMENTS

The research is part of collaboration of TU Delft, PUSAIR, and Institut Teknologi Bandung within The Adaptive Delta Management (ADM) project, funded by The Netherland Organization for Scientific Research (NWO-WOTRO). The authors great-fully acknowledge the financial support granted and also like to thank The Adaptive Delta Management (ADM) Team for their involvement in this project.

REFERENCES

Abidin, H.Z., Andreas, H., Gumilar, I., Fukuda, Y., Pohan, Y.E. & Deguchi, T. (2011). Land Subsidence of Jakarta (Indonesia) and its Relation with Urban Development. Natural hazards, 59(3), 1753-1771.

Akhtar, M.K. (2011). A System Dynamics Based Integrated Assessment Modelling of Global-Regional Climate Change: A Model for Analyzing the Behaviour of the Social-Energy-Economy-Climate System, *PhD Thesis*, The University of Western Ontario.

Asian Development Bank. (2013). *Asian Water Development Outlook 2013- Measuring Water Security in Asia and Pacific. Philippines*. Asian Development Bank.

Bappenas. (2007). Hasil Penilaian Kerusakan dan Kerugian Pascabencana Banjir Awal Februari 2007 di Wilayah Jabodetabek (Jakarta, Bogor, Depok, Tangerang, dan Bekasi). *Jakarta, Kementrian Negara Perencanaan Pembangunan Nasional BAPPENAS*, 1-11.

Budiyono, Y., Aerts, J., Brinkman, J., Marfai, M.A. & Ward, P. (2015). Flood Risk Assessment for Delta Mega-Cities: a Case Study of Jakarta. *Natural hazards*, 75(1), 389-413.

Cook, C. & Bakker, K. (2012). Water Security: Debating an Emerging Paradigm. *Global Environmental Change*, 22(1), 94-102.

DKI Jakarta, B.P.S.P. (2014). *Statistik Air Bersih DKI Jakarta 2011-2013*, DKI Jakarta, Badan Pusat Statistik Provinsi.

Forrester, J.W. (1968). *Principles of Systems*. Text and Workbook Chapters 1 through 10. Wright, Allen Press, Inc. Cambridge, Massachusetts USA, 121-122

Forrester, J.W. (1994). System Dynamics, Systems Thinking, and Soft OR. *System Dynamics Review*, 10(2-3), 245-256.

Global Water Partnership. (2000). *Towards Water Security: A Framework for Action. Second World Water Forum*. The Hague, Global Water Partnership.

Grey, D. & Sadoff, C.W. (2007). Sink or Swim? Water Security for Growth and Development. *Water Policy*, 9(6), 545-571.

Haasnoot, M. (2009). Exploring Sustainable Pathways for River Deltas into an Uncertain Future. Technology, Policy and Management. Delft, TU Delft, *Ph.D*. Delft University of Technology Delft

PAM Jaya. (2015). Service Coverage. Retrieved January, 2016, from www.pamjaya.co.id/cakupan-layanan, (Accessed 4/1/2015).

Pruyt, E. (2013). *Small System Dynamics Models for Big Issues: Triple Jump Towards Real-World Complexity*. TU Delft Library.

Sehlke, G. & Jacobson, J. (2005). System Dynamics Modeling of Transboundary Systems: the Bear River Basin Model. *Ground Water*, 43(5), 722-730.

Van Beek, E. & Arriens, W.L. (2014). *Water Security: Putting the Concept into Practice*. Global Water Partnership Technical Committee (TEC), Background Paper(20), 1-55.

©2017, IAHR. Used with permission / ISSN 1562-6865 (Online) - ISSN 1063-7710 (Print)

Proceedings of the 37th IAHR World Congress
August 13 – 18, 2017, Kuala Lumpur, Malaysia

ASSESSMENT OF WATER STORAGE VARIABILITY USING GRACE AND GLDAS DATA IN THE ARABIAN COUNTRIES CONSIDERING IMPLICATIONS FOR WATER RESOURCES MANAGEMENT

MOHAMED SABER[(1)], SAMEH A. KANTOUSH[(2)] & TETSUYA SUMI[(3)]

[(1)] DPRI, Kyoto University (Gokasho, Uji, Kyoto 611-0011, Japan)
mohamedmd.saber.3u@kyoto-u.ac.jp, msaber_75@yahoo.com
[(2)] DPRI, Kyoto University (Gokasho, Uji, Kyoto 611-0011, Japan)
kantoush.samehahmed.2n@kyoto-u.ac.jp
[(3)] DPRI, Kyoto University (Gokasho, Uji, Kyoto 611-0011, Japan)
sumi.tetsuya.2s@kyoto-u.ac.jp

ABSTRACT

Water scarcity is a critical issue in the Arabian countries. Water resources are subjected to threats such as natural variability, pollution, overexploitation and climate changes. Therefore, proposing and developing good management strategies for the available water resources are urgently needed to overcome the water demand for increasing the population and industrialization as well as urbanization. The sustainable water management is hindered by the data deficiency, and water variability and in some cases due to the political situation. Therefore, the main goal of this research is to use the Satellite Remote Sensing Data (Gravity Recovery and Climate Experiment; GRACE) and Global Land Data Assimilation (GLDAS) to assess and evaluate the total water storage variability over the Arabian countries due to their limited water resources. The total water storage anomalies were estimated from GRACE showing that most of the Arabian countries are suffering from declining and decreasing the total water storage within the time period from 2002-2015. Besides, the same situation was observed from the groundwater storage estimated from both GRACE and GLDAS. It was found that groundwater storage and soil moisture exhibit high spatiotemporal variability from one country to the others. A comparison study between all the countries was conducted in terms of total water storage and groundwater variability. The present study provide some implications and results which in turn will be a guide for all stakeholders including government, civil society and the private sector to develop control and manage their water availability based on this long term analysis. The method is characterized by providing spatiotemporal maps for water storage changes over all Arabian countries using Satellite products of GRACE and GLDAS data.

Keywords: Water resources management; GRACE, GLDAS; Arab region; total water storage; groundwater.

1 INTRODUCTION

The water scarcity in the Arab region and the increased in gap between demand and available water supply, due to growth of population, and urbanization is hindering the human development. Currently, Water scarcity is a great challenge for the human life, society and environment in the Arab region. Most of the Arabian countries are located in arid regions, where drought condition results in water scarcity. This is considered as one of the main challenges against any sustainable development in the Arab Region. Over 60% of the water demands are covered by fossil groundwater at the Gulf Cooperation Council (GCC) countries only (Al-Rashed and Sherif, 2000). The average annual volume of rainwater in the Gulf countries is estimated at 205.93 billion m3 (ACSAD, 1997). Arab countries cover about 10 per cent of the world's area but receive only 2.1 per cent of its mean annual precipitation. Most of the region is classified as arid or semi-arid (desert), receiving less than 250 millimeters of rainfall annually (Ragab, 2013).

The GRACE satellite data has been developed to monitor Terrestrial Water Storage (TWS) globally (Tapley et al., 2004). Since April 2002, it has been offering monthly gravity field solutions, and has been used as an applicable tool to infer groundwater storage changes by subtracting contributions from other components (Tiwari et al., 2009; Rodell et al., 2009; Famiglietti et al., 2011; Chen et al., 2014; Richey et al., 2015). The spatial variability of TWS is dependent and dominated by variations in ice and snow, surface water, and soil moisture (Rodell and Famiglietti, 2001). The spatial resolution of GRACE-TWS grids is 1 degree in both latitude and longitude (around 111 km at the equator) (Landerer and Swenson, 2012).

This paper aims to assess and evaluate the water resources variability at the Arabian countries using the Satellite Remote Sensing Data (Gravity Recovery and Climate Experiment; GRACE) and Global Land Data Assimilation (GLDAS). The total water storage variability over the Arabian countries due to their limited water resources will be discussed. Thus, we estimated the total water storage anomalies and groundwater storage anomalies in space and time throughout the time period from 2002-2015.

 ©2017, IAHR. Used with permission / ISSN 1562-6865 (Online) - ISSN 1063-7710 (Print)

2 STUDY AREA

The Arab countries covers an area about 13,781,751 km2. It consists of 22 countries as shown in the map except Comoros (Figure 1). The Arab world also known as the Arab nation consists of the 22 Arabic-speaking countries of the Arab League. The population has increased by the rate of 8E+6 person every year from 2002-2015 (World Bank, 2017).

Based on the report of IPCC (2008), it was expected that North Africa and the Middle East region over the next century, declining rainfall (10 -25 %); declining soils moisture (5 -10 %), declining runoff (10 -40 %), and increasing evaporation (10 -20 %) (IPCC, 2008). Generally, water management has suffered from poor accountability (both external to service users and internal within resource management and service delivery organizations). Therefore, more and more investments are being required to remedy the deferred maintenance of already installed hydraulic infrastructure in the Arab region (World Bank, 2007). In March 2007, the World Bank report has addressed that (1) water is scarce and has challenging uses which needs a management strategy to find engineering solutions, (2) To improve water management, accountability that needs to be deliberately promoted, (3) To improve water management, policies outside the water sector often are as important as those within the sector (World Bank, 2007). Not only water scarcity problem but also, Groundwater resources in most Arab countries are also threatened by pollution from agricultural, industrial and domestic activities. ‘‘Over the last two decades, irrigated areas in Gulf countries grew 100-300 per cent. Irrigation water is often used inefficiently, without considering the economic opportunity cost for urban domestic and industrial purposes’’ (Ragab, 2013).

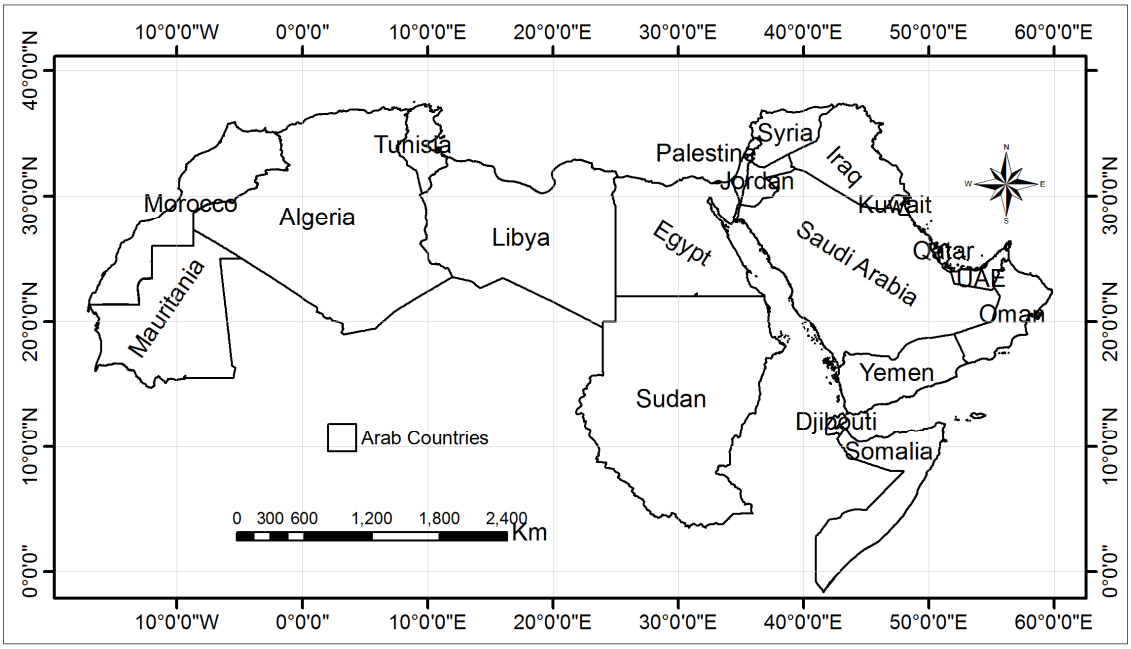

Figure 1 Location map of the Arabian countries.

3 METHODOLOGY AND DATA PROCESSING

In this study, GRACE and GLDAS data were used to estimate the total water storage and groundwater changes over the Arab region. Thus, we used the scaled version of GRACE data processed and archived by Landerer and Swenson (2012) to assess the total water storage variability at the study region. The data of GRACE TWS is available at (1°×1°) spatial resolution and monthly temporal resolution, version, RL05 (CSR). Additionally, the corresponding scaling factors were provided for the correction of GRACE data errors (such as, the leakage errors due to signal leakage from neighboring grids, and measurement errors due to raw GRACE data processing). GRACE TWS estimates at the target region were corrected by multiplying the GRACE pixels by the corresponding scaling factors. Groundwater storage changes were analyzed and assessed at different scales as at regional district (Huang et al., 2015) and for watershed scale (Billah et al., 2015) with spatial areas in the range from 30 to 7000 km2. Therefore, in the present study, GRACE TWS data were used with annual time scales starting from Oct. 2002-Sept. 2015 along with GLDAS data to estimate the groundwater anomalies at the Arab region.

GLDAS data was introduced and sponsored by NASA Goddard Space Flight Centre (GSFC) and the National Oceanic and Atmospheric Administration (NOAA) to calculate the variations in both ocean and land mass fluxes (Rodell and Famiglietti, 2001; Rodell et al., 2009; Rodell et al., 2004). GLDAS NOAH Ver.1 were processed to estimate the TWS components (e.g. Soil moisture, canopy water, surface runoff). It is available at spatiotemporal scales (1° pixels and monthly resolutions). The total Soil Moisture (SM) was estimated as the total summation of soil moisture values of 4 layers: (0–10, 10–40, 40–100, and 100–200 cm). The total soil

©2017, IAHR. Used with permission / ISSN 1562-6865 (Online) - ISSN 1063-7710 (Print)

moisture (SM) and other components were then subtracted from GRACE TWS to calculate groundwater storage changes Eq. (1). The first step, GRACE TWS were processed to estimate the variability of total water storage over the region, then the groundwater storage anomalies were also estimated to assess the variability over the study area.

In order to evaluate the groundwater storage variabilities, the water components of GLDAS such as surface water, snow water, and canopy water and soil moisture storage were subtracted from the GRACE data Eq. [2]. The annual total average for all parameters were estimated first, then the anomalies were calculated by subtracting the average over the time period (Oct. 2002- Sept. 2015) from every month value.

$$\Delta S_{TWS} = \Delta S_{SW} + \Delta S_{SM} + \Delta S_{GW} + \Delta S_{cpy} + \Delta S_{SWE} \quad [1]$$

where, ΔS : is (the monthly, seasonal, or annual changes), SM: is soil moisture, SW: is surface water, cpy: Canopy water, SWE: Snow water equivalent, and GW is groundwater storage.

$$\Delta S_{GW} = \Delta S_{TWS} - (\Delta S_{SW} + \Delta S_{SM} + \Delta S_{cpy} + \Delta S_{SWE}) \quad [2]$$

4 RESULTS AND DISCUSSIONS

As we have discussed in the previous sections, how much the importance of evaluating the total water storage variability and ground water resources at the Arab region as very important region. It is characterized the low water resources with very high variability of water availability.

4.1 Total water storage anomalies

GRACE TWS were downloaded and processed to estimate the annual anomalies of total water storage over the study area within the time period from Oct. 2002-Sept. 2015. Spatial and temporal analysis were conducted to understand the variability in both space and time at the study region. Figure 2 shows the time series of TWSA for all Arabian countries indicating a remarkable decline trend of total water storage over the whole region except for four countries (Sudan, Somalia, Mauritania, and Djibouti). The shortage or decline water volumes (Figure 3) estimated based on the linear time series trend varies from -10775.92 Million Cubic Meter in Saudi Arabia to -4.7 MCM in Bahrain. Sudan is the highest country showing an increase in the total water storage of about +1586.9 MCM, and the second country is Somalia of about 1099.3 MCM. The most declining water storages were recorded from high to low as follow (Saudi Arabia, Iraq, Algeria, Libya, Egypt, Syria, and Jordan). The reason might be due to increasing the water demand and usage as a result of population growth in those countries in addition to agriculture and domestic uses. It was noticed that there are two stages for the total water storage variability based on the time series data, the first one was stable stage (not highly changeable) from 2002 to 2008, but the second stage was highly changeable showing a decreasing trend in all countries after 2008 to 2015 (Figure 2).

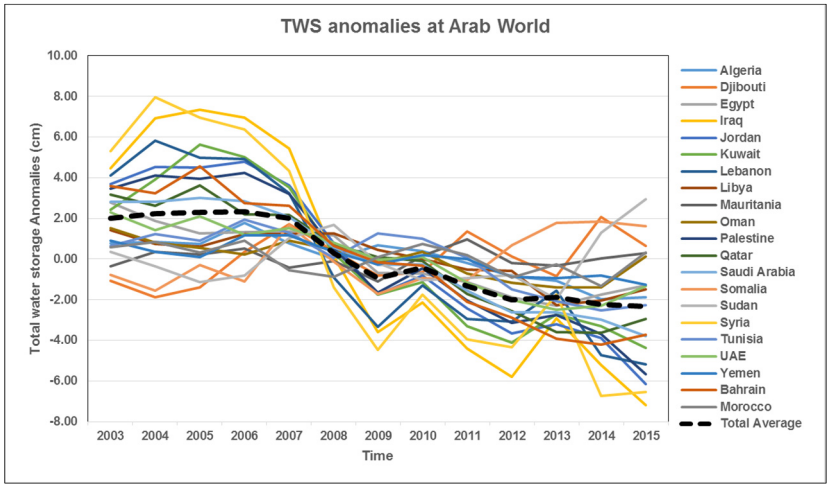

Figure 2. GRACE Total Water Storage Anomalies (TWSA) estimated for all Arab countries, showing a declining trend in all the countries except four countries (Sudan, Somalia, Mauritania, and Djibouti).

 ©2017, IAHR. Used with permission / ISSN 1562-6865 (Online) - ISSN 1063-7710 (Print)

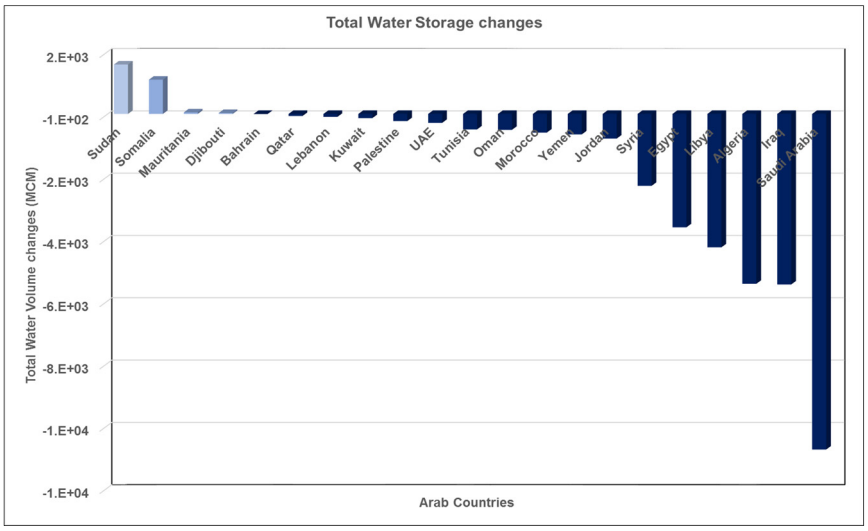

Figure 3. Total Water Storage changes estimated from TWSA from Oct. 2002 to Sept. 2015 decline estimated for all Arab countries, showing a decrease in the water storage at most of the Arab world except (Sudan, Somalia, Mauritania, and Djibouti).

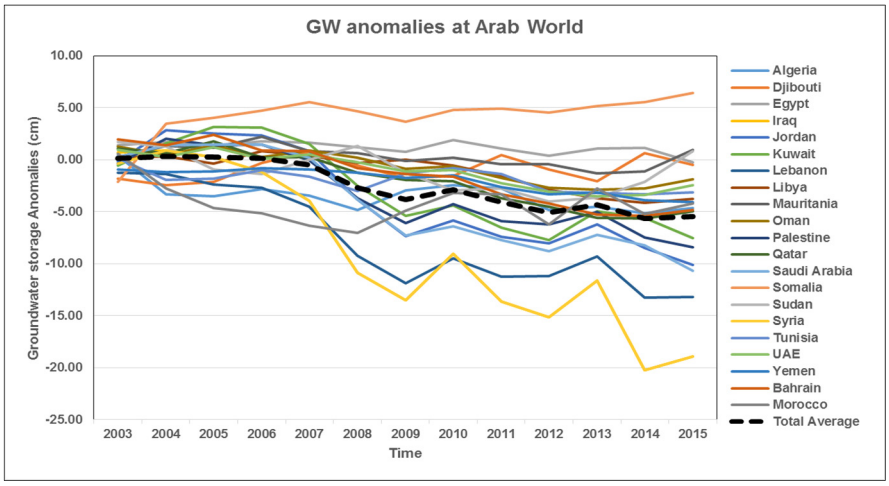

Figure 4. Groundwater Storage Anomalies estimated from Oct. 2002 to Sept. 2015 for all Arab countries, showing a declining trend in all the countries except four countries (Somalia and Djibouti).

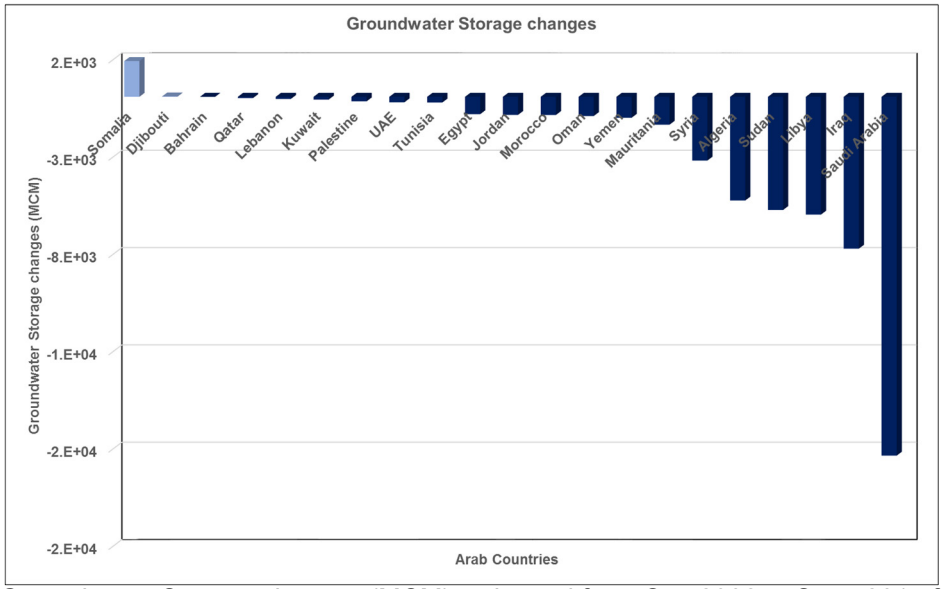

Figure 5. Groundwater Storage changes (MCM) estimated from Oct. 2002 to Sept. 2015 for all Arab countries, showing a decrease in the water storage at all the countries except four countries (Somalia and Djibouti).

©2017, IAHR. Used with permission / ISSN 1562-6865 (Online) - ISSN 1063-7710 (Print)

4.2 Groundwater storage anomalies

The groundwater storage variability was also conducted by using GRACE and GLDAS data. The results of time series analysis revealed that the groundwater storage changes (Figure 4) over the time period from 2002-2015 is declining in all countries except (Somalia and Djibouti). Saudi Arabia was also the highest user of groundwater showing the highest declining in groundwater volume about -18437.2 MCM from 2002-2015, and the lowest user was Bahrain where groundwater storage decreased about -4.3 MCM. Groundwater shortage during the time period from 2002-2015 shows high variability from one country to the others (Figure 5). The highest levels of groundwater uses were observed and ordered from high to low at (Saudi Arabia, Iraq, Algeria, Libya, Egypt, and Syria).

4.3 Spatiotemporal variability of total water storage and groundwater

Spatial distribution maps for total water storage and groundwater anomalies were developed to investigate the changes in both space and time from one country to another and from over the time as well. Figure 6 shows that TWSA from 2002-2015 is variable from one region to the others. For instance, the north eastern part of the Arab region exhibit an increase in TWSA from 2002 to 2007, but after 2007 to 2015, shows a decrease in TWSA. On the other hand, the western and southern regions exhibit a decrease in TWSA from 2002-2007, but starts to increase again after 2008-2015 (Figure 7). In case of groundwater storage anomalies (Figure 8), it was noticed that the spatiotemporal variability is remarkable in most of the countries. In Saudi Arabia, Syria, and Iraq, groundwater are always decreasing gradually from 2002-from 2006, however, after 2006, it is dramatically decreasing until 2015. In South Sudan, the situation is different as we noticed that groundwater is increasing or stable almost during the analyzed time period. The results revealed that TWSA and groundwater storage anomalies were highly variable on both space and time from one region to the others.

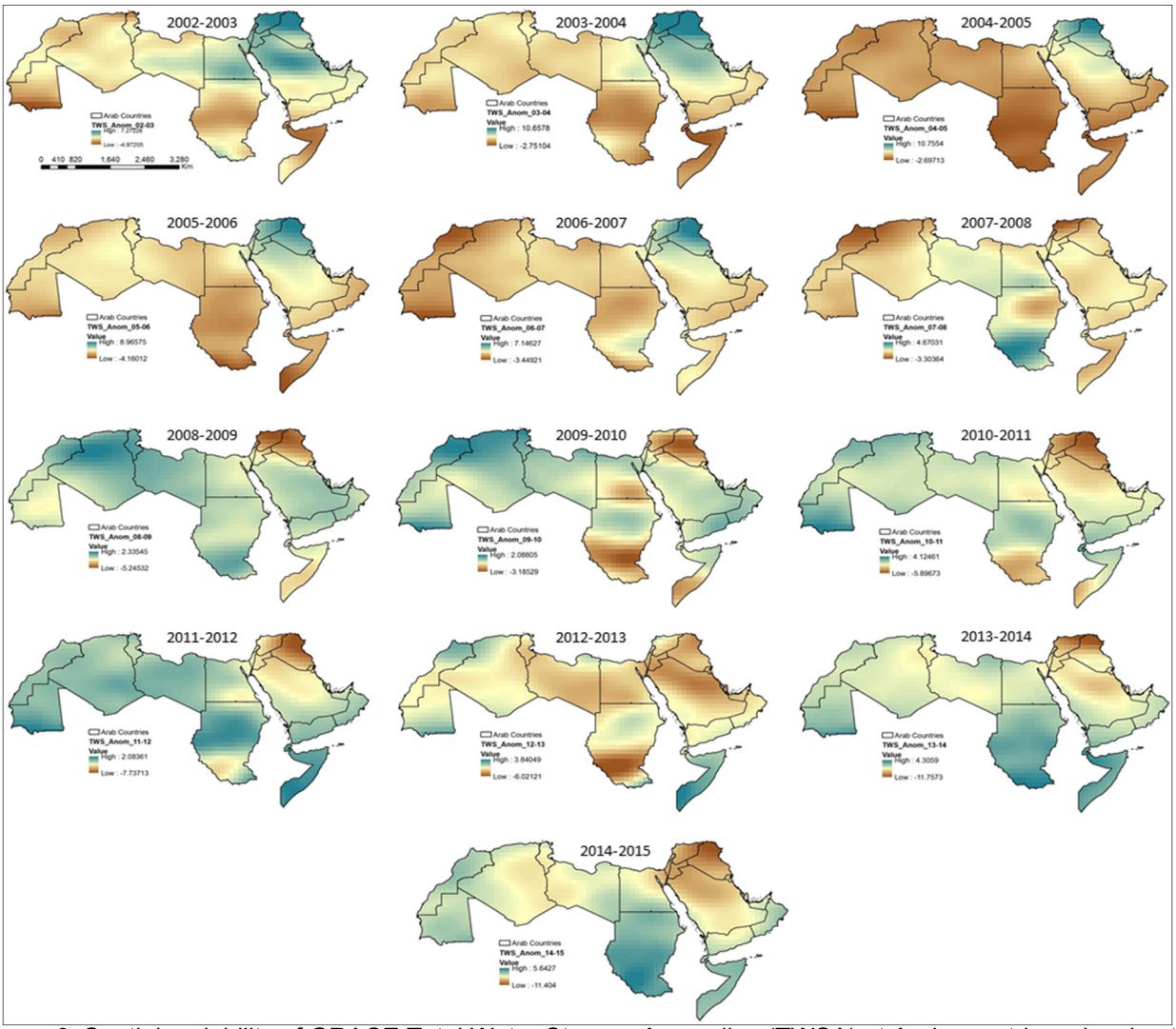

Figure 6. Spatial variability of GRACE Total Water Storage Anomalies (TWSA) at Arab countries, showing the spatial changes from one country to the others and also high variability along the time period from Oct. 2002 to Sept. 2015.

 ©2017, IAHR. Used with permission / ISSN 1562-6865 (Online) - ISSN 1063-7710 (Print)

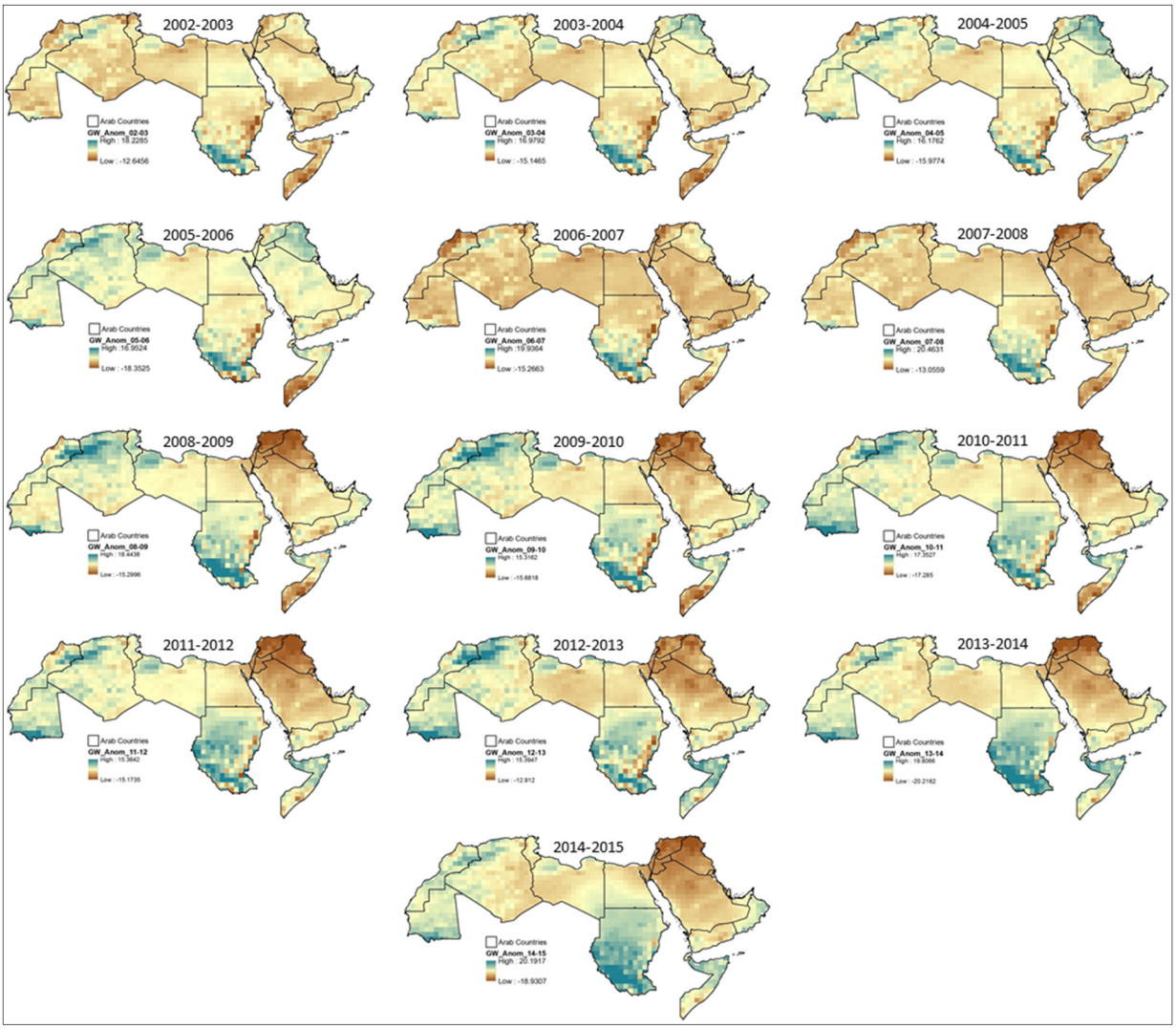

Figure 7. Spatial variability of Groundwater Storage Anomalies (TWSA) at Arab countries, showing the spatial changes from one country to the others and also high variability along the time period from Oct. 2002 to Sept. 2015.

5 CONCLUSIONS

The Arab region lie mainly in arid to semi-arid zones and renewable water resources are exceptionally low compared to other regions over the world. In this study, the cheap tools such as Satellite based data were used successfully to evaluate the water resources availability and variability in the Arab region. GRACE data and GLDAS data were used together to estimate the Total Water Storage Anomalies (TWSA) and groundwater storage anomalies for all countries. It was found that TWSA and groundwater are highly variable in both space and time. Most of the countries are suffering from dramatic declining in the total water storage and groundwater except Sudan and Somalia. Saudi Arabia, Iraq, Algeria, Libya, Egypt, Syria, and Jordan are the highest countries users showing very extreme shortage in their water resources. Somalia and Sudan shows increase in TWSA as total average, these might be due to less development in terms of urbanization and agriculture activates. The most vital contribution of this study is stating that the water in the Arab regions is showing an increase in water scarcity over the time. This urge the policy and decision makers in those countries to consider supply and demand management strategies for the future. The present study could provide spatiotemporal analysis for the water resources availability in all Arab countries, this would be the way forward for better water management in the future. Additional analysis considering land use, rainfall, and evaporation variabilities as well as linkage with the actual data for water usage and shortage will be addressed in the near future work.

ACKNOWLEDGEMENTS

This work was supported by the SPIRIT Project. We also acknowledge Kyoto University for support to this research.

©2017, IAHR. Used with permission / ISSN 1562-6865 (Online) - ISSN 1063-7710 (Print)

REFERENCES

ACSAD (1997). *Annual Technical Report*, Department of Studies of Animal Wealth, the Arab Center for the Studies of Arid Zones and Dry Lands.

Al-Rashed, M.F. & Sherif, M.M. (2000). Water Resources in The GCC Countries: An Overview. *Water Resources Management,* 14(1)**,** 59-75.

World Bank (2017). *Arab World Population Data.* Retrived online through World Bank Data, Popolation IndicatorAvailable: http://data.worldbank.org/indicator [Accessed January 2017].

World Bank (2007). *Making the Most of Scarcity: Accountability for Better Water Management in the Middle East and North Africa*, MNA Development Report on Water.

Billah, M.M., Goodall, J.L., Narayan, U., Reager, J., Lakshmi, V. & Famiglietti, J.S. (2015). A Methodology for Evaluating Evapotranspiration Estimates at the Watershed-Scale Using GRACE. *Journal of Hydrology,* 523**,** 574-586.

Chen, B., Gong, H., Li, X., Lei, K., Ke, Y., Duan, G. & Zhou, C. (2014). Spatial Correlation Between Land Subsidence and Urbanization in Beijing. China. *Natural Hazards,* 75**,** 2637-2652.

Famiglietti, J., LO, M., Ho, S., Bethune, J., Anderson, K., Syed, T., Swenson, S., DE LINAGE, C. & Rodell, M. (2011). Satellites Measure Recent Rates of Groundwater Depletion in California's Central Valley. *Geophysical Research Letters,* 38, 1-4.

Huang, Z., Pan, Y., Gong, H., Yeh, P. J. F., Li, X., Zhou, D. & Zhao, W. (2015). Subregional-Scale Groundwater Depletion Detected by GRACE for Both Shallow and Deep Aquifers in North China Plain. *Geophysical Research Letters,* 42**,** 1791-1799.

IPCC (2008). *Climate Change and Water*, Technical Paper of the Intergovernmental Panel on Climate Change. Geneva, Switzerland, IPCC Secretariat.

Landerer, F. & Swenson, S. (2012). Accuracy of Scaled GRACE Terrestrial Water Storage Estimates. *Water Resources Research,* 48(4), 1-11.

Ragab, R. (2013). *Water Governance in the Arab Region: Managing Scarcity and Securing the future.* United Nations Development Programme, Regional Bureau for Arab States (RBAS).

Richey, A.S., Thomas, B.F., Lo, M.H., Reager, J.T., Famiglietti, J.S., Voss, K., Swenson, S. & Rodell, M. (2015). Quantifying Renewable Groundwater Stress with GRACE. *Water Resources Research,* 51(7)**,** 5217-5238.

Rodell, M. & Famiglietti, J. (2001). An Analysis of Terrestrial Water Storage Variations in Illinois with Implications for the Gravity Recovery and Climate Experiment (GRACE). *Water Resources Research,* 37(5)**,** 1327-1339.

Rodell, M., Houser, P., Jambor, U., Gottschalck, J., Mitchell, K., Meng, C., Arsenault, K., Cosgrove, B., Radakovich, J. & Bosilovich, M. (2004). The Global Land Data Assimilation System. *Bulletin of the American Meteorological Society,* 85(3)**,** 381-394.

Rodell, M., Velicogna, I. & Famiglietti, J.S. (2009). Satellite-Based Estimates of Groundwater Depletion in India. *Nature,* 460(7528)**,** 999-1002.

Tapley, B.D., Bettadpur, S., Ries, J.C., Thompson, P.F. & Watkins, M.M. (2004). GRACE Measurements of Mass Variability in The Earth System. *Science,* 305(5683)**,** 503-505.

Tiwari, V., Wahr, J. & Swenson, S. (2009). Dwindling Groundwater Resources in Northern India, from Satellite Gravity Observations. *Geophysical Research Letters,* 36(18), 1-5.

 ©2017, IAHR. Used with permission / ISSN 1562-6865 (Online) - ISSN 1063-7710 (Print)

INVESTIGATING RESERVOIR REGULATIONS UNDER CLIMATE CHANGE SCENARIOS

CHO THANDA NYUNT [1] & YOSHIHISA KAWAHARA [2]

[1,2] Department of Civil and Environmental Engineering, Hiroshima University
nyunt11@hiroshima-u.ac.jp; kawahr@hiroshima-u.ac.jp

ABSTRACT

Climate change alters the hydrological cycle in river basins and threatens the future of the surface water resources under the stress of the rapid urbanization and population growth in many cities. Haji dam, located upstream of the Gono river in Chugoku region in Japan, is a very important green energy resource for urban water supply, hydropower generation, irrigation and flood control. Therefore, the assessment of the projected inflow and capacity under the present operating rule is very important for the multi-purpose reservoir. This study shows that the estimated maximum 100-year probable rainfall will be a surplus of at least 5 % of the whole river basin as well as the approximately 35 - 60 mm of rainfall surcharge in July and +5 to +20 mm extra rainfall in September that will fall on the east, west and middle of the basin in near future. The increasing trend in inflow is significant with 50 m^3/sec/year in the annual basic and around 100 to 150 m^3/sec/month during the wet season. It is necessary to revise the release ratio before and during the flood if the current flood control allocation wants to keep it constant and reservoir water level is continuously retained under the flood alarm level for reservoir safety. However, the present operating rule assures enough capacity after the flood season or from September for the multi-purpose reservoir.

Keywords: Reservoir regulations; climate change impact; CMIP5; Haji Dam; water resources management.

1 INTRODUCTION

Climate change impacts on water resources management and countermeasures for the water balance variation in the river basins have been very crucial especially for a multipurpose reservoir with mixed functions such as irrigation, industrial and municipal water use, hydropower, and flood control. Under rapid urbanization and population growth in many cities, its impacts on multi-purpose reservoirs, which runs for the blended directions of water use under the limited constraint capacity, can be concerned with hydropower generation, a green energy resource with no fuel consumption and no greenhouse gas emission to the environment. By taking the advantages of the multi-global climate models (GCMs) output from the Intergovernmental Panel on Climate Change Fifth Assessment Report (IPCC AR5) such as the future projected precipitation, the impact assessments towards future risk on water resources and water related disaster risk reduction can be achieved. Therefore, it is necessary to analyze the future changing trend of precipitation in a basin to assure the safety and security of the community. Not only the change in precipitation but also the change in hydrological circulation within a basin is very crucial for the resilient watershed minimizing the water-related hazards and assuring the water security. This study analyzed the possible future change of Haji reservoir inflow simulation using a hydrological model as well as the related reservoir regulations by combining a set of GCM runs, which are driven by concentration or emission scenarios consistent with representative concentration pathways (RCPs). Therefore, this study has an objective to evaluate the current reservoir regulations whether they are still applicable for the future variation of reservoir inflows under climate change scenarios.

2 STUDY AREA AND DATA

The Gono River starts its origin from the Chugoku Range in Hiroshima Prefecture and ends at the Sea of Japan near Gotsu city in Shimane Prefecture. Haji dam is located at 34° 39' N, 132 ° 38' E after the convergence of Tabusa River and Shijihara River. Its watershed covers an area of 307.5 km^2 and is located on the northern side of Hiroshima, Japan. A Haji reservoir in Gono River, Japan covers a small watershed, but is a very important water resource for multi-blended direction of water use such as urban water supply, irrigation, hydroelectric power, recreation and wildlife environment ecology and also flood control. Moreover, there is a diversion channel connecting to other trans-basin named Ota river that contributes mainly to the water supply of Hiroshima city residences. This means that Haji Dam is very important for municipal water supply to a total of five cities including Hiroshima and other trans-basin's socio-economy. A total of 25 in-situ daily precipitation are provided by the Hiroshima Prefectural Government. The distribution of observation networks over the Gono River basin as well as the location of Haji Dam and its catchment can be seen in Figure 1. In the Coupled Model Inter-comparison Project 5 (CMIP5), total 28 GCM gridded daily precipitation

©2017, IAHR. Used with permission / ISSN 1562-6865 (Online) - ISSN 1063-7710 (Print)

are available from the Data Integration and Analysis System (DIAS) server of the University of Tokyo. In this study, we considered 1981-2000 as the baseline period and 2046-2065 as the projected period covering RCP 4.5 emission scenarios.

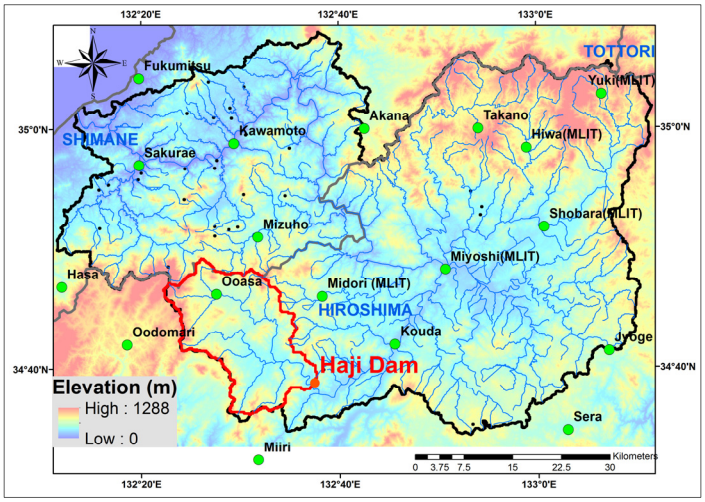

Figure 1. Locations of in-situ stations, Gono River basin and Haji Dam watershed.

3 METHODS

3.1 Multi-GCM selection

The multi-GCMs selection was carried out based on the performance of each GCM by evaluation the distinguished climatological characteristics over the target area such as the Baiu monsoon rain band over Asia, which is mainly contributed by the regional scale circulation. The capturing of the local climate was also investigated in all of the GCMs to give rank according to the scores. However, the scoring system is 1, 0, -1, which was given based on the mean value of all GCMs' spatial correlation and root mean squared error (RMSE) of a particular parameter. It should be noted that the point of this selection method is not to choose the best GCM but it is the way to reject the poor GCM, which has a lower score than the average of all GCMs (Nyunt et al., 2014).

In this study, local scale analysis parameters are precipitation, outgoing long wave radiation, while the regional analysis parameters are sea surface temperature, sea level pressure, zonal wind, meridional wind and air temperature. These are important in the large-scale circulation and regional seasonal evolution, which influences the local seasonal precipitation. After scoring, the GCMs are ranked according to the total scores of each parameter performance and selected GCMs are listed in Table 1.

Table 1. Selected GCMs list.

GCM	INSTITUTION
CESM1 (CAM5)	National Center for atmospheric Research, USA
CNRM-CM5	Centre National de Recherches Meteorologiques, France
MRI-CGCM3	Meteorological Research Institute, Japan
HadGEM2-ES	Met office Hadley Centre, UK
IPSL-CM5A-MR	Institute Pierre-Simon Laplace, France
MIROC4h	Atmosphere and Ocean Research Institute, Japan

3.2 Statistical bias-correction

Without prior bias correction, neither GCM nor RCM (Regional climate model) precipitation can be useful for hydrology simulation and other impact studies. GCM precipitation is often characterized by biases and coarse resolution, which are the main barrier for the direct use of the basin or national level analysis (Wood et al., 2004). The main biases of GCM daily precipitation are the underestimation of heavy precipitation, a low number of no rain day or dry days and inadequacy to present the seasonal variation. Here, the extreme underestimation was solved by using the peak over threshold (POT) series, which composed of the extreme values above a certain threshold regardless of the year of occurrence and allow more than one event per year. The generalized Pareto distribution (GPD) has been used to model POT (Hosking and Wallis, 1987). The GPD function is as follow:

 ©2017, IAHR. Used with permission / ISSN 1562-6865 (Online) - ISSN 1063-7710 (Print)

$$F(x) = 1 - \left[1 - \frac{\kappa(x-\xi)}{\alpha}\right]^{1/\kappa} \quad [1]$$

where, $F(x)$ = the probability of GPD
x = precipitation
κ = shape parameter
α = scale parameter
ξ = location parameter

In this study, the location parameter must be predefined extreme precipitation threshold for PDS fitting. The top 1% of the total rain days in the descending order is defined as the trial threshold for the fitting of the extreme GPD.

The number of extreme rainy days are the same in both the observation and GCM gridded series to make the same probability correction. After the GPD fitting of observation and GCM, the bias-corrected GCM was calculated from the inverse GPD probability between observed value and GCM value. After that, the estimated probable of maximum intensity for different return periods can be estimated by using the following equation.

$$X_T = \xi + \frac{\alpha}{\kappa}\left[1 - (\lambda T)^{-\kappa}\right] \quad [2]$$

where, X_T = recurrences of the maximum precipitation
T = return period in years
λ = average number of extreme events per year above the threshold ξ

The next step is to correct the frequency of dry or wet day errors, which was done by exceedance probability. All GCM rainfalls beyond the intensity of the last rank of observed rain day become zero. The same threshold will apply to the future GCM rainfall series because the future is unknown and the changing of the future trend of dry spell or wet spell can be known. For normal rainfall, a two-parameter gamma distribution function (GDF) was used and grouped into twelve months for each GCM. We assumed all of the normal rainfall follow GDF and fit the daily GCM and historical observed rainfall to twelve months of GDF using the following equation. The shape and scale parameters of the gamma distribution were determined by the methods of moment estimation (Ines and Hansen, 2006). Detailed of statistical bias correction can be found in Nyunt et al. (2013) and Nyunt et al. (2014).

$$F(x;\alpha,\beta) = \frac{1}{\beta^{\alpha}\Gamma(\alpha)} x^{\alpha-1} \exp\left(-\frac{x}{\beta}\right) \quad [3]$$

where, α = shape parameter
β = scale parameter
$\Gamma(\alpha)$ = Gamma function

3.3 Reservoir inflow simulation

To understand the projected inflow to Haji Dam, we used a water and energy budget based on distributed hydrological model called WEB-DHM. This model has a combined structure of simple biosphere SiB2 (Yongjiu and Qingcun, 1997) and a hill slope hydrological model (Yang et al., 2004). The main advantage of WEB-DHM is that it allows consistent description of water, energy and CO2 fluxes at the basin scale (Wang et al., 2009). Digital elevation map from Japan, land use of USGS global land cover dataset for Gono river, and soil data from FAO, Leaf Area Index (LAI) and fraction of photo synthetically active radiation (FPAR) from NOAA AVHRR PAL 16km satellite dataset are also prepared. Meteorological forcing parameters such as air temperature, specific humidity, air pressure, wind velocities, downward solar radiation and long wave radiation are available from JRA-25 Reanalysis data. Model simulation was done by using observed precipitation that are interpolated to 1km by Thiessen polygon method and parameter tuning was done through model

©2017, IAHR. Used with permission / ISSN 1562-6865 (Online) - ISSN 1063-7710 (Print)

calibration and validation. Then, present and projected bias-corrected GCM precipitation were used to simulate the reservoir inflow and investigate the effect of the current operating rule on the reservoir storage capacity.

4 RESULTS AND DISCUSSIONS

4.1 Bias correction of GCM precipitation

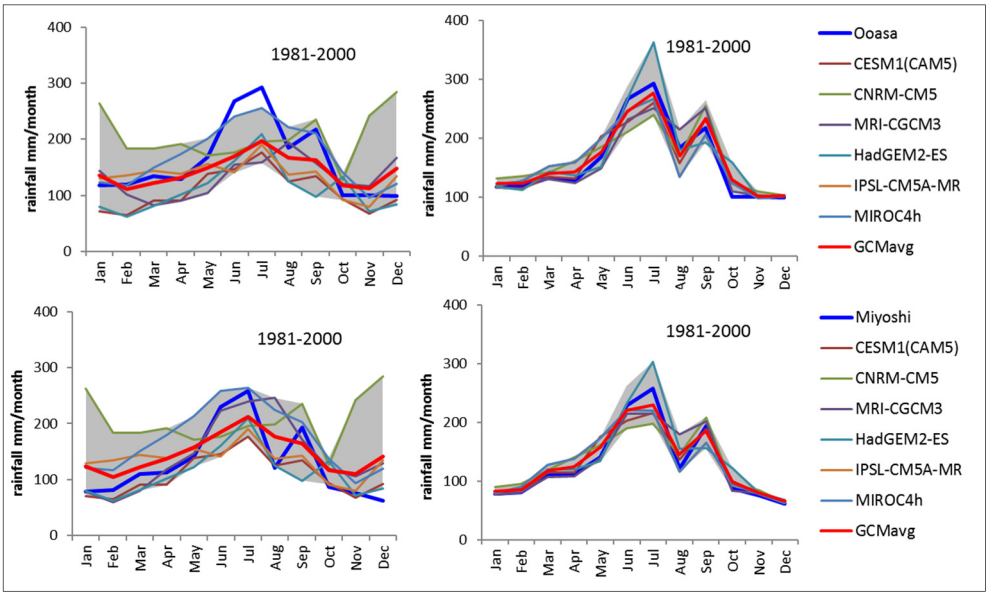

Figure 2. 1981-2000 monthly climatology at Ooasa and Miyoshi station before and after bias correction.

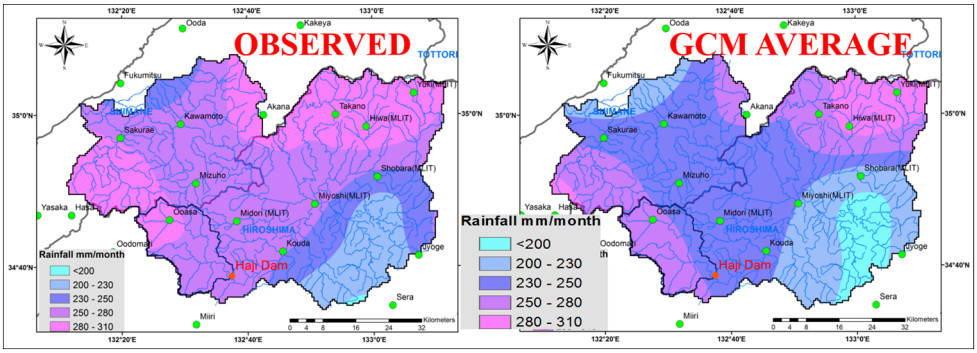

Figure 3. Multi-ensemble GCM mean of (1981-2000) bias-corrected July climatology precipitation compared to the observation.

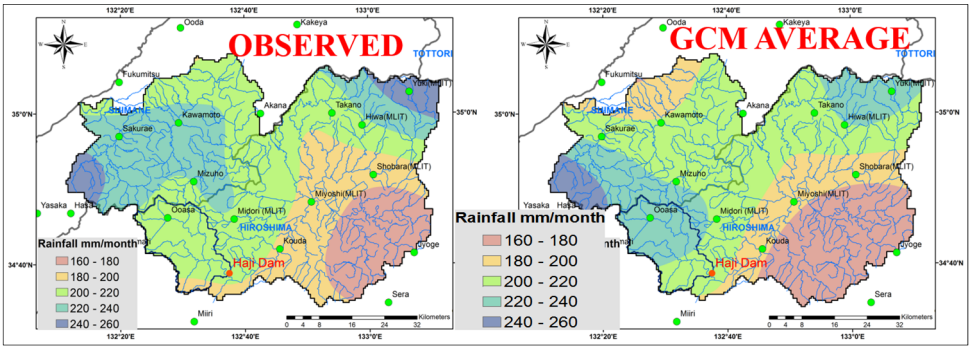

Figure4. Multi-ensemble GCM mean of (1981-2000) bias-corrected September climatology precipitation compared to the observation.

Six GCM model outputs are bias-corrected and downscaled through the observed rain gauges to discard the error contributed by the large-scale simulation compared to local historical climate. Figure 2 shows GCMs climatology monthly precipitation before and after bias-correction at Ooasa station, a station within a Haji watershed, and Miyoshi station. It can be seen easily that a wide range of error exists in the original GCMs

 ©2017, IAHR. Used with permission / ISSN 1562-6865 (Online) - ISSN 1063-7710 (Print)

output before bias-correction (left) and that bias in 20-year climatology is controlled very well after bias-correction (right). The basin wide performance was evaluated by the spline interpolation in GIS using the information at every station within the Gono river basin. As in Figure 3 and Figure 4, multi-ensemble GCMs mean of bias corrected precipitation during July and September (two flood peak seasons) climatology were compared to the observed distribution. But GCM mean shows negative bias in the east and center region of the basin in July especially in Haji watershed as in Figure 3. September result looks similar but positive error is found in the upper part of Haji watershed (Ooasa) and negative error is in the northern part of Gono basin as in Figure 4.

4.2 Projected changes in precipitation over Gono River basin

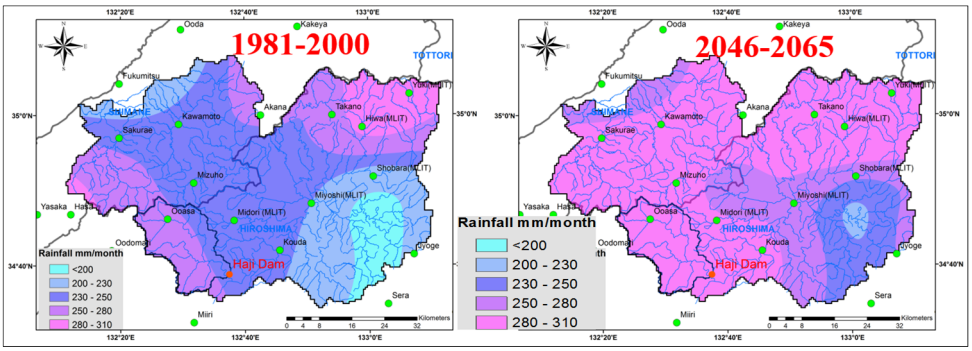

Figure 5. Average of GCM July climatology comparison between 1981-2000 and 2046-2065.

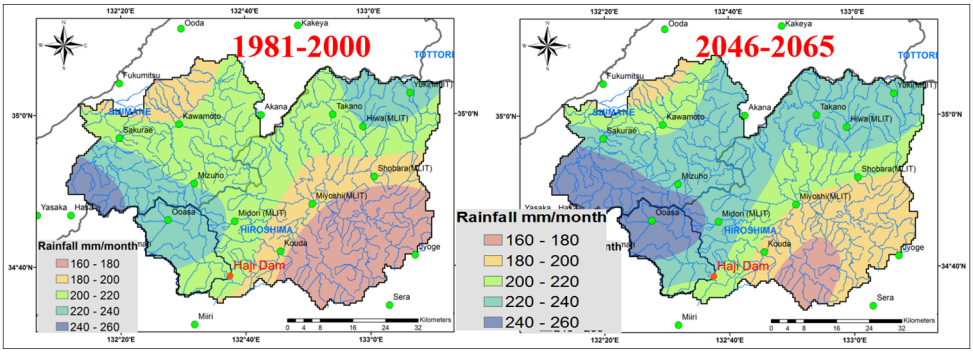

Figure 6. Average of GCM September climatology comparison between 1981-2000 and 2046-2065.

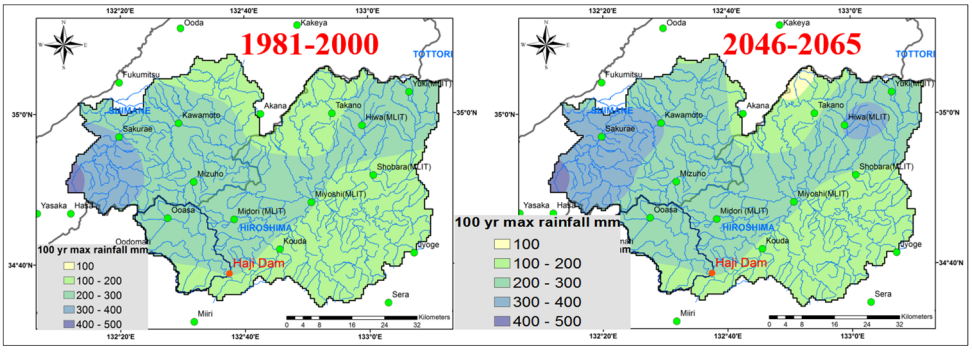

Figure 7. 100-year probable maximum rainfall comparison between 1981-2000 and 2046-2065.

Generally, total rainfall in July will increase over the whole basin and approximately around 35-60 mm will be the surplus rainfall in the near future as in Figure 5. In September, when comparing the past and future, there is a change in total intensity of +5 to + 20 mm in the east, west and middle part of the basin although the distribution pattern turns into a similar shape with a small difference as in Figure 6. The projected change in the estimated maximum 100-year probable is the surplus rainfall of at least 5% in the west of Gono river basin near the Sea of Japan as in Figure 7. Downstream of the Gono River should be prepared for more intense extreme rainfall during the wet season especially in the intense rainy period, which is in July.

©2017, IAHR. Used with permission / ISSN 1562-6865 (Online) - ISSN 1063-7710 (Print)

4.3 Assessment of Haji Dam operation rule using projected inflow

Moreover, historical climate and future scenario results are coupled with a river routing model named WEB-DHM, which is a water and energy balanced distributed hydrological model including a reservoir model for accessing the future hydrologic condition. Projected streamflow in the reservoir from the ensemble GCMs during 2046-2065 are likely to increase mainly in the flood seasons of July and September as in Figure 8. Relative change of inflow is shown by the bar graph. As a result, the increasing trend is significant with 50 m^3/sec/year in the annual basic and around 100 to 150 m^3/sec/month during the wet season. Therefore, there is a higher risk of flood that should be paid attention to, particularly in the wet season and there will be no concern regarding water shortage.

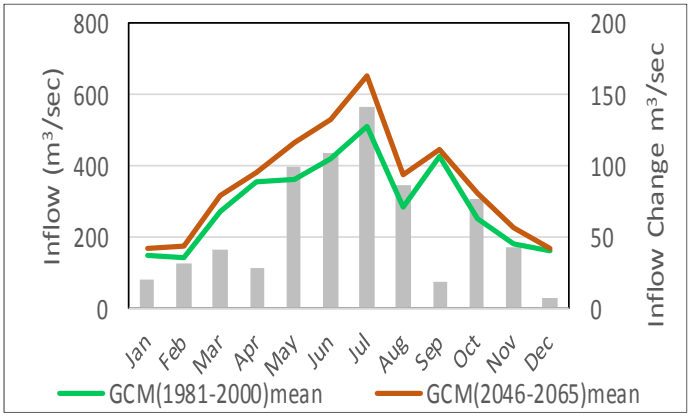

Figure 8. Seasonal change of Haji Dam Inflow between 1981-2000 and 2046-2065.

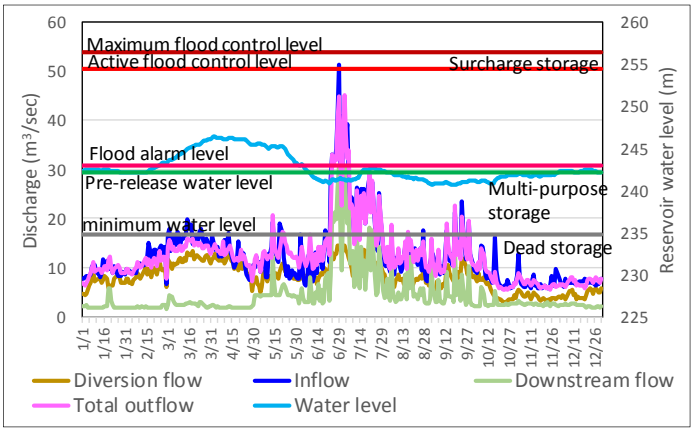

Figure 9. Observed (1981-2000) mean of inflow, total outflow, diversion, discharge to downstream and reservoir water level.

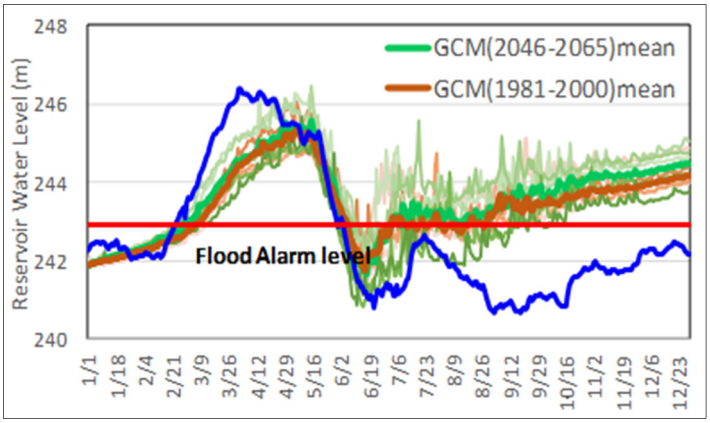

Figure 10. Comparison of yearly average daily GCM simulated reservoir water level between (1981-2000) and (2046-2065).

The general operational rules of Haji Dam are found in the link http://www.cgr.mlit.go.jp/haji. According to the website and 1981-2000 observed outflow, the water level and volume data are summarized in Figure 9.

©2017, IAHR. Used with permission / ISSN 1562-6865 (Online) - ISSN 1063-7710 (Print)

During the early flood period in spring or from March, a minimum amount of inflow is released to supply the needs of irrigation, drinking water, industrial uses, and minimum river flow for river ecology until the end of May. From June, MLIT releases mostly all of the inflow to set aside the space for upcoming flood and to keep a specific water level. As most of high inflow, it is apparent at the end of June and July, then halts in August and a few peak flows occur in September again. The change in the water level (blue line) is noticeable and it goes down under flood alarm level (red line) during this period. After September, the inflow rate is significantly reduced and most of the inflow is ruled to be stored but it will be ensured not to reach the flood warning level especially in the autumn. During winter, the flow into the dam shows an increase from middle of February and is followed by the inflow in the spring because of the snow melting in the high land area. During the spring, the reservoir continuously stores a proportion of the inflow for the approaching summer and the water level is elevated beyond the flood alarm water level in that period. During the flood period, when the control upstream station inflow reaches 200 m^3/sec, operation rule is changed to special flood control scheme and modified to secure both downstream inundation and reservoir safety. The outflow consists diversion channel flow and downstream discharge. Maximum diversion flow was found as 22 m^3/sec, which could produce 38,000 kWh on the way and 300,000 m^3/day water supply to the irrigation, five cities including Hiroshima and the industrial water use.

Consequently, whether the current reservoir rule curve can be managed or not is ambiguous under the high risk of flood and other water use. Therefore, this study investigates whether the standard operating policy (SOP) using current monthly average operating rule curve derived from the recorded data is trustworthy for increasing water demand together with the high potential of flood risk. It can be seen that the possibility of hydropower and municipal water use are likely to increase after wet season as well as increasing flood risk during the second flood of the peak season compared to the reservoir water level managed by the present rules (blue line) as shown in Figure 10. This is due to the inconsistent timing of flood peak between the recorded rule and GCM scenario results. In addition, the current pre-release amount is set aside for the next coming flood, there is not enough capacity for other flood peaks after the largest flood in July. This study suggests that the reservoir regulation for the allocation of flood control allocation before and during flood season should be required to be revised if the present safety reservoir water level (blue line) needs to be kept constant because there will be a probability of increase of inflow under the climate change scenarios. However, the present operating rule assures enough capacity after flood season or from September for multi-purpose reservoir.

ACKNOWLEDGMENTS

This research was supported by the grant of Chugoku regional technology development program provided by Kensetsu Kousaikan. The author would like to thank the data providers, Haji Dam authorities, MLIT Hiroshima, Hiroshima and Shimane Prefecture governments. We are grateful to the EDITORIA science team for the permission to use DIAS server.

REFERENCES

Hosking, J.R.M. & Wallis, J.R. (1987). Parameter and Quantile Estimation for the Generalized Pareto Distribution. *Technometrics*, 29(3): 339-349.

Ines, A. V., & Hansen, J. W. (2006). Bias Correction of Daily GCM Rainfall for Crop Simulation Studies. *Agricultural and Forest Meteorology*, 138(1), 44-53.

Nyunt, C.T., Koike, T., Sanchez, P.A.J., Yamamoto, A., Nemoto, T. & Kitsuregawa, M. (2013). Bias Correction Method for Climate Change Impact Assessments in the Philippines. *Annual Journal of Hydraulic Engineering, JSCE*, 69(4), 19-24.

Nyunt, C.T., Koike, T., Yamamoto, A., Nemoto, T. & Kitsuregawa, M. (2014). Application of Statistical Bias Correction Method to the Yoshino River Basin. *Annual Journal of Hydraulic Engineering JSCE*, Ser.B1, 70(4), 193-198.

Wang, L., Koike, T., Yang, K., Jackson, T. J., Bindlish, R. & Yang, D. (2009). Development of a Distributed Biosphere Hydrological Model and Its Evaluation with the Southern Great Plains Experiments (SGP97 and SGP99). *Journal of Geophysical Research: Atmospheres*, 114(D8), 1-15.

Wood, A.W., Leung, L.R., Sridhar, V. & Lettenmaier, D.P. (2004), Hydrologic Implications of Dynamical and Statistical Approaches to Downscaling Climate Model Outputs. *Climatic Change*, 62(1-3), 189-216.

Yang, D., Koike, T. & Tanizawa, H. (2004). Application of a Distributed Hydrological Model and Weather Radar Observations for Flood Management in the Upper Tone River of Japan. *Hydrological Processes*, 18(16), 3119-3132.

Yongjiu, D. & Qingcun, Z. (1997). *A Land Surface Model (IAP94) for Climate Studies Part I: Formulation and Validation in Off-Line Experiments. Advances in Atmospheric Sciences*, 14(4), 433-460.

©2017, IAHR. Used with permission / ISSN 1562-6865 (Online) - ISSN 1063-7710 (Print)

Proceedings of the 37th IAHR World Congress
August 13 – 18, 2017, Kuala Lumpur, Malaysia

MANAGEMENT STRATEGY BASED ON JOINT PROBABILITY ANALYSIS OF WATER QUANTITY AND QUALITY FOR CHAO RIVER, NORTH CHINA

XUAN WANG[1], NAN ZANG[2] & PEIYU LIANG[3]

[1,2] State Key Laboratory of Water Environment Simulation, Beijing Normal University, Beijing, China
wangx@bnu.edu.cn
[1,2] Key Laboratory for Water and Sediment Sciences of Ministry of Education, Beijing Normal University, Beijing, China
1095919733@qq.com
[3] IER Environmental Protection Engineering Technique co., Ltd, Shenzhen, China
lpyjx1990@whu.edu.cn

ABSTRACT

As a main tributary into the Miyun Reservoir, the only surface drinking water source of Beijing City, the Chao River plays an important role in ensuring the water safety of the reservoir. Taking the discharge as a representative indicator of the water quantity, as well the total nitrogen (TN) concentration and the total phosphorus (TP) concentration as indicators of the water quality, this research calculated joint probability of the water quantity and the water quality indicators of the river by applying the Frank copula function on the basis of analysis of their marginal probability distributions. Then, some water resource management strategies associated with water environment risk were proposed under various combination scenarios of water quantity and water quality variations from 2000-2010. The results showed the following: (1) the Frank copula was suitable for joint analysis of the water quantity and the water quality; (2) from the perspective of water safety of the river, TP concentration had a greater risk than TN concentration for the inflow of the reservoir due to high occurrence probabilities, and then water resource protection measures were provided accordingly. It could provide an effective means of risk analysis for comprehensive management of the water quantity and the water quality in the reservoir inflows.

Keywords: Joint probability analysis; water quantity and quality; water environment risk; Chao River.

1 INTRODUCTION

With the rapid development of the world economy, water resources shortage has become an increasingly serious problem due to double effects of both global climate change and human activities. As the water quantity and the water quality of inflow tributaries have a decisive impact on the water supply safety of the reservoir, it has drawn more attention to accurately analyze the status of quantity and quality of inflows with the aim to reduce the water security risk of the inflow river to the reservoir in recent years.

The water quantity and the water quality of inflows are coexisting and inevitably affect each other, and their mutual influence is complex and synergetic. Thus, some researchers have emphasized the need to jointly consider water quality and quantity issues for integrated water resources management. However, less attention has been given to describe the combined effect of the quantity and quality of inflows in previous studies. Therefore, it is urgently needed to detect dependence structures of water quality and quantity of inflows with joint probability analysis for the management of the reservoir inflow. The multivariate distribution has been more common and easier for describing the correlated hydrologic variables since the copulas function was popularized (Genest et al., 1995). In the past decades, they have been widely used for detecting characteristics of rainfall, droughts, floods and other multivariate extreme events in the field of hydrology (Salvadori and De Michele, 2010; Yu et al., 2016). The copulas function has provided an easy way to estimate multivariate joint distribution functions with known marginal distribution functions (Sklar, 1959), and is expected to be applied into the coexistence analysis of the water quantity and the water quality of inflows to the reservoir.

Therefore, this paper aimed to achieve the following tasks: (1) investigate marginal probability distributions of the water quantity and the water quality of the Chao River, an inflow of the Miyun Reservoir; (2) establish the joint probability distribution function of the water quantity and the water quality of that river; (3) identify its risk sources based on joint probabilities analysis.

2 STUDY AREA AND DATA SOURCE

The Miyun Reservoir is the largest reservoir in North China, between 40°31′–40°45′N and 115°56′–117°10′E. With a 188 km^2 surface area, it is the most important surface water source for Beijing City. It provides nearly 7.0×10^9 m^3 of water to Beijing City each year, accounting for 50% of the total surface water supply. The Chao River is an inflow river flowing into the Miyun Reservoir, with the drainage areas about 8575

 ©2017, IAHR. Used with permission / ISSN 1562-6865 (Online) - ISSN 1063-7710 (Print)

km^2. The surface runoffs of the river has large interannual fluctuations and uneven distributions throughout the year. With the rapid growth of the society and economy, the watershed has showed a clear decreasing trend from 1957 to 2009, and its water quality has shown a tendency toward degradation (Ma et al, 2010). Consequently, the water supply security of Beijing City could be threatened. Therefore, it is of great significance to water supply security for Beijing city to identify major risks to the reservoir inflow that may result from interactions between the water quantity and the water quality of the Chao River for taking appropriate precautions to prevent changes of water security in the reservoir inflow.

Monthly statistical data of water quantity and quality indicators including total nitrogen (TN) concentration and total phosphorus (TP) concentration of the Chao River were used to establish the joint distribution probability model. The observational data were obtained from the "Hydrological Year Book" provided by the Miyun Reservoir Administration Office. The time series of observational data were recorded at the Xinzhuang Station covering the period from 1960 to 2011.

3 CONSTRUCTION OF JOINT DISTRIBUTION PROBABILITY MODEL

In order to describe the relationships between the water quality and the water quantity of the Chao River and further identify its major risk source, the joint distribution probability model was established. This model can consider the water quantity and the water quality of the river together through the copulas function, and provide reasonable suggestions for decision-makers. The process of constructing a joint distribution was decomposed into two steps: (1) Establishment of the marginal distribution for the water quantity and the water quality for the river. Marginal distribution function of the water quantity was developed based on P-III distribution, and the moment approach (Wan et al., 2015) was applied to the parameter estimation for P-III distribution. Marginal distribution function of water quality was developed based on the log-normal distribution. (2) Construction of suitable copula joint distribution function according to dependence structure measure to calculate the joint distribution probabilities of the water quantity and the water quality of the river. Then, the joint distribution probabilities under various combinations of the water quantity and the water quality of the river were obtained to reveal the water security risk for providing management advices of the Miyun Reservoir inflow.

3.1 Construction of marginal probability distributions

3.1.1 Marginal probability distributions of the water quantity

The P-III distribution is a common parameter estimating method in hydrologic frequency analysis, and can describe the marginal probability distribution of the water quantity. When its probability density curve passes the origin of the coordinates, it is known as the gamma distribution ($\Gamma - \mathrm{distribution}$). Its probability density function is:

$$f(x) = \frac{\beta^{\alpha}}{\Gamma(\alpha)} x^{\alpha-1} e^{-\beta x}, \ \ 0 \le x < \infty, \beta > 0 \qquad [1]$$

where $f(x)$ is the probability density function; α and β are the distribution shape and size, respectively, for which $\alpha, \beta \ge 0$; $\Gamma(a)$ is the gamma function. The two parameters, α and β can be calculated through Eq. (2):

$$\alpha = \frac{4}{C_s^2}, \ \ \beta = \frac{2}{\bar{x} C_v C_S} \qquad [2]$$

where C_s is deviation coefficient, C_v is variation coefficient, $\bar{x}$ is mathematical expectation.

The relationship of α and β are as follow:

$$\bar{x} = \frac{\alpha}{\beta}, \ \ C_v = \frac{1}{\sqrt{\alpha}}, \ \ C_s = \frac{2}{\sqrt{\alpha}} \qquad [3]$$

In general, for the frequency analysis of annual rainfall and runoff, $\frac{C_v}{C_s} = \frac{1}{2}$.

3.1.2 Marginal distribution of water quality

Uncertainties of the river's water quality dataset have determined that characteristics of water quality data are obvious abnormal. The studies of multivariate distributions have been dominated by the normal distribution and log-normal distribution. The log-normal probability density can be deduced by the normal probability density, and it can be easily converted to normal distribution on the basis of the definition of log-normal distribution in practical application. Take one-dimensional continuous random variable x as example, the probability density function of log-normal distribution as follows:

©2017, IAHR. Used with permission / ISSN 1562-6865 (Online) - ISSN 1063-7710 (Print)

$$f(x) = \frac{1}{x\sigma\sqrt{2\pi}} exp\left(\frac{-(lnx-\mu)^2}{2\sigma^2}\right), \ x > 0 \quad [4]$$

where μ and σ are logarithmic mean deviation and logarithmic standard deviation of a random variable x, respectively. The relationships between the mean and standard deviation of normal distribution and those of log-normal distribution are as follow:

$$EX(X) = exp\left(\frac{\mu+\sigma^2}{2}\right), \ VAR(X) = \left(exp(2\mu+\sigma^2)\right)(exp(\sigma^2)-1) \quad [5]$$

where *EX(x)* is mathematical expectation; *VAR(x)* is variance.

3.2 Construction of joint probability distribution

3.2.1 Dependence structure measure

Pearson classical correlation coefficient is a widely used statistical indicator to indicate close degree and direction of correlative relationship between two variables with the linear correlation. The sample calculation formula of Pearson classical correlation coefficient r_n used for dependence structure measure is:

$$r_n = \sum_{i=1}^{n}(x_i - \bar{x})(y_i - \bar{y}) / ((n-1)\sqrt{s_x^2 s_y^2}) \quad [6]$$

where n is the length of sample; $\bar{x}$ and $\bar{y}$ are means of x_i and y_i, respectively; S_x^2 and S_y^2 are variances of x_i and y_i.

3.2.2 Establishment of copula function

Sklar (1959) showed that any multivariate probability distribution function H of some random vector $X = (x_1, x_2, \dots, x_n)$ can be represented with a copula function. Let $H(x_1, x_2, \dots, x_n)$ be a n-dimensional random vector with uniformly distributed margins $F_1(x_1), F_2(x_2), \dots, F_n(x_n)$, then there exists an n dimensional copula C such that for all the real values x in R_n as follows:

$$H(x_1, x_2, \dots, x_n) = C(F_1(x_1), F_2(x_2), \dots, F_n(x_n)) \quad [7]$$

where C denotes the copula function. If $F_1(x_1), F_2(x_2), \dots, F_n(x_n)$ are all continuous, then C is unique.

Copula functions have many types. Among them, Archimedean copulas can be constructed easily and have many good properties, thus it is a very popular copula family and has a wide range of applications in finance, hydrology and water resources (Serinaldi and Grimaldi, 2007). Frank copula function, as the most common Archimedean copula, can be applied whether the correlation between variables are positive or negative and there is no limit to the degree of correlation. It can be defined by the following form:

$$C(u_1, u_2) = -\frac{1}{\theta} ln\left[1 + \frac{(exp(-\theta u_1)-1)(exp(-\theta u_2)-1)}{exp(-\theta)-1}\right]; \ \theta \neq 0, \quad [8]$$

where u_1, u_2 are the empirical distribution functions of random variables; $C(u_1, u_2)$ is a two-dimensional copula function of u_2, u_1 with $u_1 = F_1(x_1), u_2 = F_2(x_2)$; and θ is the connection parameter of the joint distribution. The following integral relationship between τ and θ can be obtained based on the definition of Pearson correlation coefficient:

$$\tau = 1 + \frac{4}{\theta}\left[\frac{1}{\theta}\int_0^\theta \frac{t}{exp(t)-1} dt - 1\right], \ \tau \in [-1,1]\backslash\{0\} \quad [9]$$

where τ is the rank correlation of Kendall.

 ©2017, IAHR. Used with permission / ISSN 1562-6865 (Online) - ISSN 1063-7710 (Print)

4 RESULTS AND DISCUSSION

4.1 Optimization of marginal probability distributions of the water quantity and the water quality

Considering that summer is a season with significantly changing runoff and that nitrogen and phosphorus are major nutrients to cause eutrophication to degrade the water quality of the Miyun Reservoir (Wang et al., 2015), August was selected as a study period. Additionally, TN and TP concentrations were used as representative water quality indicators. With the moment method, parameters of marginal probability distributions of the water quantity for the P-III distribution curve of the Chao River were estimated: $\bar{x} = 30.91$, C_v = 1.25 , and $C_s = 2.50$. The fitting degree between the theoretical and experimental cumulative frequency was higher than 97%, and the examined calculated value of the Kolmogorov–Smirnov (K–S) test reached at 0.05 significant level, indicating that the selected model was suitable for the analysis of variables of the water quantity.

The maximum likelihood method was used to estimate the distribution parameters of TN and TP concentrations of the Chao River. Parameter estimation and fitting degree evaluation results are shown in Table 1 and Figure 1. It can be concluded that the results with K-S test reached at 0.1 and 0.05 significant level for TN and TP concentrations, respectively, indicating that the log-normal distribution was the suitable fitting distribution type of TN and TP concentrations in the Chao River.

Table 1. The maximum likelihood parameter estimation and Fitting degree evaluation results for the Chao River.

	EX	VAR	Fitting degree	K-S test
TN	1.1266	0.4678	0.8778	0.2678**
TP	-2.7635	1.4683	0.9934	0.1045*

Note: *correlation is significant at the 0.05 level, **correlation is significant at the 0.1 level.

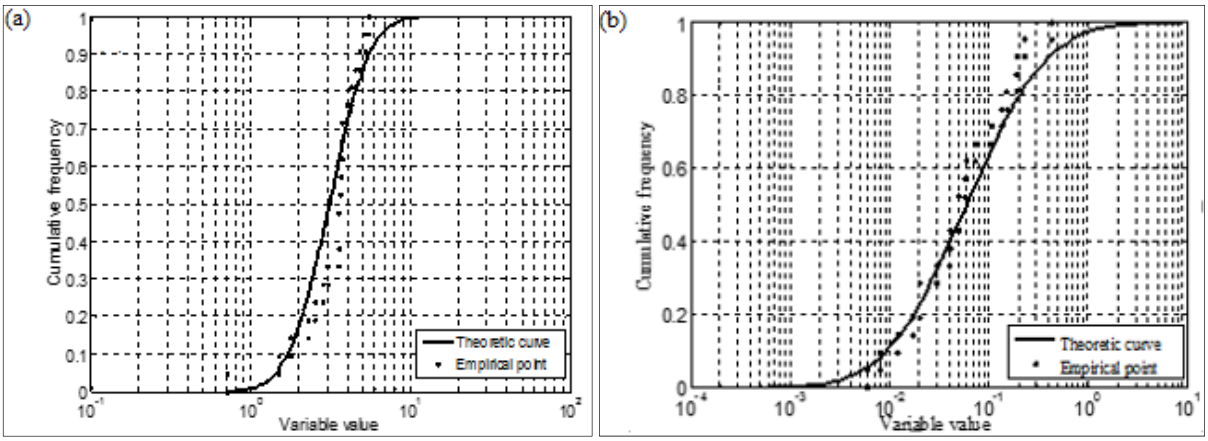

Figure 1. Log-normal distribution cumulative curves of (a) TN concentration and (b) TP concentration for the Chao River.

4.2 Joint probability distribution of the water quantity and the water quality

As a classical statistics, Pearson correlation coefficient analysis was widely used to measure the dependence strength of random variables. The Pearson correlation coefficient of the water quantity and the TN concentration, and the water quantity and the TP concentration was -0.118 and 0.414 respectively, indicating that the water quantity had a poor linear correlation with TN and TP concentrations in the Chao River. According to the results of dependence structure measure, Frank Copula was selected to calculate the joint probability distribution of the water quantity and the water quality, with parameters being estimated by the correlation index method (Table 2).

4.3 Identification of risk sources for the Chao River

The Chao River has shown significant variations in the recent 50 years. In order to determine the influence of the water quantity and the water quality of the Miyun reservoir, reasonable multiple scenarios were conducted. In this study, the average monthly water quality and water quantity indicators from 2000-2010 were calculated for use as a benchmark for setting current scenarios. These three scenarios were: favorable, medium, and adverse. Among them, the scenario where the water quantity was greater than measured mean and the water quality was less than measured mean is defined as the favorable scenario; the scenario where the water quantity was less than measured mean and the water quality indicator (i.e., TN and TP concentrations) was greater than measured mean is defined as the adverse scenario, and other combinations

©2017, IAHR. Used with permission / ISSN 1562-6865 (Online) - ISSN 1063-7710 (Print)

of the water quantity and the water quality were considered as medium scenario. The probabilities of these three combinations were calculated by corresponding joint probability functions of the water quantity and the water quality indicators (i.e., TN and TP concentrations). The results are shown in table 3. From table 3, we can see that the order of joint probabilities in three scenarios for Q-N was: medium > favorable > adverse. The joint probability in adverse scenario was only 16.51% lower than others, and that in medium scenario reached 56.22%, was significant higher than others. However, the order of joint probabilities in three scenarios for Q-P was: favorable > medium > adverse scenario. Relative to the other two scenarios, the joint probability in adverse scenario was low. To sum up, from the perspective of two indicators, the combination of the water quantity and TP was more likely to be in medium and favorable scenarios, and the combination of the water quantity and the TN concentration was more likely to be in medium scenario. Therefore, it was more important to enhance control of the TP concentration.

The Chao River is a seasonal streamflow and its flow mainly depends on rainfall runoff. Due to its large population density, relatively active agricultural activities and the large number of chemical fertilizer, the Chao river basin mainly brings nitrogen and phosphorus and other inorganic pollutants into the Miyun Reservoir. Actually, the scouring of rainfall runoff will lead to a large number of nitrogen and phosphorus pollutants flow into the watercourse. Accordingly, the pollution loads of nitrogen and phosphorus in this watershed are basically in accordance with rainfall season and mainly concentrate in July to September. Therefore, in a whole year, managers should pay special attention to monitor the water quality in the rainy season. In a wet year, managers should also be concerned about the risk of pollution to reservoirs due to the increased losses of nitrogen and phosphorus.

Table 2. Joint probability distribution of the water quantity and the water quality for the Chao River.

	Parameter	Joint pobability distribution function
Q-N	-1.130	$C(u_1,u_2)=\frac{1}{1.130}ln\left[1+\frac{\left(exp(\,1.130\,F(u_1))-1\right)\left(exp(\,1.130\,F(u_2))-1\right)}{exp(\,1.130\,)-1}\right]$ $u_1 \sim P-\mathrm{III}(0.640, 0.0207, 0), \quad u_2 \sim LogN(1.1266, 0.4678)$
Q-P	1.921	$C(u_1,u_2)=-\frac{1}{1.921}ln\left[1+\frac{\left(exp(-1.921\,F(u_1))-1\right)\left(exp(-\,1.921\,F(u_2))-1\right)}{exp(-1.921\,)-1}\right]$ $u_1 \sim P-\mathrm{III}(0.640, 0.0207, 0), \quad u_2 \sim LogN(-2.7635, 1.4683)$

Note: Q-N represents the joint distribution of the water quantity and the TN concentration, and Q-P represents the joint distribution of the water quantity and the TP concentration.

Table 3. Joint probabilities of multiple combinations for the Chao River (unit: %).

		Favorable scenario		Medium scenario	Adverse scenario	
		Marginal probability	Joint probability	Joint probability	Marginal probability	Joint probability
Q-N	Q	55.84	27.27	56.22	44.16	16.51
	N	54.92			45.08	
Q-P	Q	55.84	38.94	37.82	44.16	23.24
	P	59.86			40.14	

Note: Q-N represents the joint distribution of the water quantity and the TN concentration in the Chao River, and Q-P represents the joint distribution of water quantity and the TP concentration in the Chao River.

5 CONCLUSIONS

A methodology based on the copulas function was developed to construct a joint probability analysis of the water quantity and the water quality indicators (i.e., TN and TP concentrations) of the Chao River, an important inflow river of the Miyun Reservoir, North China. The P-III distribution curve was adopted to fit the marginal probability distribution of the water quantity, and the log-normal distribution function was selected by evaluations of goodness of fit to describe water quality in the Chao River. Furthermore, Frank Copula function was selected to develop joint probability distribution function on the basis of the results about the relativity between the water quantity and the water quality indicators of TN and TP concentrations. Ultimately, we analyzed and identified the major risk affecting the water quality security of Miyun reservoir according to the analysis of multiple current and future scenarios under various combinations of the water quantity and the water quality. Thus, the major risk sources for water stress of tributaries to the reservoir inflow were recognized. The results showed that TP indicator was a great risk sources in the Chao River.

This study illustrated that it is feasible to build a joint distribution of the water quantity and the water quality by applying the copula function. The advantage of using copulas function was that sophisticated joint distribution modeling was reduced to investigating the relationship between correlated random variables under the given univariate marginal distributions. This method can provide an effective way for risk analysis for integrated management of the water quantity and the water quality in the reservoir inflow. Therefore, in the future study, researchers need to select more appropriate probability distribution functions to analyze the applicability for corresponding variables, so as to obtain more reasonable results for practical management.

 ©2017, IAHR. Used with permission / ISSN 1562-6865 (Online) - ISSN 1063-7710 (Print)

ACKNOWLEDGEMENTS

This research was financially supported by the National Natural Science Foundation of China (Grant No. 51421065, 51439001, 51679008), and National key research and development program (Grant No. 2016YFC0401302), and Opening Foundation of MOE Key Laboratory of water and Sediment Sciences in China.

REFERENCES

Ma, H., Yang, D., Tan, S.K., Gao, B. & Hu, Q. (2010). Impact of Climate Variability and Human Activity on Streamflow Decrease in the Miyun Reservoir Catchment. *Journal of Hydrol*ogy, 389, 317–324.

Genest, C., Ghoudi, K. & Rivest, L.P. (1995). A Semiparametric Estimation Procedure of Dependence Parameters in Multivariate Families of Distributions. *Biometrika*, 82(3), 543-552.

Salvadori, G. & De Michele, C. (2010). Multivariate Multiparameter Extreme Value Models and Return Periods: A Copula Approach. *Water. Resource Research*, 46(10), 219-233.

Yu, S., He, L. & Lu, H. (2016). An Environmental Fairness Based Optimisation Model for the Decision-Support of Joint Control over the Water Quantity and Quality of a River Basin. *Journal of Hydrology*, 535, 366-376.

Sklar, A. (1959). Fonctions de Répartition a N Dimensions Et Leur Marges, *Publ. Inst. Stat. Paris*, 8, 131–229.

Wan, Z., You, Z., Chen, J. & Wang, M., (2015). Modeling of Aggregation Kinetics by a New Moment Method. *Applied Mathematical Modeling,* 39(22), 6915-6924.

Serinaldi, F. & Grimaldi, S. (2007). Fully Nested 3-Copula: Procedure and Application on Hydrological Data. *Journal of Hydrology Engineering*, 12, 420-430.

Wang, X., Hao, G., Yang, Z., Liang, P., Cai, Y. & Li, C. (2015). Variation Analysis of Streamflow and Ecological Flow for the Twin Rivers of the Miyun Reservoir Basin in Northern China from 1963 to 2011. *Science of the Total. Environment*, 536, 739-749.

©2017, IAHR. Used with permission / ISSN 1562-6865 (Online) - ISSN 1063-7710 (Print)

Proceedings of the 37th IAHR World Congress
August 13 – 18, 2017, Kuala Lumpur, Malaysia

PREDICTING THE IMPACT OF CLIMATE CHANGE ON A WATER SUPPLY RESERVOIR

ZATI SHARIP[(1)], ABD. JALIL HASSAN[(2)], MOHD ZAKI MAT AMIN[(3)], SAIM SURATMAN[(4)] & AZUHAN MOHAMED[(5)]

[(1)] Lake Research Unit, Water Quality and Environment Research Centre, National Hydraulic Research Institute of Malaysia (NAHRIM), zati@nahrim.gov.my
[(2)] River Net Consulting Sdn. Bhd., Shah Alam, Malaysia, abdjalil.hassan@gmail.com
[(3)] Water Resources and Climate Change Research Centre, NAHRIM, zaki@nahrim.gov.my
[(4)] Independent Consultant, Batu Caves, Malaysia, drsaim97@gmail.com
[(5)] NAHRIM, Seri Kembangan Malaysia, azuhan@nahrim.gov.my

ABSTRACT

Climate change is acknowledged to affect hydrological processes and water resources sustainability. Predicting the impact of changing climate on reservoir water quantity and quality is necessary to ensure adequate supply of reasonable quality of raw water. An integrated hydrological and catchment management model is developed for Sg. Terip Reservoir using Infowork Integrated Catchment Model by means of hydrology Probability Distributed Moisture model to simulate the changes of reservoir inflow and capacity, and quality. Rainfall data at three nearby stations are used to calibrate the hydrological model over the period of 2010-2013. Future hydroclimate projection data at the lake catchment based on the downscaled of coarse resolution global climate model projection to 6km grid resolution by means of a regional hydroclimate model over Peninsular Malaysia are used to simulate the climate change impact on the water balance and water quality. The existing water balance of Sg. Terip reservoir is largely impacted by the river water abstraction at the nearby water supply intake and the water source from two water transfer schemes. Inflows from main tributaries are small. Existing water quality assessment showed good water quality throughout the measurement period. Long droughts will have large impact on the reservoir storage capacity. Impact assessment is carried out based on 3 time slices: 2010-2040, 2040-2070, and 2070-2100. Hydroclimate projection under the worst case scenario, IPCC SRES A1FI of the global circulation model - CCSM3 shows that the lake catchment will receive lower rainfall amount in the mid of 21st century (2040-2070) and higher rainfall amount at the end of the 21st century (2070-2100). Simulation results indicate that lake water quality will change only slightly with alteration in these future rainfall events due to low pollution sources. Reservoir water quality may be influenced by the quality of water transferred into the water body.

Keywords: Drought; lake basin; hydrology; hydrodynamic model; water transfer.

1 INTRODUCTION

Water supply reservoir has been continuously created for storage of water to support socio-economic developments. In Malaysia alone, more than 60 reservoirs have been constructed to date for water supply purposes since the first dam was built in 1896 (NAHRIM 2016). The size of the water supply reservoir ranges between 0.05 to 695 km^2 (NAHRIM 2016). The water availability and storage capacity of these reservoirs are very much shaped by the meteorological conditions and water abstraction. Changes in climate are expected to alter water availability by altering the hydrologic cycle, specifically precipitation and evapotranspiration, and other meteorological parameters such as temperature subsequently affects water balance and quality in the water bodies. A study in the Great Lakes region, for example, showed that a change in climate and land use affects the regional hydrology by increasing the percentage of precipitation resulting in increased surface runoff from 17.1% to 21.4% (Barlage et al., 2002). Similarly, projected climatic changes will lead to significant hydrologic response in the Californian Mono Lake Basin including more frequent droughts that ranges from 15% to 22%, a decrease up to 15% in occurrence of wet hydrologic years and a decrease by 15% of annual stream flows (Ficklin et al., 2013). Such changes in hydrological patterns will eventually affect water quality in the reservoirs including increase in nutrient run-off, alteration in thermal stratification and frequent algal bloom (Sahoo et al., 2013; Trolle et al., 2011). In Peninsular Malaysia, a downscale of the regional hydroclimate model predicted significant changes in rainfall pattern over the Peninsula (Amin et al., 2017; Shaaban et al., 2012). How these hydrologic changes affects water bodies in particular the water quality has not been investigated.

 ©2017, IAHR. Used with permission / ISSN 1562-6865 (Online) - ISSN 1063-7710 (Print)

As water supply reservoirs were created based on past hydrology and water resources studies, the impact of climate change may not be incorporated in the original dam design. For example, a low rainfall pattern resulting from climate change may lead to water scarcity in the reservoir while an extreme rainfall event may disrupt the dam ability to store water and lead to excess water release or downstream flooding. Understanding how future climate change affects water quantity and quality in a reservoir is the goal of this study. Sg Terip reservoir in the Linggi Basin is one of the water supply reservoirs in Malaysia that is located within the water stress areas. The reservoir supplies water to 800,000 people in the district of Seremban and Nilai in Negeri Sembilan. The reservoir has recently been affected by frequent droughts induced by El Nino effects which affect its storage capacity. The lake water quality was reported to be in good condition while trophic state was within the mesotrophic to eutrophic in 2012 (Sharip et al., 2014).

The main objective of this study was to investigate the impact of future climate change, specifically rainfall pattern on the water balance and water quality of the water supply reservoir in tropical setting. The work is based on the development of an integrated catchment model comprising hydrological model and water quality model of a lake catchment.

2 STUDY AREA

This research was carried out in Sg Terip Reservoir, Negeri Sembilan (102° 00' 17'' E, 2° 45' 30'' N). The reservoir was selected as research site due to the 2014 state water crisis where water level drops to the critical level. Sg Terip reservoir was created in 1987 for water supply purposes. It has a total surface area of 2.43 km^2 and catchment area of 25.9 km^2. The dam has a full supply level at 103 m above sea level corresponding to 47.7 MCM while the minimum operating level is 79.9 m above sea level contributing to an active storage of 44 MCM (SAINS 2010). The reservoir received water from three tributaries namely Sg Anak Buaya, Sg Terip and Sg Gantor. Two water transfer schemes provide source of water to Sg. Terip reservoir namely the Kelinchi-Talang Reservoirs (98 MCM) and Triang water supply scheme. The existing water balance of Sg. Terip reservoir is largely impacted by the river water abstraction by the nearby water supply intake (Sg. Terip Water Treatment Plant, 136 Mld) and the water source from the transfer schemes.

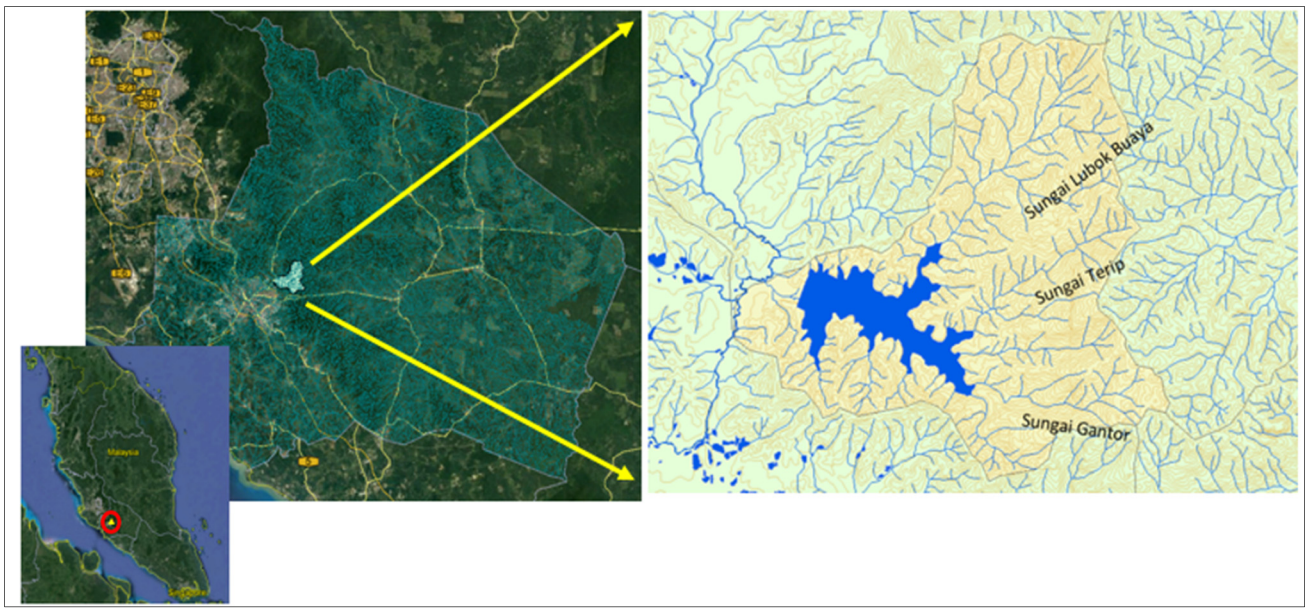

Figure 1. Sg Terip reservoir and its catchment. Inset the study location.

3 MATERIALS AND METHODS

3.1 Data collection

Water quality sampling was carried out in 2014 and 2016 involving measurement of physico-chemical parameters such as temperature, dissolved oxygen (DO), pH and turbidity using multi-parameter probe (YSI 6600) and water sampling. Sampling in 2014 was carried out once while sampling in 2016 was performed about 3-4 times. All sampling was done during the dry period. Water samples were analyzed for nitrate, ammonium suspended solids and phosphorus.

Bathymetric survey was carried out in September 2014 using a single-beam Reson-210 model of echo sounder unit. Depth soundings were acquired along 2.5 km^2 spaced at 100m intervals. In addition, a cross-lane was also established perpendicular to the main survey lines with symmetry with the survey lines to provide the cross-check comparison data needed to evaluate the consistency of the bathymetric data.

©2017, IAHR. Used with permission / ISSN 1562-6865 (Online) - ISSN 1063-7710 (Print)

Temporary tide level observation station was established near to the over-section Sg Terip Dam. All the measured tidal data corrected with the TBM value that flied from the Department of Survey and Mapping Malaysia's Temporary Bench Mark (TBM) to the tidal monitoring site. Rainfall and water level data were obtained from the Drainage and Irrigation Department of Malaysia and Syarikat Air Negeri Sembilan (SAINS). Rainfall data at three nearby stations (Kg Baru Pantai, Setor JPS and Ulu Bendul) were checked with rainfall data measured near the Sg Terip dam. Rainfall data were processed and analyzed for missing values and areal estimates. Water level data between 2003 and 2009 were assessed to understand trend and pattern of existing water balance.

3.2 Model development

The model platform utilized for this research is the Infowork two-dimensional Integrated Catchment Model (ICM) together with of the hydrology Probability Distributed Moisture (PDM) model, developed by HR Wallingford-CEH. ICM simulated the hydrodynamic flow and water quality pattern in the reservoir while the PDM model simulated the hydrology of the catchment taking into consideration the continuous rainfall and soil moisture (Moore, 2007). The 2-D ICM model is based on the shallow water equations known as the depth-average version of the Navier-Stokes equations, Eq. [1-3] assuming that the flow is predominantly horizontal while the variation of the velocity over the vertical coordinate is negligible (Innovyze 2015).

$$\frac{\partial h}{\partial t} + \frac{\partial (hu)}{\partial x} + \frac{\partial (hv)}{\partial y} = q_{1D} \quad [1]$$

$$\frac{\partial (hu)}{\partial t} + \frac{\partial}{\partial x}\left(hu^2 + \frac{gh^2}{2}\right) + \frac{\partial (huv)}{\partial y} = S_{0,x} - S_{f,x} + q_{1D}u_{1d} \quad [2]$$

$$\frac{\partial (hv)}{\partial t} + \frac{\partial}{\partial y}\left(hv^2 + \frac{gh^2}{2}\right) + \frac{\partial (huv)}{\partial x} = S_{0,y} - S_{f,y} + q_{1D}v_{1d} \quad [3]$$

where,

h is the water depth; u and v are the velocities in the x and y directions;
$S_{0,x}$ and $S_{0,y}$ are the bed slopes in the x and y directions;
$Sf_{,x}$ and $S_{f,y}$ are the friction slopes in the x and y directions;
q_{1D} is the source discharge per unit area; U_{1D} and V_{1D} are the velocity components of the source discharge q_{1D} in the x and y directions, respectively

Long duration continuous rainfall runoff model using PDM, which is available in InfoWorks was used for hydrological analysis. The hydrological analysis aimed at determining the rainfall-run off within the catchment which flows into the lake. The runoff from the sub-catchment will then be used as input to the 2D lake model. The catchment was divided into 29 sub-catchments to provide inflow from various tributaries (Figure 2). The water flowing directly to Sg Terip reservoir from Kelinchi through tunnel was included as inflow into the lake while the water abstracted to Sg Terip water treatment plant was included as outflow from the lake. Inflow from Triang Dam which was piped to Sg Terip reservoir since middle of 2016 was not included for model calibration. The survey data were imported into the ICM as ground model and interpolated using mesh technologies to capture the variation of the lake shape.

The water quality model process as described in Toriman et al. (2011) is simulated in 2-dimensional setting in ICM. Water quality determinants configured includes temperature, dissolved oxygen, pH, and nutrients such as nitrate, ammonium and total phosphorus.

3.3 Model calibration and future climate projection

The model was calibrated based on rainfall data at three nearby stations and water level data for the period of 2010-2013. This calibration period was chosen due to availability of reasonably quality rainfall data. We used future hydroclimate projection data at the Sg. Terip catchment based on the downscaled of coarse resolution global climate model projection to 6km grid resolution to simulate the climate change impact on the water balance and water quality. The downscaled model was based on a regional hydroclimate model over Peninsular Malaysia developed by the National Hydraulic Research Institute of Malaysia (NAHRIM 2014a). Impact assessment was carried out using the hydroclimate projection under the worst-case scenario, IPCC SRES A1FI scenario of the global circulation model - CCSM3 and was based on 3 slices period: 2010-2040, 2040-2070, and 2070-2100.

 ©2017, IAHR. Used with permission / ISSN 1562-6865 (Online) - ISSN 1063-7710 (Print)

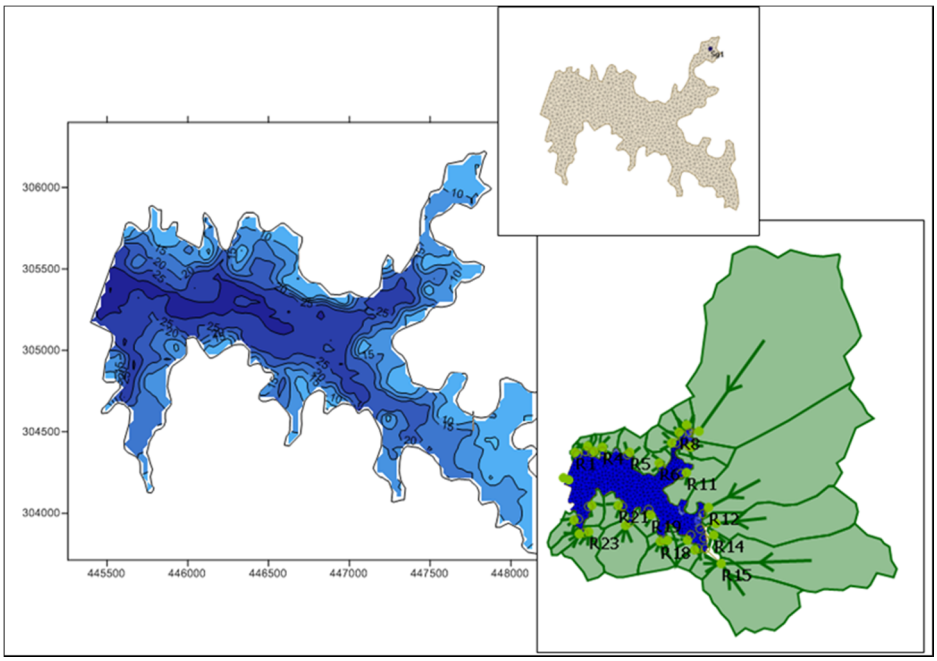

Figure 2. Bathymetry and two dimensional hydrodynamic and catchment model set up for Sg Terip reservoir.

4 RESULTS AND DISCUSSIONS

4.1 Measurement and calibration

Measurement over the period of July to October 2016 showed mean total inflows from main tributaries were small ranging between 0.8 – 2.8 m^3/s. These low inflows were very much influenced by small catchment and long drought. Mean annual rainfall in 2016 was 1876.5 m^3 compared to mean rainfall in 2015 (1911.1 m^3). Figure 3 shows the variation of annual rainfall in all four stations. Average rainfall is about 2000 mm/year.

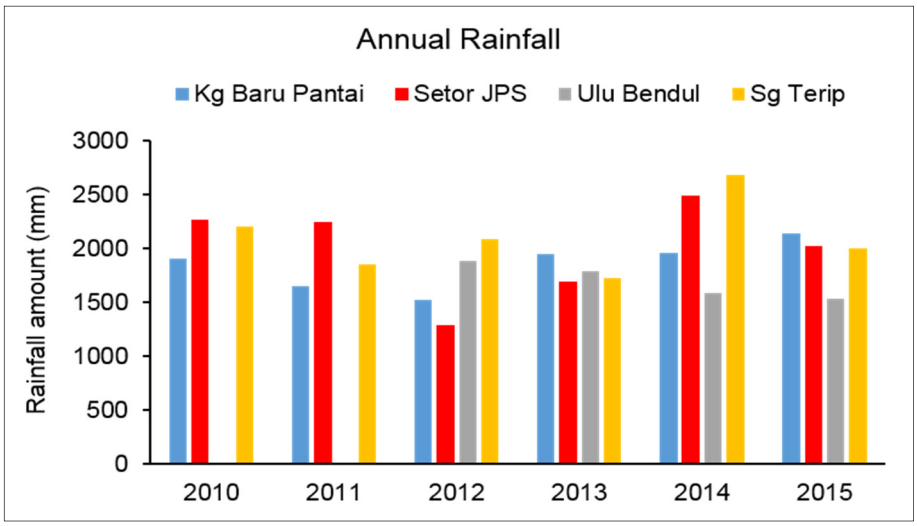

Figure 3. Annual rainfall at few stations near Sg Terip reservoir.

The calibration process for the PDM uses similar approaches as described in Azad et al. (2016) which include analysis of rainfall data, correlation between rainfall data and water level and rainfall factor. In this study, the calibrated parameter consists of rainfall factor, moisture storage distribution and time constant for surface flow. Model calibration showed reasonable match to the measured water level (Figure 4). However, it under-estimated the water level during the dry season likely due to differences in areal rainfall pattern, surface water evaporation and varying amount of water abstraction.

©2017, IAHR. Used with permission / ISSN 1562-6865 (Online) - ISSN 1063-7710 (Print)

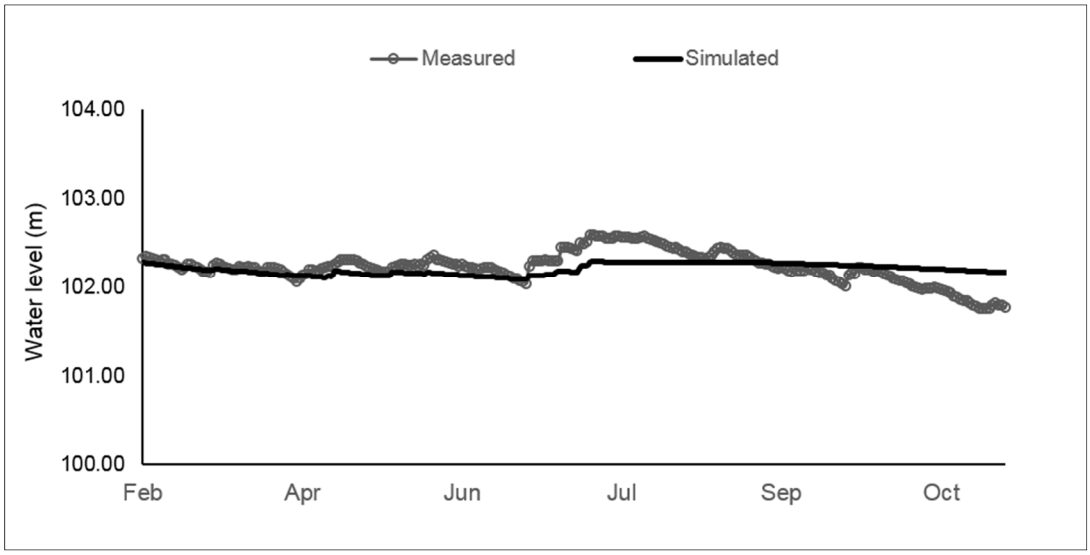

Figure 4. Measured and simulated water level in 2010.

4.2 Existing conditions

4.2.1 Water quantity assessment

Based on the annual dam water level, the water level during 2016 was the lowest compared to the water level between 2010 to 2015 but showed similar trend of water level pattern for 2015 (Figure 5a). The water level in 2016 was about 2 m lower than the water level in 2015. Lower water level in 2016 could also be related to the small increase in dam level in 2015 which was likely to be related to longer dry season. Low water level in 2015-2016 were similar to the low water level in 2003-2006 (Figure 5b). Three-year water level of 2011-2014 showed similar pattern with three-year water level of 2007-2010 with no significant monthly variations.

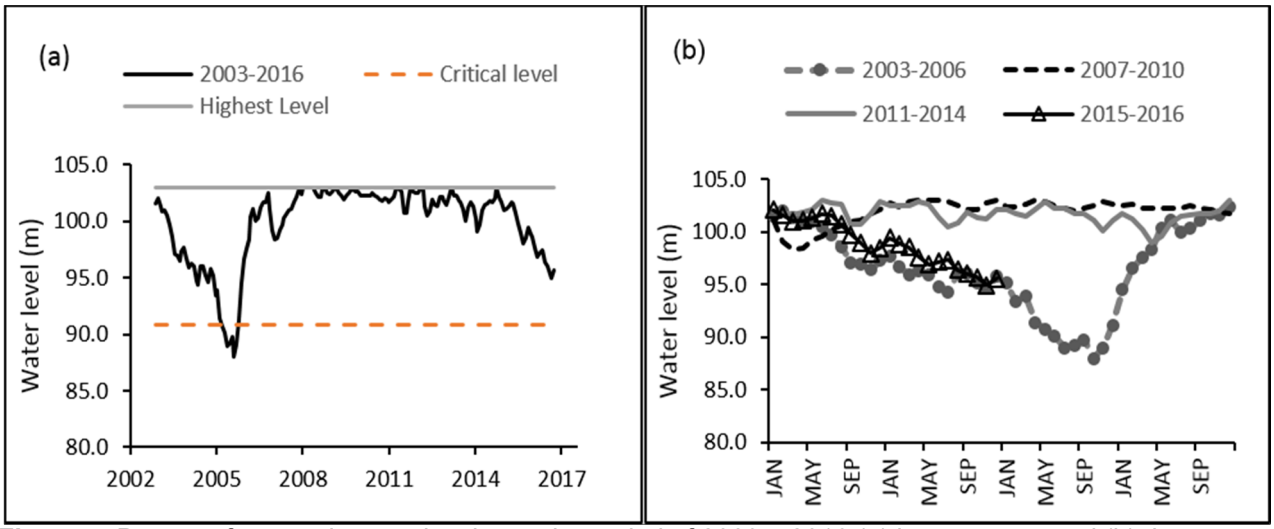

Figure 5. Pattern of reservoir water level over the period of 2003 – 2016 (a) long-term annual (b) three-year.

4.2.2 Water quality assessment

Existing water quality assessment showed good water quality condition throughout the measurement period. Mean values for temperature, DO, pH and turbidity were 30.5 °C, 7.8 mg/L, 6.8 and 5.1 NTU respectively. Based on the Department of Environment Water Quality Index (WQI), the overall water quality in Sg Terip Reservoir was at Class II or clean with WQI ranging between 90 and 93. Water in the lake was observed to be clear and good transparency. Chlorophyll concentrations were generally low in this reservoir (<10 µg/L), with mean value of 3.72 µg/L and higher value >5 µg/L occurred at around 5 m depth. This is consistent with transparency of about 1.5m where photosynthetic active radiation may be penetrated to deeper water column to provide the light environment for plankton growth. However, low nutrient levels may limit growth of plankton communities. TP concentration fluctuated from 0.01 to 0.24 mg/L. Chlorophyll-a and TP values reported in this study are consistent with prior findings (Sharip et al., 2014). However, transparency level was much lower compared to the transparency value of 2.7 m reported in 2012 (Sharip et al., 2014).

 ©2017, IAHR. Used with permission / ISSN 1562-6865 (Online) - ISSN 1063-7710 (Print)

Vertical temperature profile in 2016 showed isothermic conditions indicating the non-existence of thermal stratification likely due to the artificial de-stratification system. DO remained above 4 mg/L in the surface layer until depth ~20m. Depth below 20 m has low DO nearing hypoxic conditions. Horizontal and vertical variation of water quality is shown in Figure 6.

The water quality of the incoming water is mostly clean. The stream temperature is colder < 29°C and transparent indicating undisturbed catchment. The estimation of sediment loading based on measurement of three main tributaries namely Gantor, Anak Buaya and Terip rivers in 2016 showed TSS load ranging between 0.13 to 2600 kg/d while TP and nitrate load ranged between 0.04 to 31.4 kg/d. Higher turbidity was recorded in water from Triang river that transferred into the reservoir (unpublished data SAINS). However, water quality in nearby areas measured between the period of September – November 2016, after the pipe is in operation, showed mild increase in nutrient and TSS.

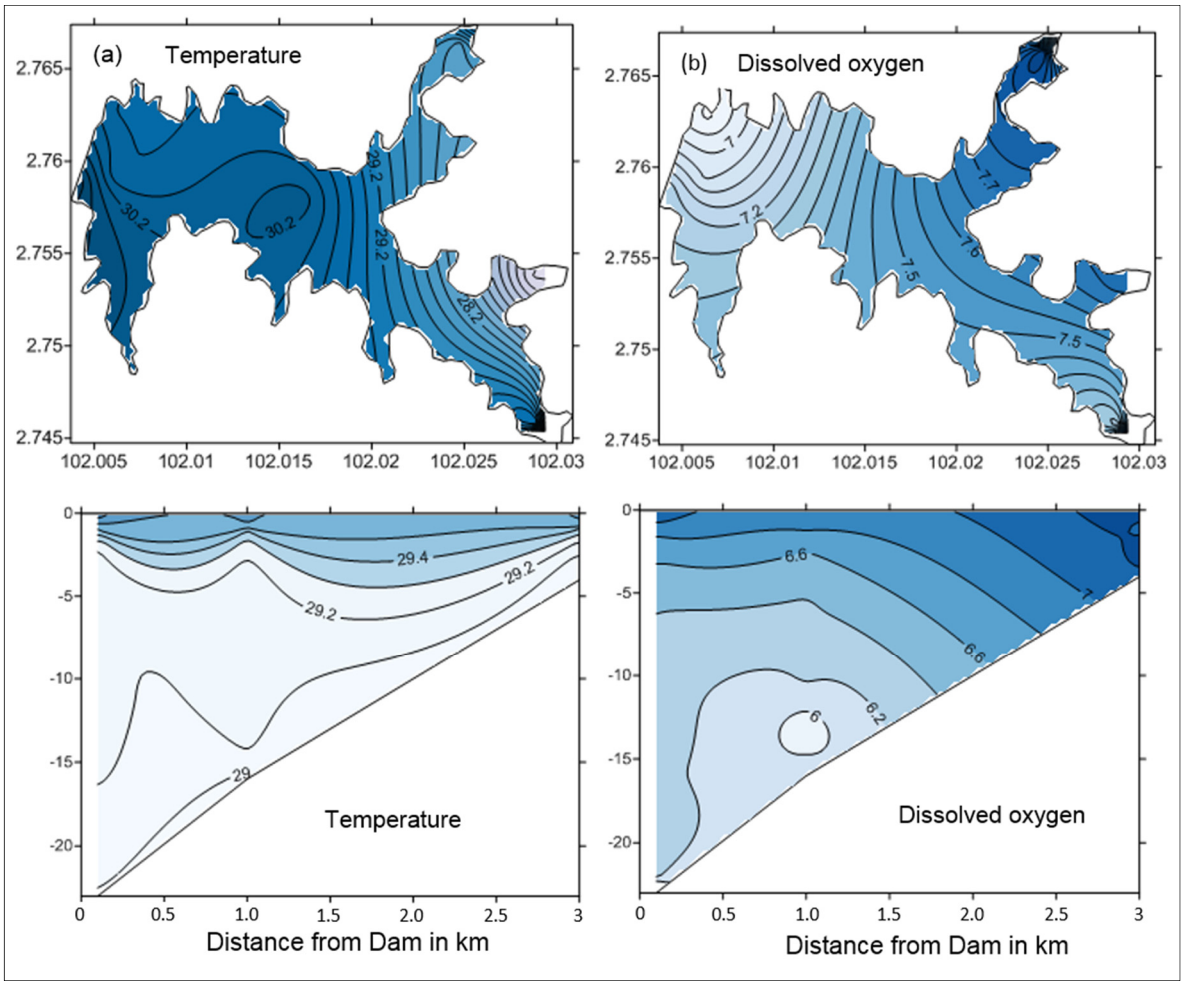

Figure 6. Horizontal and spatial variation of water quality.

4.3 Conditions under future climate projection

4.3.1 Water quantity assessment

Rainfall pattern during future hydroclimate period using IPCC SRES A1FI scenario is shown in Figure 7. Based on hydroclimate projection under the worst case scenario of the global circulation model - CCSM3, Sg Terip lake catchment will receive lower rainfall amount in the mid of 21st century (2040-2070) and higher rainfall amount at the end of 21st century (2070-2100). The mean and maximum rainfall amount during the mid 21st century was 2.8 mm and 225 mm per day, while the mean and maximum rainfall amount during the end of 21st century was estimated at 6.6 mm and 689 mm per day respectively.

©2017, IAHR. Used with permission / ISSN 1562-6865 (Online) - ISSN 1063-7710 (Print)

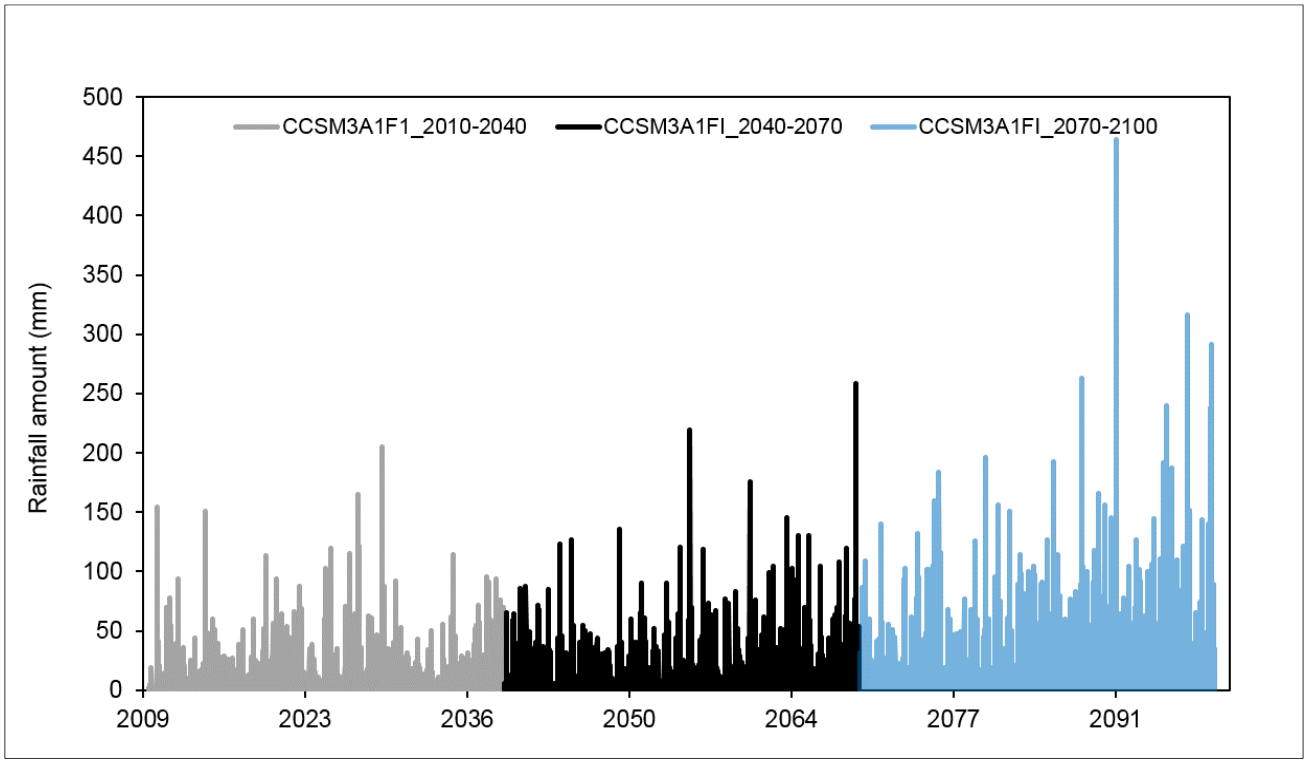

Figure 7. Daily rainfall pattern during future hydro-climate period.

Under the present inflow, future climate projection during 2040-2070 will lead to a decrease in water level below the 100 m above sea level while future climate projection during 2070-2100 will lead to increase in water level exceeding 104.9 m. The simulated water level pattern during 2040-2050 and 2090-2100 is shown in Figure 8. The drop in water level to 98 m above sea level which is equivalent to 80.7% of storage capacity. This value is still high compared to the lowest dam level recorded at 87.64m which was registered on 6 October 2005 (unpublished data, SAINS). Lower water level such as observed in 2005 and 2016 could be associated to lower rainfall within the catchment, higher evaporation rate in the lake and higher water abstraction. The varying changes in evaporation rate, which is associated to temperature, and changes in the amount of water transfer and intake need to be included to improve further the model.

Future climate change projection 2070-2100 suggest that frequent flood will occur especially during 2092-2100 resulting from simulated water level exceeding the spillway level of 103 m above sea level. The excess water can be tapped for future use, and is recommended to be stored in bunded storage to avoid flood to downstream areas. This is consistent to an earlier study that predicts flooding as a major problem for the Sg Terip reservoir (NAHRIM 2014b). The earlier study which simulation was based on HEC-RESSIM model also reported that the reservoir will be free of drought, defined as the simulated water level exceeding the dead storage level (NAHRIM 2014b). This work assume no changes in reservoir storage and catchment land use. The reservoir storage will change with time and land use due to deposition of sediments from eroded catchment areas. However, this effect was not consider in the analysis.

©2017, IAHR. Used with permission / ISSN 1562-6865 (Online) - ISSN 1063-7710 (Print)

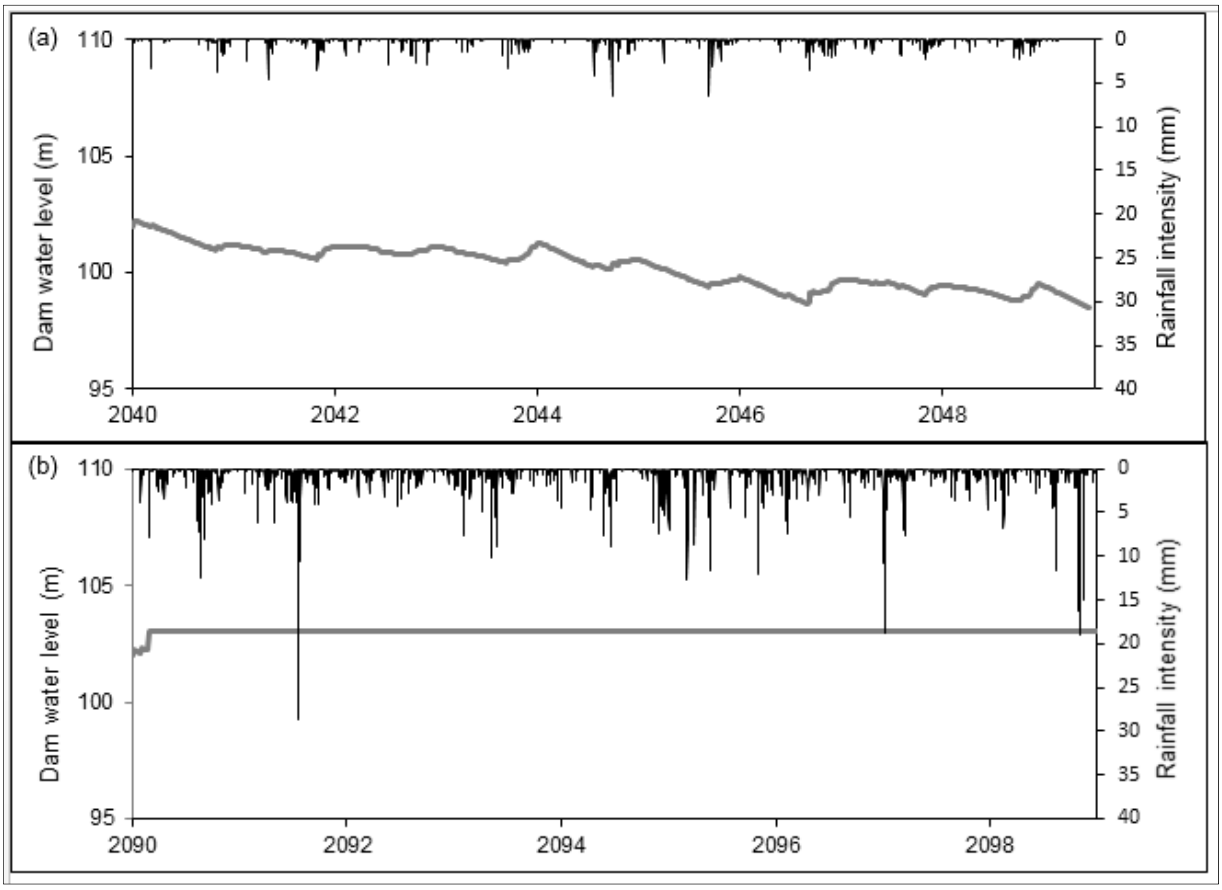

Figure 8. Rainfall pattern and dam water level during future hydro-climate (a) period 2040-2050 (b) period 2090-2100.

4.3.2 Water quality assessment

Simulation results indicated that lake water quality will change only slightly with alteration in these future rainfall events due to low pollution sources. The water quality simulation shows small changes in water quality and pollutant transport due to very slow water movement and flow within the lake, and low pollution levels. Surface DO concentration remains above 7 mg/L under the future climate projection during 2040-2070 and 2070-2090. High DO is probably associated to the atmospheric flux and low oxygen demand due to moderate biological productivity. Higher rainfall amount under the climate projection during 2070-2100 may weaken potential intermittent stratification and improve the water quality through frequent flushing effects. Stratification dynamic, however, was not modelled in this study. Under the assumption of intact catchment, deterioration in water quality will remain small for this reservoir. Some studies reported that increased rainfall associated with climate change will result in increase in suspended and nutrient loadings (Riverson et al., 2013; Mooij et al., 2007). In this reservoir, water quality, however may be influenced by the quality of water that transfer into the waterbody.

5 CONCLUSIONS

Simulation results indicated that flood will occur resulting from excess in rainfall during the end of 21st century while drought will occur resulting from low rainfall amount during the mid of 21st century. Water quality simulation indicated slight change with alteration in these future rainfall events due to low pollution sources. Reservoir water quality may be impacted by the quality of water transferred into the waterbody. This study explores the prediction of the impact of extreme future hydroclimate projection on the condition of a water supply reservoir. However, the results of the study need to be verified further with flood rule curve and probable maximum precipitation/flood in order to enhance the model findings. Further testing of the model with other hydroclimate projection scenarios is also necessary and currently been undertaken to improve the model results and enhance the usefulness of the model for determining alternate management options.

ACKNOWLEDGEMENTS

This project was funded by the Ministry of Natural Resources and Environment Malaysia through vote of Kajian Lanjutan Impak Perubahan Iklim Ke atas Sumber Air (vote No. P23170000190001). The first author would like to thank M. Azril Hilmi Shapiai and Mohd Hafiz Zulkifli for their technical support at field.

©2017, IAHR. Used with permission / ISSN 1562-6865 (Online) - ISSN 1063-7710 (Print)

REFERENCES

Amin, M.Z.M., Shaaban, A.J., Ercan, A., Ishida, K., Kavvas, M.L., Chen, Z.Q. & Jang, S. (2017). Future Climate Change Impact Assessment of Watershed Scale Hydrologic Processes in Peninsular Malaysia by a Regional Climate Model Coupled with a Physically-Based Hydrology Modelo. *Science of the Total Environment,* 575, 12-22.

Azad, W.H., Sidek, L.M., Basri, H., Fai, C.M., Saidin, S. & Hassan, A.J. (2016). 2 Dimensional Hydrodynamic Flood Routing Analysis on Flood Forecasting Modelling for Kelantan River Basin. *MATEC Web of Conferences*, 87, 1-7.

Barlage, M.J., Richards, P.L., Sousounis, P.J. & Brenner, A.J. (2002). Impacts of Climate Change and Land Use Change on Runoff from a Great Lakes Watershed. *Journal of Great Lakes Research*, 28, 568-582.

Ficklin, D.L., Stewart, I.T. & Maurer, E.P. (2013). Effects of Projected Climate Change on the Hydrology in the Mono Lake Basin, California. *Climatic Change*, 116, 111-131.

Innovyze (2015). *Basic 2D Hydraulic Theory*.

Mooij, W.M., Janse, J.H., Domis, L.N.D.S., Hulsmann, S. & Ibelings, B.W. (2007). Predicting the Effect of Climate Change on Temperate Shallow Lakes with the Ecosystem Model Pclake. *Hydrobiologia,* 584, 443-454.

Moore, R.J (2007). The PDM rainfall-runoff model. *Hydrology and Earth System Sciences Discussion* 11(1) 483-499

NAHRIM (2014a). *Extension Study of the Impacts of Climate Change on the Hydrologic Regime and Water Resources of Peninsular Malaysia*. National Hydraulic Research Institute of Malaysia, Seri Kembangan, 429.

NAHRIM (2014b). *Study on Vulnerability, Adaptation and Assessment for Water Resources and Dam Storage Capacity under Climate Change Impact Scenarios*. National Hydraulic Research Institute of Malaysia, Seri Kembangan, 255.

NAHRIM (2016). *Blueprint for Lake and Reservoir Research and Development (R&D) in Malaysia.* National Hydraulic Research Institute of Malaysia, Seri Kembangan, 91.

Riverson, J., Coats, R., Costa-Cabral, M., Dettinger, M., Reuter, J., Sahoo, G. & Schladow, G. (2013). Modeling the Transport of Nutrients and Sediment Loads into Lake Tahoe under Projected Climatic Changes. *Climatic Change* 116, 35-50.

Sahoo, G.B., Schladow, S.G., Reuter, J.E., Coats, R., Detingger, M., Riverson, J., Wolfe, B. & Costa-Cabral, M. (2013). The Response of Lake Tahoe to Climate Change. *Climatic Change*,116, 71-95.

Shaaban, A.J., Amin, M.Z.M., Chen, Z.Q. & Ohara, N. (2012). Regional Modeling of Climate Change Impact on Peninsular Malaysia Water Resources. *Journal of Hydrologic Engineering* 16, 1040-1049.

Sharip, Z., Zaki, A.T.A., Shapai, M.AH., Suratman, S. & Shaaban, A.J. (2014). Lakes of Malaysia: Water quality, Eutrophication and Management. *Lakes & Reservoirs: Research & Management*, 19, 130-141

Toriman, O.E., Hashim, N., Hassan, A.J., Mokhtar, M., Juahir, H., Gasim, M.B. & Abdullah, M.P. (2011). Study on the Impact of Tidal Effects on Water Quality Modelling of Juru River, Malaysia. *Asian Journal of Scientific Research,* 4, 129-138.

Trolle, D., Hamilton, D.P., Pilditch, C.A., Duggan, I.C. & Jeppesen, E. (2011). Predicting the Effects of Climate Change on Trophic Status of Three Morphologically Varying Lakes: Implications for Lake Restoration and Management. *Environmental modelling & software*, 26, 354-370.

 ©2017, IAHR. Used with permission / ISSN 1562-6865 (Online) - ISSN 1063-7710 (Print)

SWAT-BASED OPTIMZATION FOR AGRICULTURAL NONPOINT SOURCES POLLUTION CONTROL

CHAO DAI[1], XIAOSHENG QIN[2] & HUAI CHENG GUO[3]

[1,2] School of Civil and Environmental Engineering, Nanyang Technological University, Singapore
xsqin@ntu.edu.sg
[3] College of Environmental Science and Engineering, Peking University, Beijing, China

ABSTRACT

Excessive agricultural non-point source (ANPS) loads such as nitrogen and phosphorus has aroused serious concern around the world due to their stimulation effects on lake eutrophication. The best management practices (BMPs) are deemed effective approaches in mitigating the ANPS pollutions. However, identification of BMP placement schemes is a challenging task and involves many considerations, like cost benefits, hydrological processes, landscape condition, and water quality responses. In this study, we attempt to rely on the soil and water assessment tool (SWAT) and the genetic algorithm (GA) to find out the optimal allocations of BMPs for controlling ANPS at a watershed level. Methodology wise, the SWAT model help forecasting nutrient dynamics under different BMPs scenarios and the GA tool aided solving the optimization model to explore the best spatial placement of BMPs. The objective of the optimization model is to minimize the overall system cost of deploying the BMPs, and its constraints comprised control of exceedance frequencies for both total nitrogen (TN) and total phosphorus (TP). This study investigated the feasibility of combing different BMPs cost-effectively by using an optimization model and shed some lights for watershed managers on how to conduct a scientific decision-making under complex conditions.

Keywords: Best management practices; SWAT; agricultural nonpoint sources genetic algorithm.

1 INTRODUCTION

Best management practices (BMPs) have been effective tools for agricultural nonpoint sources (ANPS) pollution control, mainly through attenuating the nutrient loads from the surface runoff. Many BMPs, such as parallel terrace (PT), grade stabilization structure (GS) and filter strips (FS), were widely applied in many watersheds (Arabi et al., 2006; Gaddis et al., 2014; Shen et al., 2015; Sweeney et al., 2004). Placement of suitable schemes of BMPs involves many considerations, like cost benefits, hydrological processes, landscape conditions, and water quality responses. As a proven tool for simulating the related processes, soil and water assessment tool (SWAT) have been extensively used in many studies (Santhi et al., 2006; Liu et al., 2013). In general, scenario analysis through SWAT is a straightforward approach as the best alternative of management could be evaluated directly. However, the decision space of choosing combinations of BMPs is huge, which can hardly be covered by a limited number of predefined scenarios. Genetic algorithm (GA) can solve such problem through a directional global searching. Previously, SWAT-based GA approach was tested in a number of BMPs placement cases located in United States (Kaini et al., 2012; Ahmadi et al., 2013) and China (Chen et al., 2015). However, such a method has not been tested in the Lake Dianchi watershed, one of the representative polluted lake watersheds in China. Hence, this research aims to apply a SWAT-based optimization method aided by a GA solver to help identify suitable BMPs placement schemes in a tributary basin of Lake Dianchi watershed, in consideration of nutrient control and system cost.

2 METHODOLOGY

2.1 Study area

To improve the aquatic environment of the Lake Dianchi, China, the excessive nutrient loads from the tributaries need to be controlled. The Baiyuhe (BYH) River (as shown in Figure 1) is one of the tributaries of the Lake Dianchi (Dai et al., 2016), with its water environmental function deemed for recreational purpose. Accordingly, the protection target of BYH River belongs to grade IV, and the controlled discharge concentrations of TN and TP are 1.5 and 0.3 mg/L, respectively. In 2009, the exceedance frequencies of TN and TP at the BYH River are 28.6 and 3.0%, respectively. In this study, for demonstration purpose, we assume a control target of improving the TN and TP exceedance frequencies by 30 and 50%. To achieve such a goal, three potential BMPs, including PT, GS and FS, are considered for the studied river basin, with their unit construction costs being 26 $/m, 10,000 $/structure and 4.6 $/m, respectively (Maringanti et al., 2011; Park et al., 2013).

©2017, IAHR. Used with permission / ISSN 1562-6865 (Online) - ISSN 1063-7710 (Print)

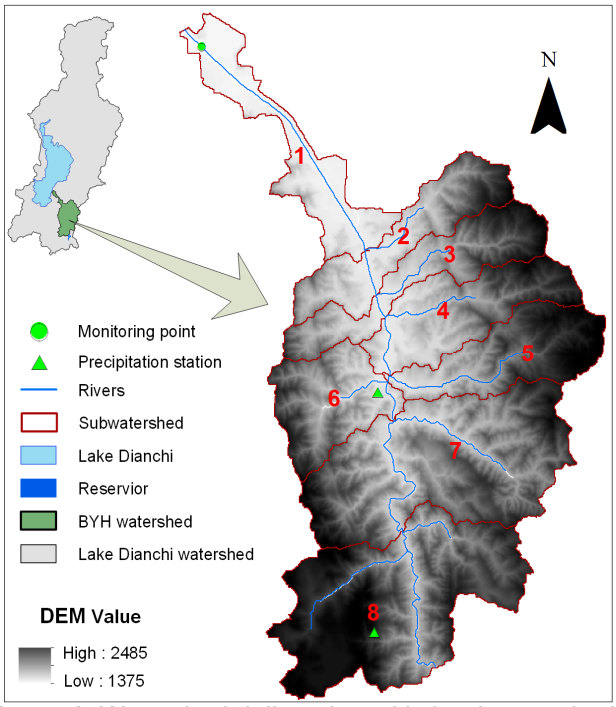

Figure 1. Watershed delineation with 8 subwatersheds.

2.2 Setup of SWAT model

The digital elevation model (DEM), soil map, and land over data obtained from different sources (Fao and Isric, 2009) are used for subwatershed delineation. The BYH river basin is subdivided into 8 subwatersheds (as shown in Figure 1), with a monitoring point at the estuary of the BYH river. The SWAT model has been calibrated by using the mean monthly flow and nutrient concentrations from 2005 to 2010, where the details can found in Dai (2016). SWAT could help evaluate the effect of implementing BMPs by changing the corresponding parameters (Panagopoulos et al., 2012). For technical details, readers can refer to Arabi et al. (2006), Kaini et al. (2012) and Maringanti et al. (2011).

2.3 Setup of optimization model for BMP placement

The optimization model for the BMP placement management can be formulated as follows:

$$Min\ c^* = \left[1 + \eta^m \cdot \frac{(1+\rho)^N - 1}{\rho \cdot (1+\rho)^N}\right] \cdot \sum_{i=1}^{8}\sum_{j=1}^{3} x_{i,j} \cdot b_{i,j} \cdot \mu_j \quad [1]$$

Subject to:

$$1 - \frac{\sum_{t=1}^{365} sign_t\left[s_{N,t}(x_{i,j}) - o_N\right]}{365} \Big/ \gamma_N \geq \upsilon_N \quad [2]$$

$$1 - \frac{\sum_{t=1}^{365} sign_t\left[s_{P,t}(x_{i,j}) - o_P\right]}{365} \Big/ \gamma_P \geq \upsilon_P \quad [3]$$

where c^* is the total cost (\$), involving both construction and maintenance costs; i is the index of subwatershed; ρ is the interest rate (%), representing value fluctuations (this study it is set to 9%); j is the index of BMPs; $x_{i,j}$ is the binary decision variable, which denotes whether if the BMPs are implemented in the ith subwatershed; $b_{i,j}$ is the implementation level of the PT, GS and FS; μ_j is the unit construction cost of the jth BMP (\$/m, \$/structure and \$/m for PT, GS and FS, respectively); η^m is the ratio of the maintenance cost to the construction cost (3%); t is the daily index of SWAT simulation and $t = 1,2,\ldots,365$; γ_N and γ_P are the TN and TP exceedance frequencies (%) during the reference year (i.e., in 2009), respectively;o_N and o_P are the TN and TP discharge limits, respectively (mg/L); υ_N and υ_P denote the expected improvement rates related to TN and TP exceedance frequencies, respectively (%); $s_{N,t}(x_{i,j})$ and $s_{P,t}(x_{i,j})$, as the outputs from the SWAT model, are the TN and TP concentrations on the tth day (mg/L), respectively. In such optimization model, a binary decision variable is used to judge if a specific BMP (i.e., PT, GS and FS) should be implemented. The

 ©2017, IAHR. Used with permission / ISSN 1562-6865 (Online) - ISSN 1063-7710 (Print)

objective is to seek the lowest system cost and the constraints mainly include control of nutrient exceedance. GA is used to search the solutions for the model, where each chromosome consists of 24 genes (which is the multiplicative result of the number of subwatersheds and the types of BMPs), denoting the binary variables (Arabi et al., 2006; Panagopoulos et al., 2013).

3 RESULTS AND DISCUSSIONS

Figure 2 shows the optimal spatial distribution of the three BMPs (i.e., FS, GS and PT) based on the solutions of the binary decision variables. For subwatersheds 1, 2, 3, and 7, GS is suggested to be implemented. Moreover, PT is recommended to be installed at the subwatershed 3, 4, 5, 7 and 8. For FS, it is suggested to be installed at the subwatersheds 3, 5, 6 and 8. Interestingly, subwatershed 3 would consider all three BMP options. Figure 3 presents the BMP implementation cost at the 8 subwatersheds. It appears that subwatersheds 1 and 2 would need the lowest implementation cost (i.e., $\$11.93 \times 10^3$) while the BMP implementation in subwatershed 8 would be the most expensive (i.e., $\$453.26 \times 10^3$). Figure 4 shows the implementation cost of different BMPs in the entire watershed. The results indicate that (i) a majority of the overall system cost (i.e. 86%) would be allocated to install PT; (ii) GS has the lowest investment as only 4% of the system cost is suggested to be allocated.

The study has a number of limitations. The strategies of PT, GS and FS were considered as the potential BMPs because their representation methods in the SWAT modeling system have been well developed in Kaini et al. (2012) and Maringanti et al. (2011). However, other BMPs, such as detention wetland, may also be considered. Thus, increasing the candidate pool to include more potential BMPs could lead to better BMP placement schemes. Moreover, a hybrid combination of decision variables (i.e., mixture of discrete and continuous decision variables) could help identify the optimal locations, types and sizes for placing potential BMPs. This study only considers the 0-1 discrete decision variables, which are only suitable for identifying locations and types of BMPs. Further study on including size optimization is desired.

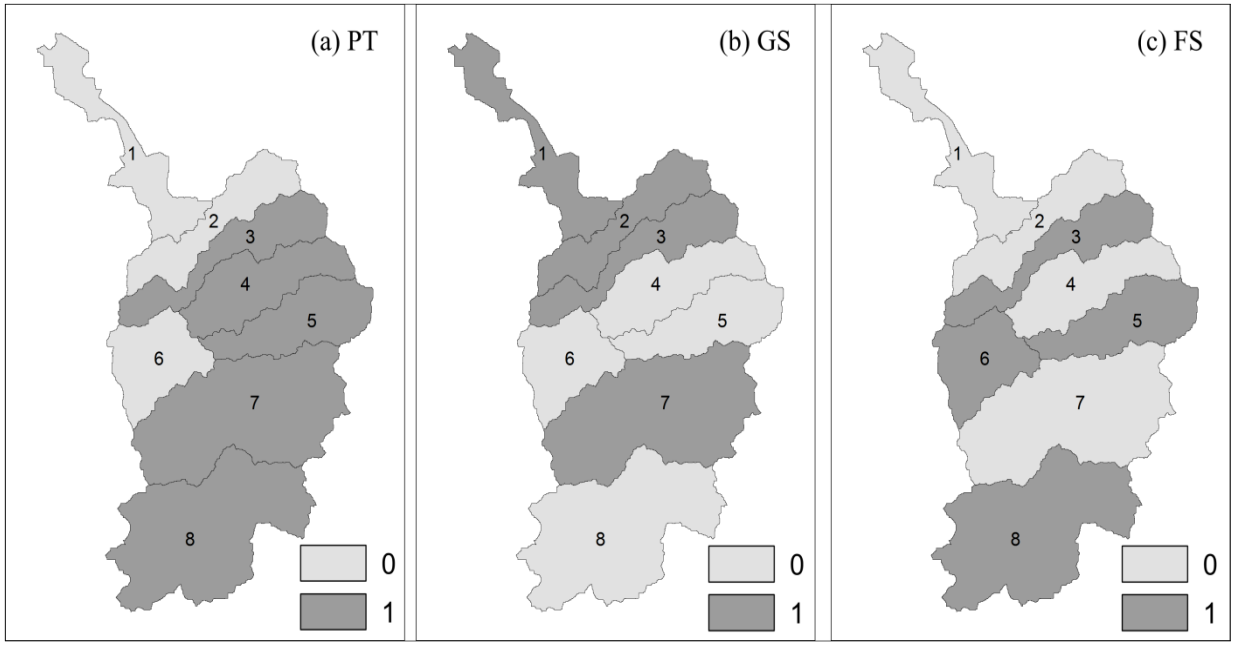

Figure 2. The optimal spatial distribution of FS, GS and PT based on the solutions of the binary decision variables (note: 0 denotes no application, and 1 denotes application).

©2017, IAHR. Used with permission / ISSN 1562-6865 (Online) - ISSN 1063-7710 (Print)

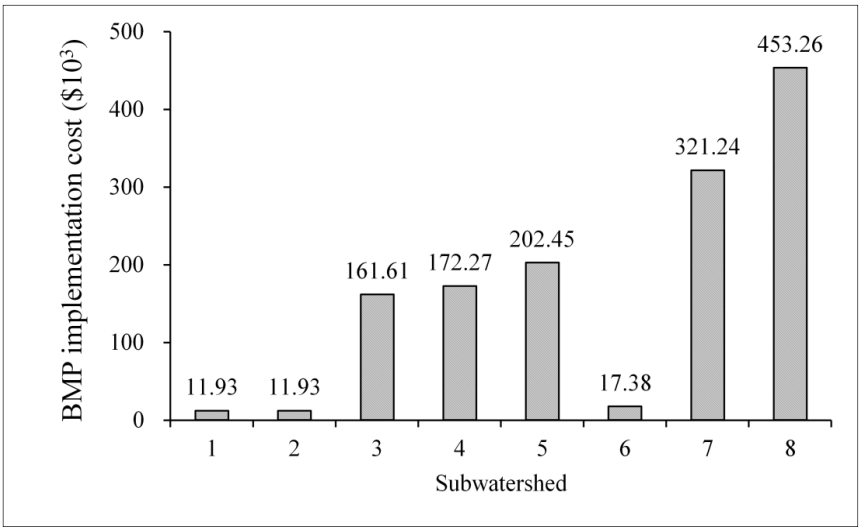

Figure 3. The BMP implementation cost at the 8 subwatersheds.

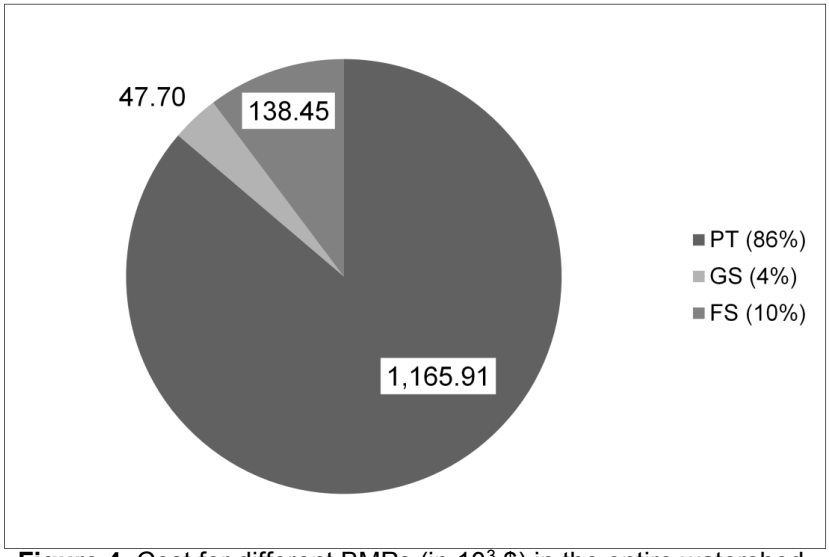

Figure 4. Cost for different BMPs (in 10^3 $) in the entire watershed.

4 CONCLUSIONS

In this study, a SWAT-based optimization method aided by GA was applied for optimizing BMP placement in agricultural non-point source pollution control problem in the BYH river basin. The SWAT model was used to simulate the hydrological process and nutrient fate under different BMPs scenarios and the GA tool was applied for solving the optimization model. Three BMPs, involving FS, GS and PT, were planned for the 8 subwatersheds. The result indicated that PT was the most popular option but would need over 80% of the total investment. GS investment only occupied 4% of the overall investment. From this study, it was found that the applied SWAT-based optimization model was effective in seeking optimal placement scheme of BMPs at a watershed scale and could help watershed managers make better decisions. Further studies are still needed to consider the saving of computational time and tackling of system uncertainties.

ACKNOWLEDGEMENTS

This material is based on research/work supported by the Major Science and Technology Program for Water Pollution Control and Treatment of China (2013ZX07102-006), and in part by Singapore's Ministry of Education (MOE) AcRF Tier 1 Project (Ref No. RG170/16; WBS No.: M4011766.030).

REFERENCES

Ahmadi, M., Arabi, M., Hoag, D.L. & Engel, B.A. (2013). A mixed Discrete-Continuous Variable Multiobjective Genetic Algorithm for Targeted Implementation of Nonpoint Source Pollution Control Practices. *Water Resources Research*, 49, 8344-8356.

Arabi, M., Govindaraju, R.S. & Hantush, M.M. (2006). Cost-effective Allocation of Watershed Management Practices using a Genetic Algorithm. *Water Resources Research*, 42(10), 1-14.

 ©2017, IAHR. Used with permission / ISSN 1562-6865 (Online) - ISSN 1063-7710 (Print)

Chen, L., Qiu, J., Wei, G. & Shen, Z. (2015). A Preference-Based Multi-Objective Model for the Optimization of Best Management Practices. *Journal of Hydrology*, 520, 356-366.

Dai, C. (2016). Study on the Spatio-Temporal Optimization and Regulation of the Water Quantity and Water Quality for the Water Resources System of the Lake Watershed. *Ph.D. Thesis* of Peking University (In Chinese).

Dai, C., Cai, Y., Lu, W., Liu, H. & Guo, H. (2016). Conjunctive Water use Optimization for Watershed-Lake Water Distribution System under Uncertainty: A Case Study. *Water Resources Management*, 30, 4429-4449.

Fao, I. & Isric, I. (2009). *JRC: Harmonized World Soil Database (version 1.1)*. FAO, Rome, Italy and IIASA, Laxenburg, Austria.

Gaddis, E.J.B., Voinov, A., Seppelt, R. & Rizzo, D.M. (2014). Spatial Optimization of Best Management Practices to Attain Water Quality Targets. *Water Resources Management*, 28, 1485-1499.

Kaini, P., Artita, K. & Nicklow, J.W. (2012). Optimizing Structural Best Management Practices using SWAT and Genetic Algorithm to Improve Water Quality Goals. *Water Resources Management*, 26, 1827-1845.

Liu, R., Zhang, P., Wang, X., Chen, Y. & Shen, Z. (2013). Assessment of Effects of Best Management Practices on Agricultural Non-Point Source Pollution in Xiangxi River Watershed. *Agricultural Water Management*, 117, 9-18.

Maringanti, C., Chaubey, I., Arabi, M. & Engel, B. (2011). Application of a Multi-Objective Optimization Method to Provide Least Cost Alternatives for NPS Pollution Control. *Environmental Management*, 48, 448-461.

Panagopoulos, Y., Makropoulos, C. & Mimikou, M. (2012). Decision Support for Diffuse Pollution Management. *Environmental Modelling & Software*, 30, 57-70.

Park, Y.S., Engel, B.A., Shin, Y., Choi, J., Kim, N.W., Kim, S.J., Kong, D.S. & Lim, K.J. (2013). Development of Web GIS-based VFSMOD System with Three Modules for Effective Vegetative Filter Strip Design. *Water* 5, 1194-1210.

Santhi, C., Srinivasan, R., Arnold, J.G. & Williams, J. (2006). A Modeling Approach to Evaluate the Impacts of Water Quality Management Plans Implemented in a Watershed In Texas. *Environmental Modelling & Software*, 21, 1141-1157.

Shen, Z., Hou, X., Li, W., Aini, G., Chen, L. & Gong, Y. (2015). Impact of Landscape Pattern at Multiple Spatial Scales on Water Quality: a Case Study in a Typical Urbanised Watershed in China. *Ecological Indicators*, 48, 417-427.

Sweeney, B.W., Bott, T.L., Jackson, J.K., Kaplan, L.A., Newbold, J.D., Standley, L.J., Hession, W.C. & Horwitz, R.J. (2004). Riparian Deforestation, Stream Narrowing, and Loss of Stream Ecosystem Services. *Proceedings of the National Academy of Sciences of the United States of America*, 101, 14132-14137.

©2017, IAHR. Used with permission / ISSN 1562-6865 (Online) - ISSN 1063-7710 (Print)

Proceedings of the 37th IAHR World Congress
August 13 – 18, 2017, Kuala Lumpur, Malaysia

SINGLE-RESERVOIR OPERATION OPTIMIZATION USING JAYA ALGORITHM FOR JAYAKWADI-1 DAM, INDIA

VARTIKA PALIWAL[1], ANIRUDDHA D GHARE[2] & ASHWINI B MIRAJKAR[3]

[1,2,3] Civil Engineering Department, VNIT, Nagpur, India,
vartikapaliwal19@gmail.com; adghare@yahoo.co.in; ashmirajkar@gmail.com

ABSTRACT

In the present study, an attempt is made to implement the new optimization algorithm called Jaya algorithm for reservoir operation. The algorithm works on the principle moving towards the best and away from the worst solution. The objective of the study is to minimize the annual sum of square deviation of the releases and storages from their target values (demands) and the model is formulated with 75% probable inflows for Jayakwadi stage-1 Reservoir, Upper Godavari basin, India. The optimization model for the mentioned objective is coded in MATLAB. Total releases (Left bank canal (LBC) + Right bank canal (RBC) + Industrial and urban releases) for the month of June, July, August, September, October, November, December, January, February, March, April, May are 9.65, 6.33, 6.65, 7.90, 7.93, 15.02, 10.78,17.21,10.78, 27.29, 9.09, 26.09 Million Cubic Meter (MCM) respectively. The algorithm has been successfully applied to real world water resources management problem. The study can further be extended for multi-reservoir planning and operation.

Keywords: Reservoir operation optimization; Jaya algorithm; probable inflows; Jayakwadi stage-1 reservoir.

1 INTRODUCTION

Water is a preeminent natural resource for the sustenance of all living creatures on earth. Therefore its sustainable use is very important. In India, huge and growing population is leading to the depletion in water level. Scarcity of water has been felt in many zones of India especially, Marathwada region of Maharashtra state, India. Marathwada region receives 770 mm of annual rainfall on an average, still the area faces drought in some parts. Main source of water for Marathwada region is Jayakwadi project which is on Godavari River. In present situation, it is important to manage the available water resources as the rainfall over the catchment shows decreasing trend over the last 30 years. For the management of available resources, proper planning and management of the projects (reservoir) is necessary. Simulation and optimization are the available techniques for proper reservoir planning and management. Optimization is the process of achieving the best from the available resources. Many studies have been conducted and various models were formulated for efficient management and reservoir operation. Simonovic (1992) presented a review on the mathematical model used in reservoir operation and management and presented conclusions reached by the previous Studies Yeh (1982), Wurbs et al. (1985). Combined Linear Programming (LP) and Dynamic Programming (DP), (Yeh and Becker, 1982) was implemented for real time reservoir optimization. Mousavi et al. (2004) developed Fuzzy State Stochastic Dynamic Programming (FSDP) model which was successfully applied to the Zayandeh–Rud river–reservoir system in Isfahan, the central part of Iran. There are various studies on systems analysis techniques which deeply explore the system and provide complete information and are increasingly applied to the real-life problem as a result of wider computer application, software availability and better understanding of the approach (Srivastava and Awchi, 2009). Moreover, every method has its own pros and cons so it is difficult to advocate that a particular method will be well suited to all real world problems (Labadie, 2004).The choice of methods depends on the characteristics of the system, data availability, its objective and restrictions (Yeh, 1985).

The newly developed Jaya algorithm has proved its effectiveness in solving a number of constrained and unconstrained benchmark functions (Rao, 2016) but has not yet been implemented in the field of water resources. In order to check its effectiveness in the field of water resources, Jaya algorithm has been applied for optimization of reservoir operation and its performance is evaluated using indices such as Monthly Frequency Deficit (MFD), Monthly Average Deficit (MAD), Annual Frequency Deficit (AFD), Annual Average Deficit (AAD) (Jothiprakash and Shanthi 2009; Mirajkar and Patel 2016).

2 STUDY AREA

The mathematical model has been formulated for, Jayakwadi project (Latitude: 19.4841°N and Longitude - 75.3735°E) located at the site of Jayakwadi village in Paithan taluka of Aurangabad district, Maharashtra, India, with gross storage capacity of 2909.04 MCM and live storage capacity of 2170.04 MCM respectively.

 ©2017, IAHR. Used with permission / ISSN 1562-6865 (Online) - ISSN 1063-7710 (Print)

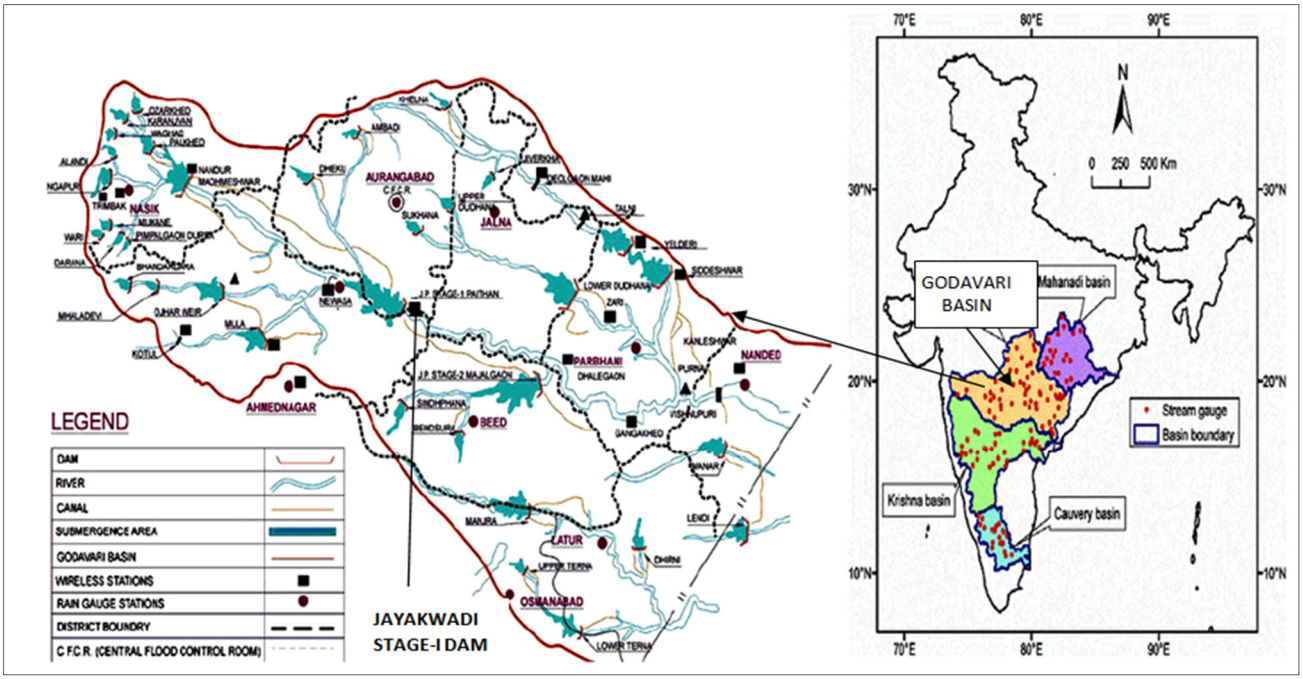

Figure 1. Index map of Upper Godavari basin.

3 MODEL FORMULATION FOR RESERVOIR OPTIMIZATION

3.1 Objective

The Objective of the study is minimization of sum of square deficit of actual total releases and actual storages from maximum total demands and target storages respectively. Mathematically it is represented as follows:

$$F(SQDV) = minimization \sum_{t=1}^{12} [w_1(R_t - D_t)^2 + w_2(S_t - TS_t)^2] \quad [1]$$

where,
w_1= Weightage for release function
w_2= Weightage for storage function
$t = 1,2,3 \ldots .12 \ \{1 = june \ldots 12 = may\}$
$F(SQDV)$ = Square deficit function to be optimised.
R_t= Total release for time period 't' in MCM= [$R_{1,t} + R_{2,t} + R_{3,t}$]
$R_{1,t}$ =Left bank canal release for time period 't' in MCM
$R_{2,t}$=Right bank canal release for time period 't' in MCM
$R_{3,t}$=Industrial and urban release for time period 't' in MCM
D_t= Total demand for reservoir for time period 't' in MCM.

3.2 Constraints

The model is subjected to the following constraints.

3.2.1 Storage Continuity constraint

Change in storage is the difference between inflow and outflow. This balancing equation is defined as continuity equation, mathematically it is expressed as follows:

$$S_{t+1} = S_t + I_t + I'_t - (R_t + E_t + O_t) \quad [2]$$

where,
I_t= Inflow in to reservoir for time period 't' in MCM
O_t = Overflow from the reservoir for time period 't' in MCM
I'_t = Reservoir lift for time period 't' in MCM
E_t = Evaporation loss from the reservoir for time period 't' in MCM
S_t= Storage of reservoir at the beginning of time period 't' in MCM

©2017, IAHR. Used with permission / ISSN 1562-6865 (Online) - ISSN 1063-7710 (Print)

S_{t+1} = Storage of reservoir at the end of time period '*t*' in MCM

3.2.2 Constraint of storage limit

Storage of a reservoir lies between its dead storage and its gross storage capacity.

$$Smin \leq S_t \leq Smax \quad [3]$$

where,
$Smin$ = Dead Storage in MCM
$Smax$ = Maximum Storage capacity of the reservoir at F.R.L. in MCM

3.2.3 Canal carrying capacity constraints

Release through a particular canal is less than or equal to its capacity.

$$R_{1,t} \leq C_{1,max} \quad [4]$$

and

$$R_{2,t} \leq C_{2,max} \quad [5]$$

where,
$R_{1,t}$ =Left bank canal (LBC) release for time period '*t*' in MCM
$R_{2,t}$=Right bank canal release (RBC) for time period '*t*' in MCM
$C_{1,max}$ = Maximum canal carrying capacity for LBC in MCM
$C_{2,max}$ = Maximum canal carrying capacity for RBC in MCM

3.2.4 Constraint of Irrigation and industrial Demands

Releases from the reservoir for its purposes like irrigation, domestic and industrial water supply should lies between its minimum requirement and maximum demand.

$$Min\ D_{x,t} \leq R_{x,t} \leq Max\ D_{x,t} \quad [6]$$

where,
$x = 1,2,3$ & $t = 1,2,3..12$
$R_{x,t}$ = Release from supply-x for time period '*t*' in MCM
$D_{x,t}$= Demand for x^{th} supply for time period '*t*' in MCM

3.2.5 Overflows constraint

Overflow occurs when storage exceeds maximum storage value. Overflow constraint developed by Chavez-Morals et al. (1987) is used in the present study, the overflow constraint is given:

$$O_t \geq S_t + I_t + I'_t - R_t - E_t - S_{max} \quad [7]$$

where,
O_t = Overflow from the reservoir for time period '*t*' in MCM
I_t = Inflow in to reservoir during the month for time period '*t*' in MCM
I'_t = Reservoir lifts for time period '*t*' in MCM.
R_t= Total release for time period '*t*' in MCM= [$R_{1,t} + R_{2,t} + R_{3,t}$]
E_t = Evaporation loss from the reservoir for time period '*t*' in MCM
S_t= Storage of reservoir at the beginning of time period '*t*' in MCM
S_{max} = Maximum Storage capacity of the reservoir at F.R.L. in MCM

4 JAYA ALGORITHM

Jaya algorithm (Rao, 2016) is parameter less algorithm and has tendency to move towards the best solution and away from the worst solution.

If F(x) is the function to be maximized or minimized, population size or candidate solution (number of solution set) = n and design variables=m. Suppose F(x) is minimization function and among the population size of n, the best candidate solution is the one providing best function value that is minimum F(x) among the population size and similarly the worst candidate solution is the one providing worst function value that is maximum F(x) among the population size. The values of the variable are updated successively as per Eq. [8].

 ©2017, IAHR. Used with permission / ISSN 1562-6865 (Online) - ISSN 1063-7710 (Print)

$$X'_{j,k,i} = X_{j,k,i} + r_{1,(j,i)}\left[(X_{j,best,i}) - \left|(X_{j,k,i})\right|\right] - r_{2,(j,i)}\left[\left(X_{j,worst,i}\right) - \left|(X_{j,k,i})\right|\right] \quad [8]$$

where,
$X_{j,k,i}$=Old value of variable
j= Position of variable, k= Candidate solution, i= Iteration
$X'_{j,k,i}$= Updated value of the variable
$X_{j,best,i}$= j[th] variable corresponding to the best candidate
$X_{j,worst,i}$= j[th] variable corresponding to the worst candidate
$r_{1,(j,i)}$ and $r_{2,(j,i)}$ = Random variable for j[th] variable during i[th] iteration ranging between 0 to 1.

If function value corresponding to the updated value of the variable is better than the old value, then the scheme replaces the old value of the variable with the updated value, else the old value is retained. Final output of the iteration will be the best solutions corresponding to the old and updated value with respect to the candidate solution. Solution of this iteration will be the input for next iteration (Rao, 2016).

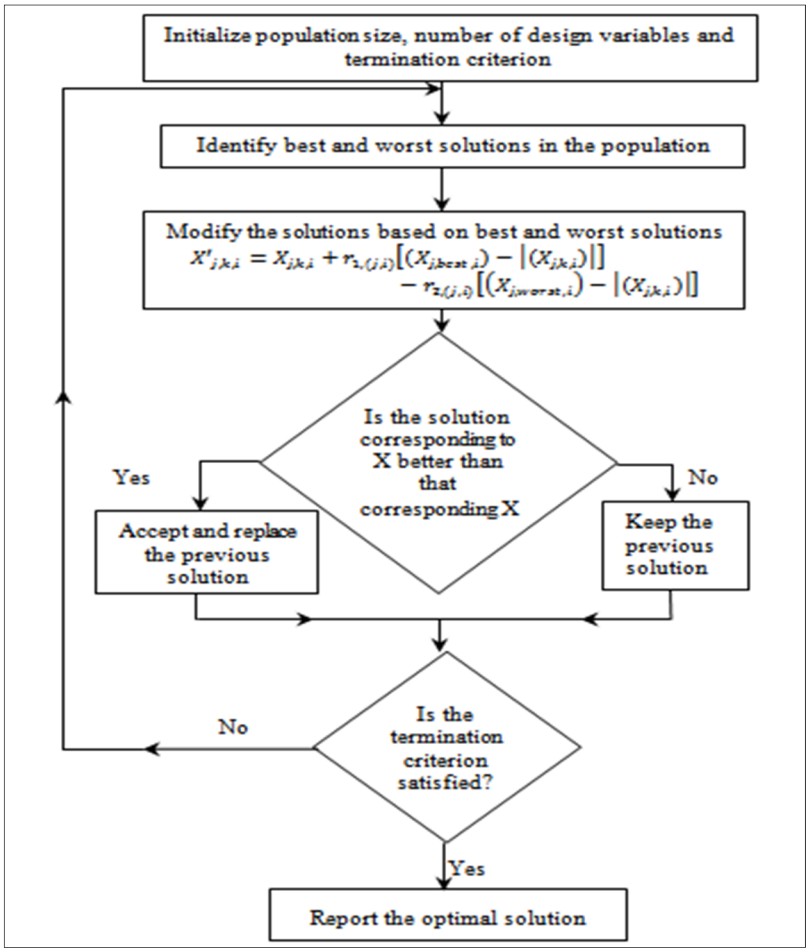

Figure 2. Flow chart for Jaya algorithm (Rao, 2016).

5 RESULTS AND DISCUSSIONS

Jaya algorithm has been applied to Jayakwadi stage-I reservoir for 75% probable inflows (for 23-year historical data) with the objective function as minimization of sum of square deficit of monthly total releases and monthly storages from actual monthly maximum total releases and monthly target storages (Sharma et al., 2016) respectively. The results were obtained in the terms of LBC releases, RBC releases, industrial and urban releases, total releases and corresponding storages in MCM which were compared with the actual data(LBC releases, RBC releases, industrial and urban releases, total releases and storages in MCM) corresponding to 75% probable inflows. Graphical presentation of the results that is obtained values with their respective target values (actual values of the year having inflow corresponding to 75% probable inflow) is shown in Figure 3 for LBC releases, Figure 4 for RBC releases, Figure 5 for industrial and urban releases, Figure 6 for total releases and Figure 7 for storages. Table 1 represents the comparative values of releases and storages for actual values (values of the year corresponding to 75% probable inflow that is year having annual inflow value nearest to the 75% probable inflow calculated annually).

©2017, IAHR. Used with permission / ISSN 1562-6865 (Online) - ISSN 1063-7710 (Print)

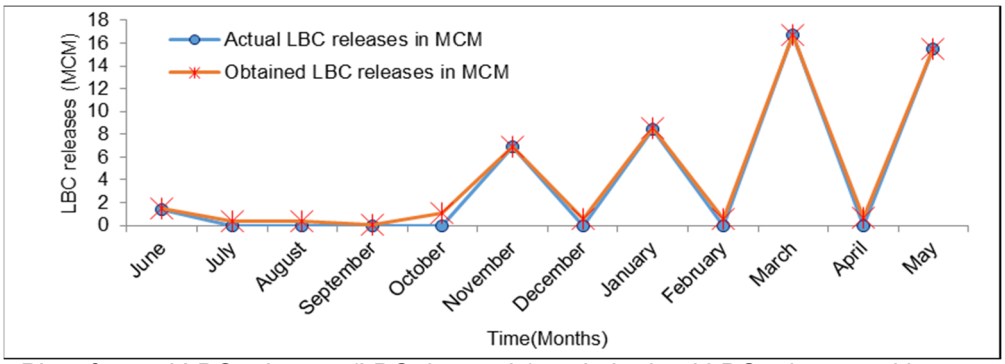

Figure 3. Plot of actual LBC releases (LBC demands) and obtained LBC releases with respect to time (months).

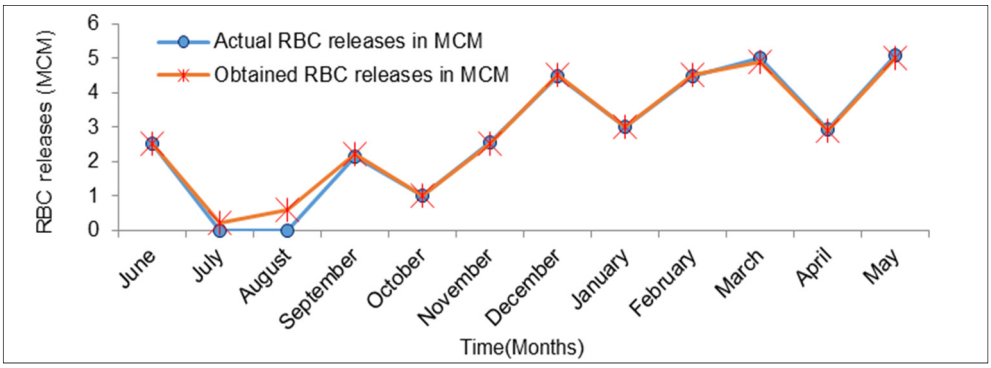

Figure 4. Plot of actual RBC releases (RBC demands) and obtained RBC releases with respect to time (months).

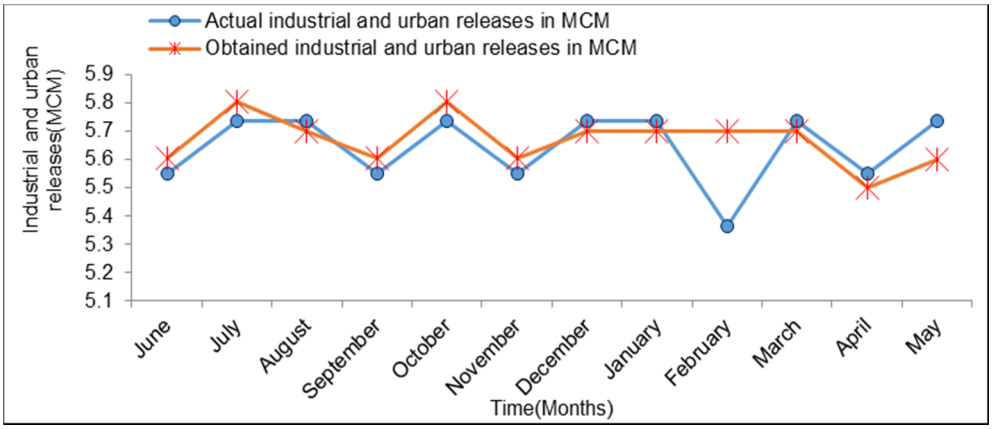

Figure 5. Plot of actual industrial and urban releases (demands) and obtained industrial and urban releases with respect to time (months).

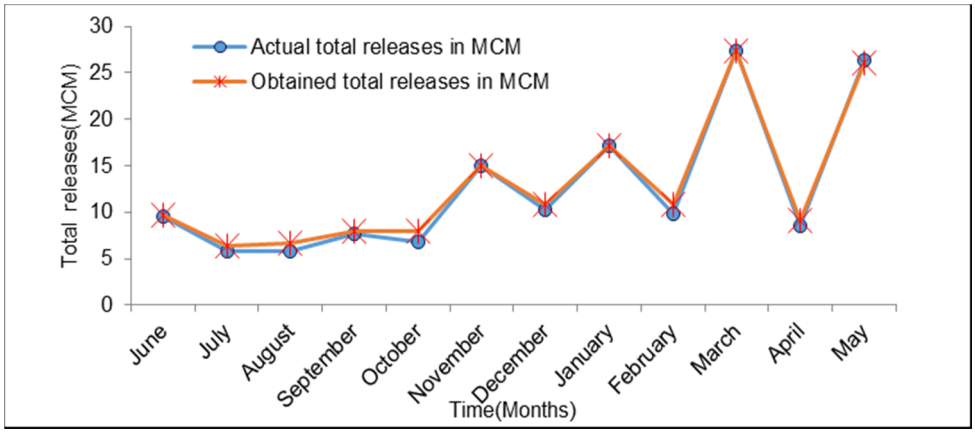

Figure 6. Plot of actual total releases (total demands) and obtained total releases with respect to time (months).

©2017, IAHR. Used with permission / ISSN 1562-6865 (Online) - ISSN 1063-7710 (Print)

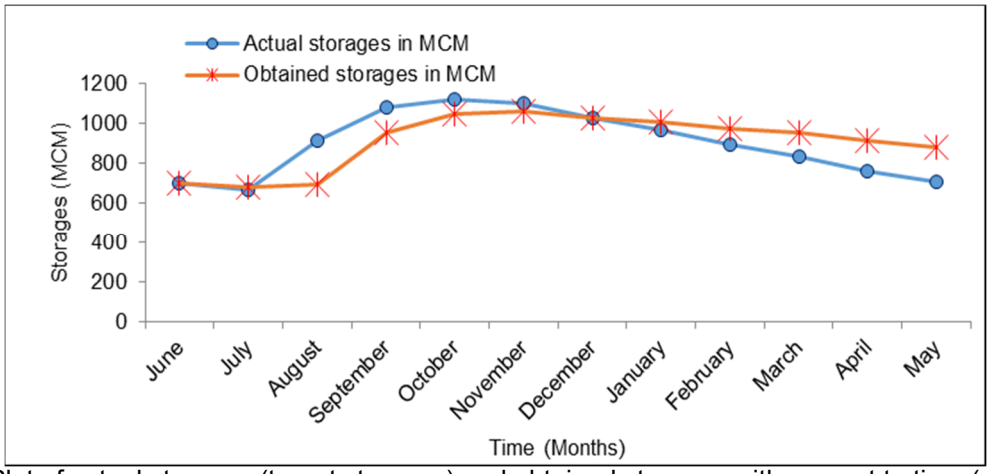

Figure 7. Plot of actual storages (target storages) and obtained storages with respect to time (months).

Table 1. Comparison of actual values and obtained values annually.

Cases	Actual in MCM	Obtained in MCM
LBC releases	48.92	52.96
RBC releases	33.17	33.77
Industrial and urban releases	67.71	68.00
Total releases	149.81	154.72
Storages	10776.53	10895.87

The performance of the Jaya algorithm for this reservoir was assessed using a simulation model with the same objective function as that of the model. Simulation is carried out using 9 years of historical data. Graphical representation of the results obtained from the simulation model is shown in Figure 8 for LBC releases, Figure 9 for RBC releases, Figure 10 for industrial and urban releases, Figure 11 for total releases and Figure 12 for storages. The performance of the developed model was evaluated on the basis of following parameters: 1) Monthly Frequency Deficit (MFD), 2) Monthly Average Deficit (MAD), 3) Annual Frequency Deficit (AFD), 4) Annual Average Deficit (AAD), were calculated for LBC releases, RBC releases, Industrial and urban releases and total releases (Jothiprakash and Shanthi 2009) is presented in Table 2 which were found to be satisfactory.

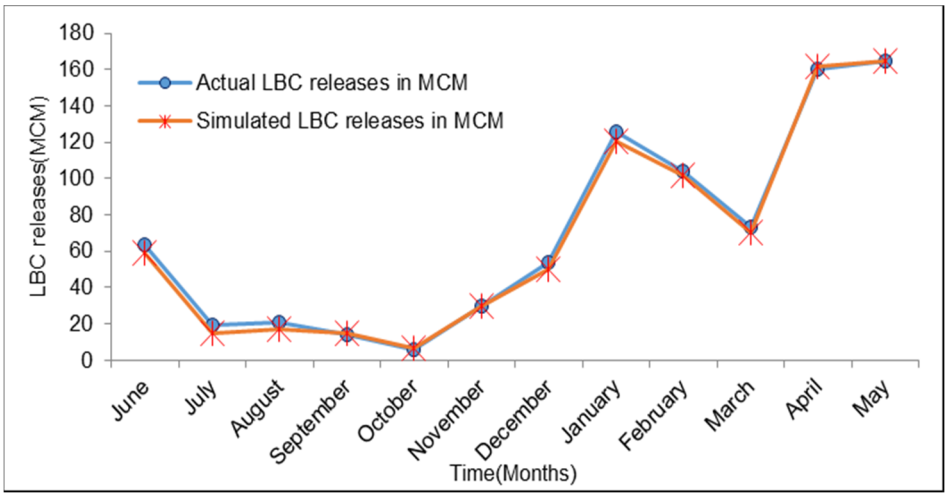

Figure 8. Plot of actual LBC releases (LBC demands) and simulated LBC releases with respect to time (months).

©2017, IAHR. Used with permission / ISSN 1562-6865 (Online) - ISSN 1063-7710 (Print)

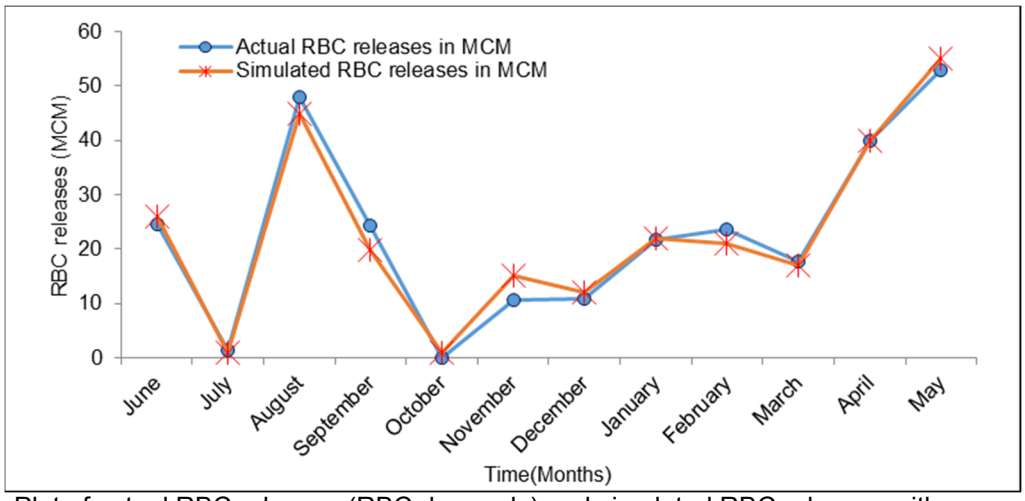

Figure 9. Plot of actual RBC releases (RBC demands) and simulated RBC releases with respect to time (months).

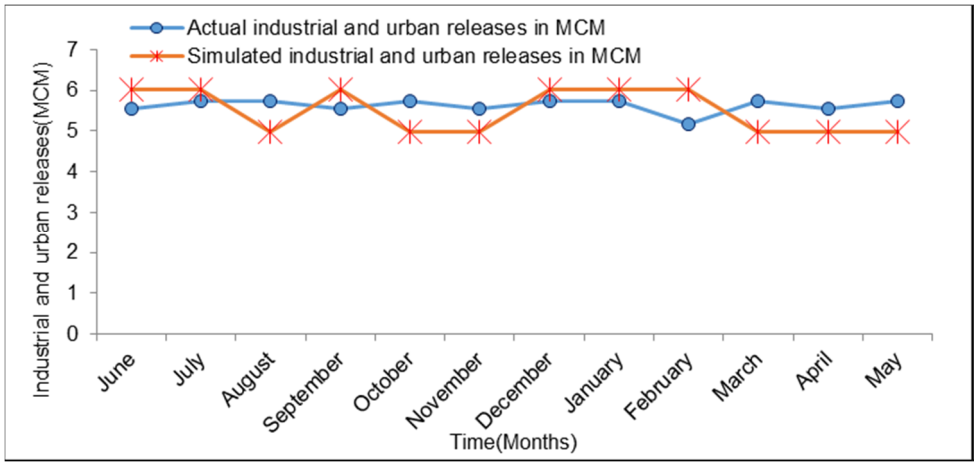

Figure 10. Plot of actual industrial and urban releases (demands) and simulated industrial and urban releases with respect to time (months).

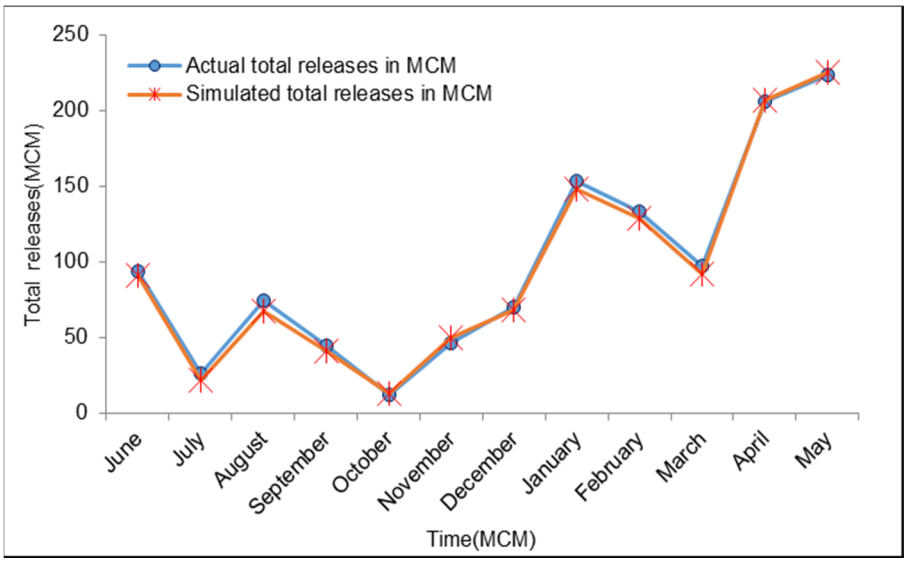

Figure 11. Plot of actual total releases (total demands) and simulated total releases with respect to time (months).

©2017, IAHR. Used with permission / ISSN 1562-6865 (Online) - ISSN 1063-7710 (Print)

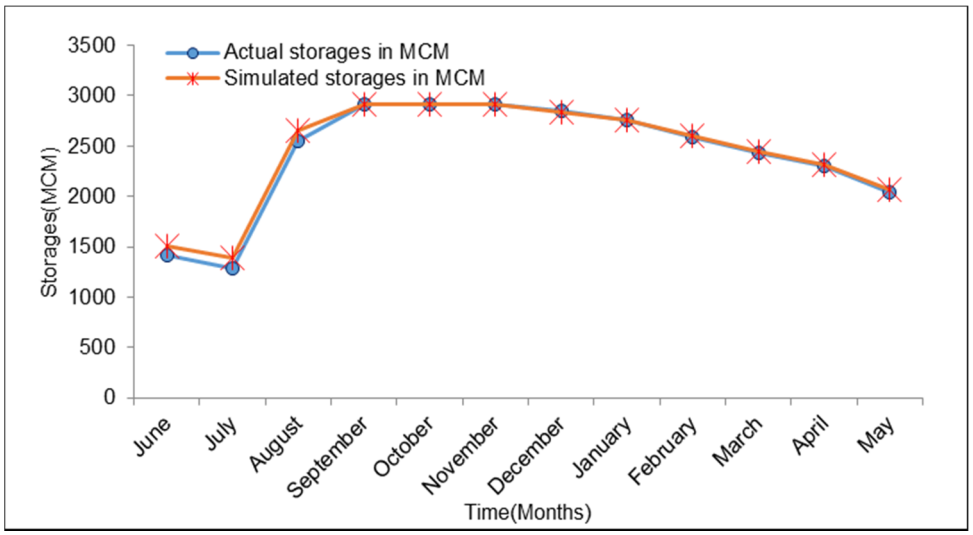

Figure 12. Plot of actual storages (target storages) and simulated storages with respect to time (months).

Table 2. Performance evaluated for the cases derived from Jaya model.

Cases	MFD	MAD in MCM	AFD	AAD in MCM
LBC releases	0.426	1.412	0.778	9.281
RBC releases	0.389	0.786	0.889	4.126
Industrial and urban releases	0.472	0.431	0.889	2.75
Total releases	0.491	1.754	0.889	11.623

6 CONCLUSIONS

Jaya model is developed for Jayakwadi stage-I reservoir located at the site of Jayakwadi village in Paithan Taluka of Aurangabad district, Maharashtra, India. Model is formulated with the objective function as minimization of sum of square deficit of releases and storages from their target values to be optimized. Model is optimized for 75% probable inflows obtained from 23 years of historical data. With the same objective function, model is simulated using 9 years of historical data. The model proved to be successful in this case study, as seen from the results obtained in simulation model. Further, the study can be extended for sensitivity analysis with different percentages of probable inflows and also for multi-reservoir system.

The scope of the present study was to check the applicability of Jaya algorithm for optimization of reservoir operation. Further investigations are to be carried out for ascertaining possibility of obtaining the global solution.

ACKNOWLEDGEMENT

Authors are thankful to Command Area Development Authority (CADA) Aurangabad, Maharashtra, India for providing the actual data of Jayakwadi stage-I reservoir.

REFERENCES

Jothiprakash, V. & Shanthi, G. (2009). Comparison of Policies Derived from Stochastic Dynamic Programming and Genetic Algorithm Models. *Water Resources Management,* 23(8), 1563-80

Labadie, J.W. (2004). Optimal Operation of Multireservoir Systems: State –of-the-Art Review. *Journal of Water Resources Planning and Management,* 130(2), 93-111.

Mirajkar, A.B. & Patel, P.L. (2016). Multiobjective Two-Phase Fuzzy Optimization Approaches in Management of Water Resources. *Journal of Water Resources Planning and Management,* 142(11).

Mousavi, S.J., Karamouz, M. & Menhadj, M.B. (2004). Fuzzy-State Stochastic Dynamic Programming for Reservoir Operation. *Journal of Water Resources Planning and Management, ASCE,* 130(6), 46-470.

Rao, R.V. (2016). Jaya: A simple and New Optimization Algorithm for Solving Constrained and Unconstrained Optimization Problems. *International Journal of Industrial Engineering Computations* 7, 19–34.

Sharma, P.J., Patel, P.L. & Jothiprakash, V. (2016). Efficient Discretization of State Variables in Stochastic Dynamic Programming Model of Ukai Reservoir, India. *ISH Journal of Hydraulic Engineering*, 22(3), 293-304.

Simonovic, S.P. (1992). Reservoir System Analysis: Closing the Gap between Theory and Practice. *Journal of Water Resources Planning and Management,* 118(3), 262-280.

Srivastava, D.K. & Awchi, T.A. (2009). Storage-Yield Evaluation and Operation of Mula Reservoir, India. *Journal of Water Resources Planning and Management,* 135(6), 414-425.

©2017, IAHR. Used with permission / ISSN 1562-6865 (Online) - ISSN 1063-7710 (Print)

Wurbs, R.A., Tibbets, M.N., Cabezas, L.M. & Roy, L.C. (1985). *State-of-the-art Review and Annotated Bibliography of Systems Analysis Techniques Applied to Reservoir Operation,* Report TR-136, Texas Water Resour. Inst., Texas A & M Univ.

Yeh, W.G. (1982). *State-of-the-Art Review: Theories and Application of Systems Analysis Techniques to the Optimal Management and Operation of a Reservoir System*. Report UCLA-ENG-82-52, Civ. Engg. Dept., Univ. of California, LosAngeles, Calif.

Yeh, W.G. (1985). Reservoir Management and Operations Models: A State-of-the-Art Review. *Water Resources Research*, 21, 1797-1818.

Yeh, W.G. & Becker, L. (1982). Multiobjective Analysis of Multireservoir Operations. *Water Resources Research,* 18, 1326-1336.

 ©2017, IAHR. Used with permission / ISSN 1562-6865 (Online) - ISSN 1063-7710 (Print)

A REVIEW FOR POLLUTION PROPAGATION MODELING IN RIVERS AND ITS SIGNIFICANCE FOR WATER RESOURCES MANAGEMENT

DANIELI MARA FERREIRA[1], CRISTOVÃO VICENTE SCAPULATEMPO FERNANDES[2] & ELOY KAVISKI[3]

[1, 2, 3] Federal University of Paraná, Curitiba, Brazil,
danielimaraferreira@gmail.com
cvs.fernandes@gmail.com
eloy.dhs@ufpr.br

ABSTRACT

Water quality simulations have been applied for management purposes in several countries. Despite the fact that numerous models with reliable numerical solutions are available today, several important questions remain challenging, such as sampling frequency (which affects the quality of modeling results), flow representation (water pathway, volume and velocity have direct impact in pollutants transport), and calibration parameters (responsible for uncertainties in results). In this context, this paper reviews and discusses distinct approaches to evaluate the aspects involved in water quality simulations, and the impacts for water resources management. The discussions presented in this research emphasizes the future perspectives that water modeling should contemplate, such as: (i) identification of appropriate reaction coefficients, (ii) reliable data to simulate water quantity and quality, and (iii) development of new strategies for interpreting results evaluation as water quality frequency curves.

Keywords: Assessment of water quality; water quantity modeling; water resources planning and management.

1 INTRODUCTION

Efforts to understand and predict water quality dynamic have increased over the years. Events such as floods and droughts, contamination of drinking water and stricter laws have intensified public awareness for a correct management of this resource (Chigor et al., 2012; Ascott et al., 2016).

Water quality degradation can be the result from multiple activities, including pollution related to point sources, originating from a single waste load allocation, and nonpoint sources, that include diffused pollution loads. While point sources can be easily identified, nonpoint loadings are often difficult to attribute to a particular location, and have been recognized as a major threat to water resources throughout the world (Lee et al., 2010; Wang et al., 2012).

Identification and representation of physical, chemical and biological dynamics give the administrators an opportunity to design and to manage appropriate water policies for different uses. Water resources modeling is an important tool in this context: besides providing a full description of quality conditions and establishing requirements to attain standards, mathematical simulations give an efficient way to predict the response of a water body to interventions and management actions before its implementation.

Mathematical models have been used since 1925, when Streeter and Phelps first developed a mass balance expression to reproduce the assessment of dissolved oxygen (DO) in the Ohio River. This model incorporates the two primary mechanisms governing the fate of DO in rivers receiving sewage: decomposition of organic matter and atmospheric aeration. Since this pioneering study, several environmental agencies and educational institutions have developed modeling strategies to represent water quantity and quality in natural systems. They differ mainly by the flow representation and by the complexity level of interaction between physical, chemical and biological processes affecting the distribution of pollutants.

Planning, designing and managing water resources systems inevitably involve impact prediction, for which mathematical modeling techniques are an important tool. The main problem in this area relies in the representation of processes and data evaluation, that involve chemical, physical and biological processes, besides questions related to economic, social and politics matters.

This paper aims to discuss the main characteristics of water quantity coupled with quality modeling in streams, in order to identify gaps in knowledge and to give background to conduct future monitoring and research efforts. These systems are the main destination of wastewater from different activities, and integrate important processes that affect environmental degradation in a watershed, which are atmospheric transport and deposition, surface flow, loads generations and movement, and subsurface flow in groundwater zones (Novotny, 2002). The water quantity aspect is related to discharges and the way water flow varies spatially

©2017, IAHR. Used with permission / ISSN 1562-6865 (Online) - ISSN 1063-7710 (Print)

and temporally, while water quality incorporates mass distribution (concentration) of different constituents in aquatic systems.

2 CONCEPTUAL ASPECTS OF RIVER WATER QUALITY MODELING

Even though every modeling evaluation has its own characteristics, all of them are configured by three main modules, which are presented in figure 1: (I) water quantity, (II) water quality and (III) water resources management. The first module provides the velocity field and hydraulic features of the channel, which are used to solve the water quality module, along with external loadings, dispersion and kinetic coefficients. The results are concentrations of a substance over space and time, which are used for water resources management purposes in the third module. Monitoring plans have an important role in this context, in order to define parameters, boundary and initial conditions, and posterior calibration and verification.

In the first module, several approaches provide not only the advection field, but also estimations of pollution generation at the source and its transport from the source area to the receiving watercourse (Larentis et al., 2008; Fonseca et al., 2014; Salla et al., 2014). These models usually link hydrological processes and land use in the watershed, resulting in hydrographs and concentrations histograms (pollutographs) at a specific location of the basin.

The water quality module solves the advection-dispersion-reaction equation (ADR), thus predicting the distribution of a specific pollutant. This expression represents the balance between the transfer of matter through the contours and control volume influence, besides changes that occur within the system. Advection and dispersion control mass exchanges, while losses or gains arise from chemical (chemical reactions in general), physical (particulate settling, for example) or biological processes (such as algae growth and death). The distribution of a species in the water body is also affected by point and nonpoint contributions.

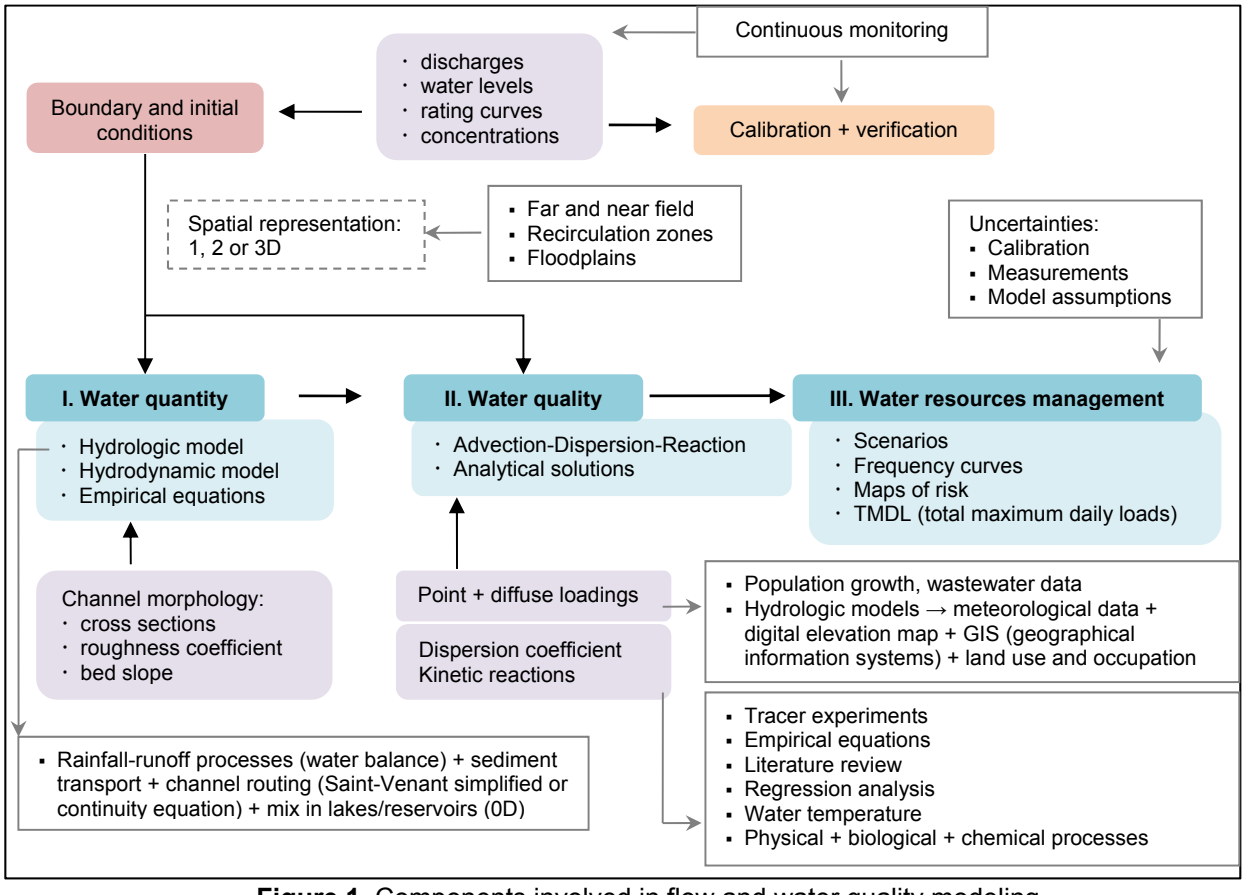

Figure 1. Components involved in flow and water quality modeling.

2.1 Spatial variation

Flow in rivers have three-dimensional (3D) characteristics due to cross sections variations and irregularities, presence of curves, meanders and several others barriers. The expression for mass conservation combined with the Navier-Stokes equations provide a complete description of the velocity field in these cases. This approach is the closest representation to reality, but it requires several data, which are usually not available. Three-dimensional models have been applied to branched network of rivers or only in small stretches (Sinha et al., 2013; Sokolova et al., 2015).

 ©2017, IAHR. Used with permission / ISSN 1562-6865 (Online) - ISSN 1063-7710 (Print)

In streams, the longitudinal scale is significantly larger than vertical and transversal scales. Therefore, the flow can be modeled through one-dimensional (1D) equations. In this approach, it is assumed that the longitudinal concentration gradients prevail and there is instant mixture in vertical and transverse directions.

Benedini and Tsakiris (2013) stated that the hypotheses made for the one-dimensional analysis are not valid particularly in large rivers, in which an injected pollutant requires some time before reaching an acceptable uniform distribution in the cross section. The pollutant presence is conceived in the form of a two or three-dimensional plume that expands on the cross section along a very long stretch of the river. Moreover, large rivers may have zones of slow stream, stagnant water or floodplains, in which the substance transport occurs in a different way from that in the main stream. Key components of the flow field, such as flow separations and recirculation zones, should also be reproduced by two-dimensional models (USACE, 1993; Olsen, 2007).

Nevertheless, Benjankar et al. (2015) call attention to the fact that despite their inability to resolve flow details, 1D models are very useful as they are computationally efficient and allow simulations for first-order conditions over much larger stream domains and over much longer periods than 2D models.

Additionally, the 1D approach is fundamental for analytical methods, which are considered the most reliable way for solving the fundamental differential equation in simple geometrical configurations, such as channels with uniform flow or prismatic cross sections. Indeed, a common practice is to use this analysis to verify numerical solutions (Juxiang, et al., 2011; Estabragh et al., 2012), although it is still applied to predict the impact of contaminants in water bodies (Fan et al., 2013). In spite of the simplifications involved, analytical solutions yield straight and fast results, which is important in the cases of accidental spills, for example.

2.2 Assessment of temporal variation

The flow characteristics at a position change very slowly over time under some circumstances. Consequently, it is assumed that the system may be assumed to be under steady state conditions. In this approach the flow is estimated using discharge coefficients or the Manning equation (Parmar and Keshari, 2012; Babbar, 2014). This type of representation has the disadvantage of fewer scenarios possibilities, but it requires less data and is easier for computational implementation. While considering low flow occurrences, this representation have been considered adequate when the cause of degradation is a steady point source, or if the studied reach receive less pollution loads (Novotny, 2002; Ferreira et al., 2016).

Some specific processes can also achieve steady conditions after a short time and therefore can be modeled by a simplified approach. According to Bowie et al. (1985), a few processes can be represented including bacterial decay and distribution and also recycling of nutrients. Another strategy is to consider unsteady flow represented by a series of steady flow, as an approach to superimpose a potential unsteady analysis through a sequence of steady-state conditions (Seo et al., 2011; Noh et al., 2015).

As stated by Dortch and Johnson (1992), crude estimations for hydraulic transport allow reasonable results because Kinect processes can outweigh the effects of transport. Natural systems have an unsteady behavior, especially in urban areas. Discharges dynamic in rivers occurs duo to multiple uses of water and morphological changes over time, natural or anthropogenic influence (such as wave propagation related to rainfall-runoff processes in the watershed contributing to the river, propagation of waves generated by the operation of reservoirs or navigation sluices, watershed drainage patterns and sewage discharges).

In addition, many processes (algal growth and respiration, chemical kinetic reactions) have a time-varying influence due to seasonal changes in water temperature and solar radiation (Bailey and Ahmadi, 2014). Furthermore, non-point loads that have an important role in rivers pollution, are controlled mainly by land use and meteorological conditions, which continuously change over time.

2.3 Flow representation

Discharge and elevation estimations have a fundamental role in water quality assessment. Flow velocity directly controls the transport of dissolved and particulate substances in water bodies. In addition, advection changes and morphological characteristics can affect kinetic processes, such as reaeration, volatilization, and photolysis (Ambrose et al., 1988). Flow conditions may also cause resuspention of sedimented material, able to promote the release of contaminants (Zuo et al., 2015).

Considering problems, which cause the water conditions to change rapidly (during a storm event, for example), a transient analysis is required. In order to represent a wave characteristics in time and space, usually hydrologic or hydrodymic models are applied. The first simulated precipitation-runoff processes usually are associated with flow routing methodologies, which include the unsteady continuity equation and part of the momentum equation. According to Saleh et al. (2013), this approach is preferable for flow routing at regional scale. These models use simplified techniques, which generally are based on linear/non-linear reservoirs that include the Muskingum routing method, the cascade of linear reservoirs, and the Muskingum-Cunge approach, among others.

Hydrological models coupled with water quality simulations have the capacity of integrate processes in a watershed. Therefore, this approach has been used to develop water quality indexes (Torres-Bejarano et al., 2011), to analyze the impacts of discharged sewage on downstream water quality (Sokolova et al, 2015), to

©2017, IAHR. Used with permission / ISSN 1562-6865 (Online) - ISSN 1063-7710 (Print)

study scenarios (population growth and industrial sector, installations of hydro-electric power stations) (Larentis et al., 2008), and development of risk maps (Zhou et al., 2011).

However, Rode et al. (2010) claimed that critical problems can arise when modeling catchment-scale water quality. Frequently, the basin has a substantial spatial variability, difficult to represent, and it is necessary to describe the water and mass fluxes and transformation processes in different compartments, like soil, surface water transportation, stream-aquifer interactions etc.

On the other hand, hydrodynamic models, that include the full one-dimensional unsteady continuity and momentum equations, have the capability to accurately simulate a wide spectrum of waterway characteristics. The continuity equation describes the balance between input, storage and output in a section of river, and the momentum equation relates the change in momentum to the applied forces (Liggett, 1975).

These equations are fit to simulate the downstream propagation of kinematic and diffusive waves, while remaining valid when downstream backwater effects or significant tributary inflows are present, or when upstream propagation of a wave, such as from large tides and storm surges, occurs, (Saleh et al., 2013). In order to gain satisfactory results in hydrodynamic modeling, it is critical to have a correct description of bed channel (roughness and slope) and reliable rating curves (Saleh et al., 2013; Benjankar et al., 2015). The uncertainties in these later can induce unrealistic estimates for the roughness coefficient (Domeneghetti et al., 2012).

Concerning hydrodynamic simulations coupled with water quality, studies have recommended the mechanisms to maintain maximum allowable limit for pollutants, mainly through improvement of treatment efficiencies in wastewater plants and enforcement of effluent standards (Kanda et al., 2015). Hydrodynamic simulations also allow one to predict changes in water quality trough hydraulic modifications in the channel, such as gate operations (Hwang et al., 2014) and sluice regulation (Zuo et al., 2015).

2.4 Water quality parameters

A wide number of substances are expected to be found in superficial waters, originating from urban and industrial wastewater or natural contact of water with soil and sediment: ions (calcium, magnesium, nitrates, chlorides, carbonates and others), inorganic compounds (sulphur, chromium, arsenic, cadmium and nickel) and organic compounds. The latter comes from the decomposition of organic matter of plants and animals including residues from agricultural areas and wastes of domestic and industrial sources (Porto et al, 1991).

Many of these substances are nonconservative and undergo changes when in contact with water. The most frequent pollutants simulated are compounds of oxygen, nitrogen and phosphorus, whose transformations can be described by means of specific biochemical processes (Sincock et al., 2003; Mannina and Viviani, 2010; Salla et al., 2014).

In the aquatic environment, the organic matter plays an important role in production and consumption cycles. This material is composed of protein compounds, carbohydrates, fats, oils, urea, surfactants, phenols, pesticides and other components in lesser amounts. However, in studies of water quality, usually only carbonaceous matter is analyzed, since this is the portion that consumes oxygen. Organic matter is traditionally represented by biochemical and chemical demand of oxygen in modeling studies (Zhou et al., 2011; Salla et al., 2014).

Although these parameters are recommended to evaluate pollution by legal regulations in Brazil, some analytical limitations may compromise the interpretation results. The biochemical demand of oxygen (BOD) test identifies only the biodegradable fraction of the organic compounds, while the chemical demand of oxygen (COD) do not allow to differentiate the sample portion that may be oxidized biologically.

In addition, the BOD quantifies only the fraction of oxygen consumed by microorganisms adapted; consequently, the presence of heavy metals or other toxic substance may restrict their action. To overcome such limitations, the organic carbon has been proposed as parameter for the overall determination of organic pollution in water and wastewater.

Sorribas et al. (2012) presented a distributed modeling of carbon in a watershed with low anthropic influence, combining hydrological processes and terrestrial and aquatic cycles. In modeling under steady state, Knapik, (2014) presented a simplified model for the balance and transport of organic carbon for the Iguaçu River (Paraná, Brazil).

Recent studies have recommended the identification of emerging substances - hormones, pharmaceutical, caffeine etc - as indicatives of anthropogenic pollution, and as a complement to organic matter (Ide et al., 2013; Santos et al., 2016).

Caffeine is recognized as one of the pharmacologically active chemical substances of higher consumption worldwide (100-200 mg/person), and may be found in the composition of food, medicines, flavorings, among others. This substance is indicative of potential pollution of water bodies in areas of intense urbanization, since anthropogenic sources are responsible for the presence of this compound in aquatic systems (Seiler et al., 1999).

Dombroski et al. (2013) called attention to the fact that few studies have been dedicated to analyze the impact that the presence of this compound have on the aquatic ecosystem and in its transport and decomposition processes. Many of the researches involving modeling of this parameter have a strong

 ©2017, IAHR. Used with permission / ISSN 1562-6865 (Online) - ISSN 1063-7710 (Print)

investigative character of decay processes, adsorption and transformation in the water column of aquatic systems, since the mechanisms are not completely known.

2.5 Sampling frequency

Contrary to hydrological data, that are often available in the form of continuous daily records, water quality data usually are limited or scarce (Fonseca et al., 2014). Frequency and detail of the data that are routinely monitored do not match with the requirements of the model, and this can be a responsible of the fact that only a few case-studies are available on model application worldwide (Sharma and Kansal, 2013; Langeveld et al., 2013).

Table 1 summarizes several modeling studies for water quality under transient regime, showing the parameters more often simulated, and the frequency of data available for simulations. Most of these studies have conducted water quality simulations under unsteady state using monthly data, or even quarterly campaigns. Continuous time series for measured concentrations are usually obtained for parameters directly measured with sondes (Langeveld et al., 2013; Adams et al., 2016).

Table 1. Common parameters simulated in rivers and monitoring data used in water quality modeling under unsteady conditions.

Reference	Study case	Parameters and time series
Larentis et al. (2008)	Area: 26000 km^2, with low population density, livestock, agriculture and industrial activities; river length: 550 km, 6 monitoring points	Quarterly data for TP (total phosphorus), DO (dissolved oxygen) and fecal coliforms; simulations for the period 1993-2002
Adams et al. (2016)	Basin with 125 km^2; 90% grassland	30 min data for phosphorus (P) and 15 min for suspended solids (SS); hourly simulation
Fonseca et al. (2014)	Watershed: 176 km^2, livestock, piggeries and domestic wastewater; 3 quality stations	Monthly data for temperature, fecal coliforms, DO, BOD, total SS, nitrates, orthophosphates and pH
Sincock et al. (2003)	Watershed: 2463.7 km^2; approximate river length: 30 km	Daily data for BOD, nitrate, DO and temperature; simulations: 27th of August to the 21st of December 1974
Mannina and Viviani (2010)	Catchment area: 160 km^2; rural ephemeral river with 6 km	Measured data at approximately each 10 min for BOD and DO; 300 min simulation
Zhou et al. (2011)	Watershed: 9750 km^2, high population and economic density; river length: 1600 km	4 values for 30h simulation: chemical oxygen demand (COD)
Inthasaro and Wu (2012)	Reach length: 214 km	Approximately 8 to 80 measured values for 10 years simulation: ammonia, nitrate, PCB, phosphate and biomass (zooplankton, forage and predatory fish)
Kanda et al. (2015)	River length: 50 km; 5 sampling points	Monthly water quality data: BOD and DO
Hwang et al. (2014)	River length: 18.5 km	Measurements of Aug. 10 and Oct. 19, 2006 at 30 min: nitrogen and phosphorous compounds, SS, COD, BOD and chlorophyll-a
Langeveld et al. (2013)	River length: 146 km	1 and 2 min data for ammonium and DO
Zuo et al. (2015)	Basin: 28150 km^2, with high population density	5 experimental values for 3 days of simulation: permanganate index and ammonia

Although sampling frequency is a common concern in research regarding water quality modeling (Zhou et al., 2011; Sorribas et al., 2012; Langeveld et al., 2013), it have not been given enough attention to a careful assessment of modeling requirements prior to field studies. According to Martin and McCutcheon (1999), the lack of information could result in sampling efforts with missing critical data, loss of important gradients, or failure to close flow and mass balances.

As stated by Meals et al. (2013), 80 to 90 % of annual load may be delivered in 10 to 20 % of time, indicating that choosing when to sample could be as important as how often the sampling was. In this context, Richards (1998), for example, showed in his study that monthly series gave only a very crude representation of the daily load flux, but it was better than expected because it included the peaks of two of the four major storms of the year. A monthly series based on dates about 10 days later than these would have included practically no storm observations, and would have underestimated the suspended solids load. Quarterly samples resulted in a poor fit on the actual daily flux pattern in this study.

3 FUTURE PERSPECTIVES AND RESEARCH NEEDS

A recent approach for water quality modeling emphasizes the need to consider hydrological regimes that meet human and ecosystem needs, rather than setting constant reference discharges to address water management plans (Souza et al., 2008). In such context, unsteady modeling approaches have been indicated

as an appropriate tool (Melching et al., 2003; Ferreira et al., 2016). One advantage of this kind of modeling is it represents the dynamic between discharges and concentrations of pollutants in a stream, which is highly variable (Zhou et al., 2011).

In order to evaluate results and predict management plans, frequency curves offer an interesting strategy to associate water quantity and quality. This concept, derived from the hydrological field, has been generally used since 1915 (Searcy, 1959). This curve associates the variable of interest to a probability, indicating the time percentage in which a value is equaled or exceeded during a given period; it combines in one curve the characteristics of a stream throughout the range of variability, without regarding the sequence of occurrence. This concept allows evaluation of the inherent uncertain behavior of different variables and standards transgression (Cunha et al, 2011; Cho and Lee, 2015).

This approach have been evaluated through simulations under steady (Brites, 2010; Calmon et al., 2016) and unsteady state (Ferreira et al., 2016), hydrological modeling (Cho and Lee, 2015), monitoring data from rivers (Oliveira et al., 2011) and reservoirs (Cunha et al., 2011).

The development of technologies in industry and agriculture, as well as the dynamic in land use and occupation, affects directly the list of pollutants that can reach the watercourses. Therefore, the number of parameters indicating water quality is still open. This fundamentally depends on the discovery of new compounds, following the improvement of analytical methods that are able to detect even a trace of concentration of substances.

Consequently, it is expected to intensify the problem of detecting and controlling new pollutants in superficial waters, highlighting the role of mathematical models for assessment of environmental conditions. At the present time, among the main difficulties are the identification of the appropriate reaction coefficients (that represent the physical-chemical-biological transformations that the substances go through when in contact with water), specific for each pollutant and able to interpret its behavior in river water. This also falls under the scope of aquatic chemistry, geochemistry, biology and toxicology (Benedini and Tsakiris, 2013).

Often unknown, kinetic coefficients are used as calibration parameters, which may induce errors or mismatch of the reality. A given set of reaction coefficients may overlap the actual effects of transport on the distribution of pollutants in the canal.

Model calibration is a critical phase, since different criteria may produce significantly distinct results, which interfere in the decision making process. Automatic techniques may provide higher precision to the desired results, which assist in the analysis of uncertainty associated with the transformation terms.

Additionally, the calibration phase requires reliable data, which implies continuous monitoring of water quantity and quality. However, monitoring plans have limitations, such as high costs, analytical uncertainties etc.

The methodologies to obtain continuous time series include the use of automatic samplers flow driven (Langeveld et al., 2013; Sokolova et al., 2015; Kozak, 2016), synthetic pollutographs (Prodanoff, 2005) and statistical analysis (Arya and Zhang, 2014; Miller et al., 2014). However, this subject is still challenging, considering that the dynamic of chemical, biological and physical processes together with the dynamic of activities in a watershed, are difficult to identity and represent.

While acknowledging the increasingly important role of modeling in water resources planning and management, it is important to recognize the inherent limitation of models as representations of a real system.

When selecting or developing a model, the user should evaluate the goals of the study, appropriate time and spatial scales, and identify system components that must be represented, in order to interpret the results correctly.

REFERENCES

Adams, R., Quinn, P.F., Perks, M., Barber, N.J., Jonczyk, J. & Owen, G.J. (2016). Simulating High Frequency Water Quality Monitoring Data using A Catchment Runoff Attenuation Flux Tool (CRAFT). *Science of the Total Environment*, 572, 1622-1635.

Ambrose, R.B., Wool, T.A., Connolly, J.P. & Schanz, R.W. (1988). *WASP4, A Hydrodynamic and Water Quality Model-Model Theory,* User's Manual and Programmer's Guide.

Arya, F.K. & Zhang, L. (2014). Time Series Analysis of Water Quality Parameters at Stillaguamish River using Order Eeries Method. *Stochastic Environmental Research and Risk Assessment*, 29(1), 227-239.

Ascott, M.J., Lapworth, D.J., Gooddy, D. C., Sage, R. C. & Karapanos, I. (2016). Science of the Total Environment Impacts of Extreme Flooding on Riverbank Filtration Water Quality. *Science of the Total Environment,* 554(555), 89-101.

Babbar, R. (2014). Pollution Risk Assessment Based on QUAL2E-UNCAS Simulations of A Tropical River in Northern India. *Environmental Monitoring and Assessment*, 186(10), 6771-6787.

Bailey, R.T. & Ahmadi, M. (2014). Spatial and Temporal Variability of in-stream Water Quality Parameter Influence on Dissolved Oxygen and Nitrate within A Regional Stream Network. *Ecological Modelling*, 277, 87-96.

Benedini, M. & Tsakiris, G. (2013). *Water Quality Modelling for Rivers and Streams*. Texas A&M University.

 ©2017, IAHR. Used with permission / ISSN 1562-6865 (Online) - ISSN 1063-7710 (Print)

Benjankar, R., Tonina, D. & McKean, J. (2015). One-Dimensional and Two-Dimensional Hydrodynamic Modeling Derived Flow Properties: Impacts on Aquatic Habitat Quality Predictions. *Earth Surface Processes and Landforms*, 40(3), 340-356.

Bowie, G.L., Mills, W.B. & Porcella, D. B. (1985). *Rates, Constants, and Kinetics Formulations in Surface Water Quality Modeling*. 2. ed. California: Environmental Protection Agency.

Brites, A.P.Z. (2010). *Enquadramento dos Corpos de água através de metas Progressivas: Probabilidade de ocorrência e custos de despoluição hídrica*. Tese (Doutorado em Engenharia) - Universidade de São Paulo.

Calmon, A.P.S., Souza, J.C., Reis, J.A.T. & Mendonça, A. S. F. (2016). Uso Combinado de Curvas de permanência de qualidade e Modelagem da Autodepuração como Ferramenta para suporte ao processo de enquadramento de cursos d'água superficiais. *Revista Brasileira de Recursos Hídricos*, 21(1), 118–133.

Chigor, V.N., Umoh, V. J.,Okuofu, C.A., Ameh, J.B., Igbinosa, E.O. & Okoh, A.I. (2012). Water Quality Assessment : Surface Water Sources used for Drinking and Irrigation in Zaria, Nigeria are a Public Health Hazard. *Environment Monitoring Assessment*, 3389–3400.

Cho, J.H. & Lee, J.H. (2015). Watershed Model Calibration Framework Developed Using An Influence Coefficient Algorithm and A Genetic Algorithm and Analysis of Pollutant Discharge Characteristics and Load reduction in A TMDL Planning Area. *Journal of Environmental Management*, 163, 2–10.

Cunha, D.G.F., Grull, D., Damato, M., Blum, J.R.C., Lutti, J.E.I., Eiger, S. & Mancuso, P.C.S. (2011).Trophic State Evolution in A Subtropical Reservoir Over 34 years in response to Different Management Procedures. *Water Science and Technology*, 64, 2338–2344.

Dombroski, L.F., Fernandes, C.V.S., Knapik, H.G., Muhlenhoff, A.P. & Froehner, S.J. (2013). A importância da cafeína como parâmetro de qualidade de água para o gerenciamento de recursos hídricos. *Anais do 11º Simpósio de Hidráulica e Recursos Hídricos dos Países de Língua Oficial Portuguesa*, 1, 1–12.

Domeneghetti, A., Castellarin, A. & Brath, A. (2012). Assessing Rating–Curve uncertainty and its Effects on Hydraulic Model Calibration. *Hydrology and Earth System Sciences*, 16(4), 1191– 1202.

Dortch, M. & Johnson, B. (1992). *Hydrodynamics for Water Quality Models*. *Hydraulic Engineering Sessions at Water Forum*, Baltimore: American Society of Civil Engineers.

Estabragh, A.R., Pereshkafti, M.R.S. & Javadi, A.A. (2012). Comparison Between Analytical and Numerical Methods in Evaluating The Pollution Transport in Porous Media. *Geotechnical and Geological Engineering*, 31(1), 93-101.

Fan, F.M., Collischonn, W. & Rigo, D. (2013). Modelo Analítico De Qualidade Da água Acoplado Com Sistema de Informação Geográfica Para Simulação De lançamentos Com Duração Variada. *Engenharia Sanitária e Ambiental*, 18(4),359-370.

Ferreira, D.M, Fernandes, C.V.S. & Kaviski, E. (2016). Curvas De Permanência De Qualidade Da água Como Subsídio Para o Enquadramento De Corpos D´água A Partir De Modelagem Matemática em Regime Não Permanente. *Revista Brasileira de Recursos Hídricos*, 21(3).

Fonseca, A., Botelho, C., Boaventura, R.A. R. & Vilar, V.J.P. (2014). Integrated Hydrological and Water Quality Model for River Management: A Case Study on Lena River. *Science of The Total Environment*, 485,474-489.

Hwang, J.Y., Kim, Y.D., Kwon, J.H., Noh, J.W. & Yi, Y.K. (2014). Hydrodynamic and Water Quality Modeling for Gate Operation: A Case Study for the Seonakdong River Basin in Korea. *KSCE Journal of Civil Engineering*, 18(1), 73–80.

Ide, A.H., Cardoso, F.D., Santos, M.M., Kramer, R.D., Mizukawa, A. & Azevedo, J.C.R. (2013). Cafeína como indicador de contaminação por esgotos domésticos na Bacia do Alto Iguaçu. *Revista Brasileira de Recursos Hídricos*, 18(2), 201–211.

Inthasaro, P. & Weiming, W. (2012). A 1-D Aquatic Ecosystem/Ecotoxicology Model in Open Channels. *International Conference on Biomedical Engineering and Biotechnology*.

Juxiang, J., Haixiao, J., Changgen, L. & Jianhua, T. (2011). Hydrodynamic and Water Quality Models of River Network and its Application in the Beiyun River. *5th International Conference on Bioinformatics and Biomedical Engineering*.

Kanda, E.K., Kosgei, J.R. & Kipkorir, E.C. (2015). Simulation of Organic Carbon Loading using MIKE 11 Model: A Case of River Nzoia, Kenya. *Water Practice & Technology*, 10(2), 298.

Knapik, H.G. (2014). *Organic Matter Characterization and Modeling in Polluted Rivers for Water Quality Planning and Management*. Tese (Doutorado em Engenharia de Recursos Hídricos e Ambiental) – Universidade Federal do Paraná.

Kozak, C. (2016). *Water Quality Assessment and its Effects on Diffuse Pollution Considering A New Water Quality and Quantity Approach*. Mestrado em Engenharia de Recursos Hídricos e Ambiental – Universidade Federal do Paraná.

Langeveld, J., Nopens, I., Schilperoort, R., Benedetti, L., Klein, J., Amerlinck, Y. & Weijers, S. (2013). On Data requirements for Calibration of Integrated Models for Urban Water Systems. *Water Science and Technology*, 68(3), 728–736.

©2017, IAHR. Used with permission / ISSN 1562-6865 (Online) - ISSN 1063-7710 (Print)

Larentis, D.G., Collischonn, W. & Tucci, C.E.M. (2008). Simulação da Qualidade de Água em Grandes Bacias : Rio Taquari–Antas. *Revista Brasileira de Recursos Hídricos*, 13, 5–22.

Lee, C., Chang, C., Wen, C. & Chang, S. (2010). Agriculture, Ecosystems and Environment Comprehensive nonpoint Source Pollution Models for a Free–Range Chicken Farm in a Rural Watershed in Taiwan. *Agriculture, Ecosystems and Environment*, 139(1–2), 23–32.

Liggett, J.A. (1975). *Basic Equations of Unsteady Flow*. *In: Mahmood, K., V. Yevjevich, Unsteady Flow in Open Channels.* Fort Collins: Water Resources Publications.

Mannina, G. & Viviani, G. (2010). *River Water Quality Assessment: A Hydrodynamic Water Quality Model for Propagation of Pollutants*. Novatech.

Martin, J.L. & McCutcheon, S.C. (1999). *Hydrodynamics and Transport for Water Quality Modeling*. Lewis Publishers.

Meals, D.W., Richards, R.P. & Dressing, S.A. (2013). *Pollutant Load Estimation for Water Quality Monitoring Projects.* National Nonpoint Source Monitoring Program, 1–21.

Melching, C.S., Alp, E., Shrestha, R.L. & Lanyon, R. (2003). *Simulation of Water Quality During Unsteady Flow in the Chicago Waterway.* Watershed 2004.

Miller, C., Magdalina, A., Willows, R.I., Bowman, A.W., Scott, E.M., Lee, D., Burgess, C., Pope, L., Pannullo, F. & Haggarty, R. (2014). Spatiotemporal Statistical Modelling of Long–Term change in River Nutrient Concentrations in England & Wales. *Science of the total Environment*, 466, 914–23.

Noh, J., Choi, H. & Lee, S. (2015). Water Quality Projection in the Geum River Basin in Korea to Support Integrated Basin–Wide Water Resources Management. *Environmental Earth Sciences*, 73(4), 1745–1756.

Novotny, V. (2002). *Water Quality: Diffuse Pollution and Watershed Management*. Wiley, 2 ed.

Oliveira, P.T.S., Rodrigues, D.B.B., Sobrinho, T.A. & Panachuki, E. (2011). Integração de informações quali–quantitativas como ferramenta de gerenciamento de recursos hídricos. *Revista de Estudos Ambientais*, 13(1), 18–27.

Olsen, N. (2007). *Numerical Modelling and Hydraulics*. Department of Hydraulic and Environmental Engineering, Norwegian University of Science and Technology.

Parmar, D.L. & Keshari, A.K. (2012). Sensitivity Analysis of Water Quality for Delhi stretch of the River Yamuna, India. *Environmental Monitoring and Assessment*, 184(3), 1487–1508.

Prodanoff, J.H.A. (2005). *Avaliação da poluição difusa gerada por enxurradas em meio urbano*. Tese (Doutorado em Engenharia) – Universidade Federal do Rio de Janeiro.

Porto, R.L.L., Branco, S.M., Cleary, R.W., Coimbra, R.M., Eiger, S., Luca, S.J., Nogueira, V.P.Q. & Porto, M.F.A. (1991). *Hidrologia Ambiental*. Edusp, São Paulo.

Richards, R.P. (1998). *Estimation of Pollutant loads in Rivers and Streams: A Guidance Document for NPS Programs*. U.S. Environmental Protection Agency.

Rode, M., Arhonditsis, G., Balin, D., Kebede, T., Krysanova, V., Van Griensven, A. & Van der Zee, S.E.A.T.M. (2010). New Challenges in Integrated Water Quality Modelling. *Hydrological Processes*, 24(24), 3447–3461.

Saleh, F., Ducharne, A., Flipo, N., Oudin, L. & Ledoux, E. (2013). Impact of River Bed Morphology on Discharge and Water Levels Simulated By 1D Saint–Venant Hydraulic Model at Regional Scale. *Journal of Hydrology*, 476, 169–177.

Salla, M.R., Arquiola, L.P., Solera, A., Álvarez, J.A., Pereira, C.E., Filho, J.E.A. & Oliveira, A.L. (2014). Integrated Modeling of Water Quantity and Quality in The Araguari River basin, Brazil. *Latin American Journal of Aquatic Research*, 42(1), 224-244.

Santos, M.M., Brehm, F.D.A., Filippe, T.C., Knapik, H.G. & Azevedo, J.C.R. (2016). Occurrence and Risk Assessment of Parabens and Triclosan in Surface Waters of Southern Brazil: A Problem of Emerging Compounds in An Emerging Country. *Revista Brasileira de Recursos Hídricos*, 21(3), 603–617.

Searcy, J.K. (1959). *Manual of Hydrology: Part 2. Low–Flow Techniques–Flow Duration Curves*. Geological Survey Water–Supply Paper 1542–A.

Seiler, R.L., Zaugg, S.D., Thomas, J.M. & Howcroft, D.L. (1999). Caffeine and Pharmaceuticals as Indicators of Wastewater Contamination in Wells. Groundwater, 37(3), 405–410.

Seo, D., Lee, E. & Reckhow, K. (2011). Development of The CAP Water Quality Model and its Application to The Geum River, Korea. *Environmental Engineering Research*, 16(3), 121–129.

Sharma, D. & Kansal, A. (2013). Assessment of River Quality Models: A review. *Reviews in Environmental Science and Biotechnology*, 12(3), 285–311.

Sincock, A.M., Wheater, H.S. & Whitehead, P.G. (2003). Calibration and Sensitivity Analysis of A River Water Quality Model under Unsteady Flow Conditions. *Journal of Hydrology*, 277(3–4), 214–229.

Sinha, S., Liu, X. & Garcia, M.H. (2013). A Three–Dimensional Water Quality Model of Chicago Area Waterway System (CAWS). *Environmental Modeling and Assessment*, 18(5), 567–592.

Sokolova, E., Petterson, S.R., Dienus, O., Nyström, F., Lindgren, P.E. & Pettersson, T.J.R. (2015). Microbial Risk Assessment of Drinking Water based on Hydrodynamic Modelling of Pathogen Concentrations in Source Water. *Science of the Total Environment*, 526, 177–186.

 ©2017, IAHR. Used with permission / ISSN 1562-6865 (Online) - ISSN 1063-7710 (Print)

Sorribas, M.V., Collischonn, W., Marques, M.D. & Fragoso, C.R. (2012). Modelagem Distribuída do Carbono em Bacias Hidrográficas. *Revista Brasileira de Recursos Hídricos*, 17, 225–240.

Souza, C., Agra, S., Tassi, R. & Collischonn, W. (2008). Desafios e Oportunidades Para A Implementação Do Hidrograma Ecológico. *Revista de Gestão de Água da América Latina*, 5(1), 25–38.

Torres-Bejarano, F., Denzer, R. & Ramírez, H., et al. (2011). Development and Integration of A Numerical Water Quality Model with The Geospatial Application suite CIDs. *19th International Congress on Modelling and Simulation*, Perth, Australia, 12–16.

USACE (United States Army Corps of Engineering). (1993). *River Hydraulics*.

Wang, X., Wang, Q., Wu, C., Liang, T., Zheng, D. & Wei, X. (2012). A Method Coupled with Remote Sensing Data to Evaluate Non–Point Source Pollution in the Xin'anjiang Catchment of China. *Science of the Total Environment*, 430, 132–143.

Zhou, N., Westrich, B., Jiang, S. & Wang, Y. (2011). A Coupling Simulation Based on A Hydrodynamics and Water Quality Model of The Pearl River Delta, China. *Journal of Hydrology*, 396(3–4), 267–276.

Zuo, Q., Chen, H. & Dou, M. (2015). *Experimental Analysis of The Impact of Sluice Regulation on Water Quality in the highly Polluted Huai River Basin*. Environmental Monitoring Assessment.

©2017, IAHR. Used with permission / ISSN 1562-6865 (Online) - ISSN 1063-7710 (Print)

Proceedings of the 37th IAHR World Congress
August 13 – 18, 2017, Kuala Lumpur, Malaysia

ASSESSING THE VULNERABILITY OF A TROPICAL DRINKING WATER RESERVOIR TO CLIMATE CHANGE

LAURA MELO VIEIRA SOARES[1], TALITA FERNANDA DAS GRAÇAS SILVA[2], BRIGITTE VINÇON-LEITE[3], JULIAN CARDOSO ELEUTÉRIO[4] & NILO DE OLIVEIRA NASCIMENTO[5]

[1, 2, 4, 5] Department of Hydraulic Engineering and Water Resources (EHR),
Universidad Federal de Minas Gerais, Belo Horizonte, Brazil
lmvsoares@ufmg.br; talita.silva@ehr.ufmg.br; julian.eleuterio@ehr.ufmg.br; niloon@ehr.ufmg.br
[3] Laboratoire Eau, Environment et Systèmes Urbains (LEESU),
École des Ponts ParisTech, Paris, France
bvl@leesu.enpc.fr

ABSTRACT

Climate change is expected to impact on lakes and reservoirs directly via atmospheric drivers and indirectly through changes in catchment characteristics and in hydrologic cycle. It is generally expected that global warming will alter the thermal structure of surface water bodies, with a shift towards earlier and more intense thermal stratification accompanied by a greater epilimnion volume, thereby increasing the potential biologically active zone. These impacts can affect frequency and/or the severity of algal bloom occurrences. The aim of this work is to assess the vulnerability of a strategic drinking water reservoir, located in a tropical metropolitan region, in face of climate change. We investigated the threats to the water security of this water supply system using a one-dimensional hydrodynamic model for simulating the thermal temperature profile and vertical stratification. We evaluated direct impacts from two scenarios of air temperature warming: increase of 0.8 ºC and increase of 2.6 ºC; and indirect impacts of climate change from two scenarios of changes in inflows discharge, which are the decrease of 0.9 % and increase of 8.1 %. The project site was Serra Azul Reservoir, located in southeastern Brazil. The results indicates prolonged duration of stratification and warmer water temperature in surface and in 15.0 m depth. We expect that the results should help to propose guidelines for the management of the reservoir and its catchment in order to reduce the vulnerability of water supply system in face of a non-stationary climate.

Keywords: Tropical reservoir; GLM-AED; reservoir modeling; mixing process.

1 INTRODUCTION

Several processes that contribute to the heat transfer through a lake surface are solar radiation, long-wave radiation of atmosphere and surface waters, sensible heat exchange, and heat flux connected with evaporation and precipitation (Imboden & Wüest, 1995). In addition, contributions of inflow and outflow of surface and groundwater as well as thermal contact with the lakebed must also be considered (Boehrer & Schultze, 2008). Climate change is expected to impact lakes and reservoirs directly via atmospheric drivers, *e.g.* air temperature increase, precipitation, wind speed and radiation (Taner et al., 2011). Impacts of climate change on inland waters are also catchment-related. Changes in weather patterns within the watershed affect streams, rivers, and groundwater, especially through changes in frequency and intensity of extreme events (Dokulil et al., 2010). In addition to the increase in precipitation, global warming is also expected to intensify the hydrological cycle by increasing evapotranspiration (Douville et al., 2012). These changes in hydrological patterns and changes in catchments characteristics result in indirectly impacts of climate changes in lakes and reservoirs.

Mean temperatures at the earth's surface are projected to increase by as much as 6 ºC by the end of the 21th century, as a consequence of anthropogenic changes to atmospheric chemistry (Bates et al., 2008) and simulated scenarios for 2050 indicate an increase of precipitation volume between 4% and 10% (Dunn et al., 2012). Several studies indicated that lakes around the world have already been impacted by changes in climate. In the western part of Europe, surface water temperature increased by 1.4 °C in Lake Windermere, between 1960 and 2000 and by 0.7 °C in Lough Feeagh between 1960 and 1997 (George et al., 2007). Mean lake temperature of Lake Zurich increased at a rate of 0.16 °C per decade from 1950 to 1990 (Livingstone, 2003). Decadal increase in mean lake temperature was 0.1 °C in Lake Constance, Switzerland, at approximately the same time (Straile et al., 2003). An exceptionally high increase of 1.6 °C per decade was reported from Lake Stensjön, Sweden (Adrian et al., 2009).

The impacts of a warmer world impose a multitude of consequences on inland waters. The effects of climate change on the physical and ecological functioning of lake can be diversed, and individual lakes may respond very differently to changes in climate due to factors such as landscape, lake history and biotic and

 ©2017, IAHR. Used with permission / ISSN 1562-6865 (Online) - ISSN 1063-7710 (Print)

abiotic interactions (Blenckner, 2005). Although, it is generally expected that the inland surface waters are directly and almost immediately affected by changes in temperature because of the close coupling between air temperature and surface water temperature (Livingstone & Lotter, 1998). Physical variables and related parameters such as mixing and stratification are primarily affected. Changes in climatic conditions affecting local meteorological forcing will therefore alter both thermal structure and vertical transport by mixing, which in turn will affect the flux of dissolved oxygen and nutrients, as well as the productivity and composition of lake ecosystems (Peeters et al., 2002).

Global warming scenarios generally indicate changes in thermal structure of surface water bodies, with a shift towards earlier and more intense thermal stratification accompanied by a greater epilimnion volume, thereby increasing the potential biologically active zone (Covich et al., 1997). The water circulation and mixing process can be related with phytoplankton dynamics (Vidal et al., 2010), iron and manganese release (Tundisi et al., 2004), phosphorus dynamics (Komatsu et al., 2006), cyanobacteria bloom (Atoui et al., 2013), and greenhouse gas emissions (Rudorff et al., 2011). There are expected impacts on the physiology of organisms, altering food-web dynamics, biodiversity, ecological productivity (Winder & Schindler, 2004), and increasing in the frequency and/or the severity of algal bloom occurrences (Thorne & Fenner, 2011). Thus, climate change is currently considered to be one of the most severe threats to the ecosystems of the lake (Bates et al., 2008).

Few studies about impacts of climate changes in tropical lakes or reservoirs have been conducted and the magnitude of their consequences should be explored. Considering that the impacts may affect water quality and can impact human water uses, the aim of this work was to assess the vulnerability of a strategic tropical drinking water reservoir in Brazil, in face of climate change. We intended to understand direct impacts of climate change on the thermodynamics of Serra Azul reservoir (Minas Gerais, Brazil) due to air temperature increase and indirect impacts through inflow discharge alterations in response to changes in hydrological patterns and catchment characteristics.

An efficient approach to support and complement the understanding of physical processes in reservoirs is the use of hydrodynamic modelling (Liu, 2007). One of the advantages to this approach is the possibility to simulate real and hypothetical scenarios, as well as the ability to simulate various processes simultaneously (Curtarelli et al., 2014). Because of the importance of the thermal structure on vertical mixing and its influence on lake dynamics and aquatic life, the General Lake Model (GLM), a lake hydrodynamic 1D model, was used in this work to determine the impacts of climate change on the thermal stratification of Serra Azul reservoir. Due to smaller horizontal gradients, the vertical gradients, temperature and salinity are considered laterally homogeneous and a one-dimensional model can represent the hydrodynamics occurring in lake or reservoir.

2 PROJECT SITE

Serra Azul reservoir (19.97º S, 44.34º W) is located in the Metropolitan Region of Belo Horizonte city (MRBH), Minas Gerais, southeastern Brazil. The reservoir has an area of 7.5 km^2, its volume is 8.8 x 10^7 m^3 and the maximum depth is 40.3 meters (Fernandes, 2012). This reservoir was built in 1981 and it is exclusively used to supply 2.5 $m^3.s^{-1}$ of drinking water to approximately 800 thousands inhabitants in MRBH. Serra Azul reservoir has seven tributaries and its catchment has a surface of 263 km^2. The climate in the region is sub-humid tropical (Cwb) with a wet season from October to March and a dry season from April to September. Average annual temperature is 20 ºC (Christofoletti, 1974). The reservoir catchment is subjected to anthropic pressures mainly due to mining activities and agriculture.

3 METHODOLOGY

3.1 General lake model (GLM)

The General Lake Model (GLM) is a one-dimensional hydrodynamic model developed for simulating lake dynamics. It simulates vertical stratification of lakes and lentic water bodies and computes vertical profiles of temperature, salinity and density by accounting for the effect of inflows and outflows on the water balance, in addition to surface heating and cooling, and vertical mixing (Hipsey et al., 2014). GLM adopts a one-dimension layer structure based on the importance of vertical density stratification over horizontal density variations with destabilizing forces such as wind stress and surface cooling abbreviated to ensure a one-dimensional structure (Tanentzap et al., 2007).

The Lagrangian design assumes each layer as a ‘control volume’ that can change thickness by contracting and expanding in response to inflows, outflows, mixing with adjacent layers, and surface mass fluxes. Each layer has a homogeneous density which is based on the local salinity and temperature. When sufficient energy becomes available to overcome density differences between the adjacent layers, they will merge thus accounting for the process of mixing. Layer thicknesses were adjusted throughout the water column by the model in order to sufficiently resolve the vertical density gradient with fine resolution occurring in the thermocline and thicker cells where mixing is occurring.

©2017, IAHR. Used with permission / ISSN 1562-6865 (Online) - ISSN 1063-7710 (Print)

3.2 Model inputs

GLM requires daily volume, temperature, and salinity of major inflows (Hipsey et al., 2014). Seven tributaries contribute to inflow volume to Serra Azul reservoir but only the discharge of the main tributary, Serra Azul creek, is monitored by a fluviometric station. For this reason the inflows were grouped to one contribution and a correction factor was used to estimate the contribution of the other tributaries. It was considered that the catchment has the same physical characteristics and the inflows are proportional to the drainage area of the tributaries. Daily inflows were obtained from Jardim station (code 40811100), which is located at 20.05º S, 44.41º W, about 3 km upstream from the reservoir. Missing data values were replaced by linear interpolation. Water temperature data were obtained from Serra Azul station (code 02044054), located at 20.09º S, 44.43º W. Missing values were replaced by correlation relationship with air temperature. Both stations are operated by the Geological Survey of Brazil. Salinity was calculated from chlorinity concentrations using the empirical relationship Salinity = 1.80655 x [Cl^-] (IOC, 2010).

The daily outflow corresponds to water withdrawal for drinking water production and for downstream flow maintenance. Hourly meteorological inputs were short wave radiation (W/m^2), air temperature (ºC), air relative humidity (%), wind speed ($m.s^{-1}$), and precipitation (m). Meteorological data are monitored by the National Weather Institute (INMET) and were obtained from Florestal station located about 11 km from Serra Azul reservoir. Missing data values were rare and were replaced by linear interpolation. GLM estimates long wave radiation and cloud cover from a theoretical approximation based on the Bird Clear Sky insolation model.

The hypsographic curve for Serra Azul reservoir was obtained in Fernandes (2012), which performed a bathymetric map of the reservoir in 2009 using an echo-bathymetry with an accuracy of ± 0,025 m. The initial conditions of the reservoir include temperature and salinity profile for the first day of the simulation. Salinity was calculated and temperature data were based on time series monitored on a tributary of the reservoir by the sanitation company (COPASA). These data have been monitored every two months since 1980 from the surface until bottom of the reservoir. Water temperatures measured in the reservoir body from surface until 15.0 m depth were used to calibrate and validate the model.

3.3 Modelling

A sensitivity analysis of model parameters was carried out in order to assess the most important parameters of Serra Azul reservoir model. Eighteen parameters and their respective range of variation were selected from literature (Tanentzap et al., 2007; Weinberger & Vetter, 2012; Rigosi & Rueda, 2012; Hetherington et al., 2015) and were assessed using one-at-a-time method. A sensitivity index (SI) was used to identify the parameters that most affect water temperature simulated by the model. The sensitivity index was calculated as follows:

$$SI = \frac{\Delta Y/Y}{\Delta X/X} \qquad [1]$$

where, Y is the model performance (*e. g.* the RMSE value) at the parameter value X, which is varied by ΔX causing a ΔY .

Model calibration was then carried out from January 2009 to September 2012 focusing on the more sensitive parameters according to sensitivity analysis results. Manual trial-and-error approach was used in order to obtain the best fit model for simulating water temperature in Serra Azul reservoir. The model performance was assessed by calculating Root Mean Square Error (RMSE) between simulated and observed mean of daily water temperature at different depths. The calibrated model was validated from October 2012 to July 2016.

In order to preliminarily assess the potential impacts of climate change on the thermal dynamics of Serra Azul reservoir, a sensitivity analysis on meteorological and hydrological variables was carried out. Model simulations were performed from January 2009 to July 2016 while considering the following: (i) two scenarios of air temperature warming according to a projection for 2050 (IPCC, 2002), which are the increase of 0.8 ºC and the increase of 2.6 ºC and; and (ii) two scenarios of changes in inflows discharge based in projection from 2032 to 2042 (Lauri et al., 2012), which are the decrease of 0.9 % and increase of 8.1 %. Those scenarios were then compared to the reference scenario (current conditions) in terms of temperature in the water column, mean water temperature at 0.5 m and 15.0 m depth, annual number of mixing events, their average duration and the duration of stratification.

4 RESULTS AND DISCUSSION

4.1 Model performance

Parameters sensitivity analysis indicates that 12 parameters (from the 18 assessed parameters) as the most sensitive to Serra Azul reservoir model. Calibrated parameters, their range of variation, obtained calibrated values and sensitivity index are shown in Table 1.

 ©2017, IAHR. Used with permission / ISSN 1562-6865 (Online) - ISSN 1063-7710 (Print)

Table 1. Calibrated parameters and sensitivity index.

Parameter	Range of variation	Calibrated value	SI
Wind factor	0.40 – 1.10	1.05	0.6485
Inflow slope angle (º)	0.01 – 7.00	5.2	0.3564
Ozone concentration (atm-cm)	0.25 – 0.30	0.26	0.3491
Sensible heat transfer coefficient	0.0010 – 0.0025	0.011	0.2659
Aerosol optical depth at 380 nm	0.015 – 0.045	0.04	0.2453
Inflow factor	0.1 – 3.0	0.89	0.2075
Transfer of momentum coefficient	0.002 – 0.004	0.0028	0.1693
Maximum layer thickness (m)	0.5 – 7.0	0.55	0.1499
Light extinction coefficient (m^{-1})	0.2 – 0.9	0.4	0.1319
Inflow drag coefficient	0.001 – 1.000	0.001	0.0961
Shear production efficiency	0.06 – 0.30	0.245	0.0860
Wind stirring efficiency	0.02 – 1.00	0.8	0.0226

Model performance during calibration and validation period was quite satisfactory. Comparison between daily simulated and observed water temperatures indicates that RMSE is 0.95 ºC in the calibration period and 1.53 ºC in the validation period. Considering the whole period from January 2009 to July 2016, RMSE was 1.24 ºC. Figure 1 shows observed and simulated water temperature for calibration and validation period at 0.5 m and 15.0 m depth. One could note that simulations have successfully captured the dynamics of temperature in both the surface and bottom layers. In the next steps of this research, automatic calibration of parameters will be implemented in order to improve model performance.

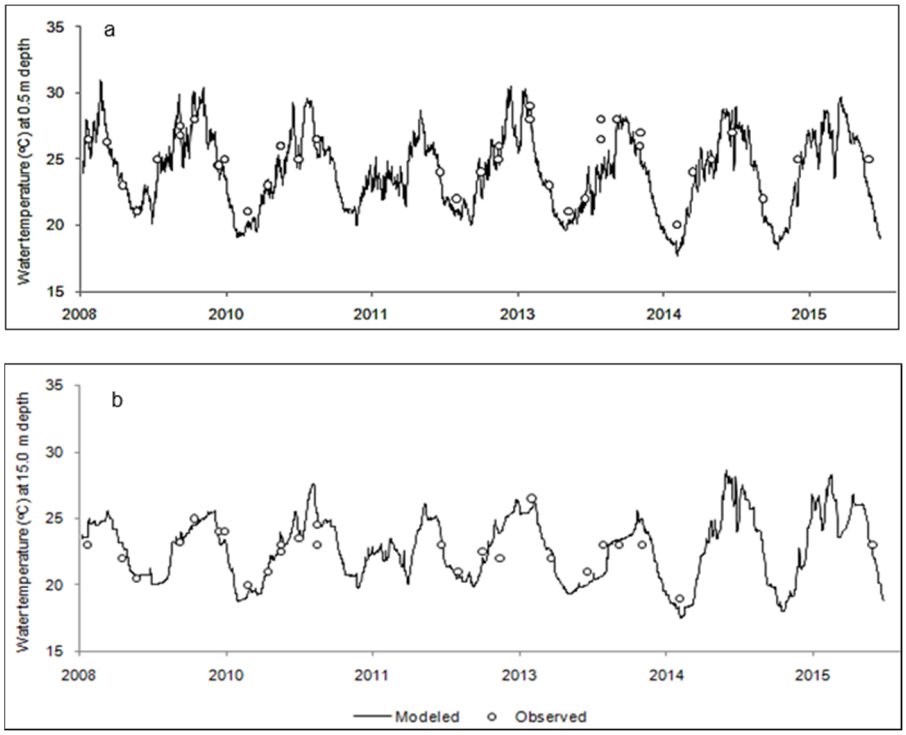

a) 0.5 m depth; and b) 15.0 m depth

Figure 1. Observed and simulated water temperature in calibration and validation period:

4.2 Impacts of meteorological and hydrological changes on Serra Azul reservoir

In this section, we compare the current conditions of Serra Azul reservoir from January 2009 to July 2016 (the reference scenario) with the different scenarios of considering the increase in air temperature and changes of inflow into the reservoir. Figure 2 shows the simulated thermal dynamics of Serra Azul reservoir in the reference scenario. One could note the occurrence and duration of stratification events mainly in warm and wet season and mixing events mainly in dry and cold season. Figure 3 shows simulated thermal dynamics of Serra Azul reservoir in AT_0.8 (Figure 3.a) and AT_2.6 (Figure 3.b) scenarios. Comparison between reference scenario and air temperature of the increased air temperature scenarios indicates that stratification and mixing events are maintained. However, in the AT_0.8 and AT_2.6 scenarios, bottom layers are colder than in the reference scenario which results in stronger stratification.

©2017, IAHR. Used with permission / ISSN 1562-6865 (Online) - ISSN 1063-7710 (Print)

Figure 4 shows simulated thermal dynamics of Serra Azul reservoir in IN_-0.9 (Figure 4.a) and IN_+8.1 (Figure 4.b) scenarios. In IN_-0.9 scenario, reduction of inflow has impacted bottom layers temperature in a similar way to air temperature increase scenarios. On the other hand, higher inflow (IN_+8.1 scenario) has minor impact on bottom layers temperature. The white spots in Figures 2, 3 and 4 represents the depletion of the reservoir due to the extreme dry period.

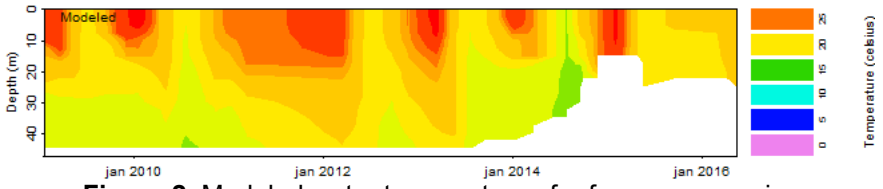

Figure 2. Modeled water temperature of reference scenario.

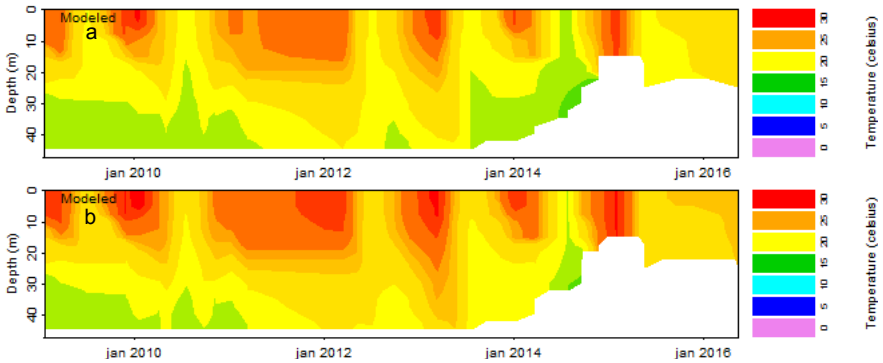

Figure 3. Modeled water temperature: a) Air temperature + 0.8 ºC; b) Air temperature + 2.6 º C.

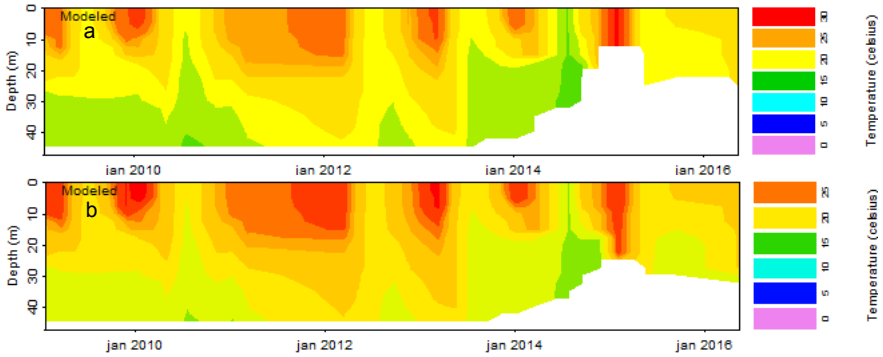

Figure 4. Modeled water temperature: a) Inflow - 0.9 %; b) Inflow + 8.1%.

Water temperature at 0.5 m depth will increase by 0.60 ºC and 1.94 ºC for AT_0.8 and AT_2.6 scenarios, respectively (Table 2). At 15.0 m depth, the water temperature will increase by 0.54 ºC (AT_0.8) and 1.79 ºC (AT_2.6). The reduction of 0.9% in inflow did not impact the water temperature at both depths. Increased inflow (IN_+8.1 scenario) leads to small reductions in water temperature (Table 2). Warmer surface water temperature creates stronger buoyancy forces which are an obstacle to turbulence, favoring the thermal resistance to vertical mixing. Furthermore, warmer water implies smaller density and stronger stratification.

Table 2. Mean water temperature (º C) for each scenario and its standard deviation

Depth	Reference scenario	AT + 0.8 º C	AT + 2.6 º C	IN - 0.9%	IN + 8.1%
0.5 m	24.07 (2.89)	24.67 (2.87)	26.01 (2.83)	24.09 (2.93)	24.00 (2.85)
15.0 m	22.74 (2.40)	23.28 (2.37)	24.53 (2.28)	22.75 (2.40)	22.52 (2.81)

The occurrence of mixing events was defined by comparing the depth of the top and bottom layers of the metalimnion. If top and bottom layers has the same depth, with no transition from warm surface water to cooler bottom water, we consider that a mixing event occurred; if top and bottom layers has different depths, and indicating rapid changes in water temperature, we considered that a stratification event occurred. The number of mixing events per year is most impacted by the AT_2.6 scenario. For this scenario, the number of mixing events reduces, but their average duration is almost doubled, increasing from 43 to 77 days per year (Figure 5). The duration of stratification events increases for all scenarios, except for IN_-0.9 scenario (Figure 6). Longer water column stratification may be related to dissolve oxygen reduction in bottom waters and shifts

 ©2017, IAHR. Used with permission / ISSN 1562-6865 (Online) - ISSN 1063-7710 (Print)

in species abundance and composition throughout the food web. Indeed, as the metalimnion acts as a barrier between the epilimnion and hypolimnion, the latter is essentially cut off from dissolved oxygen exchange with the atmosphere and it is often too dark for plants and algae to grow and to produce oxygen by photosynthesis (Ji, 2007). Longer period of stratification raises the risk of hypolimnetic anoxia as its supply of oxygen is consumed by bacteria and other bottom-dwelling organisms (Foley et al., 2012).
Vertical temperature profiles are very significant in elucidating possible impacts on the reservoir ecology. In most case, cyanobacteria species grow better at higher temperatures, although there are exceptions at lower temperatures (Hendry et al., 2006). Based on the results presented here and on previous studies, simulated scenarios indicate a need to investigate the impacts of direct and indirect drivers on phytoplankton populations.

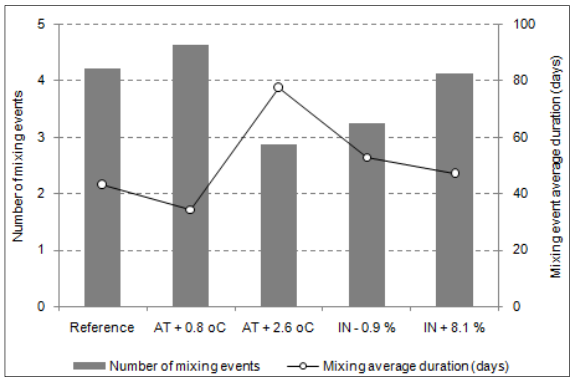

Figure 5. Number of mixing events and their average duration for each scenario

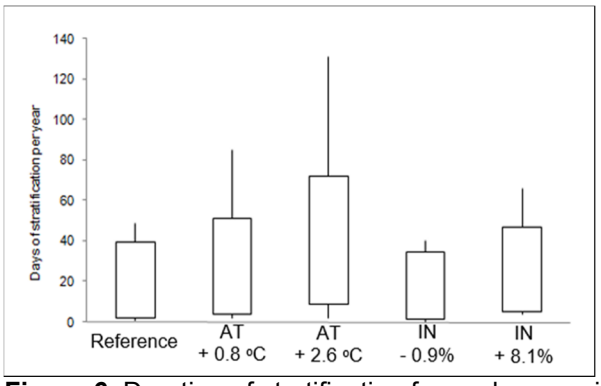

Figure 6. Duration of stratification for each scenario

Direct driver (increase in air temperature) seems to cause more intense impacts on the thermal hydrodynamic of Serra Azul reservoir when compared to the impacts caused by indirect driver (inflow changes). Higher air temperatures result in warmer water temperature on the surface and in 15.0 m depth and also prolonged the duration of stratification. The impacts are more pronounced in AT_2.6 scenario. These results are in agreement with other studies conducted in temperate regions (Lauri et al., 2012; Hetherington et al., 2015).

Changes of inflow do not represent an impact to water temperatures at 0.5 m depth, neither at 15.0 m depth. The observed impacts in stratification and mixing processes were smaller than in the air temperature scenarios. Despite all of this, it is worth to mention that inflow is contributed as a primary source of sediments and nutrients to the reservoir. Climate changes may cause more intense rainfall events leading to higher nutrient load into lakes and reservoirs which may cause algal blooms (Ji, 2007). In the next steps of this research, further investigation will be conducted in order to evaluate the impact of inflows in terms of water quality and ecodynamics.

5 CONCLUSIONS

The study presented here contributed to a better understanding of the thermal dynamics of Serra Azul reservoir and its potential sensitivity to climate change. The one-dimensional model GLM was successfully calibrated and validated for water temperature simulation at different depths. The hydrodynamic model is suitable for further ecological and limnological studies.

The results obtained indicate that Serra Azul reservoir is vulnerable to climate change, especially to air temperature increase which may lead to warmer water temperature and longer stratification periods. Impacts caused by changes in inflow discharges are smaller in terms of hydrodynamic processes, but the influences on water quality should be evaluated.

In the next steps of this research, impacts of climate change on phytoplankton communities and reservoir ecodynamics will be investigated through coupling GLM with an ecological model. Assessing thermal and ecological dynamics of Serra Azul reservoir will help to propose guidelines for its management, as well as for its catchment, aiming at reducing the reservoir vulnerability to future climate changes.

ACKNOWLEDGEMENTS

The authors are grateful to the National Agency of Water (ANA) and the Coordination of Improvement of Higher Level Personnel (CAPES) for the financial support of this research and master scholarship. We are also grateful to the sanitation company for providing measured data and for collaboration.

©2017, IAHR. Used with permission / ISSN 1562-6865 (Online) - ISSN 1063-7710 (Print)

REFERENCES

Adrian, R., O'Reilly, C.M., Zagarese, H., Baines, S.B., Hessen, D.O., Keller, W., Livingstone, D.M., Sommaruga, R., STraile, D., Van Donk, E., Weyhenmeyer, G.A. & Winder, M. (2009). Lakes as Sentinels of Climate Change. *Limnol Oceanogr*, 54(6), 2283-2297.

Atoui, A., Hafez, H. & Slim, K. (2013). Occurrence of Toxic Cyanobacterial Blooms for the First Time in Lake Karaoun, Lebanon. *Water Environmental J*ournal, 27, 42-49.

Bates, B.C., Kundzewicz, Z.W., Wu, S. & Palutikof, J.P. (2008). *Climate Change and Water. Technical paper of the Intergovernmental Panel on Climate Change*, Intergovernmental Panel on Climate Change (IPCC) Secretariat, Geneva, 210.

Blenckner, T.A. (2005). Conceptual Model of Climate-Related Effects on Lake Ecosystems. *Hydrobiologia*, 533, 1-14.

Boehrer, B. & Schultze, M. (2008). Stratification of Lakes. *Reviews of Geophysics*, 46, 1-27.

Christofoletti, A. (1974). *Geomorfologia*. Blücher, 184.

Covich, A.P., Fritz, S.C., Lamb, P.J., Marzolf, R.D., Matthews, W.J., Poiani, K.A., Prepas, E.E., Richman, M.B. & Winter, T.C. (1997). Potential Effects of Climate Change on Aquatic Ecosystems of the Great Plains of North America. *Hydrological Process*es, 11, 993-1021.

Curtarelli, M.P., Alcântara, E., Rennó, C.D., Assireu, A.T., Bonnet, M.P. & Stech, J.L. (2014). Modelling the Surface Circulation and Thermal Structure of a Tropical Reservoir using Three-Dimensional Hydrodynamic Lake Model and Remote-Sensing Data. *Water and Environment Journal,* 28, 516-525.

Dokulil, M.T., Teubner, K., Jagsch, A., Nickus, U., Adrian, R., Straile, D., Jankowski, T., Herzig, A. & Padisak, J. (2010). The Impact of Climate change on Lakes in Central Europe. *Aquatic Ecology Series*, 4, 387–409.

Douville, H., Ribes, A., Decharme, B., Alkama, R. & Sheffield, J. (2012). Anthropogenic Influence on Multidecadal Changes in Reconstructed Global Evapotranspiration. *Nature Climate Change*, 3, 59–62.

Dunn, S.M., Brown, I., Sample, J. & Post, H. (2012). Relationships Between Climate, Water Resources, Land use and Diffusive Pollution and Significance of Incertainty in Climate Change. *Journal of Hydrology*, 434, 19-35.

Fernandes, D.P. (2012). Indícios De Degradação Ambiental Em Um Reservatório Oligotrófico (Reservatório de Serra Azul, MG – Brasil): Avaliação limnológica, morfometria, batimetria e modelagem hidrodinâmica, *MSc Thesis.* Universidade Federal de Minas Gerais.

Foley, B., Jones, I.D., Maberly, S.C. & Rippey, B. (2012). Long-term changes in Oxygen Depletion in A Small Temperate Lake: Effects of Climate Change and Eutrophication. *Freshwater Biology,* 57, 278-289.

George, D.G., Hewitt, D.P., Jennings, E., Allott, N. & McGinnity, P. (2007). The Impact of Changes in the Weather on The Surface Temperatures of Windermere (UK) and Lough Feeagh (Ireland). *Fourth Inter-Celtic Colloquium on Hydrology and Management of Water Resources*, Portugal, 86–93.

Hendry, K., Sambrook, H., Underwood, C., Waterfall, R. & Williams, A., (2006). Eutrophication of Tamar Lakes: A Case Study of Land-use Impacts, Potential Solutions and Fundamental Issues for the Water Framework Directive. *Water and the Environment Journal,* 20, 159-168.

Hetherington, A.L., Schneider, R.L., Rudstam, L.G., Gal, G., Degaetano, A.T. & Walter, M.T. (2015). Modelling Climate Change Impacts on the Thermal Dynamics of Polymictic Oneida Lake, New York, United States. *Ecological Modelling*, 300, 1-11.

Hipsey, M.R., Bruce, L.C. & Hamilton, D.P. (2014). *GLM - General Lake Model: Model Overview and User Information*. The University of Western Australia, 42.

Imboden, D.M. & Wüest, A. (1995). *Mixing mechanisms in lakes*. In: Physics and Chemistry of Lakes. Springer Verlag, 83-138.

Intergovernmental Oceanographic Comission (IOC). (2010). *The International Thermodynamic Equation of Seawater*, Calculation and use of Thermodynamic Properties. Intergovernmental Oceanographic Commission, Manuals and Guides No. 56, 196.

Intergovernmental Panel on Climate Change (IPCC). (2002). *Climate Change and Biodiversity.* Technical Paper V, 86.

Ji, Z. (2007). *Hydrodynamics and Water Quality Modeling Rivers, Lakes, and Estuaries*. Wiley, 702 pp.

Komatsu, E., Fukushima, T. & Shiraishi, H. (2006). Modeling of P-Dynamics and Algal Growth in a Stratified Reservoir. Mechanisms of P-Cycle in Water and Interaction between Overlying Water and Sediment. *Ecological Modelling*, 197, 331-349.

Lauri, H., De Moell, H., Ward, P.J., Rasanen, T.A., Keskinen, M. & Kummu, M. (2012). Future Changes in Mekong River hydrology: Impact of Climate Change and Reservoir Operation on Discharge. *Hydrology and Earth System Sciences*, 16, 4603-4619.

Liu, W.C. (2007). Modelling the Effects of Reservoir Construction on Tidal Hydrodynamics and Suspended Sediment Distribution in Danshuei River Estuary. *Environmental Modelling and Software,* 22, 1588-1600.

Livingstone, D.M. (2003). Impact of Secular Climate Change on the Thermal Structure of a Large Temperate Central European Lake. *Climatic Change*, 57, 205-225.

 ©2017, IAHR. Used with permission / ISSN 1562-6865 (Online) - ISSN 1063-7710 (Print)

Livingstone, D.M. & Lotter, A.F. (1998). The Relationship between Air and Water Temperatures in Lakes of the Swiss Plateau: A Case Study with Palæolimnological Implications. *Journal of Paleolimnology,* 19, 181-198.

Peeters, F., Livingstone, D., Goudsmit, G., Kipfer, R. & Forster, R., (2002). Modeling 50 Years of Historical Temperature Profiles in a Large Central European Lake. *American Society of Limnology and Oceanograph*, 47, 186-197.

Rigosi, A. & Rueda, F.J. (2012). Propagation of Uncertainty in Ecological Models of Reservoirs: From Physical to Population Dynamic Predictions. *Ecological Modelling*, 247, 199-209.

Rudorff, C.M., Melack, J., MacIntyre, S., Barbosa, C.C.F. & Novo, E.M.L.M. (2011). Seasonal and Spatial Variability of CO_2 Emission from a Large Floodplain Lake in the Lower Amazon. *Journal of Geophysical Research*, 116, 1-12.

Straile, D., Jöhnk, K. & Rossknecht, H. (2003). Complex Effects of Winter Warming on the Physicochemical Characteristics of a Deep Lake. *Limnology Oceanographic*., 48, 1431-1438.

Tanentzap, A.J., Hamilton, D.P. & Yan, N.D. (2007). Calibrating the Dynamic Reservoir Simulation Model (DYRESM) and Filling Required Data Gaps for One-Dimensional Thermal Profile Predictions in a Boreal Lake. *Limnology and Oceanography: Methods*, 5, 484-494.

Taner, M.U., Carleton, J.N. & Wellman, M. (2011). Integrated Model Projections of Climate Change Impacts on A North American Lake. *Ecological Modelling*, 222, 3380-3393.

Thorne, O. & Fenner, R.A. (2011). The Impact of Climate Change on Reservoir Water Quality and Water Treatment Plant Operations: A UK Case Study. *Water and Environment Journal*, 25, 74-87.

Tundisi, J.G., Matsumura-Tundisi, T., Arantes Junior, J.D., Tundisi, J.E.M., Manzini, N.F. & Ducrot, R. (2004). The Response of Carlos Botelho (Lobo, Broa) Reservoir to The Passage of Cold Fronts as Reflected By Physical, Chemical, and Biological Variables. *Brazalian Journal of Biology*, 64, 177-186.

Vidal, J., Moreno-Ostos, E., Escot, C., Quesada, R. & Rueda, F. (2010). The Effects of Diel Changes in Circulation and Mixing on the Longitudinal Distribution of Phytoplankton in a Canyon-Shaped Mediterranean Reservoir. *Freshwater Biology*, 55, 1945-1957.

Weinberger, S. & Vetter, M. (2012). Using the Hydrodynamic Model DYRESM Based on Results of A Regional Climate Model to Estimate Water Temperature Changes at Lake Ammersee. *Ecological Modelling*, 244, 38-48.

Winder, M. & Schindler, D. (2004). Climate Change in Couples Trophic Interactions in an Aquatic Ecosystem. *Ecology*, 85, 2100-2106.

©2017, IAHR. Used with permission / ISSN 1562-6865 (Online) - ISSN 1063-7710 (Print)

Proceedings of the 37th IAHR World Congress
August 13 – 18, 2017, Kuala Lumpur, Malaysia

STATISTICAL CHARACTERISTICS OF EXTREME DROUGHT OF KOREA USING PALEO CLIMATIC DATA

JOO-HEON LEE[1], HO-WON JANG[2], SEO-YEON PARK[3], HYUN-PYO HONG[4] & TAE-WOON KIM[5]

[1,2,3,4] Department of Civil Engineering, Joongbu University, Goyang, Republic of Korea
leejh@joongbu.ac.kr; hs980216@hotmail.com; bin_t@naver.com, apapzk@gmail.com
[5] Department of Civil and Environmental Engineering, Hanyang University, Ansan, Republic of Korea
twkim72@hanyang.ac.kr

ABSTRACT

This study aims to provide a historical extreme drought information of Korea using the long-term precipitation for longer than 300 years that were observed by the Korean Meteorological Administration (KMA) during 1908~2015, and paleo-climate data by the Korea's ancient rain gauge (Chuk Woo Kee) during 1777-1907 and future climate change scenario from 2017-2099. Basic statistical analysis was performed such as annual/seasonal average, trends, periodicities, and outliers for the precipitation in order to compare the statistical characteristics of 2 different observed data as well as climate change scenario. The analysis results showed that annual average precipitation and seasonal precipitation were considerably different between records by Chuk Woo Kee and records by the KMA. Precipitation data by Chuk Woo Kee has seriously decreasing trends but KMA observed data show significant increasing trends because of climate change effect. While, Outliers analysis (±1.5σ) using annual precipitation data show very interesting repetition of dry (-1.5σ) and wet (+1.5σ) year period during 230 years which show extreme flood and drought periods.
SPI (6) was calculated in order to analyze severity and magnitude of the extreme drought by the drought index. Dry spell using SPI (6) indicated that extreme drought was more frequent during spring season in Chuk Woo Kee data, while KMA data show much frequent extreme drought during autumn. Such trends represented that occurrence of extreme drought was shifted from spring to autumn season. Further, the severest drought event was in the year 1901 in Seoul area with the mean drought severity -1.9 and for a duration of 12 months. As a multi-year continuous drought event, the 1899~1907 drought period was the severest drought event in Seoul with the mean severity -1.4, and for a duration of 73 months.

Keywords: Extreme drought; Chuk Woo Kee; Periodicity; Trends, Magnitude.

1 INTRODUCTION

Recently, abnormal symptoms due to climate changes are frequently witnessed in the global village. Climate anomalies are detected from many places in the world. While Uruguay River in Argentina made a record of maximum water level due to heavy rainfall in 100 years, Colombia faces problem in hydroelectric power generation due to the drought. Natural disasters are frequently followed by climate anomalies. Drought among these climate anomalies is continuing throughout a long duration, is difficult to be recognized as is the case of flood, and is also difficult to be predicted due to uncertainty of the long-term meteorological forecasts.

Drought indices such as standardized precipitation index (SPI) and Palmer drought severity index (PDSI) are mainly used to analyze drought quantitatively and various researches for the drought using precipitation data by each duration have been continuously progressed. However, long-term observation data for longer than few decades are required in order to quantitatively analyze extreme droughts. In this respect, precipitation data from 2016 based on the precipitation records from Chuk Woo Kee whose observed records are preserved since the late 1700s and the climate change scenarios in Seoul area will be very useful in analyzing the past, present, and future drought.

In order to analyze the statistical characteristics of extreme drought events in Seoul area, this study was carried out to investigate statistical characteristics of the precipitation in Seoul. Ancient rainfall data (1777-1907) restored through archives such as Seungjungwon Diary and Ilsungrok, modern observed precipitation at Seoul (1908～1949, 1953～2015) for longer than 100 years by the automatic weather station (AWS), RPC 8.5 scenario's precipitation data (2016 ~ 2099) from HadGEM2-AO were used for the analysis. We also aim to quantitively evaluate the extreme droughts in Seoul area by analyzing severity, duration, and magnitude of the drought.

 ©2017, IAHR. Used with permission / ISSN 1562-6865 (Online) - ISSN 1063-7710 (Print)

2 ANALYZED DATA

2.1 Precipitation

In this study, three different time window's precipitation data were used to perform drought studies using long-term rainfall data for Seoul area. Firstly, the rainfall data during Joseon period (1777～1907) restored by Cho and Moon (1997) and Jhun and Moon (1997) by Chuk Woo Kee records in the Seungjongwon Diary and Iseongrok were used. Secondly, of the six observatories that have more than 100 years of observation data in the automated synoptic observing system (ASOS) of the Korea Meteorological Agency, the precipitation data of the Seoul observatory (1908-1949, 1953-2015) were used. Thirdly, we used precipitation data (2016-2099) for Seoul area generated through the RCP 8.5 scenario, which was obtained by ensemble the climate change prediction model HadGEM2-ES.

2.2 Missing Precipitation data for Chuk Woo Kee

Considering that the data by Chuk Woo Kee were observed as a daily unit in this study, as an alternative to statistically supplementing the missing data of less than 2mm of daily precipitation, the average daily precipitation of 2mm per each month for 56 years during 1960～2015 of the Seoul Station, Korean Meteorological Administration (KMA) was estimated as shown in Table 1. Furthermore, to supplement missing snowfall observation data during winters, a monthly snow cover during Nov.~ Mar. in 1960～2015 of Seoul Station, KMA was estimated and each of monthly mean snowfall was estimated as shown in Table 1.

Table 1. Monthly average observed precipitation (less than 2mm/day) and monthly snowfall (mm) during 1960-2015 for the Seoul Station, KMA.

	Jan	Feb	Mar	Apr	May	Jun	Jul	Aug	Sep	Oct	Nov	Dec	Sum
Less than 2mm of precipitation	2.62	1.74	2.17	2.14	2.22	2.47	3.56	2.34	1.87	1.52	2.84	3.16	28.65
Snowfall	11.36	8.78	6.58	0.00	0.00	0.00	0.00	0.00	0.00	0.00	1.96	7.76	36.44

2.3 Drought Index

In order to quantitatively evaluate the drought at Seoul, the SPI which is a representative meteorological drought index that can be estimated from the rainfall data was calculated. Figure 1 shows the SPI (6) estimation results using the monthly precipitation data in Seoul area during 1777～2099. The estimated results were categorized into ancient (1777～1907), modern (1908～2010), and future (2011～2099) periods. It was observed that most of the drought events occurred during the ancient period when the precipitations were observed by Chuk Woo Kee. Particularly, the severe droughts in large scales were occurred continuously throughout the entire period during and around the 1900s, which was the end of the Joseon Dynasty in the ancient period. On the other hand, the future drought conditions based on climate change scenarios appeared to be much more mitigated than in the past.

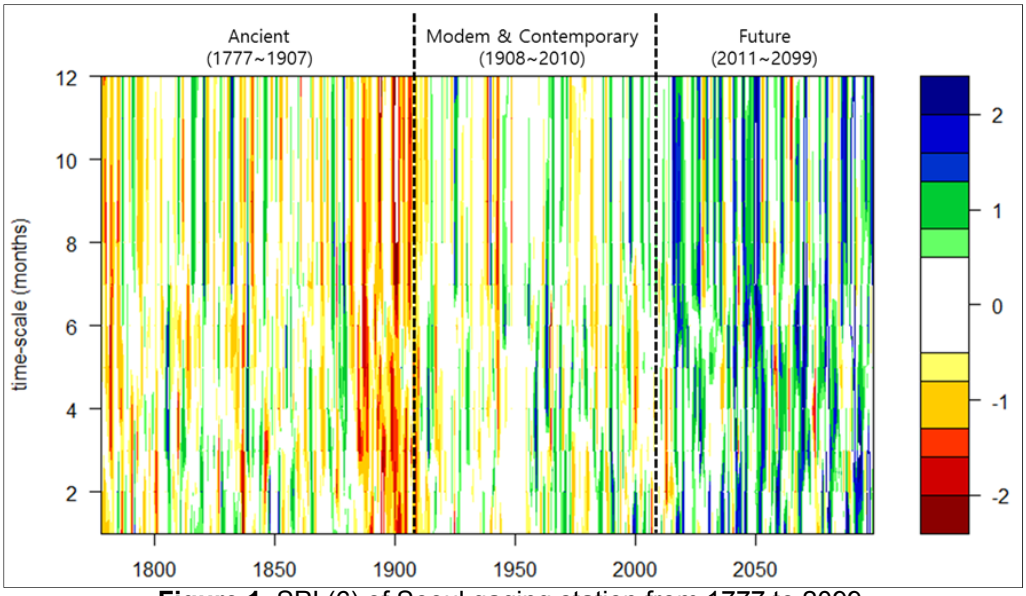

Figure 1. SPI (6) of Seoul gaging station from 1777 to 2099.

©2017, IAHR. Used with permission / ISSN 1562-6865 (Online) - ISSN 1063-7710 (Print)

3 ANALYSIS OF STATISTICAL CHARACTERISTICS

3.1 Analysis of Basic Statistical Data

Table 2 shows the basic statistical data per each period by estimating annual precipitations during 1777～2099. For the entire period, annual mean precipitation was 1380.3mm with the standard deviation 478.4mm, showing a large deviation more than ±400mm.

In case of the precipitation during ancient period, the annual average precipitation for the missing observation data before calibration was 1133.4 mm, while it was 1202.1mm after calibration. The minimum precipitations for missing observation date before and after calibration were 368.3mm and 437.1mm, respectively, showing the least precipitation throughout entire period. Whereas, during modern period, the annual mean precipitation was 1339.9mm, which was larger by around 140mm as compared with the annual mean precipitation observed by Chuk Woo Kee. During the future period for which the climate changes scenario was reflected, the annual mean precipitation was 1708.9mm with the standard deviation 567.2mm, showing the largest annual average precipitation and STD.

Table 2. Statistics seasonal precipitation for three different eras(unit : mm).

Era		Min	Max	Mean	Standard deviation
Entire period		437.0	3355.2	1380.3	478.4
Ancient (1777-1907)	Before Calibration	368.3	2566.1	1133.4	392.0
	After Calibration	437.1	2634.6	1202.1	392.0
Modern (1908-2015)		623.5	2355.5	1339.9	347.6
Future (2016-2099)		704.6	3355.2	1708.9	567.2

3.2 Trends Analysis

The Mann-Kendall test was carried out to determine the trends of annual precipitation and seasonal precipitation. Table 3 displays the trends analysis results for annual precipitation and seasonal precipitation during each period. The annual precipitation showed decreasing trends during the ancient period as well as the future period with a prominent decreasing tendency during the ancient period. Whilst, it was an increasing trend during the modern period. Particularly, during the modern period, increasing trend for the annual precipitations was statistically significant. Meanwhile, the seasonal trends analysis for the ancient period showed that the decreasing trends were prominent during autumns with statistical significances. However, the increasing trend of the precipitation was statistically significant during summers in the modern period.

Table 3. The result of Mann-Kendall test for seasonal rainfall.

	Ancient		Modern		Future	
Season	**MK-Stat***	**+ & -**	**MK-Stat***	**+ & -**	**MK-Stat***	**+ & -**
Spring	0.13	+	0.82	+	-0.33	-
Summer	-1.35	-	1.82	+	-0.80	-
Autumn	-1.81	-	1.26	+	0.39	+
Winter	0.25	+	-0.66	-	0.82	+
Annual	-1.46	-	2.61	+	-0.17	-

*Statistically significant($p < 0.10$)

3.3 Analysis of Outliers

Figure 2 shows the outliers' analysis results obtained using the annual precipitation data. From the outlier value ±1.0σ as a standard, the years having less precipitations were categorized as dry years, while the years having more precipitation were categorized as the wet years. From Figure 2, the changes of precipitation that could not be observed in the preceding researches using the precipitation data during 1974~2014 by Jang et al. (2016) can be confirmed through the long-term data. As seen in Figure 2, the dry years during the ancient period were changed to the wet years in the future period starting from the modern period. Particularly, the dry years started from the 1880s lasted until 1910s, indicating that the severe droughts occurred at the end of the Joseon Period.

 ©2017, IAHR. Used with permission / ISSN 1562-6865 (Online) - ISSN 1063-7710 (Print)

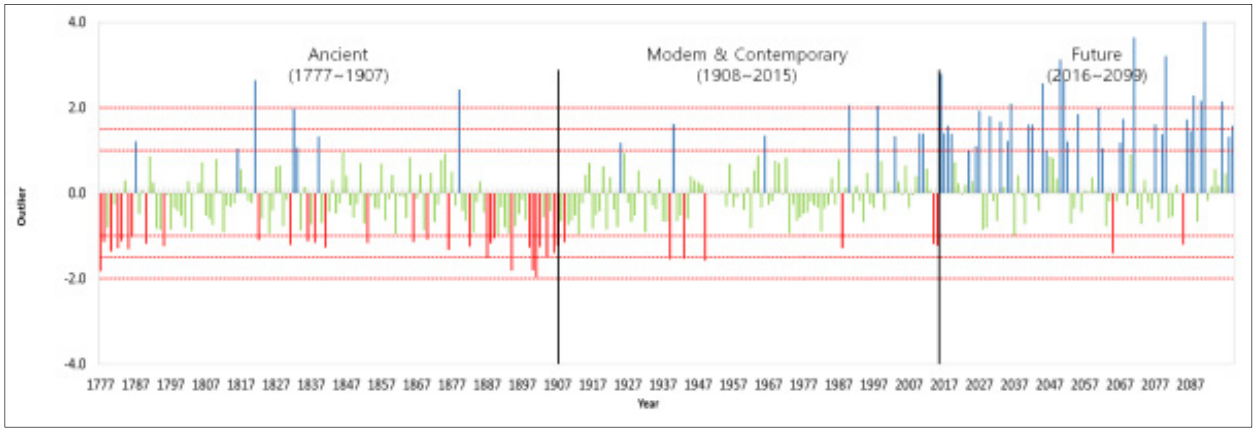

Figure 2. Wet & Dry year analysis using outlier (±1δ≥) of annual precipitation.

4 Analysis of Extreme Drought Scenario

4.1 Analysis of Drought Periodicity

The Wavelet transform analysis was carried out by using the SPI (6) for the estimated entire period to understand the periodicity of the droughts that occurred during the subjected period. Figure. 3 shows the periodicity analysis results. During the ancient period when the precipitation was measured by Chuk Woo Kee (1777-1907), statistically significant strong spectrums appeared between 60～75 months (5～6 years). Furthermore, during the modern period (1908-2015), the strong spectrums were displayed between 64～80 months (5～6 years) similarly as in the ancient period. The tendencies are in good agreement with the existing preceding research results which dealt the periodicity analysis for the droughts (Lee et al., 2012; Lee et al., 2016).

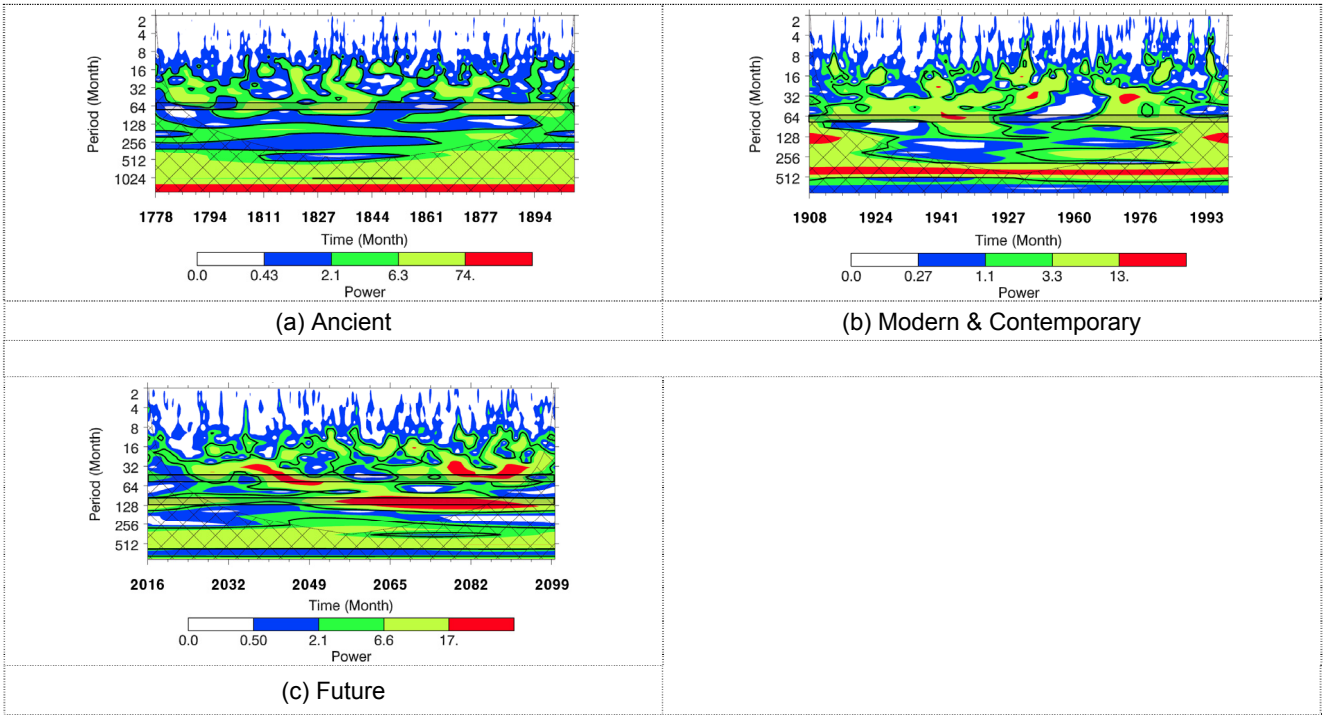

Figure 3. Wavelet analysis of SPI (6) for 3 different time window.

4.2 Analysis of Drought Magnitude

Table 4 displays the drought years in terms of the rank until top 15 by analyzing the average severity, duration, and magnitude for the entire period. As for the average severity of the drought, the year 1901 showed –2.06, representing the severest drought throughout the period as well as the largest magnitude with the value –24.67. The year 1901 stands out as the severest drought year in Seoul area among the long-term droughts data for the period of longer than 300 years.

©2017, IAHR. Used with permission / ISSN 1562-6865 (Online) - ISSN 1063-7710 (Print)

Meanwhile, during the modern period (1908-2015), the year 1943 and 1949 were the severest drought years within the rank of 15. The severest drought years in Seoul area were during the ancient period during which precipitation was observed by Chuk Woo Kee.

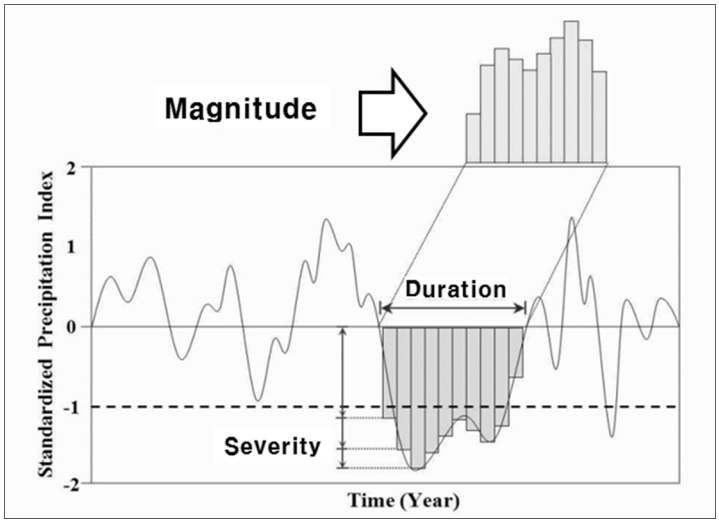

Figure 4. Concept of drought severity, duration and magnitude.

Table 4. Drought severity, duration and magnitude of drought year.

Rank	Year	Severity	Duration(months)	Magnitude
1	1901	-2.06	12	-24.67
2	1900	-1.77	12	-21.24
3	1894	-1.87	9	-16.80
4	1887	-1.64	10	-16.35
5	1943	-1.61	10	-16.11
6	1782	-1.51	10	-15.14
7	1904	-1.25	12	-15.02
8	1902	-1.25	12	-15.00
9	1876	-1.35	11	-14.88
10	1895	-1.31	11	-14.42
11	1888	-1.20	12	-14.42
12	1899	-1.29	11	-14.24
13	1909	-1.16	12	-13.90
14	1949	-1.51	9	-13.62
15	1939	-1.50	9	-13.52

4.3 Analysis of Long Lasted Extreme Drought Years

Table 5 shows the drought years continued for a long duration by analyzing the continued period from the selected extreme drought years ranked within top 30 during each period among each drought year. The continued drought analysis results showed that a total of four continuous droughts was drawn during 1899～1902, 1887～1889, 1893～1895, and 1782～1783 in the ancient period. Among these years, the severest continued droughts occurred for four consecutive years in 1899～1902 with the average severity –1.60, for a duration of 47 months, and magnitude of the drought –75.15. Whilst, during the modern period, the years 2014～2015 were found as the severe continued drought years with the average severity –1.09, drought period for 34 months, and magnitude of the drought –26.15. However, during the future period, a continued drought event for longer than two years did not appeared.

 ©2017, IAHR. Used with permission / ISSN 1562-6865 (Online) - ISSN 1063-7710 (Print)

Table 5. Drought magnitude for consecutive multiyear droughts.

Rank	Year	Successive year	Average Severity	Duration(months)	Magnitude
1	1899～1902	4	-1.60	47	-75.15
2	1893～1895	3	-1.26	34	-42.99
3	1887～1889	3	-1.25	34	-42.64
4	1782～1783	2	-1.25	22	-27.59
5	2014～2015	2	-1.09	24	-26.15

While, the drought record during Joseon Era can be confirmed from the Annals of the Joseon Dynasty. The severe drought that started from the end of the Joseon Period 1886 (The year of King Gojong 24), lasted for four years until 1889, and continued for another three years from 1893 (The year of King Gojong 31) until 1895 following the weak drought events for consecutive three years. Again, the weak droughts were continued for three years, followed by the severe drought events for six years from 1899 (The year of King Gojong 37) until 1904, recording the severest long-term drought in the Korean history.

5 CONCLUSIONS

The statistical analysis of precipitation for the Seoul showed that all the climate change data simulated with the observation data by Chuk Woo Kee that were restored from the archives and those from the Korea Meteorological Agency are well reflected in the climate characteristics of South Korea. With the basic statistical analysis for all the period for the Seoul area, the increasing trend of the precipitation throughout a long period was clearly indicated. The outliers' analysis in Seoul also detected long-term climate changes of transforming from dry years during the past to wet years during the future period starting from the modern period. In addition, the drought periodicity in Korea was for 5~6 years as analyzed by the wavelet transform analysis, and it is expected that drought would have occurred with the period of 8~10 years in the future which is longer than the drought duration in the past due to increases in the precipitation. The year 1901 has been the severest drought year in the Korean history in terms of the magnitude of drought. Meanwhile, the severest continued droughts occurred during 1899～1902 including the year 1901 in Seoul area which was severer than consecutive drought year 2014～2015. Particularly, the long-term continued drought for longer than ten years at the end of Joseon Dynasty (The year of King Gojong) was evaluated as the severest drought in the Korean history.

ACKNOWLEDGEMENTS

This research was supported by a grant (14AWMP-B082564-01) from Advanced Water Management Research Program funded by Ministry of Land, Infrastructure and Transport of Korean government.

REFERENCES

Cho, J.G. & Moon. B.K.(1997). Restorations and Analyses of Rainfall Amount Observed by Chukwookee. *Asia-Pacific Journal of Atmospheric Sciences*, 33, 691-707.

Jang, H,W., Cho, H.W., Kim, T.W. & Lee, J.H. (2016). Quantitative Characterization of Historical Drought Events in Korea Focusing of Outlier Analysis of Precipitation. *Journal of Korea Water Resources Asso*ciation, 49(2), 145-153.

Jhun. J.G. & Moon. B.K.(1997). Restorations and Analyses of Rainfall Amount Observed by Chukwookee. *Journal of Korean Meteorlogical Society*, 33(4), 691-707.

Lee, J.H., Kwon, H.H., Jang, H.W. & Kim, T.W. (2016). Future Changes in Drought Characteristics Under Extreme Climate Change over South Korea. *Hindawi Publishing Corporation Advances in Meteorology*, 19.

Lee, J.H., Seo, J.W. & Kim, C.J. (2012). Analysis on Trends, Periodicities and Frequencies of Korean Drought using Drought Indices. *Journal of Korea Water Resources Association*, 45(1), 75-89.

©2017, IAHR. Used with permission / ISSN 1562-6865 (Online) - ISSN 1063-7710 (Print)

Proceedings of the 37th IAHR World Congress
August 13 – 18, 2017, Kuala Lumpur, Malaysia

WATER RESOURCES DECREASE ISSUE AND COORDINATION STRATEGY OF GREEN WATER AND BULE WATER IN THE TAIHANG MOUNTAIN REGION

YANGWEN JIA[1], JUNKAI DU[2], CHUNFENG HAO[3], CUNWEN NIU[4] & YAQIN QIU[5]

[1,2,3,4,5] State Key Laboratory of Simulation and Regulation of Water Cycle in River Basin, China Institute of Water Resources & Hydropower Research (IWHR), Beijing, China,
jiayw@iwhr.com
[1,2,4,5] Department of Water Resources, China Institute of Water Resources & Hydropower Research (IWHR), Beijing, China,
[3] Department of Hydraulic and Hydropower Engineering, Tsinghua University, Beijing, China

ABSTRACT

The Taihang Mountain Region (140,000 km^2) is the water source area of the North China Plain, where the variations of river runoff (i.e. blue water) and rain water used by vegetation system (i.e. green water) are attributed to the climate variation and the land-use and land-cover change (LUCC). The quantitative simulation of water cycle and the attribution of water resources variation have been performed based on establishment and validation of the distributed hydrological model WEP-L (Water and Energy transfer Processes in Large river basins), as well as the remote sensing data (Landsat), meteorological data and social-economic data in the region, to analyze the inter-annual variations of blue water and green water and corresponding change rules with elevation. The results illustrate that climate variation is the main reason for the blue water decrease in the region, while the human activities including soil conservation dominate green water variation. Although the green water utilized by improved vegetation system would increase, its impacts on the blue water should not be neglected, and the coordinate strategy of the green water and the blue water in the region to realize an optimal national land space is discussed.

Keywords: Water resources; green water; blue water; climate variation; LUCC.

1 INTRODUCTION

The concept of green water has been brought forward by Sweden scientist Malin Falkenmark in 1993. Related researches on green water have been undergoing in some international organization and institutes, such as the Stockholm International Water Resources Research Center (SIWI), Food and Agriculture Organization (FAO), the International Water Management Institute (IWMI), the International Fund for Agricultural Development (IFAD), the Global Water System Project team (GWSP), and so on. The blue water and green water, highly concerned in the field of hydrology and water resources, provide a new perspective for water resources assessment, management and planning, yet corresponding concept system and assessment methodology are still in early development (Rockstrom et al., 2010). The assessment methodology of blue water consists of statistical analysis methods and hydrological models, while for green water assessment, biological methods, hydrological models and coupled biological and hydrological methods are developed (Cheng and Zhao, 2006). The hydrological models capable of temporal and spatial evaluation of water cycle factors have a significant advantage in the researches of blue water and green water. To be clear in the paper, the blue water is defined as the river runoff, and the green water is the evapotranspiration from vegetation to atmosphere (i.e. rain water used by vegetation system).

At present, related researches on green water and blue water mainly focus on large scale regions, basins and global system with detailed studies in typical mountainous regions are rarely reported. China is a mountainous country with 69% of its total land spread by mountains, hills and highlands. Moreover, hydrological processes of mountainous regions reveal distinct vertical zonality. Hence, corresponding studies on vertical distribution and variations of blue water and green water are helpful to promote hydrological processes studies in mountainous regions.

The Taihang Mountain is one of the most important mountain chains and geographical boundaries in eastern China with the Loess Plateau to the west and North China Plain to the east. The North China Plain occupies an important place in national politics, economy and culture and faces severe water resources and environment situation with rapid socio-economic development (Xia et al., 2004). The Taihang Mountain Region (TMR) is the main water source area of the North China Plain. The studies on the impacts and attributions of climate variation and land-use and land-cover change (LUCC) on blue water and green water so as to allocate rationally limited water resources between human society and ecological system are of great meaning for regional sustainable development.

In this study, the water cycle and energy transfer processes in TMR is simulated by using the distributed hydrological model Water and Energy transfer Processes in Large river basins (WEP-L) to discover the

 ©2017, IAHR. Used with permission / ISSN 1562-6865 (Online) - ISSN 1063-7710 (Print)

vertical distribution and variation of blue water and green water, as well as the impacts and attribution of climate variation and LUCC on regional blue water and green water.

2 STUDY AREA AND DATA

2.1 Study area

The Taihang Mountain, located in the eastern margin of the second stage of China terrain and regarded as eastern boundary of the Loess Plateau with Shanxi Plateau to the west and the North China Plain to the east, stretches over 400 km from the Xishan Mountain of Beijing in the north to the Wangwu Mountain of transboundary region of Henan and Shanxi provinces in the south. The Taihang Mountain Region (TMR, 140,000 km^2) is situated in the transitional zone of semi-humid region and semi-arid region, from 34°36'N, 110°10'E to 40°47'N, 116°35'E, spreading across four provincial administrative units of Beijing, Hebei, Shanxi and Henan and two first-class water resources regions of the Haihe River basin part (HRBP, 98,000 km^2) and the Yellow River basin part (YRBP, 42,000 km^2). The main vegetation type of its eastern part near the North China Plain is broad leaved deciduous forest, while its western part near the Loess Plateau is forest-steppe zone and steppe zone. The summer is hot and rainy while the winter is cold and dry because of continental climate, and average annual precipitation is about 600 mm with uneven distribution throughout the year. Main river system are consist of the Yellow River stem and its tributaries of the Qin River and the Dan River, as well as The Haihe River' tributaries of the Chaobai River, the Yongding River, the Daqing River, the Hutuo River, the Fuyang River and the Zhang River from north to south. Rivers and sub-basin division of the Taihang Mountain Region is shown in Figure 1 and the land cover map of TMR in 1990s is shown in Figure 2.

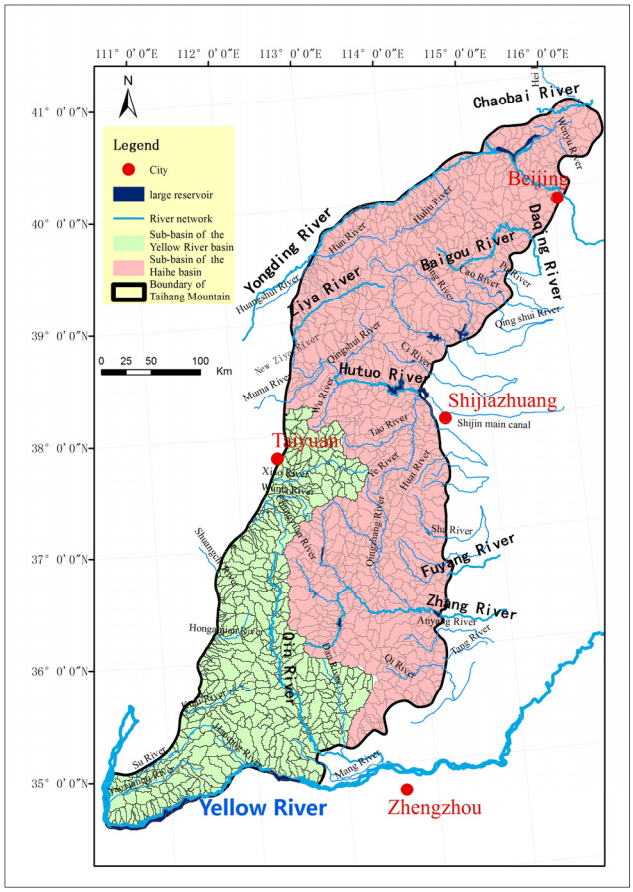

Figure 1. Rivers and sub-basin division of the Taihang Mountain Region.

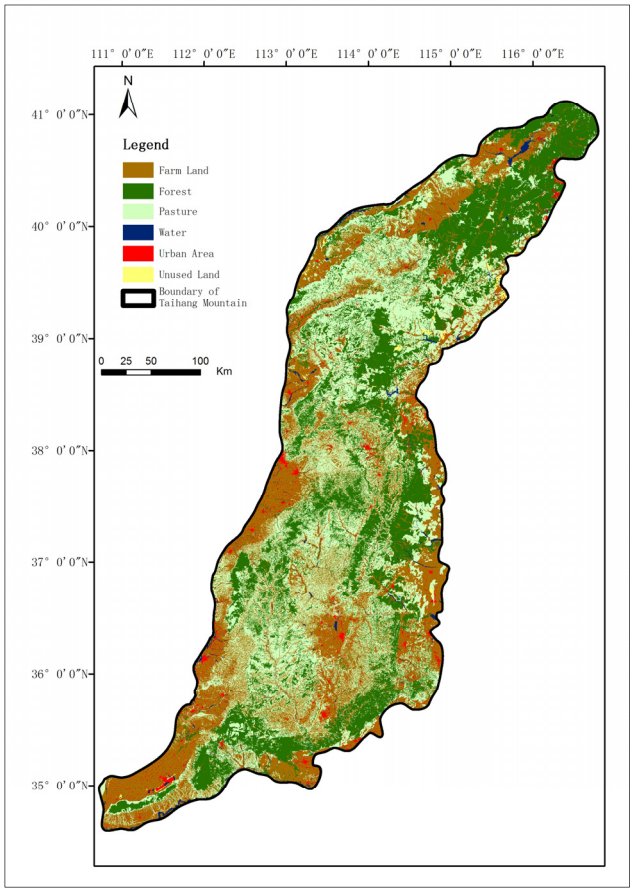

Figure 2. Land cover map of the Taihang Mountain Region (1990S).

2.2 Data source

The DEM data for WEP-L model establishment are derived from Global 30 Arc-Second Elevation (GTOPO30) by the EMOS data center of the U.S. geological survey (USGS). The measured daily meteorological data from 1980 to 2000, including precipitation, air temperature, related humidity, wind velocity and sunshine duration, are obtained from national and local meteorological and hydraulic departments, involving 536 stations in the Haihe River basin and 904 stations in the Yellow River basin. The land use and land cover data of 1986, 1996 and 2000 are from international scientific data sharing platform and extracted results of Landsat and NOAA/AVHRR images. The soil and its characteristic information are from the second

©2017, IAHR. Used with permission / ISSN 1562-6865 (Online) - ISSN 1063-7710 (Print)

national general survey of soil with the resolution of 1:100,000. The runoff series are from monitoring data of hydrological stations including 356 stations in the Haihe River basin and 132 stations in the Yellow River basin.

3 METHODOLOGY

3.1 Model introduction

The Water and Energy transfer Processes in Large river basins (WEP-L) model (Jia et al., 2001; Jia et al., 2005) is developed on basis of the Water and Energy transfer Processes (WEP) model for the water cycle simulation in large scale basins. To ensure the rapidity and accuracy of the overall hydrological processes simulation, the advantages of water cycle hydrological model and land surface model (SVATS model) are integrated in the model for the coupled simulation of water cycle and energy transfer, and the Varying Source Area (VSA) theory is embedded in for dynamic simulation of surface water, groundwater and soil water. The model sets the contour belts within the sub-basins as its basic calculation units and varied time steps as its calculation interval. Detailed description on the structure and approaches of the WEP/WEP-L models are referred to in (Jia et al., 2006a; Jia et al., 2006b). The WEP-L model is qualified for fine simulation of water cycle processes with great potential on water resources assessment under various meteorological and underlying surface conditions due to its physical foundation of hydrological and eco-hydrological mechanism and accessible parameters based on characteristics of the study area.

3.2 Model establishment and validation

There is no hydraulic connection between the two basins within TMR, hence two distributed hydrological models are established separately, in which 1634 sub-basins and further 7351 basic calculation units (contour belts) are set according to the terrain, including 1634 sub-basins and 5096 contour belts in the part of the Haihe River basin, and 507 sub-basins and 2435 contour belts in the part of the Yellow River basin. The division of sub-basins is shown in Figure 2.

Monthly runoff from 1980 to 2000 are simulated by the WEP-L model and validated by observed data. The results indicate good accuracy of model simulation with relative error (RE) below 10%, Nash efficiency coefficient (NEC) above 0.7 and correlation coefficient above 0.8. The comparison of monthly simulated runoff and observed runoff at the Wuzhi station in the Yellow River basin (NEC is 0.83 and RE is -2.0%) is shown in Figure 3. The comparison of monthly simulated runoff and observed runoff at the Guantai station in the Haihe River basin (NEC is 0.80 and RE is -2.9%) is shown in Figure 4.

3.3 Scenarios

On basis of the model validation, continuous daily simulations of 21 years water cycle processes in TMR from 1980 to 2000 were implemented with the same modeling parameters. The spatial and temporal variation rule and attribution of blue water and green water in the two catchments are brought forward. Two scenarios of prescribed conditions were designed for quantitative analysis of the impacts of climate variation and underlying surface change considering 1980-1990 as the pre-impact period (EP) and 1991-2000 as the post-impact period (OP).

In Scenarios 1, the historical underlying land cover data are adopted in the water cycle process simulation, and the variations of EP and OP are regarded to be integrated impacts of climate variation and land cover change.

In Scenarios 2, the underlying land cover data in 1980 are adopted throughout the 21 years remaining other factors unchanged as Scenarios 1, and the variations of EP and OP are just effected by climate variation.

In Scenarios 1:

$$\Delta R^{blue} = R_1^{blue} - R_2^{blue} \quad [1]$$

$$\Delta R^{green} = R_1^{green} - R_2^{green} \quad [2]$$

where, R_1^{blue} is annual average blue water of EP (mm), R_2^{blue} is annual average blue water of OP (mm), ΔR^{blue} is variation of average blue water of EP and OP (mm), R_1^{green} is annual average green water of EP (mm), R_2^{green} is annual average green water of OP (mm), ΔR^{green} is variation of average green water of EP and OP (mm).

In Scenarios 2:

$$\Delta R_{climate}^{blue} = R_1'^{blue} - R_2'^{blue} \quad [3]$$

$$\Delta R_{climate}^{green} = R_1'^{green} - R_2'^{green} \quad [4]$$

 ©2017, IAHR. Used with permission / ISSN 1562-6865 (Online) - ISSN 1063-7710 (Print)

where, $R_1'^{blue}$ is annual average blue water of EP under 1980 underlying surface(mm), $R_2'^{blue}$ is annual average blue water of OP under 1980 underlying land cover (mm), $\Delta R_{climate}^{blue}$ is variation of average blue water of EP and OP effected by climate variation(mm), $R_1'^{green}$ is annual average green water of EP under 1980 underlying land cover (mm), $R_2'^{green}$ is annual average green water of OP under 1980 underlying land cover (mm), $\Delta R_{climate}^{green}$ is variation of average green water of EP and OP effected by climate variation (mm).

Comparing Scenario1 and Scenario 2:

$$\Delta R_{LUCC}^{blue} = \Delta R^{blue} - \Delta R_{climate}^{blue} \quad [5]$$

$$\Delta R_{LUCC}^{green} = \Delta R^{green} - \Delta R_{climate}^{green} \quad [6]$$

where, ΔR_{LUCC}^{blue} is variation of average blue water of EP and OP effected by LUCC, $\Delta R_{climate}^{green}$ is variation of average green water of EP and OP effected by LUCC.

The contribution rates of climate variation and LUCC on blue water and green water are defined as following:

$$\eta_{climate}^{blue} = \Delta R_{climate}^{blue} / \Delta R^{blue} \quad [7]$$

$$\eta_{LUCC}^{blue} = \Delta R_{LUCC}^{blue} / \Delta R^{blue} \quad [8]$$

$$\eta_{climate}^{green} = \Delta R_{climate}^{green} / \Delta R^{green} \quad [9]$$

$$\eta_{LUCC}^{green} = \Delta R_{LUCC}^{green} / \Delta R^{green} \quad [10]$$

where, $\eta_{climate}^{blue}$ is contribution rate of climate variation on blue water, η_{LUCC}^{blue} is contribution rate of LUCC on blue water, $\eta_{climate}^{green}$ is contribution rate of climate variation on green water, η_{LUCC}^{green} is contribution rate of LUCC on green water.

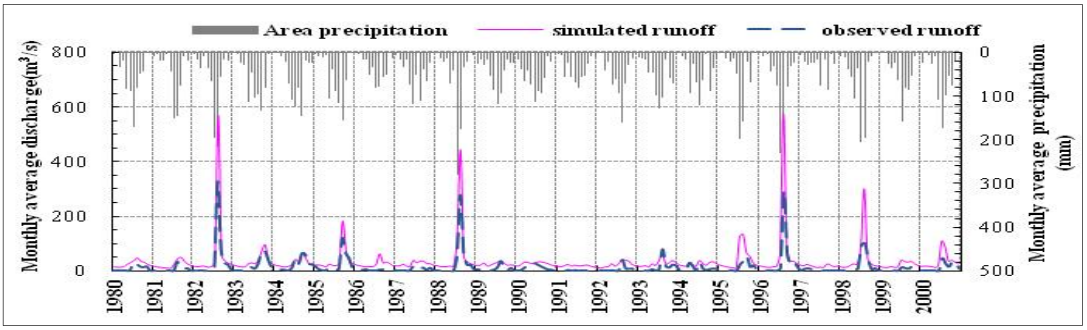

Figure 3. Comparison of monthly simulated runoff and observed runoff at the Wuzhi station in the Yellow River basin.

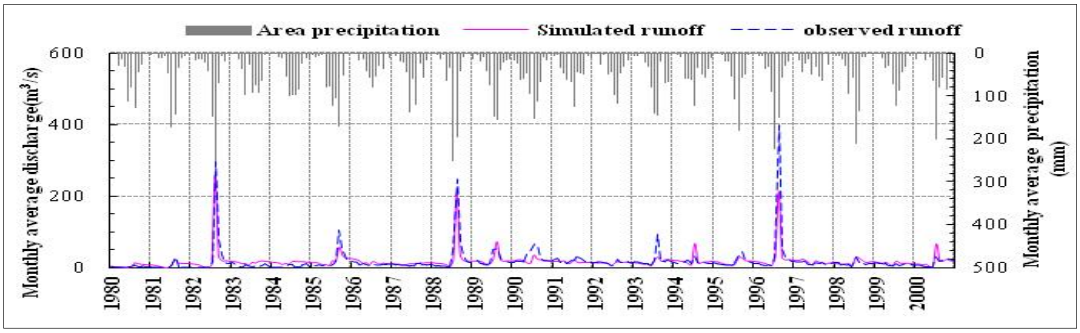

Figure 4. Comparison of monthly simulated runoff and observed runoff at the Guantai station in the Haihe River basin.

©2017, IAHR. Used with permission / ISSN 1562-6865 (Online) - ISSN 1063-7710 (Print)

4 ANALYSIS ON DISTRIBUTION AND ATTRIBUTION OF BULE WATER AND GREEN WATER

4.1 Evolution rules

TMR is a significant boundary of clime, vegetation and geography, and the hydrological factors and evolution processes of the two sides of the mountain chain are obviously different. Figure 5 and Figure 6 show the evolution rules of precipitation, blue water and green water of the TMR from 1980 to 2000, indicating increasing precipitation and blue water and decreasing green water in the Haihe River part, but the opposite trends in the Yellow River part.

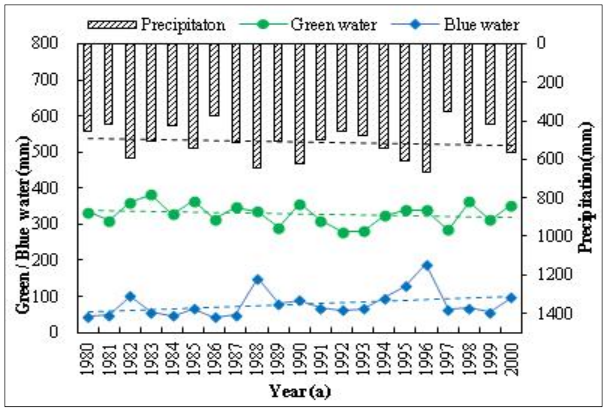

Figure 5. Evolution of precipitation, blue water and green water of the Haihe River basin part of the Taihang Mountain Region from 1980 to 2000.

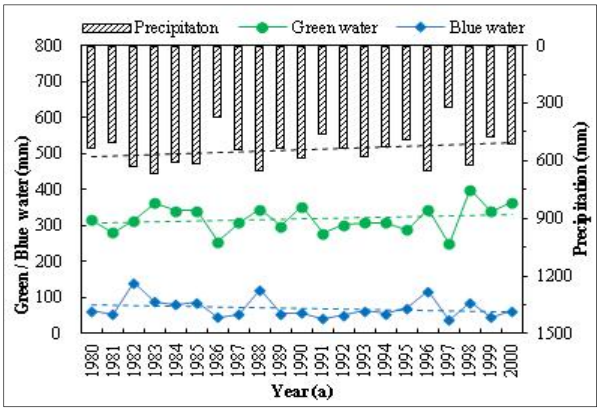

Figure 6. Evolution of precipitation, blue water and green water of the Yellow River basin part of the Taihang Mountain Region from 1980 to 2000.

4.2 Vertical distribution and variation rules

In Scenario 1, according to the modeling results, vertical distribution and variation of blue water and green water in both of the HRBP and the YRBP under Scenario 1 is shown in Figure 7 and Figure 8. The solid line in the figure represents EP (1980-1990) annual average value while the dashed line represents that of OP (1991-2000).Generally, in the HRBP, green water of OP is less than that of EP, yet blue water is becoming bigger. The peak of blue water appears at 200-400m elevation. In the YRBP, the blue water decreases with elevation, and the green water is smaller. The green water of OP is smaller than that of EP below 800m elevation, while it becomes bigger in OP than in EP above 800m elevation.

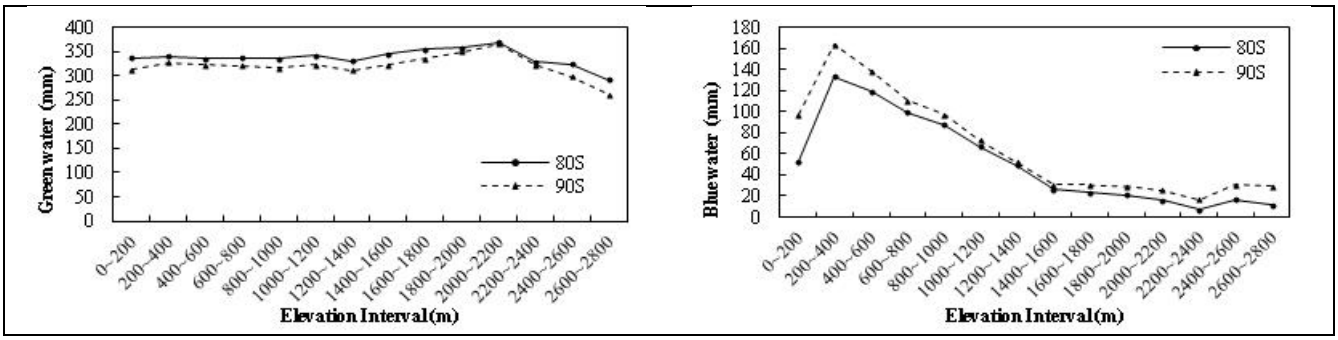

Figure 7. Vertical distribution of blue water and green water of the HRBP of the Taihang Mountain Region in Scenario 1 in 1980-1990 (80s) and 1991-2000 (90s).

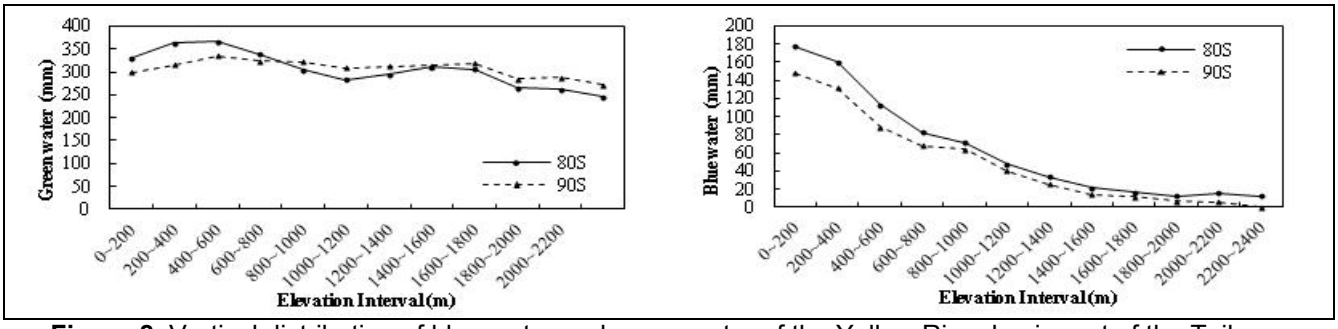

Figure 8. Vertical distribution of blue water and green water of the Yellow River basin part of the Taihang Mountain Region in Scenario 1 in 1980-1990 (80s) and 1991-2000 (90s).

 ©2017, IAHR. Used with permission / ISSN 1562-6865 (Online) - ISSN 1063-7710 (Print)

In Scenario 2, vertical distribution and variation of blue water and green water in both of the HRBP and the YRBP under Scenario 1 is shown in Figure 9 and Figure 10. In the HRBP without consideration of LUCC, the green water makes little change in EP and OP, while the blue water increases. In the Yellow River part without consideration of LUCC, both of the green water and blue water are smaller in OP than those in EP. Moreover, the green water and blue water generally decline with elevation in the Yellow River part as the rules in Scenario 1.

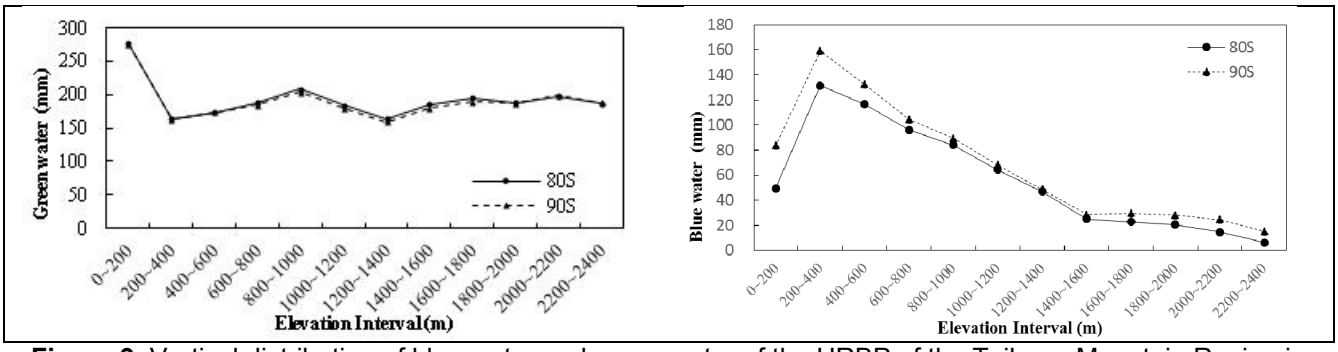

Figure 9. Vertical distribution of blue water and green water of the HRBP of the Taihang Mountain Region in Scenario 2 in 1980-1990 (80s) and 1991-2000 (90s).

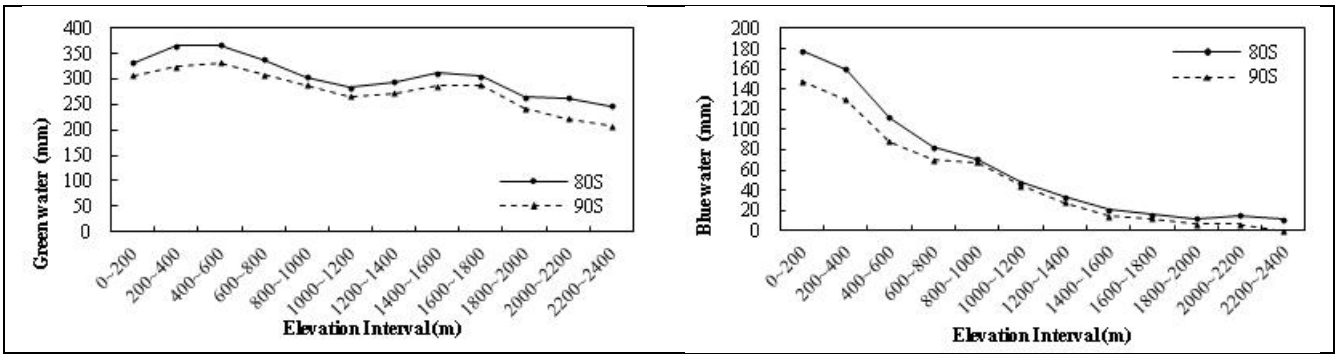

Figure 10. Vertical distribution of blue water and green water of the Yellow River basin part of the Taihang Mountain Region in Scenario 2 in 1980-1990 (80s) and 1991-2000 (90s).

4.3 Attribution analysis

For HRBP, the attribution results on variation of blue water and green water are shown in Figure 11 and Table 1, according to the methodologies illustrated by formulas in section 3.3. It's suggested that green water in HRBP decreases by 19.40mm in OP than in EP, in which the climate variation accounts for -3.29mm and the LUCC accounts for -16.11mm, hence the LUCC plays a dominant role for the green water variation. While for the blue water variation, the climate change makes up 14.74mm increment of blue water and the LUCC 4.26mm, and the total blue water increases by 19.00mm in OP than in EP. The green water changes greatly at low and middle altitude area, while the blue water increase most in low altitude area, and that of high altitude area is next.

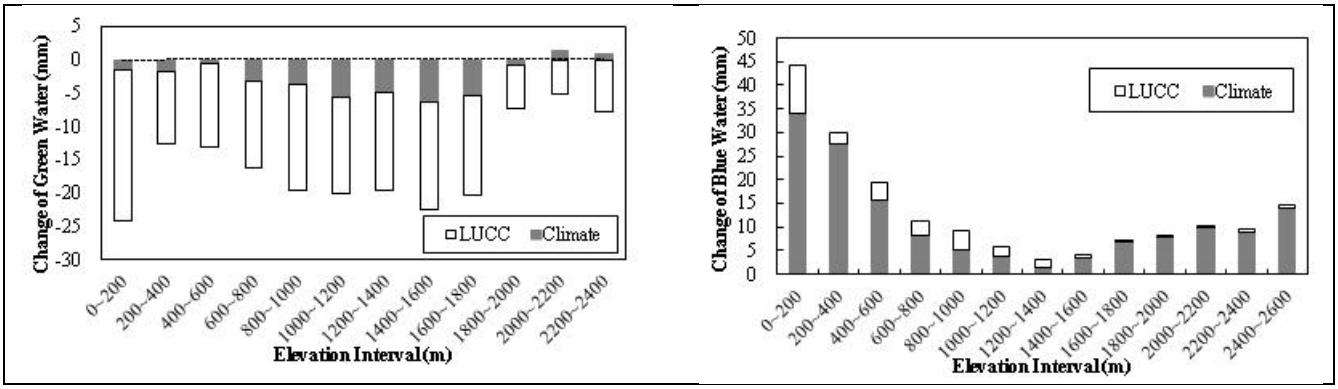

Figure 11. Attribution of climate variation and LUCC on vertical variation of the blue water and green water of the Haihe River basin part of the Taihang Mountain Region.

Table 1. Attribution results of climate variation and LUCC on vertical variation of the blue water and green water of the Haihe River basin part.

Elevation (m)	ΔR^{green} (mm)	$\Delta R^{green}_{climate}$ (mm)	ΔR^{green}_{LUCC} (mm)	ΔR^{blue} (mm)	$\Delta R^{blue}_{climate}$ (mm)	ΔR^{blue}_{LUCC} (mm)
0~200	-24.17	-1.49	-22.69	44.09	34.12	9.98
200~400	-12.59	-1.86	-10.72	29.90	27.70	2.20
400~600	-13.10	-0.66	-12.45	19.56	15.80	3.76
600~800	-16.33	-3.16	-13.17	11.23	8.30	2.93
800~1000	-19.52	-3.82	-15.70	9.36	5.30	4.06
1000~1200	-19.98	-5.59	-14.39	5.91	3.89	2.01
1200~1400	-19.71	-4.80	-14.91	3.13	1.52	1.61
1400~1600	-22.50	-6.25	-16.25	4.12	3.53	0.59
1600~1800	-20.33	-5.33	-15.01	7.25	6.91	0.35
1800~2000	-7.40	-0.88	-6.52	7.87	7.75	0.13
2000~2200	-3.93	1.29	-5.22	10.20	9.86	0.34
2200~2400	-6.94	0.95	-7.88	9.41	8.98	0.43
0~2400	-19.40	-3.29	-16.11	19.00	14.74	4.26

For YRBP, the attribution results on variation of blue water and green water are shown in Figure 12 and Table 2. The green water in the HRBP increases by 20.05mm in OP than in EP, in which the climate variation accounts for -27.82mm and the LUCC accounts for 47.87mm, indicating the opposite impacts of climate and LUCC on the green water. The climate change leads the blue water variation accounting for 6.27mm decrement of blue water, and the total blue water decreases by 8.19mm in OP than in EP. The LUCC raise the green water at low altitude area, but reduce it at high altitude area, while the climate variation reduces the green water at all altitude area. The climate variation and LUCC reduce the blue water at all altitude area, and at low and high altitude area the climate variation plays a dominant role.

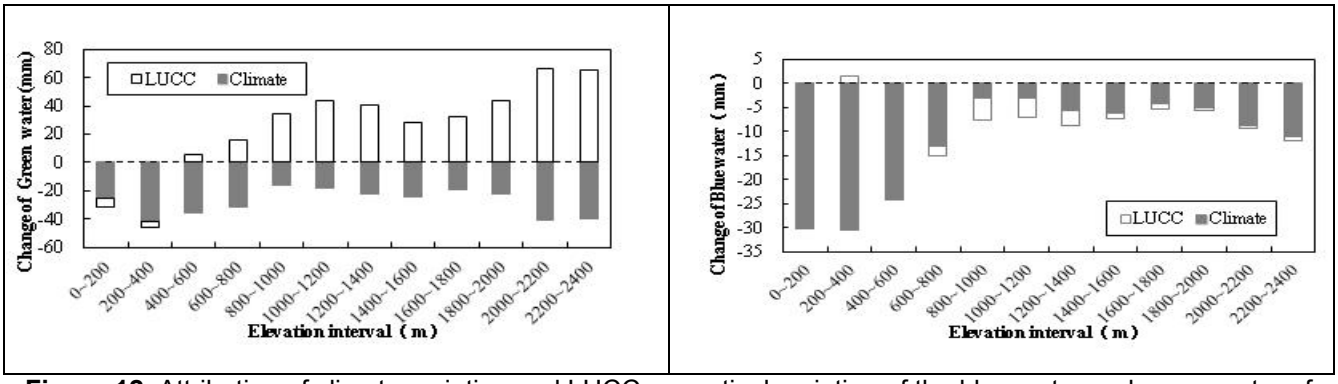

Figure 12. Attribution of climate variation and LUCC on vertical variation of the blue water and green water of the Yellow River basin part of the Taihang Mountain Region.

Table 2. Attribution results of climate variation and LUCC on vertical variation of the blue water and green water of the Yellow River basin part.

Elevation (m)	ΔR^{green} (mm)	$\Delta R^{green}_{climate}$ (mm)	ΔR^{green}_{LUCC} (mm)	ΔR^{blue} (mm)	$\Delta R^{blue}_{climate}$ (mm)	ΔR^{blue}_{LUCC} (mm)
0~200	-31.75	-25.29	-6.46	-30.06	-29.80	-0.26
200~400	-46.28	-41.40	-4.89	-28.70	-30.34	1.64
400~600	-30.6	-35.79	5.19	-24.11	-24.04	-0.07
600~800	-14.93	-31.10	16.17	-15.17	-12.99	-2.18
800~1000	18.11	-16.13	34.25	-7.52	-2.98	-4.54
1000~1200	25.59	-17.99	43.58	-7.13	-3.05	-4.08
1200~1400	18.38	-22.66	41.04	-8.67	-5.52	-3.15
1400~1600	3.25	-24.55	27.8	-7.34	-6.20	-1.14
1600~1800	13.63	-18.87	32.51	-5.22	-4.19	-1.03
1800~2000	21.19	-22.70	43.88	-5.63	-5.08	-0.54
2000~2200	25.28	-40.67	65.94	-9.38	-8.72	-0.66
2200~2400	25.36	-39.47	64.82	-12.04	-11.10	-0.94
0~2400	20.05	-27.82	47.87	-8.19	-6.27	-1.92

©2017, IAHR. Used with permission / ISSN 1562-6865 (Online) - ISSN 1063-7710 (Print)

In the whole, the green water of TMR declines from 1980 to 2000 while the blue water increases, as is shown in Table 3. Moreover, the variation of the blue water and green water in the HRBP varies is consistent with the whole TMR, while that of the YRBP is just opposite.

The contribution rates of climate variation and LUCC to the blue water and green water changes in TMR and its two catchments are shown in Table 4. For the HRBP, the climate and LUCC both raise the green water and the LUCC is the most important factor accounting for 83.0%, while for the YRBP and the whole region, the LUCC increases the green water and the climate change reduces it, and the impacts of the LUCC is greater than the climate variation. As for the blue water, the climate variation dominates its evolution accounting for more than 75% in all three statistical units.

Table 3. Attribution results of the green water and blue water changes in TMR.

Statistical Unit	Area (10^4km^2)	ΔR^{green} (mm)	$\Delta R^{green}_{climate}$ (mm)	ΔR^{green}_{LUCC} (mm)	ΔR^{blue} (mm)	$\Delta R^{blue}_{climate}$ (mm)	ΔR^{blue}_{LUCC} (mm)
The Haihe River basin part	9.8	-19.40	-3.29	-16.11	19.00	14.74	4.26
The Yellow River basin part	4.2	20.05	-27.82	47.87	-8.19	-6.27	-1.92
The Taihang Mountain Region	14.0	-6.72	-11.18	4.46	10.26	7.98	2.27

Table 4. Contribution rate of climate variation and LUCC to the green water and blue water changes.

Statistical Unit	$\eta^{green}_{climate}$	η^{green}_{LUCC}	$\eta^{blue}_{climate}$	η^{blue}_{LUCC}
The Haihe River basin part	17.0%	83.0%	77.6%	22.4%
The Yellow River basin part	-138.7%	238.7%	76.6%	23.4%
The Taihang Mountain Region	-166.4%	66.4%	77.3%	22.7%

5 DISCUSSIONS

5.1 Rationality analysis

The climate variation reduces the green water and raises the blue water of TMR, while the LUCC raises both of the green water and blue water. However, it differs in the east side and the west side of the Taihang Mountain Chain. The climate variation and LUCC in the HRBP result in decreasing green water and increasing blue water, but in the YRBP the climate variation reduces both of the green water and blue water, and the LUCC raises the green water and reduces the blue water.

As the precipitation is the total input of terrestrial water cycle, there is positive correlation between local precipitation and the green water and blue water. But in contrast, the influencing mechanism of the LUCC on water cycle processes is complicated. Under the same climate condition, higher vegetation cover may increase the entrapment evapotranspiration, raise the capability of soil infiltration and soil moisture, and enhance regional evaporative capacity and integrated evapotranspiration. Intensive vegetation may not only raise regional roughness and then attenuate the flood peak, but also increase the base flow by higher soil moisture. Hence, the increment of vegetation coverage would raise the green water in general and the blue water in dry seasons, and reduce the blue water in wet seasons.

As shown in Figure 5 and Figure 6, the precipitation of the HRBP increases and that of the YRBP decreases. The vertical vegetation coverage variation of the HRBP in EP and OP is shown in Figure 13. The total of forest land, grass land and farm land in OP is 2696.33 km^2 less than in EP with forest land decreasing by 1297.52 km^2, grass land increasing by 991.54 km^2 and farm land decreasing by 2390.95 km^2. The forest land changes the most at 800-1600m altitude, the grass land 0-600m altitude, and the farm land 0-400m altitude, which is in accordance with green water variation intensity of the HRBP.

The vegetation coverage increases greatly from 1980 to 2000 in the YRBP as shown in Figure 14. The total of forest land, grass land and farm land in OP is 2330.37 km^2 more than in EP with forest land increasing by 1699.78 km^2 (mainly at 0-400m altitude and 800-1400m altitude), grass land increasing by 1319.60 km^2 (mainly at 600-1400m altitude) and farm land decreasing by 689.01 km^2 (mainly at 0-600m altitude). The contribution rate of LUCC to the green water of the YRBP is negative at 0-400m altitude and positive at high altitude area which meets the analysis results on the LUCC.

©2017, IAHR. Used with permission / ISSN 1562-6865 (Online) - ISSN 1063-7710 (Print)

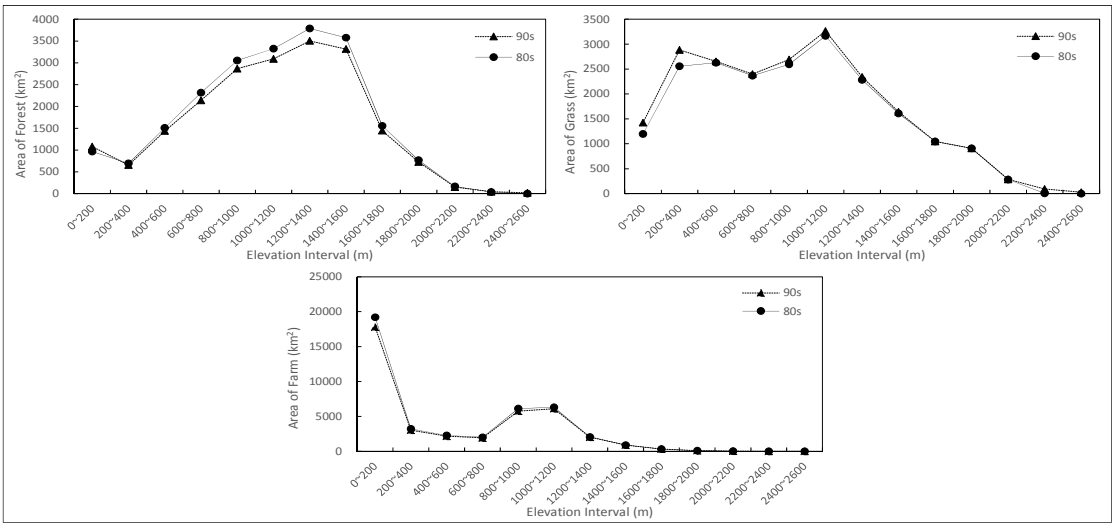

Figure 13. Vertical distribution of forest, grass and farm land of the Haihe River basin part of TMR in 1980-1990 (80s) and 1991-2000 (90s).

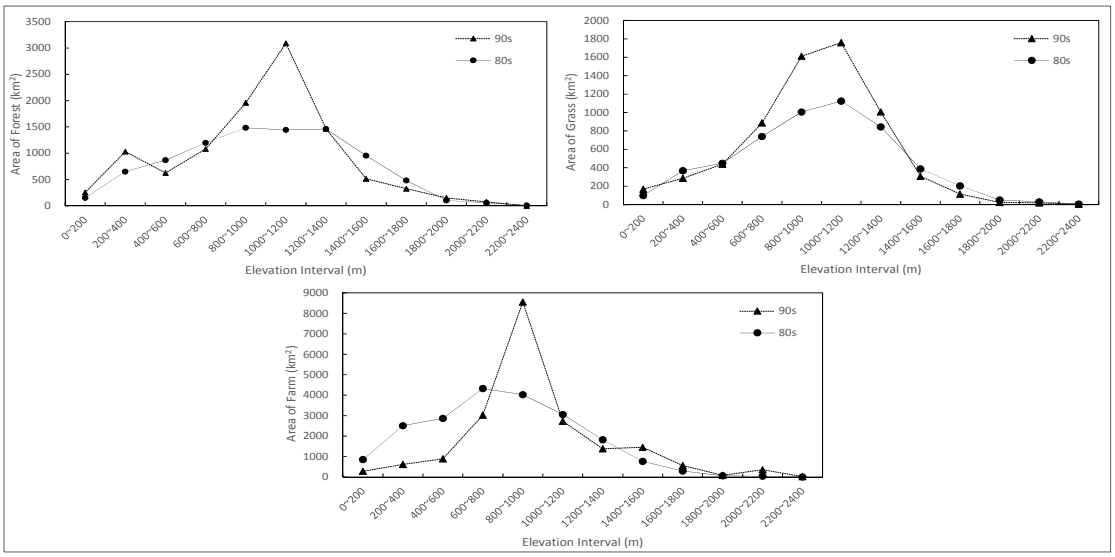

Figure 14. Vertical distribution of forest, grass and farm land of the Yellow River basin part of TMR in 1980-1990 (80s) and 1991-2000 (90s).

5.2 Existed issues

The paper completes the variation and attribution analysis on the green water and blue water of the two catchments of the TMR. The results indicate that the LUCC is the dominant factor of green water variation and the climate variation plans a leading role in blue water variation. Besides, the analysis of vegetation coverage in the HRBP and the YRBP support the results of attribution.

The simulation and attribution results show that the climate variation accounts for 77.3%, 77.6% and 77.3% of the blue water variation of TMR, the HRBP and the YRBP. Some previous studies have brought out related conclusions on the attribution of runoff (i.e. blue water in the paper) variation in the Yellow River basin. The contribution rate of climate variation to runoff reduction of the middle Yellow River basin is 43% (Liu and Zhang, 2004). The land use and land cover change in 11 typical basins of the Yellow River basin accounts for no less than 50% of the runoff reduction (Zhang et al., 2009). The average contribution rate of precipitation decrease for runoff reduction in 38 basins of the Yellow River basin is 49.3% (Yang et al., 2015).

Comparing with previous studies, the paper focuses on TMR where the human activity intensity and the underlying land surface variation are relatively small. That may be one of the reasons for bigger contribution rate of climate variation to runoff variation in the paper than in other studies, yet the impacts of LUCC on the blue water may still be underestimated.

The accuracy and resolution of the input data of the distributed hydrological model WEP-L may bring uncertainty for the simulation results. The land use data used in the model is produced according to the China national standard GB/T 21010-2007, in which the first grade classification forest land only contains wood land, shrub land and other forest land, grass land is further classified to three subclasses of natural grass land, artificial grass land and other grass land. The input land use data are unable to comprehensively reflect

 ©2017, IAHR. Used with permission / ISSN 1562-6865 (Online) - ISSN 1063-7710 (Print)

regional LUCC because of rough classification of land use type. The community structure of vegetation would improve after forest planting and the LAI (Leaf Area Index) may vary greatly in different periods which will significantly influence the processes of runoff generation and confluence. Besides, the accuracy of the distribution of precipitation and other meteorological factors may be affected due to sparse monitoring stations especially at high altitude area.

6 CONCLUSIONS

This study has established the distributed hydrological model on the HRBP and the YRBP of TMR, simulated the water cycle processes from 1980 to 2000, explained the temporal and spatial distribution and evolution of the green water and the blue water and analyzed the contribution of climate variation and LUCC. Main conclusions of the study are as follows:

(1) The evolution rules of the green water and blue water of the two catchments at the west and the east sides of TMR are distinctly different. The green water of the HRBP in 1990s is smaller than in 1980s while the blue water is bigger. The variation trend of the YRBP is just opposite;

(2) The climate variation plays a leading role in the blue water variation of the TMR, while the LUCC dominates the green water variation;

(3) The water cycle processes present obvious vertical characteristic and varies at the two sides of TMR. The blue water declines and the green water slightly decreases with elevation increase. The blue water changes the most at 0-1000m altitude for the whole region. The blue water shows dramatic alternation at 800-1800m altitude of the HRBP. At low altitude area of the YRBP, the green water reduces and at high altitude area it raises;

(4) To deal with the water shortage problem in TMR, different strategies should be adopted in the HRBP and the YRBP. In 1990s, the precipitation of the HRBP is relatively big, yet the green water reduces, indicating the contradiction of water use by regional human activities and ecological system. Hence, the reduction of socio-economic water use by water saving and adaptive development is the key point for the coordination of human society and nature. Meanwhile, the blue water of the YRBP in 1990s increases with relatively small precipitation due to soil conservation activities and forest planting, yet high vegetation coverage may reduce the blue water.

With the development of information technology and remote sensing network, the geographic data of high temporal and spatial resolution, the data assimilation of various sources and the data mining under big data framework are key research tasks for the further hydrological simulation in the mountain region.

ACKNOWLEDGEMENTS

This study is funded by the National Key Basic Research Program of China (2015CB452701) and the Chinese Academy of Engineering Consulting Project (2016-ZD-08).

REFERENCES

Cheng, G.D. & Zhao, W.Z. (2006). Green Water and its Research Progress. *Advances in Earth Science*, 21(3), 221-227.

Jia, Y.W., Ni, G.H., Kawahara, Y. & Suetsugi, T. (2001). Development of WEP Model and its Application to an Urban Watershed. *Hydrological Processes*, 15, 2175-2195.

Jia, Y.W., Wang, H., Qiu, Y.Q. & Zhou, Z.H. (2006a). Generalized Water Resources Assessment Based on Water Shed Hydrologic Cycle Model I. Assessment Approach. *Journal of Hydraulic Engineering*, 37(9), 1051-1055.

Jia, Y.W., Wang, H., Wang, J.H., Luo, X.Y., Zhou, Z.H., Yan, D.H. & Qin, D.Y. (2005). Development and Verification of a Distributed Hydrologic Model for the Yellow River Basin. *Journal of Natural Resources,* 20(2), 300-308.

Jia, Y.W., Wang, H., Zhou, Z.H., Qiu, Y.Q., Luo, X.Y., Wang, J.H., Yan, D.H. & Qin, D.Y. (2006b). Development of the WEP-L Distributed Hydrological Model and Dynamic Assessment of Water Resources in the Yellow River Basin. *Journal of Hydrology*, 331(3), 606-629.

Liu, C.M. & Zhang, X.C. (2004). Causal Analysis on Actual Water Flow Reduction in the Mainstream of the Yellow River. *ACTA GEOGRAPHICA SINICA*, 59(3), 323-330.

Rockström, J., Karlberg, L., Wani, S.P., Barron, J., Hatibu, N. Oweis, T., Bruggeman, A., Farahani, J. & Qiang, Z. (2010). Managing Water in Rainfed Agriculture - the Need for a Paradigm Shift. *Agricultural Water Management*, 97(4), 543-550.

Xia, J., Liu, M.Y., Jia, S.F., Song, X.F., Luo, Y. & Zhang, S.F. (2004). Water Security Problem and Research Perspective in North China. *Journal of Natural Resources,* 19(5), 550-560.

Yang, D.W., Zhang, S.L. & Xu, X.Y. (2015). Attribution Analysis of Runoff Decline in Yellow River Basin During Past Fifty Years Based on Budyko Hypothesis. *SCIENCE CHINA Technological Sciences,* 45, 1024-1034.

Zhang, X.P., Zhang, L., Zhao, J., Rustomji, P. & Hairsine, P. (2009). Responses of Streamflow to Changes in Climate and Land Use/Cover in the Loess Plateau, China. *Water Resources Research*, 44(7), 2183-2188.

©2017, IAHR. Used with permission / ISSN 1562-6865 (Online) - ISSN 1063-7710 (Print)

Proceedings of the 37th IAHR World Congress
August 13 – 18, 2017, Kuala Lumpur, Malaysia

TOWARDS AN INTEGRATED MUNICIPAL WATER DEVELOPMENT: OCOTLAN DE MORELOS, OAXACA, MEXICO

FERNANDO J. GONZÁLEZ VILLARREAL[1], JORGE ALBERTO ARRIAGA MEDINA[2] & JORGE IVÁN JUÁREZ DEHESA[3]

[1,2,3] National Autonomous University of Mexico (UNAM), Mexico CIty, Mexico
fgv@pumas.iingen.unam.mx; jarriagam@iingen.unam.mx; jjuarezd@iingen.unam.mx

ABSTRACT

This paper presents the results achieved by the Water Development Support Program of the states of Oaxaca, Puebla and Tlaxcala (PADHPOT, in Spanish) in Ocotlan de Morelos, Oaxaca, Mexico. The National Autonomous University of Mexico (UNAM) created this program to help municipalities with a range of 10 and 100 thousand inhabitants to improve their water supply systems. Firstly, it explains the origins and methodology used by the program. Then, the document describes the geographical and socioeconomic conditions related to the municipal water supply system. Finally, the text describes the goals achieved by PADHPOT in the community, focusing in the fact that an integrated view is needed in order not to only build hydraulic infrastructure but to promote institutional development and local capacity building as well.

Keywords: Best management practices; integrated water resources management; municipal water development; water utilities.

1 INTRODUCTION

Discussions about hydraulic development focus mainly in large urban centers, however, one of the main challenges related with water and sanitation services is with medium and small sized cities. Urban centers with more than one hundred thousand inhabitants, thanks to their economic and political influence, receive more attention in Mexico's water public policy. As a result, those communities have the highest percentages of coverage and public investments. On the other hand, medium and small cities have not received the necessary attention to effectively solve their technical, institutional and economic issues.

In 1983, the article 115 of the Mexican Constitution was reformed in order to transfer the operation of water and sewerage services to the municipalities. Nevertheless, this legislative decision was not accompanied by a coordinated public policy aimed to strengthening decentralization, especially in cities with low capacities and lack of economic resources to cope with the complex work of providing drinking water to all their inhabitants.

After three decades that the decentralization process in water sector was started, most municipal water utilities continue to work according to the problems that they face in short term, with reactive actions, without planning and without performance indicators (Domínguez, 2014). This reality prevents them from providing their communities with adequate, regular and good quality water and sewerage services. On the contrary, the water utilities, particularly of municipalities with populations between ten thousand and a hundred thousand inhabitants, have the following characteristics: (González-Villarreal and Arriaga, 2014).

(a) Inefficiency in organizational, technical and commercial management.
(b) Lack of qualified technical personnel in the operation and administration.
(c) Low participation of citizens in the design and implementation of water programs.
(d) Persistence of water fees and taxes that do not reflect the cost of services.
(e) Absence of sufficient economic resources to ensure their sustainability.

Having in mind that water utilities in small and medium cities in Mexico are facing major challenges to provide water and wastewater services, the National Autonomous University of Mexico designed PADHPOT in 2012. The intention was to share with the society regarding the results, knowledge and experience achieved during eight years of operation of its Water Management, Use and Reuse Program PUMAGUA inside their campuses (González-Villarreal et al., 2013). The PADHPOT aims to ensure water management and wastewater services are done in an efficient and sustainable way in cities with a population between ten thousand and one hundred thousand inhabitants, by promoting not only hydraulic infrastructure construction, but also social involvement.

To reach this goal, the program structures its work in two areas: Water and Sanitation and Water Observatory. While the former is a tool for technical support to improve quality of the services provided by water utilities and transmit theoretical knowledge, the latter is conceived as a strategy of information, research, planning, human resources training and water monitoring in each of the selected cities.

 ©2017, IAHR. Used with permission / ISSN 1562-6865 (Online) - ISSN 1063-7710 (Print)

As a first stage, PADHPOT selected the following eight small and medium cities: Ocotlán de Morelos, San Francisco Telixtlahuaca y Zimatlán de Álvarez, Oaxaca; Cuetzalan del Progreso, Izúcar de Matamoros, San Martín Texmelucan y Tehuitzingo, Puebla; and El Carmen Tequexquitla, Tlaxcala.

2 METHODOLOGY

Recognizing that hydraulic planning at a municipal scale is particularly complex, PADHPOT has developed a methodology that promotes the construction of hydraulic infrastructure and also institutional strengthening, informed participation of the population and mechanisms of transparency and accountability. Both elements are necessary to raise the level of water systems and to promote their sustainability. This methodology consists of the following four stages: 1) Municipal water system diagnosis, 2) Solution options proposal, 3) Implementation and 4) performance indicator evaluation.

2.1 Municipal water system diagnosis

The diagnosis allows for knowing how the water system is currently working in a structural and organizational way. It combines quantitative and qualitative methods in both infrastructure and social organization. The diagnosis contains the following actions:

Data sheets. It contains information about technical, commercial, operational, institutional and water quality issues. The information was obtained by asking the authorities of different levels about official documents and interviews to managers and water authorities.

Field research. The work of the Water and Sanitation area consisted of visiting, positioning with a GPS and lifting the main elements of hydraulic infrastructure, such as sources of supply, water lines and regulation and flow-control tanks. In addition, the operation of the chlorination systems was reviewed and the pressure in the water supply network was measured. On the other hand, the Water Observatory applied a survey in order to understand the perceptions, behaviors and attitudes towards water use. The survey allowed identifying the sociodemographic profile of the interviewees, the main source of supply, practices related on payment for the services, and attitudes towards water use. The data obtained by the survey were analyzed using the statistics software STATA and the results were confirmed with opinions collected directly from the inhabitants through participatory workshops.

Data validation. After field research, PADHPOT's team interviewed the crew that is in charge of water utilities management. In this stage, it was possible to know the way that water systems are working at technical, operative and managerial level. Information about operation hours of electromechanical equipment, service areas, customer service, inventories management, among other, was obtained by visiting water utilities for a few days.

Municipal water system diagnosis. Using the information obtained during the previous stages, PADHPOT's team proceeded to develop a diagnosis. The technical team constructed a representation of the water network using the software EPAnet 2.0 to analyze and evaluate their current conditions. The model showed data such as prediction of pressure parameters, load losses, flow-control tanks levels, demand behavior, velocity and flow in different nodes of the water network, etc. Figure 1 shows an example. The social involvement team, on the other hand, computed the results of the survey and produced specific reports on administrative policies and participatory workshops. These tools made it possible to create a diagnosis to improve the municipal drinking water system from an integral perspective.

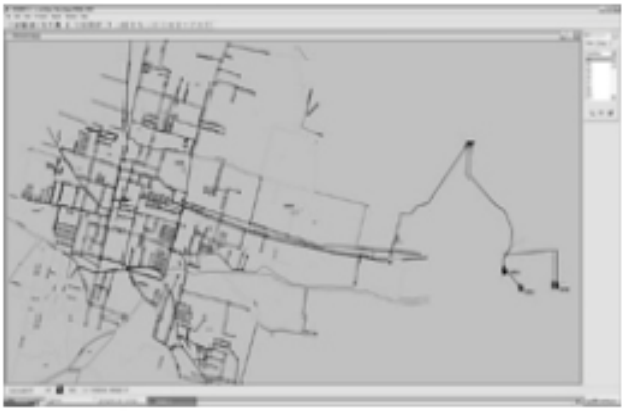

Figure 1. Representation of the water network using EPAnet 2.0.

2.2 Solution options proposal

The areas for improvement identified in the diagnosis, although they differ in each of the municipalities assisted, are usually related to the following factors: low physical efficiencies, caused by the high number of leaks in the water network due to their operation policies and the useful life of the materials that were used in the construction. Low supply of drinking water to the inhabitants that, in some cases, is not enough to assure

©2017, IAHR. Used with permission / ISSN 1562-6865 (Online) - ISSN 1063-7710 (Print)

the quantity that is suggested in the human right to water. Poor administrative system, characterized by the absence of transparent accounting systems, fees that do not reflect the cost of the service and minimum levels of payment. Lack of information and qualified personnel, both in the operation of the hydraulic system and in its administration. Inefficient water governance due to the absence of institutions that ensure citizen participation and accountability.

In general, the activities contained in the proposal of the Water and Sanitation area are directed to the sectorisation of the water network. The aim is to increase hydraulic efficiency and exercise greater operational control of parameters such as pressure, water quantity, leak detection, as well as water quality. The sectorisation allows starting a leaks control program based on a high-level analysis that applies water networks simulators and controlling measurements.

The sectorisation of water networks stablishes hydraulically isolated elements and is interconnected only by connecting lines or primary circuits. Thus, the design of each sector considers topography, location and hydraulic capacity of each region, flow-control tanks and pipelines. The sectors also contain the minimum cuts, connections, valve movements and piping installations. Therefore, the sectors have irregular forms and their dimensions depend on water availability and the existing infrastructure (González-Villarreal et al., 2015). In addition, the proposal considers replacement of electromechanical equipment, pipelines and water lines, as well as the rehabilitation of flow-control tanks and the expansion of the water network, as required in each municipality.

For its part, the Water Observatory work team proposed strategies aimed at institutional strengthening, introduction of transparency and accountability mechanisms, promotion of citizen participation and human resources training. According to the Dublin Statements, water development and management should be based on a participatory approach, involving all the stakeholders at all levels. Integrated Water Resources Management therefore means that water users can participate in public hearings for the purpose of discussing policies, programs, projects and legislation, but not only that, consumer representatives should be able to be part of the boards in charge of water management. For this mechanism to be effective, the planning system must be able to provide relevant information, for example, on what type and quality of water is available and where, who is using it and for what purpose (Gonzalez-Villarreal and Solanes, 1998).

Bearing in mind the Dublin Statements, Water Observatory has five lines of action: communication, research, planning and monitoring, training, and transparency and accountability. Among the proposed actions are the creation of a municipal water documentation center, which concentrates all the information related to municipal water resources, such as water network construction plans, laws and regulations, executive projects, activity reports, among others. The documentation center is publicly accessible through a web page and seeks, on one hand, to empower citizens with pertinent and truthful information about the state of their municipal water system, and on the other hand, to solve the lack of information that is a result of constant administration changes.

Since some municipalities do not have a formally constituted water utilities, PADHPOT works on the integration of Water Boards. Water Boards are institutions for municipal water decision-making that do not need to generate high costs resulting from creating a water utility with all its areas. In addition to the presence of municipal authorities, in Water Boards participate representatives of State Water Commissions and users, to reduce the possibility of the system's politicization. This institution also includes the presence of an external auditor, called Commissioner, whose duties include monitoring that resources administration is done in accordance with the law, programs and budgets approved by the Board, and conducting financial and technical audits (González-Villarreal y Arriaga, 2014).

The absence of water utilities is also associated to the lack of an accounting system that exclusively registers operations related to drinking water service. Water accounting is often mixed with income from other services provided by the municipality, such as property taxation or civil registration. To address this problem, Water Observatory suggested the introduction of a simplified accounting system whose operation allows the municipality to know the income and expenses made by the water system. This information is published monthly on the web page for public knowledge. The introduction of the simplified accounting system makes resources management more transparent and, in the medium and long term, improves people's confidence in raising collection levels and, if deemed appropriate, raising fees to make the system self-sustaining.

2.3 Implementation

Community and municipal authorities agreed the strategies proposed in the previous stage, which allows for greater legitimation and appropriation. According to their impacts, actions are prioritized in short, medium and long term. In addition, all the actions pursue the fulfillment of the objectives established by the State Water Commissions and the National Water Commission. This raises the possibility of using public resources, specifically, through the Program for Drinking Water, Sewerage and Sanitation in Urban Zones (APAZU, in Spanish). In those strategies that, by their very nature, cannot be financed by programs specifically designed for construction and rehabilitation of infrastructure, resources are requested from municipalities or private institutions.

 ©2017, IAHR. Used with permission / ISSN 1562-6865 (Online) - ISSN 1063-7710 (Print)

PADHPOT's work team, in coordination with municipal and state authorities, concentrates the proposals in executive projects that fulfill the requirements established by the rules of operation of the federal programs. Under the current legislation, the federal government, through the National Water Commission, can fund up to 100% of the executive projects, when the municipalities are registered in another federal program whose mission is to help the poorest localities in the country. This situation, however, is exceptional. Generally, federal funding reaches 80%, leaving the remaining 20% to the counterpart, which may be municipalities or some private entity.

Construction or rehabilitation of hydraulic infrastructure is developed by the state or by the municipality who, in turn, conduct a public tender among companies. In this stage, the work of PADHPOT is to provide technical advice and supervise that construction is in line with that written in the executive projects. At the same time, the Water Observatory added, to the previous action, the development of workshops on water culture to students in basic education, the organization of fairs to stimulate the participation of citizens in the management of their water resources, and training the system's operational staff to improve their practices.

2.4 Performance indicator evaluation

At the beginning of the formulation process, a set of indicators, both technical and social, were established to evaluate the program's performance. Indicators include drinking water and sanitation coverage, service continuity, physical and commercial efficiency, influence on electrical energy, macro and micro metering coverage, water tax collection levels, among others. During the diagnosis, a baseline was created in order to compare the information once the hydraulic infrastructure was put into operation. The results allow for making corrections to the implemented methodology and proposing new stages of intervention.

3 STUDY AREA

The municipality of Ocotlan de Morelos is located in the region of central valleys of Oaxaca, about 32 km from the capital. It has an area of 1,237 km2, which represents 0.13% of Oaxaca's territory. Its orography is generally flat, although some mountainous areas are present. According to the National Population Council, the municipality has a population of more than 20 thousand inhabitants, organized in 29 localities, and it is classified medium in the marginalization index. In terms of climate, it has a temperature range from 64 to 72 °F and a precipitation between 600 and 700 mm (INEGI, 2015). More than 40% of the population has some level of overcrowding, almost 30% have dirt floors and more than 35% of the inhabitants over 15 years did not finish primary education or are illiterate (INAFED, 2015). Despite its low degree of development, Ocotlan de Morelos is considered a regional development pole thanks to its population growth and its tourist attractions, which include the Santo Domingo de Guzman Temple, the home of the Painter's Rodolfo Morales and the traditional Friday market, one of the oldest and most popular markets in Oaxaca Valley.

Ocotlan crosses Ocotlan River, which joins Atoyac river basin, as well as Chilana, Santa Rosa, La Iglesia, Chichicapam and San Pablo rivers. The municipality also has some streams with intermittent flow during the rainy season; however, the main source of drinking water is groundwater. The coverage of drinking water and sewage is estimated at 90% and 60%, respectively. New settlements, as product of urban population growth and those who are located in high areas are not connected to water network (INEGI, 2015).

4 RESULTS: THE CASE OF OCOTLAN DE MORELOS, OAXACA

4.1 Municipal water system diagnosis

Ocotlan de Morelos has a supply system with infrastructure that surpasses 25 years. Among its main components were five deep wells, which contribute an average flow of 14.9 l / s to water network. Water is stored in two tanks with a combined capacity of 1,225 m3, which, in turn, distribute water to the municipal water network. The municipality is divided into 10 service areas, which are provided with drinking water for eight hours every ten days. This way of operating wears out the pipes and reduces their useful life up to ten times (Lambert, 2001). According to the measurements made in field, it was estimated that the 14.9 l / s injected into the system, only 5.0 are consumed, so about 9.9 are lost, representing a loss of 65%. A flow of 8.0 l / s is discharged into drainage system, considering the consumption of tank trucks and bottled water. Of this water, 6 l / s are treated in the treatment plant and 2 l / s of wastewater is directly discharge into the river.

The existing infrastructure presented the following conditions. Of the five wells, only three were fit to be rehabilitated, since the remainders had insufficient production. As for the existing tanks, one of them had 1,200 m3 capacity and showed infiltrations around the base and in the walls. Additionally, the earthenware showed cracks and detachments. Additionally, several illegal tapping were detected through water network. Finally, water network had a high rate of leakage.

Water quality parameters were analyzed by a certificate laboratory using samples collected on February 13 and 14, 2013 from the five wells in place in the municipality (well 1, well Olegario, well 3, well Tocuela and well Huaje). The water quality parameters measured were the ones that are established in the Mexican regulation (NOM-127-SSA1-1994). This standard establishes permissible limits of bacteriological characteristics, such as fecal coliforms and total coliforms; physical and sensory characteristics (color, smell,

©2017, IAHR. Used with permission / ISSN 1562-6865 (Online) - ISSN 1063-7710 (Print)

taste and cloudiness); chemical characteristics (which include 34 parameters, such as aluminum, arsenic, barium, etc.), as well as treatment methods which should be applied according to the pollutants encountered. Analysis indicated that all parameters accomplished permissible limits established in the Mexican regulations; hence, water quality was not a factor threatening people's health in the municipality.

The survey on knowledge, perceptions, behaviors and attitudes towards water, surveyed in 100 households during November 2014, showed that only 63.5% of the interviewees had access to water service. This data represents a difference of 26.5% respect to the coverage data established by INEGI. The population without water access was provided through tank trucks (25.9%) and private wells (7.7%). Those who have piped water receive it less than once a week. Due to the inefficiency of the service, 95% of households have storage infrastructure, such as water tanks, cisterns and other containers.

The survey also showed a very high consumption of bottled water. Eighty-eight percent of the interviewees said they bought bottled water, spending an average of 15 dollars a month. Adding the cost of buying bottled water to the payment for tank trucks, some families allocate up to 16% of their monthly income to supplement the inefficiency of the municipal water service. Regarding the above, people in the community expressed to payed a monthly water fee of 0.6 dollars. Although 81% of the sample expressed that they pay their water bill, the municipality reports a collection of only 30%.

4.2 Solution options proposal

In order to address the issues identified by the diagnosis, PADHPOT formulated three different proposals. The activities include responding technically to the needs and incorporating, as far as possible, the concerns expressed by the population through participatory workshops. After an analysis of the proposals by PADHPOT's work team and municipal and state authorities, it was decided to design a master plan that considered the following actions, which are infrastructure construction to protect three wells, in order to ensure their integrity, and installation of a new electromagnetic meter, data logger and manometer, which will enable to have a record of the water extracted and its pressures. It was also decided of the demolition of the current tank and the construction of a new one with similar dimensions; replacement of the network that goes from flow-control tanks to water network, with same trajectory but using steel instead of concrete.

Regarding water network, it was suggested regarding the construction of a main hydraulic circuit around the downtown to ensure adequate pressure throughout the water network. The hydraulic circuit does not contemplate connections of home takes, the reason why the only exits will be for the entrances of the sectors. In the case of the secondary water network, the pipes that showed more leaks were substituted. This action was complemented by the creation of five isolated hydraulic sectors. Valves that were placed in the main hydraulic sector control the flow that comes directly from the flow-control tank.

About institutional strengthening, mechanisms for transparency and accountability, and the promotion of citizen participation, the following activities were proposed and approved. Creation of a municipal water documentation center, the implementation of a communication campaign thorough publication of news in local and national newspapers and the creation of a web page and social networks management. The results of the survey of knowledge, perceptions, behaviors and attitudes towards water were published in indexed journals and popular science magazines.

Training and capacity building were also promoted through workshops on better practices related to water use in basic educations, training courses to the water utility staff, participatory workshops with inhabitants of the community and the establishment of a scholarship program to develop local professionals. Finally, the strategy to enhance transparency and accountability was based on the introduction of a simplified accounting system and the creation of the Water Board.

4.3 Implementation

The construction and replacement of hydraulic infrastructure in the municipality was quoted at about 1.7 million dollars. According to the rules for APAZU operation, for communities such as Ocotlan, the federal level funds up to 70% of the total investment, leaving the remaining 30% to the municipality. Having in mind that Ocotlan is a municipality with is classified medium in the marginalization index and does not have the amount of resources to execute a work of this magnitude; it was decided to divide the master plan into three stages.

The first stage began in the first quarter of 2015 and included the construction of the flow-control tank with a capacity of 1,200 m^3 and the replacement of the water network that goes from one of the wells to the flow-control tank. 1,503 meters of tubing was also changed with standard steel astm-a-ML 53 of 10 "in diameter. The infrastructure construction can be seen in Figure 2. This stage also included the expansion of the water network to some areas that did not have the service.

 ©2017, IAHR. Used with permission / ISSN 1562-6865 (Online) - ISSN 1063-7710 (Print)

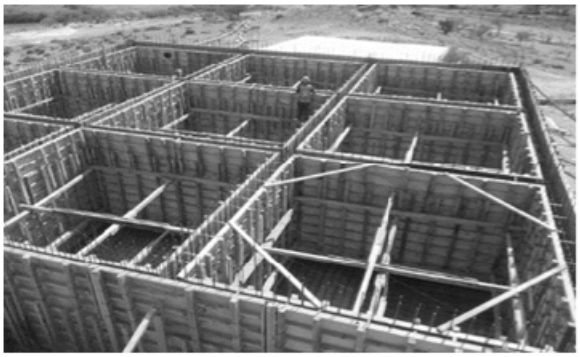

Figure 2. Construction of the flow-control tank.

The second stage of construction began in February 2016 and its goal was to create the main hydraulic circuit, constituted by 2,623.50 meters of hydraulic PVC pipe of 10" diameter and by 3,302.66 meters of 6" hydraulic PVC pipe. In addition, the water network that goes down from the flow-control tank to the supply network was constructed, with a length of 3,300 meters of 10” hydraulic PVC. These actions are still under way, but at the end of the third stage, the volume of water extracted is expected to increase by at least 30%. This construction will benefit more than 12 thousand inhabitants, in addition to avoiding losses in the network, having a better control in the disinfection process and maintaining a record of measurement of the extracted volume in the supply sources. A new water quality analysis is expected after the construction is ended.

For its part, the Water Observatory created the municipal water documentation center, available to all users through the web page. So far, the information center contains about 120 documents with relevant information to municipal water management, such as municipal and state legislation on the subject, drinking water network plans, copies of executive projects to be implemented, among others. To ensure access to information, a computer is available within the facilities of the municipality.

On January 22, 2015, in a public event, the Water Board was instituted. Among its attributions are to establish municipal water policy guidelines, authorize the program and annual, approve investment projects and propose the modification of water fees. The Water Board is integrated by a President, who is the municipal president, a Secretary, member of the municipal authorities, and three vowels, who came from the State Water Commission, home users and industrial users. According to the regulations approved for its establishment, the Board relies on a Commissioner, outside the municipal structure, who ensures that the administration of resources is done as approved by the Board and practices financial and technical audits. Figure 3.

Figure 3. Water Board establishment.

Since January 2016, the municipality has been working on the introduction of the simplified accounting system. After an analysis of the existing commercial systems and the practices already performed by the municipality administration, an instrument was designed to fit to the particular needs of the community. The accounting system allows for keeping a register by charging user fees, opening and closing cash per day, a daily revenue ratio, an inventory control and a count of expenses incurred by items such as payroll, electrical energy, purchase of equipment, etc. The system also generates monthly reports of income and expenses that are shared with the population through the web page. This is expected to generate greater confidence on the citizens to increase the rate of collection and, in medium term, raise awareness of the need to raise water fees in order to promote the self-sustainability of the drinking water system.

The above-mentioned actions have been complemented by the workshops to students of basic education, in order to promote a more responsible use of the resource. In addition, PADHOTs team held participatory workshops that, unlike at the diagnostic stage, are intended to inform the population about the progress of the program, promote their participation and try to reduce the discontent caused by the opening of roads for the

©2017, IAHR. Used with permission / ISSN 1562-6865 (Online) - ISSN 1063-7710 (Print)

construction and replacement of hydraulic infrastructure. A communication campaign was also implemented through social networks and digital and print newspapers.

5 CONCLUSIONS

In recent years, all three-government levels have recognized the need to improve the performance of drinking water and sanitation systems at the national level. To this end, subsidy programs have been implemented, such as the Program for the Improvement of Efficiency in the Drinking Water and Sanitation Sector (PROME) or the Program for Drinking Water, Sewerage and Sanitation in Urban Zones (APAZU). Despite the growing political will to strengthen the subsector, the proposed models continue to offer solutions without questioning the predominant institutional framework (IMCO, 2014). Although there is a consensus on the weakness of a large number of municipalities to provide efficient drinking water and sanitation services, little has been debated on the need to amend article 115 of the Constitution to ensure a broader and more coordinated participation of Federal and state authorities.

Even under the current institutional scheme, other difficulties persist to promote municipal water development. In particular, there is no communication in federal programs to support infrastructure construction and training of local human resources and to promote social involvement. By working in isolation, these programs give rise to new problems that escalate those purely related to water. For example, transferring resources for infrastructure construction directly to the municipality without ensuring, on the one hand, that what was projected during the design stage is actually executed, and, on the other, that there are mechanisms of transparency and accountability, generates social polarization, a discretionary use of money and water infrastructure, and, in some cases, conflicts over the control of municipal drinking water and sanitation systems.

According to the experience developed by PADHPOT, the merely construction of hydraulic infrastructure is not directly related to a greater efficiency of the municipal drinking water and sanitation system. Even less when there are no monitoring schemes for the results and the population to which it is intended to benefit does not participate in the decisions on the water resources management. In this regard, it is necessary to move from traditional participation schemes by invitation to a true institutional strengthening, in which the regulation contemplates the presence of citizens in the decision-making process.

REFERENCES

IMCO (2014). *Guía Para la Creación de Organismos Metropolitanos de Agua Potable y Saneamiento en México*. IMCO-Embajada Británica en Mexico, Mexico, 154.

INAFED (2015), *Sistema Nacional de Información Municipal*, SEGOB, on line http://www.snim.rami.gob.mx/

INEGI (2015), *Prontuario de Información Geográfica municipal de los Estados Unidos Mexicanos. Ocotlán de Morelos, Oaxaca*, INEGI, on line http://www3.inegi.org.mx/sistemas/mexicocifras/datos-geograficos/20/20068.pdf

Lambert, A. (2001), Water Losses Management and Techniques, *Water Science and Technology*: Water *Supply*, 2, 1-20.

González-Villarreal, F. & y Arriaga, J. (2014). Sistemas de Agua Potable y Saneamiento en Comunidades Medias de México. *Revista Ingeniería Civil*, 542, 10-14.

González-Villarreal, F., Lartigue, C. & Rocha, J. (2015). Sectorización y Control de Presiones en Ciudad Universitaria. *Revista Ingeniería Mexicana*, 6, 29-31.

González-Villarreal, F. & y Solanes, M. (1998). *Los Principios de Dublín Reflejados en una Evaluación Comparativa de Ordenamientos Institucionales y Legales Para una Gestión Integrada del Agua*, Asociación Mundial del Agua, Estocolmo.

González-Villarreal, F., Val, R., Domínguez, M., Lartigue, C. & Arriaga, J. (2013). Un Modelo de Gestión Integral. *Ciudades*, 99, 30-38.

PADHPOT (2011). *Formulación de un Programa de Apoyo al Desarrollo Hidráulico de Los Estados de Oaxaca, Puebla y Tlaxcala, México*, Red del Agua UNAM-Instituto de Ingeniería, Mexico, 52.

PADHPOT (2012). *Diagnóstico: Organismos operadores, Oaxaca, Ocotlán de Morelos, México*, Red del Agua UNAM-Instituto de Ingeniería, Mexico, 120.

PADHPOT (2015). *Encuesta Sobre Conocimientos, Percepciones, Conductas y Actitudes Hacia el Agua, Ocotlán de Morelos, México*, Red del Agua UNAM-Instituto de Ingeniería, Mexico, 36.

 ©2017, IAHR. Used with permission / ISSN 1562-6865 (Online) - ISSN 1063-7710 (Print)

A FUNDAMENTAL STUDY FOR IMPACT ASSESSMENT OF CLIMATE CHANGE ON OPERATION OF RESERVOIR SYSTEMS FOR WATER SUPPLY IN JAPAN

SHUNSUKE SUZUKI[(1)], DAISUKE NOHARA[(2)], TOMOHARU HORI[(3)] & YOSHINOBU SATO[(4)]

[(1)] Graduate School of Engineering, Kyoto University, Japan
suzuki.shunsuke.25e@st.kyoto-u.ac.jp
[(2,3)] Disaster Prevention Research Institute, Kyoto University, Japan,
[(4)] Faculty of Agriculture, Ehime University, Japan

ABSTRACT

Impact assessment of climate change on operation of reservoir systems and river discharges in Japanese river basins have been conducted as a fundamental study in order to develop a method to operate reservoirs more effectively under the expected future climate condition. Current climate data (1979-2003) and future climate data (2075-2099) projected by MRI-AGCM3.2S, a high resolution AGCM developed by Meteorological Research Institute, are used as meteorological input. River discharges in both climates are respectively estimated from climate data by use of Hydro-BEAM (Hydrological River Basin Environment Assessment Model), a cell concentrate type hydrological model, integrating operation of reservoirs for water supply and water intake in the target river basins. The assessment is conducted in the Yoshino River basin where droughts often occur, and the Mogami River basin where snow melting water contributes to river discharge significantly. The results suggested that the potential changes in river discharge that may increase a risk of drought in the future. The assessment also demonstrates that the model considering anthropogenic river flow regulation such as reservoir operation or water intake can provide a different result of impact assessment compared to those without considering anthropogenic regulation, indicating importance of consideration of reservoir operation in the assessment of climate change impacts.

Keywords: Climate change; water supply; reservoir operation; Hydro-BEAM; future river discharge.

1 INTRODUCTION

Water resource management systems in river basins may be threatened by changes of hydrological systems associated with climate changes. The concern is that, severe flood and drought events may occur more often in the future due to the changing climate. In order to assess changes in risks of water-related disasters such as floods or droughts, river discharge under the future climate condition need to be assessed quantitatively.

From this point of view, many researches about impact assessment of climate change on river discharges have been conducted in recent years. Sato et al. (2009) predicted the impact assessment of disaster environment in the Yoshino River basin in Japan due to climate change using a super-high-resolution atmospheric general circulation model (AGCM). Tachikawa et al. (2011) constructed a cell concentrate type hydrological model targeting the Japanese islands. With that model, runoff analysis was investigated in all major river basins in Japan, using the outputs of a super high resolution atmospheric model (MRI-AGCM20km). Furthermore, several researches were conducted with consideration of reservoir operation for controlling river discharges (Yoshimura et al., 2015).

As river discharge is regulated by reservoirs in many river basins, it is important to consider the effect of reservoir operation when future river discharge is evaluated. It is also considered important to analyze the capability of reservoirs to mitigate the impacts of climate change by changing their operation in order to develop a robust operation method of water resources systems as a measure of adaptation to changing climate. Sayama et al. (2008) investigated the flood impact on river discharges and reservoir by integrating operation of reservoirs with the model in the target river basins. However, only a few researches consider impact assessment of climate change on water supply operation of reservoir systems in Japan. Consideration of anthropogenic river flow regulation such as reservoir operation or water intake in the assessment on impacts of climate change can provide a different result compared to those without considering anthropogenic regulation.

Considering the issues described above, impact assessment of climate change on operation of reservoir systems and river discharges in Japanese river basins was conducted as a fundamental study considering reservoir operation for water supply in order to develop a method to operate reservoirs more effectively under the expected future climate condition. The assessment was conducted for two river basins with different hydrological characteristics, namely the Yoshino River basin where droughts often occur, and the Mogami River basin where snow melting water contributes to river discharge significantly. Current climate data (1979-2003) and future climate data (2075-2099) projected by MRI-AGCM3.2S, a high resolution AGCM developed

©2017, IAHR. Used with permission / ISSN 1562-6865 (Online) - ISSN 1063-7710 (Print)

by Meteorological Research Institute (MRI), were used as meteorological input for the assessment. River discharges both in the current and future climates were respectively estimated from climate data by use of Hydro-BEAM (Hydrological River Basin Environment Assessment Model), a cell concentrate type hydrological model, integrating operation of reservoirs and water intake in the target river basins.

2 METHODOLOGY

2.1 Super-high-resolution atmospheric general circulation model

In this study, a high resolution AGCM developed by Meteorological Research Institute (MRI-AGCM3.2S) was used for the climate model. This model was developed as an improvement of MRI-AGCM3.1S. The difference of the two models are described in Mizuta et al. (2012). The model has a horizontal resolution of triangular truncation 959(TL959), and the transform grid uses 1920×960 grid cells, corresponding to approximately a 20 km grid interval with 64 vertical layers. Two climate projections by the model are available: current climate data (1979-2003) and future climate data (2075-2099), both of which were used as meteorological input to the assessment model developed in this study. Future climate dataset were simulated under the RCP8.5 scenario of the Special Report on Emission Scenarios in the Fifth Assessment Report of the Intergovernmental Panel on Climate Change.

2.2 Hydrological model

The Hydrological River Basin Environment Assessment Model (Hydro-BEAM; Kojiri, 2006) was used for the hydrological simulation. Hydro-BEAM is a cell concentrate type distributed hydrological model that divides each grid cell into two pairs of rectangular hill slopes and one river channel in the middle. The spatial resolution is 1 km.

Four land types are used to determine land surface roughness according to Manning's equation (forest: 0.7, grassland: 0.3, urban: 0.03, water: 0.04). River channels run through the lowest part of each grid mesh and flow to the adjacent mesh with the steepest slope. If a depression sink occurs before the river mouth is reached, the elevation of the mesh is modified to allow flown down to the nearest lowest mesh among four directions; north, south, east and west. All input data for Hydro-BEAM such as precipitation were interpolated to 1 km grid mesh data by using inverse distance weighting (IDW) method (Sato et al., 2013).

Kinematic wave model is used to calculate surface flow and subsurface flow from the upper soil (layer A). Also, by integrating Manning's formula for surface flow and Darcy's formula for subsurface flow, the equation of kinematic wave model is described as:

$$\frac{\partial h}{\partial t}+\frac{\partial q}{\partial x}=fr(x,t) \quad [1]$$

$$q=\begin{cases}\alpha(h-d)^{\frac{5}{3}}+ah \\ ah\end{cases},\quad when\begin{cases}h\geq d \\ h<d\end{cases} \quad [2]$$

$$\alpha=\frac{\sqrt{\sin\theta}}{n},\quad a=K\frac{\sin\theta}{\lambda} \quad [3]$$

where h is water depth (m), q is discharge per unit width (m^2/s), r is input effective rainfall intensity (mm/s), d is the effective soil depth of the layer A (m), sinθ is hill slope angle, n is Manning's friction coefficient, K is saturated hydraulic conductivity (=0.0001m/s), α is the constant of Manning's equation and a is the constant of Darcy's equation. A multi-layers linear storage function model to calculate base flow from the lower soil (layers B and C) which is described as:

$$\frac{dS}{dt}=I-O \quad [4]$$

$$O=kS \quad [5]$$

where S is water storage (m), I is inflow (m/s), O is outflow (m/s), and k is the runoff coefficient (1/s). In case the maximum water storage in each layer is larger than annual precipitation amount, no return flow will occur to the upper layer.

 ©2017, IAHR. Used with permission / ISSN 1562-6865 (Online) - ISSN 1063-7710 (Print)

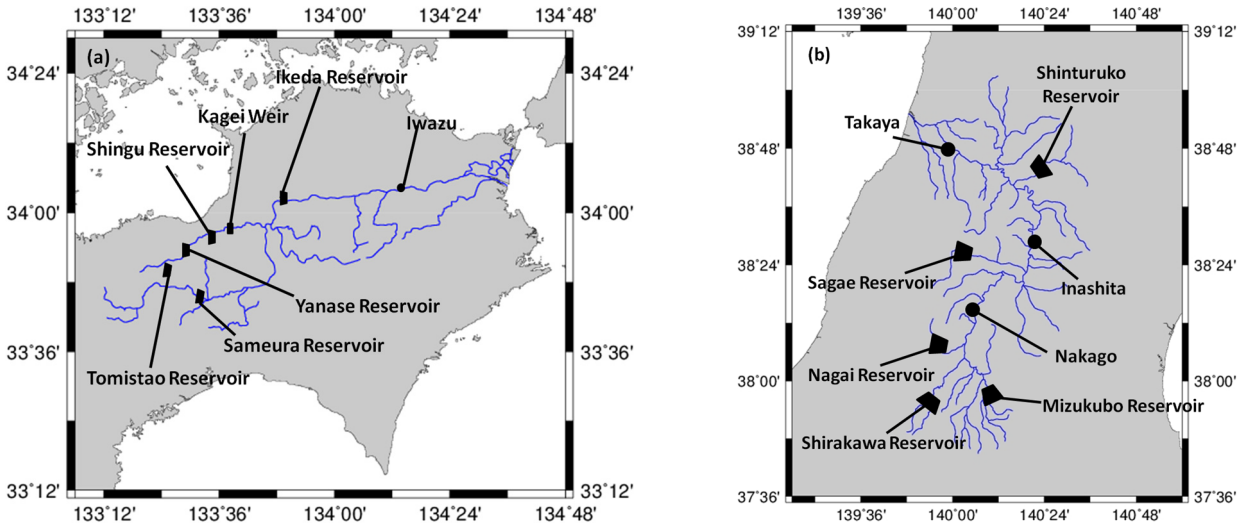

Figure 1. Channel network of the Target Rivers: (a) the Yoshino River, and (b) the Mogami River.

2.3 Study area

The assessment on impacts of climate change on river discharge and reservoir operation for water supply was conducted in the Yoshino River and the Mogami River basins in this study. The location of the two river basins are shown in Figures 1(a) and 1(b). The Yoshino River basin is a river basin with the total area of 3,750 km^2, located in Shikoku Island in the southwest part of Japan. The reference point for planning and management of the Yoshino River is located in Iwazu, where the river has the drainage area of 2,740 km^2. As this river basin has suffered from floods or droughts frequently, assessing impacts of climate change is significantly important to analyze risks of severe water-related disasters which may occur more frequently under the future climate. On the other hand, the Mogami River basin is located in Tohoku region, the northern of the main island of Japan. Total area of the Mogami River basin is 7040 km^2, and the reference point is located in Takaya with the drainage area of 6497km^2. This region is a snow dominated region, and snow-melting water is an important source of river water in this region. Under the present climate, the snowfall season is mainly from November to February, and snow-melting is observed from March to May. However, due to higher temperature expected in future climate, it is considered that not only the total amount of rainfall but also the amount of snowfall will decrease which shifts the snowmelt season earlier. This will impact traditional water utilization especially in agriculture, as most farmers start planting rice taking a lot of river water increased in the snow-melting season. When the snow-melting season shifts earlier, total water storage amount will decrease for the current irrigation season, which might lead to the lack of water. Therefore, it is concerned that the seasonal operation of reservoirs currently applied may not be suitable under the future climate.

2.4 Reservoir operation model

Reservoir operation for water supply was modeled in order to assess impacts of climate change considering operation of reservoirs. Roles and coordination in operation of reservoirs generally differs among basins. An operation model for reservoir systems for water supply was therefore developed for each target river basin.

2.4.1 Reservoir operation model for the Yoshino River basin

There are five major multi-purpose reservoirs in the Yoshino River basin: Sameura Reservoir and Ikeda Reservoir, both of which are located in the mainstream of the Yoshino River, and Tomisato, Yanase and Shingu reservoirs that are located in the Dozan River, a tributary of the Yoshino River. Basically, operation of reservoirs for water supply is conducted separately between the Dozan River basin and the other sub basins in the Yoshino River basin. In Dozan River basin, river water is mostly trapped and stored by the three reservoirs to divert water across the mountains to coastal areas along the Seto Inland Sea in Ehime Prefecture, a region outside of the Yoshino River basin. Thus, only a limited amount of water joins the Yoshino River from the Dozan River. Normally, only a small amount of water is released from the Kagei Weir, which locates in the downstream of the three reservoirs in the Dozan River, in order to keep river flow of 0.17 m^3/s in the downstream of the weir for the environmental purpose.

Considering the actual river water management practices described above, operation of reservoirs in the Dozan River was modelled as follows for simplification in this study. Firstly, the three major multi-purpose reservoirs which locate in series in the Dozan River were assumed as one integrated reservoir at Shingu, and were assumed to be operated to release water for the environmental flow. In this modelling, water intake for diversion to the coastal area in Ehime Prefecture and water release of 0.17 m^3/s from the integrated reservoir

©2017, IAHR. Used with permission / ISSN 1562-6865 (Online) - ISSN 1063-7710 (Print)

at Shingu (called as Shingu Reservoir hereafter) were subtracted from the total storage of the three reservoirs considering their inflow. Water release of 0.17 m^3/s from the Shingu Reservoir joins to the Yoshino River through the Kagei Weir in this modelling. When the total storage exceeds the storage capacity for water utilization in the three reservoirs, the exceeding amount were released from the Shingu Reservoir in adittion to the release for environmental flow, which also joins to the Yoshino River. Water of the Dozan River flows into the Yoshino River just upstream the Ikeda Reservoir, as it is in actual.

On the other hand, Sameura Reservoir has a significant role in water supply in the other sub basins in the Yoshino River while Ikeda Reservoir does not have a large storage capacity and is operated just to increase river water level so as to make water intake in the upstream of the reservoir easy. The assessed point of water flow amount in the Yoshino River basin is located just upstream of the Ikeda Reservoir, where much water is taken for canals including the Kagawa Canal and the Hokugan Canal. Sameura Reservoir is operated to release water so as to meet water demand at the assessed point (Ikeda Reservoir) considering runoff to the Yoshino River from sub basins in the downstream of the Sameura Reservoir. Considering these operation practices, operation of reservoirs along the main stream of the Yoshino River was modelled as follows. At first, the target water release volume from the Sameura Reservoir is determined to meet water demand at the Ikeda Reservoir together with water flow from the Dozan River (0.17 m^3/s basically) and runoff water flowing into the Yoshino River between the Sameura and Ikeda reservoirs. Inflow of the Ikeda Reservoir is calculated by the sum of releases from the Sameura and Shingu reservoirs as well as runoff water from the other sub basins in the upstream of the Ikeda Reservoir. The model did not consider storage capacity in Ikeda reservoir, and flow regulation by the Ikeda Reservoir is neglected in the model. Release from the Ikeda Reservoir was calculated by subtracting water intake from the Ikeda Reservoir for two major canals, the Kagawa and the Hokugan canals, from inflow of the Ikeda Reservoir. River discharge at Iwazu, which is the hydrological station of the Yoshino River basin for flood management, was calculated by the sum of the amount of water released from the Ikeda Reservoir release and runoff between Ikeda and Iwazu. Because the Kagawa Canal takes water to a region outside of the Yoshino River basin, the amount of water taken for the Kagawa Canal is just subtracted from the water in the Yoshino River in this study. Water taken for the Hokugan Canal, which is an irrigation canal, was also subtracted from water in the Yoshino River in this study, as it mostly joins into the Yoshino River again in the downstream of Iwazu and does not affect the amount of river flow at Iwazu, which is the most downstream point considered in this study for the Yoshino River. Those operations were calculated on daily basis.

Equations to calculate water release from the reservoirs and river flow in the Yoshino River basin are summarized as follows. Inflow of the Ikeda Reservoir is firstly calculated as:

$$Q_I(i) = R_S(i) + R_G(i) + O_A(i) \quad [6]$$

where $Q_I(i)$ is inflow of the Ikeda Reservoir (m^3/s) at daily time step i, $R_s(i)$ is release from the Sameura Reservoir (m^3/s), $R_G(i)$ is release from Shingu Reservoir(m^3/s) and $O_A(i)$ is the runoff between the Ikeda Reservoir and the Sameura and Shingu reservoirs (m^3/s), respectively. The release from the Shingu Reservoir $R_G(i)$ can be calculated by considering operation of reservoirs and water intake in the Dozan River which is described as below. First, the three major reservoirs in the Dozan River were modeled as one integrated reservoir, and release amount from the Shingu Reservoir, which locates in the most downstream in the series of the three reservoirs, was calculated considering continuous formula of the reservoir by the following equations:

$$S_G(i+1) = S_G(i) + \left[Q_G(i) - R_G(i) - W_G(i)\right] * T_S \quad [7]$$

$$R_G(i) = \max\left\{S_{G,\mathrm{sur}}(i)/T_S,\ \min\left[D_G(i),\ S_{G,\mathrm{avl}}(i)/T_S\right]\right\} \quad [8]$$

$$S_{G,\mathrm{sur}}(i) = S_G(i) + Q_G(i)\cdot T_S - S_{G,\max}(i) \quad [9]$$

$$S_{G,\mathrm{avl}}(i) = S_G(i) + Q_G(i)\cdot T_S \quad [10]$$

where $S_G(i)$ is the total storage of Tomisato, Yanase and Shingu reservoirs (m^3/s), $Q_G(i)$ is total inflow at Shingu Reservoir (m^3/s), $W_G(i)$ is water intake amount for outside basin from three reservoirs, which was estimated by historical data (m^3/s), T_s is number of seconds in one time step (86,400 seconds), $D_G(i)$ is target release volume from the Shingu Reservoir (0.17m^3/s in this study), and $S_{G,\max}(i)$ is maximum storage amount in three reservoirs (m^3/s), respectively. Release from the Sameura Reservoir $R_s(i)$ was also calculated in a similar fashion. Water storage volume and release rate of the Sameura Reservoir were calculated as:

$$S_S(i+1) = S_S(i) + \left[Q_S(i) - R_S(i)\right] * T_S \quad [11]$$

 ©2017, IAHR. Used with permission / ISSN 1562-6865 (Online) - ISSN 1063-7710 (Print)

$$R_S(i) = \max\left\{ S_{S,\mathrm{sur}}(i)/T_S \,,\, \min\left[D_S(i),\ S_{S,\mathrm{avl}}(i)/T_S \right] \right\} \quad [12]$$

$$S_{S,\mathrm{sur}}(i) = S_S(i) + Q_S(i)\cdot T_S - S_{S,\max}(i) \quad [13]$$

$$S_{S,\mathrm{avl}}(i) = S_S(i) + Q_S(i)\cdot T_S \quad [14]$$

$$D_S(i) = Q_i^* - R_G(i) - O_A(i) \quad [15]$$

where $S_S(i)$ is storage volume of the Sameura Reservoir (m^3/s), $Q_S(i)$ is water inflow at the Sameura Reservoir (m^3/s), $D_S(i)$ is target release rate from the Sameura Reservoir (m^3/s), $S_{S,\max}(i)$ is maximum storage amount in the Sameura Reservoir (m^3/s), and $Q_I^*(i)$ is the target river discharge at Ikeda reservoir point, respectively. By using $Q_I(i)$ calculated by Eq. [3], release from the Ikeda Reservoir was calculated as:

$$R_I(i) = Q_I(i) - W_I(i) \quad [16]$$

where $R_I(i)$ is release rate from the Ikeda Reservoir (m^3/s), and $W_I(i)$ is water intake rate for the Kagawa and Hokugan canals (m^3/s), which was estimated from historical data, respectively. River discharge at Iwazu was calculated as:

$$Q_W(i) = R_I(i) + O_B(i) \quad [17]$$

where $Q_W(i)$ is river discharge at Iwazu point (m^3/s) and $O_B(i)$ is the sum of residual runoff (m^3/s) between the Ikeda Reservoir and Iwazu, respectively. Runoff and river flows which are not affected by reservoir operation were calculated by Hydro-BEAM for each point.

2.4.2 Mogami River basin reservoir operation model

In Mogami River basin, there are three major multi-purpose reservoirs: Sagae Reservoir, Nagai Reservoir and Shirakawa Reservoir, and two major irrigational reservoirs: Mizukubo Reservoir and Shitsuruko Reservoir. Nagai Reservoir was constructed in 2009, thus the operation of the reservoirs was modeled without considering the operation of Nagai Reservoir. In addition, there are three reference points in Mogami River basin and each hydrological station has a water demand to satisfy: Nakago with $8m^3/s$, Inashita with $27m^3/s$ and Takaya with $57m^3/s$.

Since irrigational reservoirs are mainly operated for agricultural water, these reservoirs are conducted independent from the whole basin. Therefore, the operation for irrigational reservoirs were modeled by setting target water release volume based on regulations of water supply and irrigational water.

On the other hand, Sagae Reservoir and Shirakawa Reservoir have a significant role for water supply in this river basin in order to satisfy the water demand at each hydrological stations. Shirakawa Reservoir is operated to release water so as to meet water demand at the hydrological station (Nakago) considering the release water from Mizukubo Reservoir and runoff to Mogami River from sub basins in the downstream of the Shirakawa Reservoir. Sagae Reservoir is operated in the same way as Shirakawa Reservoir. This reservoir is operated to satisfy water demand at Inashita and Takaya considering the release water from Shintsuruko Reservoir and runoff to Mogami River from sub basins in the downstream of the Sagae Reservoir. Considering these operation practices, operation of reservoirs along the main stream of the Mogami River was modelled as follows. At first, the target water release volume from the Shirakawa Reservoir is determined based on water demand at Nakago together with water release from Mizukubo Reservoir and the runoff water flowing into the Mogami River between the Shirakawa and Nakago. River discharge of the Nakago is calculated by the sum of releases from the Shirakawa and Mizukubo reservoirs as well as runoff water from the other sub basins in the upstream of the Nakago. Next, the target water release volume from Sagae Reservoir is determined to meet the water demand at the Inashita as well as Takaya, together with water release from Shitsuruko Reservoir and the runoff water flowing into Mogami River from downstream of Sagae Reservoir. River discharge at Inashita is calculated by the sum of release from Sagae Reservoir and river discharge at the Nakago. In addition, river discharge at the Takaya is calculate by the sum of release from Shintsuruko Reservoir and river discharge at Inashita as well as runoff water from the other sub basins in the upstream of the Takaya, which is the most downstream point considered in this study for the Mogami River. Equations to calculate water release from the reservoirs and river flow in the Mogami River basin are summarized as follows. Water flow at the Nakago is firstly calculated as:

$$Q_N(i) = R_M(i) + R_{Sh}(i) + O_1(i) \quad [18]$$

where $Q_N(i)$ is the river discharge at the Nakago (m^3/s) at daily time step i, $R_M(i)$ is release from the Mizukubo Reservoir (m^3/s), $R_{Sh}(i)$ is release from the Shirakawa Reservoir (m^3/s) and $O_1(i)$ the runoff between the Nakago and the Shirakawa and Mizukubo Reservoirs (m^3/s), respectively. The release from Mizukubo

©2017, IAHR. Used with permission / ISSN 1562-6865 (Online) - ISSN 1063-7710 (Print)

Reservoir $R_M(i)$ can be calculated by considering the operation of reservoir for irrigation, which was calculated considering continuous formula of the reservoir by the following equations:

$$S_M(i+1) = S_M(i) + \left[Q_M(i) - R_M(i)\right] * T_S \quad [19]$$

$$R_M(i) = \max\left\{S_{M,\mathrm{sur}}(i)/T_S,\ \min\left[D_M(i),\ S_{M,\mathrm{avl}}(i)/T_S\right]\right\} \quad [20]$$

$$S_{M,\mathrm{sur}}(i) = S_M(i) + Q_M(i)\cdot T_S - S_{M,\max}(i) \quad [21]$$

$$S_{M,\mathrm{avl}}(i) = S_M(i) + Q_M(i)\cdot T_S \quad [22]$$

where $S_M(i)$ is the total storage of Mizukubo Reservoir (m^3/s). $Q_M(i)$ is total inflow at Mizukubo Reservoir (m^3/s) $D_M(i)$ is target water release from Mizukubo Reservoir. $S_{M,\mathrm{sur}}(i)$ is surplus water amount at Mizukubo Reservoir (m^3/s). $S_{M,\max}(i)$ is maximum water storage amount in Mizukubo Reservoir (m^3/s). $S_{M,\mathrm{avl}}(i)$ is available storage amount in Mizukubo Reservoir (m^3/s), respectively. Release from the Shirakwa Reservoir $R_{sh}(i)$ was also calculated in a similar fashion. Water storage volume and release rate of the Shirakawa Reservoir were calculated as:

$$S_{Sh}(i+1) = S_{Sh}(i) + \left[Q_{Sh}(i) - R_{Sh}(i)\right] * T_S \quad [23]$$

$$R_{Sh}(i) = \max\left\{S_{Sh,\mathrm{sur}}(i)/T_S,\ \min\left[D_{Sh}(i),\ S_{Sh,\mathrm{avl}}(i)/T_S\right]\right\} \quad [24]$$

$$S_{Sh,\mathrm{sur}}(i) = S_{Sh}(i) + Q_{Sh}(i)\cdot T_S - S_{Sh,\max}(i) \quad [25]$$

$$S_{Sh,\mathrm{avl}}(i) = S_{Sh}(i) + Q_{Sh}(i)\cdot T_S \quad [26]$$

where $S_{Sh}(i)$ is the total storage of Shirakawa Reservoir (m^3/s). $Q_{Sh}(i)$ is total inflow at Shirakawa Reservoir (m^3/s), $D_{Sh}(i)$ is target water release volume from Shirakawa Reservoir. $S_{Sh,\mathrm{sur}}(i)$ is surplus water amount at Shirakawa Reservoir (m^3/s). $S_{Sh,\max}(i)$ is maximum storage amount in Shirakawa Reservoir (m^3/s) and $S_{Sh,\mathrm{avl}}(i)$ is available storage amount in Shirakawa Reservoir (m^3/s), respectively. By using $Q_N(i)$ calculated by Eq. [10], river discharge at Inashita was calculated as:

$$Q_{In}(i) = Q_N(i) + R_{Sa}(i) + O_2(i) \quad [27]$$

where $Q_{In}(i)$ is the river discharge at Inashita (m^3/s), $R_{Sa}(i)$ is release from Sagae Reservoir (m^3/s) and $O_2(i)$ is runoff water release between Nakago to Inashita (m^3/s), respectively. Sagae reservoir's storage volume and release volume are then calculated as:

$$S_{Sa}(i+1) = S_{Sa}(i) + \left[Q_{Sa}(i) - R_{Sa}(i)\right] * T_S \quad [28]$$

$$R_{Sa}(i) = \max\left\{S_{Sa,\mathrm{sur}}(i)/T_S,\ \min\left[D_{Sa}(i),\ S_{Sa,\mathrm{avl}}(i)/T_S\right]\right\} \quad [29]$$

$$S_{Sa,\mathrm{sur}}(i) = S_{Sa}(i) + Q_{Sa}(i)\cdot T_S - S_{Sa,\max}(i) \quad [30]$$

$$S_{Sa,\mathrm{avl}}(i) = S_{Sa}(i) + Q_{Sa}(i)\cdot T_S \quad [31]$$

where $S_{Sa}(i)$ is the total storage of Sagae Reservoir (m^3/s). $Q_{Sa}(i)$ is total inflow at Sagae Reservoir (m^3/s), $D_{Sa}(i)$ is target water release from Sagae Reservoir. $S_{Sa,\mathrm{sur}}(i)$ is surplus water amount at Sagae Reservoir (m^3/s). $S_{Sa,\max}(i)$ is maximum water storage amount in Sagae Reservoir (m^3/s) and $S_{Sa,\mathrm{avl}}(i)$ is available storage amount in Sagae Reservoir (m^3/s), respectively. Release from Shintsuruko Reservoir was also calculated in a similar fashion. Water storage volume and release rate of the Shintsuruko Reservoir were calculated as:

$$S_{St}(i+1) = S_{St}(i) + \left[Q_{St}(i) - R_{St}(i)\right] * T_S \quad [32]$$

$$R_{St}(i) = \max\left\{S_{St,\mathrm{sur}}(i)/T_S,\ \min\left[D_{St}(i),\ S_{St,\mathrm{avl}}(i)/T_S\right]\right\} \quad [33]$$

$$S_{St,\mathrm{sur}}(i) = S_{St}(i) + Q_{St}(i)\cdot T_S - S_{St,\max}(i) \quad [34]$$

$$S_{St,\mathrm{avl}}(i) = S_{St}(i) + Q_{St}(i)\cdot T_S \quad [35]$$

where $S_{St}(i)$ is the total storage of Shinturuko Reservoir (m^3/s). $Q_{St}(i)$ is total inflow at Shinturuko Reservoir (m^3/s), $D_{St}(i)$ is target water release from Shinturuko Reservoir. $S_{St,\mathrm{sur}}(i)$ is surplus water amount at Shinturuko

 ©2017, IAHR. Used with permission / ISSN 1562-6865 (Online) - ISSN 1063-7710 (Print)

Reservoir (m^3/s). $S_{St,max}(i)$ is maximum storage amount in Shinturuko Reservoir (m^3/s). $S_{St,avl}(i)$ is available storage amount in Shinturuko Reservoir (m^3/s). Observed amounts and target volume for Mizukubo and Shinturuko Reservoir were based on the "Yamagata prefecture agricultural irrigation and drainage facilities maintenance regulation" and "Water Information System of Ministry of Land, Infrastructure, Transport and Tourism". Consideing the release calculated at Eq. [15] river discharge at Takaya was calculated as:

$$Q_T(i) = Q_{In}(i) + R_{St}(i) + O_3(i) \quad [36]$$

where $Q_T(i)$ is the river discharge at Takaya (m^3/s), $R_{St}(i)$ is release volume from Shinturuko reservoir (m^3/s) and $O_3(i)$ residual runoff release between Inashita to Takaya (m^3/s), respectively. Runoff and river flows which are not affected by reservoir operation were calculated by Hydro-BEAM for each point.

3 RESULTS AND DISCUSSIONS

3.1 Reproducibility of current climate by AGCM

For meteorological inputs of Hydro-BEAM in this study, hourly precipitation and daily evapotranspiration were derived from MRI-AGCM3.2S. Amounts of evapotranspiration were estimated by AGCM and SVAT model in the similar way used in the existing study (Sato et al., 2009). Figure 2 shows the comparison of basin average precipitation in seasonal variation of the Yoshino River basin and the Mogami River basin between observation and estimation by AGCM. In the Yoshino River basin, values simulated by AGCM were underestimated mainly in summer season while AGCM overestimated precipitation in the other seasons. In the Mogami River basin, values calculated by AGCM were underestimated mainly in winter season. As river discharges in Yoshino River basin and Mogami River basin calculated from precipitation estimated by AGCM using Hydro-BEAM, bias was seen in comparison to the observed river discharge amounts. Such trend of the bias was similar with that detected in precipitation. Therefore, bias correction of precipitation values calculated by AGCM was conducted.

3.2 Bias correction of AGCM precipitation output

Bias correction of AGCM precipitation output was conducted based on the method employed in Tanaka et al. (2008). Considering that the trend of bias differs by seasons, bias correction ratio was set for each month from January to December. Bias correction ratio for each month was respectively calculated by dividing the sum of observed precipitation in each month for 25 years from 1979 to 2003 by that of AGCM precipitation outputs for for 25 years of experiment under the current climate condition. AGCM precipitation outputs for each month were then modified by multiplying the estimated ratio as bias correction respectively. The calculation formula was described the following equation:

$$x'(n,m,i) = \alpha(m) \cdot x(n,m,i) \quad [37]$$

$$\alpha(m) = \frac{\sum_k \sum_i x_0(k.m.i)}{\sum_k \sum_i x(k,m,i)} \quad [38]$$

$$[n, k = 1, \dots, 25, m = 1, \dots, 12, i = 1, \dots, I(m)] \quad [39]$$

where $\alpha(m)$ is bias correction ratio for month m (m = 1-12), $x'(n,m,i)$ is daily precipitation derived from AGCM output after bias correction for day i, month m, year n in the present or future climate experiment period, $x(n,m,i)$ is AGCM precipitation output before bias correction for day i, month m, year n, $x_o(n,m,i)$ is observed precipitation on day i, month m, year k in the present climate experiment period, and $I(m)$ is total days in month m.

3.3 Reproducibility of river discharge on current climate by after bias correction of precipitation

Considering AGCM evapotranspiration outputs and the bias corrected AGCM precipitation outputs as meteorological inputs, river discharges at Iwazu point in the Yoshino River basin and Takaya point in the Mogami River basin were respectively calculated by use of Hydro-BEAM with consideration of the proposed reservoir operation model. Figure 3 shows comparison in monthly average between observed and simulated river discharges at Iwazu in the Yoshino River and at Takaya in the Mogami River. Monthly mean observed river discharge averaged over 25 years (1979-2003), river discharge simulated by Hydro-BEAM without bias correction, and that with bias correction are shown in Figure 3. For the results for the Yoshino River basin, reproducibility of river discharge by Hydro-BEAM generally improved after introduction of bias correction in AGCM precipitation outputs. However, river discharge amount were still underestimated by Hydro-BEAM in August, and overestimated in November. On the other hand, bias correction only in precipitation was not enough in Mogami River. River discharges were highly underestimated throughout the snowfall season from November to February and in the snowmelt season from March to May. The difference in river discharge amounts is especially great in March and April. This is mainly because bias correction in snowpack or in

©2017, IAHR. Used with permission / ISSN 1562-6865 (Online) - ISSN 1063-7710 (Print)

snowmelt, which is also important hydrological process in the Mogami River, was not considered in this study. Therefore it can be considered necessary to consider these processes in bias correction in order to reproduce river discharge in this river basin well.

3.4 Comparison of river discharge and reservoir operation under current climate and future climate

Figure 4 shows river discharges at the hydrological stations of the two river under the current climate and future climate conditions, all of which were calculated by Hydro-BEAM. For the Yoshino River, the result showed that the total amount of river discharge at Iwazu decreased in the future climate condition. River discharge especially decreased in summer season. The period where river discharge largely decreased in the future climate condition corresponds to irrigation season. In addition, river discharge decreased also in winter season. Droughts often occur and are considered as a severe issue in the Yoshino River basin under the current climate. The results shown in Figure 4 suggests an increased risk of frequent drought occurrence in this river basin under the future climate condition. On the other hand, for the Mogami River, river discharge at Takaya under the future climate was highly different from that under the current climate. Changes distinct especially from December to May. This can be considered because snow-melting period becomes earlier in the future climate due to high temperature. The peak of snowmelt shifts to March or early April in the future climate from May in the current climate. Since the Mogami River basin highly depends on snow-melting water for water usage, it can be considered that reservoir operation rules need to be changed to mitigate adverse impacts of these changes in river discharge in the future climate condition as an adaptation to climate change.

Figure 5 shows examples of trajectory of water storage and release in the Sameura Reservoir in the Yoshino River in a year under the experiments for the current climate and future climate conditions. Due to the changes in river discharge under the future climate condition as shown in Figure 3, storage volume of the Sameura Reservoir starts decreasing from the end of May, when water use in irrigation usually starts increasing, and remains small until the end of the year. Similar characteristics of reservoir operation were seen in the simulation for other years in the future climate. Therefore, if it is supposed that the reservoir is operated based on the current operation rules, much severe drought event may occur frequently under the future climate condition.

Figure 6 shows examples of trajectory of water storage and release in the Shirakawa Reservoir in the Mogami River in a year under the experiments for the current climate and future climate conditions. In the Shirakawa Reservoir, change of the snow-melting period occurs directly to the change of the water storage volume. Under future climate, capacity of the water storage volume became full with water earlier than current climate. Water use capacity of the Shirakawa Reservoir were operated to decrease in summer season. Therefore, even though snow-melting period became earlier under future climate, it did not affect much to the reservoir operation. However, the result was peculiar to the Shirakawa Reservoir. In the other reservoirs which does not decrease the capacity of water use, the change of snow-melting season can be critical. Therefore, in future climate, water storage volume will decline faster which may lead to long term drought after summer season.

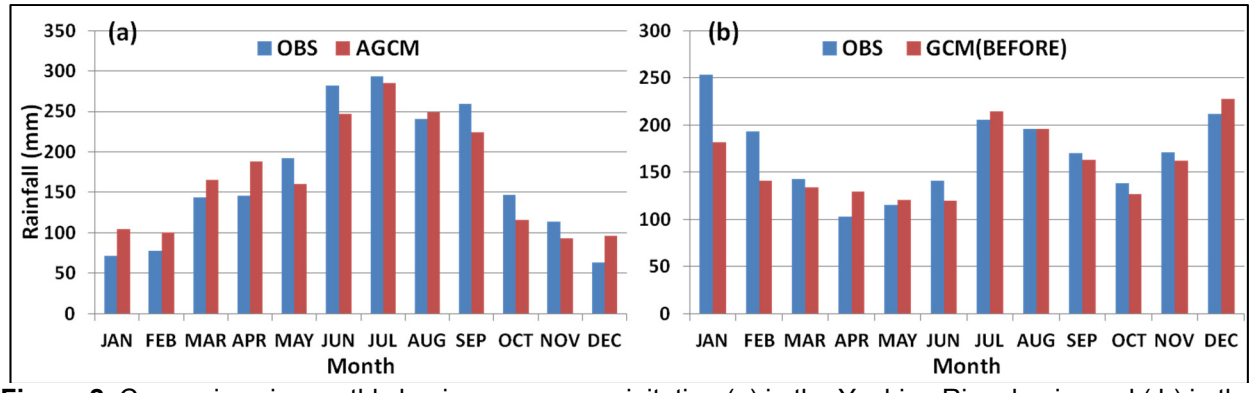

Figure 2. Comparison in monthly basin average precipitation (a) in the Yoshino River basin, and (b) in the Mogami River basin.

 ©2017, IAHR. Used with permission / ISSN 1562-6865 (Online) - ISSN 1063-7710 (Print)

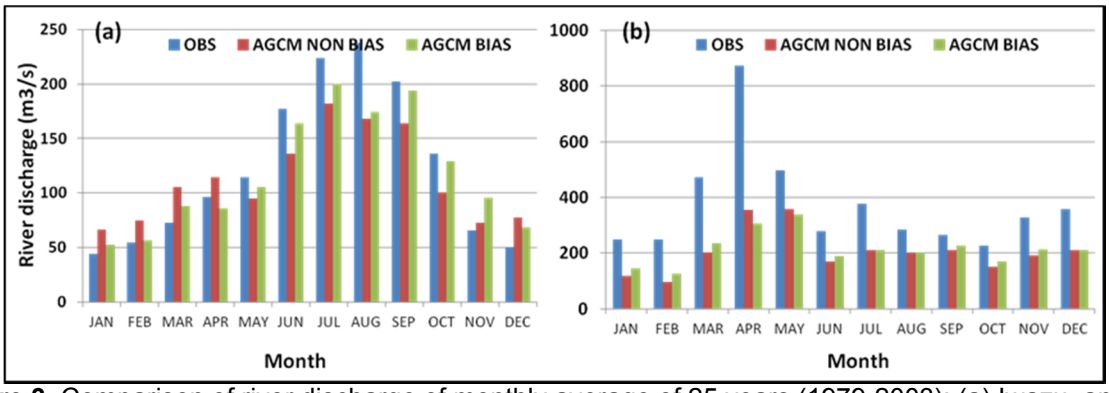

Figure 3. Comparison of river discharge of monthly average of 25 years (1979-2003): (a) Iwazu, and (b) Takaya.

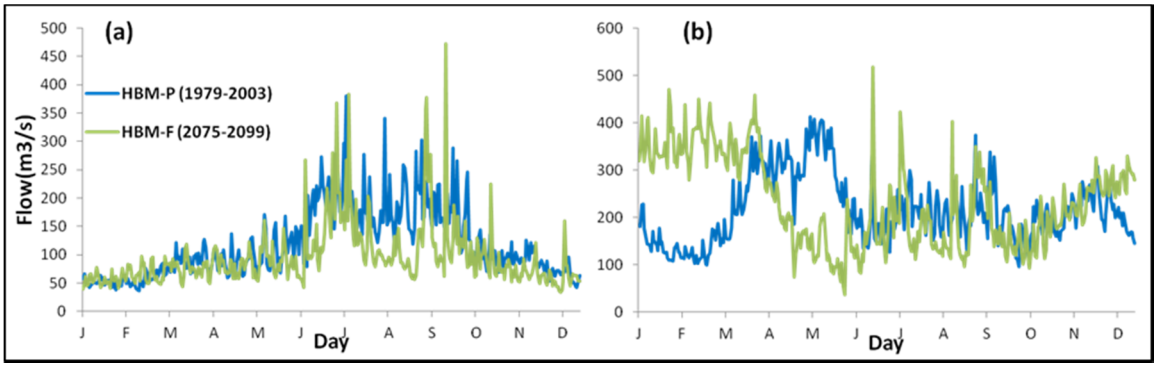

Figure 4. Comparison of river discharge of 25 year average under current climate and future climate : (a) Iwazu, and (b) Takaya.

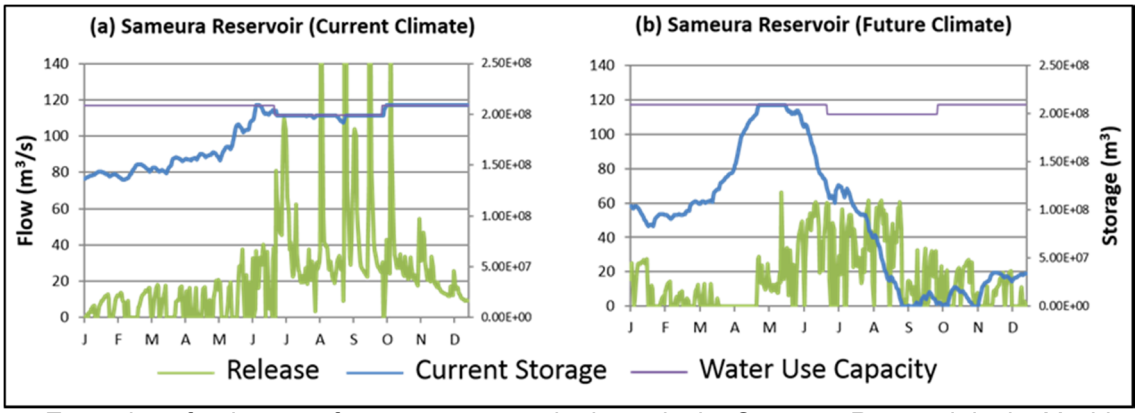

Figure 5. Examples of trajectory of water storage and release in the Sameura Reservoir in the Yoshino River in a year: under the experiments for (a) the current climate and (b) future climate conditions.

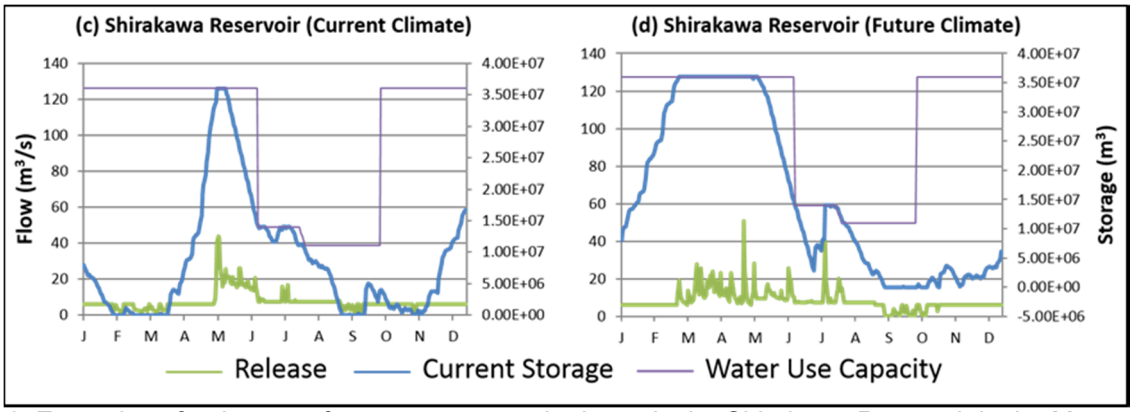

Figure 6. Examples of trajectory of water storage and release in the Shirakawa Reservoir in the Mogami River in a year: under the experiments for (a) the current climate and (b) future climate conditions.

©2017, IAHR. Used with permission / ISSN 1562-6865 (Online) - ISSN 1063-7710 (Print)

4 CONCLUSIONS

In this study, impact assessments of climate change on operation of reservoir systems and river discharges in the Yshino River basin and Mogami River basin were conducted as a fundamental study considering reservoir operation for water supply for the expected future climate condition. Using current climate data (1979-2003) and future climate data (2075-2099) projected by MRI-AGCM3.2S, river discharges both in the current and future climates were respectively estimated by use of Hydro-BEAM integrating operation of reservoirs and water intake in the target river basins.

With consideration of reservoir operation, river discharge amount in Iwazu point were still predicted to decrease especially in summer season. Therefore, under such condition, improvement of reservoir operation are necessary, and if current reservoir operation were used, simulation were made that drought may continue after summer season. In the Mogami River basin, snow melting season were simulated to shift earlier, from March-May to December-April. Under current reservoir operation rules, water storage volume was lowered before May to prepare for water produced by snow melting. Therefore, in future climate, water storage volume will not recover after March, due to the effect of snow melting season shifting earlier, which may lead to a long term drought from the summer season.

Reservoir operation model conducted in this study were constructed without the consideration of small reservoirs especially for power generation and other river discharge regulation faculties. In addition, only the bias of rainfall were corrected for the meteorological inputs by MRI-AGCM3.2S. Therefore, the reproducibility of river discharge in the Mogami River were not considered to be reliable enough due to the underestimation which was largely seen through the snowfall and snowmelt seasons. Bias correction of snowpack or snowmelt processes needs to be tackled in the future in order to estimate reliable changes in river discharges in these regions.

ACKNOWLEDGEMENTS

This work was supported by “Theme D Problem Oriented Accurate Impact Assessment” of the Japanese Program for Risk Information on Climate Change (SOUSEI). Data related to the Yoshino River basin was provided by Japan Water Agency. The authors would like to express sincere appreciation to all of them.

REFERENCES

Kojiri, T. (2005). Hydrological River Basin Environment Assessment Model (Hydro-BEAM). In *Watershed models* .CRC Press, 613-626.

Mizuta, R., Yoshimura, H., Murakami, H., Matsueda, M., Endo, H., Ose, T., Kamiguchi, K., Hosaka, M., Sugi, M., Yukimoto, S., Kusunoki, S. & Kitoh, A. (2012). Climate Simulations using MRI-AGCM3.2 with 20-km Grid. *Journal of Meterological Society of Japan,* 90A, 233-258.

Sato, Y., Tanaka, K., Nakakita, E. & Kojiri, T. (2009). Anticipatory Adaptation to Flood and Drought Disaster due to Climate Change. In *Proceedings of 33rd IAHR Congress: Water Engineering for a Sustainable Environment,* 1701-1707.

Sayama, T., Tachikawa, Y., Takara, K., Masuda, A. & Suzuki, T. (2008). Evaluating the Impact of Climate Change on Flood Disasters and Dam Reservoir Operation in the Yodo River Basin. *Journal of Japan Society of Hydrology and Water Resources*, 21(4), 296-313.

Tachikawa, Y., Takino, S., Fujioka, Y., Yorozu, K., Kim, S., & Shiiba, M. (2011). Projection of river discharge of Japanese river basins under a climate change scenario. *Journal of Japan Society of Civil Engineering,* 1, 1-15.

Tanaka, K., Hagizawa, Y., Sakuma, R. & Kojiri, T. (2008). Bias Detection and Correction of Climate Model Output. *Annuals of Disaster Prevention Research Institute,* Kyoto University*,* No. 51B.

Yoshimura, K. & Koike, T. (2015). Dam Volume Reallocation between Flood Control and Water use as an Adapting Policy under Climate Change in Kino River Basin. *Journal of JSCE*, 71(4), 385-390.

 ©2017, IAHR. Used with permission / ISSN 1562-6865 (Online) - ISSN 1063-7710 (Print)

REDUCING WATER LOSSES IN THE UPPER NILE RIVER BASIN

NESMA ADWY[1], HAYTHAM AWAD[2], MOHAMED ABOUROHIM[3] & ALAA ELDEEN YASSIN[4]

[1,2,3,4] Faculty of Engineering, Alexandria University, Alexandria, Egypt,
eng_nesma_adwy@yahoo.com; haytham.awad@alexu.edu.eg; mrohim76@yahoo.com; ayeco70@hotmail.com

ABSTRACT

It has been recognized that there is a possibility to increase the overall availability of water in the Nile Basin by reducing 'losses' of water through evaporation. The marshes became a subject of research by planners to save water by reducing the evaporation (losses) from the marshes such as the Machar Marshes which lies north of the Sobat River in southern Sudan. During the flood season, a small amount of water from the Machar Marshes enters the White Nile, northeast of Malakal, due to the water losses mostly by evaporation. Based on the very limited data available over the Machar region, remote sensing is conducted to compute Machar area and annual evapotranspiration from these wetlands, after that the monthly water balance will be simulated. Landsat-7 and Landsat 8 imagery for wet and dry seasons of the Machar area are studied to assess the historical land use change between 2001 and 2014. It is found that the areas are 724 km^2, 9221 km^2 for April and September respectively for the year 2001, and 494 km^2, 6161 km^2 for April and September respectively for the year 2014. A remote sensing technique is used assess actual evapotranspiration (Eta) across Machar marshes using and applies the theory of the Surface Energy Balance Algorithm for Land (SEBAL) model. It is found that the annual evapotranspiration is 1404 mm. The Machar Canal is designed to bypass the marshes and direct downstream a proportion of the water that is 'lost' from the Nile each year by spill and evaporation in the swamps. In order to analyze and investigate the amount of water saving by this scenario, Hec-ResSim model is used to calculate this simulation which reveals that an amount of 4.299 to 5.8BCM can be saved.

Keywords: Machar marshes; South Sudan; remote sensing; classification; SEBAL.

1 INTRODUCTION

It has long been recognized that there is potential to increase total water availability in the Nile Basin by reducing 'losses' of water through evaporation and infiltration to groundwater from both natural and man-made water bodies and other irrigation schemes. There are three mechanisms proposed for achieving this purpose: (i) the conversion of flows from natural wetlands; (ii) management of man-made storage to reduce evaporation; and (iii) improving the efficiency of irrigation.

The Machar marshes are one of the wetland areas located along the Nile in southern Sudan between Sobat in the east and Malakal in the north. The overall objective of this study is to assess the water balance to improve understanding of hydrology and variability in relation to spatial and temporal aspect in the Machar marshes region. The estimation of the flooded area of Machar and spatial variation of evaporation in a watershed is essential for many applications in the field of water resources and climate modeling. Evaporation and marshes area are a major component of the water budget in a wetland, but it has proven difficult to measure accurately. So some researchers have developed many methods to estimate evaporation and area.

It has to be noted that, the area of Machar marshes used in previous studies differs greatly from one study to another. Hurst et al. (1950) is the first one who analyzed the water losses from Baro, above Sobat head. This analysis estimates the Marshes' area to be about 6500 km^2. The second is the Jonglei investigation team JIT (1954), bringing above investigation up to date; this study focuses on the spillover from Baro between Jun-Nov. The study found the annual spill of about 2.820 km^3, and rainfall measured from 1940-1952 estimated an average of about 788 mm/yr over the area. The Jonglei investigation team (JIT, 1954) estimated annual spill of 2.8 BCM/yr from Baro towards Machar Marches, plus the annual flow of 1.7 BCM/yr from the eastern catchment, and an outflow of 0.5 BCM/yr. El Hemry and Eagleson (1985) studied the Machar area. They used Landsat imagery to map the extension of Machar marshes, and vegetation distribution. The results obtained by Sutcliffe and Parks (1999) show that estimated areas of flooding vary between about 1500 and 6000 km^2 over the 5-year period.

The spatial and temporal distribution of evapotranspiration ET can be mapped from remote sensing techniques without going through excessive ground truth data collection (Franks and Beven, 1999). Several models have been developed to spatially estimate ET; among them are the Surface energy balance algorithms for land (SEBAL; Bastiaansen et al., 1998), the Mapping Evapotranspiration with Internalized Calibration (METRIC; Allen et al., 2007) model, the Remote Sensing of Evapotranspiration method, and the Analytical Land Atmosphere Radiometer Model (ALARM; Suleiman et al., 2009). SEBAL was developed to

©2017, IAHR. Used with permission / ISSN 1562-6865 (Online) - ISSN 1063-7710 (Print)

estimate ET over large areas using satellite surface energy fluxes (Bastiaanssen et al., 1998). SEBAL is said to be capable of estimating ET without prior knowledge on the soil, crop, and management conditions (Bastiaanssen et al., 2005). This method has been used widely including locations in the U.S.A., Africa, Europe and other parts of the world.

2 SITE DESCRIPTION

The river Sobat makes up approximately half of the White Nile's water, and 1/6 of the entire Nile. It spills into the Machar marshes during years of heavy rainfall. The Sobat has two main tributaries the Pibor and Baro. The Machar Marshes are the least known of the southern Sudan wetlands. It lies north of the main channel of the Baro as shown in figure (1). These are seasonal wetlands that receive water from both rainfall and over-bank spills of the Sobat and the Baro. In the rainy season these wetlands expand to cover a large area east of Malakal and north of the Baro River, included by latitude 9º to 10º North, and longitude 32º 45' to 33º 30' East, Figure 1. During the flood season, a small amount of water from the Machar Marshes enters the White Nile, northeast of Malakal, due to the water losses mostly by evaporation, (Sutcliffe and Parks, 1999).

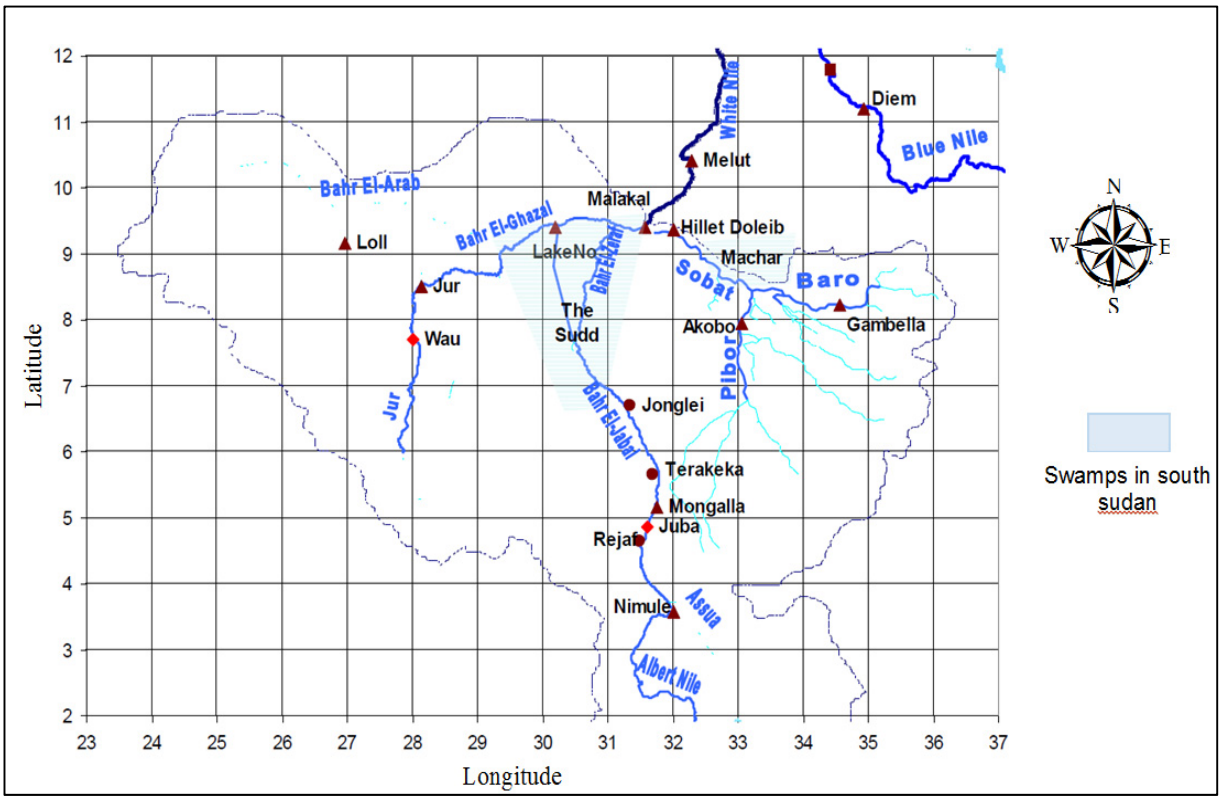

Figure 1. Location of Machar marshes source: Elshamy (2006).

3 MACHAR AREA

3.1 Data sets

Remote sensing has been used to classify and map wetlands cover and uses different techniques and data sets (Ozesmi and Bauer, 2002).

In the present study, multi-temporal satellite images dated April & September 2000 and January, April & September 2014 were used to perform Machar Marsh's classification and change detection analysis. Different types of data have been used to accomplish the study; Landsat 7 ETM+ 30 m, Landsat 8 OLI and TIRS +30, the Shuttle Radar Topographic Mission (SRTM) 90 m, and land cover map were the primary data sources used, as shown in Table 1.

Table 1. Global data set sources.

Type of data	Date of acquisition	Resolution (m)	Source
Landsat 7 172/53&172/54	8 April 2000&12 September 2000	30	USGS
Landsat 8 172/53&172/54	23 April 2014 &11 September 2014	30	USGS
SRTM 43_10& 43_10		90	CGIR
land cover	22-May-07		FAO-Africover

©2017, IAHR. Used with permission / ISSN 1562-6865 (Online) - ISSN 1063-7710 (Print)

During the selection process, it was important that the satellite scenes contained minimal cloud cover or were totally free of such and acquired within the same season (as was the case in this study) to ensure uniformity (Coppin et al., 2004; Malingreau et al., 1995) as shown in figure 2.

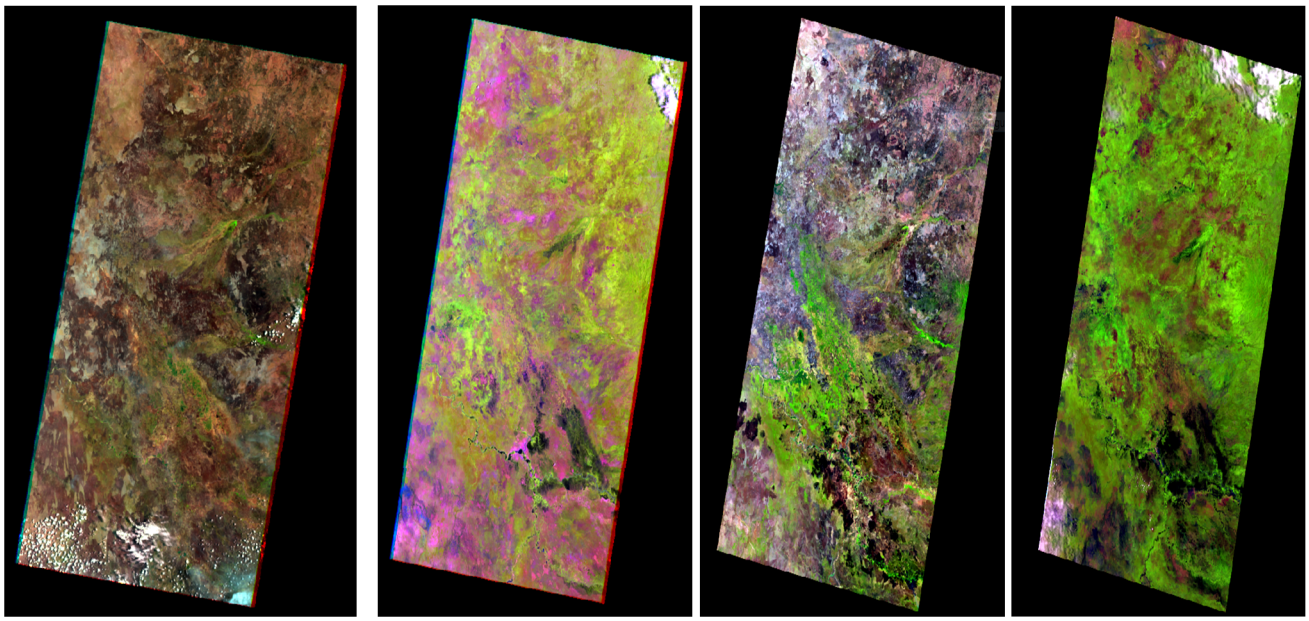

(a) April2000 (b) September 2000 (c) April 2014 (d) September 2014

Figure 2. Landsat tiles in different seasons and years covered Machar marshes.

3.2 Data pre-processing

The LANDSAT images were downloaded from the USGS, unzipped. The most important image preprocessing implemented using ERDAS IMAGINE Software is, layer stacking of the bands is used for combining the bands of each image to create composite images.

3.3 Classification

An important part of image analysis is identifying groups of pixels that have similar spectral characteristic and to determine the various features or land cover classes represented by these groups. This form of analysis is known as classification. The result of a classification is that all pixels in an image are assigned to particular classes resulting in a classified image that is essentially a thematic map of the original image. Signatures were generated for field identification of the classes and as training the supervised classification. The land cover classes were categorized into seven major classes namely shrubs, tree savannah, water body, open woody vegetation, herbaceous vegetation, woody vegetation on flooded land and other land classes. This classification scheme was based on the Sudan Land cover map (http://www.un-spider.org/links-and-resources/data-sources/land-cover-sudan-africover-fao) and from GIS the attribute table was created. The source of data used for deriving both training and testing data included historic reference data, digital elevation map (DEM), Google Earth, and visual interpretation of the images during image classification. The accurate assessment of the marshes maps was performed using the Accuracy Assessment command in ERDAS Imagine.

3.4 Results of Machar area

Table 2 shows the result of the remote sensing in the calculation of Machar area which differs from study to another. In addition, table 3 shows the comprehension of the area of Machar in the dry and wet season. Two selected years show the compression of the area, which differs from one year to other, depend on the rainfall and evapotranspiration amount.

Table 2. Machar area results.

Month	Jan	Feb	Mar	Apr	May	Jun	Jul	Aug	Sep	Oct	Nov	Dec
Area calculated in this study Km^3	4080	3101	1800	724	1920	4900	6300	8741	9221.2	9003	8100	6609

©2017, IAHR. Used with permission / ISSN 1562-6865 (Online) - ISSN 1063-7710 (Print)

Table 3. Comprehension of area of Machar in dry and wet season.

Month	Area in km2	
	2001	2014
April (Dry Season)	724	494.469
Sep (wet season)	9221.6	6161.98

4 ESTIMATION OF EVAPOTRANSPIRATION (ET)

Latent heat flux (vapor transference to the atmosphere through the process of vegetal transpiration and soil water evaporation) was computed by the simple difference between the radiation balance cards, soil heat flux and sensible heat flux. The Surface Energy Balance Algorithm for Land (SEBAL) model computes a complete radiation and energy balance along with the resistances for momentum, heat and water vapour transport for each pixel. Evapotranspiration is derived in terms of instantaneous latent heat flux, λET (W/m2), and it is computed as the residual of the surface energy balance equation at the moment of satellite overpass on a pixel-by-pixel basis:

$$\lambda ET = (Rn - G - H) \quad [1]$$

where, R_n is Net radiation (W/m^2), G is the soil heat flux (W/m^2), and H is the sensible heat flux (W/m^2).

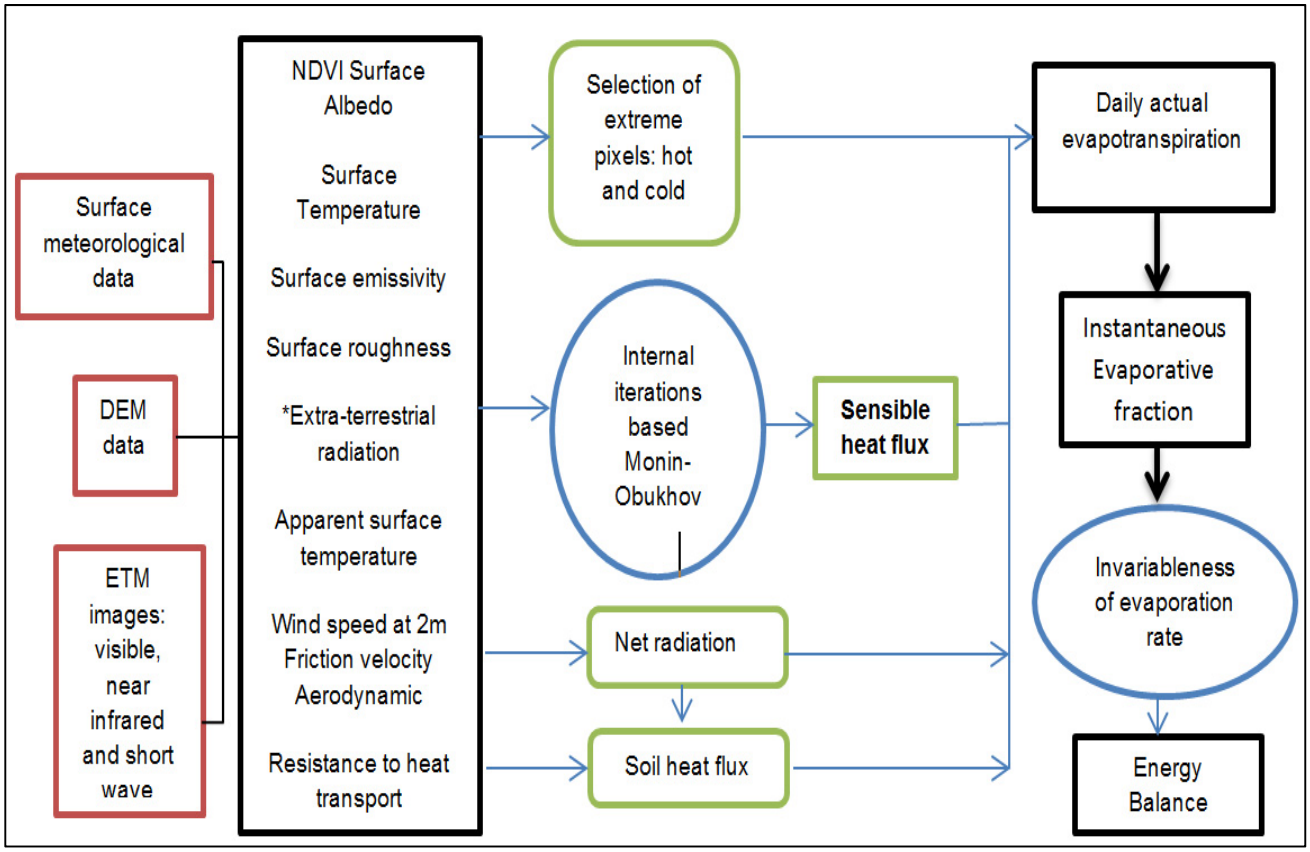

Figure 3. Flowchart of daily ET estimation by using ETM images and SEBAL model.

A number of publications have been released on SEBAL approach and its applications describing the entire procedure (Bastiaanssen, 1998) the flowchart for the SEBAL model is shown by figure 3. SEBAL requires spatially distributed visible, near-infrared and thermal infrared data together with routine weather data. The algorithm computes net radiation (R_n), sensible heat flux (H) and soil heat flux (G) for every pixel and the latent heat flux (λE) is acquired as a residual in energy balance equation. This is accomplished by first computing the regional surface radiation balance, followed by the regional surface energy balance.

4.1 Calculation of the net radiation flux

The net surface radiation Rn can be estimated, as gain-losses which can be expressed by the following equation:

$$R_n = (1 - \alpha)R_s \downarrow + R_L \downarrow - R_L \uparrow - (1 - \varepsilon_0)\, R_L \downarrow \quad [2]$$

©2017, IAHR. Used with permission / ISSN 1562-6865 (Online) - ISSN 1063-7710 (Print)

The net shortwave radiation available at the earth surface depends on the incoming solar radiation (R_s) and the surface albedo (α). The incoming long wave radiation ($R_L \downarrow$) is calculated using the Stefan–Boltzmann equation with an empirically determined atmospheric emissivity (ε_a) and the field measurements of air temperature *(T).* Outgoing long wave radiation ($R_L \uparrow$) is obtained using the Stefan–Boltzmann equation with an empirically determined surface emissivity (ε_0) and surface temperature (T_o) acquired by the satellite after atmospheric correction. The final term in radiation balance equation,$(1-\varepsilon_0)\, RL\downarrow$ represents the fraction of $RL\downarrow$ that is lost from the surface due to reflection.

4.2 Soil heat flux (G)

Soil heat flux is the rate of heat storage into the soil and vegetation due to conduction. Consequently, it is computed according to the following equation:

$$G/R_n = \frac{T_s}{\alpha}(0.0038\alpha + 0.007\alpha^2)(1 - 0.98NVDI^4) \quad [3]$$

where,

T_s : The surface temperature (C°),
α: The surface albedo,
$NVDI$: The Normalized Difference Vegetation Index, and
G: The readily calculated by multiplying G/R_n by the value forR_n.

4.3 Sensible heat flux (H) estimation

The basic calculation of H is performed by using the bulk aerodynamic method using Eq. [4] below:

$$H = \rho_a * C_{pa} * (T_o - T_a)/rah \quad [4]$$

where ρ_a is the air density of moist air (kg/m3), C_{pa} is specific heat of dry air (~1004 J/kg/K); T_a is average air temperature (*K*) at screen height (typically at 2 m), T_o is the average surface aerodynamic temperature (*K*). To is not measured and may be difficult to estimate, thus some users substitute radiometric surface temperature (T_s) for T_o. The sensible heat flux (H) for the whole image is calculated iteratively until convergence in the successive value is found.

4.4 Latent heat of flux (λET)

Finally, latent heat flux is the rate of latent heat loss from the surface as a result of evapotranspiration. It can be computed for each pixel as a residual term of the surface energy balance using Eq. [1]. An equivalent amount of instantaneous ET is also calculated by dividing the latent heat flux by the latent heat of vaporization (λ), according to following equation:

$$ET_{ins} = 3600\frac{\lambda ET}{\lambda} \quad [5]$$

where, ET_{ins} is the hourly evapotranspiration (mm/hr), 3600 is the time conversion from seconds to hours and *L* is the latent heat of vaporization or the heat absorbed when a kilogram of water evaporates (Jkg-1).

4.5 Application of Sebal Technique on Machar Marshes

Eq. [1] was applied to compute the energy balance components and hence to derive the component of this equation on a pixel-by-pixel basis over the area, covering of Machar marshes. SEBAL has been applied for 12 images acquired during individual days of the year 2000.

In order to perform the operation, the software ERDAS and manual SEBAL have been applied in Machar, the 24-hour ET amount and its distribution are calculated with this model. It is found that the ET amount is verifiable and the ET distribution is in accordance with the land type.

4.6 Evaporation results

The estimation of pixel-scaled ET_a was conducted via SEBAL using Landsat-7 ETM+ images, DEM and meteorological data. The monthly (actual) evaporation E_a is given in Table (4). The difference in E_a through the year is caused by both the dominant evaporation mechanism and the areal extent of the swamp. Due to the lack of field data, therefore, the results are compared with the previous results. Comparison of the monthly (actual) evaporation E_a in the present study against actual evaporation due to Batiaanssen (2005) calculated by SEBAL and average evaporation by Sutcliffe and Parks (1999) is given in Table (4). The value used for evaporation in current study(1404 mm/yr) is in good agreement with the SEBAL estimates of the Machar by Batiaanssen (2005) (1288 mm/yr). The difference between two studies due to Batiaanssen (2005) calculated

©2017, IAHR. Used with permission / ISSN 1562-6865 (Online) - ISSN 1063-7710 (Print)

the average actual evaporation for all Sobat basin, but in this study, actual evaporation was calculated for Machar only. Sutcliffe and Parks (1999) used open water evaporation, estimated by the Penman method from temperature, humidity, sunshine and wind speed at Bor near sudd wetland, south sudan, which should provide a reasonable estimate for the Machar marshes. Because of the evaporation by Sutcliffe (1999) is approximate so results are inaccurate.

Table 4. Different estimates of evaporation over the Machar marshes.

	Evaporation rate (mm/month)												
Source	Jan	Feb	Mar	Apr	May	Jun	Jul	Aug	Sep	Oct	Nov	Dec	Total
Current Study	130	118	96	107	113	122	120	121	141	125	102	109	1404
Batiaanssen (sebal) 2005	121	102	84	91	115	113	111	117	125	128	83	98	1288
Sutcliffe and Parks (1999)	217	190	202	186	183	159	140	140	150	177	189	217	2150

5 INFLOW

The inflow to the Machar swamps is supplied from two sources.

1. The spilling from the Baro.
2. The run-off from the eastern tributaries coming from the Ethiopian foothills.

Raafet (2015) studied the Baro-Akobo-sobat basin to understanding of hydrology, hydrological complexity and variability with respect to spatial and temporal aspect in the basin. And describe the locations and relative size of Swamps in the basin. Raafet estimate losses from Baro River epically to Machar marches as shown in Table 5.

Table 5. Spilling from Baro River (Raafet, 2015).

Month	Jan	Feb	Mar	Apr	May	Jun	Jul	Aug	Sep	Oct	Nov	Dec
U.S Machar	55	9.4	10	34.1	157.5	483.9	893.5	1048.5	1052	842.8	520.8	220
Spill to Machar	0	0	0	0	0	0	353.5	508.5	512	302.8	0	0

The second source is the run-off from the eastern tributaries coming from the Ethiopian foothills. These tributaries are the Khor Ahmar, Tombak, Yabus, Daga and Lau and the areas of their basins are 600, 900, 4300, 2900 and 1600 km2, respectively. Considering an annual run-off coefficient of 14% and an annual rainfall depth of 1.0 m, the annual run-off reaches 1.44 mlrd m3/yr (Hurst et al., 1966). The total inflow from these five tributaries is given in Table 6.

Table 6. Flow from eastern torrents Sutcliffe and Parks (1999).

	Jan	Feb	Mar	Apr.	May	Jun	Jul	Aug	Sep	Oct	Nov	Dec
Total Estimated Inflow From Eastern torrents	23	12	7	8	29	68	156	401	423	398	158	61

6 RAINFALL

The rainfall in the machar area varies from an average of 800 mm/year in the northern part (Malakal) to 1000 mm/year in the southern part (Mongalla). The rainy season extends from April to October, with the peak in July/August.

The Climate Forecast System Reanalysis (CFSR) was designed and executed as a global, high resolution, coupled atmosphere-ocean-land surface-sea ice system to provide the best estimate of the state of these coupled domains over this period. The CFSR creates the opportunity to select user defined areas to collect rainfall data. The results of the analysis of the average monthly precipitation in the Machar area for year 2000 are given in table 7.

 ©2017, IAHR. Used with permission / ISSN 1562-6865 (Online) - ISSN 1063-7710 (Print)

Table 7. Input data of the Machar marshes for year 2000.

	Flooded area	Precipitation	Evaporation	Inflow to Machar	
Month	**Area calculated in this study (Km^3)**	***P*** **(mm/month)**	***E*** **sebal calculated from this study (mm/month)**	**Spill from Baro towards Machar BCM**	**total estimated inflow from eastern**
Jan	4080	0	130	0	23
Feb	3101	0	118	0	12
Mar	1800	4.634855	96	0	7
Apr	724	22.31856	107	0	8
May	1920	229.3714	113	0	29
Jun	4900	116.2396	122	0	68
Jul	6300	257.4097	120	353.5	156
Aug	8741	201.4738	121	508.5	401
Sep	9221.2	199.1332	141	512	423
Oct	9003	135.8597	125	302.8	398
Nov	8100	18.95485	102	0	158
Dec	6609	0.387955	109	0	61

7 THE WATER BALANCE

The Machar marshes can be treated as a reservoir whose storage is dependent on inflow and outflow data, estimates of rainfall and evaporation data, as shown also in table 6.

According Sutcliffe and Parks (1999) the Sudd water balance can be calculated using the equation of continuity for a time interval *Δt*:

$$\frac{dV}{dt} = (Q_{in} + P) - (Q_{out} + E) \quad [6]$$

where V is the volume of water stored in the flooded area (Km^3), Q_{in} is the inflow (Mm3/month), Q_{out} is the outflow (mm^3/month), P is the precipitation (mm^3/month) and E is the evaporation (Mm^3/month).

Monthly parameters of water balance equation have been computed for the Machar marshes. The results of the water balance are provided in table 8.

Table 8. The monthly change of volume of flooding in Machar region.

Total Inflow m^3/month	losses m^3/month	*dv/dt* BCM/month
23000000	530400000	-0.5074
12000000	365918000	-0.35392
15342739.78	172800000	-0.15746
24158634.71	77468000	-0.05331
469393012.2	216960000	0.252433
637574230.3	597800000	0.039774
2131181099	756000000	1.375181
2670582695	1057661000	1.612922
2771246854	1300189200	1.471058
1923944614	1125375000	0.79857
311534272.5	826200000	-0.51467
63563993.93	720381000	-0.65682

8 THE OPERATION OF THE MACHAR CANAL

The Machar Canal was designed to bypass the marshes and direct downstream a proportion of the water that is 'lost' from the Nile each year by spill and evaporation in the swamps.

©2017, IAHR. Used with permission / ISSN 1562-6865 (Online) - ISSN 1063-7710 (Print)

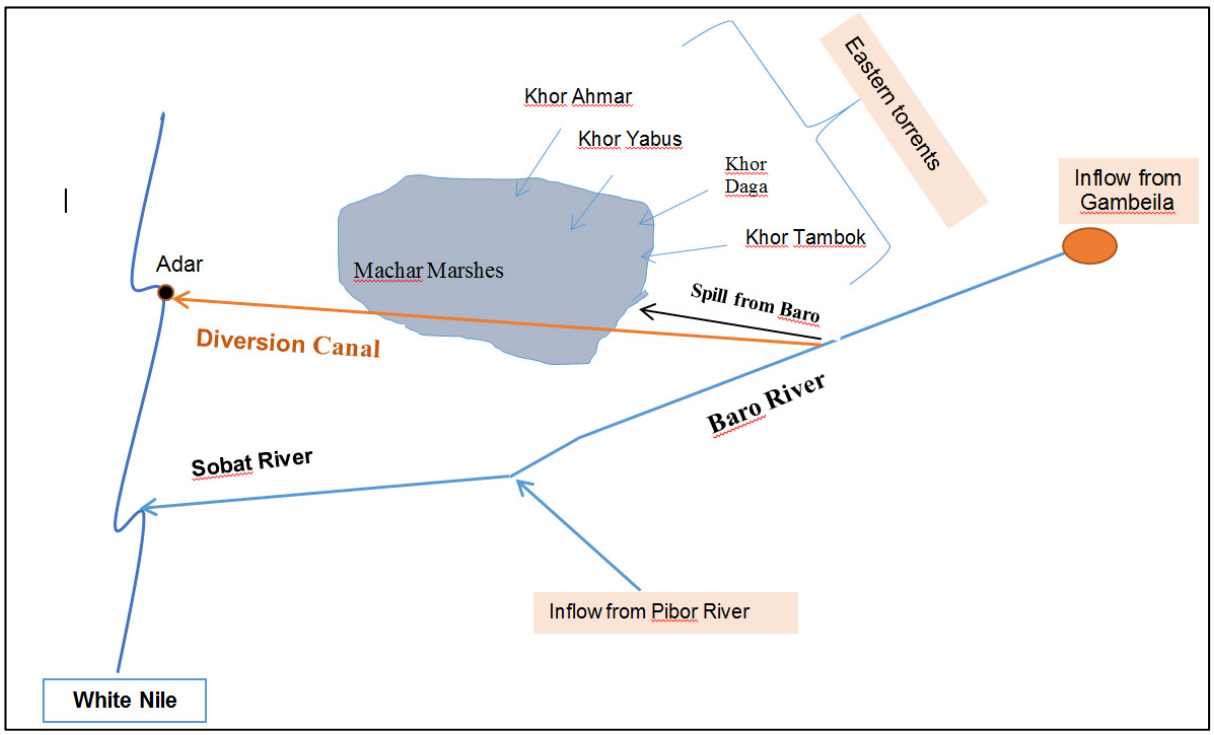

Figure 4. Shows the location of new canal.

This canal project in the southern Sudan will be considered as a water resources development project as well as a way for saving water which would be lost by evaporation in marshes and promoting the social standards and economic life of the population in the project area. The Machar Canal was designed to connect Khor Machar to Khor Adar to collect the spilling from Baro River and eastern torrents to prevent marshes formation. As shown in figure 4 this canal will be about 238 km in length with slope 8 cm/km.

For the difficult of understanding the nature of land cover, so the estimation of surface runoff becomes very difficult. So that to calculate surface run off, it is assumed as a percentage from rainfall over the mashes with 10%, 15%, 20%, 25%, 30%. All data used in Hec_Ressim model are shown in Table 9 in cms.

Table 9. The total saving of water by new canal.

	water saving				
% surface run off	10% rainfall	15% rainfall	20% rainfall	25% rainfall	30% rainfall
Jan	43655285	43720128	43787934.3	43854339.6	43920691.6
Feb	17107076	17107200	17107133.4	17107162.2	17107190.8
Mar	10320617	10528704	10740219.2	10950075.8	11159893.2
Apr	8698312	9306144	9912469.31	10121402.1	11126717.6
May	41780263	53283744	64788936	76293207	87797464.3
Jun	98167249	123323904	148480231	173635946	198792042
Jul	4.02E+08	458301888	514188949	570074992	625962751
Aug	9.01E+08	988093728	1075379580	1162655470	1249936632
Sep	1.1E+09	1191356640	1281246517	1371116616	1460997025
Oct	1.01E+09	1087636032	1167094413	1246541133	1325994742
Nov	5.3E+08	537423552	572267157	607111328	641955726
Dec	1.36E+08	141847200	147451876	153053274	158654870
Tot	4.3E+09	4661928864	5052445417	5442514945	5833405745

9 CONCLUSIONS

The following conclusions were reached by analyzing the results of model outcomes:

- The study demonstrated the use of remote sensing techniques to delineate headwater marshes from non-wetlands and determine the dynamics of areas over different months through year;

 ©2017, IAHR. Used with permission / ISSN 1562-6865 (Online) - ISSN 1063-7710 (Print)

- The spatial distribution of the Machar area was analyzed in combination with the land cover map by using supervised classification. Landsat images were handled using ERDAS IMAGINE software to classify the image to identify the swamps, water and other classes;
- The application of the SEBAL technique was conducted to map spatial variation in actual evapotranspiration (ETa) of the Machar marshes, using Landsat7 ETM+ images of 2000. And the prediction of ETa was compared with the study of Batiaanssen (sebal) (2005) and Sutcliffe and Parks (1999);
- The estimated daily ETa ranged from 0 for bare soil and town constructed land to 8 mm/day for open waters and reed swamps with the average ETa value of about 4.7 mm/day for the whole area. The variation of estimated ETa over different kinds of land use was allowed with the evapotranspiration theory, which hints the application of the SEBAL approach with some detailed field information such as crop or land use type;
- It was found that the open water body and swamp were at a high evapotranspiration rate, while the crop land, grassland and rural residential land took the second place, and bare soil was at the lowest evapotranspiration rate, which accorded with the evapotranspiration theory;
- For saving water from evaporation in marshes, the scenario of Machar canal was made in this study using Hec-Ressim model.

ACKNOWLEDGEMENTS

I would like to thank my supervisors, Prof. Alaa Eldeen Yassin, Prof. Mohamed Abourohim, and Prof. Haytham Awad, they gave me the opportunity to start with my study. Also, I would like to thank Dr. Ahmed Mohamed Abdelrazek for his help in my study. Special thanks are extended to the Hydraulic and irrigation department, Alexandria University.

REFERENCES

Allen, R.G., Tasumi, M. & Trezza, R. (2007). Satellite-based Energy Balance for Mapping Evapotranspiration with Internalized Calibration (METRIC)—Model. *Journal of irrigation and drainage engineering*, 133(4), 380-394.

Bastiaanssen, W.G., Menenti, M., Feddes, R.A., & Holtslag, A.A.M. (1998). A Remote Sensing Surface Energy Balance Algorithm for Land (SEBAL). 1. Formulation. *Journal of hydrology*, 212, 198-212.

Bastiaanssen, W.G.M., Mohamed, Y.A., Van den Hurk, B.J.J.M. & Savenije, H.H.G. (2005). Impact of the Sudd Wetland on the Nile Hydroclimatology. *Water resources research*, 41(8), 1-14.

Coppin, P.I., Jonckheere, K., Nackaerts, B. & Lambin, E. (2004). Review Article Digital Change Detection Methods in Ecosystem Monitoring: A Review*. International Journal of Remote Sensing*, 25, 1565-1596.

El Hemry, I.I. & Eagleson P.S. (1985). *Water Balance Estimates of the Machar Marshes*. Department of Civil Engineering, Massachusetts Institute of Technology, Report No. 260.

Franks, S.W. & Beven, K.J. (1999). Conditioning a Multiple-Patch SVAT Model using Uncertain Time-Space Estimates of Latent Heat Fluxes as Inferred From Remotely Sensed Data. *Water Resources Research*, 35(9), 2751-2761.

Hurst, H.E. & Black R.P. (1950). *The Nile Basin.* Vol. VI. Government Press, Cairo, 575.

Raafet, A. (2015). Assessment of the Impacts of Proposed Water Resources Development Projects in Baro-Akobo-Sobat Basin on High Aswan Dam, *Msc. Thesis. Cairo University.*

Jonglei investigation team JIT. (1954). *The Equatorial Nile Project and Its Effects in the Anglo-Egyptian Sudan*. Report of the Jonglei Investigation Team, *Sudan Government, Khartoum, Sudan*.

Malingreau, J., Achard, F., D'souza, G., Stibig, H., D'souza, J., Estreguil, C. & Eva, H. (1995). AVHRR for Global Tropical Forest Monitoring: The lessons of the TREES project. *Remote Sensing Reviews*, 12(1-2), 29-40.

Ozesmi, S.L. & Bauer, M.E. (2002). Satellite Remote Sensing Of Wetlands. *Wetlands Ecology and Management*, 10, 381-402.

Suleiman, A.A., Bali, K.M. & Kleissl, J. (2009). Comparison of ALARM and SEBAL Evapotranspiration of Irrigated Alfalfa. *2009 ASABE Annual International Meeting*.

Sutcliffe, J.V. & Parks, Y.P. (1999). *The hydrology of the Nile*. IAHS special publication No. 5. IAHS Press, Oxfordshire, UK, 192.

©2017, IAHR. Used with permission / ISSN 1562-6865 (Online) - ISSN 1063-7710 (Print)

Proceedings of the 37th IAHR World Congress
August 13 – 18, 2017, Kuala Lumpur, Malaysia

MOBILISING LOCAL COMMUNITIES TOWARDS INVOLVEMENT IN RIVER MANAGEMENT: LESSONS LEARNT FROM THE SUNGAI PINANG RIVER COMMUNITY ENGAGEMENT PROJECT IN PENANG, MALAYSIA

CHEE HUI LAI[(1)], NGAI WENG CHAN[(2)], HUI WENG GOH[(3)] & NOR AZAZI ZAKARIA[(4)]

[(1,3,4)]River Engineering and Urban Drainage Research Centre (REDAC), Universiti Sains Malaysia, Engineering Campus, Nibong Tebal, Penang, Malaysia
laicheehui.usm@gmail.com
[(2)] School of Humanities,Universiti Sains Malaysia, Penang,Malaysia
Nwchan@usm.my

ABSTRACT

In the era of sustainable development, collaboration is needed from all stakeholders to sustainably manage rivers and water resources. Non-Governmental Organisations (NGOs) play a crucial role in all levels of river management, especially as a link between government and local communities in seeking solutions to river issues in the local context. This paper examines the Sungai Pinang River Community Engagement Project (SPRCEP) undertaken by a local NGO aimed at engaging local communities in conserving a river in Penang State, Malaysia. It discusses the contribution and challenges of the project in engaging local communities in river management. Findings from this paper are drawn from the lessons learned from the pilot project in engaging local communities in river conservation activities and providing practical information at the end of the paper to improve public participation in river management. The project site is located at the Sungai Pinang River (SPR) in Penang State, Malaysia. The river is one of the most polluted rivers in the state. In the project, a series of water educational programs, such as outdoor learning programs, quiz competitions, and river clean-up activities, were organised to educate the public on river conservation. Various platforms were created to enable discussions among multi-stakeholders on the causes of SPR pollution and the solutions for reducing it. At the end of the paper, challenges of effectively engaging local community in river management are discussed. In conclusion, the paper suggested that indicators for local community involvement in river management need to be developed, incentives to be given to the local communities that have made contributions to river conservation, and official platforms to be created to enable exchange of experiences and ideas, and mutual learning between all stakeholders involved in river-related issues.

Keywords: River management; stakeholder participation; local community; Non-Governmental Organisations (NGOs); river pollution.

1 INTRODUCTION

Rivers serve as sources of life, providing water supply to human society for domestic and commercial usage, irrigation for agriculture, as a means of transportation, hydroelectric power, and a source of food in fisheries (Abdullah, 2002). Rivers are also rich in ecosystems services and provide the function for storage and processing of organic matter, nutrients turnover, and energy transformation (Padmalal and Maya, 2014). In the modern era, rivers have also become important ecotourism destinations (Nor Azazi Zakaria et al., 2004). Moreover, in twenty-first century, water and river management have become more complex due to increasing uncertainties caused by climate change (Pahl-Wostl, 2002). Hence, more innovative efforts are needed to sustainably manage rivers in the world for the long term water security in every country. Despite acknowledging the importance of rivers, reasons such as rapid urbanization, industrialization, economic development, and economic growth have caused the number of degraded rivers to increase all over the world (WWAP, 2009). Managing river and water resources is a complex process, as it not only needs to consider the physical characteristics of the river basin, but also the sustainable management of rivers with contributions from all relevant stakeholders. Successful river management involves programmes ranging from organising awareness raising campaign to formulating policies, identifying issues and challenges that need to be addressed, and formulating river management plans and implementing them to ensure that a river basin can be managed sustainably (Chan, 2005).

In Malaysia, rivers are the “Life Veins” of the country as they are the historically favoured locations of cities and towns, and contribute significantly to the country’s economy and social life (Chan, 2002). However, rivers have been severely degraded over the decades. Out of 477 rivers monitored by the Department of Environment (DOE) Malaysia in 2015, 33 rivers were classified as polluted rivers and 168 rivers were found to be slightly polluted (DOE, 2015). Referring to Table 1, more than 40 percent of the rivers monitored by DOE Malaysia in the past five years were classified as slightly polluted river or polluted river. Factors such as mismanagement, poor public involvement, lack of funds, poor enforcement, and low priority on government

 ©2017, IAHR. Used with permission / ISSN 1562-6865 (Online) - ISSN 1063-7710 (Print)

agendas have caused degraded river water quality in Malaysia (Chan, 2012). To improve the effectiveness of river management in Malaysia, both structural and non-structural measures for river management will be need to be taken into account. Furthermore, river basin management needs to adopt holistic and integrated approaches, including engaging stakeholders to play a more active role in planning, monitoring, enforcement and managing river basins in the country (Abdullah, 2002).

Involving stakeholders such as local communities in river management not only improves their commitments for implementing river management plan and policy, but also changes their behavior if the stakeholders play a direct role in developing the plan or policy (Watson, 2004). In Malaysia, the public such as local communities, civil society groups and non-governmental organisations (NGOs) have started playing a more active role in various aspects of water and river management (Chan, 2012). Nevertheless, participation of individual stakeholders from local level in water management and river management is still lacking (Mokhtar et al., 2011; Lai et al., 2017). Institutional and operational challenges were faced by related authorities to engage individual stakeholders from local level to contributing to policy making for water and river management (Mokhtar et al., 2011). Generally, only a small section of Malaysian society has been actively involved in river management (Chan, 2012). This paper examines a pilot project by a local NGO to engage the local communities to conserve a river in Penang State, Malaysia. Findings from this paper are drawn from the lessons learned from the pilot project in engaging the local communities in river conservation activities and providing practical information at the end of the paper to improve public participation in river management. Specifically, the objectives of this paper are: (i) to investigate the issues and challenges in engaging local stakeholders in river management in Malaysia and (ii) to evaluate the outcomes and effectiveness of the Sungai Pinang River Community Engagement Project (SPRCEP) in engaging local stakeholders in river management.

Table 1. River water quality in Malaysia, 2005-2015.

Year	Number Of Rivers Monitored	Clean	Slightly Polluted	Polluted
2005	594	338	166	90
2006	573	335	180	58
2007	520	368	164	48
2008	579	334	197	48
2009	577	306	217	54
2010	570	293	203	74
2011	464	275	150	39
2012	477	278	161	38
2013	477	275	173	29
2014	477	244	186	47
2015	477	276	168	33

Source: Department of Environment Malaysia, 2016

2 THE SUNGAI PINANG RIVER COMMUNITY ENGAGEMENT PROJECT (SPRCEP)

2.1 Project Site

The Sungai Pinang River (SPR) (Figure 1) is a river located in the capital city of Penang State, Malaysia. Penang State is located at the northern part of Peninsula Malaysia and is one of the smallest states in Malaysia but has the second highest population density among all the Malaysian states. In the past few decades, the SPR has been severely polluted by rapid development, urbanization and uncontrolled garbage dumping and wastewater discharges. This river was once declared to be a dead river, as no aquatic life could be found (Chan, 2012). Referring to the Environmental Quality Report (DOE, 2015), the water quality of SPR can be classified as Class III. Domestic sewage, waste from animal husbandry areas, industrial wastes, soil erosion from construction site and urban runoff are identified as the main sources of pollution of SPR (Naemah et al., 2006). Despite years of rehabilitation efforts and high spending to clean the river, it is still classified as one of the most polluted rivers in the state, if not the country. The local community relies heavily on the efforts of the state government to solve this problem. Poor stakeholder engagement, low awareness and apathetic attitude of the local community regarding river pollution and waste management have become the primary factors that have polluted and continue to threaten the SPR (Chan, 2005). The project sites of the SPR project are illustrated in Figure 2.

©2017, IAHR. Used with permission / ISSN 1562-6865 (Online) - ISSN 1063-7710 (Print)

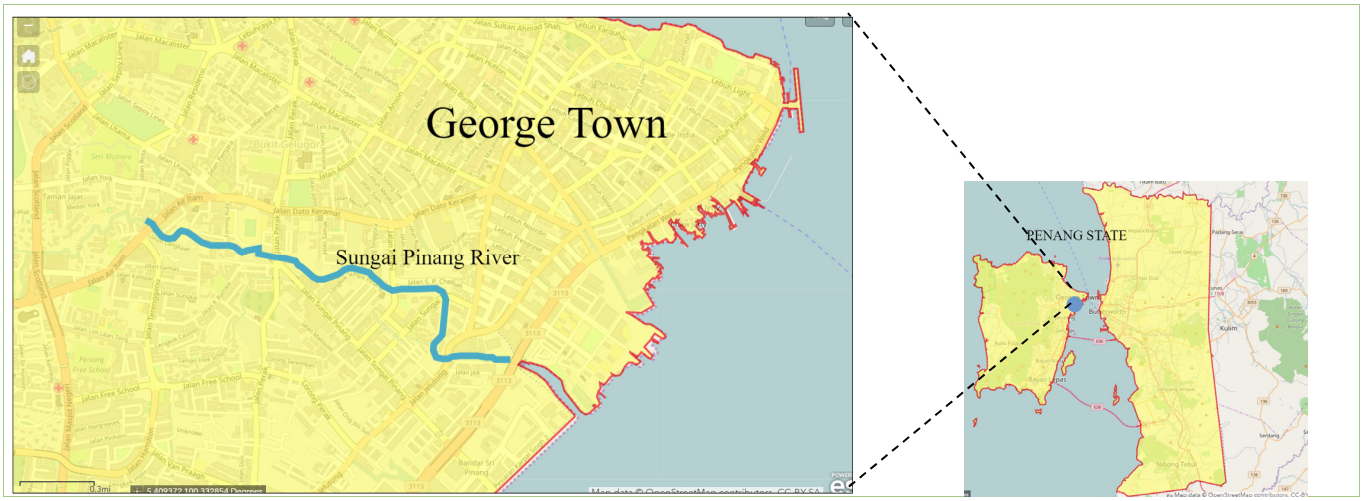

Figure 1. Location of the Sungai Penang River.

(a) Sungai Pinang River @ Taman P Ramlee

(b) Sungai Pinang River @ Rawa Village

(c) Sungai Pinang River @ Patani Street

Figure 2. Project Sites.

2.2 Sungai Pinang River Community Engagement Project (SPRCEP)

The SPR Community Project (SPRCEP) is a project undertaken by Water Watch Penang (WWP) to engage the local community to conserve the SPR. Water Watch Penang (WWP) is a Malaysian non-governmental organisation (NGO) set up in 1997 that aims to promote study, awareness, knowledge, conservation, protection and the practice of a water saving society towards the sustainable development of water resources (WWP, 2016). The SPRCEP is a two-year pilot project (2016 to 2018) by WWP, whereby the final aim of the project is to develop a river management plan to reduce the pollution of SPR via community engagement. Awareness, perception and commitment of a person will affect the personal behavior or action towards an environmental problem (Grob, 1995). Hence, to engage the local community in river conservation, the local community must have enough awareness and good knowledge regarding the SPR pollution issue. Thus, the project is divided into two phases: (i) phase 1 of the project is aimed at raising community awareness, improving their knowledge and foster multi-stakeholder discussion on the SPR pollution issue, and (2) phase 2 aims to investigate the local community perception regarding the solutions for the river pollution issue as well as developing a community-based river management plan to reduce the pollution of SPR. Basically, phase 1 of this project focused in improving local community's awareness and knowledge regarding the SPR pollution issue, whereas phase 2 focuses on developing the solutions together with the local communities for reducing the pollution of SPR. Until April 2017, phase 1 of the SPRCEP has been completed. This paper shows the findings from the activities conducted by phase 1 of the project in 2016. The specific objectives of phase 1 of this project were:

i. To raise local community's awareness and improve their knowledge regarding SPR's pollution issue.
ii. To create platform that allows the stakeholders to discuss the solutions for the SPR's pollution issue.

3 THE PROJECT ACTIVITIES AND OUTPUTS

3.1 Water and River Education Program for School Children

A series of water education programs that targeting different groups of the local communities were organised to raise public awareness and knowledge regarding the pollution of SPR. First, Water and River Educational Program that targeting children aged from 9 to 12 years old were organised. This activity aimed to

 ©2017, IAHR. Used with permission / ISSN 1562-6865 (Online) - ISSN 1063-7710 (Print)

raise the awareness of children and their parents on the SPR pollution issue, as well as to instill a sense of attachment and care in the young generation regarding river and water. As the main participants of this activity were children, the activities were conducted at the upstream of SPR, where the water and environment is safer for the children. The children were brought to the river to catch aquatic insects and macro-invertebrates to identify the water quality of the river (Figure 3). After that, a story about the SPR's pollution issue was shared with the parents to raise their awareness on SPR's pollution issue. As a result, a total of 35 children (aged from 9 to 12 years old) and 20 parents participated in this educational program. The kids were expected to have their interest on river protection instilled in their mindset after the program. The parents are expected to have their knowledge and awareness on river conservation improved after the program.

(a) (b)

Figure 3. Water and River Educational Program for School Kids.

3.2 State-Level Inter-School River Quiz Competition for School Students

A state-level interschool river quiz competition was organised for secondary schools in Penang. Students aged from 13 to 15 years old and teachers from secondary schools in Penang State were invited to participate in this quiz. The quiz acts as a tool towards furthering environmental education by offering a platform for teachers and students to learn about the importance of the precious but fragile river and the interactions of society and river, especially on how the negative interactions can harm the river while the positive interactions can conserve and rehabilitate it. A presentation about the issues and challenges of reducing pollution of SPR was given to the participants before the competition started. A total of 88 students from 16 different schools in the Penang State participated in this competition (Figure 4). Students learned about the SPR pollution issue by listening to a presentation given before the competition. Study materials and news articles related to the river conservation and river pollution issue were distributed to the students one month before the quiz. Students were expected to have more knowledge and awareness of the SPR pollution issue after participating in the quiz.

(a) (b)

Figure 4. State-Level Inter-School River Quiz Competition for Secondary School Students.

3.3 River Clean- Up Activity at the SPR for Young Adults

A river clean-up activity was held at the river bank of SPR. This activity not only collected rubbish thrown on the river banks of SPR, but also analysed the types of rubbish collected along the river. A total of 55 young people aged from 16 to 23 years old participated in this activity (Figure 5). This activity was jointly organised with a village committee, with five representatives from the village committee given responsibility to lead the river clean-up. At first, participants collected rubbish thrown along the riverside. After that, the participants

©2017, IAHR. Used with permission / ISSN 1562-6865 (Online) - ISSN 1063-7710 (Print)

analysed the collected rubbish by dividing the rubbish into two categories, *i.e.* recyclable waste (e.g. plastic, bottle, glass, paper, etc.) and non-recyclable waste (e.g. food waste, dirty waste, etc.). A total of 2087 pieces of rubbish were collected, with 88.9 percent of the collected rubbish being the recyclable waste. And among these recyclable wastes, 68.2 percent were plastic, 24.9 percent paper, and the rest were rubber, aluminum, glass and others. At the end of the activity, the participants were divided into different groups for a discussion on the causes and solutions to the SPR's pollution issue.

(a) (b)

Figure 5. Half-day River Clean-up Activity for Young Adults and Village Committee.

3.4 Public Forum on "Clean the Sungai Pinang River, Stop the Pollution at its Source"

A public forum that acted as a platform for the stakeholders to discuss about the solutions of the SPR's pollution issue was organised. Representatives from the Penang State Government, government agencies, NGOs, universities, and local communities were invited to participate in this forum to share their views on the SPR's pollution issue. The forum was officiated by the Penang State Executive Councilor for Local Government, Traffic Management and Flood Mitigation, who is one of the most important policy makers for the Penang State for the aspect of flood mitigation and river management. Five of the invited speakers were the representatives from the state's Department of Environment, Penang Island Municipal Council, Department of Irrigation of Drainage of Penang State, Water Watch Penang and River Engineering and Urban Drainage Research Centre of Universiti Sains Malaysia. A total of 130 participants who were the representatives from the community organisations, government agencies, media, non-governmental organisations, public and university were taking part (Figure 6). The forum discussed the issues and challenges of cleaning SPR. Besides, the presenters also stated that the main source of pollutants identified for the river including waste water from human settlements, industrial waste, and waste from slaughter houses, wet markets and agricultural waste, as well as rubbish thrown along the river. The forum concluded that to effectively clean the SPR, the local stakeholders should stop the pollution at its source instead of cleaning the river after it is polluted.

(a) (b)

Figure 6. Public Forum on "Clean the SPR, Stop the Pollution at its Sources".

3.5 Increasing Awareness Via Video on Social Media

A two-minute awareness raising video named "Save the Sungai Pinang River" was produced. The main aim of the video is to raise public awareness on the SPR pollution issue via mass and social media, which is the current preferred communication tool of the masses. The majority of the actors and actress of the video

 ©2017, IAHR. Used with permission / ISSN 1562-6865 (Online) - ISSN 1063-7710 (Print)

were kids aged from 7 to 10 years old. The purpose is to show that the next generation is very concerned about the SPR's pollution issue as they do not want to inherit a polluted river. This video was then shared on WWP's Facebook page as well as shared through Universiti Sains Malaysia's TV Facebook page. Until 30th March 2017, the video has accumulated about 40,233 views and it had been shared by 1,290 Facebook users. This video is now the most viewed and shared video in Universiti Sains Malaysia's TV Facebook page. The video can be viewed at https://www.facebook.com/USMTV/videos/1005068889543045/. By watching, sharing, and commenting "Save the Sungai Pinang River" Facebook video, Facebook users that have interacted with this Facebook video were expected to have gained some awareness about the SPR pollution issue. Furthermore, spreading of this awareness raising video through Facebook has initiated discussions among Facebook users regarding the issues and challenges of conserving the SPR. Table 2 summarizes SPRCEP's activities, outputs and outcomes.

Table 2. Outputs and Outcomes of SPRCEP Phase 1's Activities.

Activity	Outputs	Expected Outcomes (Contribution Of Activity)
Water & River Educational Program for School Kids	• 35 school children (9-12 years old) and 20 parents.	- Kids' and their parents' interest on river conservation was improved. Their parents were expected to be more aware about the SPR pollution issue.
State-Level Inter-School River Quiz Competition	• 88 secondary school students (13-15 years old).	- Students' knowledge and awareness on river conservation, environmental conservation, and SPR's pollution issue were improved.
Half-day River Clean-up Activity	• 55 young adults (16-23 years old) and five local people.	- Local young people' awareness and knowledge on the causes of the SPR's pollution issue were improved. The types of rubbish thrown along the SPR were identified by the local young adult.
Public Forum on SPR Pollution	• 130 attendees from village committees, government agencies, media, NGOs, public and university.	- Policy makers' and stakeholders' views on the causes of SPR pollution issue, issues and challenges of reducing SPR's pollution were discussed. The forum also served as a learning platform for the stakeholders regarding the possible causes and solution for SPR pollution issue.
Spreading of Awareness Raising Video on Social Media	• 40,233 views and shared by 1,290 Facebook users.	- Spreading of the video raised awareness of the public regarding SPR's pollution issue and fostered discussion among Facebook users regarding the causes and solution of SPR's pollution issue.

4 DISCUSSION

With the 17 Sustainable Development Goals (SDGs) of the 2030 Agenda for Sustainable Development adopted by the world leaders in United Nation Summit in September 2015 (UN, 2016), the involvement of local community in different levels of environmental management, water and river management, disaster management, city planning, etc. has been one of the indicators for sustainability in many countries. Especially in the light of climate change, involving the local stakeholders in river and water management is useful for addressing the complexity and uncertainty inherent in water and river management (Braun, 2010). At the country level, according to the 11th Malaysian Plan, the five-year country plan for 2016 to 2020 advocates the local community involvement in biodiversity conservation, natural resource conservation, green growth, and disaster risk management (EPU, 2015). In recent years, there have been many programs by the federal-state-local governments to improve local people involvement in water and river management. Nevertheless, there are many challenges to effectively engage local stakeholders in river management.

Based on the outcomes and observations made during the project's activities, educating public on river conservation and raising public awareness on the SPR pollution issues can be made via organising a series of water education programs. Referring to SPRCEP, the project demonstrated different approaches of educating local people from different age levels on the SPR pollution issue. For example, organizing indoor/ outdoor education programs, quiz with theme related to river conservation, and river clean-up activity can effectively raise public awareness on SPR pollution issue, especially the young generation. Spreading of awareness raising video through social media can spread the message of conserving SPR faster and is able to reach people faster than organising onsite programs. By spreading the awareness raising video through social media, it can also initiate discussion among users from the social media to discuss the causes of SPR pollution issue and the solution of reducing it. For the public forum, it allowed the stakeholders from different sectors to discuss the causes of river pollution issue and the solution of solving this issue in the same platform.

Nevertheless, challenges were faced to further engage the local community in conserving the SPR. Based on the observation and informal discussion with the participants of the project activities, it was found that most of the young adult and local people that took part in the project activities were aware of the SPR

©2017, IAHR. Used with permission / ISSN 1562-6865 (Online) - ISSN 1063-7710 (Print)

pollution issue. The challenge was in getting them to actively participate in the river conservation. Many participants became more aware of the causes of SPR pollution issue after participating in the river clean up activity. The next two questions are: (i) To find out how many of them will change their behavior to be more environmental friendly, and (ii) To find out how many of the participants will be actively involved in participating or organising activities related to river conservation. Traditionally, many of the community-based river clean-up activities were organised on an ad hoc basis, a mechanism must be created to initiate the actions by the local stakeholders to actively participating in river conservation activity. Policy must be developed to enable environment for local people involvement in river and water management. To overcome this barrier, NGOs, civil society groups, village committees plays a crucial role, for the role of WWP played in the SPRCEP was not only to connect the policy makers with the local stakeholders but also to educate the local people on river conservation and to raise their awareness regarding SPR pollution issue.

During an informal discussion with the representatives from the village committee, many of them responded that they knew the daily activities of the local community are one of the causes of the pollution of SPR. One of the village committee's representative said, "Since I was a kid, I have seen many people throwing rubbishes into this river. We know this river is polluted, but I think it is very difficult to change the mindset of the local community that the surrounding of this river is a dumping site, because we have practiced this since our early age." When discussing about the ways of improving local community participation in river conservation, the same representative from the village committee responded "We seldom see that the platforms provided to the local community to engage us in the decision making for the river conservation strategies. Many of the local communities were not informed regarding the state government's plan for restoring this river." In Malaysia, one of the institutional challenges for successful Integrated River Basin Management (IRBM) and Integrated Water Resource Management (IWRM) implementation is inadequate platforms for local level stakeholders participating in decision and policy making process (Mokhtar et al., 2011; Chan, 2012). For example, the public forum by SPRCEP was organised by WWP on an ad hoc basis, there have not been many similar official platforms organised to connect the local stakeholders with the policy makers for deciding river- and water-related policies and strategies. Even if a dialogue session is organised to discuss river-related matters, it was more like a closed-door meeting, which the public is not invited, as such dialogue is usually attended by the head of village committee. Moreover, there has not been an official online platform by the government on the social media for the public to share and discuss issues related to river and environment.

5 CONCLUSIONS AND PRACTICAL IMPLICATION

The SPRCEP demonstrates approaches for engaging local community in river management. It shows that NGOs not only can play a role in educating public on river conservation and empower local community in river conservation activities, but also can play a role in linking the local community with the policy maker. For young generation of the local community, classroom and outdoor learning activities act as the useful tool to educate kids, teenager, and young adult on river conservation and raise their awareness on river pollution issues. Especially the outdoor activity, the young participants have a chance to learn outside the classroom and gain awareness and sensitivity toward river and environment conservation when they get to go into the river. Secondly, spreading message of river conservation can be done faster by spreading the news through social network. By choosing the right platform in the social media, such message can reach more people in a shorter time as compared to the onsite projects, it is effective for raising public awareness regarding an environment issue. Thirdly, the onsite community engagement activity is suggested to jointly organised with the local stakeholder to ease the resistance of local people to participate in the project's activity. For instance, SPRCEP's river clean-up activity was jointly organised by WWP and the village committee, with the assistance and explanation from the representatives from the village committee. The participants of the river clean-up activity gained more exact information regarding the possible causes of SPR pollution issue. Finally, SPRCEP's public forum demonstrates the approach of engaging multi-stakeholders to discuss the causes of SPR's pollution issue and the solution of solving it in the same platform, it fosters exchange of ideas and learning in between the stakeholders regarding the challenges and solution for reducing SPR's pollution issue.

Based on the lesson learned from this project, some recommendations are given for improving the local community engagement in river management in Malaysia:

a) Indicators must be developed for evaluating the participation rate of local community in various aspects of river management. For example, the number of local people consulted in developing policy related to river and water resource management and the number of local people/ representatives direct involved in state- or municipal-level river-related committee for deciding policy/ strategy.
b) Incentives is suggested to be given to initiate the local community's movement to start organising more river conservation activities. For instance, incentive or acknowledgement can be given to the village committees that keep the riverside clean by organising river clean-up activity.
c) Platforms must be created to enable the local community to have chance to communicate with the technical experts, river management committee, and the high-level policy makers for exchanging their

 ©2017, IAHR. Used with permission / ISSN 1562-6865 (Online) - ISSN 1063-7710 (Print)

views and thoughts regarding river-related issue as well as discussing the solution for solving it. Public forum, workshop, and dialogue can be useful tools for engaging different level of local stakeholder. Besides, online platform can be created to allow the internet users to participate in discussing the solution to river and environmental related issue.

ACKNOWLEDGEMENTS

The project reported herein is funded by Eco-Peace Leadership Centre and Yuhan-Kimberly. The authors would like to thank WWP's staff and volunteer for their involvement in this project.

REFERENCES

Abdullah, K. (2002). Integrated river basin management. *Rivers: Towards Sustainable Development***,** 3-14.

Braun, R. (2010). Social Participation and Climate Change. *Environ Dev Sustain,* 12**,** 777-806.

Chan, N. W. (2005). Sustainable management of rivers in Malaysia: Involving all stakeholders. *International Journal of River Basin Management,* 3**,** 147-162.

Chan, N. W. (2012). Managing Urban Rivers and Water Quality in Malaysia for Sustainable Water Resources. *International Journal of Water Resources Development,* 28**,** 343-354.

DOE (2015). Malaysia Environmental Quality Report 2015. *In:* MALAYSIA, D. O. E. (ed.). Selangor: Department of Environment Malaysia.

EPU (2015). Eleventh Malaysia Plan. *In:* MALAYSIA, G. O. (ed.). Kuala Lumpur: Percetakan Nasional Malaysia Berhad.

Grob, A. (1995). A structural model of environmental attitudes and behaviour. *Journal of Environmental Psychology,* 15**,** 209-220.

Lai, C. H., Chan, N. W. & Roy, R. (2017). Understanding Public Perception of and Participation in Non-Revenue Water Management in Malaysia to Support Urban Water Policy. *Water,* 9**,** 26.

Mokhtar, M., Toriman, M., Hossain, M. A. A. & Tan, K. W. (2011). Institutional challenges for integrated river basin management in Langat River Basin, Malaysia. *Water and Environment Journal,* 25**,** 495-503.

Naemah, F., Saadi, M., Norulaini, N., Rahmani, N. A., Kadi, M. O. A. & Omar, F. M.(2006). Identification of Pollution Sources within the Sungai Pinang River Basin. Malaysian Research Group International Conference, 2006 Manchester, United Kingdom. 478-485.

Padmalal, D. & Maya, K. (2014). Sand Mining. *Environmental Impacts and Selected Case Studies.* Springer Netherlands.

Pahl-Wostl, C. (2002). Towards sustainability in the water sector – The importance of human actors and processes of social learning. *Aquatic Sciences,* 64**,** 394-411.

PROGRAMME, W. W. A. (2009). The United Nation World Water Development Report 3: Water In a Changing World. Paris.

UN.(2016). *The Sustainable Development Agenda* [Online]. Available: http://www.un.org/sustainabledevelopment/development-agenda/ [Accessed 10/04/2017].

Watson, N. (2004). Integrated river basin management: A case for collaboration. *International Journal of River Basin Management,* 2**,** 243-257.

WWP. (2016). *Our Aim* [Online]. Available: http://waterwatchpenang.org/ [Accessed 10/04/2017].

©2017, IAHR. Used with permission / ISSN 1562-6865 (Online) - ISSN 1063-7710 (Print)

Proceedings of the 37th IAHR World Congress
August 13 – 18, 2017, Kuala Lumpur, Malaysia

MULTI-OBJECTIVE RISK ANALYSIS OF RESERVOIR FLOOD CONTROL OPERATION BASED ON COPULA-MONTE CARLO METHOD

YANG PENG[1], ZHIYI WU[2] & KAI CHEN[3]

[1,2,3] School of Renewable Energy, North China Electric Power University, Beijing 102206, China
pengyang@ncepu.edu.cn; wuzhiyi18@foxmail.com; chenkai2014@ncepu.edu.cn

ABSTRACT

Flood control operation of a reservoir system is a multi-objective decision making process and the uncertainty in flood will bring risk to flood control operation. In this study, the flood control risk caused by the uncertainties of floods in mainstream and tributary is investigated, and a multi-objective risk analysis method for explicitly describing the risks of reservoir flood control operation is proposed by using the Copula-Monte Carlo (CMC) method. The joint distribution of the mainstream and tributary is established through the copula function, and the flood hydrographs of mainstream and tributary are calculated according to the peak discharge ratios of the simulated flood to the corresponding observed flood. As a result, flood risk rates and the corresponding objective values are estimated by using Monte Carlo (MC) method through the reservoir flood and multi-objective flood control scheduling on the simulated floods of mainstream and tributary. In addition, Technique for Order Preference by Similarity to an Ideal Solution (TOPSIS) method based on combinational weight is used to evaluate each operation schemes. This method is applied to a case study in Xiangjiaba Reservoir to analyze the risks of flood control operation. A non-inferior set for risk rate of each objective and the corresponding values are obtained, and optimal solutions with different weights are derived. The results demonstrate that the proposed method is a useful tool to reduce the flood risks while maintaining the reservoir benefit, which can provide technical support for multi-objective decision-making of reservoir operation.

Keywords: Multi-objective risk analysis; flood uncertainty; copula-monte carlo method; optimal operation of reservoir flood control; mainstream and tributary.

1 INTRODUCTION

Reservoir flood control operation is an important non-engineering measure for reducing flood losses. It is a typical multi-stage, multi-constraint, and multi-objective decision making problem, of which reservoir safety, flood control objectives at both upstream and downstream, and numerous constraints should be considered. The actual operation sometimes cannnot achieve the expected scheduling targets due to the influences of objective uncertainty of rainfall, flood, structure status, and subjective factors of various anthropogenic scheduling managements. This would not only affect the reservoir safe operation and comprehensive benefits during flood season, but also brings the risk to scheduling decision. Therefore, it is necessary to study the multi-objective risk analysis of reservoir flood control operation.

Since 1980s, several Chinese scholars have studied the risk of reservoir operation and have proposed a series of methods such as probability combination method (Fu et al., 1999), First Order Second Moment method (Zeng et al., 2003), Fault Tree Analysis (Cheng and Chen, 2005), and Monte Carlo (MC) method (Diao and Wang, 2010). Among these approaches, the MC method is often used to estimate the risk caused by the uncertainties of inflow runoff and flood (Diao et al., 2010). For instances, Li et al. (2009) simulated stochastically forecasting error of inflow flood in the Three Gorges Reservoir and made the decisions on the risk of flood control schemes to use the Grey Correlation method. Qin et al. (2011) estimated the risk of reservoir flood control operation under hydrological uncertainty by using MC method, and proposed a multi-attribute risk decision-making method based on relative dominance of the scheme in sorting and selection. On the basis of considering the flood forecasting accidental error and the correlation between the upstream and downstream reservoir inflow, Wang et al. (2014) estimated the flood control risk of cascade reservoirs by using MC Method and maximum entropy theory. Zhou et al. (2010) made the risk analysis on reservoir flood regulation by using MC Method while considering the uncertainty of interval flood, the uncertain relationship between storage capacity and water level, and uncertain discharge capacity. Besides the uncertainty of inflow flood, the uncertainty of inflow in tributaries between reservoir and flood control area downstream would bring certain risks to the flood control area downstream. Yan et al. (2010; 2013) used Copula function to construct the joint distribution of the annual maximum flood occurrence dates, magnitudes and the 15-days flood volume and its interval between Yangtze River and Qingjiang River, and analyzed the flood encountering risk between the two rivers. Liu et al. (2015) established the joint distribution of floods in mainstream and its tributaries based on Copula function, and calculated the flood probabilistic distribution under the influence of upstream reservoir regulation by using MC method. Despite the advanced achievements in the above studies

 ©2017, IAHR. Used with permission / ISSN 1562-6865 (Online) - ISSN 1063-7710 (Print)

where the uncertainty of floods in mainstream and tributaries is considered, the influence of the uncertainty of the floods on reservoir regulation is still rarely studied.

In this paper, the influence of the uncertainties of floods in mainstream and its tributary on reservoir flood control operation is considered, and a Copula-Monte Carlo (CMC) method for multi-objective risk estimation for reservoir flood control operation is proposed. The Copula function is used to describe the joint probability distribution of peak discharges of mainstream and tributary, and the flood hydrographs of mainstream and tributary are calculated according to the peak discharge ratios of the simulated flood to the observed flood correspondingly. In addition, the Monte Carlo (MC) method (Yan et al., 2015; Yan and Moradkhani, 2016a) is used to estimate the flood risk rates and the corresponding objective values based on the reservoir flood multi-objective flood control scheduling on the simulated floods of mainstream and tributary. Next, Technique for Order Preference by Similarity to an Ideal Solution (TOPSIS) method based on combinational weight is used to evaluate each operation schemes. Finally, the proposed method is applied to estimate the multi-objective risk of flood control operation of Xiangjiaba Reservoir, and an optimal operation scheme that balanced the requirements of the upper and lower flood control objectives is obtained.

2 STOCHASTIC SIMULATION OF FLOODS IN MAIN STREAM AND ITS TRIBUTARY

For flooding control downstream of reservoir with tributary streamflow, the safety of flooding control downstream is affected by the reservoir outflow and the encountered tributary flood. Therefore, the floods in the mainstream and tributaries were simulated by CMC method, in which the joint relationship between the two floods was considered.

According to the Sklar theorem (Sklar, 1959), a two-dimensional joint distribution can be formulated through two independent marginal distributions and a Copula function. Flood peak discharges of mainstream and its tributary are termed as random variables X and Y in this study, and their marginal distributions are expressed as $\mathrm{u} = \mathrm{F_X(x)}$ and $\mathrm{v} = \mathrm{F_Y(y)}$, which are uniformly distributed in [0,1]. Thus, the bivariate joint probability distribution of flood peaks of mainstream and its tributary can be calculated by using the Copula function(Guo et al., 2008), which is expressed as

$$F(x, y)=C_\theta[F_X(x), F_Y(y)]=C_\theta(u, v) \quad [1]$$

Where $F(x, y)$ is the joint distribution; θ is Copula parameter to be estimated.

Following the studies of Nelsen (1999) and Salvadori et al. (2007), the conditional distribution function of X given $Y = y$ was expressed as

$$F(x|Y=y)=P(X\leq x|Y=y)=\frac{\partial C(x,y)/\partial y}{dF_Y(y)/dy}=\frac{\partial C(u,v)}{\partial v}=\frac{\partial F(x,y)}{\partial F_Y} \quad [2]$$

The conditional distribution of $F(x|Y = y)$ is also uniformly distributed in [0,1], and the steps about simulation of flood peaks of mainstream and its tributary by using CMC method can be given as follows: firstly, generate the two-dimensional random numbers m_1 and m_2, and make v equal to m_1; secondly, calculate the value of u by solving the equation of $m_2=C(u|v)$; and thirdly, obtain the values of X and Y from their marginal distributions since the marginal distributions u and v were the probabilities that random variables X and Y did not exceed their certain values.

According to the simulated flood peaks of mainstream and its tributary, the flood hydrographs in mainstream and its tributary can be calculated according to the peak discharge ratios of the simulated flood to the observed flood correspondingly for their typical flood processes.

3 OPTIMAL OPERATION OF FLOOD CONTROL

There are three major tasks of reservoir flood control operation, which include ensuring the safety of the dam, alleviating flood disaster downstream of reservoir and reducing the inundation loss on the upper reaches. In this paper, the safeties of reservoir and downstream flood control area were mainly considered. The minimum of the highest water level of reservoir and the minimum flood peak discharge in the downstream flood control area were chosen as objective functions of flood control optimal scheduling model, which can be expressed as follows

$$Z_m=\min(\max Z(t)) \quad [3]$$

$$q\_m=\min(\max(Q\_ck\ (t)+Q\_qj\ (t)) \quad [4]$$

where, $Z(t)$ is the water level of reservoir in the *t*th period, $Q_{ck}(t)$ is the outflow discharge from reservoir in the *t*th period, $Q_{qj}(t)$ is the discharge of interval flood in the *t*th period.

©2017, IAHR. Used with permission / ISSN 1562-6865 (Online) - ISSN 1063-7710 (Print)

The constraints include water balance limit, water releasing ability limit of dam, water level limit at the end of scheduling period, outflow discharge limit, water stage storage capacity limit and flood control regulations etc. (Chen, 2008).

The above multi-objective optimization model can be reduced to a single objective model by using weight coefficient method (Jia et al., 2015) and non-inferior solutions were obtained by solving the model with dynamic programming.

4 ESTIMATION OF RISK RATE

When considering the uncertainties of inflows in mainstream and its tributary, the flood control objective values and their risk rates under different scheduling schemes were the important issues to the decision-makers. Therefore, it was necessary to estimate the risks of each scheduling scheme, and determine the probability of each objective exceeding its safety threshold.

Taking the above obtained flood hydrographs in mainstream and its tributary as input data of the model, the highest water level series $\{Z_m\}$ and the maximum discharge series $\{q_m\}$ under different scheduling schemes can be obtained by solving the above flood control optimal scheduling model (Eqs. [3] and [4]). Risk probabilities of both reservoir and flood control downstream can be estimated with the number of times that the highest water level and the maximum discharge exceeded their safety thresholds, which were upper water level for flood control and safety discharge of flood control point respectively.

5 MULTI-OBJECTIVE RISK DECISION- MAKING

The aim of reservoir flood control optimal operation is to maximize the flood control benefit with minimizing the losses caused by flood as much as possible. It is necessary to evaluate flood control schemes and get an optimal scheme. Both target values and risks of each scheme should be considered during the evaluation. In this paper, mean values of the highest water level series and the maximum discharge series and risk probabilities of reservoir and the flood control were regarded as decision-making indexes.

There are many methods for comprehensive evaluation of non-inferior schemes in multi-objective decision-making. To get the maximal flood control benefit, Technique for Order Preference by Similarity to an Ideal Solution (TOPSIS) method (Yue, 2003) is an effective evaluation method that can reflect the closeness degree between the objective value and the optimal value. Due to the different relative importance of each target, TOPSIS method were combined with weighing coefficients of evaluation index, in which both subjective weight and objective weight were considered. This method is called TOPSIS method based on combinational weight.

The whole decision-making process was divided into two steps: firstly, calculate combination weight as $w_j=\alpha w_{zj}+(1-\alpha)w_{kj}$, in which w_{zj} is subjective weight determined by analytic hierarchy process (AHP), w_{kj} is objective weight determined with entropy method (Wang et al., 2011), and α is empirical factor and $0 \leq \alpha \leq 1$, which reflects a decision-maker's preference for the subjective consideration and the objective (Wang & Yang, 2010); and secondly, rank the preference order of the non-inferior schemes by using TOPSIS method based on combination weight, and select the optimal one.

6 A CASE STUDY

Xiangjiaba Reservoir, which is located in the lower reach of Jinsha River, was selected for a case study. Xiangjiaba hydropower project is the third-largest hydropower plant in China. Its primary purpose is hydroelectric power generation with an installed capacity of 7,750 MW. Additionally, as a reverse regulation reservoir of the upstream Xiluodu project, Xiangjiaba hydropower project provides for flood control, sediment deduction, and improving navigation conditions at both upstream and downstream. The reservoir normal capacity is 51.63×10^8 m^3 with flood control capacity of 9.03×10^8 m^3. Min River, a branch of Jinsha River, mingles with Jinsha River at about 29.7 kilometers upstream of the dam. There is a flood control point, named Lizhuang Station, located about 45.2 kilometers downstream of Xiangjiaba Reservoir. The coincidence of floods of Jinsha River and Min River will increase the flood risk of Lizhuang Station. For the flood protection downstream of Xiangjiaba Reservoir, the discharge of Lizhuang Station is required to not exceed its safety rate (40,000 $m^3 \cdot s^{-1}$). Their locations are shown in Figure 1.

 ©2017, IAHR. Used with permission / ISSN 1562-6865 (Online) - ISSN 1063-7710 (Print)

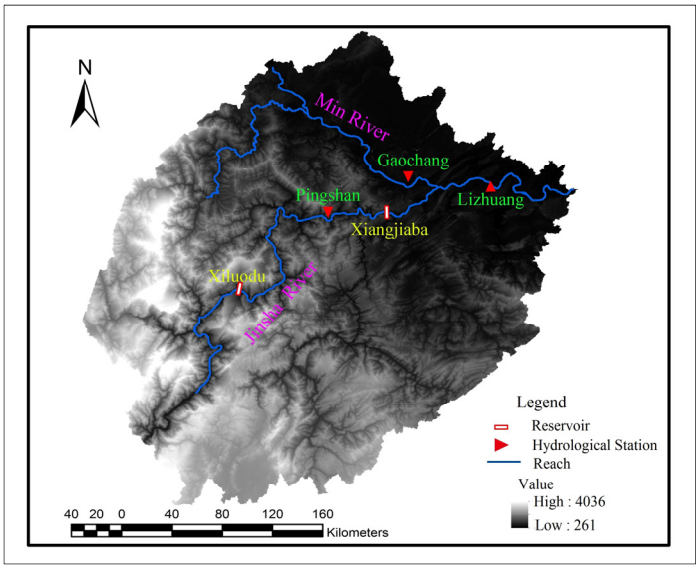

Figure 1. Location of the studied reservoir.

The data used for fitting the marginal distributions of peak discharges of Jinsha River and Min River were from two hydrological stations, namely Pingshan and Gaochang, which are located in Jinsha River and in Min River, respectively (Fig. 1). Annual flood series were extracted from the daily average streamflow records of the two stations in the period from 1950 to 2010 (61-year long time series) and historical flood data (Wang, 1999; Xiao and Zhao, 2002). The Pearson Type III (P3) Distribution was used to quantify the marginal distributions, and parameters of the P3 distributions were estimated by the L-moment method (Hosking and Wallis, 1997; Yan and Moradkhani, 2015; 2016b). The chi-squared goodness-of-fit test was performed to test the validity of the assumption (H_0) that the flood peak followed the P3 distribution. Parameters and hypothesis test results of the P3 distributions were given in Table 1.

Table 1. Parameters and hypothesis test results of P3 distributions.

Control Station	Mean Value $/m^3 \cdot s^{-1}$	Shape	Scale	Location	χ^2 Test
Pingshan	17,871	2.778	0.000,311	8,935.51	3.21 (5.99)
Gaochang	17,068	2.441	0.000,262	7,733.94	3.68 (5.99)

It can be seen from Table 1 that the value of chi-squared test statistic does not exceed the critical value, which means that the assumption (H_0) is valid at the 0.05 significance level. Videlicet, the P3 distribution is valid for flood peaks at the two sites.

The dependence of AM flood series of the two stations was estimated. Empirical estimation value of the bivariate Kendall's tau (τ) of peak discharges is 0.123. This means that the correlation between the two variables is positive, and Clayton copula was therefore used to describe their joint distribution. The formula of the bivariate Clayton copula is given as

$$C(u, v)=\left(u^{-\theta}+v^{-\theta}-1\right)^{-1/\theta} \quad [5]$$

where θ is parameter of Clayton copula which is calculated according to $\tau = \theta/(2+\theta)$ (Nelsen 1999).

With $\tau = 0.123$, the computed value of parameter of Clayton copula (θ) is 0.28. Hence the joint probability distribution of peak discharges of the two rivers can be stated as follows

$$F(x,y)=\left[F_X(x)^{-0.28}+F_Y(y)^{-0.28}1\right]^{-1/0.28} \quad [6]$$

where $F_X(x)$ and $F_Y(y)$ are marginal distributions of peak discharges of Jinsha River and Min River, respectively.

A set of flood peaks of Jinsha River and Min River with 10,000 MC probabilities were simulated by using the above CMC method, which is shown in Figure 2. The flood occurred in the period from August 8 to September 6 in 1998 was selected as a typical case in this study. A set of 10,000 MC flood hydrographs of Jinsha River and Min River can be obtained by multiplying the value of discharge by the peak discharge ratios of the simulated flood to the observed flood.

©2017, IAHR. Used with permission / ISSN 1562-6865 (Online) - ISSN 1063-7710 (Print)

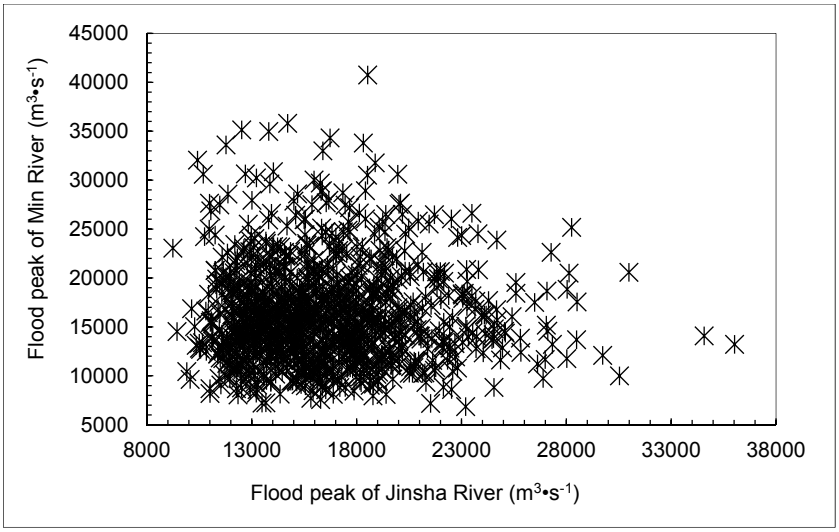

Figure 2. Simulated flood peaks of Jinsha River and Min River.

Nine sets of 10,000 non-inferior solutions were obtained by solving the above flood control optimal scheduling model (Eq. (3) and (4)) with the input data of the 10,000 MC flood hydrographs of Jinsha River and Min Rive. The mean of each set of 10,000 non-inferior solutions can be regarded as the target values of flood control operation under each non-inferior scheme, which are shown in Figure 3.

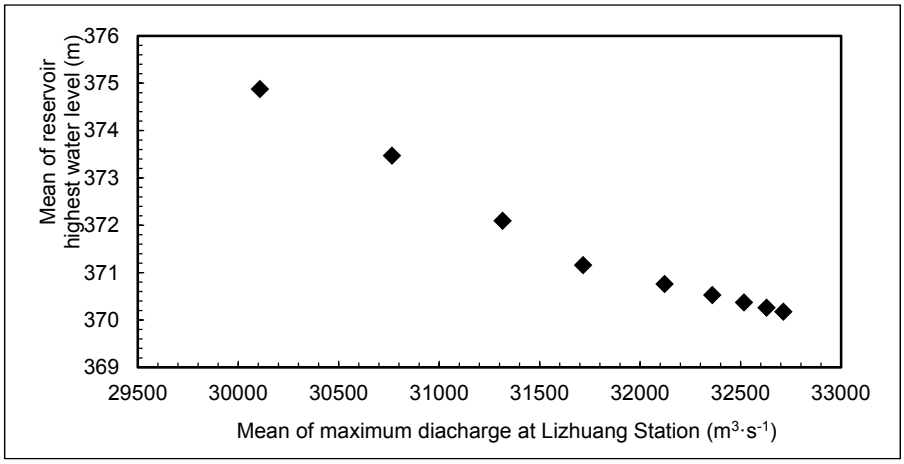

Figure 3. Non-inferiority between target values of flood control operation in Xiangjiaba Reservoir.

For Xiangjiaba Reservoir, the upper water level for flood control is 380 m and the safety discharge at Lizhuang Station is 40,000 $m^3 \cdot s^{-1}$. Risk probabilities of reservoir and the flood control downstream under each non-inferior scheme can be estimated with the numbers of times that the highest water level of reservoir and maximum discharge at Lizhuang Station exceeded 380 m and 40000 $m^3 \cdot s^{-1}$, respectively, according to each set of 10,000 non-inferiority solutions. The target values and risk rates of flood control operation under each non-inferiority scheme were shown in Table 2.

Table 2. Target values and risk rates under each non-inferior scheme.

Non-inferior Schemes	Highest Water Level of Reservoir		Maximum Discharge at Lizhuang Station	
	Mean Value ($m^3 \cdot s^{-1}$)	Risk Rate (%)	Mean Value ($m^3 \cdot s^{-1}$)	Risk Rate (%)
1	370.32	0.02	32,576.3	12.31
2	370.47	0.02	32,428.3	11.81
3	370.65	0.03	32,238.2	11.09
4	370.90	0.03	31,982.2	10.37
5	371.26	0.03	31,615.8	9.15
6	371.87	0.03	31,386.2	8.68
7	373.26	0.53	30,860.8	7.56
8	375.26	1.92	29,929.6	5.64
9	377.45	4.08	28,971.1	4.03

 ©2017, IAHR. Used with permission / ISSN 1562-6865 (Online) - ISSN 1063-7710 (Print)

It can be shown in Table 2 that from scheme 1 to scheme 9, the highest water level and the corresponding risk rate increase, while the maximum discharge at Lizhuang Station and the corresponding risk rate decrease. A higher water level of reservoir results in a greater risk to the reservoir, a smaller flow discharger at Lizhuang Station, and a smaller risk of flood control area downstream.

The target values and risk rates in Table 2 are regarded as original decision-making indexes, which are cost-type indicators. The indexes can be normalized according to the standard 0-1 transformation (Grus, 2015), and their normalized values are shown in Table 3.

Table 3. Normalized decision-making indicators.

Non-inferior schemes	Highest Water Level of Reservoir		Maximum Discharge at Lizhuang Station	
	Mean Value	Risk Rate	Mean Value	Risk Rate
1	1	1	0	0
2	0.980	1	0.041	0.060
3	0.953	0.998	0.094	0.147
4	0.918	0.998	0.165	0.234
5	0.867	0.998	0.266	0.385
6	0.782	0.998	0.330	0.438
7	0.588	0.874	0.476	0.574
8	0.307	0.532	0.734	0.803
9	0	0	1	1

The objective weights of each decision-making index were calculated by entropy method according to their normalized values shown in Table 3. Two set of subjective weights of decision-making index were given according to two kinds of decision's preferences: whether preference is on the safety of reservoir or on the safety of flood control area of downstream. The empirical factor in combination weight calculation was set as 0.5. The coefficients of objective weights, subjective weights and combination weights of decision-making indexes are shown in Table 4.

Table 4. Weights of different evaluation index.

Objective Weights	Preference on Safety of Reservoir		Preference on Safety of Downstream	
	Subjective Weights	Combination Weights	Subjective Weights	Combination Weights
0.295	0.40	0.312	0.25	0.237
0.281	0.20	0.201	0.15	0.176
0.223	0.25	0.273	0.40	0.348
0.201	0.15	0.216	0.20	0.241

The optimal scheme were obtained by ranking the preference order of the non-inferior solutions in Table 2 using TOPSIS method based on combination weight, and the computed preference orders are shown in Table 5.

Table 5. Orders of non-inferior schemes.

Non-inferior Schemes	Preference on Safety of Reservoir		Preference on Safety of Downstream	
	Closeness	Order	Closeness	Order
1	0.516	8	0.488	9
2	0.525	7	0.496	8
3	0.539	6	0.509	7
4	0.557	4	0.527	6
5	0.592	2	0.562	4
6	0.598	1	0.574	3
7	0.591	3	0.597	2
8	0.547	5	0.607	1
9	0.484	9	0.540	5

It can be seen from Table 5 that the optimal scheme differs from the interests of decision-makers. When the decision-makers paid more attention on the safety of reservoir, the weight of the highest water level of reservoir is bigger than the other three indexes. Therefore, the optimal scheme is scheme 6 with a lower water level and a smaller risk of reservoir, which has a great discharge and a greater risk of flood control area downstream. When decision-makers paid more attention on the safety of flood control area downstream, the weight of the maximum discharge at Lizhuang Station is bigger than the other three indexes, so the optimal

©2017, IAHR. Used with permission / ISSN 1562-6865 (Online) - ISSN 1063-7710 (Print)

scheme is scheme 8 with a smaller discharge and a smaller risk of flood control area downstream, which has a higher water level and a higher risk of reservoir. Therefore, different weights embody the interests of decision-makers on the safeties of reservoir and downstream. The optimal scheme is a balanced scheme for the safeties of reservoir and downstream.

7 CONCLUSIONS

This paper proposed a Copula-Monte Carlo method for multi-objective risk analysis on reservoir flood control operation, where the uncertainties of floods in mainstream and its tributary are considered as the main risk factors. The Copula-Monte Carlo method was used to simulate the floods in mainstream and its tributary, in which the joint relationship between the two floods was considered. Flood risk rates and the corresponding objective values were estimated by using Monte Carlo (MC) method through the reservoir flood multi-objective flood control scheduling on the simulated floods of mainstream and tributary, and the optimal scheme was selected by using TOPSIS method based on combination weight. The main conclusions of this study are summarized as follows: (1) the presented method can estimate, evaluate and make decision on the risks caused by the uncertainties of floods in main stream and its tributary in the reservoir flood control operation, which can help decision-makers to formulate an optimal scheme with consideration of both benefits and risks; (2) a lower discharge rate in the flood control area downstream resulted in a smaller risk that the discharge exceeds its safety discharge, but the highest water level of reservoir and its risk that exceed its upper water level for flood control will be increased. Therefore, the decreased discharge in the flood control area downstream resulted in an increased risk of reservoir; and (3) the optimal scheme differed with the interests of decision-makers. Decision-makers need to handle the contradiction of the safeties between reservoir and flood control area downstream with more care when evaluating the schemes.

ACKNOWLEDGEMENTS

The research reported herein is funded by the National Natural Science Foundation of China (51679088 and 51179069), National Key R&D Program of China (2016YFC0402308 and 2016YFC0402309), and CRSRI Open Research Program (CKWV2015201/KY).

REFERENCES

Chen, S.L. (2008). *Operation and Scheduling of Hydropower Station*. Beijing: China Electric Power Press.

Cheng, W.S. & Chen, J. (2005). Systematic Risk Evaluation Model for Flood-Control System. *Advances in Water Science*, 01, 114-120.

Diao, Y.F. & Wang, B.D. (2010). Risk Analysis of Flood Control Operation Mode with Forecast Information Based on a Combination of Risk Sources. *Science in China: Technology and Science*, 53, 1949−1956.

Fang, Z.G., Liu, S.F. & Zhu, J.J. (2009). *Decision Theory and Method*. Beijing: Science Press.

Fu, X., Wang, L.P. & Ji, C.M. (1999). Estimating Flood Hazard Risk value of Flood Control Region under Flood Encountering Combination. *Hydroelectric Energy*, 04, 23-26.

Grus, J. (2015). *Data Science from Scratch*: *First Principles with Python*. O'Reilly Media, Inc.

Guo, S.L., Yan, B.W., Xiao, Y., Fang, B. & Zhang, N. (2008). Multivariate Hydrological Analysis and Estimation. *Journal of China Hydrology*, 03, 1-7.

Hosking, J.R.M. & Wallis, J.R. (1997). *Regional Frequency Analysis: An Approach Based on L-moments*. Cambridge University Press, Cambridge.

Jia, B.Y., Zhong, P.N., Chen, J. & Wu, Y.A. (2015). Coordinated Optimal Operation Model of Complex Flood Control System. *Advances in Water Science*, 04, 560-571.

Li, Y.H., Zhou, J.Z., Zhang, Y.C., Liu, L. & Qin, H. (2009). Risk Decision Model for the Optimal Operation of Reservoir Flood Control and Its Application. *Water Power*, 04, 19-21.

Liu, Z.J., Guo, S.L., Hu, Y., Yang, G. & Ying, J.B. (2015). Flood Probability Distribution Estimation under the Influence of Upstream Reservoir Regulation Based on Monte Carlo Method. *Water Power*, 08, 17-22.

Nelsen R.B. (1999). *An Introduction to Copulas*. Springer, New York.

Qin, H., Li, Q.Q. & Zhou, J.Z. (2011). A Multi-Attribute Risk Decision-Making Method Based on Relative Dominance for Reservoir Flood Control Operation. *Journal of Yangtze River Scientific Research Institute*, 12, 58-63.

Sklar, A. (1959). *Fonctions de Répartition à n Dimensions et Leurs Marges*. Publ. l'Institut Stat. l'Université Paris 8, 229–231.

Wang, H.B. & Yang, X. (2010). A New Method of Ascertaining Weight Based on Analytic Hierarchy Process and Rough Set Theory. *Journal of Safety Science and Technology*, 06, 155-160.

Wang, L.F. (1999). Overview of the Jinsha River's Historical Floods Features. *Sichuan Water Conservancy*, 20(3), 46-48.

Wang, L.P., Huang, H.T., Zhang, Y.K. & Xu A.N. (2014). *Flood Control Risk Estimate Model of Cascade Reservoirs*, China Rural Water and Hydropower.

Wang, L.P., Zhang, Y.K., Ji, C.M. & Li, J.Q. (2011). Risk Calculation Method for Complex Engineering System. *Water Science and Engineering*, 4(3), 345-355.

 ©2017, IAHR. Used with permission / ISSN 1562-6865 (Online) - ISSN 1063-7710 (Print)

Xiao, T.G. & Zhao, T.Y. (2002). Floods in The Min River. *Express Water Resources and Hydropower Information*, 23(2), 29-30.

Yan, B.W., Guo, S.L. & Yu, W. (2013). Coincidence Risk of Flood Hydrographs between Yangtze River and Qing River. *Journal of Hydroelectric Engineering*, 01, 50-53.

Yan, B.W., Guo, S.L., Chen, L. & Liu, P. (2010). Flood Encountering Risk Analysis for Yangtze River and Qingjiang River. *Journal of Hydraulic Engineering*, 05, 553-559.

Yan, H. & Moradkhani, H. (2015). A Regional Bayesian Hierarchical Model for Flood Frequency Analysis. *Stochastic Environmental Research and Risk Assessment,* 29(3), 1019-1036.

Yan, H., DeChant, C.M. & Moradkhani, H. (2015). Improving Soil Moisture Profile Prediction with the Particle Filter-Markov Chain Monte Carlo method. *IEEE Transactions on Geoscience and Remote Sensing*, 53(11), 6134-6147.

Yan, H. & Moradkhani, H. (2016a). Combined Assimilation of Streamflow and Satellite Soil Moisture with the Particle Filter and Geostatistical Modeling. *Advances in Water Resources*, 94, 364–378.

Yan, H. & Moradkhani, H. (2016b). Toward More Robust Extreme Flood Prediction by Bayesian Hierarchical and Multimodeling. *Natural Hazards*, 81(1), 203-225.

Yue, C.Y. (2003). *Decision Theory and Method*. Beijing: Science Press.

Zeng, Y.H., Hu, M.L. & Liang, Z.C. (2003). Threshold Value and Risks Analysis for Flood Control System. *Journal of Wuhan University of Hydraulic and Electric Engineering*, 06, 27-30.

Zhou, Y.L. & Mei, Y.D. (2010). Risk Analysis for Flood Regulation Based on Copula Function and Monte Carlo Method. *Water Resources and Power*, 08, 37-39.

©2017, IAHR. Used with permission / ISSN 1562-6865 (Online) - ISSN 1063-7710 (Print)

Proceedings of the 37th IAHR World Congress
August 13 – 18, 2017, Kuala Lumpur, Malaysia

SPATIAL WATER QUALITY VULNERABILITY ASSESSMENT OF HAN RIVER BASIN USING MULTI-CRITERIA DECISION MAKING METHOD

PATRICIA JITTA ABDULAI[1],EUN-SUNG CHUNG[2] & YEONJOO KIM[3]

[1,2] Department of Civil Engineering, Seoul National University of Science and Technology, Seoul 01811, Korea, eschung@seoultech.ac.kr; patriciajabdulai@gmail.com
[3] Department of Civil and Environmental Engineering, Yonsei University, Seoul 03722, Korea, Yeonjoo.kim@yonsei.ac.kr

ABSTRACT

Assessing water resources vulnerability is very significant to keep water resources safely in a basin. This study uses the three sub-components of vulnerability as defined and suggested by the IPCC (i.e. exposure, sensitivity, and adaptive capacity). The aim of this study is to compare the significance of using different weighting methods to assess the spatial water quality vulnerability in the Han River Basin using TOPSIS among the multi-criteria decision making (MCDM) methods and applied to the unit basin including indicators of hydrological and socio-economic factors. Thirteen (13) water quality indicators are selected to quantify the vulnerability using the Technique for Order of Preference by Similarity to Ideal Solution approach (TOPSIS). Environmental and socioeconomic data are obtained from the national statistics database and is used to simulate results by the Soil and Water Assessment Tool (SWAT) model. The results shows relatively high maximum consecutive dry days with distinct distribution of water quality indices. Therefore, this study shows the significance of comparing Subjective and objective weights in order to help decision makers of spatial water quality vulnerability in prioritization of water sustainability and water policy planning in maintaining the water quality in the Han River basin.

Keywords: Water quality vulnerability; Han River basin; TOPSIS; shannon entropy.

1 INTRODUCTION

The Han River basin is the biggest basin of South Korea with an area of (34,428 km2) approximately a quarter of the country and located in the middle of the Korean peninsula at 36º30'-38º55' N and 126º24'-129º02' E, including part of North Korea. The basin consists of two metropolitan cities (Seoul, and Incheon) and four provinces (Gyeonggi-do, Gangwon-do, Chungcheongbuk-do, and Gyeongsangbuk-do). This study constructed 237 unit sub-basins across the Han River basin and applied our index for a total 205 unit sub-basins, disregarding nearby areas including North Korea. In addition, the Han River basin was divided into four sub-regions, Imjin-River (W1), North Han-River (W2), South Han-River (W3), and Han-River (W4), as shown in Figure 1.

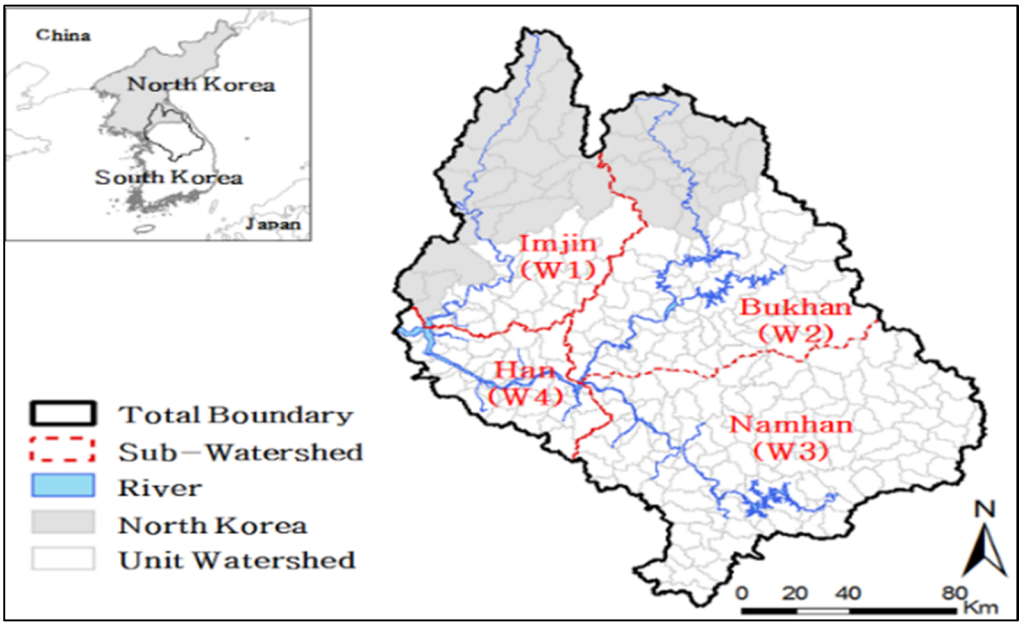

Figure1. Illustration of the study area (Han River basin).

©2017, IAHR. Used with permission / ISSN 1562-6865 (Online) - ISSN 1063-7710 (Print)

The basin has a population of about 24 million including densely populated area of Seoul metropolitan. The quality of water in the Han River basin has continued to deteriorate due to increasing economic activities in the basin altering the landscape which has substantial influence on basin hydrology and water quality. This leads to variation of river ecosystem and also threatens public health and socio economic sustainability. With reference to that, water quality along with hydrology in the Han River basin, plays an important role in the spatial dynamics of a range of ecological patterns and processes which is also often a key component of river health assessments. Hence this draws us to the focus in this study.

Moreover, vulnerability is generally used to describe a weakness or flaw in a system, and its susceptibility to a specific threat and harmful event. Spatial water resources vulnerability including water quantity and quality using various approaches has been frequently assessed in a quantitative manner. (Chung et al., 2009; Jun et al., 2011; Adger et al., 2004; Chung et al., 2014; IPCC, 2001; UN/ISDR, 2004; Gleick, 1990; Eakin, 2003). Common to most is the concept that vulnerability is a function of the exposure and sensitivity of a system to a climate hazard and the ability to adapt to the effects of the hazard (Eakin and Luers, 2006; Adger et al., 2004). The International Strategy for Disaster Reduction (UN/ISDR) defines vulnerability as the conditions determined by physical, social, economic and environmental factors or processes which increase the susceptibility of a community to the impact of hazards UN/ISDR, (2004), whereas the IPCC defined vulnerability as a function of the character, magnitude, and rate of climate variation to which a system is exposed, its sensitivity and its adaptive capacity IPCC (2001). For the purpose of this study, we follow the IPCC definition of vulnerability.

Many researches are underway to assess water resources vulnerability using existing data. Wang et al. (2012), collects key elements of water resource vulnerability watershed in the northern part of China. Kim and Chung (2014) quantify water quantity and water quality vulnerability using TOPSIS and taking into consideration various climate scenarios. Kim et al. (2012) uses Fuzzy-TOPSIS and weighted sum method to measure flood weakness and performed quantified rank correlation analysis. KEI (2014) developed a sustainable water use index wherein sulfur was assessed and verification of global water use index was conducted. Moreover, many of the indicators used are to ensure the reliability of calculating weights and applied them in various ways.

Nevertheless, the aim of this study is to compare the significance of using different weighting methods to assess the spatial water quality vulnerability in the Han River Basin using TOPSIS among the multi-criteria decision making (MCDM) methods and applied to the unit basin including indicators of hydrological and socio-economic factors. The integrated vulnerability indices were quantified using the Technique for Order of Preference by Similarity to Ideal Solution approach (TOPSIS). Likewise, to determine the weight of each criterion, Delphi weights and Shannon's entropy methods were used to include various opinions. Hence, this study investigates the significance of comparing subjective weights with objective weights) to water quality vulnerability giving an understanding in terms of decision making and prioritization of water resource vulnerability planning.

2 MATERIALS AND METHODS

2.1 Procedure

As mentioned earlier, we follow the IPCC-based vulnerability framework in this study wherein vulnerability (V) can be numerically defined as follows:

$$V = \alpha \times E + \beta \times S - \gamma \times AC \qquad [1]$$

where α, β and γ are the weights for E, S and AC, respectively.

The study used four steps as shown in Figure 2 below. First, we select all available and appropriate vulnerability indicators that objectively describe the hydrologic condition. Second step, we construct all dataset of sub-basins for the all indicators. Third, derivation of objective and subjective weighting values using entropy and Delphi methods and lastly was to quantify the vulnerability using TOPSIS method with all combined weighting value sets with objective and subjective values.

©2017, IAHR. Used with permission / ISSN 1562-6865 (Online) - ISSN 1063-7710 (Print)

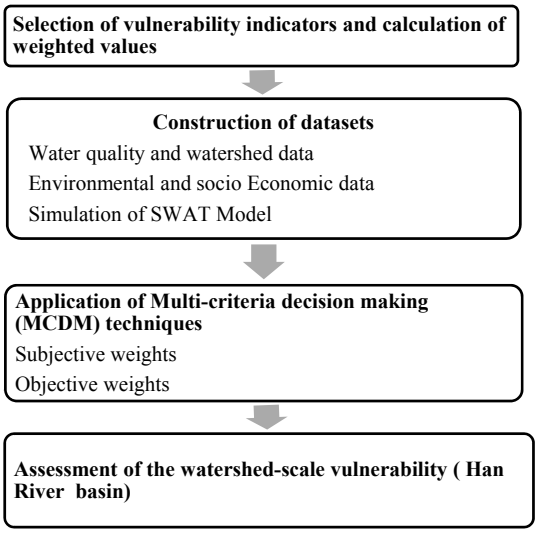

Figure 2. Procedure of spatial water quality vulnerability used in this study.

2.2 Weights determination

In the MCDM process, the relative levels of importance of multiple objectives to system-level performance have to be determined. This study used two different weights: objective weights from Shannon entropy method and subjective weights from Delphi technique. Subjective methods determine weights based on the preference or judgments of the decision makers. Entropy is generally understood as a measure of uncertainty in the information, as defined by Shannon and Weaver (1948). It indicates that a broad distribution represents more uncertainty than does a sharply peaked one Deng et al. (2000). The author further states that, objective weighting is particularly applicable if reliable subjective weights cannot be obtained. In the entropy-based weighting approach, greater entropy values result in smaller entropy weights, smaller differences of alternatives in this specific criterion, less information provided by the specific criteria and less importance of this criterion in the decision-making (Zou et al., 2006; Wang and Lee, 2009). This paper used Shannon entropy-based weights (Wang and Lee, 2009) as an objective weighting approach which are determined using Eq. [1], [2], and [3]. For the MCDM problem with criteria C_i (*i=1… m*) and alternative A_j (*j=1… n*), the best x_i^* and worst x_i^- values of all of the criteria functions are determined according to the benefit and cost functions. Thus, the normalized performance is calculated using Eq. [1] Shannon (1948):

$$r_{ij} = \frac{x_{ij} - x_i^-}{x_i^* - x_i^-} \quad [2]$$

The entropy of ith indicator is defined as:

$$H_i = -k \sum_{j=1}^{n} f_{ij} \ln f_{ij} \quad [3]$$

where $f_{ij} = r_{ij} / \sum_{j=1}^{n} r_{ij}$; $k = 1/\ln n$ and is assumed when $f_{ij} = 0$; $f_{ij} \ln f_{ij} = 0$. The entropy-based weight of *i*th indicator could be defined as:

$$w_i^{ent} = \frac{1 - H_i}{m - \sum_{i=1}^{m} H_i} \quad [4]$$

where $0 \le w_i^{ent} \le 1, \sum_{i=1}^{m} w_i^{ent} = 1$

2.3 Technique for Order Performance by similarity to Ideal Solution (TOPSIS)

The TOPSIS method developed by Hwang and Yoon (1981) is based on order preference by similarity to the ideal solution. It is a rational and relatively simple method where the underlying concept is that the most preferred alternative should not only have the shortest distance from 'ideal' solution, but also the longest distance from an 'anti-ideal' solution. The technique is based on the concept that the ideal alternative has the best values for all attributes, whereas the negative ideal is the alternative with all of the worst attribute values.

The chosen alternative should have the ''shortest distance" from the ideal solution and the ''farthest distance" from the ''negative-ideal"

Given the normalized performance matrix in Eq. [3], the weighted normalized value v_{ij} is calculated as follows:

 ©2017, IAHR. Used with permission / ISSN 1562-6865 (Online) - ISSN 1063-7710 (Print)

$$v_{ij} = w_j \times r_{ij} \quad [5]$$

Then the weighted normalized matrix $V = [v_{ij}]_{mxn}$ is constructed. Then, positive ideal solutions (PIS) A^+ and negative ideal solutions (NIS) A^- are calculated as follows:

$$A^+ = (v_1^+, v_2^+, \ldots, v_n^+) \quad \& \quad A^- = (v_1^-, v_2^-, \ldots, v_n^-)$$

$$\text{where } v_j^+ = \max_i v_{ij} \quad \& \quad v_j^- = \min_i v_{ij} \quad [6]$$

Here the PIS (NIS) for each criterion is the maximum (minimum) of weighted normalized values regardless of benefit and cost criteria, as they are already considered in the normalization process.

3 RESULTS AND DISCUSSIONS

3.1 Identification of vulnerability Indictor

Identification of the key indicator of water quality sector under the IPCC (2001) vulnerability concept consisting of Exposure, Sensitivity and Adaptive capacity was carried out in this study involving specialist discussions, researchers and civil servants with a total of 13 indicators of water quality as shown in Table 1. Water quality of climate-related indicators were chosen as many environmental phenomena such as heat waves and droughts which could potentially cause water-quality problems. Sensitivity except for forest area ratio and all proxies were positively related to vulnerability. The forested area tends to minimize surface runoff, soil erosion and thus sediment transport, tending to lead the system in resilience to climate and adaptive capacity

Table 1. Descriptions of water quality indicators (Chung et al., 2016).

Criteria		Indicator		Description of indicator	Reference	Period
Exposure	Climate	B1	Consecutive dry days (day)	Maximum number of consecutive days with daily precipitation < 1 mm	KMA	2010-2014
		B2	Heat wave days (day)	Number of days with maximum temperature > 33°C		
	Pollution sources	B3	Nitrogen loading (kg/km²/day)	Nitrogen pollutant load	KEI	2009-2011
		B4	Phosphorus loading (kg/km²/day)	Phosphorus pollutant load		
		B5	Sediment loading (g/m²·yr)	Amount of potential soil loss	KEI, ME	
		B6	BOD loading (kg/km²/day)	Biochemical Oxygen Demand	KEI	
Sensitivity	Watershed environment	B7	Forest (%)	Ratio of forest area	ME	2008
	Water supply	B8	Sewerage distribution rate (%)	Ratio of population receiving sewerage system services	ME	2013
		B9	River water use (%)	Ratio of annual water demand and average annual runoff	MOLIT, SWAT	2011, 2005-2014
Adaptive capacity	Water supply	B10	Waterworks distribution rate (%)	Ratio of population receiving waterworks supply	ME	2013
	Economy	B11	Fiscal self-reliance ratio (%)	Ratio of the local government's own revenue to its total revenue expenditure	MOI	2015
		B12	GRDP (10^8won)	Gross regional domestic product	KOSIS	2013
	Governance	B13	Number of official for water management (person/km²)	Number of official for water management (Waterworks and Sewerage)	ME	2013

KMA : Korea Meteorological Administration, KEI : Korea Environment Institute, ME : Ministry of Environment, WAMIS : Water Management Information System, MOLIT : Ministry of Land, Infrastructure and Transport, MOI : Ministry of the Interior, KOSIS : Korean Statistical Information Service, SWAT : SWAT modeling result

©2017, IAHR. Used with permission / ISSN 1562-6865 (Online) - ISSN 1063-7710 (Print)

3.2 Data collection and standardization

The data on selected indicators of water quality as described in Table 1 were provided by the administrative district of source materials and were utilized for statistical data of the country's report. Hydrologic data for water quality were obtained from SWAT simulations. All values of selected indicators are incommensurable because of their different units. Therefore, values of indicators were individually normalized as shown in Figure 3. According to the distribution, the raw data was logarithmically transformed. In addition, some indicators of exposure and sensitivity of the overall index (effective rainfall, groundwater, forest cover rate, sewerage penetration) were standardized to fit the orientation of the vulnerability. Higher values indicate weaker vulnerabilities and are therefore vulnerable. The forested area tends to minimize surface runoff, soil erosion and, thus, sediment transport, tending to lead the system in resilience to climate change and variability. In addition, the results show relatively high contaminant loadings, and low penetration sewer as show in (Figure 3 B5). The result also shows that, high dry consecutive dry days, heat waves and water works distribution rate which are important factors in terms of water quantity vulnerability which could also potentially cause water quality problems with low phosphorus nitrogen loadings which are significant in river health assessments as they determine the conditions of aquatic life. (Figure B3, B4).

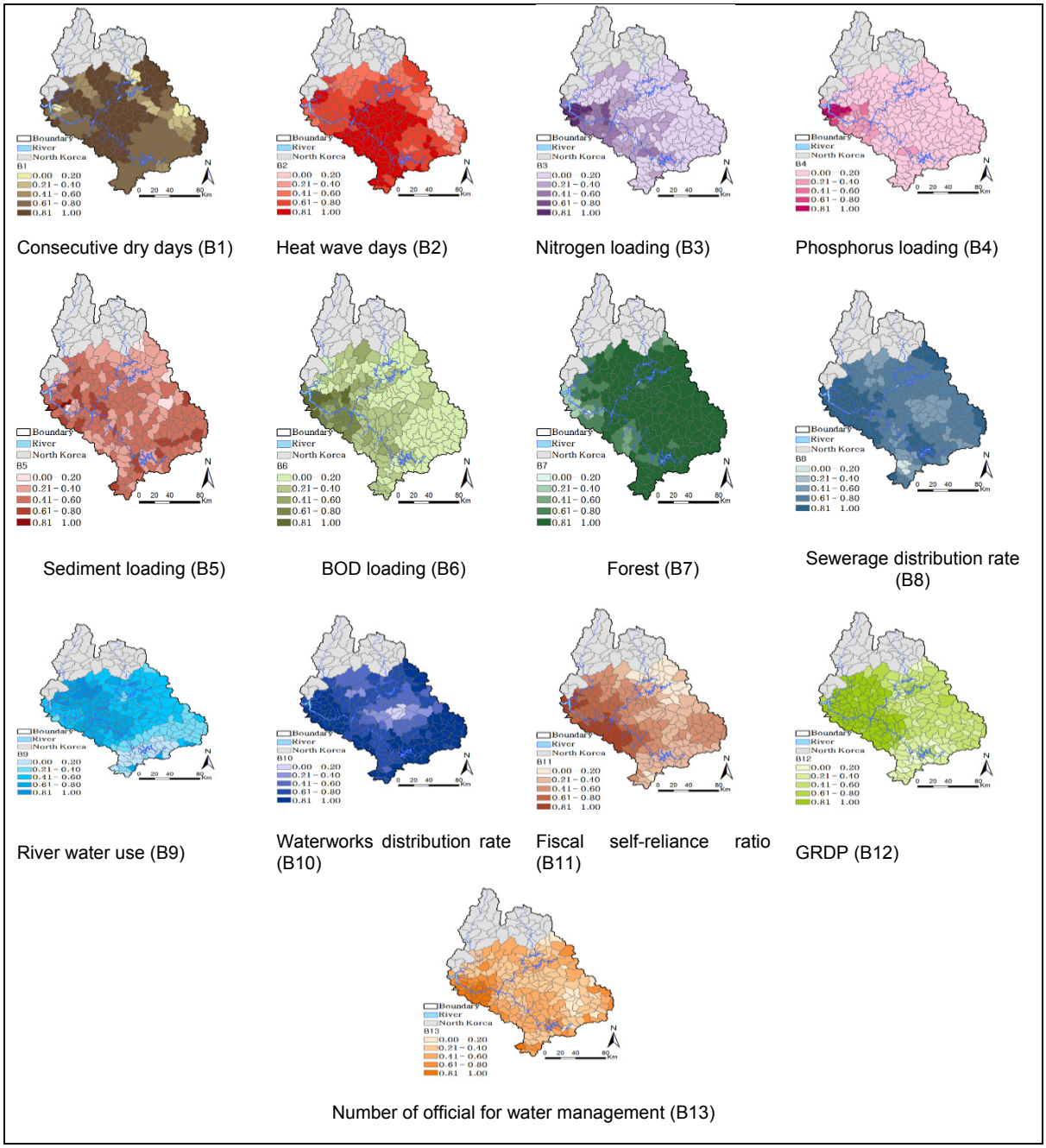

Figure 3. Normalization of water quality vulnerability indicators (Chung et al., 2016).

 ©2017, IAHR. Used with permission / ISSN 1562-6865 (Online) - ISSN 1063-7710 (Print)

3.3 Derivation of objective and subjective weights

The weighting factors for key indicators and vulnerability components were determined with two approaches: expert survey and entropy-based estimation for subjective and objective weights, respectively. For the subjective weight, we performed the expert surveys and estimated the average weight for each indicator (Figure 4). Distributions of weights for each indicator shows variable patterns; in some cases, weights tend to distribute around the mode, but in other cases weights tend to split into two extremes. Many experts pointed out the significance of forest ratio in water quality. While for the objective weight, the Shannon entropy-based method was employed to estimate the weights without expert's opinions. Based on the entropy concept, all indicators for water quality vulnerability, percentage of forest and phosphorus loading were derived to be relatively important proxies

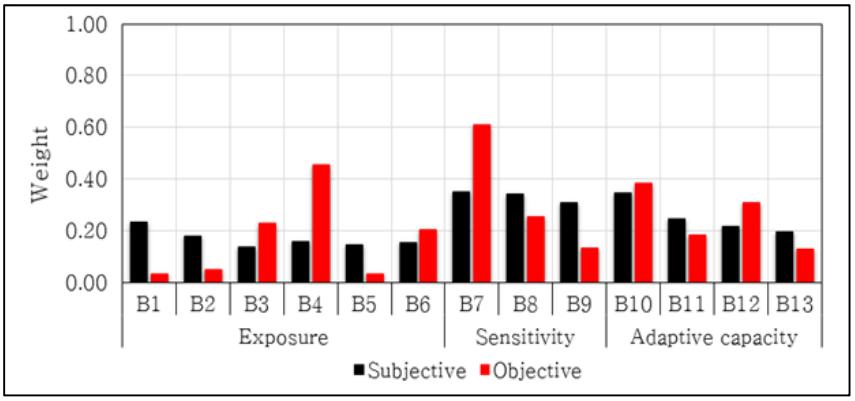

Figure 4. Comparative representation of subjective and objective weights.

3.4 Water quality vulnerability ranking using TOPSIS

In each normalized index, the data of the subjective and objective weights were applied to TOPSIS techniques to integrate the indicators in relation to water quality and the vulnerability of sub-basins were calculated and their rankings compared as shown in Figure 5 and 6 based on the weighting method. As a result, it was definitely found that, water quality vulnerability rankings in Figure 6 show common differences in the weighting method and most were from the metropolitan area. The subjective weight shows higher vulnerability of the metropolitan area except for Seoul where the objective weights show conflicting results according to the weighting method. In some areas, vulnerabilities appear higher in the metropolitan area and are largely represented including Seoul as shown in Figure 3.

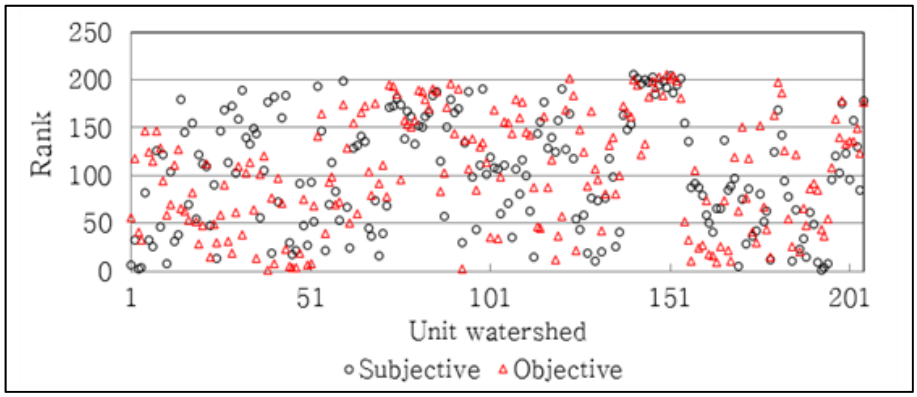

Figure 5. Vulnerability ranking for subjective and objective weights.

In Figure 7, a division of four detailed results (i.e. W1, W2, W3 and W4) are confirmed from the overall along the river flow. The water quality shows distinct results depending on the basin, wherein the sensitivity and adaptive capacity index values are low when compared to those in other basins. Moreover, the adaptive capacity index of W4 is the highest. On the other hand, the ranking of water quality vulnerability, of W2 has the highest from subjective weights while that of W4 has the highest from objective weights.

©2017, IAHR. Used with permission / ISSN 1562-6865 (Online) - ISSN 1063-7710 (Print)

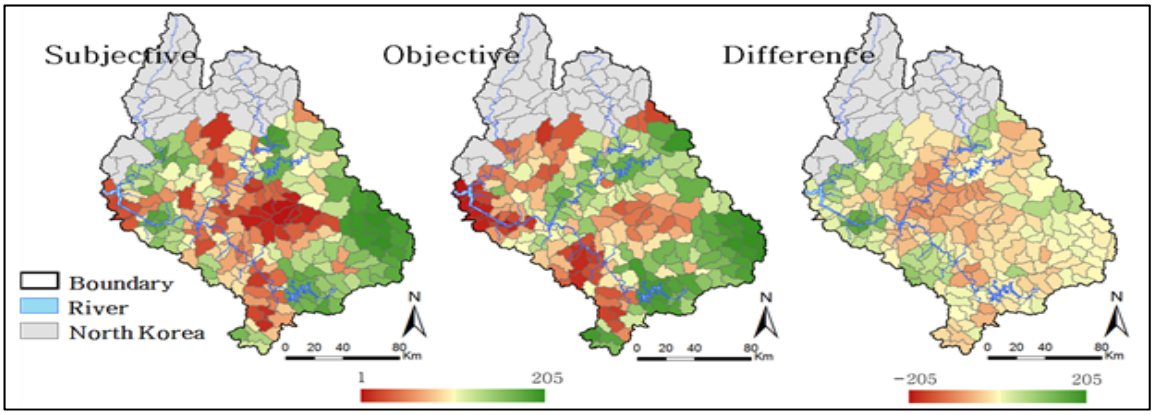

Figure 6. Comparative analysis for water quality vulnerability ranking.

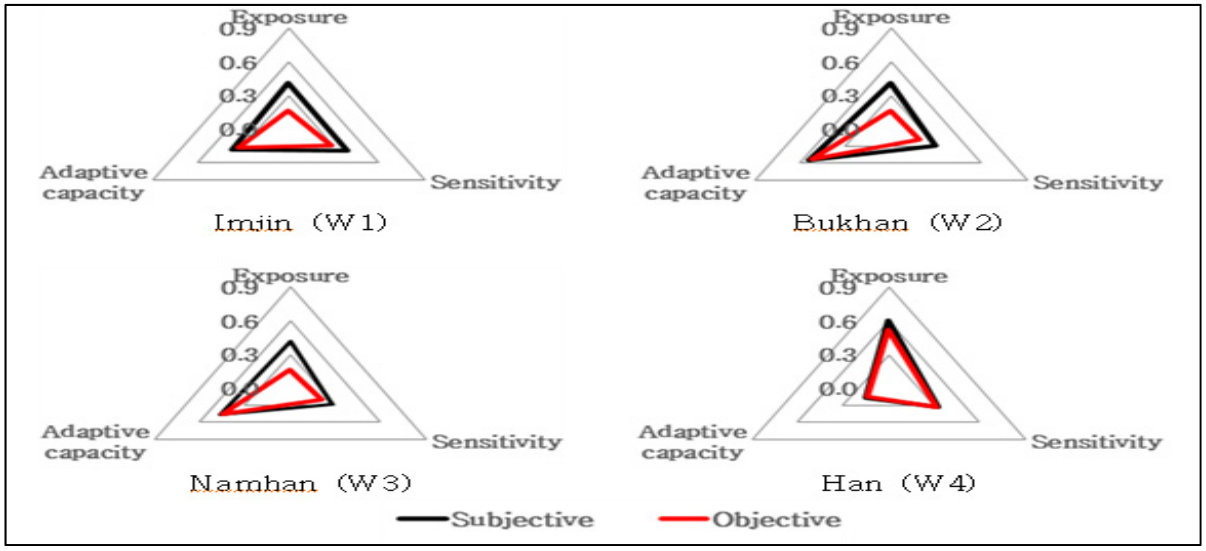

Figure 7. Vulnerability indices of Exposure, Sensitivity and Adaptive capacity for four sub-basins.

3.5 Vulnerability correlation for two weighting methods

This study was conducted to analyze Spearman correlation coefficient of water resources vulnerability in accordance with the results of the weighted method. The water quality vulnerability has a relatively low correlation compared to the quantity estimated to have been 0.51. In this case of applying the entropy of water quality indicators, have been able to give much weight to the sensitivity index. The big differences between the indictor values are included in Exposure and Sensitivity classification with low correlation.

4 CONCLUSIONS

This study evaluated the vulnerabilities of water quality in the Han River basin. For estimating the weighted values for each indicator, expert surveys for subjective weight and data-based Shannon's entropy method for objective weight were utilized. The water quality, vulnerable sub-basins showed relatively high maximum consecutive dry days and temperature and the distribution of water quality indices were quite distinct according the weight methods. Moreover, the results also shows relatively high pollutant loadings. The ranking of water quality vulnerability, W2 has the highest based subjective weights while objective weights of W4 has the highest. The water quality vulnerability has a significantly low correlation of 0.51. Such results suggest that, the approach to consider different weighting methods would be important for reliably assessing the spatial water resource vulnerability. Then the required strategies to the vulnerable area can be considered to be implemented with caution. In addition, this study also suggests the importance of comparing subjective and objective weights for better decision making processes and prioritization of water quality planning and management in the Han River Basin.

ACKNOWLEDGEMENTS

This research was supported by a grant (14AWMP-B082564-01) from the Advanced Water Management Research Program funded by the Ministry of Land, Infrastructure and Transport of the Korean government. Also, this study was supported by a grant (NRF-2016R1D1A1B04931844) funded by National Research Foundation of Korea.

 ©2017, IAHR. Used with permission / ISSN 1562-6865 (Online) - ISSN 1063-7710 (Print)

REFERENCES

Adger, W.N., Brooks, N., Bentham, G., Agnew, M. & Eriksen, S. (2004). *New Indicators of Vulnerability and Adaptive Capacity*, Technical Report 7, Tyndall Centre for Climate Change Research: Norwich, UK.

Chung, E.-S. & Lee, K.S. (2009). Identification of Spatial Ranking Of Hydrological Vulnerability Using Multi-Criteria Decision Making Techniques: Case Of Korea. *Water Resour Mana*ge. 23, 2395–2416.

Chung, E.-S., Won, G.J., Kim, Y. & Lee, H. (2014). Water Resources Vulnerability Characteristics by District's Population Size in a Changing Climate Using Subjective and Objective Weights. *Sustainability*, 6, 6141–6157.

Chung, E.S. & Lee, K.S. (2009). Identification of Spatial Ranking of Hydrological Vulnerability using Multi-Criteria Decision Making Techniques: Case Study of Korea. *Water resources management*, 23(12), 2395-2416.

Chung, E.S., Abdulai, P.J., Park, H., Kim, Y., Ahn, S.R. & Kim, S.J. (2016). Multi-Criteria Assessment of Spatial Robust Water Resource Vulnerability Using the TOPSIS Method Coupled with Objective and Subjective Weights in the Han River Basin. *Sustainability*, 9(1), 29.

Deng, H., Yeh, C.H. & Willis, R.J. (2000). Inter-Company Comparison using Modified TOPSIS with Objective Weights. *Computers and Operations Research*, 27(10), 963–973.

Eakin, H. (2003). The Social Vulnerability of Irrigated Vegetable Farming Households in Central Puebla. *The Journal of Environment & Development*, *12* (4), 414-429.

Eakin, H., & Luers, A. L. (2006). Assessing the vulnerability of social-environmental systems. *Annual Review of Environment and Resources*, 31, 365-394.

Gleick, P.H. (1990). Vulnerability of water systems. *Climate Change and US Water Resources. New York: John Wiley and Sons, Inc*.

Hwang, C.L. & Yoon, K. (1987). Multiple Attributes Decision Making Methods and Applications; Springer: Heidelberg, Germany, 104, 83.

Intergovernmental Panel on Climate Change (IPCC). (2001). *Impacts, Adaptation Vulnerability. In Contribution of Working Group II to the Third Assessment Report of the Intergovernmental Panel on Climate Change*, United Nations Environment Programme (UNEP)/World Meteorological Organization (WMO), Geneva, Switzerland.

Jun, K.S., Sung, J.Y., Chung, E.-S. & Lee, K.S. (2011). Development of Spatial Water Resources Vulnerability Index Considering Climate Change Impacts. *Science of the total environment*, 409(24), 5228-5242.

Korea Environment Institute (KEI). (2014). Development and Application of Sustainable Water Use Indicators, *KEI*, 08, (14-45-01).

Kim, Y. & Chung, E.S. (2014). An Index-Based Robust Decision Making Framework for Watershed Management in a Changing Climate. *Science of the Total Environment*, 473, 88-102.

Kim, Y.K., Chung, E.S. & Lee, K.S. (2012). Fuzzy TOPSIS Approach to Flood Vulnerability Assessment in Korea. *Journal of Korea Water Resources Association*, 45(9), 901-913.

Shannon, C.E. (1948). A Mathematical Theory of Communications. *Bell Systems Technical Journal*, 27, 379-423.

United Nations Office for Disaster Risk Reduction (UN/ISDR). (2004). *Living with Risk: A Global Review of Disaster Reduction Initiatives*; UNISDR: Geneva, Switzerland.

Wang, T.C. & Lee, H.D. (2009). Developing a Fuzzy TOPSIS Approach based on Subjective Weights and Objective Weights. *Expert Systems with Applications*, 36(5), 8980-8985.

Wang, X., Ma, F.B. & Li, J.Y. (2012). Water Resources Vulnerability Assessment based on the Parametric-System Method: A Case Study of the Zhangjiakou Region of Guanting Reservoir Basin, North China. *Procedia Environmental Sciences*, 13, 1204-1212.

Zou, Z.H., Yi, Y. & Sun, J.N. (2006). Entropy Method for Determination of Weight of Evaluating Indicators in Fuzzy Synthetic Evaluation for Water Quality Assessment. *Journal of Environmental Sciences*, 18(5), 1020-1023.

©2017, IAHR. Used with permission / ISSN 1562-6865 (Online) - ISSN 1063-7710 (Print)

Proceedings of the 37th IAHR World Congress
August 13 – 18, 2017, Kuala Lumpur, Malaysia

ANALYSIS OF METEOROLOGICAL AND HYDROLOGICAL DROUGHT EVENTS IN PENINSULAR MALAYSIA

MD MUNIR HAYET KHAN[1], NUR SHAZWANI MUHAMMAD[2] & AHMED EL-SHAFIE[3]

[1,2] Department of Civil & Structural Engineering, Universiti Kebangsaan Malaysia (UKM), 43600 Bangi, Selangor, Malaysia, shihab.bd@gmail.com; shazwani.muhammad@ukm.edu.my
[3] Department of Civil Engineering, Faculty of Engineering, University of Malaya (UM), 50603 Kuala Lumpur, Malaysia, elshafie@um.edu.my

ABSTRACT

Drought events have affected peninsular Malaysia several times during the last decades. Therefore, analysis of drought episodes is important for drought management operations. Drought indexing is a practical approach to assimilate large amounts of data into quantitative information which can be applied in drought forecasting, declaring drought levels, contingency planning and impact assessments. This paper analyzes the meteorological drought events for 44 years of historical rainfall data using the Standardized Precipitation Index (SPI) and hydrological drought events from 56 years of streamflow data using Streamflow Drought Index (SDI). The objective is to determine the frequency and severity of droughts and whether or not they have increased or decreased during this time period in Peninsular Malaysia. The computed monthly SPI shows that there are trends only for January, March, April and August, all of which are upward trends. In contrast, the computed monthly SDI shows that there are trends in the month of October, November, March, May and July that move downwards. However, the SDI and SPI drought trend analysis with all longer time scales were able to detect significant trends. Additionally, the researchers found that the SPI and SDI had very little correlations between them for drought trend analysis.

Keywords: Meteorological; hydrological; drought indices; SPI & SDI.

1 INTRODUCTION

Drought has been regarded as one of the most severe types of hazard that the earth could face. Occurrence of drought can initiate a series of continued chain reactions over a long period of time. A simple definition of drought is the absence of water. One half of the world's population will confront severe conditions of water crisis by the year 2025 particularly in South Asia, Middle East and Africa (Diwan, 2002). More than 10 million people have died in the last century between 1900 to 2005 (Wilhite, 2000; Below et al., 2007). In Malaysia, there have been so many occurrences of drought episodes in the past, but the most famous one was in 1997-98 whereby an El Nino related drought caused extensive impact to the environment and society across the whole nation. The worst hit region during the drought was the capital city of Kuala Lumpur and part of Selangor where water rationing had to be exercised affecting some 3.2 million people for about 5 months from April to September. The affected areas were from Perlis, the northern states of Peninsular Malaysia, up to the southern states of Negeri Sembilan and Melaka. The drought was also being observed in Sarawak and Sabah, which are the East of Malaysia. All the divisions of Sabah state experienced high rainfall deficits for a period ranging from 4 to 9 months, affecting more than 2,797 km^2 and 170,000 people living in that region (Shaaban and Low, 2002).

A common tool that was utilized to monitor drought conditions is a drought index (DI). Several drought indices can be used (i.e. SPI, SDI, EDI, RDI, NDVI etc.) to forecast the possible evolution of an ongoing drought in order to adopt appropriate mitigation measures and drought policies for water resources management. This is because a DI is expressed by a numeric number, which is believed to be far more functional than raw data during decision-making process. The objective of this study is to investigate the characteristics & trends of meteorological and hydrological droughts from historical data in and around Selangor state of Peninsular Malaysia.

2 METHODOLOGY

2.1 Streamflow drought index (SDI)

The SDI method, as proposed by Nalbantis (2008) was used to assess drought severity. Cumulative Stream flow volumes from different time scales were used to study the distribution and variation of drought severity at different durations. The drought severity of the study area, frequency of drought occurrence and occurrence of cycles can be obtained by this method. It was first assumed that the time series of monthly streamflow volumes (Q_{ij}) were successive, which were then accumulated according to the time duration k. The cumulative streamflow volume for the i-th hydrological year for a duration k was obtained as below:

 ©2017, IAHR. Used with permission / ISSN 1562-6865 (Online) - ISSN 1063-7710 (Print)

$$V_{i,k} = \sum_{j=1}^{3k} Q_{i,j} \quad \text{i= 1,2, ……. J= 1,2, ….., 12 , k = 1,2,3, 4} \qquad [1]$$

where $Q_{i,j}$ refers to monthly streamflow volumes, *i* refers to the hydrological year, *j* refers to the month of that year, *k* refers to the time duration of the period and $V_{i,k}$ is the cumulative streamflow volume for the *i*-th hydrological year with a period duration of *k*. In the next step, the SDI for the *i*-th hydrological year with period duration *k* was defined using the cumulative streamflow volumes $V_{i,k}$:

$$SDI_{i,k} = \frac{V_{i,k} - \bar{V}_k}{S_k} \qquad i\text{= 1,2,….., k= 1,2,3,4} \qquad [2]$$

where V_k and S_k are the long-term mean and standard deviation of cumulative streamflow volumes, respectively. When assessing a SDI value, the data for analysis must follow a normal or log-normal distribution. However, in small basins, streamflows might follow a skewed probability distribution, whose distribution pattern is similar to that of the Gamma distribution. Therefore, when using SDI to analyze streamflow data, the first step is to transform the statistical distribution.

$$SDI_{i,k} = \frac{y_{i,k} - \bar{y}_k}{S_k} \qquad i\text{= 1,2,….., k= 1,2,3,4} \qquad [3]$$

$$y_{i,k} = \ln(V_{i,k}),\ \text{i= 1, 2,…… k=1,2,3, 4} \qquad [4]$$

where, $y_{i,k}$ are the natural logarithms of cumulative streamflow with mean y_k and standard deviation $s_{y,k.}$. The SDI suggested by Nalbantis (2008) is shown in Table1 below.

Table 1. Hydrological Drought Classification by SDI.

SDI Values	Classification
SDI ≥ 0.0	Non-drought
-1.0 ≤ SDI ≤ 0.0	Mild drought
-1.5 ≤ SDI ≤ -1.0	Moderate drought
-2.0 ≤ SDI ≤ -1.5	Severe drought
SDI < -2.0	Extreme drought

2.2 Standardized precipitation index (SPI)

The SPI is a drought defining and monitoring tool. The SPI calculation for any location is based on the long-term precipitation records during a desired period. This long-term records were fitted to a probability distribution, which were then transformed into a normal distribution so that the mean SPI for the location and desired period is zero (Edwards and McKee, 1997). The SPI can easily be computed by dividing the difference between the normalized seasonal precipitation and its long-term seasonal mean by the standard deviation as given in Eq. [5]. Thus:

$$SPI = \frac{Xi_j - \bar{X}}{\sigma} \qquad [5]$$

where, (x_{ij}) is the seasonal precipitation at the i^{th} rain gauge and j^{th} observation, ( ) is the long-term seasonal mean and () is its standard deviation. This method requires only a set of precipitation data for 30 or more years. The most frequent time scales being 1, 3, 6, 12 and 24 months of duration. Table 2 shows the classification of drought levels according to SPI.

Table 2. Classification of drought conditions according McKee et al. (1995).

SPI Values	Classification
2.0 or more	Extremely wet
1.5 to 1.99	Very wet
1.0 to 1.49	Moderately wet
-0.99 to 0.99	Near normal
-1.0 to -1.49	Moderately dry
-1.5 to -1.99	Severely dry
-2 or less	Extremely dry

©2017, IAHR. Used with permission / ISSN 1562-6865 (Online) - ISSN 1063-7710 (Print)

2.3 Mann-Kendall test

Mann Kendall test was used to identify the monotonicity in a time series (Yue et al., 2002; Kumar et al., 2010; Caloiero et al., 2011; Jain et al. 2013; Adarsh and Reddy, 2015). Being a non-parametric test, the problem due to data skew can be evaded easily (Swain et al., 2015).
The Mann-Kendall statistic, *S* is given as:

$$S = \sum_{k=1}^{n-1} \sum_{j=k+1}^{n} sgn(x_j - x_k) \quad [6]$$

The trend test was applied to a time series x_k that was ranked from k = 1, 2 …n-1, and x_j, which was ranked from j = k+1, 2 ….n. Every data point x_k was taken as a reference point to compare with all the other data points, x_j. For a positive difference between the data points, the so-called S statistic was increased by +1, while it was decreased by −1 for a negative difference. It was observed that when n ≥ 8, the statistic S was approximately normally distributed i.e. with zero mean and variance given by:

$$VAR(S) = \frac{1}{18}[n(n-1)(2n+5) - \sum_{i=1}^{m} t_i(t_i-1)(2t_i+5)] \quad [7]$$

where, t_i represents the number of ties up to sample i. The test statistic *Z* was calculated from *VAR(S)*-:

$$\begin{aligned} Z &= \frac{S-1}{[VAR(S)]^{1/2}} \; if\; S > 0 \\ &= 0 \qquad\qquad if\; S = 0 \\ &= \frac{S+1}{[VAR(S)]^{1/2}} \; if\; S < 0 \end{aligned} \quad [8]$$

Z was assumed to follow a standard normal distribution. Hence, its value being positive indicates a rising trend and that of negative indicates a decreasing trend. A significance level α was also utilized for testing monotonicity of trend (a two-tailed test). If *Z* is greater than Zα/2 where α depicts the significance level, then the trend is considered to be significant (Babar and Ramesh, 2014).

2.4 Sen's slope estimator test

Sen's slope estimator was the most frequently used method to detect a linear trend (Yue and Hashino, 2003; Jain and Kumar, 2012; Swain et al., 2015). The slope (T_i) of all data pairs is given as below (Sen, 1968). T_i was calculated for each of the *N* data pairs, where, *N = n(n-1)/2*:

$$T_i = \frac{x_j - x_k}{j-k} \text{ for i= 1, 2, 3……N} \quad [9]$$

where x_j and x_k are considered as data values at time j and k (j>k), respectively. The Sen's estimator of slope is given by the median of these N values of T_i, which is projected as the slope estimator and the median of these *N* individual slopes.

$$\begin{aligned} \widehat{Q} &= median\; slope \\ &= T_{\left[\frac{(N+1)}{2}\right]} \qquad\qquad if\; N\; is\; odd \\ &= \frac{1}{2}\left(T_{[N/2]} + T_{[(N+2)/2]}\right) if\; N is\; even \end{aligned} \quad [10]$$

It is very similar to the Mann-Kendall test whereby the positive and negative values of slope estimator represent a positive and negative trend, respectively.

3 STUDY AREA & DATA COLLECTION

The selected stations *Sekolah Kebangsaan Kampung Sg Lui* rainfall station in Langat river basin in Selangor state and *Sg. Teriang di Juntai* streamflow station in Pahang river basin in Negeri Sembilan state are shown on Figure 1 below. These stations were selected because Langat is the largest basin and most of the drought events occurred here. The streamflow station was chosen based on its closeness to a rainfall station and to different river basins in different states. Table 3 provides the details of hydrological stations used in this study.

 ©2017, IAHR. Used with permission / ISSN 1562-6865 (Online) - ISSN 1063-7710 (Print)

Figure 1. Locations of study.

Table 3. Details of hydrological stations.

Gauging Station	Station No.	Coordinate		Period (year to year)	Duration (years)	Missing Data (%)
		Latitude (N)	Longitude (E)			
Sek. Keb. Kg. Sg. Lui	3118102	03° 10' 25"	101° 52' 20"	1971-2014	44	8
Sg. Teriang di Juntai	3022431	03° 04' 30"	102° 13' 05"	1960-2016	56	9

Necessary rainfall and streamflow data to be used were collected from Drainage and Irrigation Department (DID, Malaysia) according to completeness. Figures 2 and 3 below display the mean and median of monthly rainfall and streamflow of both stations. Dry months are generally observed from January to March and June to September in Malaysia.

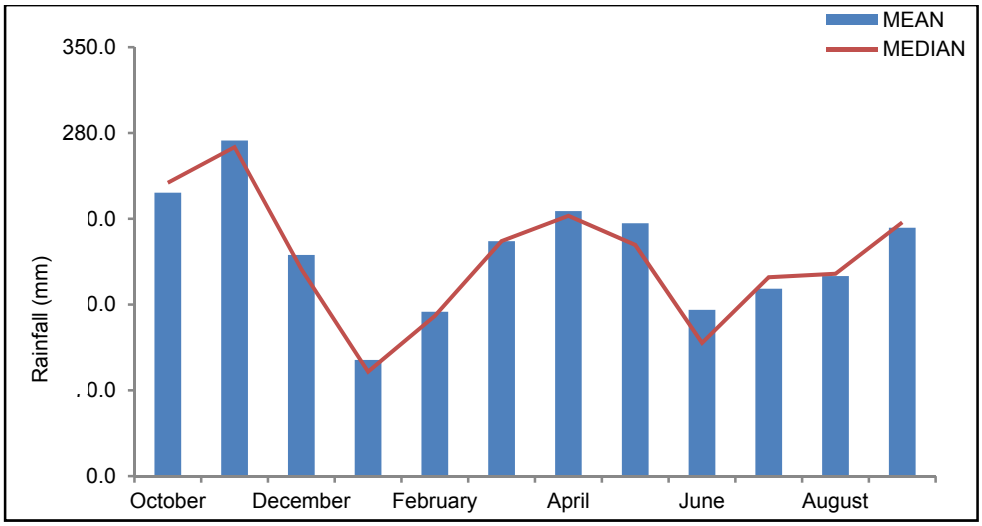

Figure 2. Mean and median of monthly rainfall at Sekolah Kebangsaan Kampung Sungai Lui.

©2017, IAHR. Used with permission / ISSN 1562-6865 (Online) - ISSN 1063-7710 (Print)

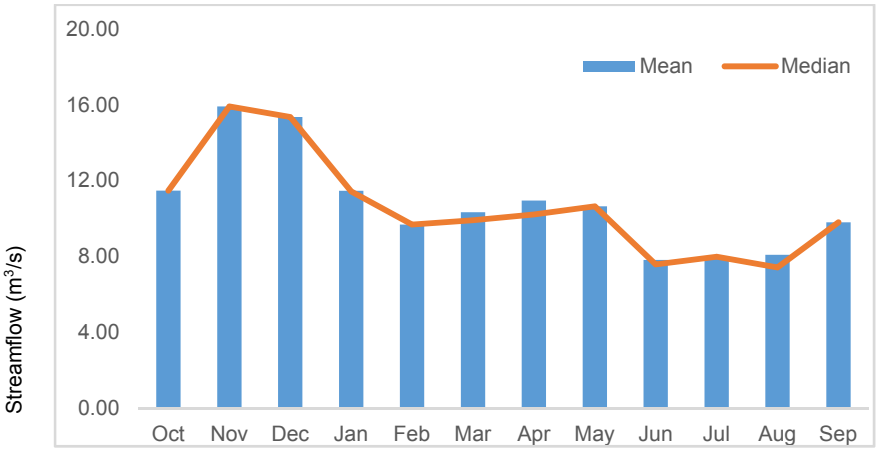

Figure 3. Mean and median of monthly streamflow at Sg. Teriang.

4 RESULTS

Trends in annual (starting October), 1-3 months (Oct.-Dec), 1-6 (Oct.- March) months and 1-9 (Oct.-June) months' time scales were investigated in the study area. The trend analysis result as shown in Table 4 and 5 are based on rainfall data of 44 years. Monthly SPI for the historical series shows that trends were only detected for the months of January, March, April and August. All of which are slightly positive (increasing) trends. Similarly, 3-monthly SPI shows that there are trends for all 4 quarters and are positive too. It also shows that 6-monthly and yearly trends are also increasing.

Table4. Trend Analysis based on monthly SPI values (α = 0.05).

Monthly SPI	Kendall's tau	S (Statistic)	p-value (Two-tailed)	Z (Test Statistic)	Trend Detection (Yes/No	Sen's Slope
Oct	-0.015	-13.000	0.897	Null	No	-0.002
Nov	0.159	137.000	0.141	Null	No	0.014
Dec	0.038	33.000	0.730	Null	No	0.005
Jan	0.318	274.000	0.003	2.959	Yes	0.035
Feb	0.120	103.000	0.271	1.105	No	0.009
Mar	0.272	234.000	0.012	2.525	Yes	0.030
Apr	0.357	307.000	0.001	3.316	Yes	0.034
May	-0.051	-44.000	0.641	-0.466	No	-0.003
Jun	0.016	14.000	0.888	0.141	No	0.002
Jul	0.015	13.000	0.897	0.130	No	0.001
Aug	0.321	276.000	0.003	2.980	Yes	0.030
Sep	0.075	65.000	0.490	0.694	No	0.006

Table5. Trend Analyis based on different SPI series (α = 0.05).

SPI	Kendall's tau	S (Statistic)	p-value (Two-tailed)	Z (Test Statistic)	Trend Detection (Yes/No)	Sen's Slope
1-3 SPI	0.134	115.000	0.218	Null	Yes	0.014
4-6 SPI	0.332	272.000	0.002	Null	Yes	0.038
7-9 SPI	0.180	155.000	0.095	Null	Yes	0.020
10-12 SPI	0.237	204.000	0.028	2.200	Yes	0.028
1-6 SPI	0.245	201.000	0.025	2.247	Yes	0.025
7-12 SPI	0.254	219.000	0.018	Null	Yes	0.031
1-9 SPI	0.264	227.000	0.014	Null	Yes	0.030
1-12 SPI	0.312	269.000	0.003	Null	Yes	0.033

Figure 4 below describes that meteorological droughts occurrences (%) in all 12 months but maximum percentage of droughts occurred in January and March which is normally a drier period in Malaysia. In Figure 5 below, it can be seen that the decadal drought events in terms of number of occurrences. The total number of drought events was 66 times with a total 23 times drought occurrences during 1995-2004 which is the highest number in the last 40 years. The maximum number of drought events took place during 1985 – 2004

 ©2017, IAHR. Used with permission / ISSN 1562-6865 (Online) - ISSN 1063-7710 (Print)

with a total of 38 times. McKee et al. (1993) defined the criteria for a “drought event” at any time scale is when it occurs at the time when the value of the SPI is continuously negative and reaches “-1”. The event ends when the SPI becomes positive.

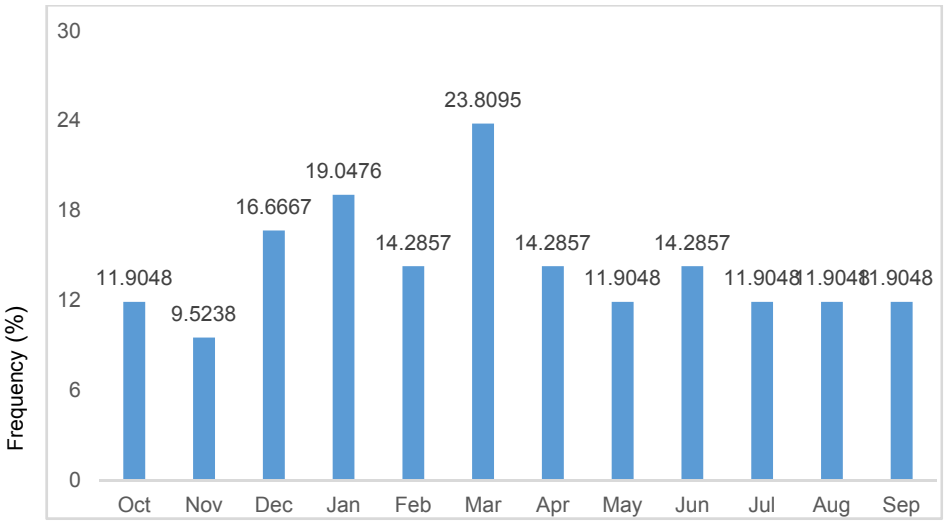

Figure 4. Monthly meteorological droughts of historical data (1971-2014).

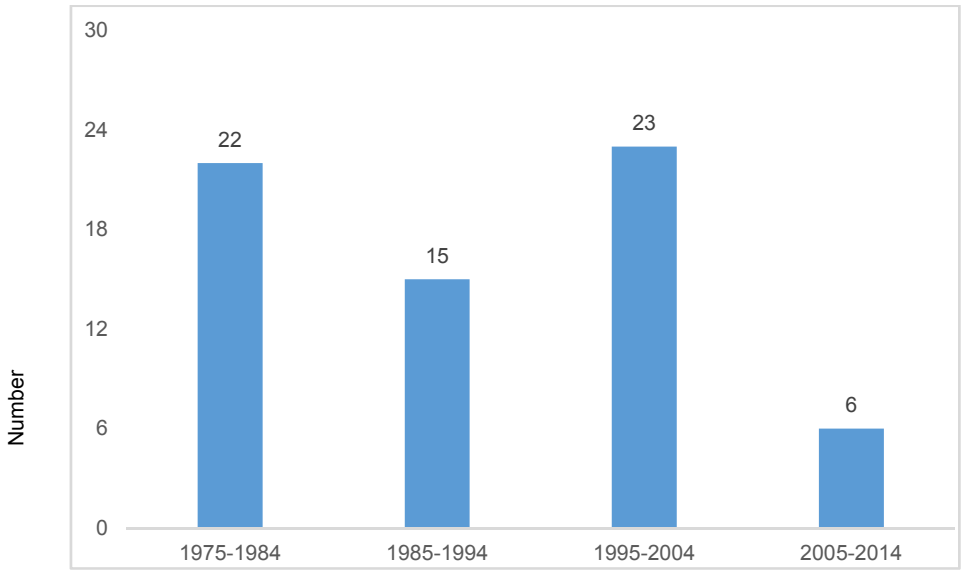

Figure 5. No. of meteorological drought in the last four (4) decades.

For hydrological drought, the trend analysis in Tables 6 and 7 show results based on streamflow data of 56 years. The values of monthly SDI for the historical series show that there are trends in the month of October, November, March, May and July. All of which are slightly negative (decreasing) trends. Similarly, 3-monthly SDI shows that there are trends for quarters of October-June which are negative as well. The 6-monthly and annual trends are also slightly decreasing. The SDI and SPI drought trend analysis at all longer time scales were able to detect significant trend. Both SPI and SDI drought trend analysis was found to be more sensitive to time scales as both were able to detect significant trends at only 5 stations each for monthly scales. Trend detection increases as the time scale increases up to annual.

©2017, IAHR. Used with permission / ISSN 1562-6865 (Online) - ISSN 1063-7710 (Print)

Table 6. Trend Analysis based on monthly SDI values (α = 0.05).

Monthly SDI	Kendall's tau	S (Statistic)	p-value (Two-tailed)	Z (Test Statistic)	Trend Detection (Yes/No	Sen's Slope
Oct	-0.254	-387.000	0.006	-2.733	Yes	-0.025
Nov	-0.235	-355.000	0.012	-2.512	Yes	-0.018
Dec	-0.125	-188.000	0.184	-1.329	No	-0.011
Jan	-0.138	-207.000	0.143	-1.466	No	-0.006
Feb	-0.130	-197.000	0.165	-1.390	No	-0.012
Mar	-0.215	-328.000	0.021	-2.315	Yes	-0.018
Apr	-0.170	-259.000	0.068	-1.828	No	-0.018
May	-0.236	-357.000	0.012	-2.526	Yes	-0.022
Jun	-0.171	-259.000	0.067	-1.831	No	-0.018
Jul	-0.199	-299.000	0.034	-2.117	Yes	-0.013
Aug	-0.074	-112.000	0.431	-0.788	No	-0.003
Sep	-0.082	-124.000	0.382	-0.874	No	-0.006

Table 7. Trend Analyis based on different SDI time scales (α = 0.05).

SDI	Kendall's tau	S (Statistic)	p-value (Two-tailed)	Z (Test Statistic)	Trend Detection (Yes/No)	Sen's Slope
1-3 SDI	-0.260	-396.000	0.005	-2.796	Yes	-0.026
4-6 SDI	-0.210	-320.000	0.024	-2.258	Yes	-0.019
7-9 SDI	-0.242	-370.000	0.009	-2.612	Yes	-0.024
10-12 SDI	-0.125	-188.000	0.184	-1.329	No	-0.012
1-6 SDI	-0.292	-448.000	0.002	-3.161	Yes	-0.026
7-12 SDI	-0.250	-383.000	0.007	-2.702	Yes	-0.024
1-9 SDI	-0.350	-538.000	0.000	-3.797	Yes	-0.029
1-12 SDI	-0.315	-484.000	0.001	-3.414	Yes	-0.029

Figure 6 below shows that hydrological droughts happened in all 12 months and it can be seen that maximum percentage of droughts occurred in April, September, October and December. Figure 7 below describes the decadal drought events in terms of number of occurrences. It can be seen that a total of 31 times of drought occurred during 2006-2016 out of a total of 55 times in the last 40 years.

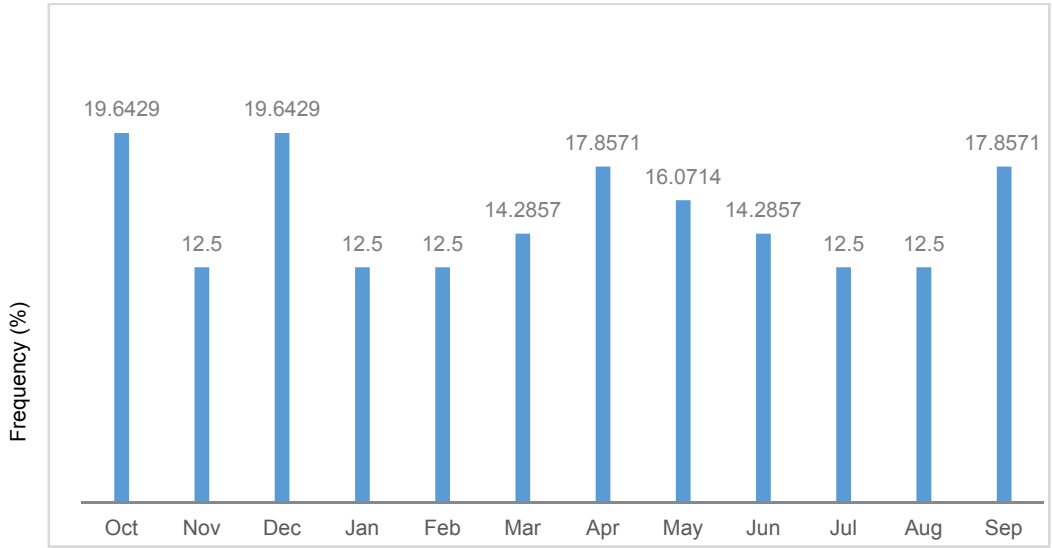

Figure 6. Monthly percentage of hydrological droughts of historical data (1965-2016).

©2017, IAHR. Used with permission / ISSN 1562-6865 (Online) - ISSN 1063-7710 (Print)

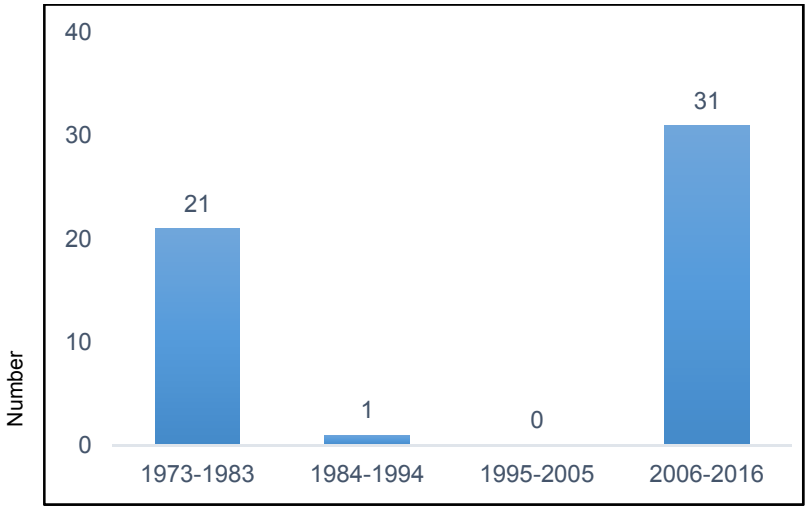

Figure 7. No. of hydrological drought events of last four (4) decades.

When the slopes (*Q*) were computed, the results show a consistency with the results of the Mann-Kendall test. It was observed that the Sen's slope for all time scales of SDI was negative (decreasing) whereas for SPI, it was positive (increasing). The correlation between SPI and SDI of monthly Sen's slope of the historical data is shown below in Figure 8. The pattern of the Sen's slope from October to January and May to August are quite similar between SPI & SDI, although the correlation is unlikely. The trend of monthly time scales could not be detected half of the time but almost all of the larger time scales were able to detect the trend for both SPI and SDI series.

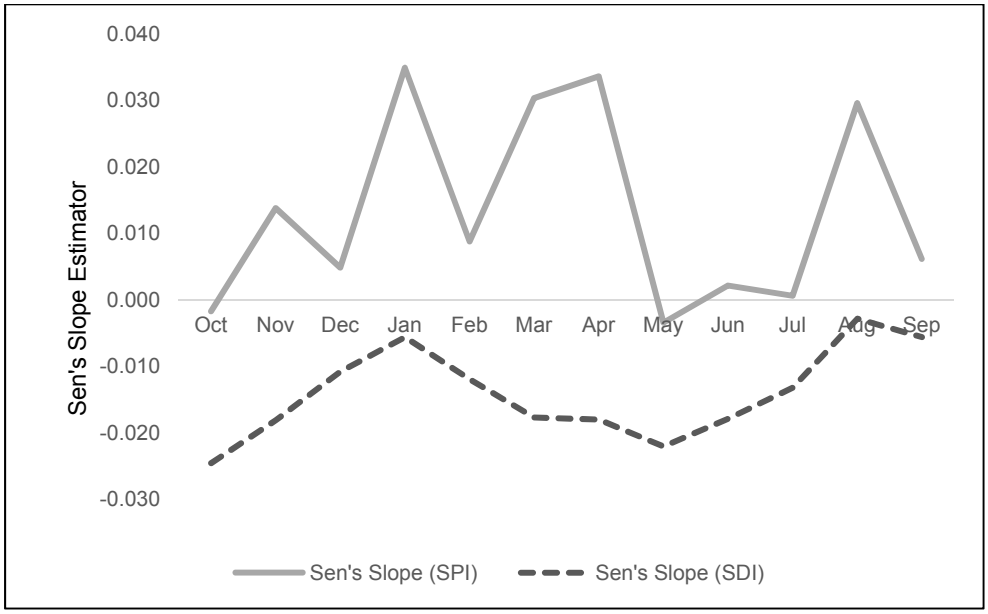

Figure 8. Correlation between Sen's Slope Estimator of Monthly SPI & SDI.

Figure 9 below shows the original SPI series and SDI series. It was observed that there was very little similarity between the two which is consistent with their correlation of trends; however, they were able to capture the major drought events of the respective river basin. For example, in 1997-1998 and 2014-2015, the occurrence of drought events managed to be captured by SPI. Streamflow drought Index (SDI) was not able to detect those drought events possibly due to the fact that the region was not affected during the stated time. The streamflow station was not in the same river basin suggesting regionalization (i.e. river basin) should be taken into consideration while analyzing droughts.

©2017, IAHR. Used with permission / ISSN 1562-6865 (Online) - ISSN 1063-7710 (Print)

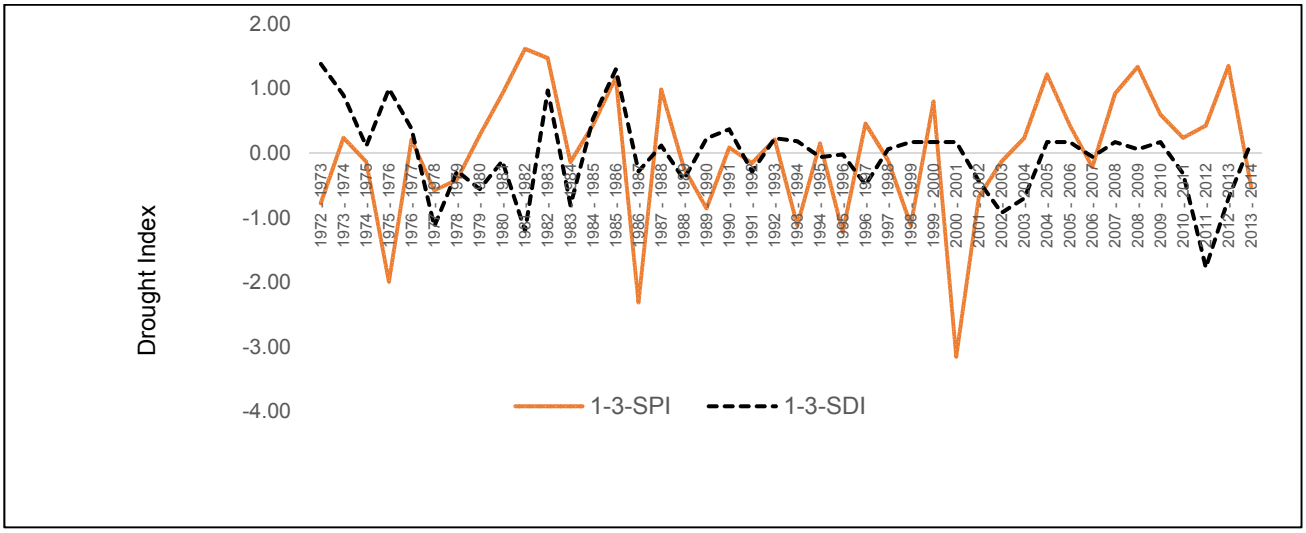

Figure 9. 3-montly SPI and SDI.

5 CONCLUSIONS

The study of drought trends is extremely important as it is related to food security and management of scarce water resource, both of which are critical in the case of drought events. In this work, the drought trend of Standardized precipitation index (SPI) at 1, 1-3, 1-6, 1-9 and 12 months time scales of monthly precipitation data for time series (1971-2014) and scales for streamflow drought index were computed using long time series (1960-2016) of monthly streamflow data of the chosen study station. The statistical significance at 95% confidence level as per Mann-Kendall and Sen's slope estimator were used for drought trend analysis over two neighbouring states. The SDI and SPI drought trend analysis at all longer time scales were able to detect significant trends. Additionally, both SDI and SPI were found to be more sensitive to multiple time scales as they were able to detect significant trends at only 5 times each for monthly scale. Trend detection increases as the time scale increases up to annual. This analysis may assist the decision-making process that is associated with droughts and allocation of water for agriculture, industry, domestic and industrial use.

ACKNOWLEDGEMENTS

The authors appreciate the supports from UKM (Universiti Kebangsaan Malaysia) and Ministry of Education (MOE) for the research fund FRGS/2/2014/TK02/UKM/03/2. The supports from INTI International University, Nilai and DID (Drainage & Irrigation Department), Malaysia are also acknowledged.

REFERENCES

Adarsh, S. & Janga Reddy, M. (2015). Trend Analysis of Rainfall in Four Meteorological Subdivisions of Southern India using Nonparametric Methods and Discrete Wavelet Transforms. *International Journal of Climatology,* 35(6), 1107-1124.

Shaaban, A.J. & Low, K.S. (2002). The 1998 Drought in the Kuala Lumpur-Bangi-Kajang Conurbation: Characterisation and Impacts. *International Conference on Urban Hydrology*, Kuala Lumpur.

Babar, S. & Ramesh, H. (2014). Analysis of Extreme Rainfall Events over Nethravathi Basin. *ISH Journal of Hydraulic Engineering*, 20(2), 212-221.

Below, R., Grover-Kovec, E. & Dilley, M. (2007). Documenting Drought-Related Disasters: A Global Reassessment. *The Journal of Environment & Development,* 16(3), 328–344.

Caloiero, T., Coscarelli, R., Ferrari, E. & Mancini, M. (2011). Trend Detection of Annual and Seasonal Rainfall in Calabria (Southern Italy), *International Journal of Climatology*, 31(1), 44-56.

Diwan, P.L. (2002). Water, Environment & Drought. Proceedings: *All India Seminar on Water & Environment Issues and challenges*, October, IIT, Roorkee, India 21-185.

Edwards, D.C. & McKee, T.B. (1997). *Characteristics of 20th Century Drought in the United States at Multiple Time Scales*. Climatology Report 97-2, Department of Atmospheric Science, Colorado State University, Fort Collins, Colorado.

Jain, S.K., Kumar, V. & Saharia, M. (2013). Analysis of Rainfall and Temperature Trends in Northeast India. *International Journal of Climatology*, 33(4), 968-978.

Jain, S.K. & Kumar, V. (2012).Trend Analysis of Rainfall and Temperature Data for India. *Current Science*, 102(1), 37-49.

Kumar, V., Jain, S.K. & Singh, Y. (2010). Analysis of Long-Term Rainfall Trends in India. *Hydrological Sciences Journal–Journal des Sciences Hydrologiques*, 55(4), 484-496.

McKee, T.B., Doeskin, N.J. & Kleist, J. (1995). Drought Monitoring with Multiple Time Scales. *Conference of Applied Climatology,* American Meteorological Society, Boston, 179-184.

Nalbantis, I. (2008). Evaluation of a Hydrological Drought Index. *European Water*, 23(24), 67-77.

 ©2017, IAHR. Used with permission / ISSN 1562-6865 (Online) - ISSN 1063-7710 (Print)

Swain, S., Verma, M., Verma, M.K. (2015). Statistical trend analysis of monthly rainfall for Raipur district, Chhattisgarh, *International Journal of Advanced Engineering Research and Studies /IV/II/* Jan-March, 87-89, 1-3.

Sen, P.K. (1968). Estimates of the Regression Coefficient based on Kendall's Tau. *Journal of the American Statistical Association*, 63(324), 1379-1389.

Wilhite, D.A. (2000). *Drought: A Global Assessment.* Volume I and II. London/New York: Routledge, 1-22.

Yue, S. & Hashino, M. (2003). Long Term Trends of Annual and Monthly Precipitation in Japan. *Journal of the American Water Resources Association*, 39(3), 587-596.

Yue, S., Pilon, P., Phinney, B. & Cavadias, G. (2002). The Influence of Autocorrelation on the Ability to Detect Trend in Hydrological Series. *Hydrological Processes*, 16(9), 1807-1829.

©2017, IAHR. Used with permission / ISSN 1562-6865 (Online) - ISSN 1063-7710 (Print)

Proceedings of the 37th IAHR World Congress
August 13 – 18, 2017, Kuala Lumpur, Malaysia

OPTIMIZING HYDROPOWER OPERATION OF RESERVOIR SYSTEM IN THE UPPER YELLOW RIVER

YUAN SI[1], XIANG LI[2], DONGQIN YIN[3], JIAHUA WEI[4], YUEFEI HUANG[5], TIEJIAN LI[6] & GUANGQIAN WANG[7]

[1,4,5,6,7] State Key Laboratory of Hydroscience and Engineering, Tsinghua University, Beijing 100084, China, siy13@mails.tsinghua.edu.cn; weijiahua@tsinghua.edu.cn; yuefeihuang@tsinghua.edu.cn; litiejian@tsinghua.edu.cn; dhhwgq@tsinghua.edu.cn
[2] China Institute of Water Resources and Hydropower Research, Beijing 100038, China, ideal.thu@gmail.com
[3] Electric Power Planning and Engineering Institute, Beijing 100120, China, yindqcq7@126.com
[3,4,5,6,7] State Key Laboratory of Plateau Ecology and Agriculture, Qinghai University, Xining 810016, China

ABSTRACT

The reservoir system in the Upper Yellow River, one of the largest hydropower bases in China, plays a vital role in the energy structure of the Qinghai Power Grid. This paper aims at studying the trade-off between power quantity (i.e., maximum power) and power reliability (i.e., firm output) of the reservoir system in case of joint operation. A total of 13 reservoirs currently in operation are involved, including two pivotal storage reservoirs on the Yellow River, which are the Longyangxia reservoir and the Liujiaxia reservoir. The multi-objective model is formulated, and with the epsilon constraint method, it can be solved by a traditional nonlinear programming algorithm. Historical hydrological data from multiple years (2000-2010) are used as inputs to the model for analysis. Results indicate that if the reservoir system is operated jointly, the firm output can reach 3110 MW (guarantee rate of 100%) and 3510 MW (guarantee rate of 90%); while the maximum power can reach 297.7, 363.9, and 411.4×10^8 KWh in typical dry, normal, and wet years, respectively. Moreover, a decrease in power generation from the Longyangxia reservoir can bring about a very large increase in firm output from the reservoir system. Furthermore, the trade-off curve between the two objectives is also provided for reference.

Keywords: Hydropower operation; multi-objective optimization; nonlinear programming; upper yellow river; Qinghai Power Grid.

1 INTRODUCTION

The characteristics of low cost, little pollution and rapid start-up/shut-down make hydropower one of the most promising renewable resources. Constructions of cascade reservoir systems have been growing vigorously in China in order to make full use of hydropower resources stored within river basins. Throughout the nation, 13 large-scale hydropower bases are planned to be built along major rivers (Cheng et al., 2012; Wang and Chen., 2010). The reservoir system in the Upper Yellow River (UYR) is one of the largest hydropower bases. According to a report from the Huanghe Hydropower Development Co., Ltd (2016), a total of 39 hydropower plants are planned along the main stream of the UYR (from the headwater to the Hekou town, see Figure 1), with the total installed capacity of around 25,000 MW. By the end of 2015, 24 power plants have been put into operation and the designed annual power generation can reach approximately 538×10^8 KWh. The UYR reservoir system plays strategic roles in conserving water resources and utilizing hydropower resources as well as other purposes for the lower basin area, such as ice/flood control, water supply, farm irrigation, and ecological sustainability.

At present, the power balance situation of the Qinghai Power Grid, where the majority of installed capacity of the UYR reservoir system is located, is not promising. The power shortage is severe currently and in the near future. Hydropower is the most important component of the energy structure of the Qinghai Power Grid, occupying more than 60% power supply to the province. Therefore, exploring the hydropower potential of the current reservoir system is the key for relieving the power supply pressure on the regional power grid. Over the last several decades, lots of studies have been conducted on the benefit evaluations and comparisons under the assumption of the joint operation of a reservoir system within a river basin. Barros et al. (2003) estimated the benefits from the joint operation of the large-scale hydropower system in Brazil. Zhang et al. (2012) optimized the joint operation of the major storage reservoirs on the Upper Yangtze River and its major tributaries. Bai et al. (2015) quantified and analyzed the synergistic gains (including hydropower generation, water supply, ice/flood control and ecological flow) from the joint optimal operation of the UYR reservoir system. Researches indicate that enormous socio-economic benefits can be gained from the joint operation of reservoirs that have hydraulic, hydrological and electrical connections.

 ©2017, IAHR. Used with permission / ISSN 1562-6865 (Online) - ISSN 1063-7710 (Print)

Maximizing hydropower generation and ensuring firm output are two major concerns for evaluating performance of hydropower plants, which two are conflicting objectives and respectively represent the quality and reliability of hydropower operation (Li and Qiu, 2015). For decision makers, providing the Pareto set of solutions for multi-objective reservoir operation is more acceptable for making decisions than a single solution. The traditional way for solving a multi-objective optimization problem is using the weighting or epsilon constraint methods, and finding the Pareto set of solutions (i.e., the non-dominated solutions) with several runs. For instance, Yeh and Becker (1982) used the epsilon constraint method to study the multi-reservoir system of California Central Valley Project, considering the objective combinations of hydropower production, fish protection, water quality maintenance, water supply and recreation. Li et al. (2015) modeled the reservoir operation for analyzing the trade-off between water supply and power generation objectives, and used the epsilon constraint method and the nonlinear programming to solve the problem; and moreover, the ability of the nonlinear programming solver embedded in the LINGO software to find the global optimality was demonstrated for problems with large computing scale.

This paper aims at studying the joint optimal operation of the UYR reservoir system under the current water regulation policies and analyzing the trade-off between the maximum power and the firm output for the Qinghai Power Grid. To achieve this goal, first, we collect the hydrological data in the UYR basin and the operating rules for the reservoir system; second, a multi-objective model is formulated and solved by the nonlinear programming solver; finally, the Pareto set of solutions is presented and the results of typical years are selected for analysis.

2 MATERIALS

2.1 The reservoir system in the Upper Yellow River

The reservoirs that supply energy to the Qinghai Power Grid, where the majority of the installed capacity of the UYR reservoir system is located, are considered. Along the flow direction, these are the Banduo, Longyangxia (LYX), Laxiwa, Nina, Lijiaxia, Zhiganglaka, Kangyang, Gongboxia, Suzhi, Huangfeng, Jishixia, and Dahejia reservoirs, as shown in Figure 1. Moreover, the Liujiaxia (LJX) reservoir, although not a constituent of the Qinghai Power Grid, is also included in this study due to its large regulation capacity and great significance for the middle and lower basins, which constrains the bounds on releases from the reservoir system. Therefore, the system is composed of 13 reservoirs. The main characteristics of the reservoirs in the UYR are listed in Table 1.

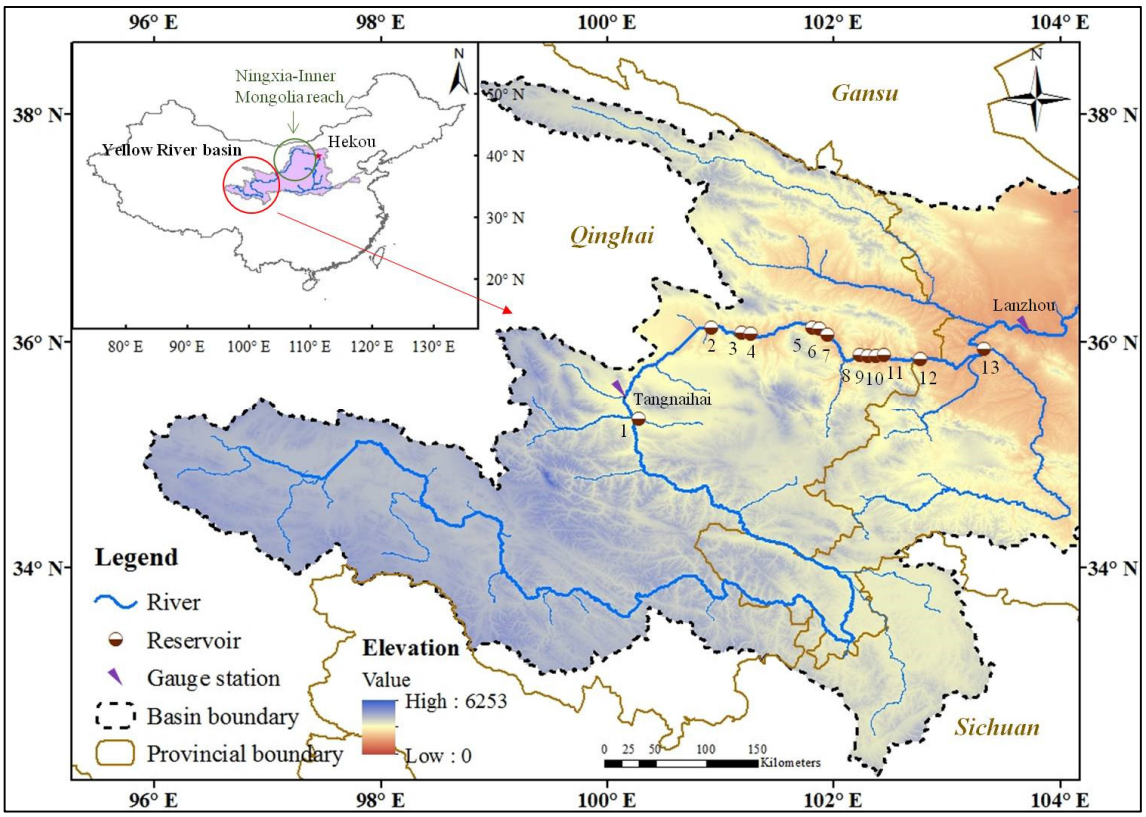

Figure 1. Map of the study area.

Table 1. Main characteristics of reservoirs in the UYR.

No.	Reservoir	Normal water level (m)	Dead water level (m)	Design water head (m)	Total storage (10^8 m^3)	Installed capacity (MW)
1	Banduo	2760	2757	35.5	0.108	360
2	Longyangxia	2600	2530	122	247	1280
3	Laxiwa	2452	2440	205	10.79	4200
4	Nina	2235.5	2231	14	0.262	160
5	Lijiaxia	2180	2178	122	16.5	2000
6	Zhiganglaka	2050	2048	12.5	0.154	192
7	Kangyang	2033	2031	18.7	0.288	280
8	Gongboxia	2005	2002	99.3	5.50	1500
9	Suzhi	1900	1897.5	16	0.455	225
10	Huangfeng	1880.5	1878.5	16	0.59	220
11	Jishixia	1856	1852	73	2.38	1020
12	Dahejia	1783	1782	9.2	0.039	142
13	Liujiaxia	1735	1694	100	57	1350

Among the 13 reservoirs, the LYX and LJX reservoirs are more dominant because of their large regulation capacities. Reasonable compensation actions between them can improve comprehensive benefits for the reservoir system. The LYX is a multi-year storage reservoir with 247×10^8 m^3 of total storage capacity and 1280 MW of total installed capacity; the LJX is a yearly storage reservoir with 57×10^8 m^3 of total storage capacity and 1350 MW of total installed capacity; the others are daily storage reservoirs or run-of-river hydropower plants.

2.2 Hydrological characteristics

The UYR region experiences a typical monsoon climate, with heavy precipitation in summer and less in other seasons. The stream flow results from the rainfall during the flood season, and it is also fed by the flow recession and mountain snowpack melt during the non-flood season. As can be seen from Figure 2, the maximum flows at the Tangnaihai gauge station (the control station at the entrance of the LYX reservoir, see Figure 1) occur in July, August, and September, when the annual average flows are 1307, 1078, and 1214 m^3/s, respectively; while the minimum flows occur in December, January, February and March, when the annual average flows are 229, 168, 166, and 220 m^3/s, respectively; and moreover, the flow variations display a much wider range during the flood season than during the non-flood season.

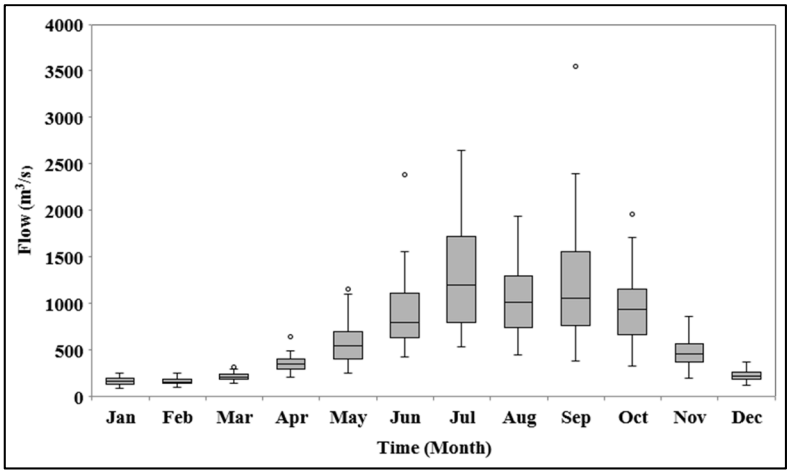

Figure 2. Temporal distribution of runoff at the Tangnaihai gauge station.

2.3 Operating rules of storage reservoirs

According to the operating rules and practice, the fore-bay water level of the LYX reservoir should be lowered below the flood limited water level 2594 m before early July (i.e., the beginning of the flood season) and maintained until the middle of September (i.e., the end of the flood season). Then, the fore-bay water level of the LYX reservoir gradually impounds as high as its normal water level 2600 m. The LJX reservoir undergoes two drawdown-refill cycles during a year. One is for flood control: the fore-bay water level of the LJX reservoir should be lowered below the flood limited water level 1726 m before early July and impounds as high as possible after the middle of September. The other is for ice control: the LJX reservoir should be pre-

 ©2017, IAHR. Used with permission / ISSN 1562-6865 (Online) - ISSN 1063-7710 (Print)

released at the end of November to reserve sufficient storage (approximately 10 - 15 billion m^3), because during ice season, the release from the LJX reservoir should be strictly limited to ensure stability of ice freeze-up and break-up in the Ningxia-Inner Mongolia reach (see Figure 1), and more water from the LYX reservoir should be released to compensate for the energy deficit during the peak energy period in the ice season. At times other than the two seasons, the fore-bay water level of the LJX reservoir can reach as high as its normal water level of 1735 m.

Furthermore, the priority of water regulation is superior to the hydropower regulation along the Yellow River. Therefore, the release from the control reservoirs should be guaranteed in order to meet the multiple utilization requirements downstream. The LJX reservoir is currently the farthest downstream storage reservoir of the system, which should be regarded as the control reservoir. The upper and lower bounds on releases from the LJX reservoir vary in periods: 1) during the flood season, the upper bound is approximately 4290 m^3/s, corresponding to the 100-year return period flood at Lanzhou gauge station; 2) during the ice season, the upper bounds range from 400 to 600 m^3/s, and the lower bounds range from 220 to 400 m^3/s, according to both practice and the literature (Chang et al., 2014); 3) during the water supply season, the lower bounds range from 700 to 950 m^3/s (particularly for farm irrigation), corresponding to the water requirement during 2010 at Lanzhou gauge station (Bai et al., 2015). It should be noted that the control releases from the LJX reservoir are presented by converting the flows at Lanzhou gauge station using the basin area ratio for the two locations.

3 METHODS

3.1 Multi-objective model

For a typical two-objective maximization problem, the mathematical model can be formulated as:

$$\max \mathbf{F(x)}=\left[F_1(\mathbf{x}), F_2(\mathbf{x})\right] \quad [1]$$

$$x_l \geq 0 \quad \forall l \quad [2]$$

$$g_k(\mathbf{x}) \leq 0 \quad \forall k \quad [3]$$

where $\mathbf{F}(\mathbf{x})$ is the vector of objectives, which includes two objectives, $F_1(\mathbf{x})$ and $F_2(\mathbf{x})$; x_l is the decision variables $l \in [1, L]$; $g_k(\mathbf{x})$ is the constraint, $k \in [1, K]$.

The two-objective maximization model Eq. [1] – [3] can be translated with the epsilon constraint method into the equivalent formulation as Eq. [4] – [7]:

$$\max F_1(\mathbf{x}) \quad [4]$$

$$F_2(\mathbf{x}) \geq F_2^{\min} + \sigma \cdot \Delta \quad [5]$$

$$x_l \geq 0 \quad \forall l \quad [6]$$

$$g_k(\mathbf{x}) \leq 0 \quad \forall k \quad [7]$$

where $F_2^{\min}$ is the minimum of objective $F_2(\mathbf{x})$; Δ is the increment of $F_2(\mathbf{x})$; σ is the integer constant, $\sigma = 0, 1, 2, \cdots$. The Pareto set of solutions of the two-objective maximization problem can be gained through solving Eq. [4] – [7] with various σ.

3.2 Objective

The objective of this study is to trade off the power quantity and power reliability associated with hydropower operation of the UYR reservoir system for the Qinghai Power Grid. For the maximum power computation, the energy produced from the LJX reservoir cannot be ignored because of its importance as mentioned earlier; while for the firm output computation, the output production of the LJX reservoir is excluded from the reservoir system because its output production is not transmitted to the Qinghai Power Grid. Therefore, the optimization model can be formulated as Eq. [8] – [9]:

$$\max\left(\sum_{t=1}^{T}\sum_{i=1}^{13} E_{i,t} - \zeta\sum_{t=1}^{T}\beta_t\right) \quad [8]$$

$$\sum_{i=1}^{12} N_t(t) + \beta_t \geq N^{\min} + \sigma\Delta N \quad [9]$$

©2017, IAHR. Used with permission / ISSN 1562-6865 (Online) - ISSN 1063-7710 (Print)

where

$$E_{i,t} = N_i(t)\Delta t = 9.81\eta_i R_i'(t)\bar{H}_i(t)\Delta t \quad [10]$$

$$R_i(t) = R_i'(t) + R_i''(t) \quad [11]$$

$$\bar{H}_i(t) = HF_i(t) - HT_i(t) - HL_i(t) \quad [12]$$

$E_{i,t}$ is the energy production of the hydropower plant at reservoir i during time step t; $N_i(t)$ is the output production of the hydropower plant at reservoir i during time step t; η_i is the hydropower plant efficiency at reservoir i; $R_i'(t)$ and $R_i''(t)$ are the power release and non-power release from reservoir i during time step t; Δt is the time interval; $\bar{H}_i(t)$ is the average head at reservoir i during time step t, which is the difference between the reservoir fore-bay water level $HF_i(t)$ and the tail-race water level $HT_i(t)$ and the water head loss $HL_i(t)$ at reservoir i during time step t; $N^{\min}$ is the minimum output production of the 12-reservoir system; ΔN is the increment of output production of the 12-reservoir system; β_t is the slack variable during time step t; ζ is the penalty factor. With the penalty term and slack variable in Eq. [8] and [9], the model can gain results when the guarantee rate of firm output from the 12-reservoir system is less than 100%.

3.3 Constraints

The operation of reservoir system is subject to the following constraints:

(1) Continuity equation:

$$\mathbf{S}(t+1) = \mathbf{S}(t) + \mathbf{I}(t) - \mathbf{M}\mathbf{R}(t) \quad \forall t \quad [13]$$

where $\mathbf{I}(t)$ is the vector of inflows to reservoirs ($i = 1,\cdots,n$) during time step t; $\mathbf{R}(t)$ is the vector of total releases from reservoirs ($i = 1,\cdots,n$) during time step t, $\mathbf{R}(t)=\left[R_1(t),\cdots,R_i(t)\cdots,R_n(t)\right]^T$; and $\mathbf{M}$ is the $n\times n$ reservoir system connectivity matrix.

(2) Initial and final reservoir storages:

$$\mathbf{S}(1) = \mathbf{S}^{initial} \quad [14]$$

$$\mathbf{S}(T+1) \geq \mathbf{S}^{final} \quad [15]$$

where $\mathbf{S}^{initial}$ and $\mathbf{S}^{final}$ are the vectors of initial and final storages of reservoirs ($i = 1,\cdots,n$).

(3) Lower and upper bounds on storages:

$$\mathbf{S}^{\min}(t+1) \leq \mathbf{S}(t+1) \leq \mathbf{S}^{\max}(t+1) \quad \forall t \quad [16]$$

where $\mathbf{S}^{\min}(t+1)$ and $\mathbf{S}^{\max}(t+1)$ are the vectors of minimum and maximum storages of reservoirs ($i = 1,\cdots,n$) at the end of time step t.

(4) Lower and upper bounds on total releases:

$$\mathbf{R}^{\min}(t) \leq \mathbf{R}(t) \leq \mathbf{R}^{\max}(t) \quad \forall t \quad [17]$$

where $\mathbf{R}^{\min}(t)$ is the vector of the required minimum releases from reservoirs ($i = 1,\cdots,n$) during time step t; and $\mathbf{R}^{\max}(t)$ is the vector of maximum allowable releases from reservoirs ($i = 1,\cdots,n$) during time step t.

(5) Lower and upper bounds on power releases:

$$\mathbf{R}'^{\min}(t) \leq \mathbf{R}'(t) \leq \mathbf{R}'^{\max}(t) \quad \forall t \quad [18]$$

where $\mathbf{R}'^{\min}(t)$ is the vector of the required minimum releases through turbines in hydropower plants at reservoirs ($i = 1,\cdots,n$) during time step t; and $\mathbf{R}'^{\max}(t)$ is the vector of maximum allowable releases through turbines in hydropower plants at reservoirs ($i = 1,\cdots,n$) during time step t.

(6) Lower and upper bounds on outputs:

$$\mathbf{N}^{\min}(t) \leq \mathbf{N}(t) \leq \mathbf{N}^{\max}(t) \quad \forall t \quad [19]$$

 ©2017, IAHR. Used with permission / ISSN 1562-6865 (Online) - ISSN 1063-7710 (Print)

where $\mathbf{N}(t)$ is the vector of outputs produced from hydropower plants at reservoirs ($i = 1,\cdots,n$) during time step t; $\mathbf{N}(t)=\left[N_1(t),\cdots,N_i(t)\cdots,N_n(t)\right]^T$; $\mathbf{N}^{\min}(t)$ is the vector of minimum required outputs from hydropower plants at reservoirs ($i = 1,\cdots,n$) during time step t; and $\mathbf{N}^{\max}(t)$ is the vector of maximum allowable outputs from hydropower plants at reservoirs ($i = 1,\cdots,n$) during time step t.

3.4 Nonlinear programming solver

The formulated optimization model is highly nonlinear and non-convex because of the complicated conversion from potential energy to kinetic energy and then to electrical energy. In this study, the LYX and LJX reservoirs are operated as storage reservoirs, while the other reservoirs are treated as run-of-river hydropower plants for simplicity. Therefore, the decision variables are the releases from the LYX and LJX reservoirs, and their storages are taken as state variables. In this study, the model is written and solved with LINGO 16.0 x64 (LINDO, 2015).The nonlinear programming solver of LINGO employs the generalized reduced gradient (GRG) algorithm, which is a nonlinear extension of simplex method for linear programming (Lasdon et al., 1978). The GRG is one of the most effective and efficient algorithm for solving the constrained nonlinear programming problem.

4 RESULTS AND DISCUSSIONS

The inflows over a recent 10-year horizon (from July, 2000 to June, 2010) were used as the inputs to the formulated model. The time period is divided into 360 time steps (each of which has a length of approximately 10 days). In practice, the water supply requirement downstream of the LJX reservoir cannot be adequately met during dry years. Therefore, it is assumed that the guarantee rates of releases from the LJX reservoir can reach 80% during the water supply seasons for the years when the hydrologic frequencies are above 80%. For analysis, three typical hydrologic years, including a dry year (2004-2005), a normal year (2008-2009) and a wet year (2005-2006), are selected, which corresponds to the hydrologic frequencies of approximately 75%, 50% and 25% in the historical record, respectively.

4.1 Trade-off between maximum power and firm output

The trade-off between maximum power and firm output of the UYR reservoir system is shown in Table 3, where 13 scenarios (S1 - S13) are listed. Both the annual average energy of 13-reservoir system (including the LJX reservoir) and 12-reservoir system (excluding the LJX reservoir) are presented. It can be seen from S1, the maximum annual average energy of the 13-reservoir system is 364.9×10^8 KWh and that of 12-reservoir system is 312.8×10^8 KWh. The annual average energy production decreases as the firm output of reservoir system increases. The firm output can reach 3110 MW if the guarantee rate is equal to 100%, whereas it can reach 3510 MW if the guarantee rate is around 90%. Note that the guarantee rate is the ratio of the number of time steps when the firm outputs are met to the total number of time steps. A small decrease in annual average energy can bring about a substantial increase in firm output from the 12-reservoir system. Specifically, a 4.5×10^8 KWh (1.42%) decrease in maximum power produces an 800 MW (34.63%) increase in firm output (i.e., S9 minus S1); a 7.7×10^8 KWh (2.46%) decrease in maximum power yields a 1200 MW (51.95%) increase in firm output (i.e., S13 minus S1). The decrease in annual average energy from the 12-reservoir system is completely from the LYX reservoir. The Pareto set of solutions is shown in Figure 3.

Table 3. Trade-off between maximum power and firm output of UYR reservoir system.

Scenario	Firm output (MW)	Annual average energy production (10^8 KWh)			
		LYX	LJX	13-reservoir system	12-reservoir system
S1	2310	51.9	52.1	364.9	312.8
S2	2410	51.8	52.1	364.8	312.7
S3	2510	51.7	52.0	364.6	312.6
S4	2610	51.5	51.9	364.4	312.4
S5	2710	51.4	51.8	364.1	312.3
S6	2810	50.8	51.9	363.6	311.7
S7	2910	49.9	52.0	362.8	310.8
S8	3010	48.8	52.1	361.8	309.7
S9	3110	47.4	51.9	360.3	308.3
S10	3210 (97.8%)	46.7	51.9	359.6	307.6
S11	3310 (95.6%)	45.7	51.9	358.5	306.6
S12	3410 (93.3%)	44.5	51.7	357.1	305.4
S13	3510 (90.6%)	44.2	51.2	356.3	305.1

*Note: the percentage after the firm output represents the guarantee rate.

©2017, IAHR. Used with permission / ISSN 1562-6865 (Online) - ISSN 1063-7710 (Print)

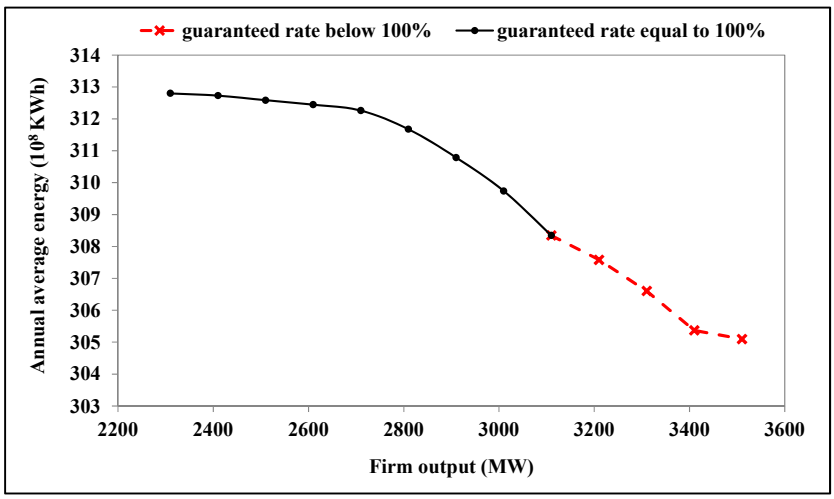

Figure 3. Trade-off between maximum power and firm output of 12-reservoir system in the Qinghai Power Grid.

4.2 Comparison of energy production under different scenarios

Four scenarios (S1, S5, S9, and S13) are selected for the following analysis. The comparison of energy production from the 12-reservoir system among various scenarios is shown in Figure 4. To maximize the energy production, the annual average energy is unevenly distributed among the various months within a year -- more energy is produced during the wet season (May, July, August, and September) while less in dry season. In S1, the maximum energy production is 36.4×10^8 KWh in May, and the minimum energy production is 16.0×10^8 KWh in February. To maximize the firm output, the annual average energy is evenly distributed. In S13, the power generation is approximately 25.0×10^8 KWh among the various months.

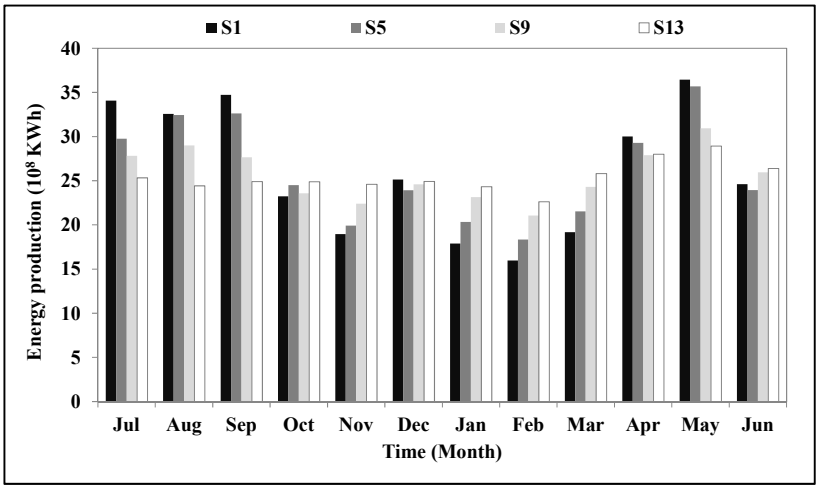

Figure 4. Comparison of energy production distribution from 12-reservoir system among various scenarios.

4.3 Comparison of power production in different hydrological years

The energy production during various hydrologic years is shown in Table 4. In S1, the maximum power of the 12-reservoir system can reach 297.7, 363.9, and 411.4×10^8 KWh, and the energy production from the LYX reservoir is 49.5, 62.8, and 71.1×10^8 KWh for the dry, normal, and wet years, respectively. In S13, the maximum power of the 12-reservoir system is 307.5×10^8 KWh, and the power generation of LYX reservoir is 35.9, 46.2, and 44.5×10^8 KWh for the three typical hydrologic years. This indicates that the LYX reservoir regulates water conditions over multiple years and distributes the water and hydropower resources from wet years to dry years to meet the firm output requirement.

 ©2017, IAHR. Used with permission / ISSN 1562-6865 (Online) - ISSN 1063-7710 (Print)

Table 4. Energy production during various hydrologic years.

Hydrologic year	Scenario	Energy production (10^8 KWh)			
		LYX	LJX	13-reservoir system	12-reservoir system
Dry	S1	49.5	50.4	348.1	297.7
	S5	44.1	47.4	323.6	276.3
	S9	35.2	45.7	318.3	272.7
	S13	35.9	53.7	361.2	307.5
Normal	S1	62.8	59.8	423.7	363.9
	S5	62.0	59.2	418.9	359.7
	S9	58.6	56.6	398.7	342.1
	S13	46.2	51.2	358.7	307.5
Wet	S1	71.1	70.2	481.6	411.4
	S5	68.0	67.8	461.7	393.9
	S9	45.2	52.7	335.6	282.9
	S13	44.5	57.3	364.9	307.5

4.4 Comparison of fore-bay water level and release

The comparison of fore-bay water level and release among the various scenarios is shown in Figure 5. It can be seen that, as the firm output increases, the release from the LYX reservoir becomes higher and flatter, resulting in a decrease in the fore-bay water level of the LYX reservoir on the whole. In S13, the water stored in the LYX reservoir plus the incoming flow to the LYX reservoir cannot maintain the increase in the release from the LYX reservoir, resulting in violations for the firm output from the 12-reservoir system during the first three years. While for the LJX reservoir, its operation is adapted to various incoming flows from upstream in the various scenarios for energy production maximization.

5 CONCLUSIONS

This paper studies the trade-off between power quantity and power reliability associated with hydropower operation of the UYR reservoir system, considering the full potential of joint operation. The following results can be made through analysis:

(1) The maximum annual average power can reach 312.8×10^8 KWh, corresponding to the firm output of 2310 MW; the maximum firm output can reach 3110 MW (guarantee rate of 100%) and 3510 MW (guarantee rate of 90%), corresponding to the maximum annual average power of 308.3×10^8 KWh and 305.1×10^8 KWh, for the 12-reservoir system in the Qinghai Power Grid. The 1.42% and 2.46% percentage reduction in maximum power, which is completely from the LYX reservoir, can get 36.63% and 51.95% percentage increase in firm output from the 12-reservoir system in return, respectively;

(2) For the typical dry, normal, and wet years, the maximum power can reach 297.7, 363.9, and 411.4×10^8 KWh, respectively; when the firm output is 3510 MW, the energy production is 307.5×10^8 KWh for all these hydrologic years for the 12-reservoir system. The LYX reservoir plays the role of multi-year regulation that distributes the water and hydropower resources from wet year to dry year so as to meet the firm output requirement;

(3) For maximizing the energy production, the fore-bay water level of the LYX reservoir should be maintained as high as possible; while for maximizing the firm output, the water from the LYX reservoir should be released as much and stable as possible;

(4) The Pareto set of solutions in the form of trade-off curve can provide important reference with managers and help support the power purchase decision from outside the Qinghai Power Grid.

©2017, IAHR. Used with permission / ISSN 1562-6865 (Online) - ISSN 1063-7710 (Print)

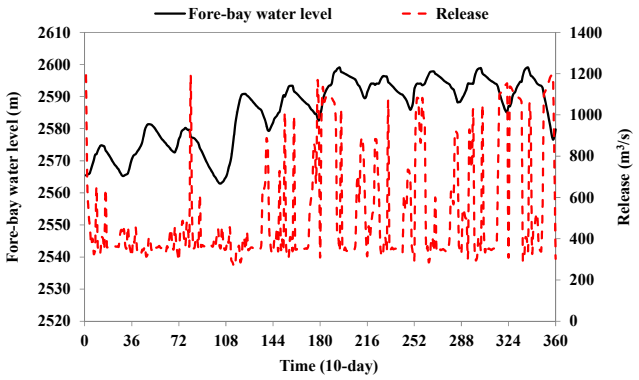

(a) LYX in S1

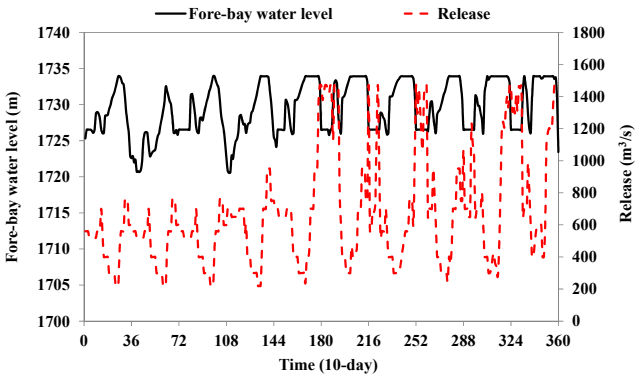

(b) LJX in S1

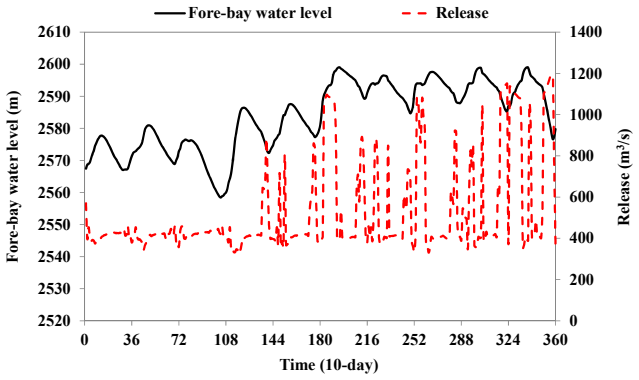

(c) LYX in S5

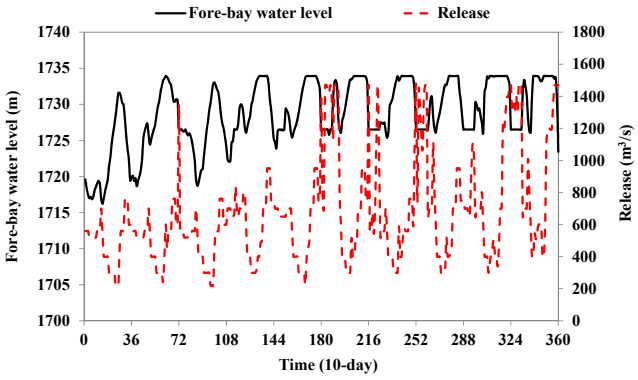

(d) LJX in S5

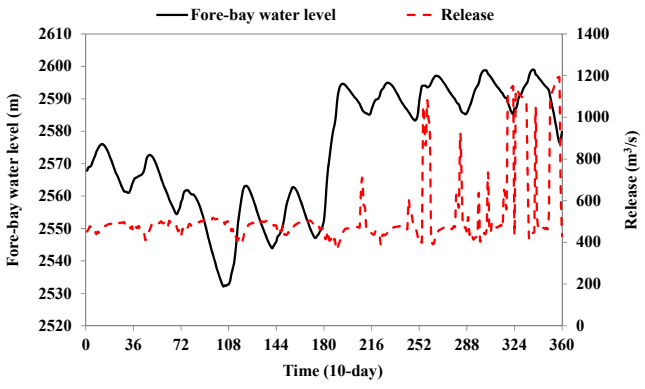

(e) LYX in S9

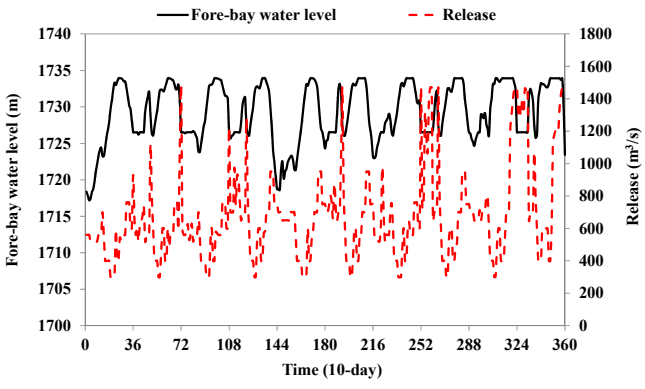

(f) LJX in S9

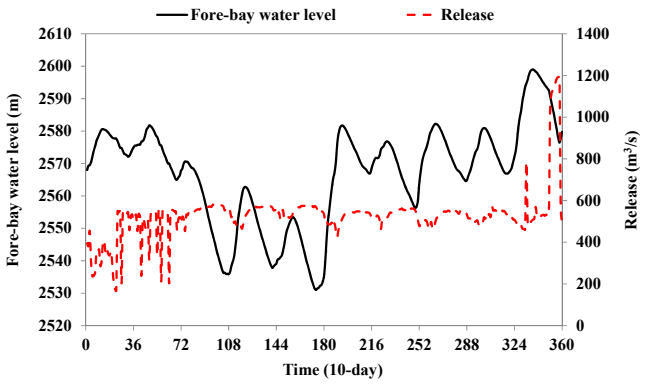

(g) LYX in S13

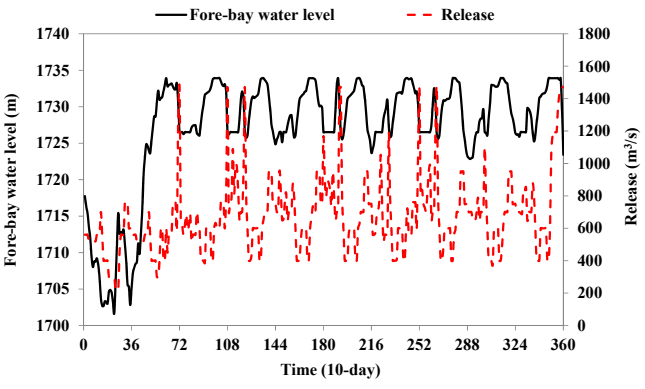

(h) LJX in S13

Figure 5. Comparison of fore-bay water level and release among various scenarios.

©2017, IAHR. Used with permission / ISSN 1562-6865 (Online) - ISSN 1063-7710 (Print)

ACKNOWLEDGEMENTS

This study is supported by the National Key Research and Development Program of China (2016YFC0401401), the National Natural Science Foundation of China (51609256, 51609122, 51522907 and 51579131), the Science and Technology Project of State Grid Corporation of China (52283014000T). The authors are very grateful to the Yellow River Conservancy Commission and the Huanghe Hydropower Development Co., Ltd for the provision of valuable study data.

REFERENCES

Bai, T., Chang, J.X., Chang, F.J., Huang, Q., Wang, Y.M. & Chen, G.S. (2015). Synergistic Gains from the Multi-Objective Optimal Operation of Cascade Reservoirs in the Upper Yellow River Basin. *Journal of Hydrology*, 523, 758-767.

Barros, M.T.L., Tsai, F.T.C., Yang, S.L., Lopes, J.E.G. & Yeh, W.W.G. (2003). Optimization of Large-Scale Hydropower System Operations. *Journal of Water Resources Planning and Management*, 129(3), 178-188.

Chang, J.X., Meng, X.J., Wang, Z.Z., Wang, X.B. & Huang, Q. (2014). Optimized Cascade Reservoir Operation Considering Ice Flood Control and Power Generation. *Journal of Hydrology*, 519, 1042-1051.

Cheng, C.T., Shen, J.J., Wu, X.Y. & Chau, K.W. (2012). Operation Challenges for Fast-Growing China's Hydropower Systems and Respondence to Energy Saving and Emission Reduction. *Renewable and Sustainable Energy Reviews*, 16(5), 2386-2393.

Huanghe Hydropower Development Co., Ltd. (2016). Available: http://www.hhsd.com.cn/develop/fd/ [Accessed on 28/12/2016]. (in Chinese)

Lasdon, L.S., Waren, A.D., Jain, A. & Ratner, M. (1978). Design and Testing of a Generalized Reduced Gradient Code for Nonlinear Programming. *ACM Transactions on Mathematical Software (TOMS)*, 4(1), 34-50.

Li, F.F. & Qiu, J. (2015). Multi-Objective Reservoir Optimization Balancing Energy Generation and Firm output. *Energies*, 8(7), 6962-6976.

Li, X., Wei, J.H., Si, Y. & Yin, D.Q. (2015). Modeling and Optimizing Reservoir Operation for Trade-Off between Water Supply and Power Generation. *South-to-North Water Transfers and Water Science & Technology*, 13(5), 973-979. (in Chinese)

LINDO. (2015). *LINGO User's Guide*, LINDO Systems Inc.

Wang, Q. & Chen, Y. (2010). Status and Outlook of China's Free-Carbon Electricity. *Renewable and Sustainable Energy Reviews*, 14(3), 1014-1025.

Yeh, W.W.G. & Becker, L. (1982). Multiobjective Analysis of Multireservoir Operations. *Water Resources Research*, 18(5), 1326-1336.

Zhang, R., Zhou, J.Z., Zhang, H.F., Liao, X. & Wang, X.M. (2012). Optimal Operation of Large-Scale Cascaded Hydropower Systems in the Upper Reaches of the Yangtze River, China. *Journal of Water Resources Planning and Management*, 140(4), 480-495.

©2017, IAHR. Used with permission / ISSN 1562-6865 (Online) - ISSN 1063-7710 (Print)

Proceedings of the 37th IAHR World Congress
August 13 – 18, 2017, Kuala Lumpur, Malaysia

CLIMATE-SMART DECISION SUPPORT SYSTEM FOR IRRIGATION AND WATER RESOURCES MANAGEMENT FOR RICE PRODUCTION

MD ROWSHON KAMAL[1]., NKULULEKO SIMEON DLAMINI[2] & MOHD AMIN MOHD SOOM [3]

[1,2] Department of Biological and Agricultural Engineering, Faculty of Engineering,
Universiti Putra Malaysia, 43400 UPM Serdang, Selangor Darul Ehsan, Malaysia,
[3] Crop Production Programme, Faculty of Sustainable Agriculture, Universiti Malaysia Sabah,
rowshon@upm.edu.my

ABSTRACT

Global water scarcity remains the main growing challenge faced by the agriculture sector. This condition is attributed partly to the tremendous increase in the demand for different water uses and the climate change phenomena. Modelling irrigation water allocation for systems such paddy fields under changing climate requires several procedures that may be tedious for water users such as farmers. Climate-smart Rice Irrigation Management Information System (CSRIMIS), is a user-friendly decision support program developed in this study to simulate water allocation deliveries in paddy fields at Tanjung Karang irrigation scheme while accounting for the impacts of climate change. The program is driven by climate data derived from 10 global climate models (GCMs) statistically downscaled under 3 emission scenarios RCP4.5, 6.0 and 8.5. A stochastic daily rainfall model is developed for forecasting future rainfall. Outputs of a hydrological model are incorporated in the program for assessing flows of the Bernam River, which is a source of irrigation water for the scheme. The program assess water requirement by adjusting the reference evapotranspiration (ETo) for projected future carbon concentration based on GCM simulations. The program comprises of 4 key modules; stochastic rainfall, reference evapotranspiration, water demand and water allocation and monitoring. MATLAB programming language is used to develop the program and its graphical user interface (GUI). The interface is the framework for linking all the modules of the program and provides the user with the ability to access data and output for the system, based on a mouse-driven approach with pop-up windows, pull-down menus and button controls. The multi-model projections show an increase in future temperature (tmax and tmin) in all respective scenarios, up to an average of 2.5 °C for under the worst-case scenario (RC8.5). This paper discusses the CSRIMIS program and presents some of its outputs as relates to the 4 modules.

Keywords: Climate change; CSRIMIS; GCM; water allocation; rice irrigation.

1 INTRODUCTION

The impact of climate change is a 21st century environmental problem which has raised worldwide concern at all government levels and research community (Wang et al., 2014). The Intergovernmental Panel on Climate Change (IPCC, 2007) has presented compelling evidence on the existence of this phenomenon. How rainfall and temperature patterns and their magnitudes have been changing over the past centuries. It is anticipated that these climatic changes might take the world into a new phase of water stress and uncertainty. Global studies reveal that climate change will impact more significantly on the hydrologic cycle and water supplies. It has been predicted that with changes in rainfall and temperature, there will be a significant increase in water demands. At the global scale, it is predicted that water demand will increase by 55 % by 2050 (Vörösmarty et al., 2005) and this increase will be felt more by the agriculture sector. It is therefore crucial to understand how water demand will change as a result of climate change for managing and planning of water resources in the short and long-term period.

A number of studies have been done to investigate the impact of climate change on hydrological and water demand in various regions (Matthews et al., 1995; Döll, 2002; Konzmann et al., 2013). At regional scale, Matthews et al. (1995) simulated climate change impacts on rice yields in Asia using two crop models and found significant spatial differences wherein in some Asian countries. Rice yield was predicted to increase while a decrease was observed in Japan and South Korea. On a global scale, the study is among the earliest global studies of climate change impacts on long-term average irrigation requirements (Döll, 2000). The Global Irrigation Model (GIM) with a spatial resolution of 0.5° x 0.5° was used to explore the impact of climate change on irrigation water requirement for all irrigated areas of the year 1995 on the globe. Two outputs from ECHAM4 and HadCM3 were used and the results show that two-thirds of the area under irrigation in the year 1995 would possibly suffer from increased water requirements. A more recent study by Konzmann et al. (2013) investigated climate impacts on global irrigation requirements using 19 GCMs, simulated with vegetation and hydrology model. They found that irrigation requirements have a high likelihood of increasing

 ©2017, IAHR. Used with permission / ISSN 1562-6865 (Online) - ISSN 1063-7710 (Print)

for some regions and lower for others. However, they stressed that the increase would have to be abst Döll (2000) racted from groundwater resources.

Most of the climate change assessment studies investigated the changes in the reference evapotranspiration, irrigation water demand, the effective rainfall during crop growing season on changes in temperature and rainfall simulated by climate models mainly based on the downscaling technique. However, many water users such as farmers have not taken seriously the realities of the impact of climate change primarily because of the way climate projections information is presented and also the fact that downscaling is a tedious and complex exercise for many people. To overcome this issue, a simple computer-based water management tool is developed in this study to reduce the task downscaling and enable farmers to simulate their long-term and daily irrigation water deliveries and allocation using climate information derived from global climate models (GCMs). It is expected that the tool proposed in this study can be used for more realistic projection of irrigation water demand and deliveries, thus contributing to long-term water resources planning and management in the context of climate change.

2 DATA AND METHODOLOGY

Analysis of water allocation on paddy fields as impacted by climate change requires the generation of climate change data), calculation of reference evapotranspiration (ETo) and water allocation estimation. Climate change data are to generate from the global climate models (GCMs using downscaling techniques). The ETo is calculated using the FAO Penman–Monteith method and water balance model for paddy field. The decision support system is developed using MATLAB programming environment.

2.1 Study area

The Tanjung Karang Irrigation Scheme (TAKRIS) Döll (2000) is one the 8 large rice schemes shown in Figure 1, located in the District of Kuala Selangor in Selangor State on a flat coastal plain and lies within 3.4°E and 100.59°N. The scheme occupies a total irrigable area of 20,000 hectares under rice production and is cultivated twice a year. That is, January to June (off-season) and July to December (main-season).

About 123 irrigation blocks receive irrigation water from the runoff of the Upper Bernam river basin which is diverted and conveyed via a 36 km long feeder canal and pumped into the scheme tertiary canal systems through the main Canal. The area receives an annual rainfall of about 1,700 mm year^{-1} and experiences a tropical climate with marked differences between the two cropping seasons. Due to insufficient flows in this river especially during the off-season, cultivation of paddy has been re-staggered into four Irrigation Service Areas (ISAs): ISA I, ISA II, ISA III and ISA IV to ensure constant water supply in paddy fields. Cases of water rationing are common during the dry season which has led to frequent water shortages for paddy fields in the past. The river discharge records are generally low during the same period.

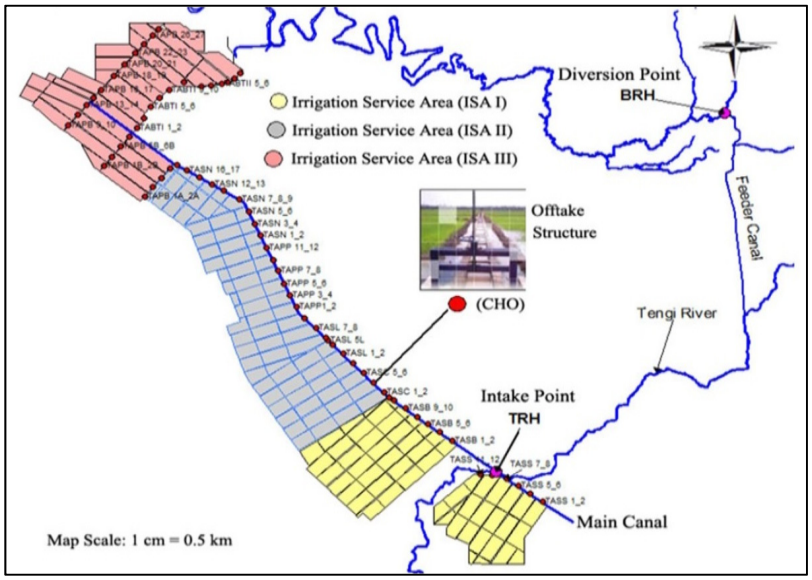

Figure 1. Tanjung Karang Rice Irrigation Scheme at Northwest Selangor (Source: Rowshon et al., 2014).

2.2 Generating climate scenarios

In this study, climate change data as impacted by carbon emissions were obtained by downscaling climate outputs from 10 GCMs using statistical downscaling and change factor techniques to produce local-scale daily weather data. In the water allocation model, we used the latest scenarios called Representative Concentration Pathways (RCPs). RCPs offer a better understanding regarding the concentration of future

©2017, IAHR. Used with permission / ISSN 1562-6865 (Online) - ISSN 1063-7710 (Print)

greenhouse gases for running climate models than previous scenarios (Meinshausen et al., 2011; Wayne, 2013). There are three available climate scenarios; RCP4.5, RCP6.0, and RCP8.5, for 10 GCMs. Data from the 10 GCMs was extracted using coordinates of the study area regarding longitude and latitude of the nearest grid to study area. Change factors were calculated in terms of the ratio of precipitation and absolute change amount for air temperature and other variables for each month and three periods, 2010–2039 (the 2020s), 2040–2069 (2050s), and 2070–2099 (2080s).

2.3 Hydrological simulation

Climate change impacts on hydrology at the Bernam catchment were quantified based on discharges simulated with the Soil and Water Assessment Tool (SWAT) hydrological model, developed by the United States Department of Agriculture (USDA) (Arnold et al., 1998). SWAT has been used for water resources planning including climate change assessments for over 20 years. SWAT is a continuous-time, semi-distributed, process-based river basin model for simulation of hydrology, sediment and non-point source pollution in big river systems by agricultural chemicals (Arnold et al., 2012). The basin minimum required daily input data for SWAT include; spatial data (soils, land use and digital elevation model), temperature (minimum and maximum) and rainfall. A natural inflow time series data is also needed for model calibration (1981-1998) and validation (1999-2006). Model performance was based on the three objective functions (Nash-Sutcliffe, the coefficient of determination and percent bias).

3 MODEL DEVELOPMENT

3.1 Software and GUI integration

A decision support system program, known as Climate-smart Rice Irrigation Management Information System (CSRIMIS) was developed. The model comprises of 4 management modules: (1) Stochastic Rainfall Generator Module; (2) Reference Evapotranspiration Module; (3) Water Demand Module; and (4) Water Allocation Module, all contained within a single computer file. The overall structure of the program is shown in Figure 2. All simulations are driven by climate models (GCMs) based on future carbon emission scenarios. The program was developed using MATLAB (R2014a) programming and graphical user interface development environment (GUIDE). The different modules are linked through the graphical user interface (GUI) and provide the user with the ability to access data and output for the system. GUI is based on a mouse-driven approach with pop-up windows, pull-down menus and button controls. Description of the program components is given in the next section.

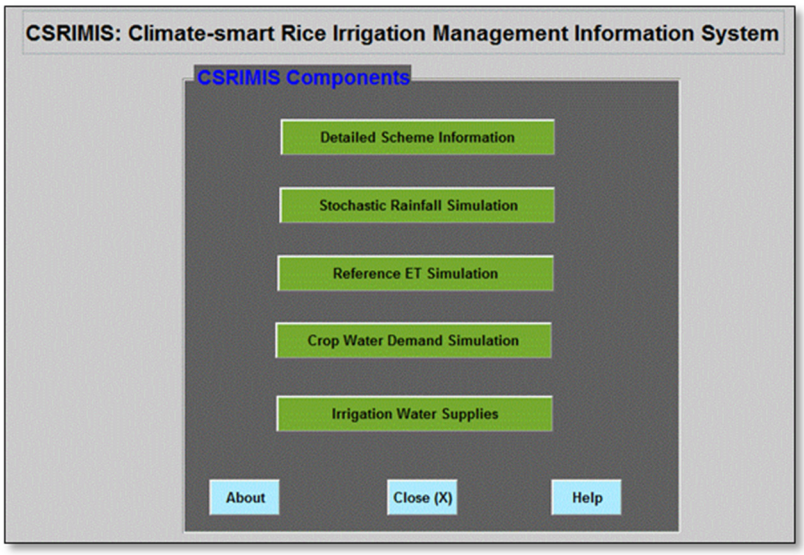

Figure 2. CSRIMIS Program main window.

3.2 Stochastic rainfall generator module

Rainfall was generated in two steps, generating rainfall occurrence and amount. For occurrence step, rainfall is described by two transitional probabilities, *P(dw)* the probability of a wet day preceded by a dry day and *P(ww)* the probability of a wet day preceded by a wet day. The 2 transitional probabilities are computed from observed rainfall series and are constant for a given month but vary between the different months. To simulate rainfall occurrence *Ps(t)* on day t, a random number U_t, ranging between 0 and 1 is generated and compared with the critical transition probability which depends on rainfall state of the previous day t-*1* where wet day = *w* and dry day = *d*. A wet day is simulated when the random number is less than the critical

 ©2017, IAHR. Used with permission / ISSN 1562-6865 (Online) - ISSN 1063-7710 (Print)

probability. Otherwise, it is simulated as a dry day. The distribution of rainfall is assumed as a gamma distribution because it is the most popular choice in rainfall studies. The graphical user interface for the Rainfall Generator Model was developed using the MATLAB. MATLAB script was developed for each component of the rainfall model including model calibration, change factor calculations from GCM outputs and perturbing model parameters for future simulations. Observed historical rainfall records (1976-2005) and GCM outputs (precipitation flux) are the main inputs in the rainfall generation module. The observed historical rainfall records are considered the 'predictand' while the precipitation flux is the 'predictor' in the model.

3.3 Reference ET computation module

Climate variables were downscaled from ten GCMs outputs using the Change Factor method and used as basic input data in the Reference ET model for calculation of the future ETo using Eq. [1].

$$ETo = \frac{0.408\Delta(R_n - G) + \gamma \frac{900}{T+273} u_2 (e_s - e_a)}{\Delta + \gamma(1 + 0.34u_2)} \quad [1]$$

where; ETo = standardized reference crop evapotranspiration for short grass (mm d-1), Rn= net radiation at the crop surface (MJ m-2 day-1), G= soil heat flux density (MJ m-2 day-1), T = air temperature at 2 m height (°C), u2 = wind speed at 2 m height (m sec-1), es – ea = saturation vapour pressure deficit (kPa), Δ = slope vapour pressure curve (k Pa °C-1), ɣ = psychometric constant (k Pa °C-1), 900 = constant factor.

3.4 Water demand module

The paddy crop consumptive use, also known as ETc, was determined using reference evapotranspiration and crop coefficients (Kc) combination. Net irrigation requirement, which is the amount of water that the paddy crop would transpire more than rainfall in the root zone of the crop, is calculated based on the crop water requirement, seepage/percolation and the expected rainfall contribution for that period Eq. [3]. Seepage-percolation rate ranging between 2-5 mm/day was adopted following the feasibility study report for the scheme by Japan International Cooperation Agency, JICA (1988).

$$ET_c = ET_o \times K_c \quad [2]$$

$$NIR = ET_c + SP - EFR \quad [3]$$

where; ETc = the crop evapotranspiration (mm/day), Kc = the crop coefficient, NIR = net irrigation requirements (mm/day), SP = seepage (mm/day), and EFR = effective rainfall (mm/day).

3.5 Water allocation module

Daily water demand in each irrigation compartment is computed based on actual planting dates and expected rainfall. The module computes the daily irrigation deliveries using a daily time step water balance model as shown in Eq. [4].

$$SW_{t+1} = SW_t + IR_t + ER_t - ET_t - SP_t - DR_t \quad [4]$$

where: SW_{t+1} = depth of standing water in the field on the *(t+1)*th day, SW_t = depth of standing water in the field on *t* th day, IR_t, = depth of applied irrigation on the *t*th day, ER_t,= depth of the effective rainfall on the *t*-th day, ET_t,= depth of crop evapotranspiration on the *t*th day, *SPt* = depth of water lost through seepage and percolation on the *t*th day, DR_t = depth of water lost through surface drainage on the *t*th day.

4 RESULTS AND DISCUSSIONS

4.1 Climate scenarios

Table 1 present future annual changes in temperature and rainfall projections in relation to the baseline period (1976-2006) under three RCP scenarios. For temperature, there is a distinct increasing trend in maximum temperature throughout the future period although this varies with period and seasons. On annual basis, under RCP4.5, 6.0 and 8.5 scenarios, the mean maximum temperature is predicted to increase by an average range of 0.9°C, 1.4°C and 2.5°C in the 2020s, 2050s and 2080s periods respectively, compared to the baseline period. The results are consistent with findings of Tan et al. (2015) who also found that projected future annual temperature may increase by 0.99 to 3.15°C in the most severe scenario (RCP 8.5) for the Johor River Basin of Malaysia.

©2017, IAHR. Used with permission / ISSN 1562-6865 (Online) - ISSN 1063-7710 (Print)

Table 1. Change in temperature (maximum and minimum) and rainfall under the RCP scenarios with respect to baseline period (1976–2005) for Tanjung Karang Irrigation Scheme, Malaysia.

Scenarios	RCP 4.5	RCP 6.0	RCP 8.5
Maximum Temperature (°C)			
2020s	0.7	0.5	0.8
2050s	1.3	1.1	1.9
2080s	1.6	1.9	3.3
Minimum Temperature (°C)			
2020s	0.7	0.6	0.9
2050s	1.4	1.2	2.0
2080s	1.8	1.9	3.4
Rainfall (mm)			
2020s	38.5	19.2	65.1
2050s	17.2	46.4	115.8
2080s	96.8	53.3	132.7

The results indicate that annual future rainfall will increase slightly from the baseline amounts for all scenarios. There was no significant difference among the eight stations within the basin with respect to future temperature and rainfall changes, possibly because of the watershed size (1,097 km^2) where all the stations fall within one GCM grid cell.

4.2 Impact of climate to future streamflow

The model was calibrated and validated using 30 years (1976–2005) of daily discharge data. The optimal combination of parameters was selected based on the coefficient of determination (R2), Nash-Sutcliffe (NS) and percent bias (PBIAS) criteria, yielding values of 0.67, 0.62 and -9.4 and 0.62, 0.61 and -4.2 for calibration and validation, respectively. These values are representative of high quality weather inputs and observed discharge and are acceptable based on the Moriasi et al. (2007) evaluation criteria. Projected rainfall changes in the context of climate change are shown in Table 2 for years 2020s, 2050s and 2080s.

Table 2 shows that there is a general decrease of flow in the dry season runoff response especially in the 2050s and 2080s periods, but less apparent in the 2020s. The largest decrease is -6.9 m^3/s during the 2080s under the RCP85 scenario. This reduction confirms the corresponding decrease in rainfall amount and temperature increase during this season. Although there is a slight increase in rainfall during May, June, and July, this does not seem to offset the decreasing flows in this season. The wet season period is characterized by an increase in streamflow of 10.7 m^3/s for the RCP85 scenario in the 2020s, followed by 9.9 m^3/s and 7.3 m^3/s in 2050s and 2080s respectively, in response to the increase in rainfall during this season. Annually, streamflow shows an increase in all scenarios and all future periods, where RCP8.5 has the smallest increase (0.4%) from the baseline in the 2080s and largest increase (14.9%) in the 2020s period.

Table 2. Comparison of streamflow between observed and projected values under RCP45, 60 and 85 scenarios.

Season	Baseline	2020s (m^3/s)			2050s (m^3/s)			2080s (m^3/s)		
	(m^3/s)	RCP4.5	RCP6.0	RCP8.5	RCP4.5	RCP6.0	RCP8.5	RCP4.5	RCP6.0	RCP8.5
Dry	40.0	2.5	- 0.2	2.8	- 2.1	- 1.5	- 3.1	0.1	- 1.8	- 6.5
Wet	50.1	3.5	7.7	10.7	4.4	5.5	9.4	2.7	6.5	7.3
Annual	45.1	3.0	3.7	6.7	1.1	2.0	3.1	1.4	2.3	0.2
		(6.6%)	(8.3%)	(14.9%)	(2.5%)	(4.4%)	(7.0%)	(3.1%)	(5.2%)	(0.4%)

Paddy production seasons: 1) Dry season: January to June; 2) Wet season: July to December

4.3 Stochastic rainfall generator module outputs

The stochastic rainfall generator model runs following the algorithm explained in section 3.2. The CSRIMIS dialog wizard for simulating rainfall is shown in Figure 3. Estimated model parameters for different months are shown in Table 3. The user makes selection of the station, GCM and emission scenario. The GCM multi-model option is recommended to reduce the inherent uncertainties exhibited by a single GCM projection. The button 'Generate time Series' will then generate the rainfall sequences. Simulation can be done for both short-term and long-term periods and the output can be saved in the output folder and displayed in tables and graphs.

 ©2017, IAHR. Used with permission / ISSN 1562-6865 (Online) - ISSN 1063-7710 (Print)

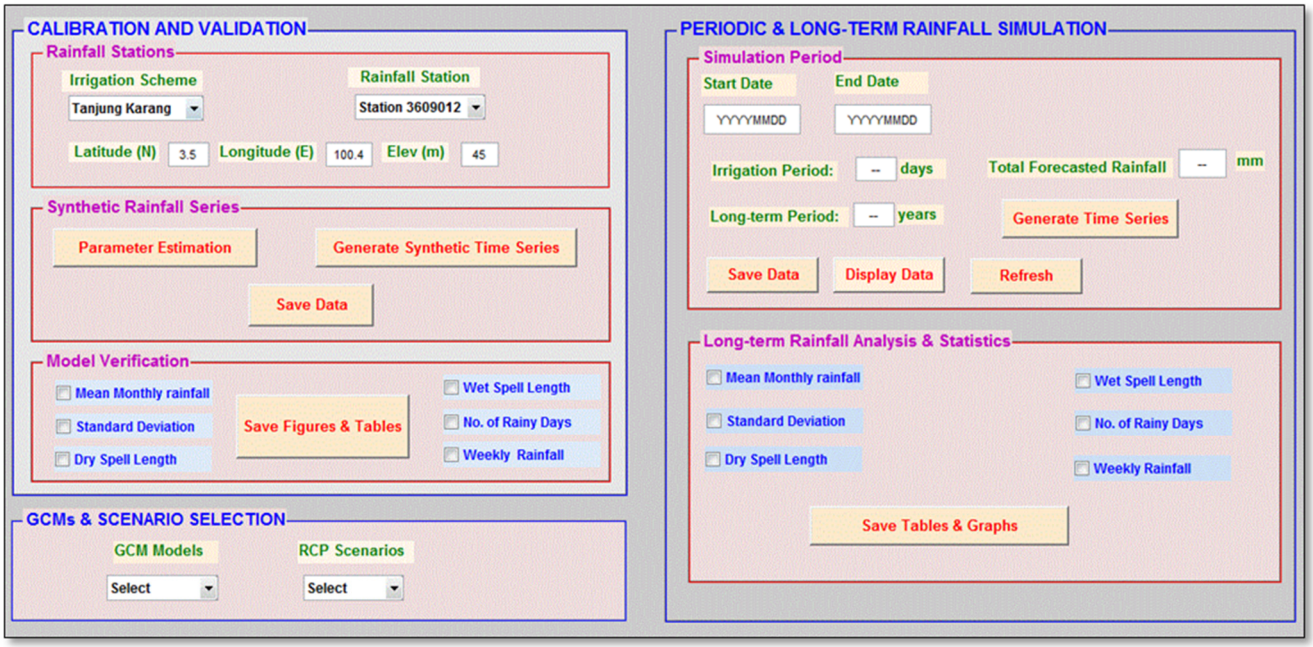

Figure 3. Stochastic rainfall generator model dialog wizard for simulation of rainfall sequences.

Table 3. Estimated model parameters for different months for the simulated period.

Gamma Parameters	Jan	Feb	Mar	Apr	May	Jun	Jul	Aug	Sep	Oct	Nov	Dec
α	0.96	0.83	0.85	0.91	0.86	0.90	0.73	0.84	0.91	0.97	0.97	1.11
β	13.09	19.93	16.94	16.75	17.42	16.34	20.6	19.28	16.54	17.46	17.04	14.27

Table 4 shows one year simulation period of 2017 from January to December. The total daily annual expected rainfall is 1,646.0 mm and 1,525.5 mm under MRI-CGCM3 model and multi-model, respectively. The single GCM overestimated rainfall by about 121 mm compared with the multi-model projection. These results illustrate the underlying inherent uncertainties in climate model projections as indicated by the large spread of the single model trajectory. However, simulated rainfall amounts are consistent with the annual expected rainfall amount for the study area, which is also around 1,600 mm.

Table 4. Stochastic daily rainfall simulation for 2017 (1 Jan – 31 Dec) under RCP4.5 scenario.

No.	Year	Month	Day	Rainfall
1	2107	1	1	0
2	2107	1	2	0
3	2107	1	3	0
4	2107	1	4	0
5	2107	1	5	0
6	2107	1	6	0
7	2107	1	7	0
8	2107	1	8	0
9	2107	1	9	0
10	2107	1	10	0
11	2107	1	11	0
12	2107	1	12	4.81
13	2107	1	13	13.27
14	2107	1	14	16.96
15	2107	1	15	0
16	2107	1	16	0
17	2107	1	17	0
18	2107	1	18	7.17
19	2107	1	19	6.83
20	2107	1	20	0
21	2107	1	21	0

Long-term rainfall simulation amount is demonstrated in Figure 4 for multi-model projection respectively, for a 10-year simulation period. Both simulations projected increase in rainfall under RCP4.5 scenario compared to the baseline period.

©2017, IAHR. Used with permission / ISSN 1562-6865 (Online) - ISSN 1063-7710 (Print)

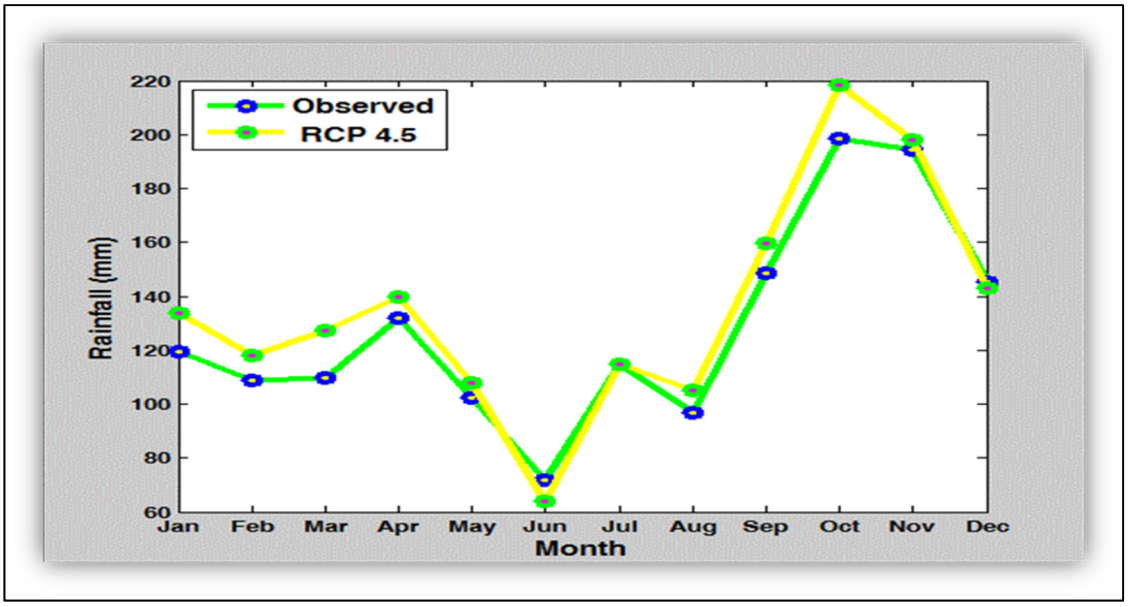

Figure 4. Simulated mean monthly rainfall for 10-year period (2017 to 2027) under RCP4.5 scenario.

4.4 Reference evapotranspiration module outputs

Reference evapotranspiration (ETo) for future projections of climate scenarios was estimated with the Penman-Monteith equation using downscaled climate variables from the GCMs outputs. The dialog wizard for daily ETo computing is shown in Figure 5. Selection criterion is similar to the one in the rainfall module previously discussed. The button 'Generate ETo Series' will generate ETo time series for any chosen simulation period.

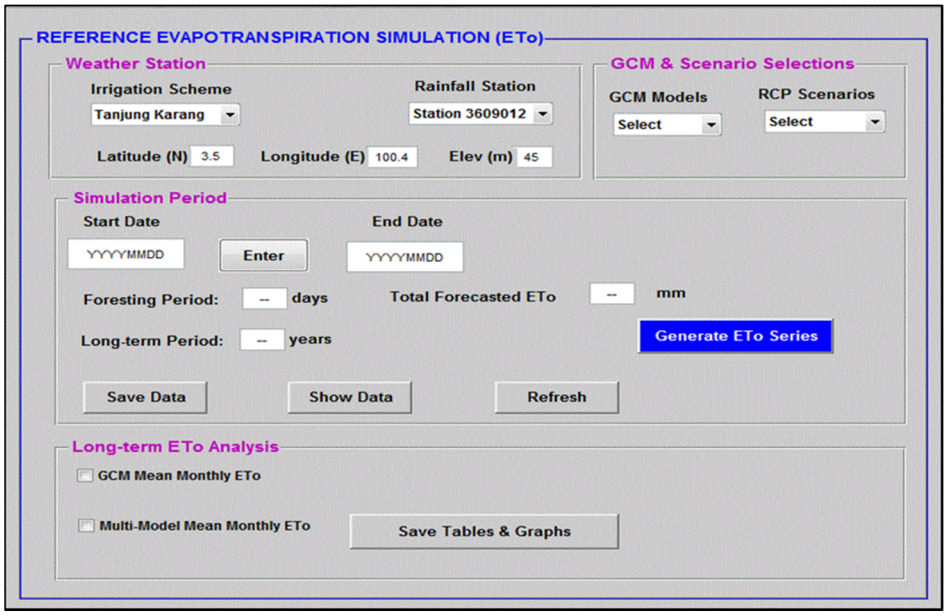

Figure 5. Dialog window for reference evapotranspiration (ETo) simulation module.

Figure 6 shows an example of daily simulated ETo values for 2017 (Jan-Dec) under RCP4.5 scenario. For the RCP4.5 scenario, the annual simulated ETo values are 1,402.5 mm and 1,391.6 mm under MRI-CGCM3 model and multi-model projection respectively. The obtained ETo values are within the expected annual ETo values for the study area. Figure 7 presents long-term ETo simulation outputs from RCP4.5 scenario simulated by a single model (MRI-CGCM3) for a 10-year simulation period (2017-2026). Average maximum monthly simulated values are 126.0 mm and 127.3 mm for MRI-CGCM3 and multi-model projections respectively, in the month of July, also consistent with the observed period.

 ©2017, IAHR. Used with permission / ISSN 1562-6865 (Online) - ISSN 1063-7710 (Print)

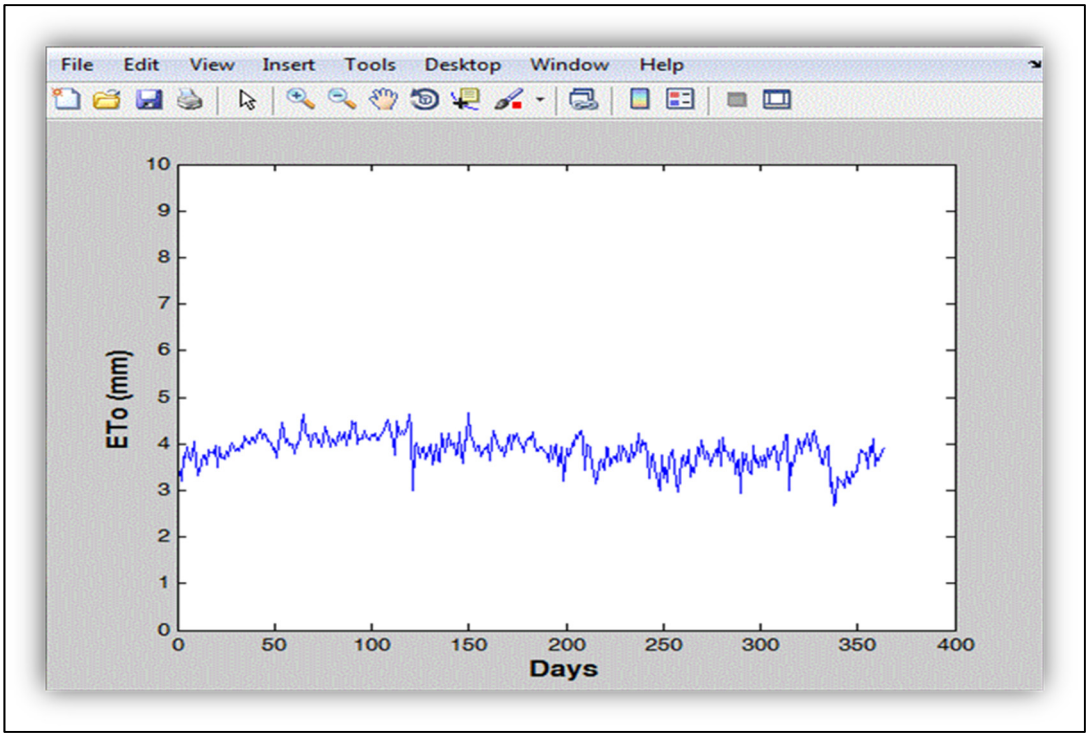

Figure 6. Simulated daily series of annual ETo for 2017 under RCP4.5 scenario.

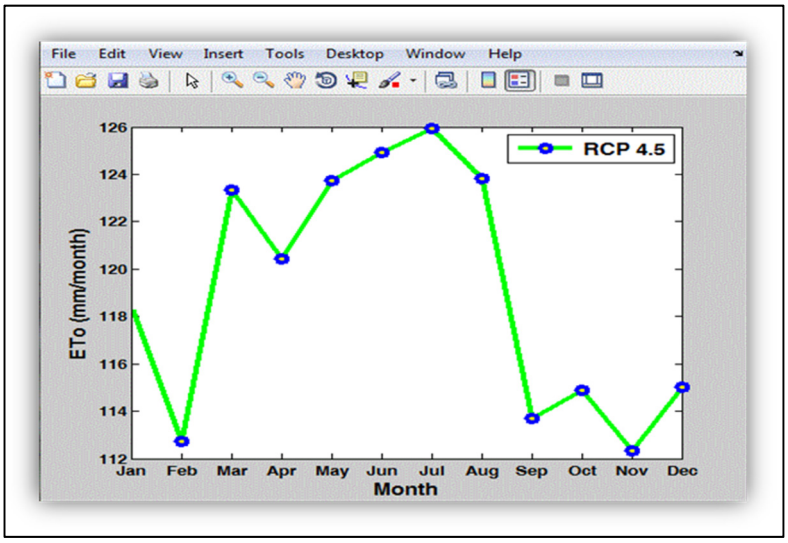

Figure 7. MRI-CGCM3 model simulated mean monthly ETo under RCP4.5 scenario for 10-year period.

4.5 Water demand module outputs

The dialog window for simulating paddy water demands is shown in Figure 8. To simulate water demand, the user has to specify the simulation period, GCMs, rice variety, planting date, daily percolation rate, pre-saturation depth and irrigation efficiency. Length of growth stages and crop factor values are displayed instantaneously upon selecting the rice variety and can be adjusted as the season advances. Some of these parameters are set as default by the model, and others such as expected rainfall and ETo are imported from previous modules using the 'Import Button' button. The Command button "Simulate Water Requirement" will initiate the simulation process according to selected period and the output is displayed in tables and graphs and saved on the output folder.

©2017, IAHR. Used with permission / ISSN 1562-6865 (Online) - ISSN 1063-7710 (Print)

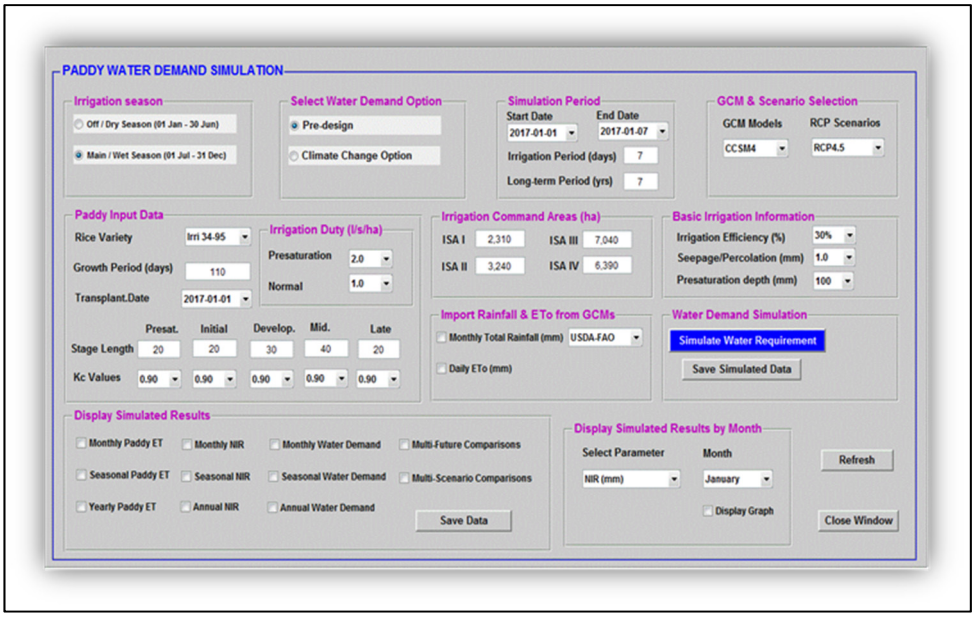

Figure 8. Dialog window for water demand simulation module of the CSRIMIS program.

This module is still being developed and currently no output is available. Outputs will be on a monthly, seasonal and annual time-scale and will include; paddy evapotranspiration (mm), irrigation water requirements (mm), gross irrigation demands and volumetric water demands (m^3), based on selected GCM-scenario combination. Water managers and farmers can use it in planning and managing of water supply, without necessarily undertaking the extraneous processes of downscaling.

5 CONCLUSIONS AND RECOMMENDATIONS

Planning irrigation water deliveries under climate change scenarios is an important aspect of water resources management. A decision support system tool for modeling irrigation water demand and deliveries has been developed. The program incorporates the uncertainty in rainfall and crop evapotranspiration under climate forcing based on the stochastic nature of rainfall. Outputs derived from the program show that the program has good ability to predict rainfall and reference evapotranspiration. Such information could assist irrigation system managers to reduce the amount of irrigation water that will be required during the coming days to meet crop water demand. The program will be validated by comparing the actual irrigation deliveries with model predicted values for both the main and off-crop seasons. It is hoped that the model will provide details in identifying periods of either excess or shortage of water in the context of climate change scenarios, and possible adaptation strategies that could be implemented.

ACKNOWLEDGEMENTS

The authors wish to acknowledge the Ministry of Higher Education in Malaysia (MOHE) and Universiti Putra Malaysia (UPM) for providing funding for this research. This research is funded by the Universiti Putra Malaysia under Putra Grant number 9406300 and the Ministry of Higher Education (MOHE) under FRGS number FRGS 5524362. We are grateful to the staff of the Department of Irrigation and Drainage (DID) and the National Hydraulic Research Institute of Malaysia (NAHRIM) for providing hydro-meteorological data. Sincere appreciation is also extended to the reviewers for their valuable critics and recommendations in improving this manuscript.

REFERENCES

Arnold, J.G., Srinivasan, R., Muttiah, R.S. & Williams, J.R. (1998). Large Area Hydrologic Modeling and Assessment Part I: Model Development1. *Journal of the American Water Resources Association*. 34(1), 73–89.

Arnold, J.G., Moriasi, D.N., Gassman, P.W., Abbaspour, K.C., White, M.J., Srinivasan, R. & Kannan, N. (2012). SWAT: Model use, Calibration, and Validation. *Transactions of the ASABE*, 55(4), 1491-1508.

Döll, P. (2002). Impact of Climate Change and Variability on Irrigation Requirements: A Global Perspective. *Climatic change*, 54(3), 269-293.

IPCC (Intergovernmental Panel on Climate Change). (2007). *Climate Change 2007: The Physical Science Basis*. Cambridge University Press, Cambridge and New York, 996.

JICA (1998). *The Study on Modernization of Irrigation Water Management System in the Granary Areas of Peninsular Malaysia*, V. 1. Main report - v. 2. Annexes, Nippon Koei Co. Ltd.

 ©2017, IAHR. Used with permission / ISSN 1562-6865 (Online) - ISSN 1063-7710 (Print)

Konzmann, M., Gerten, D. & Heinke, J. (2013). Climate Impacts on Global Irrigation Requirements under 19 Gcms, Simulated with a Vegetation and Hydrology Model. *Hydrological Sciences Journal*, 58(1), 88-105.

Moriasi D.N., Arnold J.G., Van Liew M.W., Bingner R.L., Harmel R.D. & Veith T.L. (2007). Model Evaluation Guidelines for Systematic Quantification of Accuracy in Watershed Simulations. *Transactions of the ASABE*, 50(3), 885-900.

Matthews, R.B., Martin, J.K., Dominique, B. & van Laar, H.H. (1995). *Modeling the Impact of Climate Change on Rice Production in Asia*. Int. Rice Res. Inst, 289.

Meinshausen, M., Smith, S.J., Calvin, K., Daniel, J.S., Kainuma, M.L.T., Lamarque, J.F. & Thomson, A.G. J.M.V. (2011). The RCP Greenhouse Gas Concentrations and their Extensions from 1765 to 2300. *Climatic change*, 109(1-2), 213.

Rowshon, M.K., Mojid, M.A., Amin, M.S.M., Azwan, M. & Yazid, A.M. (2014). Improving Irrigation Water Delivery Performance of a Large-Scale Rice Irrigation Scheme. *Journal of Irrigation and Drainage Engineering*, 140(8), 1-13.

Tan, M.L., Ficklin, D.L. & Yusop, Z. (2015). Impacts and Uncertainties of Climate Change on Streamflow of the Johor River Basin, Malaysia using a CMIP5 General Circulation Model Ensemble. *Journal of Water and Climate Change*, 5(4), 676-695.

Vörösmarty, C.J., Douglas, E.M., Green, P.A. & Revenga, C. (2005). Geospatial Indicators of Emerging Water Stress: An Application to Africa. Ambio: *A Journal of the Human Environment*, 34(3), 230–236.

Wayne, G.P. (2013). *The Beginner's Guide to Representative Concentration Pathways*. Skeptical science, 25.

Wang, X.J., Zhang, J.Y., Shahid, S., Guan, E.H., Wu, Y.X., Gao, J. & He, R.M. (2014). Adaptation to Climate Change Impacts on Water Demand. *Mitigation and Adaptation Strategies for Global Change*, 21(1), 81-99.

©2017, IAHR. Used with permission / ISSN 1562-6865 (Online) - ISSN 1063-7710 (Print)

Proceedings of the 37th IAHR World Congress
August 13 – 18, 2017, Kuala Lumpur, Malaysia

WATER AVAILABILITY FOR HYBRID OFF-RIVER AUGMENTATION SYSTEM (HORAS) IN LANGAT RIVER

MD MOBASSARUL HASAN[1], ZALIN AMIR[2] & ABDULLAH AL-MAMUN[3]

[1] Tropical Marine Science Institute, National University of Singapore, Singapore
tmsmha@nus.edu.sg
[2,3] Jurutera Perunding Zaaba Sdn. Bhd., Kuala Lumpur, Malaysia
zalinamir@gmail.com; mameefa@yahoo.com

ABSTRACT

Hybrid-off river augmentation system (HORAS) is a water supply system where river water is harvested through ponds and pumped into the treatment plant for processing. HORAS has been adopted in this study to solve the increasing water crisis in the district of Kuala Langat in Selangor state as a big abandoned mining pond (commonly known as MC8 & MC9) is available along the river near the village Labohan Dagang. Three different models are used to carry out the study such as Hydrological, Hydrodynamic and salinity model. The Hydrological model is used to calculate the rainfall runoff from all the catchments in the Langat Basin. Whereas the Hydrodynamic model is used to calculate available water in the river by considering rainfall runoff from upstream, and tidal action from downstream and salinity model is used to assess the salinity level in the river under different hydrological conditions. Both the Hydrological and Hydrodynamic model have been simulated for 40 years from 1975 to 2014 to gather sufficient data for reliable statistical analysis. It is evident from the rainfall runoff calculation that 95% dependable flow near the ponds is about 8.32 m^3/s when there is no intervention at Dengkil whereas it is about 1.09 m^3/s when there is intervention at Dengkil (no flow from Dengkil). On the other hand, it is found from the Low Flow Analysis that if there is no flow from Dengkil, the proposed site will still receive about 2.72 m^3/s rainfall runoff in 50-Yr ARI drought event. It is also evident from the Hydrodynamic model result that the available average flow near proposed site is about 97.95 m^3/s due to tidal action which is free from salinity intrusion even in extreme drought condition. Therefore, HORAS will be a fruitful solution for the district of Kuala Langat during extreme and prolonged drought event.

Keywords: Hybrid-off river augmentation system (HORAS); numerical model; rainfall runoff; salinity intrusion; water availability.

1 INTRODUCTION

The water shortage issue in Malaysia is a great concern nowadays. Delissio and Primack (2003), Salafsky (1998) and Walsh (1996) stated in their study that the El Nin˜o Southern Oscillation (ENSO) droughts in South-East Asia have been increasing in frequency and intensity over recent decades. On the other hand, Meehl (1997) and Timmerman et al. (1999) also added that ENSO-associated events, including droughts, are likely to become more frequent and more extreme. States of Selangor, Penang, and Kedah have already experienced this kind of drought (Angela, 2002; Rahman, 2014) which caused an extensive impact on the environment and society across the nation (Austin, 2012).

In view of the above, this is the time to take necessary action to avoid any water scarcity situation in the near future. Hybrid-off river augmentation system (HORAS) can be one of the solutions to this kind of disaster. HORAS is a water supply system where river water is harvested through ponds and pumped into the treatment plant for processing (Kusin et al., 2016). Particularly such system can ensure the continuous supply of water to the treatment plant during the drought season or any emergency closure of the river intake due to pollution or even any other reason. Seeing the increasing water stress in Southern part of Selangor State, Langat basin was selected to assess the availability of fresh water for HORAS during extreme drought condition which is considered as the main objective of this study. To carry out the study work, one existing abandoned mining pond (commonly known as MC8 & MC9 pond) near the village Labohan Dagang was selected as a part of HORAS. The study area, location of the pond and its Stage-Area-Volume curve is presented in Figure 1. It is evident from the figure that the capacity of the pond is about 20 million m^3.

 ©2017, IAHR. Used with permission / ISSN 1562-6865 (Online) - ISSN 1063-7710 (Print)

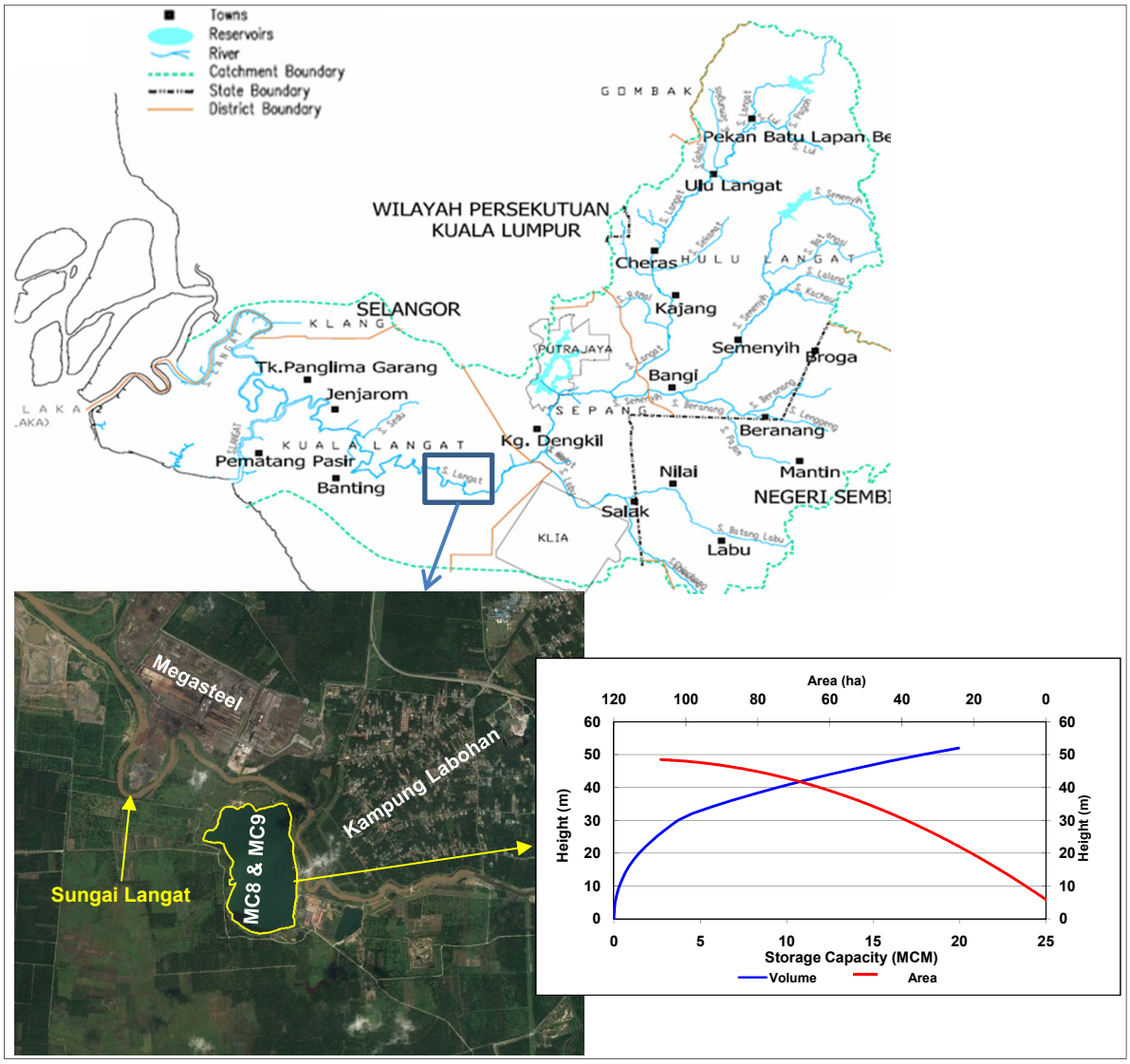

Figure 1. Study area, location of MC8 & MC9 pond, and Stage-Area-Volume curve of the pond.

2 METHODOLOGY

The flow diagram of the methodology is furnished in Figure 2 where data collection is kept at the top of the chart considering its importance on the quality of study findings. All the collected data on rainfall, evaporation, water level, discharge, salinity and cross section were checked, processed, and analyzed as per model requirement. In the beginning, a suitable Hydrological model of Langat basin was developed which was used to determine the available rainfall runoff at the proposed site. After that Hydrodynamic model of Langat River was developed to calculate the available water at the project site due to tidal action following which salinity model was developed to check the saline water intrusion through the Langat River during extreme drought condition.

©2017, IAHR. Used with permission / ISSN 1562-6865 (Online) - ISSN 1063-7710 (Print)

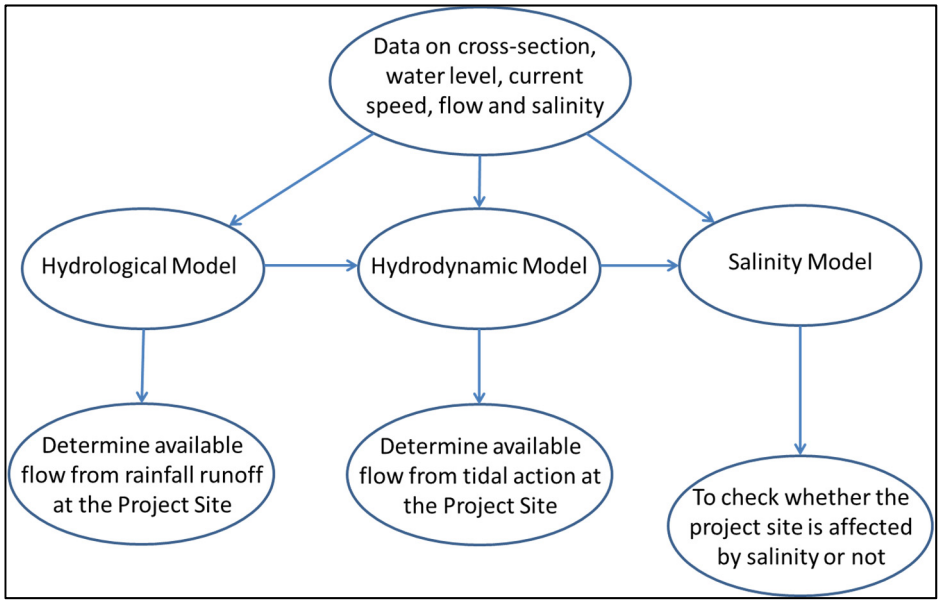

Figure 2. Flow diagram of study methodology.

3 NUMERICAL MODELLING

3.1 Hydrological model

A Hydrological model was carried out under this study to calculate rainfall runoff from all the catchments under Lagnat River basin. Rainfall runoff is the valuable data source for the study, and that is why a reliable approach is needed to adopt for the calculation. There are a lot of approaches to hydrologic forecasting that have been used in the last few decades. These can be grouped into three categories (i) lumped conceptual models, (ii) models based on physical distributions and (iii) empirical black box models. Lumped conceptual models require substantial amounts of calibration data and also need extensive experience of the user to implement and calibrate. On the other hand, physical distribution based models need a large amount of data about topology, soil, vegetation and geological characteristics of the catchment areas. However, the accuracy of empirical black box models requires good quality of observed data, and they are useful operational tools where there are not enough meteorological data available (Bojkow, 2001). Precipitation distribution, evaporation, transpiration, abstraction, watershed topography, and soil types are implicit and explicit factors which are affecting the rainfall-runoff process in the modeling (Dawson et al., 2000).

The Rational Method (McPherson, 1969), Soil Conservation Service- Curve Number Method (Maidment, 1993), and Green and Ampt Method (Green and Ampt, 1991) are the widely known rainfall runoff models identified. The Genetic Danish MIKE11 NAM (Nedbør Affstrømnings Model) is one of the complex models identified which should provide better runoff estimation (Supiah and Normala, 2002). Considering the above MIKE 11 NAM was used in this study. It is a deterministic, lumped conceptual rainfall-runoff model which is developed by Technical University of Denmark (Beck, 1987). It is a well-proven engineering tool that has been applied to a number of catchments around the world (Resfsgaard and Knudsen 1996; Thompson et al., 2004; Keskin et al., 2007; Liu et al., 2007; Kamel 2008; Makungo et al., 2010), representing many different hydrological regimes and climatic conditions.

The total area of Langat River catchment is about 2,400 km^2. There are ten dominant rainfall stations and two evaporation stations within and adjacent to the river basin. In the beginning, the whole catchment was divided into 28 sub-catchments (Figure 3) based on existing land elevation pattern. After that, Thiessen Polygons were drawn by using ARC GIS to distribute the rainfall data (from 16 stations) among different catchments according to their proportion. The model was then simulated for 40 years from 1975 to 2014 to gather sufficient data for the analysis of water availability near the proposed HORAS site. The model was also calibrated and validated for different periods (Table 2) that are described elaborately in section 3.4.

 ©2017, IAHR. Used with permission / ISSN 1562-6865 (Online) - ISSN 1063-7710 (Print)

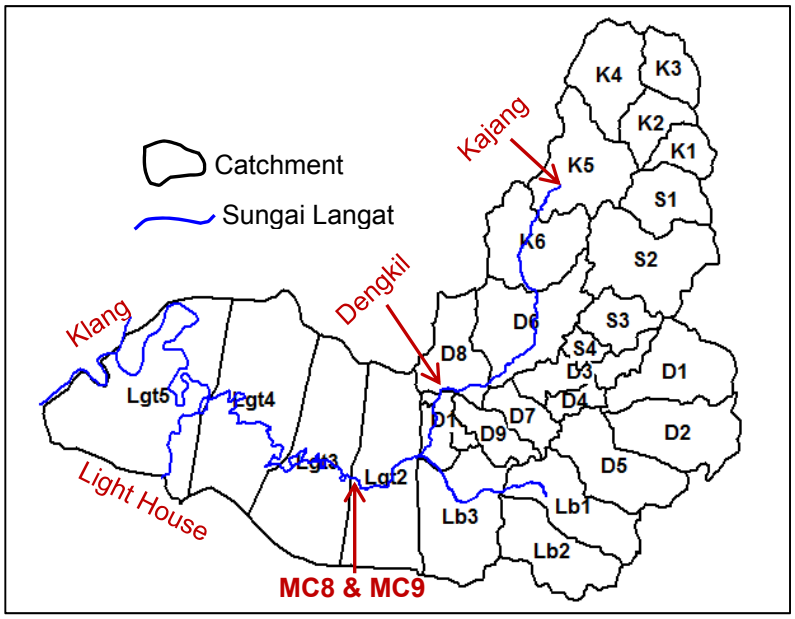

Figure 3. Delineated catchments along with river network.

3.2 Hydrodynamic model

Hydraulic model is a proven and tested technology which can be applied in assessing any impact assessment in any water body. The physically based hydrodynamic modelling system MIKE11 has been used in this study to carry out the surface water modelling work. MIKE 11 is synonymous with top quality river modelling tool covering more application areas than any other river modelling package available. It requires a large amount of high-quality data including river channel bathymetry, water level, and discharge measurements. Figure 4 shows the river network, which was used to develop Hydrodynamic model of Sungai Langat. The model is schematized from Kajang to the Malacca Strait, and the total length of the river network is about 133.5km. The details of river network and number of cross-sections used in the model are furnished in Table-1.

Table 1. River segments and number of cross-sections used in the model for each segment.

River Segments	Length (km)	No. of cross-sections
Kajang to Dengkil	26km	15
Dengkil to Light House	64km	126
Confluence to Port Klang	43.5km	26
Total	133.5km	167

It was then simulated for 40 years by using the outputs from Hydrological model result and tidal force from downstream. The downstream boundary was predicted for 40 years by using tidal constituents of Light House and Port Klang. To calculate tidal constituents, available water level at Light House and Port Klang was collected from authentic secondary sources, and a harmonic analysis was carried out for both the stations. Water level at the boundaries was then predicted by using those constituents.

After setting up the model, it enters into calibration phase. Calibration is carried out to determine its ability to reproduce the phenomena observed in the field. This is a trial and error process in which any deficiencies in the model setup and input data are rectified and model elements are fine-tuned until a reasonable agreement between simulation and observation is achieved. Details of calibration and validation of Hydrodynamic model are discussed in Section 3.4.

©2017, IAHR. Used with permission / ISSN 1562-6865 (Online) - ISSN 1063-7710 (Print)

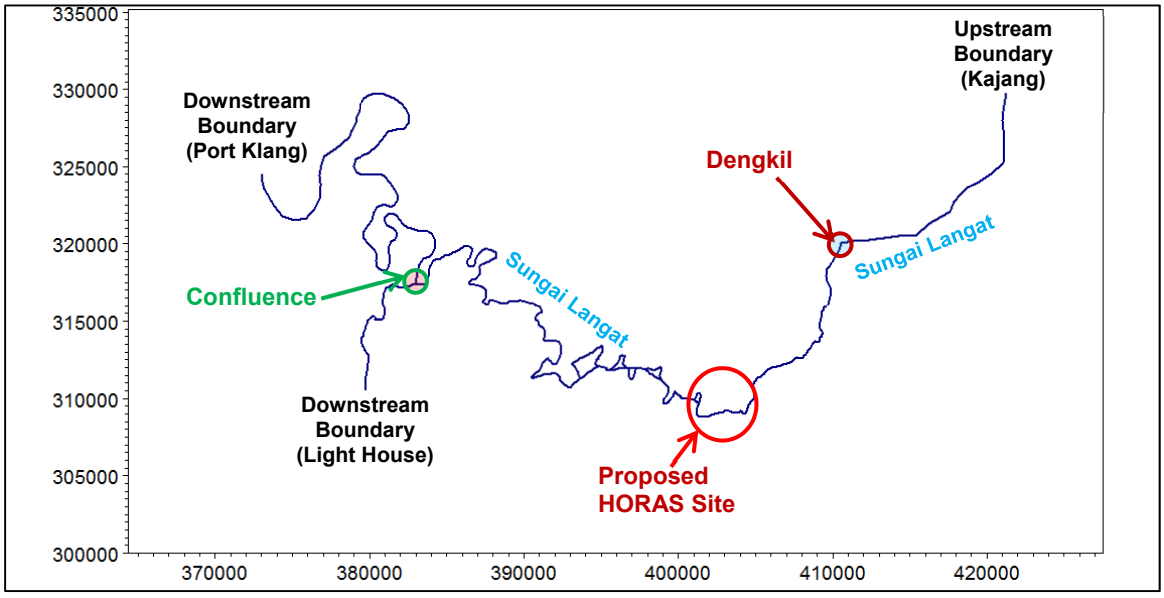

Figure 4. River Network and proposed HORAS site.

3.3 Salinity model

The Langat River model starts from Kajang Hill tracks and falls into the Malacca Strait near Light House. During high tide, salt water moves toward land and propagates toward upstream until the ebb tide comes. In general, salinity movement in any river depends on the following parameters:

- Upstream flow condition;
- Abstractions along the river;
- Riverbed slope.

In this study, the salinity model was developed to assess the salinity intrusion in the Langat River especially near the proposed HORAS site during existing condition, extreme drought condition and the worst condition when there is no flow from the upstream river. The details of the model are described below:

The salinity model was developed by using Advection and Dispersion Module of the MIKE11 Modelling System. Advection is a transport mechanism of a substance or a conserved property with a moving fluid whereas Dispersion is a system in which particles are dispersed in a continuous phase of a different composition. The module is based on the one-dimensional equation of conservation of mass of a dissolved or suspended material, i.e. the advection-dispersion equation as in Eq. [1]. The module requires output from the hydrodynamic module, in time and space, in terms of discharge and water level, cross-sectional area and hydraulic radius.

$$\frac{\partial AC}{\partial t} + \frac{\partial QC}{\partial t} - \frac{\partial}{\partial x}\left(AD\frac{\partial C}{\partial x}\right) = -AKC + c_2 q \qquad [1]$$

where,

C : concentration
D : dispersion coefficient
A : cross-sectional area
K : linear decay coefficient
C2 : source/sink concentration
q : lateral inflow
x : space coordinate
t : time coordinate

The upstream of the model is at Kajang where there is no salinity, and that is why the salinity boundary at Kajang is considered as 0 ppt. Whereas at the downstream boundary, measured data was used for calibration purpose and the maximum sea salinity 32 ppt (Amiruddin et al., 2011) was used for scenario simulation.

3.4 Model calibration and validation

Calibration is the process under which the model parameters and/or structure are determined on the basis of measurement and priori knowledge (Beck, 1987). For any kind of model, field/measured data can be used to calibrate the model at a given time by adjusting model parameter values until acceptable correlation is achieved (Ditmars,1988). In this study model calibration has been carried out against the available flow, current speed, water level and salinity. Hydrological model was calibrated against flow data whereas

 ©2017, IAHR. Used with permission / ISSN 1562-6865 (Online) - ISSN 1063-7710 (Print)

Hydrodynamic model was calibrated against flow, current speed and water level data and salinity model was calibrated against salinity level.

Once calibration is done, another simulation is performed for a different hydrological period and compared with the second set of measured/field data (Thomann et al., 1987). If the second simulation is also acceptable, the model is considered as validated and this process is called validation. It is to be noted that model parameters are not adjusted based on field data during validation. If the parameters are adjusted for simulations subsequent to calibration, then the effort is not validation but recalibration. As both the Hydrological and Hydrodynamic models were simulated for 40 years, model validation was carried out for different period to make it more reliable for further application. Sample plots of calibration and validation are furnished in the Figure 5.

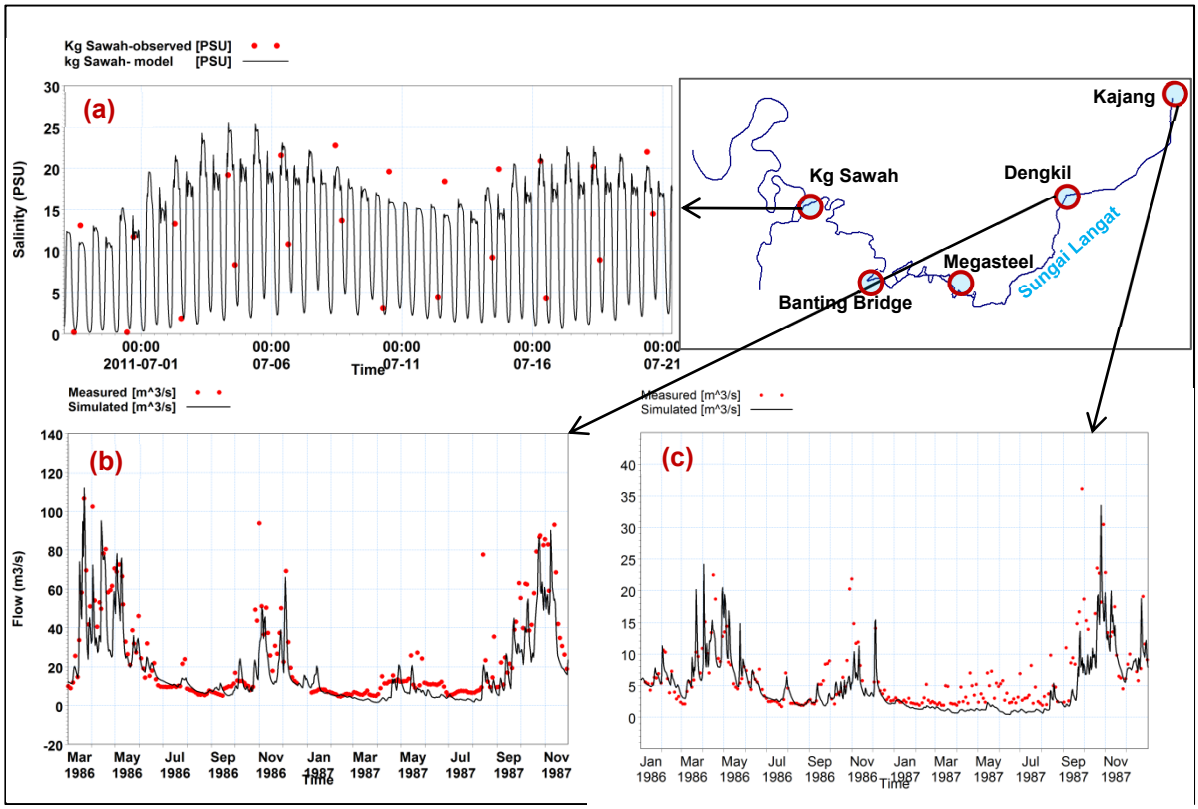

Figure 5. (a) calibration of Salinity Model at Kg Sawah, (b) validation of Hydrodynamic Model at Dengkil, and (c) validation of Hydrological Model at Kajang.

The performance of models was also assessed by introducing Quality Index as in Eq. [2]. Quality indices were calculated both for calibration and validation results of Hydrological and Hydrodynamic model, and are furnished in Table 2. It is evident from the table that almost all the results satisfy the criteria set by JPS.

$$\rho = \frac{\sum_{i=1}^{N}(me_i - \overline{me})(mo_i - \overline{mo})}{\sqrt{\sum_{i=1}^{N}(me_i - \overline{me})^2 \sum_{i=1}^{N}(mo_i - \overline{mo})^2}} \quad [2]$$

where,

quality index, ρ
me, Measured value
mo, Model value

©2017, IAHR. Used with permission / ISSN 1562-6865 (Online) - ISSN 1063-7710 (Print)

Table 2. Quality Index for Flow, water level and current speed.

Model	Stations	Item	Period	Calibrations/ Validation	Quality Index	JPS Guideline
Hydrological	Dengkil	Flow	2012 – 2014	Calibration	0.90	0.8
	Dengkil	Flow	2002 – 2003	Validation	0.82	0.8
	Kajang	Flow	2008 – 2003	Validation	0.83	0.8
	Kajang	Flow	1986 – 1987	Validation	0.87	0.8
	Kajang	Flow	1980 – 1981	Validation	0.89	0.8
Hydrodynamic	Dengkil	Flow	2012 – 2013	Calibration	0.80	0.8
	Dengkil	Flow	1986 – 1987	Validation	0.88	0.8
	Banting	Current	Spring tide-2012	Calibration	0.84	0.8
	Bridge	Speed	Neap Tide-2012	Calibration	0.70	0.8
	Megasteel	WL	2012	Calibration	0.98	0.9
	Kg Sawah	WL	2012	Calibration	0.98	0.9
Salinity	Kg Sawah	Salinity	2011	Calibration	N/A	N/A
	Kg Sawah	Salinity	2016	Validation	N/A	N/A

To quantify and qualify model performance of salinity model, goodness criteria by Moriasi et al. (2007) was used under this study as JPS does not have any guideline for that. The formula and goodness criteria are furnished below:

PBIAS(%) = (Measured mean – Model Mean)*100/Measured mean

Table 3. Goodness criteria.

PBIAS <±15	very good
±15≤ PBIAS ≤ ±30	good
±30≤ PBIAS ≤ ±55	satisfactory
PBIAS≥ ±55	unsatisfactory

PBAIS(%) was then calculated for salinity model and furnished in the Figure 6. It is evident from the figure that both the calibration and validation fall under very good criteria.

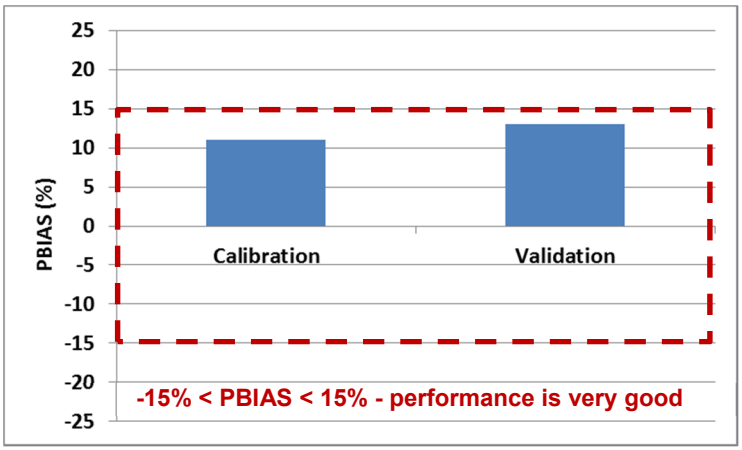

Figure 6. Model performance of salinity model.

4 LOW FLOW ANALYSIS

Statistical analysis was conducted to determine the probability of the drought event for 30, 60, 90 and 120 days low flow based on actual river flow record at Dengkil. The original flow data, however, has several gaps with missing data, and there are several periods with suspected wrong data. The latter involves extended low flow during which period, in contrary, contains several heavy rain events. Consequently, the flow record was adjusted and corrected using simulated river flow output from the Hydrological Model result. Low flow at the proposed HORAS site was also derived using Hydrological model results, and statistical analysis was carried out to determine low flows of various durations and frequencies of occurrence. All the results are shown in Table 4. It is seen from the table that 1 in 50 year drought stretched for 120 days (it matches with 1986-87 drought event) with an average low flow of 4.32 m^3/s or 374 MLD at Dengkil whereas at the proposed site it is about 7.04 m^3/s or 608 MLD. It implies that if there is no flow from Dengkil, the site will still receive 2.72 m^3/s or 236 MLD rainfall runoff during 1 in 50 year drought event. The same thing will also happen for all other durations and return periods.

 ©2017, IAHR. Used with permission / ISSN 1562-6865 (Online) - ISSN 1063-7710 (Print)

Table 4. Low Flows for Sg. Langat at Dengkil and the Proposed HORAS Site for Various Durations and Return Periods (m^3/s).

Return Period (Years)	60 Days		75 Days		90 Days		120 Days	
	At Dengkil	At the site	At Dengkil	At the site	At Dengkil	At the site	At Dengkil	At the site
2	11.49	15.65	12.70	16.96	13.70	18.21	15.96	21.66
5	6.28	9.08	6.98	9.94	7.52	10.65	8.51	12.22
10	4.91	7.37	5.39	8.06	5.76	8.59	6.24	9.42
20	4.25	6.55	4.61	7.16	4.87	7.59	5.03	7.96
25	4.12	6.39	4.45	6.98	4.69	7.39	4.77	7.65
50	3.86	6.07	4.12	6.62	4.30	6.98	4.32	7.04
100	3.73	5.91	3.95	6.43	4.10	6.76	3.89	6.63

5 ASSESSMENT OF SALINITY INTRUSION

One of the main concerns of this study is to assess whether the intake (project site) will be affected or not by saline water under extreme drought event. Therefore, salinity model was simulated for 50-Yr ARI drought event which covers the duration from November 1986 to May 1987. One more simulation was also carried out considering no flow from Dengkil (no flow from upstream) during this drought event. All the results are furnished in Figure 7. It is evident from the figure that salinity front propagates only up to 42km from the river mouth whereas our project site is about 52 km from there. It implies that the proposed site is safe from salinity intrusion under any extreme condition.

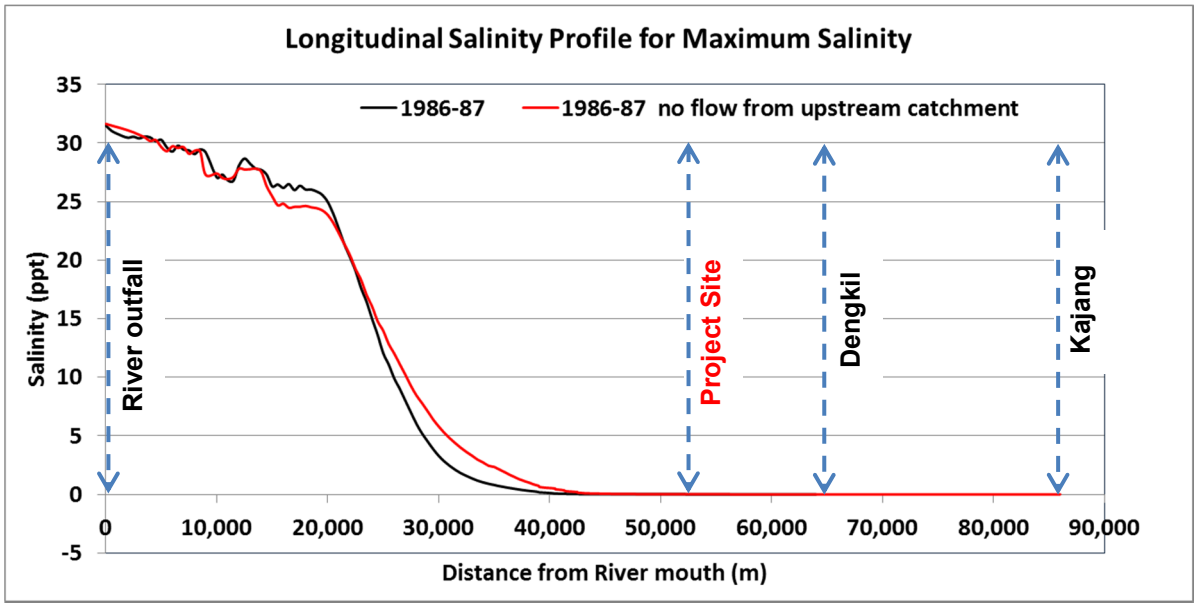

Figure 7. Longitudinal salinity profile during 50-Yr ARI drought event and no flow from upstream catchment during the same event.

6 WATER AVAILABILITY ANALYSIS

Both the Hydrological and Hydrodynamic analysis were simulated for 40 years to gather reasonable data set at the project site to carry out the water availability analysis. Rainfall runoff from Hydrological model was analyzed, and two flow duration curves were prepared (Figure 8) considering with and without flow from Dengkil. It is evident from the figure that 85%, 90% and 95% dependable flow near the pond (proposed site) are 12.85 m^3/s, 10.7 m^3/s and 8.32 m^3/s respectively if there is no intervention in the upstream whereas they are 2.42 m^3/s, 1.82 m^3/s and 1.09 m^3/s respectively if there is intervention at Dengkil (no flow from Dengkil, Table 5). On the other hand, it is evident from Hydrodynamic model result that available average flow in the river near the project site is about 97.95 m^3/s or 8,463mld (Table 6) due to tidal action from downstream. As the site is influenced by tide, it is essential to check whether the site is affected by salinity or not especially in the severe drought event. It is evident from the salinity model results that the project site is free from salinity intrusion even in severe drought condition which supports the study of Hasan et al. (2014).

©2017, IAHR. Used with permission / ISSN 1562-6865 (Online) - ISSN 1063-7710 (Print)

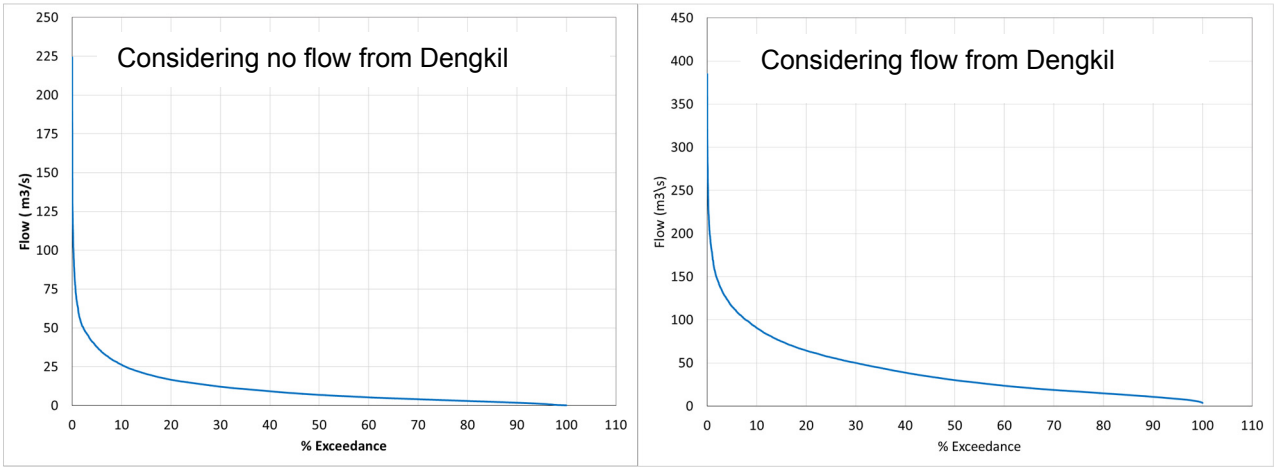

Figure 8. Flow duration curve at proposed HORAS site considering with and without flow from Dengkil.

Table 5. Dependable flow at the proposed HORAS site considering with and without flow from Dengkil.

	Flow at proposed HORAS site			
	[considering all upstream catchments]		[no flow from Dengkil]	
	(m^3\s)	(mld)	(m^3\s)	(mld)
80% dependable flow	20.31	1755	3.58	309
85% dependable flow	17.65	1525	3.00	259
90% dependable flow	15.15	1309	2.38	206
95% dependable flow	12.18	1052	1.41	122

Table 6. Average tidal flow near proposed HORAS site.

	1975-84	1985-94	1995-04	2005-14	Average
Average flow (m^3/s)	94.8	93.2	101.4	102.4	97.95
Average flow (mld)	8191	8052	8761	8847	8463

7 CONCLUSIONS

Prolonged drought is very common nowadays in Malaysia especially in Selangor state due change in weather pattern such as a change in the pattern of El Nino. The main objective of this study was to assess the availability of fresh water for Kuala Langat District in Selangor state during such prolonged drought period. Hybrid-off river augmentation system (HORAS) was adopted under this study to supply fresh water during prolonged drought period, and an abandoned pond MC8 & MC9 was selected as part of the system. To accomplish the study objective, availability from rainfall runoff was assessed by using flow duration curve, and it is found that 95% dependable flow is only 1,41 m^3/s near the pond if there is no flow from Dengkil. Low flow analysis was also carried out to get the available rainfall runoff at different return period. It is found from the analysis of measured data at Dengkil and simulated data at proposed site that the proposed site will receive 2.72 m^3/s (236 MLD) rainfall runoff even in 50-Yr ARI drought event stretched for 120 days when there is no flow from Dengkil. On the other hand, the proposed site is influenced by the tide, and the average tidal flow near the pond is about 97.95 m^3/s (8463 MLD). But it is established from the salinity model that the study area is completely free from salinity intrusion. It implies that if there is no rainfall for a long period, the HORAS can be continued using this salt-free tidal flow. However, it can be concluded that HORAS can be adopted to solve the water crisis in Kuala Langat as sufficient amount fresh water is available from rainfall runoff even in extreme and prolonged drought event.

ACKNOWLEDGEMENTS

The authors express their gratitude to JPZ, a private organization in Malaysia for the support to use the study findings in the paper.

REFERENCES

Amiruddin, A.M., Ibrahim, Z.Z. & Ismail, S.A. (2011). Water Mass Characteristics in the Strait of Malacca using Ocean Data View. *Research Journal of Environmental Sceince*, 5, 49-58.

Angela, M. (2002). No Water Rationing in Klang Valley. *The Sun*, Shah Alam, 14(03).

Austin, O.C. (2012). Risk in Malaysia Agriculture: The Need for a Strategic Approach and a Policy Refocus, *Kaijan Malaysia*, 30(1), 21–50.

 ©2017, IAHR. Used with permission / ISSN 1562-6865 (Online) - ISSN 1063-7710 (Print)

Beck, M.B., (1987). System Analysis in Water Quality Management. *Symposium Proceedings, London*, Oxford-Pergama Press 3-63.

Bojkow, V.H. (2001). *Runoff Modelling with Genetic Programming and Artificial Neural Networks*, D2K Technical Report D2K TR, 0401-1.

Dawson, C.W., Brown, M.R. & Wilby, R.L. (2000). Inductive learning approaches to rainfall-runoff modelling. *International journal of neural systems*, 10(01), 43-57.

Delission, L.J. & Primack, R.B. (2003). The Impact of Drought on the Population Dynamics of Canopy-Tree Seedlings in an Aseasonal Malaysian Rain Forest. *Journal of Tropical Ecology*, 19, 489-500.

Ditmars, J.D., (1988). Performance Evaluation of Surface Water Transport and Dispersion Models. *Journal of Environmental Engineering Division*, ASCE, 113(EE8), 961- 971.

Green, W.H. & Ampt, G.A. (1911). Studies on Soil Physics. *Journal of Agricultural Sciences*, 4, 1-24.

Hasan, M.M., Begum, M., Mamun, A.A. & Khan, Z.H. (2014). Selection of Extreme Drought Event for Langat Basin and Its Consequence on Salinity Intrusion through Langat River System. *IOSR Journal of Mechanical and Civil Engineering (IOSR-JMCE),*11(3), 62-69.

Kamel, A.H. (2008). Application of a Hydrodynamic MIKE 11 model for the Euphrates River in Iraq. *Slovak Journal of Civil Engineering*, 2, 1-7.

Kusin, F.M., Zahar, M.S.M., Muhammad, S.N., Mohamad, N.D., Zin, Z.M. & Sharif, S.M. (2016). Hybrid Off-River Augmentation System as an Alternative Raw Water Resource: The Hydrogeochemistry of Abandoned Mining Ponds. *Environmental Earth Science*, 75(230), 1-15.

Liu, H.L., Chen, X., Bao, A.M. & Wang, L. (2007). Investigation of Groundwater Response to Overland Flow and Topography using a Coupled MIKE SHE/MIKE 11 Modeling System for an Arid Watershed. *Journal of Hydrology,* 347, 448-459.

McPherson, M.B. (1969). *Some Notes on the Rational Method of Storm Drain Design*, Technical Memo, ASCE, Water Resources Research Program. Harvard University, Cambridge, USA.

Makungo, R., Odiyo, J.O., Ndiritu, J.G. & Mwaka, B. (2010). Rainfall–Runoff Modelling Approach for Ungauged Catchments: A Case Study of Nzhelele River Sub-Quaternary Catchment. *Physics and Chemistry of the Earth,* 35(13), 596-607.

Maidment, D.R. (1993). *Handbook of Hydrology*. NewYork, McGraw Hill: 1424, 1-4.

Moriasi, D.N., Arnold, J.G., Liew, M.W.V., Bingner, R.L., Harmel, R.D. & Veith, T.L. (2007). Model Evaluation, Guidelines for Systemmatic Quantification of Accuracy in Watershed Simulations. *Transactions of the ASABE*, 50(3), 885-900.

MEEHL, G. A. (1997). Pacific Region Climate Change. *Ocean and Coastal Management*, 37, 137–147.

Rahman, H.A. (2014). Water Shortage in Malaysia: Again? *ResearchGate.* Available: https://www.researchgate.net/publication/282865681_Water_Shortage_in_Malaysia_Again

Refsgaard, J.C. & Knudsen, J. (1996). Operational Validation and Intercomparison of Different Types of Hydrological Models. *Water Resources Research*, 32, 2189-2202.

Salafsky, N. (1998). Drought in the Rain Forest, Part II an Update based on the 1994 ENSO Event. *Potential Impacts of Climate Change on Tropical Forest Ecosystems* 39, 461-463.

Supiah, S. & Normala, H. (2002). Rainfall Runoff Simulation using Mike11 Nam. *Journal of civil engineering*, 15, 26-38.

Timmermann, A., Oberhuber, J., Bacher, A., Esch, M., Latif, M. & Roeckner, E. (1999). Increased El Niño Frequency in a Climate Model Forced by Future Greenhouse Warming. *Nature*, 398(6729), 694-697.

Thomann, R.V. & Muller, J.A., (1987). *Principles of Surface Water Quality Modelling and Control*. Harper and Row, New York, 91-173.

Walsh, R.P. (1996). Drought Frequency Changes in Sabah and Adjacent Parts of Northern Borneo Since the Late Nineteenth Century and Possible Implications for Tropical Rain Forest Dynamics. *Journal of Tropical Ecology*, 12(03), 385-407.

©2017, IAHR. Used with permission / ISSN 1562-6865 (Online) - ISSN 1063-7710 (Print)

Proceedings of the 37th IAHR World Congress
August 13 – 18, 2017, Kuala Lumpur, Malaysia

PROTOTYPE OBSERVATION ON ICE IN WATER TRANSFER CANAL

YAN HUA NIE[(1)], JIN BO YANG[(2)], GUO BING HUANG[(3)] & MENG KAI LIU[(4)]

[(1,2,3,4)] Hydraulics Department, Changjiang River Scientific Research Institute, Wuhan, China.
yuanauy111@126.com

ABSTRACT

Many water transfer projects have been built to solve the regional water shortage problems. For some projects in cold region, the operation regulation is very important especially in ice period. It is also a pivotal judgment standard whether the project is safe, and the water user's demand has been satisfied. Thus, it is meaningful to study the ice pattern of water transfer canal. In this paper, one whole winter prototype observation has been completed which contains data collection, measurement, photograph and video, etc. After analyzing ice observation data, the inherent patterns of the canal ice are revealed. The research results can provide some references for the canal water transfer regulation and also provide some suggestions for the project design.

Keywords: Water transfer canal; operation dispatch; ice; prototype observation.

1 INTRODUCTION

Currently, some long-distance water transfer projects have been built to solve the shortage of regional water resources and improve local ecological environment simultaneously. Most of them have long line and large span canals, some projects run from warm region to cold regions. In winter, some canal sections are frozen because of cold air temperature, and this is a major challenge to canal operation.

The process of the canal ice formation is usually affected by temperature, water flow regulation and some other control factors. In order to research the occurrence and evolution of the canal ice in winter, analyze and forecast the ice formation process, there must be first-hand data about ice evolution and extinction in canal. Since then, there are some researches about river or glacier ice (Chen, 2005; Pariset Ernest, 1961; Shen Hungtao, 1984; Hungtao, 2000; Wasantha Lal, 1991; Xia, 2000; YApa Poojitha, 1986), however, the research about canal ice is less seen in public periodicals. There are numerous differences between a canal system and river in terms of ice development. In this paper, a prototype observation on canal ice information was organized to achieve this goal.

2 ICE PROTOTYPE OBSERVATION

2.1 Summary

2.1.1 Observation target and position

A large-scale, long-distance, and inter-basin water transfer project in China across warm and semi-cold region was chosen as the observation target. The main construction of the project is an open canal with a number of sluices (control sluice, outlet sluice, and escape sluice) along it, the canal is divided into series connection pools by these sluices, and these sections are approximately 8 km to 40 km in length. Some sections are straight, and the others are curve. There are many traffic bridges and aqueducts cross the canal whose piers are in canal. In order to prevent the floating ice from colliding the gates, some ice cables were set in front of the control sluice.

The specific location of ice observation is a canal section with control sluices, outlet gates, escape sluices, aqueducts and some curves (Figure 1). There are also some bridges that pass through it. The parameters are shown in Table 1.

 ©2017, IAHR. Used with permission / ISSN 1562-6865 (Online) - ISSN 1063-7710 (Print)

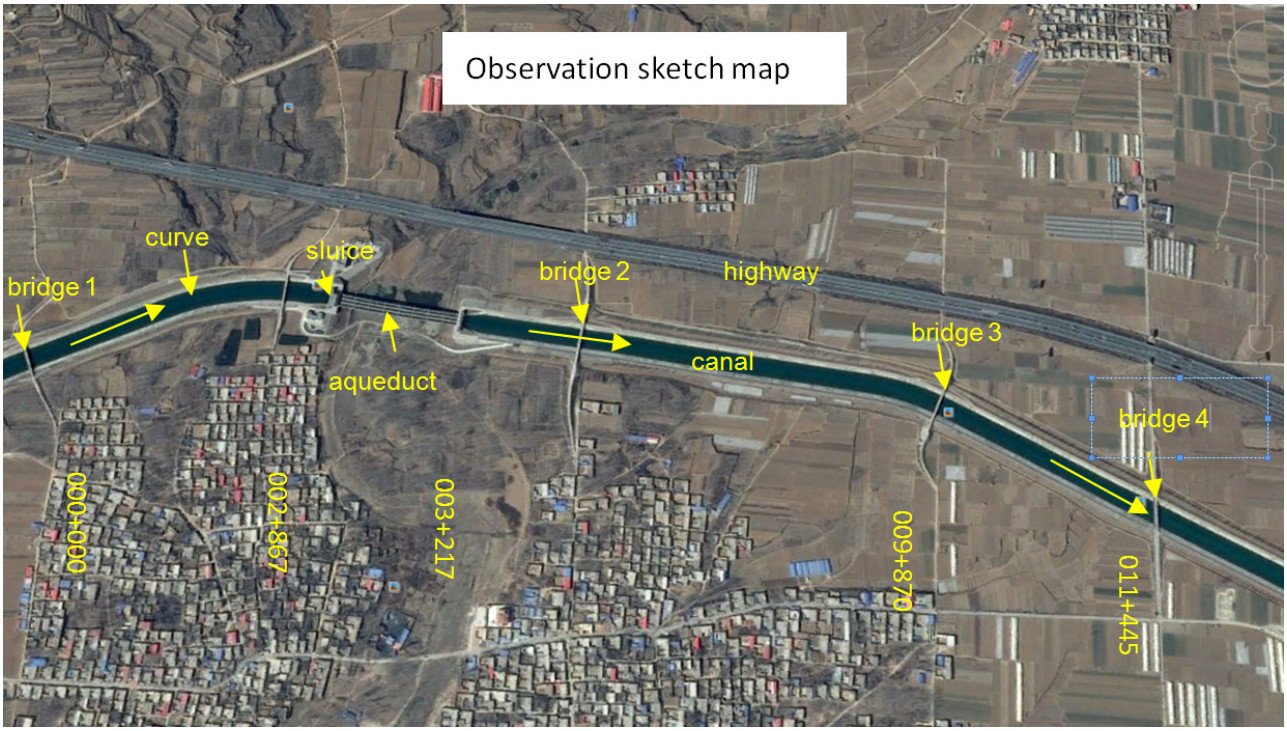

Figure 1. Sketch map of the observation.

Table 1. Parameters of the observation section.

Stake number		Length	Name	Longitudinal slope	Design bottom	Slope	Section
Begin	End	（m）		(1/i)	width (m)	coefficient	form
000+000	002+867	2867	Canal	25000	21.5	2.5	Trapezoid
002+867	003+217	350	Aqueduct			2.5	rectangle
003+217	009+870	6653	Canal	25000	21.5		Trapezoid
009+870	011+445	1575	Canal	20000	20.0	2.5	Trapezoid

There are different structures along the canal, such as sluices, aqueduct and bridge, as shown below (Figure 2):

1-1 Straight canal 1-2 Curve canal 1-3 Control sluice

1-4 Aqueduct 1-5 Bridge cross the canal

Figure 2. Different structures of canal.

©2017, IAHR. Used with permission / ISSN 1562-6865 (Online) - ISSN 1063-7710 (Print)

2.1.2 Observation time

The observation began from December 14, 2011 to March 1, 2012. During this period, the canal flow was approximately 16.5 m^3/s to 18.5m^3/s, and it lasted for 7 days with juxtaposition ice cover in the canal.

2.1.3 Observation items

The meteorology and hydraulic parameters are main observation content of the ice development process. The phenomenon of ice formation includes: shore ice, frazil ice, floating ice, ice cover, ice dam, ice jam, etc. The meteorology parameters include temperature, air pressure, wind speed and direction, ground temperature, water temperature and relative humidity, etc. Water discharge, velocity and water level belong to hydraulic parameters, as shown in Table 2-2.

Table 2. Observations item.

Item	Content
Ice phenomenon	Shore ice Frazil ice Floating ice Ice discharge Ice cover
meteorology parameters	Air pressure Wind speed Wind direction Ground temperature Water temperature and relative humidity
Hydraulics parameters	Water velocity Water discharge Water level

In addition, non-fixed-point observation was also carried out during the entire observation period, such as Ice Bridge, ice dam, ice jam, etc.

2.2 Observation results

2.2.1 Thermodynamic data

Historical weather

The winter meteorological data from 2009 to 2011 are shown in table 3，which was collected from local meteorological department.

Table 3. Meteorological data.

Time	Highest temperature (℃)	Lowest temperature (℃)	Average temperature (℃)
2008-2009	19.8	-11.2	-2.3
2009-2010	12.0	-14.8	-3.5
2010-2011	13.2	-12.0	-3.6

The average temperature was -2.3°C between 2008 and 2009, the lowest temperature was -11.2°C, and the highest temperature was 19.8°C; the winter average temperature was -3.5°C between 2009-2010, the lowest temperature was -14.8°C, and the highest temperature was 12°C; During 2010-2011, the average temperature was -3.6°C, the lowest temperature was -12°C, and the highest temperature was 13.2°C.

Observation data

The weather conditions include air temperature, water temperature, ground temperature, relative humidity, air pressure, wind speed and direction. The observation lasts for 91 days. Overall situation is shown in table 4 and other results are shown in table 5, and 6. Figure 3 shows the annual winter meteorological data curve in observation period.

Table 4. Weather conditions.

Weather conditions	Sunny	Overcast	Cloudy	Snow	Haze
Number(day)	55	11	23	2	20

 ©2017, IAHR. Used with permission / ISSN 1562-6865 (Online) - ISSN 1063-7710 (Print)

Table 5. Wind speed.

Wind speed	Speed (m/s)	Date
Highest	9.0	2012.2.6/14:00
Lowest	0	2011.12.22/8:00
Highest daily average	3.8	2012.2.6-7
Lowest daily average	0.5	2011.1.9
Average	1.38	——

Table 6. Ground temperature.

Item	10（cm）	20(cm)	40(cm)	80(cm)
Date of turning negative	2011.12.14	2011.12.20	2011.1.10	-
Date of turning Positive	2012.2.28	2012.2.29	2012.2.27	-
Lowest temperature	-7.00	-3.30	-1.40	1.10
Temperature/date	2012.1.23	2012.1.23	2012.1.25	2012.2.12
Lowest average temperature	-4.20	-2.50	-1.30	1.10
/date	2012.1.23	2012.1.23	2012.1.3	2012.2.12
average temperature	-1.30	-0.37	0.64	3.00

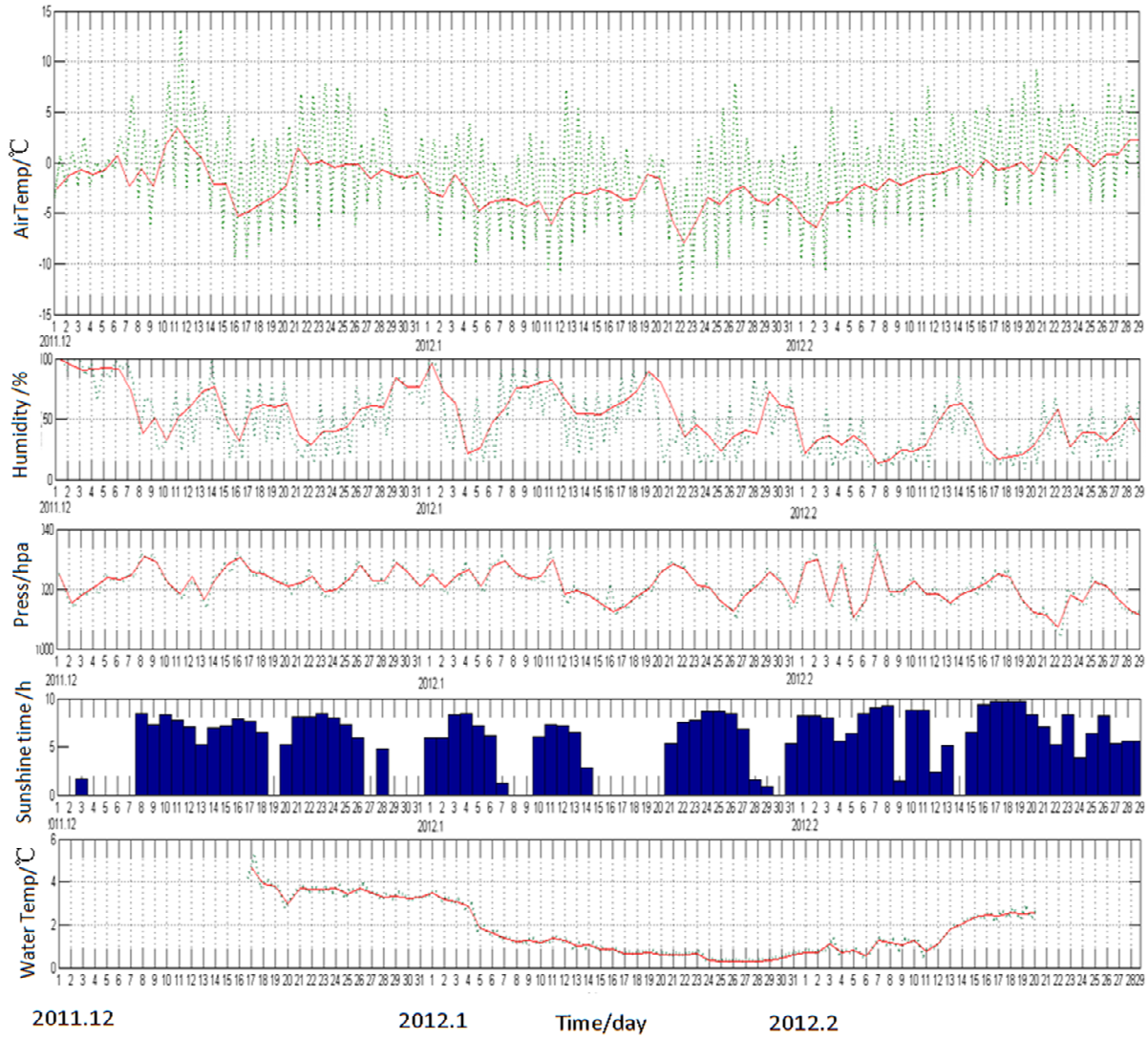

Figure 3. 2011-2012 The annual meteorological data curve.

2.2.2 Hydraulics data

Hydraulics observation contains discharge, velocity, and water level. Through analyzing the observation data, the results are as follows: (1) the discharge of the Aqueduct was between 16.6m^3/s~18.5m^3/s, (2) the water depth upstream the X-sluice was 4.29m-4.42m, and 2.60m-2.67m downstream, (3) the velocity was

©2017, IAHR. Used with permission / ISSN 1562-6865 (Online) - ISSN 1063-7710 (Print)

0.113~0.18m/s upstream the X- sluice, and 0.13 ~0.28m/s downstream, the water conditions were relatively stable throughout the observation period. Figure 4 shows the changing process of the hydraulics parameters.

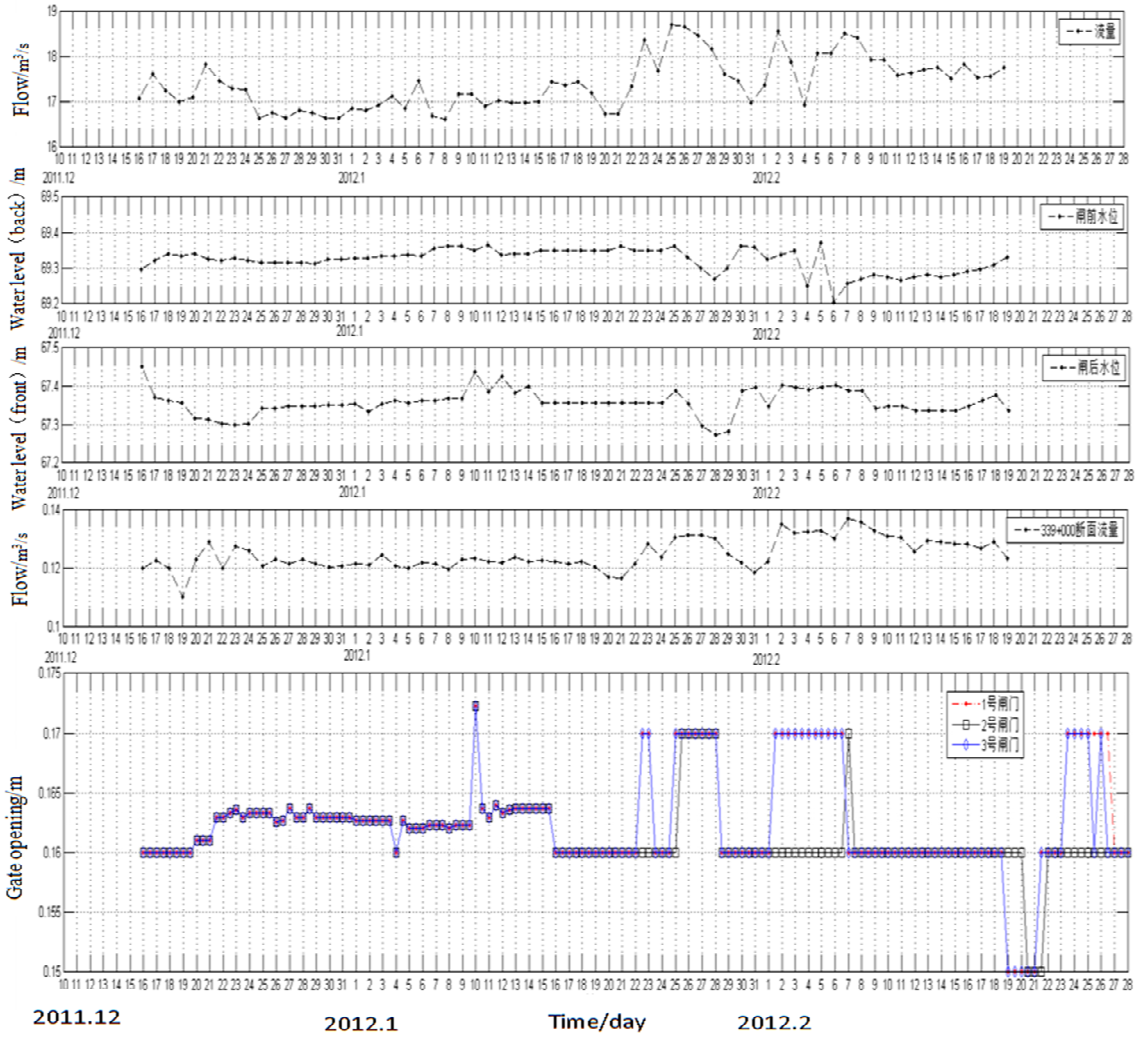

Figure 4. Hydraulics parameters curve.

2.2.3 Ice observation

In this prototype observation, the development process of the canal ice was recorded completely, some typical icing phenomena were recorded as video or photographs, which contained shore ice, frazil ice, floating ice, ice discharge, etc. The detailed descriptions are as follows:

(1) Shore ice

The whole ice evolution process can usually be divided into four periods in the entire winter, namely initial ice, drifting ice period, freezing period and melt period. Shore ice is the first phase that appeared in ice information. The details are shown in Table 7.

Table 7. Shore ice formation and development

NO	Date	Width(m)	Thickness (cm)	Shape	Description
1	2011.12.16-2012.01.03	0.05-0.3	0.1-1.1	Feather-like Array ice layer	Thin, brittle
2	2012.01.04-2012.01.21	0.3-2.5	0.6-8.0	Strip-like	Initial stage:thin,brittle Late stage: thick,
3	2012.01.22-2012.01.28	10.0-12.0	8.0-14.0	Ditch	Thick, hard
4	2012.02.29-2012.02.23	0.0-2.5	0-14.0	Drip	Off shore, melting

©2017, IAHR. Used with permission / ISSN 1562-6865 (Online) - ISSN 1063-7710 (Print)

The development process of shore ice is divided into three phases: initial ice, floating ice and freezing period. Some ice data are recorded in Table 8 and a portion of typical pictures are shown in Figure 5 (a, b, c):

Initial ice (2011.12.16-2012.01.03): The average temperature was -1.7°C in this period, and the negative accumulated temperature (NAT: the value of the negative temperature adds together) was below 50, the water temperature maintained at 2°C, the width of shore ice was thinner than 0.3cm, and the thickness was less than 1.2cm.

Floating ice (2012.1.4-2012.1.21): The average temperature was -3.5°C and the negative accumulated temperature was from 50 to 113, the water temperature was between 0.5°C and 2°C, the shore ice width was between 0.3cm and 2.5cm and the thickness was between 0.8cm and 2.5cm.

Freezing period (2012.1.22-2012.1.29): The average temperature was -4.3°C and the negative accumulated temperature was from 113 to 140, the water temperature was lower than 0.5°C; the thickness of the ice cover was between 8 and 14cm.

Table 8. Relationship between ice thickness and influencing factors.

Phase	Average temperature (℃)	NAT	Water temperature (℃)	Ice width (m)	Thickness (cm)
Shore ice	-1.7	50	2	<0.3	D<1.2
Floating ice	-3.5	50～113	0.5~2	0.3~2.5	0.8~2.5
Frozen ice	-4.3	113～140	t<0.5	--	8~14

a. Initial ice b. Floating ice

c. Ice cover period

Figure 5. Shore ice development process.

(2) Frazil ice

The purpose of the frazil ice observation is to study the original form of the canal ice in winter, it is not observed in this ice observation period.

(3) Floating ice

Floating ice is the other form of canal ice. There are two fixed positions chosen for observing, the first one is upstream the aqueduct (stake NO: 000+000) and the other one is downstream of it (stake NO:102+000). The observations data are shown in Table 9. The observation result shows that temperature (water and air) play an important role in the generation of the canal ice. Figure 6 shows the array-like floating ice moves downstream the canal.

©2017, IAHR. Used with permission / ISSN 1562-6865 (Online) - ISSN 1063-7710 (Print)

Table 9. Characteristic value of the floating ice.

Item	Time	Lowest temperature(℃)	Water temperature (℃)	Flow speed(m/s)	Remark
000+000	2012.1.4	-5.8	1.7	0.11	Array ice layer
102+000	2012.1.8	-7.7	1.1	0.24	Ice group

Figure 6. Array-like floating ice.

(4) Ice discharge

Due to those floating ice cables in front of every sluice gate, ice generated in each canal pool cannot spread through the gate and inverted siphon to next canal pool. Therefore, the ice production of each canal section can be calculated independently. In addition, the ice production is an important criterion to judge whether ice bridge and ice cover can form.

Eq. [1] shows the calculation method of ice discharge, where Qg is ice discharge, B is the width of the floating ice piece, Vg is velocity of floating ice, and Dsg represent the average thickness of the ice.

$$Qg = B\ Vg\ Dsg \qquad [1]$$

3 ANALYSIS

The entire ice information process can be divided into four stages. The first stage (2011.12.16-2012.1.3) is the initial ice period. The daily lowest temperature was -2□, the average daily temperature was below 0□, and the water temperature was higher than 2.7°C, the accumulated negative temperature reached 20.6, and shore ice was the main ice form in this period. The second stage is called the drifting ice period (2012.1.4-2012.1.21). In this period, floating ice began to appear in the canal pool and drifted downstream until the ice booms in front of these control gates. The daily lowest temperature was -5°C, the daily average temperature was below -3□, water temperature was between 0.5°C and 2.7°C, and negative accumulated temperature reached 48□. The third stage (2012.1.22-2012.1.29), which is called the ice cover stage, is the final form of the canal ice. Ice cover finally formed in this period and water run downstream under it. The coldest temperature reached -6°C, the daily average temperature was below -3° C and the water temperature was below 0.5°C, and the accumulated negative temperature reached 112□. The fourth stage (2012.1.29-2012.1.22) is called the melting ice period, and it is the last stage. In this period, as temperatures rose, the canal ice began to melt, some shore ice separated from the canal lining board and drifted downstream with the floating ice from upstream together. The daily lowest temperature was -5°C, the average daily temperature was above -3°C, and the water temperature was above 0.5°C. Specific data are shown in Table 10.

©2017, IAHR. Used with permission / ISSN 1562-6865 (Online) - ISSN 1063-7710 (Print)

Table 10. Ice cover.

Phase	Date	Ice form	Air temperature	Water temperature
Initial ice period	2011.12.16-2012.01.03	Shore ice	Lowest temperature<-2℃ Average temperature< 0℃	T>2.7℃
Drifting ice period	2012.01.04~2012-01.21	Floating ice	Lowest temperature<-5℃ Average temperature<-3℃	2.7℃>T>0.5℃
Ice cover period	2012.01.22~2012-01.28	Ice cover	Lowest temperature<-6℃ Average temperature<-3℃	T<0.5℃
Melting ice period	2012.01.29~2012-02.22	Off shore ice	Lowest temperature<-5℃ Average temperature>-3℃	T>0.5℃

3.1 Shore ice period

3.1.1 Shore ice formation conditions

Some necessary conditions can be concluded through observation results, based on which the shore ice forms initially. First, the weather condition must be satisfied. The NAT should reach more than 20 and the air temperature is below -3□ at night. Secondly, water temperature is another necessary condition, and it must be lower than 4℃. The third one is hydraulics condition where ice cannot form in swift current. The average velocity at the canal shore should be less than 0.08 m/s. In addition, the shore ice formation is also affected by the wind to some extent. The stronger the wind, the higher the waves. If the waves continue to beat the canal lining board, a stable shore ice will be prevented to form at the canal shore. Moreover, there is another character in the shore ice's information, in one day, it usually appears after 10:00 pm and the width reaches the maximum value at 8:00 am of the next day, and then melts again when the sun comes out. This process is often repeated for a period of time until the arrival of a large cold wave.

3.1.2 The conditions of shore ice detachment

As the same as the information process, shore ice melting process is also affected by temperature, solar radiation, wind and waves. By analyzing the prototype observation data, it can be found that when water temperature is above 1.0°C, the daily sunshine time is more than 8 hours and the daytime temperature is higher than 0 ℃, and the shore ice begins to separate from the canal lining board.

Since the heat capacity of concrete is larger than water, the temperature of concrete will rise faster than water under the same solar radiation. Then, the connection between shore ice and the canal lining board begin to weaken, and then shore ice break away from canal shore and move downstream.

3.2 Drifting ice period

There are two kinds of drifting ice forms in this period, namely ice flower and array ice. Ice flower is the initial form of the canal floating ice. With the decrease of temperature and time passing by, ice flowers develop into array ice flow gradually. The array ice layer is a major factor in the formation of ice cover.

3.2.1 Ice flower formation conditions

Ice flowers generally appear in the second or third cooling process, when the flow velocity is smaller than 0.3m/s, the temperature is lower than 5 degrees below zero, and the water temperature is below 1.5e, the ice flower may form in the middle of the water surface. Flow velocity has some certain effect on ice flower information. In general, they appear earlier before the control gates than behind them.

3.2.2 Formation mechanism of drifting ice

First of all, when the night temperature drops to a certain extent, small tiny solid particles floating on the water surface will gradually develop into ice crystals, with themselves as condensation nuclei. Then, these ice crystals freeze each other, spread around and finally form scattered ice flowers. Along with further reducing of the temperature and movement of channel flow, the ice flowers also have gradual increase in area and thickness. The ice thickness is generally less than 1mm at this time. This process generally occurs in the upstream portion of the single channel pool, approximately in the range of 3-5km after a control gate. The ice flower mass continues to flow downstream with the canal pool water, and the area and thickness continue to increase until it can be arrested by canal structures such as piers or bend. At this time, the ice flower group begins to gather and bond into surface ice layer.

©2017, IAHR. Used with permission / ISSN 1562-6865 (Online) - ISSN 1063-7710 (Print)

3.3 Ice cover period

3.3.1 Ice cover formation conditions

It can be seen that the key point of the ice cover formation is the relationship between the amount of ice-melting during the day and the ice production at night, and if the ice production at night is greater than the melted ice during the day, the remaining ice becomes basis of the ice cover next day.

Factors that affect the ice production and the amount of melting ice contain weather conditions and hydraulic conditions, such as air temperature, water temperature, wind speed, flow velocity, discharge, etc. In addition, it is also affected by cold wave, because it will be accompanied by sustained low-temperature weather after a cold wave every time. The ice cover form completely after the fourth cooling in this observation period.

3.3.2 Ice cover developing mode

The ice cover appears from floating ice booms in front of the control gate in every single canal pool. As mentioned earlier, the drifting ice is stopped by the ice boom block, more and more ice gather here and then spread upstream gradually. If the ice is still, it begins to freeze together, and then the whole channel water surface is frozen, ice cover information process finally finishes. If the temperature is low enough, and the time is long enough, ice cover will continue to develop upstream until the entire canal pool is covered by the ice cover.

3.4 Melting ice period

When the daily average temperature rises to a certain stage, the amount of melting ice during the day is more than the ice production at night, the canal enters to the stage of melting ice period. If hydraulic conditions do not change in this period, the canal ice will be only influenced by solar radiation. This kind of ice melting process is called civil breakup. In turn, if hydraulic condition changes, the ice covers are destroyed into pieces by external force like water level fluctuation, then melt in the migration process, this process is called military breakup. The observation result shows that the canal entered into break up period since 2012.1.29. The way of river breaking up was half civil and half military, mainly due to the opening and closing adjustments of the sluice gate in observation period.

4 CONCLUSIONS

Throughout the entire winter canal ice prototype observation, some characteristic of the development of canal ice is summed up. Mainly in the following aspects:

(1) From shore to middle
As previously mentioned, when temperature drops to a certain stage, the canal ice first appears in the form of shore ice, and if the shore ice formed at night does not melt the next day (continuous cold weather), it will thicken and expand to the center of the canal pool.

(2) From point to surface
The characteristics that are from point to surface in channel ice formation process are mainly reflected in the form of floating ice, that is from Ice crystal—Ice flower—Ice flower group—Array ice layer. Firstly, some ice crystals appear with tiny particles (dust) that float on surface of the water as the core, then these ice crystals develop into moving ice flowers gradually, more and more ice flowers bond together in the journey downstream, and finally become pieces of ice layer.

(3) From downstream to upstream
The long canal was divided into several varying length canal pools by control sluices. In order to protect the gate from ice collision, some ice booms were set in front of these gates. When array-like floating ice moves downstream, most of them were stopped by the ice booms and frozen in situ to form ice cover, and then develop upstream gradually.

(4) From north to south
The canal transition from south to north, and it is colder in the north than in the south. Therefore, generally, the canal water in north region freezes first, and the ice develops from north to south in single canal pool.

These results above are available for parameters' calibration in mathematics model on canal ice. They can enrich channel control theory and provide technical support for operation and dispatch of water diversion project, it has strong academic and practical value. This kind of observation should be carried out continuously in order to form a more complete ice data base.

ACKNOWLEDGEMENTS

This study was supported by the National Natural Science Foundation of China (Grant No. 51509015 and, 51309015) and the basic scientific research service fee of the central level Public Welfare Scientific Research Institute of Changjiang River Scientific Research Institute (No. CKSF2016016/SL)

 ©2017, IAHR. Used with permission / ISSN 1562-6865 (Online) - ISSN 1063-7710 (Print)

REFERENCES

Chen, F., Shen, H.T., Andres, D. & Jasek, M. (2005). Numerical simulation of surface and suspended freeze-up ice discharges, In *Impacts of Global Climate Change*, 1-10.

Shen, H.T., Sun, J. & Liu, L. (2000). SPH Simulation of River Ice Dynamics. *Journal of Computational Physics*, 165(2),752-770.

Pariset, E. & Hausser, R. (1961). Formation and Evolution of Ice Covers on Rivers. *Transactions of the E.I.C*, 5(1),41-49.

Shen, H.T. & Chiang, L.A. (1984). Simulation of Growth and Decay of River Ice Cover, *Journal of Hydraulic Engineering*,110(7),958-971.

Shen, H.T. & Wang, D. (1995). Under Cover Transport and Accumulation of Frazil Granules. *Journal of Hydraulic Engineering*, ASCE, 121(2),184-194.

Shen, H.T. (1996). River Ice Processes-State of Research. *13th IAHR International Symposium on ice*, Beijing, China, Aug.

Shen, H.T. (2000). River Ice Transport Theories: Past, Present and Future. *15th IAHR International Symposium on ice,* Gdansk, Poland, Aug.

Shen, H.T., Gunaratna, P.P. & Lal, A.M.W. (1990). Mathematical Model for Ice Processes in River Networks. *IAHR Ice Symp. Int. Assoc. of Hydr. Res. (IAHR)*, Espoo, Finland,726-734.

Wasantha, L.A.M. & Shen, H.T. (1991). Mathematical Model for River Ice Processes. *Journal of Hydraulic Engineering*, 117(7), 851-967.

Xia, X. & Shen, H.T. (2000). Nonlinear Interaction of Shallow Water Wave with River Ice Cover. *15th International Symposium on Ice*, Gdank, Poland, August 28-September 1.

Yapa, P. D. & Shen, H.T. (1986). Unsteady Flow Simulation for an Ice-Covered River. *Journal of Hydraulic Engineering*, ASCE, 112(11),1036-1049.

©2017, IAHR. Used with permission / ISSN 1562-6865 (Online) - ISSN 1063-7710 (Print)

Proceedings of the 37th IAHR World Congress
August 13 – 18, 2017, Kuala Lumpur, Malaysia

VALIDATION OF TRMM 3B43 MONTHLY PRECIPITATION PRODUCT WITH RAIN GAUGES DATA IN GANSU, CHINA DURING 2000-2013

CHENG CHEN [(1)], QIU WEN CHEN [(1)], JIN ZHANG [(1)], YU QING LIN [(1)], SHU HE ZHAO [(2)], ZHENG DUAN [(3)] & XIAO QI

[(1)] Center for Eco-Environment Research, Nanjing Hydraulic Research Institute, Nanjing, China
chencheng@nhri.cn
[(2)] School of Geographic and Oceanographic Sciences, Nanjing University, Nanjing, China
[(3)] Chair of Hydrology and River Basin Management, Technical University of Munich, Munich, Germany

ABSTRACT

Tropical Rainfall Measuring Mission (TRMM) precipitation data with a relatively high spatial resolution and a relatively large scope of space had been widely used to improve forecasting of extreme events in recent years. The present study is to analyze and validate the error structures of TRMM 3B43 monthly precipitation products using rain gauge measurements over Gansu province of China during the year of 2000-2013. The TRMM data at monthly, seasonal and annual scales were validated, and the errors at each rain gauge station were analyzed. The validation results show that the TRMM precipitation data are highly correlated with the rain gauges data, and the correlation degree becomes higher with the accumulation of time. In addition, the TRMM precipitation significantly overestimates the actual precipitation, and the errors at each rain gauges station are highly correlated with annual precipitation (R^2=0.81). It is demonstrated that the satellite-based TRMM 3B43 precipitation data which could capture the spatial heterogeneity of rainfall is effective for hydrological applications in the study area.

Keywords: TRMM 3B43; validation; precipitation; spatial heterogeneity; rain gauge.

1 INTRODUCTION

With global climate warming, the Intergovernmental Panel on Climate Change Fourth Assessment Report (IPCC AR4) pointed out that the energy and water cycle characteristics of global underlying surface has occurred significant changes, which had a greater impact, especially on extreme climate. Over the past several decades, China had experienced several devastating extreme hydrological events, particularly in the context of climate change (Piao et al., 2010). For instance, an unprecedented great flood of 1998 in the Yangtze River and the severe drought of 2010 in southwest China, which resulted in huge losses on national economy and people's life.

Precipitation is a major driving force in global climate change, hydrological cycle, and ecological environment, which has significant importance to agricultural irrigation, disaster prevention, and other production activities (Chen et al., 2015; Duan and Bastiaanssen, 2013; Langella et al., 2010). The traditional method to obtain precipitation data is completely dependent on the observations from point-based rain gauges. However, the method faces challenges in the mountainous and remote areas where the rain gauges sites are scarce. Remote sensing is the only choice for obtaining precipitation at a regional or global scale. Since the successful launch of the first meteorological satellite TIROS-1 in 1960, hundreds of precipitation retrieval algorithm has been developed for all kinds of sensors (Kummerow et al., 1998). Nowadays, more and more global precipitation datasets are produced, such as Climate Prediction Center (CPC) Morphing (CMORPH), Global Satellite Mapping Precipitation (GSMaP), Global Precipitation Climatology Project (GPCP), the Precipitation Estimation from Remote Sensing Information using Artificial Neural Network (PERSIANN), Tropical Rainfall Measuring Mission (TRMM) and Global Precipitation Measurement (GPM).

TRMM satellite created a new era of global precipitation monitoring, and it has been widely used in various fields in recent years, such as hydrological modeling (Immerzeel, 2008; Li et al., 2012), drought and flood disasters (Chen and Zhao, 2016), El Niño episodes (Hamid et al., 2001), fire detection (Giglio et al., 2000) and soil moisture (Stephen et al., 2010). However, numerous studies have shown that sampling errors (approximately 30%) and time errors (± 8% to ± 12% per month) are present in TRMM precipitation products (Franchito et al., 2009). In fact, satellite-based remote sensing is an indirect estimate of precipitation, inherently containing regional and seasonal systematic biases and random errors (Shen et al., 2014), and the uncertainty of TRMM precipitation products need to be evaluated when applied.

Barros et al. (2000) compared the TRMM precipitation data and rain gauge data of Nepal during the monsoon period in 1999, and the results showed that even at altitudes as high as 4,000 m the cumulative monsoon rainfall is comparable to the highest amount recorded in the Indian subcontinent. Islam and Uyeda (2005) compared TRMM 3B42 products rainfalls with surface-based rain gauge rainfall obtained at 31 stations over Bangladesh for the years between 1998 and 2002. It was found that, on an average, TRMM could

 ©2017, IAHR. Used with permission / ISSN 1562-6865 (Online) - ISSN 1063-7710 (Print)

describe about 98.24% of the surface-based rain gauge rainfall. Huffman et al. (2007) pointed out that the TRMM multi-satellite precipitation data (TMPA) could capture precipitation well on monthly scale, but less on slight and short-term precipitation. Collischonn et al. (2008) compared the daily rain gauge station and TRMM satellite precipitation data for large-scale hydrological models, and the results show that TRMM is comparable to the measured data. The TRMM PR (precipitation radar) data at seasonal scales in Brazilian were evaluated by Franchito et al. (2009). The results show that the random errors and systematic errors of the TRMM PR are more sensitive to the seasons and regions. Almazroui (2009) used TRMM 3B42 data to analyze the temporal and spatial distribution pattern of precipitation in Saudi Arabia. The results show that there is underestimation of precipitation in TRMM during rainy season, and the correlation between TRMM precipitation and the rain gauge station data is higher (0.9) at monthly scale. Chen and Zhao (2016) obtained 676 rain gauge measured data in China to verify the accuracy of TRMM 3B43 data in the whole country, and the results show that the TRMM 3B43 has a high correlation degree in different months with coefficient of determination greater than 0.74.

The uncertainty of TRMM precipitation data varies with regional and temporal scales, so it is essential to evaluate the satellite-based precipitation at different regions and multi-temporal scales over long time series. In this paper, the TRMM 3B43 precipitation data from January 2000 to December 2013 in Gansu province of China were obtained. The long time series TRMM precipitation data were validated at monthly, seasonal and annual scales with the rain gauge measured data, and the error structures at each rain gauge station were also analyzed.

2 STUDY AREA AND DATASETS

2.1 Study area

Gansu is located in the northwest inland areas of China, and the territory lies between latitudes 32° and 43° N, and longitudes 92° and 109° E (Figure 1). The elevations in Gansu province have greater disparity, and the topography is slanted downward in the northeast direction from the southwest. Hill and mountains accounted for 78.2% of the total area. Gansu is a typical arid and semi-arid region and is mainly dominated by continental climate, which leads to pronounced temperature differences between winter and summer.

Affected by various factors, such as topography, geographical location and atmospheric circulation, the spatial distribution of precipitation is of great difference in Gansu province. Because of the impact of the high mountain barrier and it is far away from the ocean, the precipitation in northwest region is relatively rare. The maximum value of annual precipitation occurs in the southeast of Gansu (700–800 mm/year), and the minimum value occurs in the northwest (Hexi Corridor, 40–200 mm/year). Most of the precipitation falls in the months of summer (May–September).

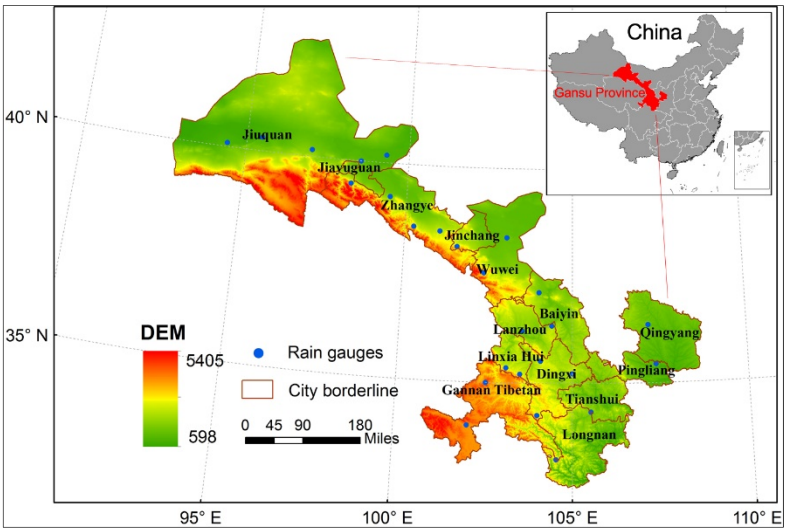

Figure 1. The elevation and rain gauges station of Gansu province in China.

2.2 Datasets

2.2.1 TRMM 3B43 data

The Tropical Rainfall Measuring Mission (TRMM) is a joint endeavor between NASA and Japan's National Space Development Agency, and the satellite was launched on November 28, 1997. TRMM 3B43 precipitation product is created using TRMM-adjusted merged microwave-infrared precipitation rate and root-mean-square precipitation error estimates. It covers areas from 50° S to 50° N latitude, 180° W to 180° E longitude. The TRMM 3B43 data is on a calendar month temporal resolution and a 0.25° by 0.25° spatial

©2017, IAHR. Used with permission / ISSN 1562-6865 (Online) - ISSN 1063-7710 (Print)

resolution, and the 3B43 dataset is the monthly version of the 3B42 dataset (Huffman et al., 2007). In this study, the TRMM 3B43 data from January 1999 to December 2013 were freely available from the NASA database (http://mirador.gsfc.nasa.gov/).

2.2.2 Rain gauges data

Measurements from 25 stations during 2000–2013 were used in this study (see Figure 1), and this datasets were obtained from the China Meteorological Data Sharing Service System (http://data.cma.cn/). The rain gauge stations information in the study area is shown in Table 1.
It could be found that the maximum annual average precipitation (604.46 mm) is in Maqu station, and the minimum value (45.54 mm) occurs in Dunhuang station.

Table 1. Rain gauges information in the study area

No.	Name	Latitude/°N	Longitude/°E	Elevation/m	Annual average precipitation/mm
1	Wudu	33.24	104.55	1079.1	453.04
2	Maqu	34.00	102.05	3471.4	**604.46**
3	Minxian	34.26	104.01	2315.0	573.48
4	Hezuo	35.00	102.54	2910.0	540.96
5	Lintao	35.21	103.51	1893.8	499.05
6	Huajialing	35.23	105.00	2450.6	463.25
7	Linxia	35.35	103.11	1917.2	514.00
8	Xifen town	35.44	107.38	1421.0	555.47
9	Yuzhong	35.52	104.09	1874.4	364.32
10	Jingyuan	36.34	104.41	1398.2	199.87
11	Huanxian	36.35	107.18	1255.6	424.11
12	Jingtai	37.11	104.03	1630.9	181.09
13	Wuwei	37.55	102.40	1531.5	168.16
14	Yongchang	38.14	101.58	1976.9	217.13
15	Minqin	38.38	103.05	1367.5	122.32
16	Shandan	38.48	101.05	1764.6	212.39
17	Zhangye	38.56	100.26	1482.7	135.53
18	Gaotai	39.22	99.50	1332.2	116.61
19	Jiuquan	39.46	98.29	1477.2	94.84
20	Jinta	40.00	98.54	1270.5	69.70
21	Dunhuang	40.09	94.41	1139.0	**45.54**
22	Yumen town	40.16	97.02	1526.0	78.99
23	Dingxin	40.18	99.31	1177.4	58.81
24	Anxi	40.32	95.46	1170.9	45.94
25	Mazongshan	41.48	97.02	1770.4	62.56

2.2.3 DEM

The Shuttle Radar Topography Mission (SRTM) is an international project spearheaded by the National Geospatial-Intelligence Agency (NGA) and the NASA (http://www.nasa.gov/). The SRTM DEM (Digital Elevation Model) data at the spatial resolution of 90 m was used in this study.

3 METHODOLOGY

Various statistical methods including R^2, Bias, RMSE, and MAE have been adopted to validate the performance of TRMM precipitation products. The coefficient of determination (R^2) which reflects the degree of linear correlation between TRMM precipitation and gauge observations was used to calculate the agreement. Formula is as follows:

$$R^2 = \left(\frac{\sum_i^N \left(M_i - \overline{M}\right)\left(P_i - \overline{P}\right)}{\sqrt{\sum_i^N \left(M_i - \overline{M}\right)^2 \left(P_i - \overline{P}\right)^2}} \right)^2 \quad [1]$$

 ©2017, IAHR. Used with permission / ISSN 1562-6865 (Online) - ISSN 1063-7710 (Print)

The relative bias (Bias) describes the systematic bias of satellite precipitation estimates. The value of Bias greater than zero indicates that TRMM precipitation is greater than the gauge observations, or vice versa. Bias is calculated as follows:

$$Bias = \frac{\sum_i^N P_i}{\sum_i^N M_i} - 1 \qquad [2]$$

The root mean square error (RMSE) is used to measure the differences between TRMM precipitation and rain gauges data. Bias is calculated in Eq. [3]:

$$RMSE = \sqrt{\frac{\sum_i^N (P_i - M_i)^2}{N}} \qquad [3]$$

The average absolute error (MAE) in Eq. [4] represents the average magnitude of the errors.

$$MAE = \frac{\sum_i^N (P_i - M_i)^2}{N} \qquad [4]$$

where, M represents the rain gauge observations, P represents the TRMM precipitation, $\overline{M}$ and $\overline{P}$ represent the mean precipitation of the rain gauges and TRMM respectively, and N represents the number of rain gauges.

4 RESULTS AND DISCUSSIONS

4.1 Multi-temporal analysis of TRMM precipitation

The TRMM 3B43 monthly data were validated using 25 effective rain gauge stations data in Gansu Province from 2000 to 2013. Considering the accuracy of TRMM precipitation data is different at different time scales, the applicability of TRMM precipitation data on monthly, seasonal and annual scales are analyzed in this paper.

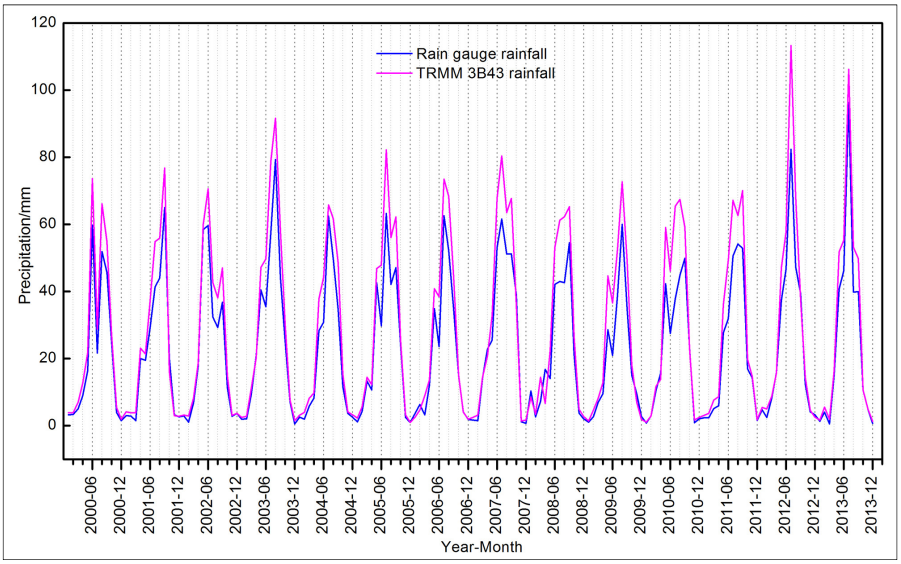

Figure 2. Average monthly precipitation from 2000 to 2013.

Figure 2 shows the average monthly rainfall of TRMM 3B43 and rain gauges data in time series from 2000 to 2013 in the study area. The average monthly precipitation was obtained by averaging the 25 stations' data. It could be seen that the average monthly precipitation of TRMM 3B43 and rain gauges in time series had the same trend, showing obvious cyclical characteristics. In the study area, precipitation is mainly concentrated in the summer, and July and August are the months with the largest precipitation. The average monthly precipitation in the study area is about 60 mm. In general, when rainfall is large, the TRMM precipitation data tend to underestimate precipitation, and this is closely related to the satellite sensor. On one hand, the satellite cannot record the whole process of rainfall. On the other hand, the emission wavelength of PR (precipitation radar) is longer than the ground radar. The longer the wavelength, the smaller the sensor's

©2017, IAHR. Used with permission / ISSN 1562-6865 (Online) - ISSN 1063-7710 (Print)

ability to sense rain attenuation. Therefore, the smaller rainfall (less than 0.7mm/h) will not be monitored by satellite sensor, resulting in relatively small satellite observations. In addition, when the rainfall is zero, the satellite observations usually indicate the presence of rainfall. The TRMM 3B43 monthly precipitation in Gansu Province significantly overestimates the actual rainfall, and the higher of rainfall, the greater overestimation of TRMM data. This phenomenon may be related to the mountainous terrain of the study area and the coarse resolution. Generally, rainfall in the more complex terrain is affected by multiple factors, which could lead to relatively larger errors of the satellite-based precipitation. It is worth mentioning that the spatial resolution of TRMM precipitation is 0.25° (about 27.5 km), which results in the difficulty to match between TRMM and rain gauge station.

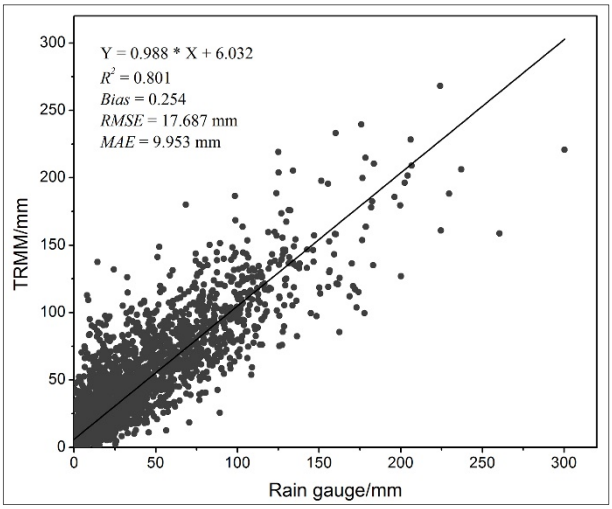

Figure 3. Fitting results of the monthly precipitation between TRMM and rain gauges.

Figure 3 shows the fitting results of monthly precipitation between TRMM and rain gauges data during 2000-2013 in 25 measured stations. The fitting results with a high determination coefficient (R^2=0.801, P<0.001) indicate that the TRMM 3B43 monthly precipitation data could basically meet the practical application requirements.

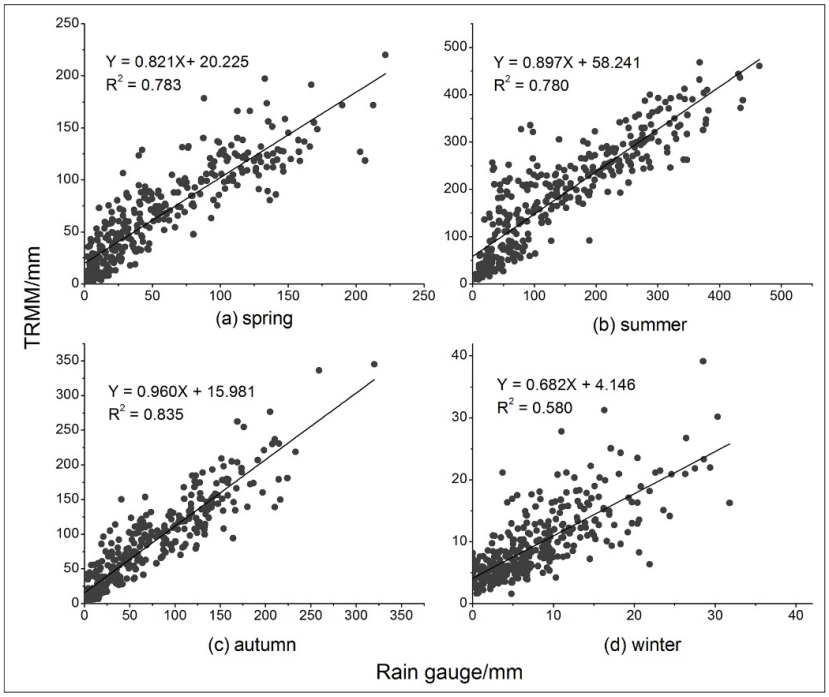

Figure 4. Fitting results of each seasonal precipitation between TRMM and rain gauges.

Figure 4 shows the fitting results of each seasonal precipitation between TRMM and rain gauges, and Figure 4(a)-4(d) represents the fitting results in spring (March to May), summer (June to August), autumn (September to November) and winter (December to February), respectively. It could be seen from Figure 4 that the fitting results are different for different seasons. The optimal fitting result occurs in autumn, while in

 ©2017, IAHR. Used with permission / ISSN 1562-6865 (Online) - ISSN 1063-7710 (Print)

winter the fitting result is the smallest (R^2=0.58) reflecting the smaller rainfall season, which has the worst accuracy. The coefficient of determination (R^2) represents the close relationship between the two datasets, but it cannot accurately reflect the deviation between two datasets. Although the TRMM satellite precipitation in winter has the lowest R^2, the MAE is smaller than that of other seasons because of the relatively small rainfall.

Table 2. Fitting results at different scales between TRMM and rain gauges.

Scale	R^2	Bias	RMSE/mm	MAE/mm
Monthly	0.801	0.254	17.687	9.953
Seasonal	0.855	0.254	39.607	23.563
Annual	0.845	0.254	107.774	78.805

Table 2 shows the fitting results at monthly, seasonal and annual scales between TRMM and rain gauges data from 2000-2013 in the study area. If compared with the monthly fitting results, the TRMM data at seasonal scale had an improvement with R^2 from 0.801 to 0.855. The TRMM precipitation at annual scale with R^2 equal to 0.846 also showed a better fitting result than monthly result and each seasonal results (Figure 4). It was demonstrated that the correlation degree between TRMM and rain gauges data becomes higher with the accumulation of time. The Bias, calculated according to Equation 3, does not change anymore at different scales, and it is because the sum of TRMM precipitation and rain gauges data are always the same at different scales. The RMSE and MAE increase from monthly to annual scales because of the accumulation of errors. The values of R^2 are larger in seasonal and annual scales, but relatively RMSE and MAE remind us that a calibration procedure should be carried out to reduce the errors when the TRMM data were used.

4.2 Validation at each single rain gauge station

Thiessen polygon first proposed by the climatologist Thiessen AH is frequently used to calculate the average rainfall of the discrete distribution of meteorological stations. In this paper, the thiessen polygon tool in ArcGIS 10.2 was used to segment 25 rain gauge stations within the study area. The monthly precipitation data from 2000-2013 (14 years/168 months) at each station were fitted, and the fitted results of R^2 are shown in Figure 5.

It could be seen from Figure 5 that the values of R^2 are ranged from 0.5 to 0.9, and the distribution in space shows an obvious trend of southeast high northwest low. This trend is similar with the average annual precipitation, demonstrating TRMM data at the sites with larger average annual precipitation have a good correlation with rain gauges data. In order to further analyze the influence factors of the spatial distribution of R^2, the DEM and mean annual precipitation data at each station were used to fit with R^2. The results are shown in Figure 6, in which the quadratic polynomial fitting is the best. It can be seen that the annual precipitation had the optimal fitting result (R^2 = 0.81), and this results are consistent with the above conclusions, that is, TRMM satellite precipitation data is in good agreement at the rain gauge where the rainfall is relatively larger. The elevation also has a positive impact on the spatial distribution of the R^2 on time series.

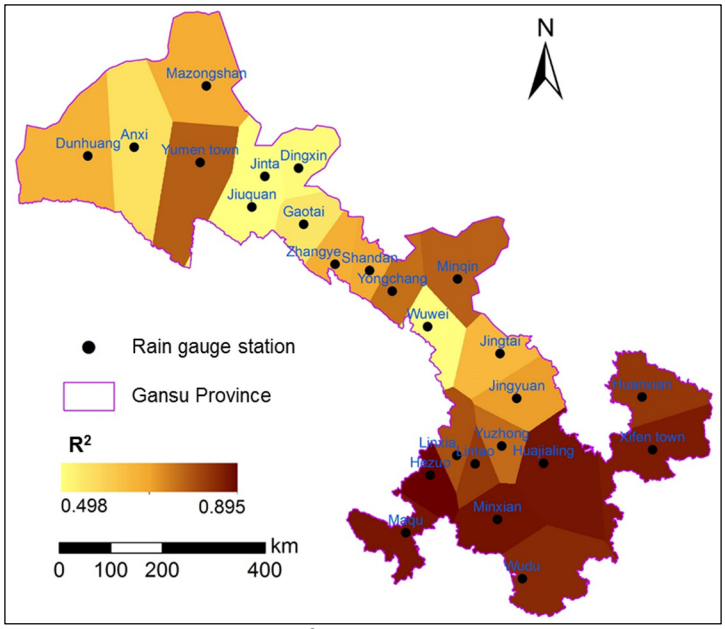

Figure 5. Spatial distribution of R^2 on time series at each rain gauge station.

©2017, IAHR. Used with permission / ISSN 1562-6865 (Online) - ISSN 1063-7710 (Print)

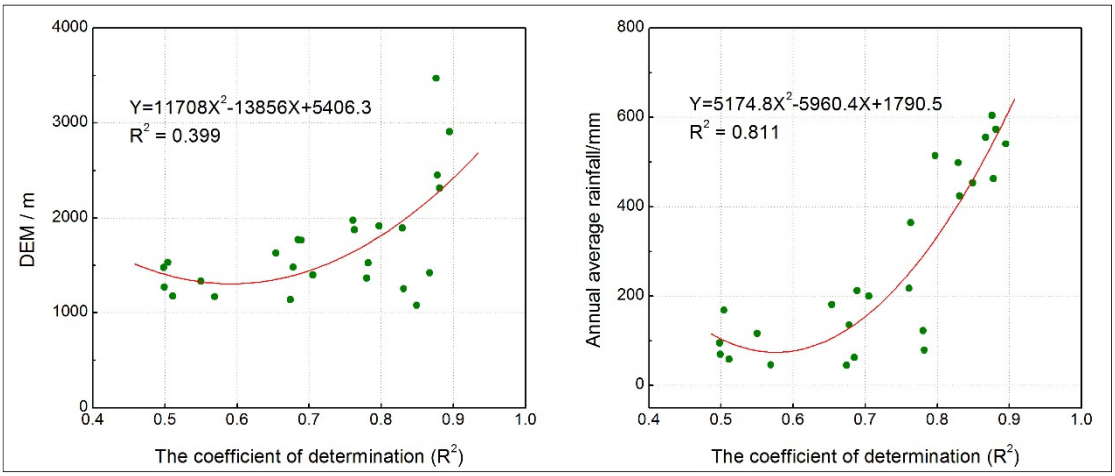

Figure 6. Fitting results between elevation, annual precipitation and R^2 on time series in the study area.

Figure 7 shows the spatial distribution of TRMM mean annual precipitation from 2000 to 2013 in Gansu Province, and the mean annual precipitation at each rain gauge is shown in Table 1. It is found that precipitation has typical spatial heterogeneity in the study area. The precipitation inside each thiessen polygon is different, thus the thiessen polygon method which represents precipitation inside each polygon using the single value is not suitable for obtaining the rainfall in space. The interpolation method which ignores the spatial heterogeneity will also have bad results, in which the number of rain gauges is sparse. The surface-based TRMM 3B43 data, which could capture the spatial heterogeneity of precipitation effectively, is suitable for hydrological applications in the study area.

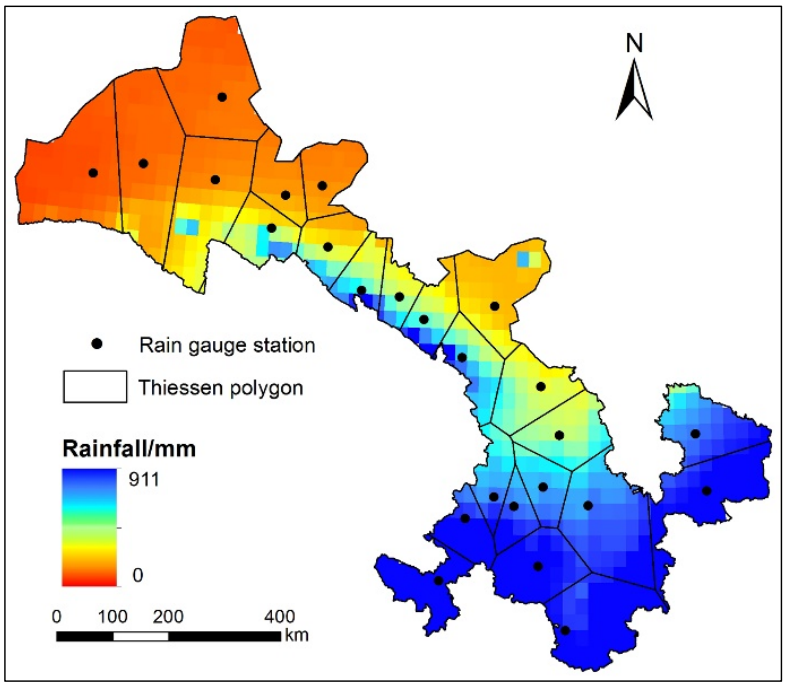

Figure 7. Spatial distribution of TRMM mean annual precipitation from 2000 to 2013.

5 CONCLUSIONS

The TRMM 3B43 monthly precipitation product in Gansu province of China from January 2000 to December 2013 at different scales were validated by 25 rain gauge stations data in this study. It was found that the TRMM precipitation data at monthly, seasonal and annual scales are highly correlated with the rain gauge stations data (with R^2 greater than 0.8) in the study area, and the correlation degree becomes higher with the accumulation of time. The coefficient of determination in autumn is the largest (0.84), while the winter has the smaller value of R^2 (0.58). The error analysis at each rain gauge station showed that the spatial distribution of R^2 (fitting results between TRMM and rain gages data on time series) is in good agreement with average annual precipitation (R^2=0.81), which has an obvious trend of southeast high northwest low. The TRMM 3B43 precipitation data which could capture the spatial heterogeneity of precipitation well in the study area are suitable for hydrological applications.

 ©2017, IAHR. Used with permission / ISSN 1562-6865 (Online) - ISSN 1063-7710 (Print)

ACKNOWLEDGMENTS

This work was supported in part by the Project funded by Nanjing Hydraulic Research Institute under Grant Y916032 and in part by the Science and Technology Promotion Project of Ministry of Water Resources under Grant TG1528.

REFERENCES

Almazroui, M. (2011). Calibration of TRMM Rainfall Climatology over Saudi Arabia during 1998–2009. *Atmospheric Research,* 99(3), 400-414.

Barros, AP., Joshi, M., Putkonen, J. & Burbank, D.W. (2000). A Study of the 1999 Monsoon Rainfall in a Mountainous Region in Central Nepal Using TRMM Products and Rain Gauge Observations. *Geophysical Research Letters*, 27(22), 3683-3686.

Chen, C. & Zhao, S. (2016). Drought Monitoring and Analysis of Huanghuai Hai Plain Based on TRMM Precipitation Data. *Remote Sensing Land Resources*, 28(1), 122-129.

Chen, C., Zhao, S., Duan, Z. & Qin, Z. (2015). An Improved Spatial Downscaling Procedure for TRMM 3B43 Precipitation Product Using Geographically Weighted Regression. *IEEE Journal of Selected Topics Applied Earth Observations and Remote Sensing*, 8(9), 4592-4604.

Collischonn, B., Collischonn, W. & Tucci, C.E.M. (2008). Daily Hydrological Modeling in the Amazon Basin Using TRMM Rainfall Estimates. *Journal of Hydrology*, 360(1), 207-216.

Duan, Z. & Bastiaanssen, W.G.M. (2013). First Results from Version 7 TRMM 3B43 Precipitation Product in Combination with a New Downscaling–Calibration Procedure. *Remote Sensing Environment*, 131, 1-13.

Franchito, S.H., Rao, V.B., Vasques, A.C., Santo, C.M. & Conforte, J.C. (2009). Validation of TRMM Precipitation Radar Monthly Rainfall Estimates Over Brazil. *Journal of Geophysical Research*, 114(D2), 1-9.

Giglio, L., Kendall, J.D. & Tucker, C.J. (2000). Remote Sensing of Fires with the TRMM VIRS. *International Journal of Remote Sensing*, 21(1), 203-207.

Hamid, E.Y., Kawasaki, Z.I. & Mardiana, R. (2001). Impact of the 1997–98 El Nino Event on Lightning Activity over Indonesia. *Geophysical Research Letters*, 28(1), 147-150.

Huffman, G.J. (2007). The TRMM Multisatellite Precipitation Analysis (TMPA): Quasi-Global, Multiyear, Combined-Sensor Precipitation Estimates At Fine Scales. *Journal of Hydrometeorology*, 8(1), 38-55.

Immerzeel, W.W. & Droogers, P. (2008). Calibration of a Distributed Hydrological Model Based on Satellite Evapotranspiration. *Journal of Hydrology*, 349(3), 411-424.

Islam, N. & Uyeda, H. (2005, July). Comparison of TRMM 3B42 Products with Surface Rainfall over Bangladesh. *IGARSS*, 4112-4115.

Kummerow, C., Barnes, W., Kozu, T., Shiue, J. & Simpson, J. (1998). The Tropical Rainfall Measuring Mission (TRMM) Sensor Package. *Journal of Atmospheric and 0ceanic Technology,* 15(3), 809-817.

Langella, G., Basile, A., Bonfante, A. & Terribile, F. (2010). High-Resolution Space Time Rainfall Analysis Using Integrated ANN Inference Systems. *Journal of Hydrology*, 387(3), 328-342.

Li, XH., Zhang, Q. & Xu, C.Y. (2012) Suitability of The TRMM Satellite Rainfalls in Driving A Distributed Hydrological Model for Water Balance Computations in Xinjiang Catchment, Poyang Lake Basin. *Journal of Hydrology*, 426, 28-38.

Piao, S. (2010). The Impacts of Climate Change on Water Resources and Agriculture in China. *Nature*, 467(7311), 43-51.

Shen, Y., Zhao, P., Pan, Y. & Yu, J. (2014). A High Spatiotemporal Gauge-Satellite Merged Precipitation Analysis over China. *Journal of Geophysical Research*, 119(6), 3063-3075.

Stephen, H., Ahmad, S., Piechota, T.C. & Tang, C. (2010). Relating Surface Backscatter Response from TRMM Precipitation Radar to Soil Moisture: Results over a Semi-Arid Region. *Hydrology Earth System Sciences*, 14(2), 193-204.

©2017, IAHR. Used with permission / ISSN 1562-6865 (Online) - ISSN 1063-7710 (Print)